University of Catania

Department of Biological, Geological and Environmental Sciences

PhD course on Earth and Environmental Sciences

XXXIV PhD Cycle

Microstructural and chemical characterization of mineral fibres of high impact for environmental pollution

———————————————

Claudia Ricchiuti

PhD supervisors

Prof. Rosalda Punturo

Prof. Andrea Bloise

Year 2022

Table of Contents

1. Introduction and aim of the work

Now-a-day, it is well known in the scientific community that the exposure to asbestos may lead to the development of health issues. Due to their physical properties, the six silicate minerals defined as asbestos (chrysotile, tremolite, actinolite, amosite, crocidolite, anthophyllite), have been widely exploited worldwide to produce Asbestos-Containing Materials (ACMs).

To date, according to the Italian law (L. 257/92), the extraction, the use and marketing of asbestos in Italy is currently banned, whereas only in the 34% of the countries in the world the use of regulated asbestos is restricted. Although the existing restriction, the human health is still endangered due to the exposure to the natural occurrence of asbestos (NOA) which represents a big concern. The term NOA refers to asbestos present in geological deposits (i.e., rocks and soils) that, due to human activities (e.g., road construction, excavation) or weathering processes (e.g., erosion), may be disturbed and release asbestos fibres into the environment thus representing a source of fibres dispersion. The risk to human health consists of the potential inhalation of asbestos fibres which may penetrate the lungs thus causing cancer pathologies (IARC, 2009). The World Health Organization (WHO) established that respirable fibres have length $> 5\mu m$, width < 3 μm and aspect ratio ≥ 3.

The main lithotypes associated with the presence of asbestos minerals are rocks from the ophiolite complexes (i.e., metabasite and serpentinite) which represent metamorphosed oceanic lithosphere; they have been of great interest to the scientific community for years. Much less literature studies refer to asbestos-bearing soils whose examination is extremely important as well (Ricchiuti et al., 2020). Derived soils inherit the mineralogical and geochemical characteristics of the bed rock (Chesworth, 1992) and may contain hazardous fibres that can be released into the air (for instance because of agricultural activities) and therefore, they may represent a source of risk to human health.

In addition to the morphometric features (e.g., morphology, size, surface area, density) of the fibres, another aspect that should not be underestimated is represented by the geochemical composition of the fibres. As a matter of fact, asbestos fibres are capable to host potentially toxic elements (PTEs) in their structure that, once inhaled, can be released into the lungs due to the dissolution processes and they may induce lung cancer (Schereier et al., 1987; Wei et al., 2014).

In this scenario, the present study aims to address a twofold aspect: *i)* the dangerousness of the fibres related to their morphometric parameters (e.g., morphology, size), and *ii)* the role of potentially toxic elements (PTEs) in inducing asbestos related diseases.

Therefore, the present work of thesis is focused on the mineralogical and geochemical characterization of serpentinite rocks and derivative soils occurring in Southern Apennines (Calabria and Basilicata region) as well as on chemical characterization of three asbestos fibres types (chrysotile, tremolite, actinolite) extracted from serpentinites samples. Due to the high impact of naturally occurring asbestos (NOA) on human health, the study areas are of great scientific interest. As a matter of fact, 70 mesothelioma deaths caused by asbestos exposure have been recorded by the Italian National Mesothelioma Register in the Calabria region between 1993 and 2015 (INAIL, 2015). Similarly, relevant excess of negative health effects NOA-correlated cases has been highlighted by epidemiological studies conducted on twelve villages of the Basilicata region (Caputo et al., 2018).

The main goals of the present study were the definition of *i)* asbestos minerals occurrence in the study area, *ii)* the morphometric parameters (e.g., morphology, size) of the fibres to identify the respirable ones, potentially dangerous to human health, *iii)* the concentration of potentially toxic elements (PTEs) firstly in asbestos-containing rocks and soils, and secondly in isolated fibres.

The outcomes of this study have been published on various scientific magazines (summarized in figure 1) with the aim of providing a contribution to the territory mapping relatively to the natural asbestos occurrences in Southern Apennines as well as a better understanding of this issue in both geological and environmental perspective. Specifically, the findings related to the mineralogical and geochemical characterization of rocks and derived soils occurring in the study area can be found in Punturo et al. (2018, 2019a) and Bloise et al. (2019, 2020a) while those related to the chemical characterization of individual asbestos fibres can be found in Bloise et al. (2020b) and Ricchiuti et al. (2021). Moreover, a review study based on the most relevant available literature, testifying the presence of fibrous minerals in soils worldwide has been conducted during the doctoral period to provide a summary of asbestos-containing soils investigation conducted so far (Ricchiuti et al., 2020). Finally, to improve the knowledge on this topic, other asbestos-containing rocks from quarries located outside the study area (i.e., serpentinites from Sierra Nevada and Sierra de los Filabres, South-eastern Spain and white marbles from Namibia, South-western Africa) have been investigated (Punturo et al., 2019b; Bloise et al., 2021). The PhD candidate contribution on the scientific study included various activities such as the use of different analytical techniques for the morphological, mineralogical, and geochemical characterization of the samples, the data processing and the papers preparation, participating as co-author or first author.
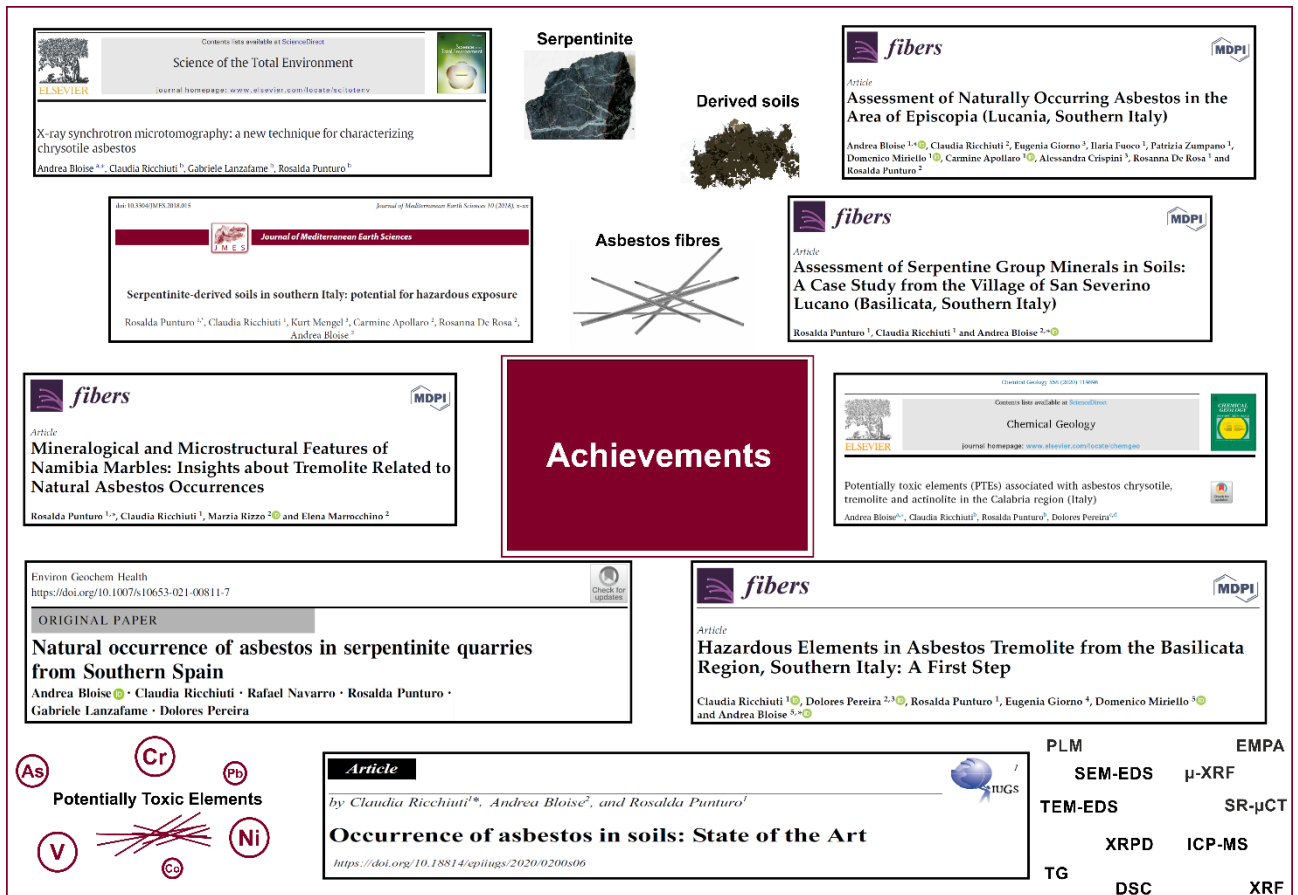
Figure 1: summary of the main goals achieved during the PhD period.

2. Asbestos: some outlines of historical background and state of the art

The name asbestos comes from the ancient Greek "ἄσβεστος" that means "inextinguishable" and refers to six fibrous silicates belonging to the serpentine (chrysotile) and amphibole (tremolite, actinolite, amosite, crocidolite, anthophyllite) groups (WHO, 1986; NIOSH, 2008; Ballirano et al., 2017).

Asbestos has been used since prehistorical times as reported by the first evidence dating back to the Persians and the ancient Romans when it was often used for ritual purposes since people were convinced of its magical properties. Due to their physical-mechanical and chemical properties, which made it an excellent material for many industrial applications, asbestos has been widely marketed and exported all over the world to create Asbestos Containing Materials (ACMs). Among its main characteristics, it is recognized the high tensile strength, the flexibility, the heat resistance as well as the fact to be chemically inert (or nearly so). Some examples of common commercial products made by asbestos include roofing, insulation, plaster, cement, textiles (McDonald, 2003).

The most ancient use of asbestos dates back to 4500 ago in what is currently Finland, where it was mixed with clay to form ceramic utensils and pots while the use as textile was known since 3000-3500 years ago in China and Greece. Due to its high versatility, asbestos began to be used in a wide range of product of daily life such as shoes and cigarette filters, reaching the highest peak of production in the 1970s. After that time, there was a drastic decreasing of asbestos production in Europe, while an important increase of its use was registered in non-EU countries (e.g., Asia, China, India, Africa, Brazil; Vogel, 2005).

The workers of asbestos factories were the most exposed to potentially inhalable fibres since they were in contact with it every day; even if they did not directly handle raw asbestos, they worked in a contaminated environment with materials containing asbestos such as factory tools or equipment (Figure 2). An example of a big asbestos factory in Italy, is represented by the Eternit factory at Casale Monferrato (North of Italy), operating from 1906 to 1986 (Figure 3). The factory was built in a territory famous for its clay (essential for cement production) and at about 100 km from Balangero that is the largest chrysotile asbestos mine in Western Europe (Meni, 2012). It was extended in an area of about 94.000 m^2 and it had up to 5000 workers.

Figure 2: photograph from the 1930s showing textile mill workers during the production of asbestos cloth at the Garlock Packing Company (New York, America) from asbestos.com

Figure 3: eternit factory at Casale Monferrato (northern Italy). (yespolitical.com)

The World Health Organization (WHO) calculated approximately the asbestos exposure during mining, milling or industrial activities, estimating about 125 million workers over the world and about 1.3 million workers in the USA, resulting in 13.885 deaths because of asbestosis between 1994 and 2010 (Diandini et al., 2013; Stayner et al., 2013).

The first evidence of the connection between the asbestos exposure and health negative effects dates to the 20th century, when Cooke (1924) showed the link between the development of lung fibrosis and occupational exposure to mineral fibres of a worker in a textile plant in Lancashire (England). In the following years many studies highlighting the development of lung diseases after the asbestos exposure were published (Nordman 1938; Wedler, 1943; Wagner et al., 1960) and asbestos was declared a human carcinogen by the US Environmental Protection Agency (EPA, 1986), the International Agency for Research on Cancer (IARC) of the World Health Organization (WHO) and the National Toxicology Program (Nicholson, 1986; IARC, 2012c).

Medical studies involving employees working in asbestos industries (occupational exposure) showed that they developed non-cancerous and cancerous pathologies. The non-cancerous ones include: *i)* asbestosis, typically caused by high exposure levels and long period of time; and *ii)* pleural changes or pleural plaques, that is often asymptomatic; while the cancerous pathologies include: *i)* lung cancer, developed as individual masses in the lungs; *ii)* mesothelioma, that is a rare cancer caused by inhaling asbestos fibres and it can form in the lining of the lungs, heart or abdomen (PHE, 2007). These tumors are characterized by prolonged latency period that begin years after the first exposure (Capella et al., 2017).

Starting in the late 1980s, more and more countries began to ban or regulate the use of asbestos containing materials (ACMs) but despite this, only in 67 over 195 countries (34%) in the world the use of regulated asbestos minerals is restricted today (Table 1; Gualtieri et al., 2017a). In the specific case of Italy, with the law No. 257 of 27/03/1992 the use and marketing of asbestos and all materials containing asbestos has been denied. Nevertheless, due to their extensive use in the past, ACMs represent a persistent source of environmental pollution despite the legal prohibitions adopted by many countries (Ricchiuti et al., 2020). As a matter of fact, it has been estimated that about 150 million m^2 of asbestos-based products and more than two thousand million m^2 of cement-asbestos roofing are still present today (Gualtieri et al., 2009). Even though ACMs are well stored, the fibrous structure of asbestos could still be maintained thus enhancing the importance of finding methods able to destroy the structure of asbestos (Kusiorowski et al., 2013).

National Asbestos Bans[1]				
Algeria	Czech Republic	Iraq	Mauritius	Seychelles
Argentina	Denmark	Ireland	Monaco	Slovakia
Australia	Djibouti	Israel	Mozambique	Slovenia
Austria	Egypt	Italy	Netherlands	South Africa
Barain	Estonia	Japan	New Caledonia	Spain
Belgium	Finland	Jordan	New Zeland	Sweden
Brazil	France	Korea (South)	Norway	Switzerland
Brunei	Gabon	Kuwait	Oman	Taiwan5
Bulgaria	Germany	Latvia	Poland	Turkey
Canada	Gibraltar	Liechtenstein	Portugal	United Kingdom
Chile	Greece	Lithuania	Qatar	Uruguay
Colombia	Honduras	Luxembourg	Romania	
Croatia	Hungary	Macedonia	Saudi Arabia	
Cyprus	Iceland	Malta	Serbia	

Table 1: list of countries where the use of all types of asbestos is banned (exemptions for minor uses are allowed in some countries listed) List compiled by Laurie Kazan-Allen and modified and revised in July 15, 2019 (http://www.ibasecretariat.org/alpha_ban_list.php).

It is worth mentioning, that many countries promote the safe use of chrysotile for industrial purpose assuming that its potential toxicity is lower than that one of amphiboles (McDonald et al., 1980; McDonald and McDonald, 1997) since it is less biodurable, and therefore they still produce and consume asbestos (i.e., China, India, Russia, Kazakhstan, Zimbabwe, Brazil etc.). The issue is object of debate and the mechanisms by which mineral fibres induce cyto- and genotoxic damage is not fully understood due to the high variability of fibres in terms of morphology, size, chemistry biopersistence, surface activity etc. (Donaldson et al., 2010).

In addition to the risks related to the use of ACMs, the environmental exposure to the naturally occurring asbestos (NOA) represents an unsolved concern. The term NOA refers to asbestos fibres occurring in rocks (e.g., serpentinite or altered ultramafic rocks) and soils, referring to those not extracted for commercial purposes (Bloise et al., 2008; Harper, 2008; Pugnaloni et al., 2013; Wroble et al., 2020).

The global territory is interested by the widespread occurrence of natural asbestos (see chapter 5) and the risk to human health is represented by the potential inhalation of asbestos fibres released into the air because of human activity and weathering processes that may disturb NOA-bearing rock or soil thus causing the production of dust containing fibres. As a matter of fact, asbestos does not pose a threat until broken or disturbed. Italy is characterized by abundant occurrence of ultramafic rocks and ophiolites in Alps and Apennines (see chapter 6) that have been mined in the

past to extract the stone for different purposes. Among the main mining and quarrying sites in our territory there are Balangero (Piedmont) and Valmalenco (Lombardy).

Balangero was the biggest chrysotile mine of Europe from 1920s to the 1990s, situated in a serpentinite body of the Lanzo Massif that is the largest ultramafic body of the Western Alps (Compagnoni et al., 1983). In Valmalenco, long-fibres of chrysotile were extracted in underground mines in the past, leaving large amount of mining waste.

The impact of NOA exposure on human health is object of great interest in the scientific community and many literature studies showed an association with neighborhood exposure to asbestos and an increased risk of deaths from lung diseases for those people who leave nearby naturally occurring asbestos deposits (Punturo et al., 2018, 2019; Bloise et al., 2019).

3. Mineral species belonging to asbestos

The name "asbestos" is a generic term referring to six silicate minerals belonging to the serpentine and amphibole groups and occurring with a fibrous habit. The Italian Legislation (D.L. 257, 15/08/91), identified chrysotile, tremolite, actinolite, amosite (i.e., the fibrous varieties of grunerite), crocidolite (i.e., the fibrous varieties of riebeckite) and anthophyllite as asbestos minerals (Table 2).

Regulatory name	Mineral name	Mineral group	Ideal chemical formula
Chrysotile	Chrysotile	Serpentine	$Mg_3Si_2O_5(OH)_4$
Tremolite asbestos	Tremolite	Amphibole	$Ca_2Mg_5Si_8O_{22}(OH)_2$
Actinolite asbestos	Actinolite	Amphibole	$Ca_2(Mg,Fe^{2+})_5Si_8O_{22}(OH)_2$
Anthophyllite asbestos	Anthophyllite	Amphibole	$Mg_7Si_8O_{22}(OH)_2$
Crocidolite	Riebeckite	Amphibole	$Na_2Fe_3^{2+},Fe_2^{3+}Si_8O_{22}(OH)_2$
Amosite	Cummingtonite-grunerite	Amphibole	$(Mg,Fe^{2+})_7Si_8O_{22}(OH)_2$

Table 2: list of asbestos minerals with regulatory name, mineral name, mineral group and related ideal chemical formulas.

3.1. Chrysotile

The mineral species belonging to serpentine group are three and are structurally distinct: *i*) chrysotile, *ii*) lizardite, and *iii*) antigorite, with ideal formula is $Mg_3(OH)_4Si_2O_5$.

Chrysotile is the fibrous variety of serpentine, and it is the most serpentine-asbestos even though antigorite, generally described as platy together with lizardite, may occur in similar fibrous shape as chrysotile (Keeling et al., 2008).

The crystallographic structure of chrysotile is layered and made up of SiO_4 tetrahedral (T) and $Mg(OH)_2$ octahedral layers (O, Brucite sheets) shearing oxygen atoms, generally separated by lateral distances of 0.305 nm in the silicate layer and 0.342 nm in the brucite layer (Virta et al., 2002; Figure 4). The typical fibrous crystal habit of chrysotile is defined by the mismatch between these two layers due to the different parameters of the T and O sheets (T sheet is the smallest), thus resulting in a differential strain responsible for a curvature of the TO layers (Ballirano et al., 2017). The curvature radius diameters of the external layers can reach 25 nm while that of internal ones ranges from 2.5 to 3.0 nm, thus producing fibrils (unit fibres) with external diameters ranging between 20 and 50 nm (Virta et al., 2002). Depending on the stacking of the T and O sheets in the

chrysotile structure, three types of chrysotile fibres can be generated: *i)* clino-chrysotile (x parallel to fibre axis), *ii)* ortho-chrysotile (x parallel to fibre axis), *iii)* para-chrysotile (y parallel to fibre axis). Therefore, the fibrils are arranged by concentrically or spirally curved layers, thus forming a tubular structure (Yada 1967; Figure 5) with hollow cores having diameter of about 5-8 nm (Cressey et al., 1994) that may be vacant or filled by silica, iron-rich amorphous phases or occupied by large ionic radii elements (Bloise et al., 2012; Lafay et al., 2014).

The substitutions of Si^{4+} and Mg^{2+} by other cations may occur in chrysotile structure. Specifically, Al^{3+} may replace both Si^{4+} in the tetrahedral layer and Mg^{2+} in the octahedral layer, Fe^{2+} and Fe^{3+} ions, can replace Mg^{2+} in the octahedral layer (Stroink et al., 1980; Hardy and Aust, 1995) and rarely Fe^{3+} may replace Si^{4+} in the T sheet (Blaauw et al., 1979; O'Hanley and Dyar, 1998). Trace elements such as Cr^{3+}, Co^{2+}, Mn^{2+}, Ni^{2+}, Zn^{2+}, Cu^{2+}, can replace Mg^{2+} in the octahedral sites (Wicks and O'Hanley 1988; Bloise et al., 2016a).
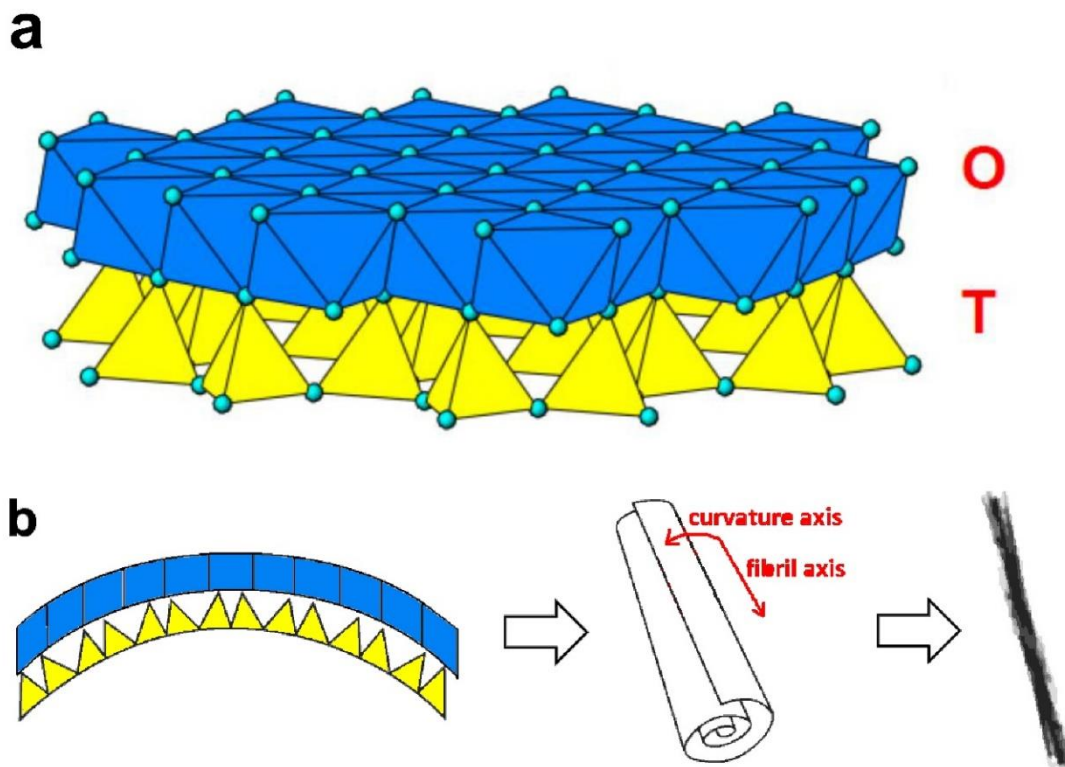

Figure 4: a) sketch of chrysotile structure with SiO_4 tetrahedral sheet joined to $Mg(OH)_2$ octahedral sheet (b-c crystallographic plane); b) TO layers bending in chrysotile asbestos (molecular scale), resulting in a rolling paper-like rolled carpet-like microstructure that is the fibril at the microscale (Modified after Gualtieri et al., 2012).
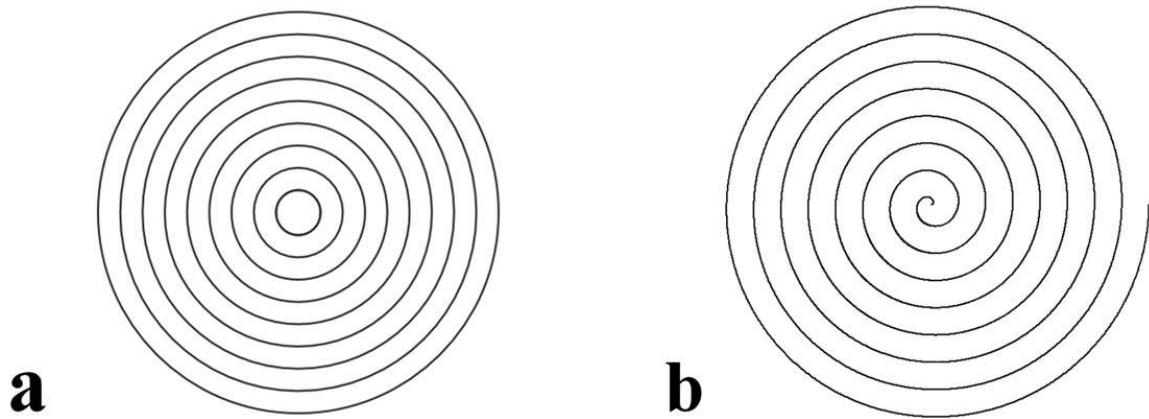
Figure 5: fibril morphology depending on the rolling mode: a) cylindrical circular (concentric) lattice; b) cylindrical spiral lattice (Gualtieri et al., 2017b).

3.2 Amphibole asbestos

As mentioned above, the amphibole species falling into the asbestos family are five and are reported in Table 1.

The crystal habit of amphiboles varies from prismatic to acicular due to the various minerogenetic conditions. Differently to chrysotile, the crystal structure of amphiboles does not lead to fibre formation. As a matter of fact, a strongly preferential mineral growth along the *c* axis is needed to generate the asbestiform habit of amphiboles (Whittaker, 1979).

From the crystallographic point of view, the structure of amphiboles consists of a double $(Si_4O_{11})^{6-}$ chains T(1) and T(2) running parallel to *c*-axis, which are bonded to octahedral strips consisting of three octahedral sites M(1), M(2), M(3). The strip of octahedra and the double chain of tetrahedra, are linked by the M(4) (the B site), and below the hexagonal ring, at the center of the cavity there is the A site with a nominal coordination of [12] (Figure 6).

The simplified formula of amphiboles (Veblen, 1981) can be expressed as follows:

$$\mathbf{A\ B_2\ C_5\ T_8\ O_{22}\ W_2}$$

A = Na, K, □ (vacancy), Ca, Li; irregular cation sites, generally in the [12] coordinated cavity

B = Na, Li, Ca, $Mn^{2+,}$ $Fe^{2+,}$ Mg; [8] coordinated cavity

C = Mg, Fe^{2+}, Mn^{2+}, Al, Fe^{3+}, Mn^{3+}, Ti^{4+}, Li; quite regular octahedral cation sites

11

T = Si, Al, Ti^{4+}; tetrahedral sites within the silicate chain

W = (OH), F, Cl, O^{2-}.

Amphiboles have high capability for hosting many trace elements (Scambelluri et al., 1997; Tiepolo et al., 2007) such as Zn, Ni^{2+}, Co^{2+}, V^{3+}, Sc, Cr^{3+} and Zr, that represent lattice substitution in certain crystallographic sites (M1, M2, M3 and M4) (Hawthorne et al., 2012).

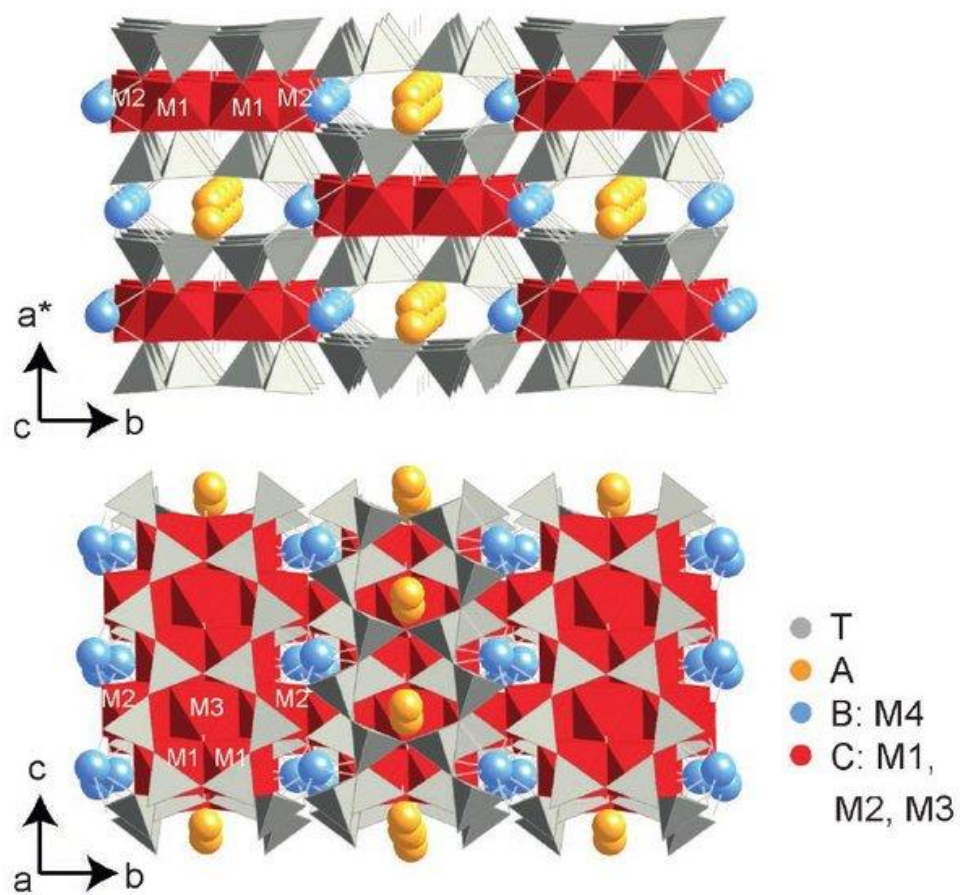

Figure 6: crystal structure of amphiboles (Biederman et al., 2015).

4. Asbestos and human health: pathological effects of asbestos fibres

Nowadays it is accepted that the exposure to mineral fibres may increase the risk of various diseases. The first systematic investigations based on health effects of minerals on human health, began around the second half of the 20th century (Guthrie, 1997) during which several cases of pleural mesothelioma in miner workers of asbestos contaminated mines located in South Africa, were documented (occupational-exposure, Wagner et al., 1960, Newhouse and Thompson, 1965). Asbestos fibres can penetrate the body by *i)* inhalation, *ii)* oral route, or *iii)* ingestion. It has been shown that, between these three ways of entry, the inhalation exposure is the one that causes most negative effects (Turci et al., 2017) since it may provoke lung cancer, pulmonary fibrosis and mesothelioma (IARC, 2012b).

Depending on their size and shape, once inhaled the largest fibres can be trapped in the mucous membranes of the nose, throat or in the oropharynx tract and be rapidly removed for instance by sneezing or swallowing (NIOSH, 2011), otherwise they can penetrate deeply into the lungs (the smallest ones) accumulating into the alveolar sacs (Broaddus, 2001) where they may have long retention time. The retention time of the fibres can last variable time depending on their bio-persistence and during this period, they change and react with the organism, firstly with body fluids and immune system cells, and dynamically interact with the biological surroundings (Turci et al., 2017). The removal mechanisms of the particles from the body are different depending on the site where the fibres are located; in the upper airways it takes place in the first 24 h of exposure by means of the mucociliary system (Sturm and Hoffman, 2009), while for particles reaching the alveolar region, the removal occurs through macrophages that is slower than mucociliary (Turci et al., 2017). The phagocytosis, or the process by which the macrophages engulf and digest the stranger particles, of the fibres is dependent on their length. As a matter of fact, the fibres shorter than 5 µm can be completely phagocytizes unlike the longer ones (length > 30 µm) that cannot be engulfed (Allison, 1974; Schinwald et al., 2012). In the latest case, takes place the coating process with the formation of the "asbestos bodies" which consist of an iron-rich layer of protein that surround the fibres (Koerten et al., 1990). The formation of asbestos bodies represents the reaction of the organism to the presence of poorly digestible fibres in the lungs or in the pleural cavity. Moreover, fibres with shorter length may reach the lymphatic system of the lungs or they can move to pleural and peritoneal spaces following patterns of lymphatic drainage (Broaddus 2001; Dodson et al., 2003). Basically, it has been demonstrated that asbestos fibres could reach all organs of the subjects exposed to asbestos (Miserocchi et al., 2008; Huang et al., 1988). In general, whether the fibres reach respiratory lung tissue, is mainly dependent on their size as well as the mechanism of defense of the body and the type of disease developed, are strictly dependent to the type and the

position of the fibres into the organism. Both non-cancer, such as asbestosis and pleural disease, and cancer such as lung cancer and mesothelioma, can be caused by breathing asbestos fibres. The World Health Organization (WHO) has estimated that about 107.000 people in the world die each year because of asbestos-related diseases (WHO, 2010) and about 43.000 because of mesothelioma (Driscoll et al., 2005).

4.1 Factors influencing the fibres toxicity

When a mineral fibre penetrates the organism, it meets biological material and provokes the occurrence of a complex series of physicochemical transformations and biological reactions.
Many interconnected factors contribute to the development of asbestos-related diseases. Firstly, it should be considered the dose of the toxic mineral that is defined as its amount into the organism over a certain period. In general, it is possible to say that the higher the dose of a toxic mineral, the greater the effects (Turci et al., 2017). Secondly, the exposure to a toxicant (i.e., any condition providing the opportunity for the toxicant to enter the body; Bernstein et al., 2005) and its duration, the exposure route (i.e., inhalation, ingestion) as well as the individual susceptibility, are all factors that influence the possible negative effects (IARC, 2012b; Drummond et al., 2016).
Moreover, intrinsic factors of the fibres such as: i) morphometric parameters (e.g., morphometry, surface area), ii) biodurability (e.g., fibre dissolution rate), iii) the crystal chemistry (e.g., iron content or the concentration of toxic elements), contribute to define the toxicity/pathogenicity of mineral fibres (Mossman et al., 1990; Qi et al., 2013).

4.1.1 Morphometric parameters

The size and shape of mineral particles are the most investigated properties, among the several factors that may influence the toxicity and carcinogenicity of the fibres. As a matter of fact, they are considered as major influencing factors for the cells' engulfment mechanism and fibres clearance from the respiratory system (Belluso et al., 2017).
It has been demonstrated by experimental studies (Donaldson et al., 2010; Lippmann, 2014; Mossman and Pugnaloni, 2017) that the length plays a key role in the toxicity, inflammation, and pathogenicity of mineral fibres. These studies highlighted that asbestos related lung diseases such as lung cancer and malignant mesothelioma are associated with the presence of fibres with length > 5 µm.

Similarly, Stanton et al. (1981) hypothesized that needle-shaped fibres with length > 8 µm cannot be removed by phagocytic cells as well as Lippman (2014) proved that fibres longer than 5 µm and thinner than 0.1 µm bring to the development of malignant mesothelioma.

Chrysotile and amphibole asbestos show visible different morphology. As a matter of fact, chrysotile generally consists of long, very thin, and flexible fibrils characterized by uniform size, occurring either singly or as bundles and aggregates; the size of each single fibril depends on the kinetics of crystal growth. Differently, fibrous amphiboles consist of rigid fibres and parallel-sided (Belluso et al., 2017) with variable size depending upon the mineral type (Case et al., 2011; Belluso et al., 2017).

In addition to the morphometric parameters, the surface chemical properties of the fibres entered the body may contribute to their overall toxicity and pathogenicity, since they interact with biological media, cells, and tissues (Turci et al., 2017). The factors of the mineral surface involved in toxicity are described in term of reactivity, or the potency of the surface to alter chemically biomolecules. Specifically, it has been shown that asbestos minerals induce the reactive oxygen species (ROS) generation in cell cultures as a result of both, highly reactive surface iron ions and frustrated phagocytosis (Manning et al., 2002). During the normal cellular metabolism, moderate levels of ROS are constantly generated and required as regulatory mediators in signaling processes and homeostasis. However, due to their high chemical reactivity ROS can react and damage DNA. The Fe ions present at the fibre surface in a poor coordination state promote the free radical generation by the surface Fenton reaction chain (Fubini and Mollo, 1995; Martra et al., 2003; Turci et al., 2011). The role of iron in asbestos toxicity is better discussed in the fibres chemistry paragraph of this chapter.

The surface area affects the biopersistence of the fibres and it is related to the dissolution rate and kinetics (Gualtieri et al., 2017c, d). In general, it is possible to consider less biodurable that fibres with greater surface area and subsequently, they should be considered toxic at a lesser extent (Gualtieri et al., 2017c).

4.1.2   Biopersistence and Biodurability

The biopersistence and biodurability of mineral fibres represent two important factors to consider for the determination of the carcinogenic potential and the health effects due to the inhalation of fibres. The biopersistence is defined as the ability of the fibres to persist in the human body even if they are subject to chemical, physical, and other physiological clearance mechanisms (Bernstein et al., 2005). The chemical solubility of the fibres when they are in contact with the organic fluids,

the crystal structure as well as the properties of the mineral surface, influence the biopersistence (Rozalén et al., 2017) and subsequently the fibres toxicity. In fact, the longer is the persistence of the fibres in the respiratory tract, the greater is the probability that they cause negative effects (Gualtieri et al., 2017c, d).

The biodurability refers to the ability of the fibres to resist chemical/biochemical alteration; biodurable fibres resist more to the action of macrophages and therefore are poorly cleared (Oberdöster, 2000; Bernstein et al., 2005) and may persist in the lungs for decades. The process taking place when the fibres are in contact with body fluids is the *dissolution,* which takes shorter or longer time (dissolution rates) depending on various factors: i) chrystal structure integrity; ii) specific surface area (i.e. higher surface area, higher is the surface exposed thus resulting in an increasing of the dissolution rate); iii) pH (i.e. the dissolution rates of fibres tend to increase as the pH decrease; Rozalén et al., 2014).

For instance, a recent literature study based on the biodurability comparison of chrysotile and fibrous crocidolite, showed that after the same exposure time of the fibres to cell cultures, chrysotile was partially dissolved and amorphized, differently to crocidolite which showed less amorphization (Di Giuseppe et al., 2019). Among the asbestos minerals, chrysotile due to its crystal structure, shows a faster dissolution rate than amphiboles (Ballirano et al., 2017; Rozalén et al., 2017; Gualtieri et al., 2017b) and some researchers suppose that his potential toxicity is much lower compared to amphibole asbestos (amphibole hypothesis). On the other hand, other researchers sustain the opposite and consider asbestos fibres as potentially toxic substances indistinctly (Dement and Brown, 1994; Stayner et al., 1996).

4.1.3   *Crystal chemistry*

Literature studies showed that crystal chemistry of mineral fibres strongly influences their interaction with the biological environment once into the body. The presence of Fe as well as its coordination represents an important factor in fibres toxicity (Bonneau et al., 1986; Turci et al., 2011). Iron in asbestos minerals may be present as a stoichiometric constituent, as in the case of crocidolite [$Na_2(Fe^{2+}, Mg^{2+})_3-(Fe^{3+})_2Si_8O_{22}(OH)_2$] and amosite [$(Fe^{2+},Mg)_7Si_8O_{22}(OH)_2$], or as a contaminant as in natural chrysotile [$Mg_3Si_2O_5(OH)_4$], in which it replace isomorphously magnesium and silicon (Schwarz and Winner ,1971; De Waele et al., 1984; Kamp and Weitzman 1999). Specifically, it has been shown that the Fe in a poor coordination state present at the fibre surface catalyzes the generation of ROS (Fantauzzi et al., 2010, 2012; Pacella et al., 2010, 2012; Turci et al., 2005). As a matter of fact, at the fibre's surface are located the reactive sites or low

coordinated surface atoms and exposed ions that may coordinate molecules thus playing a primary role in the catalytic reactions (Fubini, 1993).

Moreover, epidemiological and experimental evidence showed that trace elements such as trace metals present in asbestos fibres, may cause lung cancer (Nemery, 1990). Asbestos fibres are capable to host potentially toxic elements (PTEs; Fe, Ni, Co, Cr) in their structure and according to some researchers they may play a passive role in inducing asbestos related pathologies (Cralley et al., 1967; Harington et al., 1967) and act as a reservoir of PTEs that may be released into the intracellular or extracellular environment during dissolution processes. It has been proven that high amount of trace elements may induce lung cancer (Schreier et al., 1987; Wei et al., 2014). For instance, among the trace elements hosted in asbestos fibres structure, Ni is considered the most hazardous one since it damages DNA (Caicedo et al., 2007). Several studies focus on the capability of Ni to produce ROS as well as on its toxicity at intracellular sites (Nackerdien et al., 1991; Salnikow et al., 2000; Chen et al., 2003; Horie et al., 2009) and it has been shown that various adverse health effects such as lung fibrosis and cancer of the respiratory tract can be caused by Ni (Seilkop and Oller, 2003; Leyssens et al., 2017). Similarly, Cr especially in the hexavalent redox state can induce tissue damage, necrosis, and inflammation (IARC, 2012a). If adequate concentrations of trace elements (e.g., Ni, Cr) accumulate in the lungs, the baseline levels of these elements in normal human lung tissue may be altered, thus provoking the development of lung cancer such as mesothelioma and bronchogenic carcinoma (Dixon et al., 1970; Nemery 1990; Wei et al., 2014).

The study conducted by Bloise et al. (2016a) based on the investigation of trace elements concentration (Li, Be, Sc, V, Cr, Mn, Co, Ni, Cu, Zn, As, Rb, Sr, Y, Sb, Cs, Ba, La, Pb, Ce, Pr, Nd, Sm, Eu, Gd, Tb, Dy, Ho, Er, Tm, Yb, Lu, Th, U) in mineral fibres, showed the large capacity of chrysotile and amphiboles for hosting trace elements. By considering the short bio-persistent of chrysotile in the lungs compared to amphiboles, trace metals may be released quickly in the extracellular medium therefore the potential toxicity of metal-rich chrysotile asbestos should be reconsidered (Gualtieri et al., 2017b).

5. Natural Asbestos Occurrences (NOA)

The term NOA refers to asbestos minerals occurring in rocks and soils that have not been exploited for commercial purposes (Bloise et al., 2008; Harper, 2008; Belluso et al., 2020; Wroble et al., 2020). By the genetic point of view, asbestos minerals crystallize with fibrous habit in specific thermobaric conditions and generally, asbestos deposits mainly occur in areas where permeability and fluid flow have been enhanced as in fault or shear zones and contact metamorphic aureoles (Nichols et al., 2002).

5.1 Asbestos-containing rocks

Ophiolite rocks (i.e., serpentinite and metabasite) are the main lithotypes associated with asbestos, since asbestos minerals are the major constituents of these rocks in which they crystallize in veins or in pseudomorph structure.

The environment is characterized by the wide occurrence of natural asbestos, some examples include Appalachian Mountains (USA), chrysotile deposits in Ural Mountains in the Russian Federation (Ross and Nolan, 2003), Canada (Virta, 2006) and China, South Africa, India, Italy, Australia, Cyprus, Greece (Ross and Nolan, 2003) and other countries.

The geographic areas in the world where asbestos minerals are abundant enough to be exploited are visible in figure 7, showing the distribution of active and inactive asbestos mining sites (Turci et al., 2020). The global maps revealed that chrysotile is the most frequent occurring asbestos, followed by anthophyllite, crocidolite, tremolite, actinolite and amosite. For instance, the largest producer States in US were Arizona, California, North Carolina, and Vermont where most of the asbestos mined was chrysotile as well as in Canada, Brazil (Virta 2006).

For most of the 20th century, Italy was the second largest producer of asbestos in Europe, behind Russia, initially with tremolite asbestos and then with chrysotile (Balangero mine opening; Virta 2006). Generally, most productive commercial deposits typically contain 5-6 % of asbestos whereas only a few deposits such as the Coalinga chrysotile deposits in California, USA are reported to contain 50% or more (USGS, 2001; Virta, 2006).

Since small non-economic occurrences of asbestiform minerals are common into the environment (Lee et al., 2008), they have been included in the global map in those areas in which health-related issues were documented by mesothelioma epidemiology such as: *i)* fluoroedenite (Biancavilla, Sicily); *ii)* fibrous amphibole (Libby, Montana); *iii)* erionite (Turkey, United State and Mexico) (Turci et al., 2020).

Moreover, in addition to mafic and ultramafic rocks, asbestos may be sometimes also found in sedimentary and alluvial deposits, as a result of asbestos-containing rocks erosion, as well as in soils.
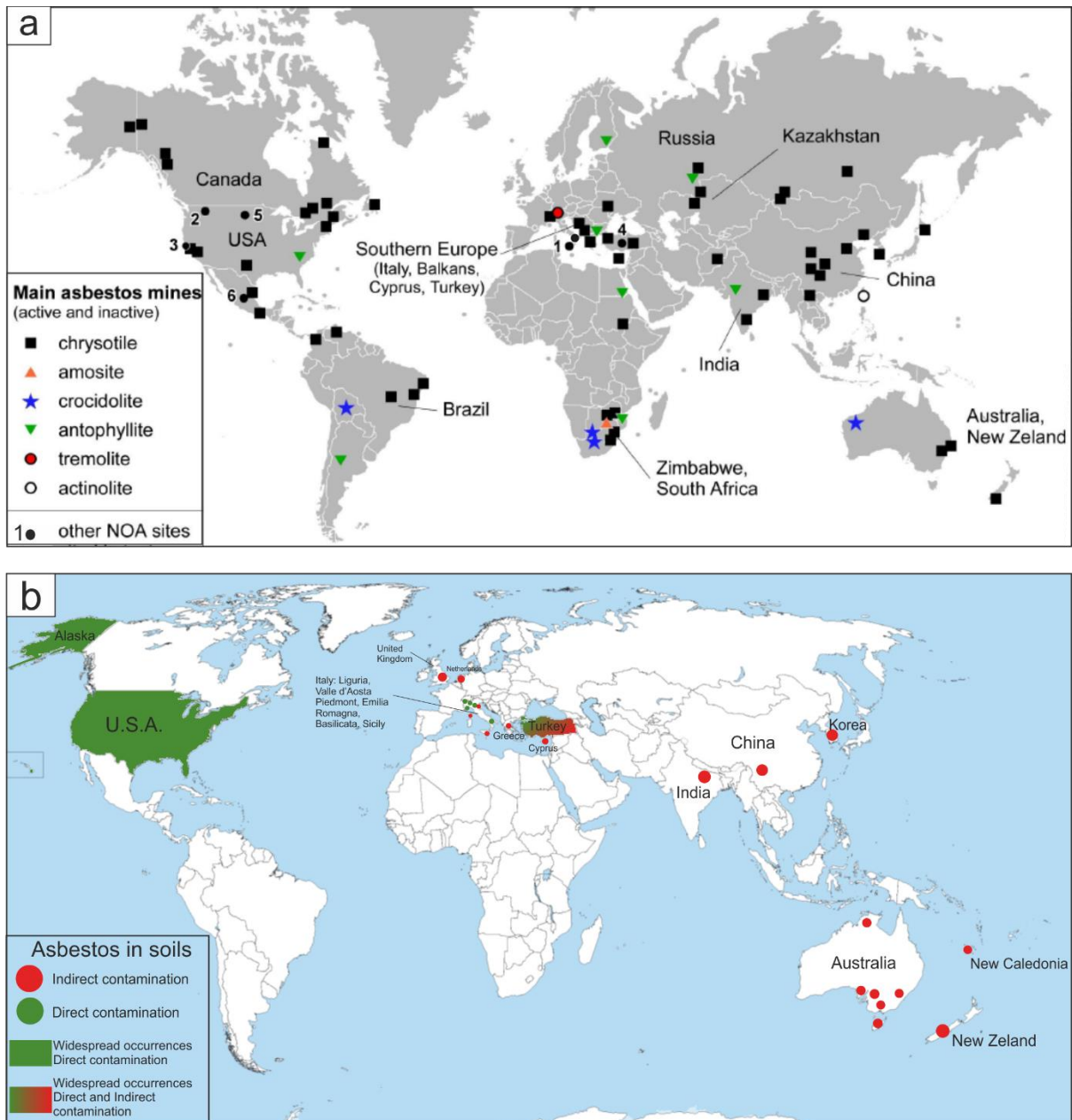
Figure 7: global map showing a) the main asbestos mines (active and inactive), modified after Turci et al., 2020; other asbestiform occurrence sites are also indicated: 1 = Biancavilla (Italy); 2 = Libby (Montana); 3 = Franciscan Complex (California); 4, 5, 6 = erionite sites in Turkey (Cappadocia), the United States (Dunn Country, North Dakota), and Mexico (Tierra Blanca de Abajo), respectively. b) occurrence of asbestos-containing soil at the state of the knowledge (Ricchiuti et al., 2020).

5.2 Asbestos-containing soils

Asbestos in soils may be found for various reasons such as: *i)* improper removal of Asbestos-Containing Materials (i.e., indirect contamination); *ii)* proximity to asbestos factory/mine (indirect contamination); *iii)* inheritance from mother rocks (natural occurrences, i.e., direct contamination). It is worth noting, that depending on the source of contamination, asbestos fibres can be found in different portion of soil. As a matter of fact, in the case of direct contamination, the sub-soil is more representative than the top-soil since the presence of fibres is not due to the deposition (as in the case of the indirect contamination) but rather to the characteristics of the mother rock (Figure 8).

The distribution of asbestos-containing soils in the global territory is reported in Figure 7b. Specifically, according to the most relevant studies the territories characterized by asbestos-containing soils due to the direct contamination include Turkey, USA and Italy (Ricchiuti et al., 2020) while the indirect contamination covers a big range of the territory. For instance, the study conducted by Metintas et al. (2017) in the Anatolia region (Turkey), revealed the presence of tremolite in soil samples whereas high occurrence of actinolite and chrysotile-containing soils were found in USA (EPA, 2009; Thompson et al., 2011; Buck et al., 2013).

As for Italy, scientific studies revealed the presence of tremolite in soils occurring in the Calabria and Basilicata region (Campopiano et al., 2018; Punturo et al., 2018, 2019; Bloise et al., 2016b; 2018 a, b; 2019; Colombino et al., 2019; Dichicco et al., 2019; Laurita and Rizzo, 2019). Tremolite asbestos, actinolite asbestos and chrysotile were found in soils occurring in the Liguria region (Militello et al., 2019) as well as the presence of serpentine asbestos were documented in Valle d'Aosta region by Gualtieri et al. (2009).

The different distribution among the soils indirectly contaminated, may be due to the fact that the high use and commercialization of asbestos in the past resulted in its exportation all over the world and therefore they are currently widespread in the territory.

Differently, since the natural occurrence of asbestos is dependent on the geology of the area the presence of contaminated soils is limited to the distribution of the mother rock outcrops (Ricchiuti et al., 2020).
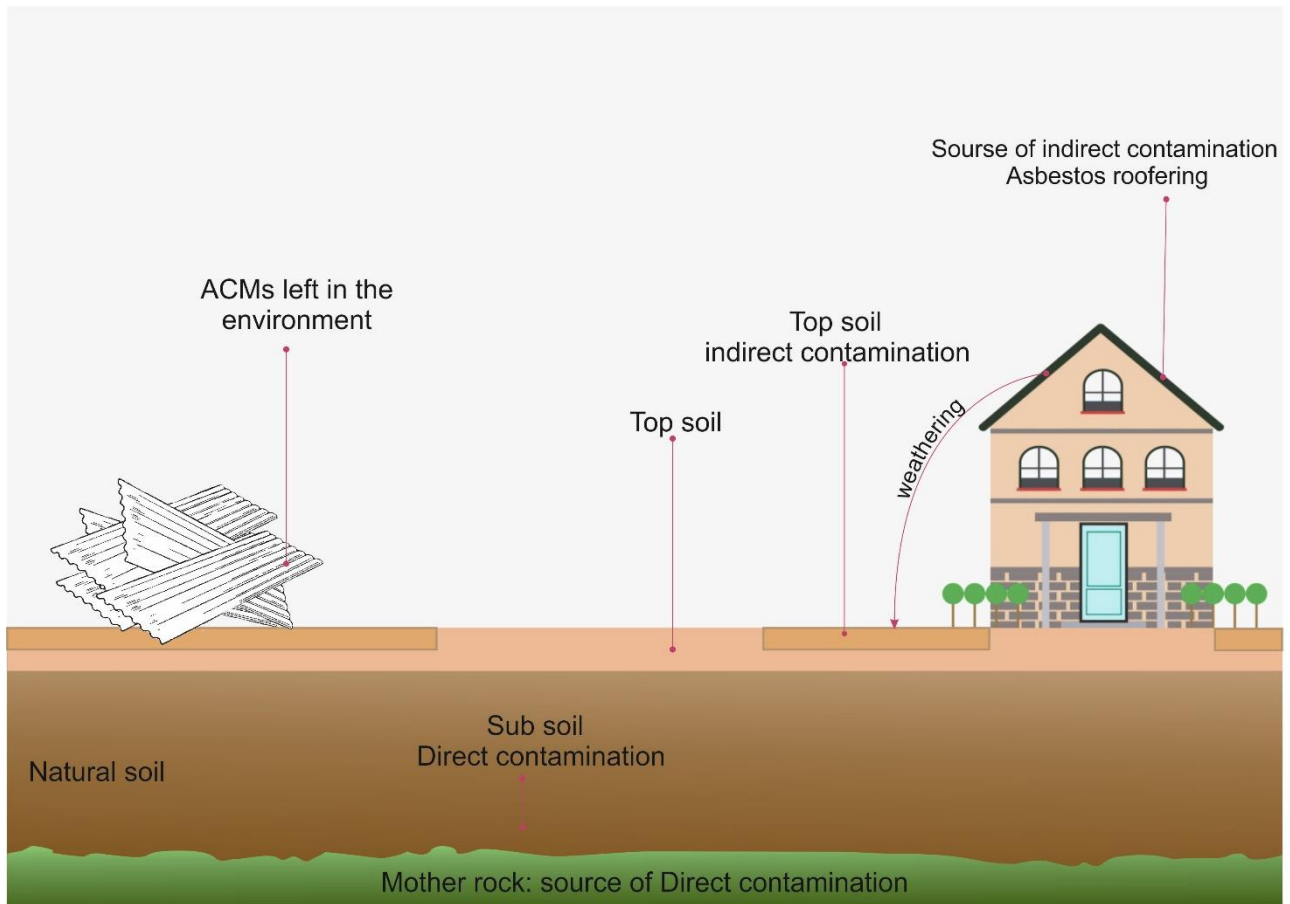
Figure 8: presence of asbestos fibres in soils depending on the source of contamination (Ricchiuti et al., 2020).

5.3 NOA in Italy

Due to the occurrence of ophiolite outcrops in specific parts of its territory, Italy is characterized by the wide occurrence of natural asbestos and based on literature data, the main asbestos varieties diffused are represented by chrysotile, tremolite asbestos, and actinolite asbestos and anthophyllite at a lesser extent (Cavallo and Rimoldi, 2013; Gaggero et al., 2013; 2017; Vignaroli et al., 2013). In general, chrysotile is often associated with serpentinized ultramafic rocks while tremolite and actinolite mainly occur in calc-schists, chlorite-schists, actinolite schists, greenschist facies metabasite and ophicarbonate rocks of metamorphis processes that affected the oceanic lithosphere, currently constituting the ophiolite complexes.

The main asbestos extraction sites in Italy include Valmalenco (Lombardy), Emarese (Aosta Valley) and the Balangero mine (Piedmont region; see chapter 2).

The NOA mapping is currently mandatory in Italy (L. no. 93/2001) and related Environment Ministry Decree no. 101/2003), and it should be carried out by the environmental protection agency (EPA) of each region.

It is worth mentioning, that many species of asbestiform silicates currently not regulated in Italy, occur in the territory (naturally occurring non-asbestos, NONA) as shown by Belluso et al., 2020 who describes the presence of NOA and NONA detected in Italy so far (Figure 9). For instance, fluoro-edenite fibres have been found in the volcanic rocks of the Etna Mountain, in the area of Biancavilla town (Sicily region, southern Italy; Famoso et al., 2012) where high incidence of malignant pleural mesothelioma was recorded (Cardile et al., 2004; Travaglione et al., 2006; Musumeci et al., 2011). Environmental studies showed no asbestos exposure of population in Biancavilla, either from occupational activities or from the use manufactured products (Paoletti et al., 2000) but rather the environmental diffusion of fluoro-edenite from the nearby sites was recognized (Paoletti et al., 2000; Gianfagna et al., 2003).

Specifically, from the north to the south the regions showing the presence of asbestos are: *i)* Lombardy, Trentino Alto Adige, Aosta Valley, Piedmont, and Liguria (characterized by ophiolitic units), *ii)* Emilia Romagna and Tuscany (characterized by flysch units containing sedimentary rocks derived from the dismantling of asbestos-bearing lithologies) *iii)* Sardinia (asbestos detected in granitoid rocks), Basilicata and Calabria regions (characterized by ophiolitic units). Therefore, the Italian territory, especially Alps and Apennines, are interested by massive presence of ophiolitic outcrops rich in serpentine (i.e., chrysotile) and amphibole fibres (i.e., tremolite, actinolite and anthophyllite). Among the regions with the largest number of these outcrops, Piedmont is known for the Lanzo Valley and in particular the ex-mine of Balangero where chrysotile was extracted (Compagnoni and Groppo, 2006).

Various localities in the central and southern Italy are interested by the presence of ophiolites hosting asbestos fibres as in the Latium (Burragato et al., 2001), Basilicata (Massaro et al., 2013; Caputo et al., 2018; Dichicco et al., 2018; Punturo et al., 2018, 2019; Bloise et al., 2019; Ricchiuti et al., 2021) Calabria region (Punturo et al., 2015; Bloise et al., 2016b) where scientific studies focused on the impact of airborne asbestos fibres dispersed during mining and milling operations have been conducted (Zakrzewska et al., 2008).
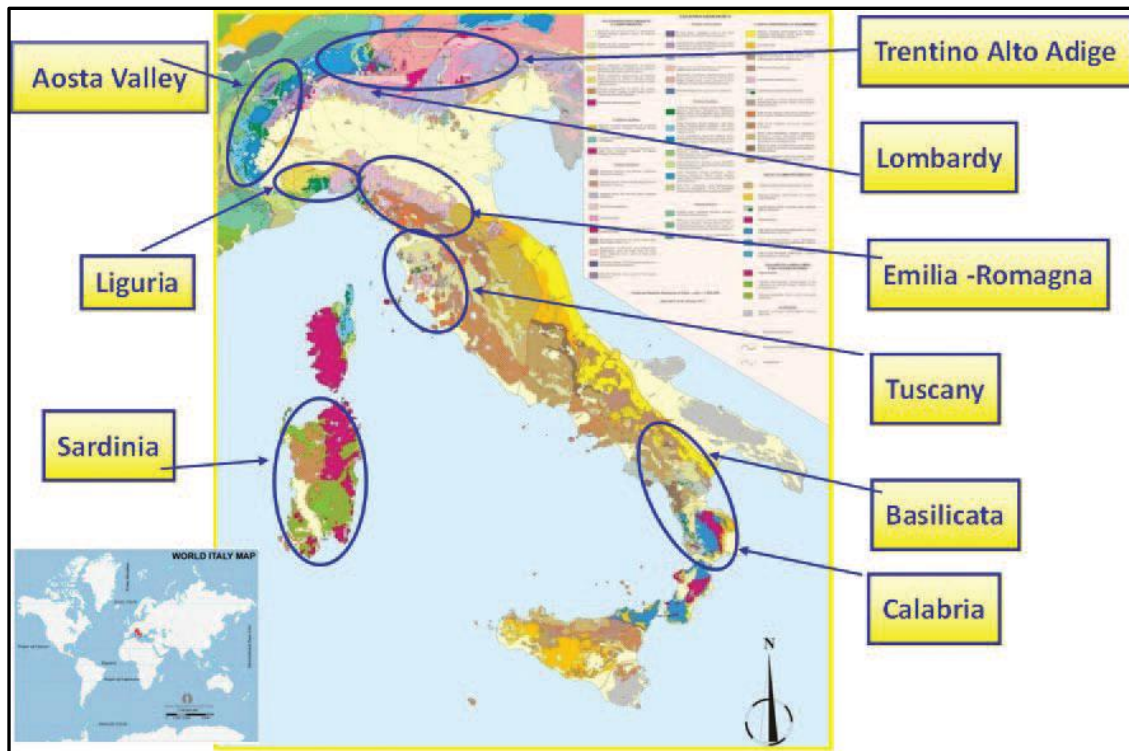
Figure 9: map of Italy showing the occurrence of asbestos in rocks at the current state of knowledge (from Belluso et al., 2020).

6. Study area description and sampling

The study area of the present work of thesis is located in the southern Apennines, precisely in northern Calabria (Gimigliano-Mount Reventino Unit, Sila Piccola area) and in the Calabrian-Lucania border (Pollino Massif).

The ophiolitic sequence of Gimigliano-Mount Reventino Unit (GMRU; Figure 10) consists of metabasites and serpentinites covered by marble alternating with calc-schists and quartzites (Punturo et al., 2015 and references therein; Bloise et al., 2016b).

Various serpentinite quarries (still active and inactive, Figure 11) are located in the study area, which comprise the towns of Gimigliano, Conflenti, Decollatura, San Mango D'Aquino together with their surroundings and Monte Reventino, where the so called "green stones" have been excavated for road construction or for using as building and ornamental stones (Zakrzewska et al., 2008).

Concerning the Calabrian-Lucania border, the study has been carried out in the northern sector of the Pollino Massif, in an area of approximately 20 km^2 in the Pollino National Park where the terrains of the Liguride Complex occur (Figure 12). The latter, consists of three main tectonic units of Upper Jurassic to Upper Oligocene age (Monaco and Tortorici, 1995): *i)* the Calabro-Lucano Flysch (Monaco et al., 1998), *ii)* the metamorphic terranes of the Frido Unit (Vezzani, 1969; Amodio Morelli et al., 1976), *iii)* syn-orogenic turbiditic sequences (Vezzani, 1966).

In the specific case of this study, serpentinite rocks belonging to the Frido Unit occurring in the surroundings of Episcopia and San Severino Lucano villages have been sampled together with derivative soils to determine the presence of asbestos minerals (Figure 13).
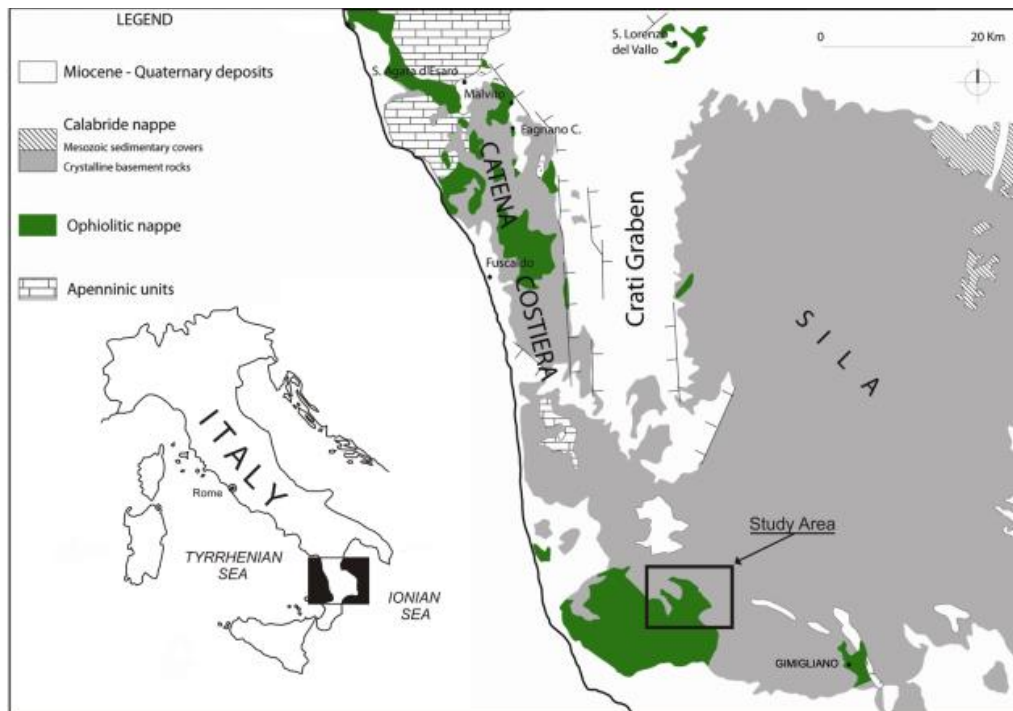
Figure 10: simplified geological map of the Northern Calabrian Arc (modified after Apollaro et al., 2011) and study area location.

Figure 11: abandoned quarry at Gimigliano town (Calabria region, southern Italy).
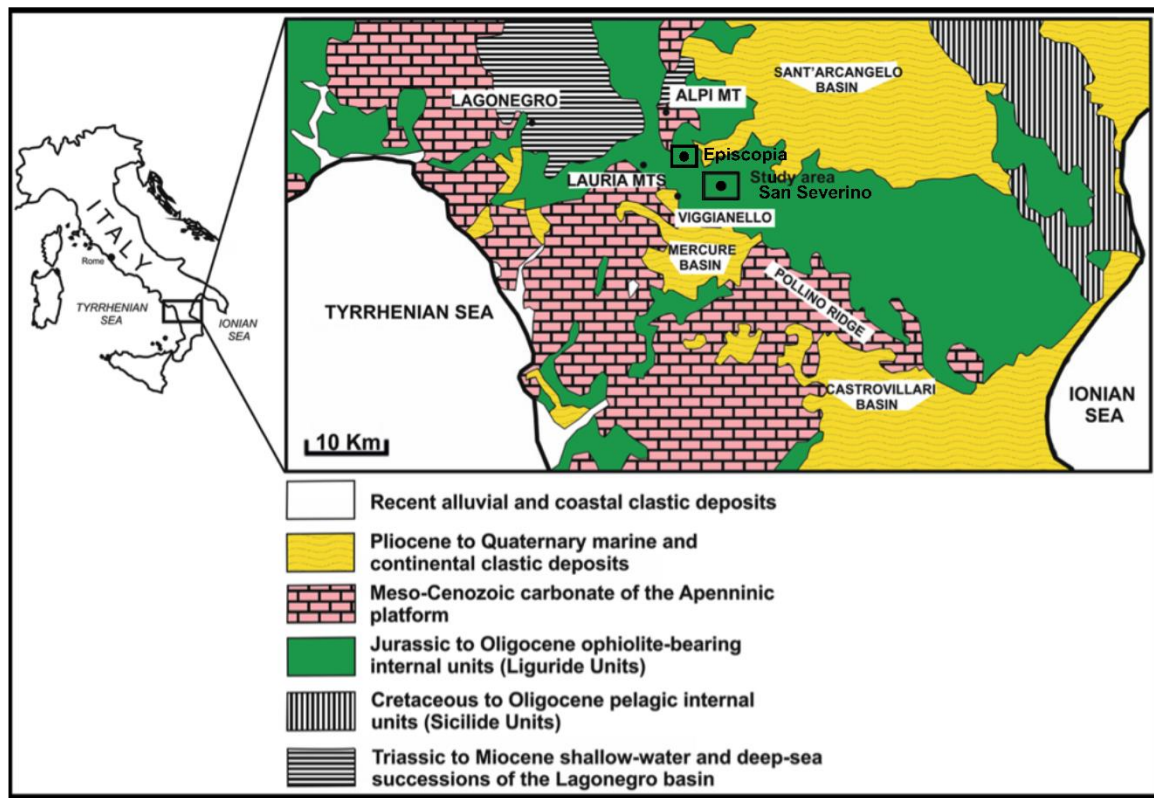
Figure 12: simplified geological map of the study areas (Episcopia and San Severino Lucano villages; Basilicata region). Modified after Punturo et al., 2018.

Figure 13: a) Distant view of the Episcopia village, with appearance of serpentinite at the road cut near to the village (the red circle encloses white fibers of asbestos tremolite); b) Serpentinite outcrops near the village of San Severino Lucano (Basilicata region, southern Italy). Modified after Bloise et al., 2019.

A total of 30 serpentinite samples, 12 derivative agricultural sub-soil and three type of asbestos (i.e., chrysotile, tremolite and actinolite) have been collected (Table 3). Specifically:

- seven serpentinite rocks from an abandoned quarry in the Gimigliano-Mount Reventino Unit (GMRU; Calabria region).
- eleven serpentinite rocks from Episcopia village (Basilicata region).
- twelve serpentinite and twelve derivative soil samples from San Severino Lucano village (Basilicata region).
- three asbestos minerals coming from ophiolitic outcrops belonging to the GMRU:

  a) chrysotile from a road cut close to San Mango D'Aquino town.

  b) tremolite asbestos from an abandoned quarry located in the area of Mount Reventino.

  c) actinolite asbestos from an abandoned quarry close to the towns of Conflenti.
- two tremolite asbestos from serpentinite rocks cropping out in the surroundings of Episcopia and San Severino Lucano villages (Basilicata region).

By the macroscopic point of view, serpentinite rocks show the typical dark green colour and massive structure, with the widespread presence of veins of various diameters and lengths mainly filled by chrysotile fibres. As visible in figure 14 showing serpentinites cropping out in the Gimigliano Mount-Reventino area, the veins do not exhibit a preferred orientation thus suggesting that they developed under various mechanisms and conditions of formation. The samples collected in the GMRU area are shown in figure 15.

Figure 16 shows serpentinite samples coming from Episcopia village, that are often characterized by widespread white parts consisting of fibrous minerals (Figure 16a), whereas serpentinite and derivative soils coming from San Severino Lucano village are shown in figure 17. The field survey carried out in these areas showed that serpentinites outcrops are rarely covered by vegetation mainly because of the toxic composition of the surface formation (soils) which is derived from these rocks. As a matter of fact, serpentinites represent hostile environment for plant life and only a few species are able to survive under these adverse chemical conditions (Garcìa Barriuso et al., 2011).

Finally, the mesoscopic appearance of asbestos fibres extracted from the rocks are reported in figures 18 and 19. To avoid the possible contamination by other mineral impurities the fibres were manually selected by using a binocular microscopy, but it must be specified that it is not possible to exclude the presence of nano-sized other species.
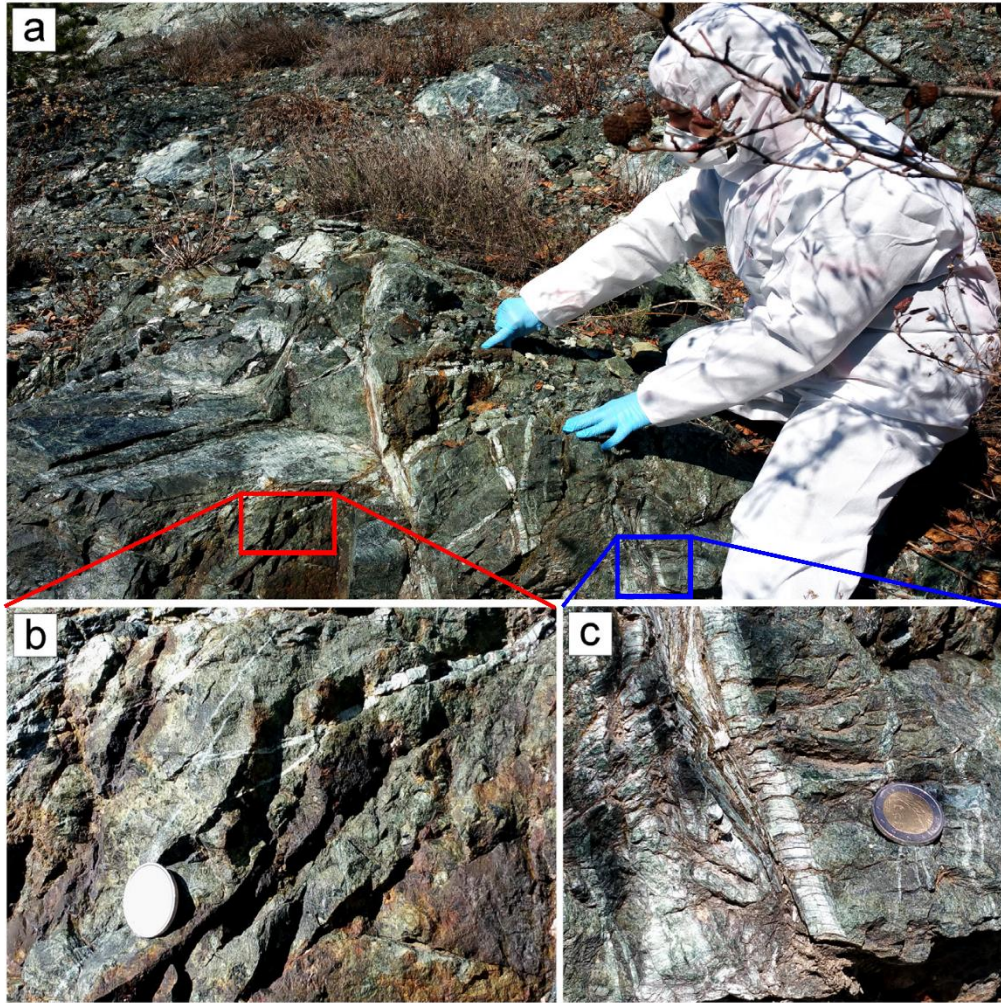
Figure 14: a) GMRU abandoned quarry; b) the red square indicates the zoom area: the vein network developing inside massive serpentinite; c) the blue square indicates the zoom area: the vein network developing inside massive serpentinite. Bloise et al., 2020a.
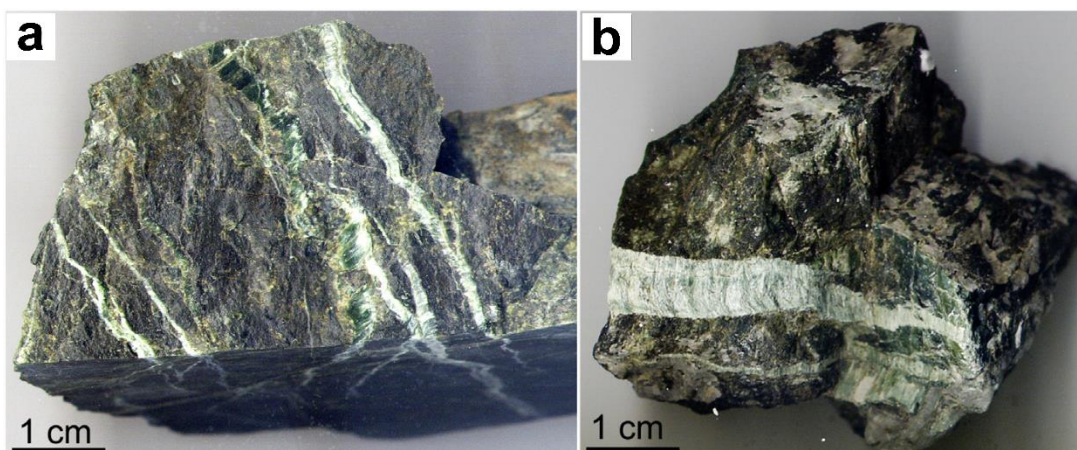
Figure 15: serpentinite samples coming from abandoned quarry in the GMRU: a) the picture shows the vivid green serpentinite veins crosscutting the sample and with variable thicknesses; b) V-shaped veins. Modified after Bloise et al., 2020a.
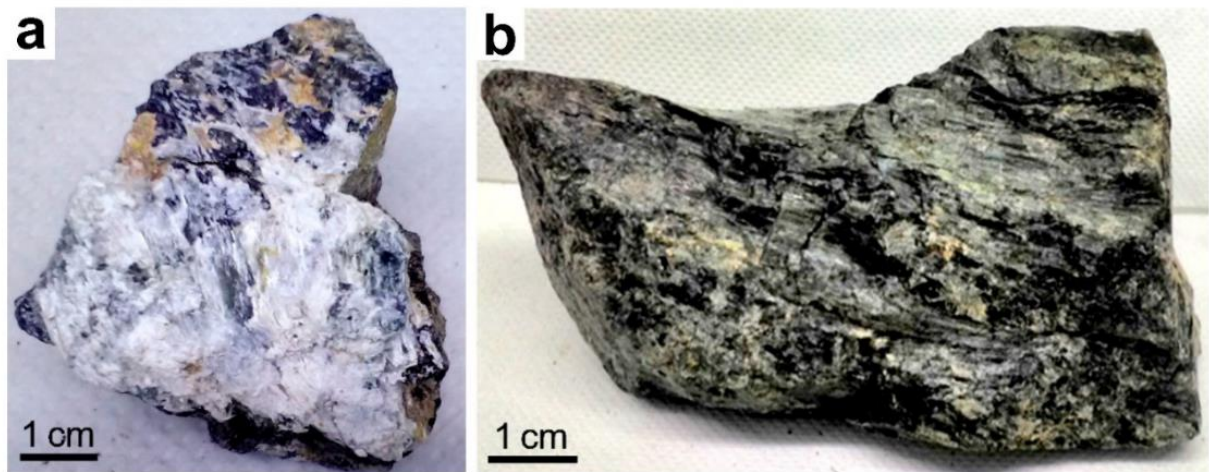
Figure 16: serpentinite samples coming from Episcopia village (Basilicata region): a) mesoscopic appearance of white and silky tremolite on the surface of the sample; b) characteristic blazing surface of serpentinite, looking like a snake's skin. Bloise et al., 2019.
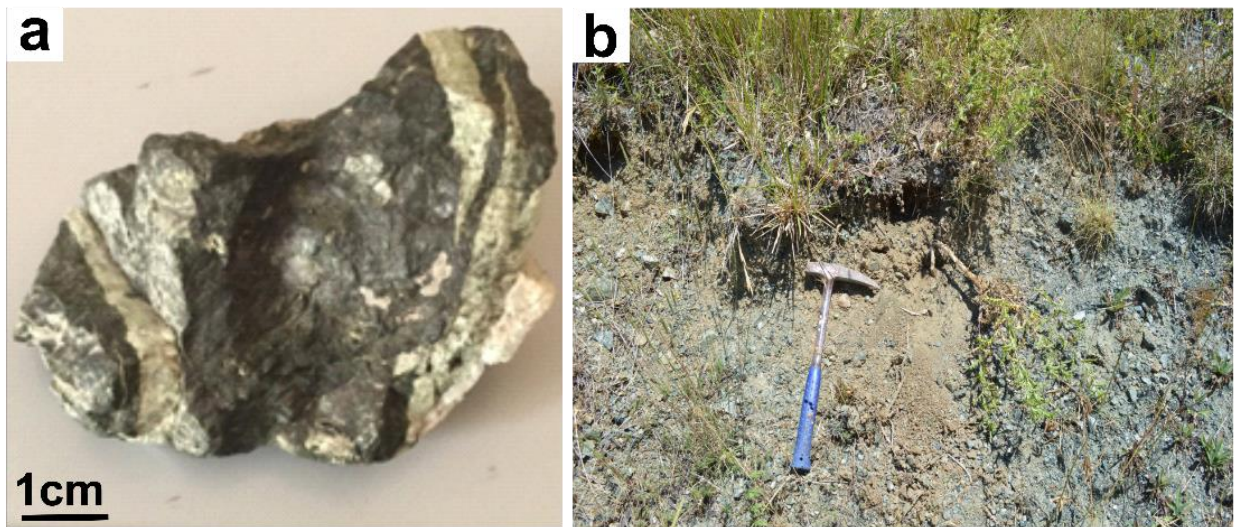
Figure 17: serpentinite samples coming from San Severino Lucano village (Basilicata region): a) serpentinite with evident fibrous veins; b) derivative agricultural soil. Modified after Punturo et al., 2018.
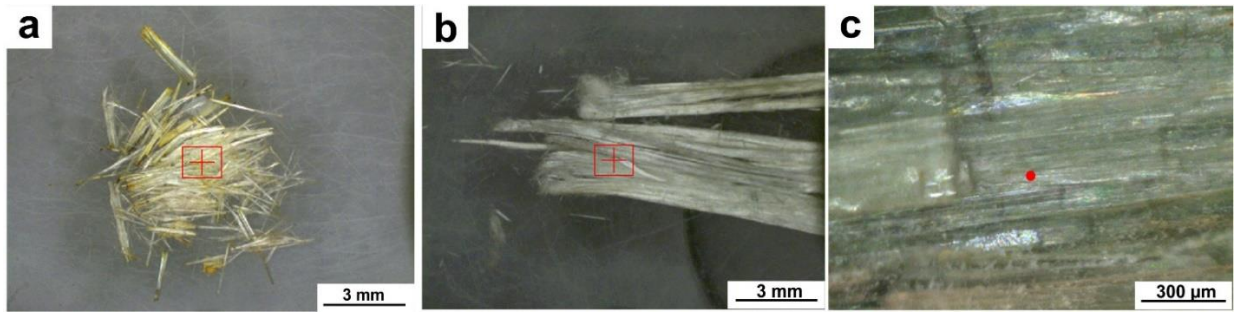
Figure 18: a) straw-yellow chrysotile fibres, from San Mango D'Aquino (Calabria Region, Italy); b) white tremolite asbestos, from an abandoned quarry in Mt. Reventino (Calabria Region, Italy); c) green actinolite asbestos, from an abandoned quarry close to the town of Conflenti (Calabria Region, Italy). Modified after Bloise et al., 2020b.

Figure 19: tremolite fibres from Episcopia (a) and San Severino Lucano villages (b). Modified after Ricchiuti et al., 2021.

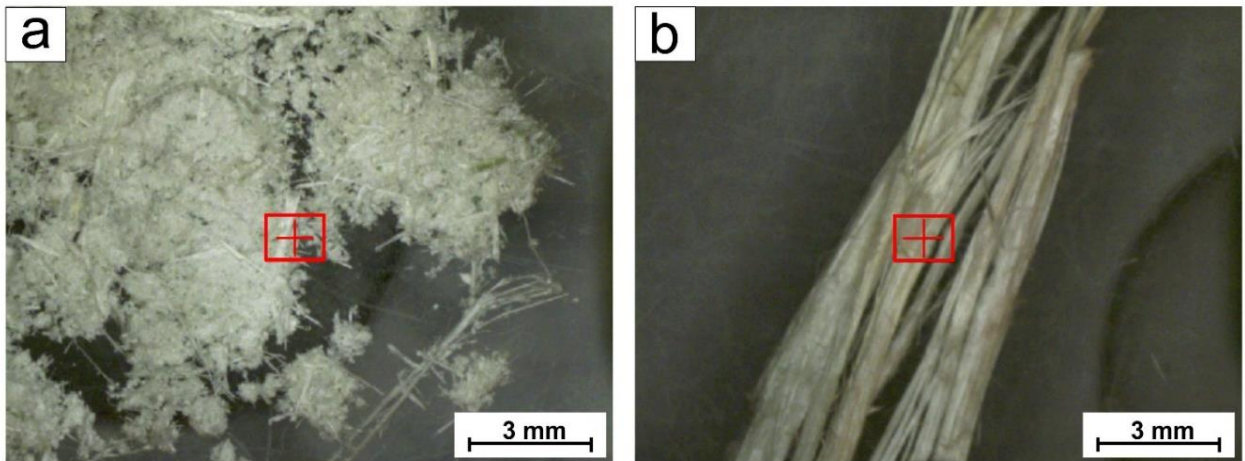|	Sample	Lithotype	Locality	Site Description	Lon (East)	Lat (North)
Rocks from GMRU	CNF 16.2	Serpentinite	Conflenti Town	Inactive quarry	610190	4326239
	CNF 16	Serpentinite	Conflenti Town	Inactive quarry	610190	4326239
	CNF 3	Serpentinite	Conflenti Town	Inactive quarry	610190	4326239
	GML 2	Serpentinite	Conflenti Town	Inactive quarry	633592	4314552
	GML 2.1	Serpentinite	Conflenti Town	Inactive quarry	633592	4314552
	GML 12	Serpentinite	Conflenti Town	Inactive quarry	632521	4315109
	GML 12.2	Serpentinite	Conflenti Town	Inactive quarry	632521	4315109
Rocks from Episcopia	E1	Serpentinite	Episcopia Village	Slope	594261	4436353
	E4	Serpentinite	Episcopia Village	Road cut	594118	4436407
	E6	Serpentinite	Episcopia Village	Slope	594031	4436259
	E8	Serpentinite	Episcopia Village	Dirt road	593457	4436029
	E8b	Serpentinite	Episcopia Village	Dirt road	593611	4436038
	E10	Serpentinite	Episcopia Village	Slope	593696	4435960
	E10b	Serpentinite	Episcopia Village	Road cut	593287	4435880
	E10t	Serpentinite	Episcopia Village	Dirt road	593332	4436037
	E11	Serpentinite	Episcopia Village	Road cut	594231	4436063
	E11b	Serpentinite	Episcopia Village	Road cut	593973	4435615
	E12	Serpentinite	Episcopia Village	Road cut	593342	4436196
Rocks from San Severino Lucano	Rpol_1	Serpentinite	S. Severino Lucano Village	Entry of the Village	597417	4429775
	Rpol_2	Serpentinite	S. Severino Lucano Village	Entry of the Village	597405	4430523
	Rpol_3	Serpentinite	S. Severino Lucano Village	Road cut outside the Village	597808	4430474
	Rpol_4	Serpentinite	S. Severino Lucano Village	Road cut outside the Village	597569	4430504
	Rpol_5	Serpentinite	S. Severino Lucano Village	Road cut outside the Village	597270	4431103
	Rpol_6	Serpentinite	S. Severino Lucano Village	Road cut outside the Village	597268	4430927
	Rpol_7	Serpentinite	S. Severino Lucano Village	Road cut outside the Village	597323	4431363
	Rpol_8	Serpentinite	S. Severino Lucano Village	Road cut outside the Village	597223	4430711
	Rpol_9	Serpentinite	S. Severino Lucano Village	At the base of the slop, outside the Village	597569	4430504
	Rpol_10-11	Serpentinite	S. Severino Lucano Village	Road cut outside the Village	596890	4430715
	Rpol_12	Serpentinite	S. Severino Lucano Village	Road cut outside the Village	596831	4430823

Continuation of table 3.

	Sample	Lithotype	Locality	Site Description	Lon (East)	Lat (North)
Soils	Spol_1	Soil	S. Severino Lucano Village	Entry of the Village	597417	4429775
	Spol_2	Soil	S. Severino Lucano Village	Entry of the Village	597405	4430523
	Spol_3	Soil	S. Severino Lucano Village	Road cut outside the Village	597808	4430474
	Spol_4	Soil	S. Severino Lucano Village	Road cut outside the Village	597569	4430504
	Spol_5	Soil	S. Severino Lucano Village	Road cut outside the Village	597270	4431103
	Spol_6	Soil	S. Severino Lucano Village	Road cut outside the Village	597268	4430927
	Spol_7	Soil	S. Severino Lucano Village	Road cut outside the Village	597323	4431363
	Spol_8	Soil	S. Severino Lucano Village	Road cut outside the Village	597223	4430711
	Spol_9	Soil	S. Severino Lucano Village	At the base of the slop, outside the Village	597569	4430504
	Spol_10	Soil	S. Severino Lucano Village	Road cut outside the Village	596890	4430715
	Spol_11	Soil	S. Severino Lucano Village	Road cut outside the Village	596890	4430715
	Spol_12	Soil	S. Severino Lucano Village	Road cut outside the Village	596831	4430823
Isolated fibres from GMRU	Ctl	Fibres	S. Mango D'Aquino Town	Road cut close to the Village	604420	4324593
	Tr	Fibres	Mount Reventino	Abandoned quarry	613821	4321875
	Act	Fibres	Conflenti Town	Abandoned quarry	612452	4323945
Isolated fibres Pollino Massif	TR_EPS	Fibres	Episcopia Village	Slope	593696	4435960
	TR_SSL	Fibres	S. Severino Lucano Village	Road cut	595423	4431099

Table 3: list of the collected samples together with their lithology, provenience, and site description.

7. Section 1 – Rocks and soils: Mineralogical, microstructural, and geochemical characterization

7.1 *Methods*

With the aim of obtaining a fully mineralogical and geochemical characterization of both serpentinite rocks and derivative agricultural soils, the collected samples have been analyzed by using various analytical techniques (Table 4). Specifically, Polarized Light Microscope (PLM), Scanning Electron Microscope with Energy Dispersive Spectrometry (SEM-EDS), Transmission Electron Microscopy with Energy Dispersive Spectrometry (TEM-EDS), X-Ray Powder Diffractometry (XRPD), Derivative Thermogravimetry (DTG), Differential Scanning Calorimetry (DSC), X-Ray Fluorescence (XRF), X-Ray synchrotron microtomography (SR-μCT), Electron Probe Micro-Analysis (EPMA) were adopted. It is worth specifying, that soil samples were pre-treated with H_2O_2 and pre-heated for 24 h at 530 °C, to remove the organic compounds.

Samples				
Methods	**Rocks_GMRU**	**Rocks_EPS**	**Rocks_SSL**	**Soil_SSL**
PLM	X		X	
SEM	X	X	X	X
TEM				X
XRPD		X	X	X
DTG-DSC		X		X
XRF			X	X
SR-μCT	X			
EPMA	X			

Table 4: list of the analytical techniques used for the analysis of the samples. Rocks_GMRU = Serpentinite samples coming from Gimigliano Mount-Reventino Unit (Calabria Region); Rocks_EPS = Serpentinite samples coming from Episcopia village (Basilicata region); Rocks_SSL = Serpentinite samples coming from San Severino Lucano village (Basilicata region); Soil_SSL = derivative soil samples coming from San Severino Lucano village (Basilicata region).

7.1.1 Polarized Light Microscopy (PLM)

The petrographic and microstructural characteristics of the investigated serpentinites were obtained by the examination of polished thin sections acquired from the collected samples by using a Zeiss Axiolab Microscope with Polarized Light (PLM).

An E3ISPM Industrial Digital Camera equipped with Sony Exmar CMOS sensor was useful for the acquisition of photomicrographs of main microstructural features.

The samples were cut to highlight the main fabric features of the serpentinite rocks, such as the massive parts and the vein occurrence.

7.1.2 Scanning Electron Microscopy (SEM-EDS)

For the morphological observation of fibrous minerals, the samples were examined without any previous grinding treatment to preserve their original crystal habit, using the Tescan-Vega\\LMU scanning electron microscope, equipped with an energy-dispersive X-ray spectrometer (EDS) Edax Neptune XM4 60, operating at 15 kV accelerating voltage and 20 nA beam current conditions, and Environmental Scanning Electron Microscope FEI QUANTA 200 (Thermo Fisher Scientific, Waltham, MA, USA), with BSE detector and equipped with an X-ray EDS suite comprising a Si/Li crystal detector model EDAX-GENESIS4000 (EDAX Inc., Mahwah, NJ, USA).

A fragment for each sample was fixed onto a SEM stub using a double-sided conductive adhesive tape and subsequently coated by graphite using a Quorum Q150T ES sputter coater.

SEM-EDS investigation was carried out at the Department of Biological, Geological and Environmental Sciences of the University of Catania and at the Department of Biology, Ecology and Earth Sciences, University of Calabria.

7.1.3 Transmission Electron Microscopy (TEM-EDS)

The analysis performed by means of TEM-EDS were useful for the determination of the size and the chemical composition of single fibers. Specifically, a Jeol JEM 1400 Plus (120 kV) Transmission Electron Microscope equipped with Jeol large-area silicon drift detector SDD-EDS (Jeol, Tokyo, Japan) were used for microanalyses.

For TEM investigation, no grinding treatment have been performed to avoid the size reduction of the mineral fibres. Each sample was put into isopropyl alcohol and then sonicated. Three drops of the obtained suspension were deposited on a Formvar carbon-coated copper grid.

TEM-EDS investigation was performed at the "Laboratorio di Microscopia Elettronica e Microanalisi" of the University of Calabria.

7.1.4 X-Ray Powder Diffractometry (XRPD)

The X-ray powder diffraction patterns (XRPD) were obtained on a Bruker D8 Advance X-ray diffractometer with CuKa radiation, monochromated with a graphite sample monochromator at 40 kV and 40 mA. Scans were collected in the range of 3°-66° 2θ, with a step interval of 0.02° 2θ, and step-counting time of 3 s.

Each sample has previously been ground and placed on the sample holder for the analysis.

To identify the mineral phases in each X-ray powder spectrum, and to obtain a semi-quantitative mineralogical composition of samples, EVA software (DIFFRACplus EVA) was used. Experimental peaks have been compared with 2005 PDF2 reference patterns.

XRPD investigation was performed at the Regional Agency for the Protection of the Environment (ARPA) of Catania, Sicilia region.

7.1.5 Thermal analyses

Thermogravimetry (TG) and differential scanning calorimetry (DSC) were performed in an alumina crucible under a constant aseptic air flow of 30 mL·min^{-1} with a Netzsch STA 449 C Jupiter (Netzsch-Gerätebau GmbH, Selb, Germany) in the 25–1000 °C temperature range with a heating rate of 10 °C·min^{-1} and 20 mg of sample powder.

Instrumental precision was checked by 5 repeated collections on a kaolinite reference sample revealing good reproducibility (instrumental theoretical T precision of ± 1.2 °C). For the identification of exo- and endothermic peaks, weight loss and derivative thermogravimetric (DTG), a Netzsch Proteus thermal analysis software (Netzsch-Gerätebau GmbH, Selb, Germany) was used. Thermic analyses were performed at the department of Biology, Ecology and Earth Sciences, University of Calabria.

7.1.6 X-Ray Fluorescence (XRF)

For the X-ray fluorescence spectrometry investigation, all samples have previously been ground by means of agate mortar.

The analysis was carried out with PAN-analytical Axios instrument on fused glass diluted by $Li_2B_4O_7$ (1:5) and by using external calibration with international rock standards (PCC-1; USGS-W-2).

L.O.I. (Loss on Ignition) was determined by gravimetric method. XRF investigation have been carried out at the Department of Mineralogy, Geochemistry, Salt Deposits of the Technical University of Clausthal.

7.1.7 X-Ray synchrotron microtomography (SR-μCT)

For the 3D study, for each serpentinite sample the parts of greatest interest for the study or the most fibrous ones such as the veins, have been selected. Therefore, the samples were cut parallelepiped shaped with size of about 4 x 4 x 20 mm and analyzed by using Synchrotron Radiation X-ray computed microtomography (SR-μCT) in phase-contrast mode (Cloetens et al., 1997) at the SYRMEP beamline of the Elettra synchrotron laboratory (Basovizza, Trieste, Italy). Experiments were performed in white beam configuration (Baker et al. 2012), employing a filtered (1 mm Si + 1 mm Al) polychromatic X-ray beam delivered by a bending magnet source in transmission geometry. A total of 1800 projections were acquired over a scan angle of 180° for each experiment, with an exposure time/projection of 2 s and sample-to-detector distance fixed at 150 mm. The employed detector was a 16 bit, air-cooled, sCMOS camera (Hamamatsu C11440 22C) with a 2048 x 2048 pixels chip. The effective pixel size of the detector was set at 1.95 x 1.95 μm^2, yielding a maximum field of view of ca. 4 mm^2. Microtomographic scans were acquired in local region of interest mode (Maire and Withers, 2014). The Syrmep Tomo Project (STP) house software suite (Brun et al., 2017) was used for the reconstruction of the 2D tomographic slices. With the aim of improving the consistency of the quantitative analysis, a single-distance phase-retrieval algorithm (Paganin et al., 2002) combined with Filtered Backprojection algorithm (Herman, 1980) was employed to the sample projections. This allowed to obtain the 3D distribution of the complex refraction index of the imaged samples and to reduce edge-enhancement effect at sample borders, thus preserving the morphology of the smallest features. In the specific case of the veins, the obtained 3D images were useful to evaluate their arrangement and their geometric relationship with the massive serpentinite. The Fiji software (Schindelin et al., 2012) was used for the 3D image treatment. The original stacks of slices were first cropped for

extracting, for each sample, the volumes of interests (VOIs). To retrieve the veins/voids phase, VOIs were segmented by manual thresholding. This procedure allowed to obtain binary (black and white) 3D images of the phase of interest that were analyzed for retrieving the porosity values, calculated as volume of pores/total volume. The 3D renderings of the VOIs were obtained by means of VGStudio Max 2.2 software.

7.1.8 Electron Probe Micro-Analysis (EPMA)

For EPMA analysis, all samples were polished, and carbon coated by graphite using a Quorum Q150T ES sputter coater. An Electron Probe Micro Analysis (EPMA) JEOL-JXA 8230 coupled with a Spectrometer EDS – JEOL EX-94310FaL1Q and five WDS Spectrometer XCE type equipped with a LDE, TAP, LIF and PETJ crystals, were used to carry out the microchemical analysis of the minerals. EPMA/WDS single-point analyses were performed using accelerating voltage of 15 kV, probe current of 10 nA, counting times of 30 s for elemental peaks and 5 s for backgrounds. The X-Ray mapping of elements was performed with a WDS system with the following condition: 50.0 nA probe current, 15 keV accelerating voltage, 15ms dwell time. The area of maps ranged between 1.1 and 0.8 mm^2 with resolutions of 800×600 $pixel^2$. A set of standards Ref. # 02757-AB (SPI Supplies, Metals & Minerals Standard, serial 4AK) containing minerals with declared compositions was used for quantification. WDS microanalysis was carried out using the standardless ZAF correction method.

7.2 Results

7.2.1 Rocks from GMRU

Polarized light microscope (PLM), scanning electron microscopy analysis combined with energy dispersive spectrometry (SEM-EDS), X-ray synchrotron microtomography (SR-μCT) and electron probe micro-analysis (EPMA) were used for the identification of asbestos fibres within serpentinite from Gimigliano Mount-Reventino Unit (GMRU).

Since asbestos fibres mainly constitute the vein infill, particular attention has been paid to their investigation.

The macroscopic observations revealed that the studied specimens are characterized by the presence of veins crosscutting the rock and showing various thickness and shape features.

As shown in Figure 20, some veins show irregular thicknesses along their length (Figure 20a, e), while other veins are V-shaped thus decreasing in width towards the pointed end (Figure 20b, d), others are similar in shape and maintain a constant width (Figure 20c, f).

Due to the various morphological characteristics of the veins, an arbitrarily method based on their average distribution width has been applied to subdivide them into distinct categories. Therefore, to determine the widths variation of the asbestos veins in the studied samples, 10 measurements on 50 single veins have been carried out (Figure 21). This method allowed the identification of four classes of veins characterizing the studied samples:

- T1 → average width < 0.3 mm
- T2 → average width ranging between 0.3 mm to 1 mm
- T3 → average width ranging between 1 mm and 2 mm
- T4 → average width > 2mm

Based on this distinction, results highlighted that most vein types belong to classes T1 (37%) and T2 (41%), whereas only 22% is represented by wider veins (11% per type; Figure 22).
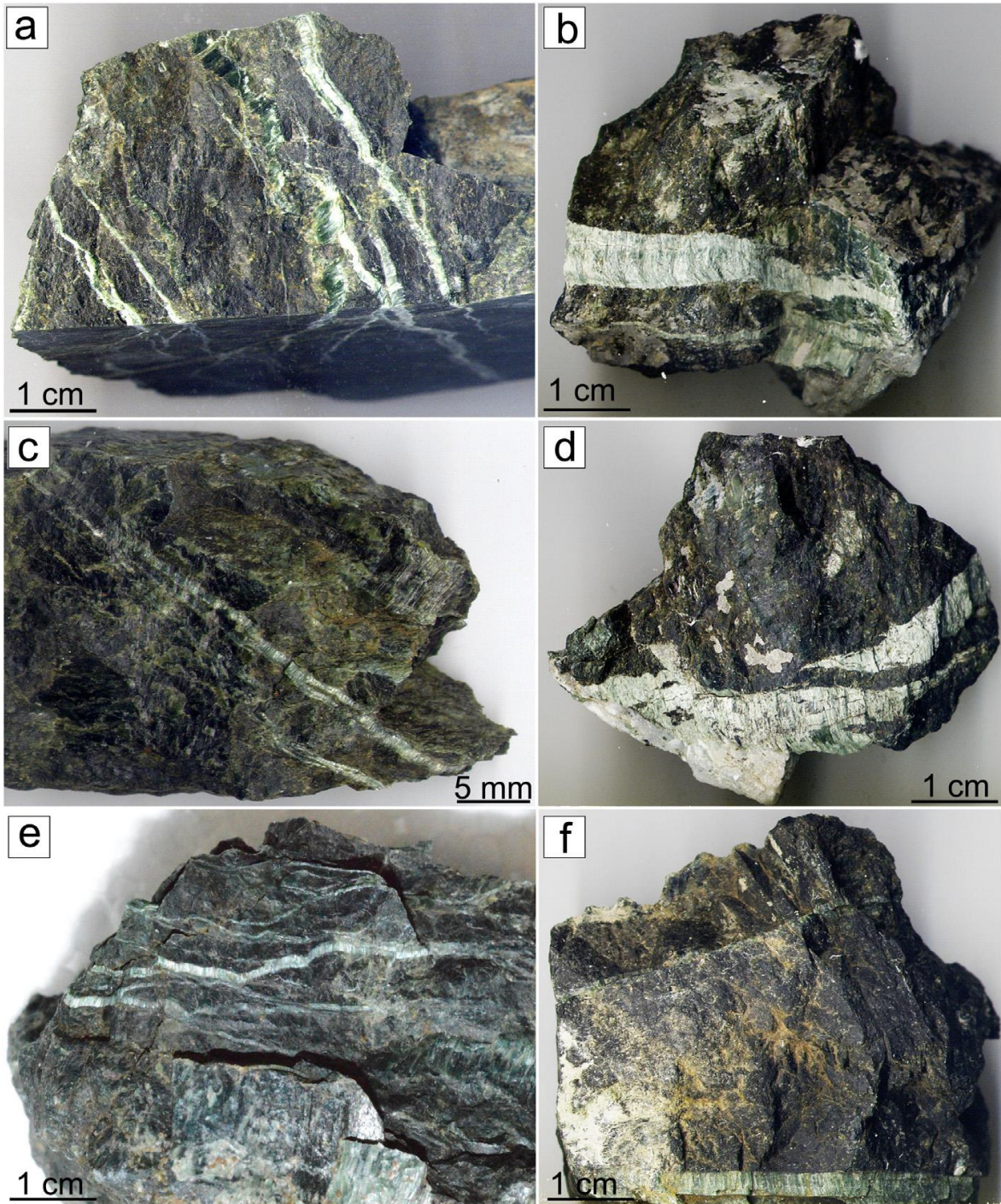
Figure 20: vein network of studied serpentinite: a-f) vivid green serpentinite veins; a,e) veins crosscut the sample showing variable thicknesses; b,d) V-shaped veins; c,f) veins characterized by constant thickness. From Bloise et al., 2020a.
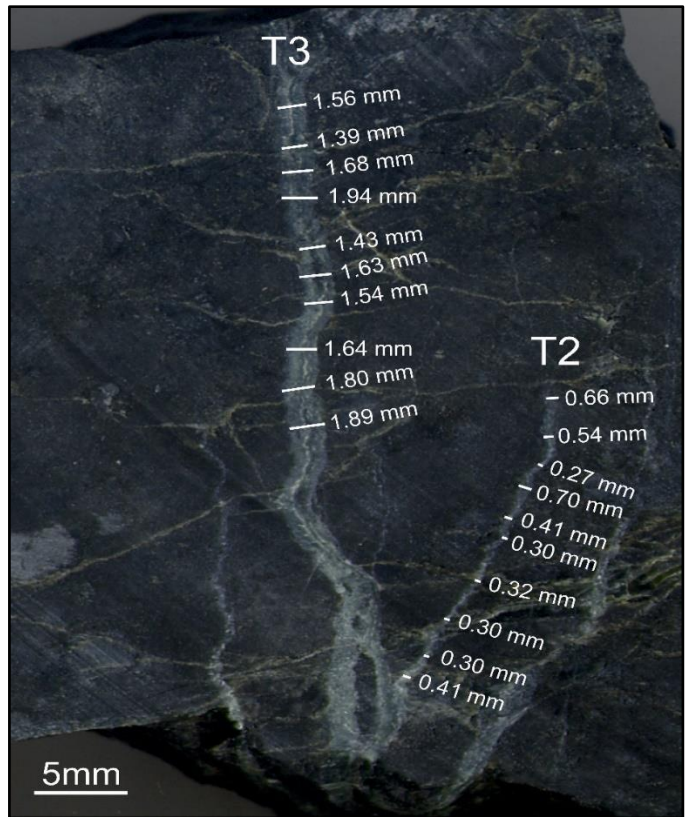
Figure 21: width measurement of the serpentinite veins in 2D (Bloise et al., 2020a).
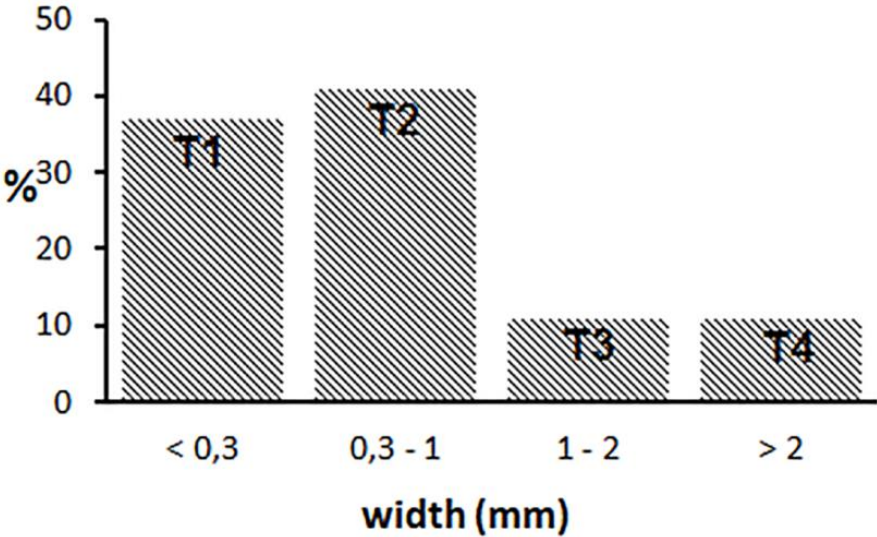
Figure 22: vein width distribution calculated on the average of 50 veins. The average value of each single vein was calculated on ten measurements (Bloise et al., 2020a).

7.2.1.1   Petrographic characterization

The results of the petrographic investigation showed that the ultramafic (peridotite) protolith of the serpentinite samples locally preserve the original texture despite the serpentinization process is almost completed. As visible in figure 23, olivine and pyroxenes as well as spinel have been replaced by serpentine minerals and by magnetite. Pseudomorph aggregates of serpentine and secondary magnetite are also present showing the typical net-like and mesh texture. Microscopic observations also showed the presence of vein systems whose infill is mainly represented by chrysotile oriented either perpendicular (cross fibres) or parallel (slip fibres) to the vein elongation directions. Moreover, chrysotile fibres fill the veins in syntaxial growth following the flow of the fracture walls. In some cases, evidence of post deformation is exhibited as by kink banding (Figure 23d).
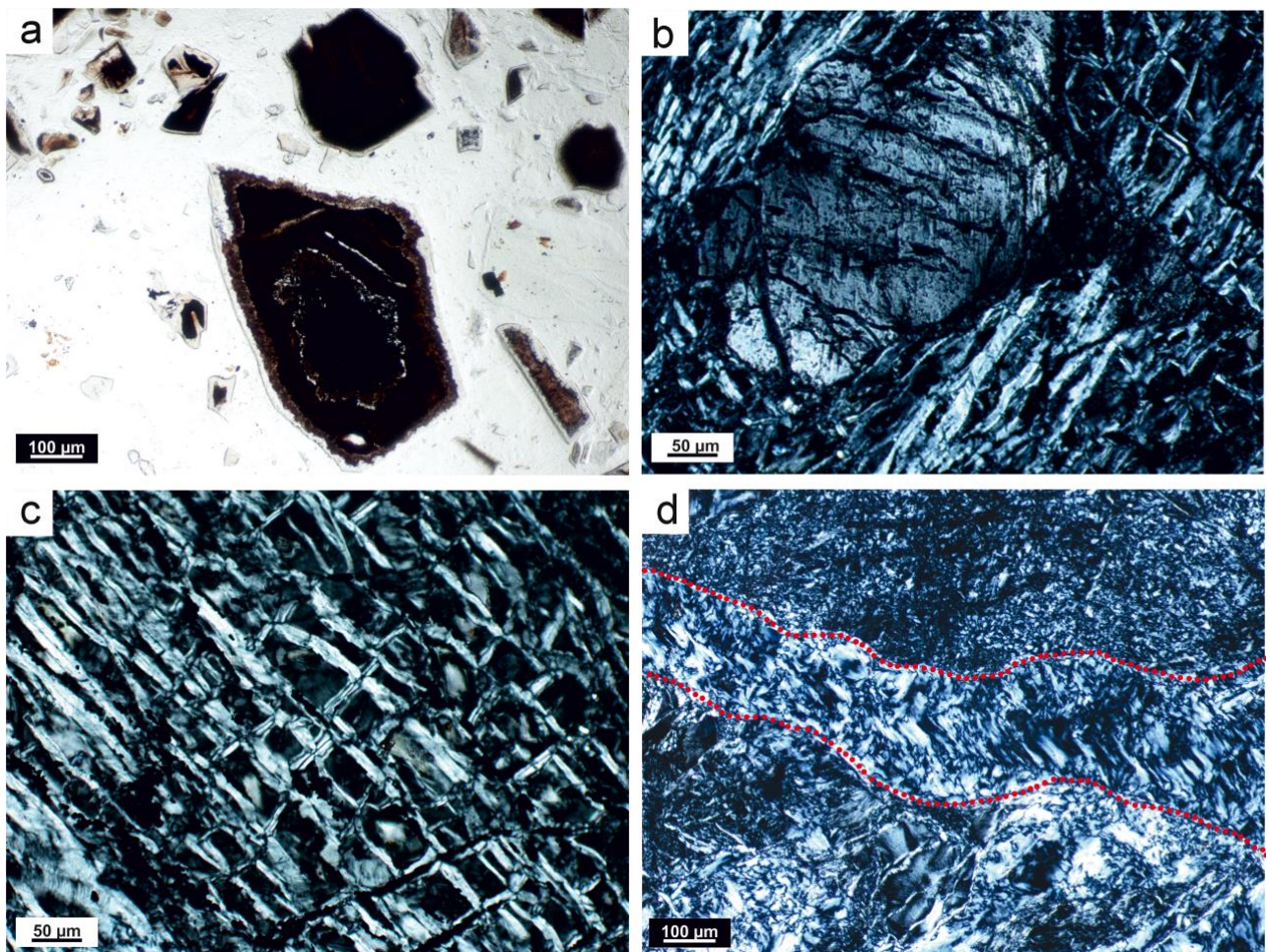
Figure 23: a) magnetite replacing spinel minerals (lower polarizer); b) olivine and pyroxenes replaced by serpentine (crossed polarizers); c) detail of mesh-like texture of serpentine (crossed polarizers); d) kink-banded serpentine veins within the mesh-like matrix (crossed polarizers). From Bloise et al., 2020a.

7.2.1.2   SEM-EDS characterization

SEM analysis allowed to observe the morphological characteristics of mineral phases present in the studied samples whose identification was carried out with the contribution of EDS chemical analysis. Serpentine minerals are present in both fibrous and non-fibrous habit. The massive portion of serpentinite samples was characterized by the occurrence of lizardite with lamellar morphology whereas chrysotile fibres were mainly found inside the veins where they are primarily arranged perpendicular to the vein elongation (Figure 24a). The fibres appear flexible and occur in bundles or as isolated fibrils. Figure 24a shows a longitudinal splitting of larger bundles into thinner while the presence of isolated fibrils is shown in Figure 24b (relative EDS point analysis showed in figure 24c).
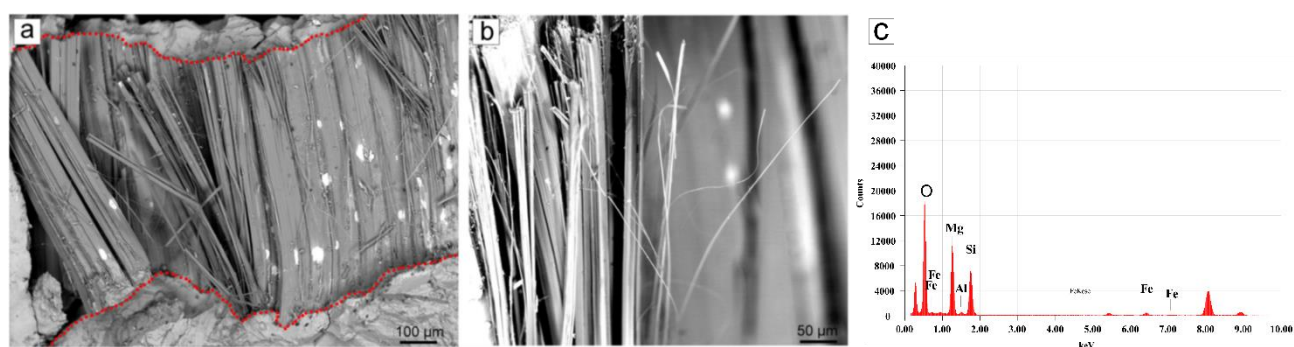
Figure 24: SEM images showing a) vein filled by chrysotile fibres bundles in which the splitting of compact fibres into tinner is visible; b) isolated fibres and chrysotile fibre bundles with the typical wavy appearance. Note the flexibility of the single fibrils. Bloise et al., 2020a.

7.2.1.3   EPMA characterization

With the aim of verifying the chemical variations between the veins and the matrix of the studied serpentinite, electron probe micro-analysis provides the elemental maps showing the element's distribution into the samples. The analyses revealed that in addition to Si and Mg that are the most abundant elements of the samples, followed by Al and Fe, other elements such as Ni, Cr and Mn are found in smaller quantities. Various consideration can be made by observing the elemental map reported in figure 25. Firstly, the color contrast between dark grey and light grey visible in Figure 25a, that is based on the difference in density of mineral phases, allowed to identify the passage from the matrix to the vein and subsequently to recognize the walls of the veins (marked with the red lines). Secondly, attributing different color to the elements it is clearly visible the different concentrations of the elements in the mapped section. Specifically, the distribution of Si

(as well as that of Mg, as reported in table 5) is uniform between the matrix and the vein differently to Al and Fe which that show distinct behavior. As a matter of fact, as shown in figure 25b, the highest concentration of Al has been revealed inside the vein (filled by chrysotile), as opposed to Fe whose highest values have been detected in the matrix. Moreover, it is notable that iron it is non-homogenously distributed in the matrix but rather it most characterizes the extremities of the vein walls. These concentrations are better visible in the Si/Al/Fe ratios showed in green, red, and blue color respectively in figure 25. It is worth mentioning, that a spot analysis specifically focused on serpentine minerals filling the veins and on those present in the matrix, was performed at the same time to avoid potential matrix effects mainly caused by magnetite. The chemical composition obtained by the several spot analyses are reported in Tables 5 and 6. The average values of Al and Fe in chrysotile that fills the vein is about 2.45 wt % and 2.00 wt% respectively (Table 5) while about 0.72 wt% of Al and 3.67 wt% of Fe (almost two times higher than Fe in the vein) was found in the matrix (Table 6).

A homogenous distribution of Mn and Ni were revealed between chrysotile that fills the veins and the matrix. Specifically, Mn content inside the vein ranges from 0.13 to 0.20 wt% with an average value of 0.16 wt% that is similar to the average concentration in the matrix (0.17 wt%; Tables 5, 6). As for Ni, the content was approximately 2-fold higher than Mn, with values ranging from 0.25 wt% in the vein infill to 0.31 wt% in the matrix (Tables 5, 6). Conversely, highly variable concentrations were revealed for Cr that was detected with the highest amount in the matrix (1.04 wt%) and even below the detection limits within the vein.
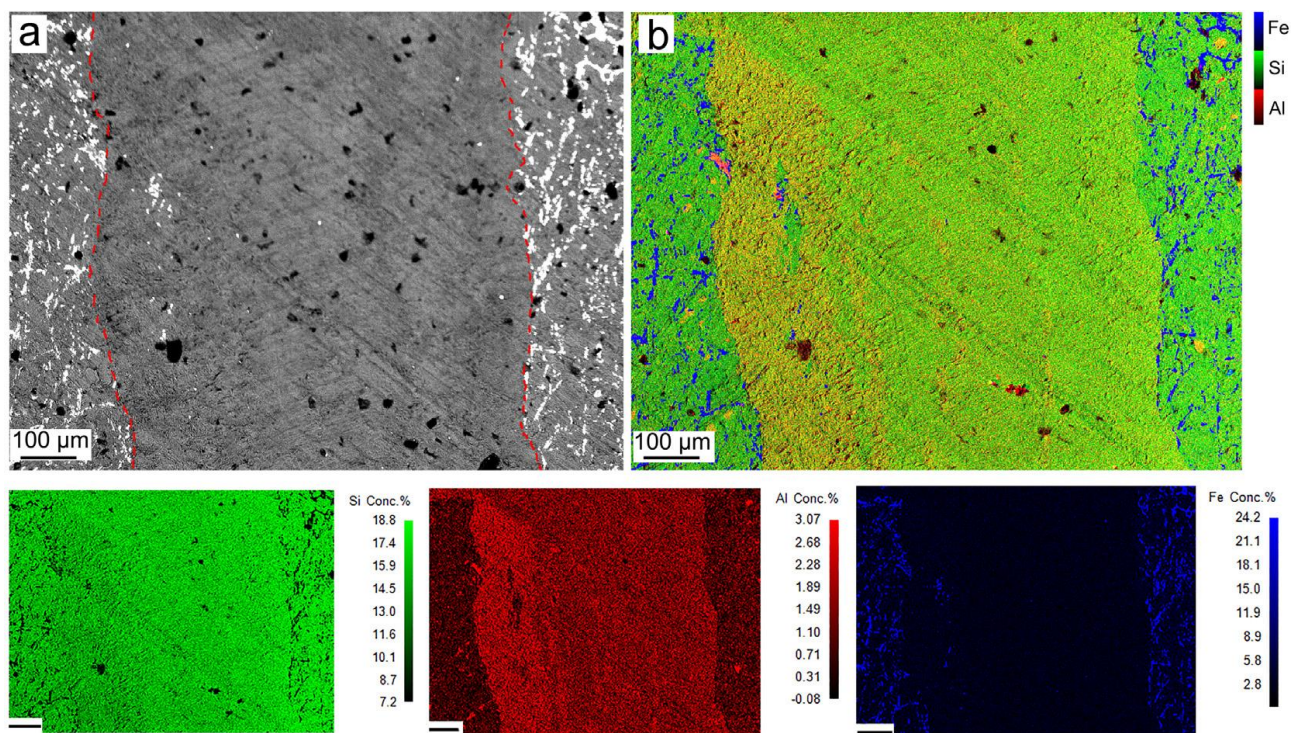
Figure 25: Si (green), Al (red), and Fe (blue) element maps with related concentrations (%) expressed by the intensity of the color (see concentration % scale on the right of each map). a) area mapped with red line highlighting the vein surface; b) area mapped with Fe/Si/Al ratios. The black bar represents 100 μm. Bloise et al., 2020a.

			Chrysotile inside the veins					
Oxide wt %	MgO	SiO$_2$	Al$_2$O$_3$	Cr$_2$O$_3$	FeO	MnO	NiO	Total
1	40.41	41.64	2.05	0.20	1.90	0.17	0.55	86.91
2	40.28	41.62	2.78	0.35	1.82	0.14	0.00	86.99
3	39.96	41.36	2.08	0.19	3.00	0.15	0.46	87.20
4	40.97	39.99	2.85	0.29	1.93	0.18	0.11	86.32
5	40.77	40.36	2.86	0.00	1.82	0.20	0.38	86.38
6	40.97	41.01	2.44	0.23	2.12	0.13	0.20	87.09
7	40.11	41.37	2.21	0.00	1.76	0.14	0.32	85.91
8	40.14	41.25	3.00	0.67	1.83	0.18	0.00	87.07
9	41.97	41.95	2.03	0.41	1.93	0.16	0.36	88.81
10	40.92	41.40	2.17	0.37	1.89	0.13	0.12	87.01
Average	40.65	41.19	2.45	0.27	2.00	0.16	0.25	86.97

Table 5: representative EPMA analyses of chrysotile inside the vein. Bloise et al., 2020a.

Matrix outside the veins								
Oxide wt %	MgO	SiO$_2$	Al$_2$O$_3$	Cr$_2$O$_3$	FeO	MnO	NiO	Tot
1	41.89	40.68	0.48	0.93	3.42	0.14	0.24	87.78
2	40.42	41.63	1.02	0.84	3.74	0.16	0.29	88.09
3	39.97	42.49	0.85	1.03	3.36	0.13	0.26	88.07
4	40.48	41.09	1.04	0.41	3.54	0.21	0.38	87.14
5	41.60	41.60	1.03	0.72	3.54	0.05	0.25	88.78
6	40.80	41.17	0.56	0.69	3.90	0.18	0.56	87.86
7	41.42	41.09	0.52	0.15	3.87	0.04	0.37	87.44
8	40.57	41.94	0.39	0.11	4.21	0.41	0.33	87.97
9	40.28	41.81	0.46	0.82	3.72	0.26	0.13	87.48
10	39.06	41.95	0.86	1.04	3.38	0.09	0.24	86.60
Average	40.65	41.54	0.72	0.66	3.67	0.17	0.31	87.72

Table 6: representative EPMA analyses of matrix outside the vein. Bloise et al., 2020a.

7.2.1.4   *Three-dimensional image analysis*

For the three-dimensional image analysis two specimens of veins from class T2 (i.e., thicknesses ranging from 0.3 to 1 mm) present in the collected samples were selected (Figure 26). This class has been chosen since it represents the most abundant vein type and because fibrous bundles are visible at the mesoscale. Specifically, T2$_{GMRU2}$ and T2$_{GMRU12}$ were selected.

The 3D rendering (Figure 27a, c) shows the geometric shape of the veins that are recognized with i) sub-parallel side; ii) lens-shape; iii) V-shape; iv) irregular shape.

In the sample T2$_{GMRU2}$ a small variation of the thickness is visible (Figure 27 a, b) with highest values of 0.580 mm, while a maximal thickness of 0.566 mm has been measured in T2$_{GMRU12}$ sample (Figure 27 c).

The SR-µCT investigation also revealed the presence of veins belonging to class T1 (average width < 0.3 mm) that were not identified at the mesoscopic scale and thanks to the 3D reconstructions the branching of the veins into the matrix is visible (Figure 27 b, d).

Thanks to the observation of 2D slices of the veins, the presence of voids in some portions of the sample has been recognized. In these voids, it is possible to identify chrysotile fibres crystallized as bundles of intertwined fibres (Figure 28).

The Fijii software (Schindelin et al., 2012) enabled us to measure the fibres width by direct measurements on 100 slices obtained from SR-µCT. Specifically, in all samples the fibres length ranges from 10 to 300 µm with aspect ratios >3:1, thus falling into the category of respirable fibres as established by the World Health Organization (WHO, 1986).

It is worth specifying, that the SR-μCT analyses is not capable of measuring fibres shorter than 2 μm.
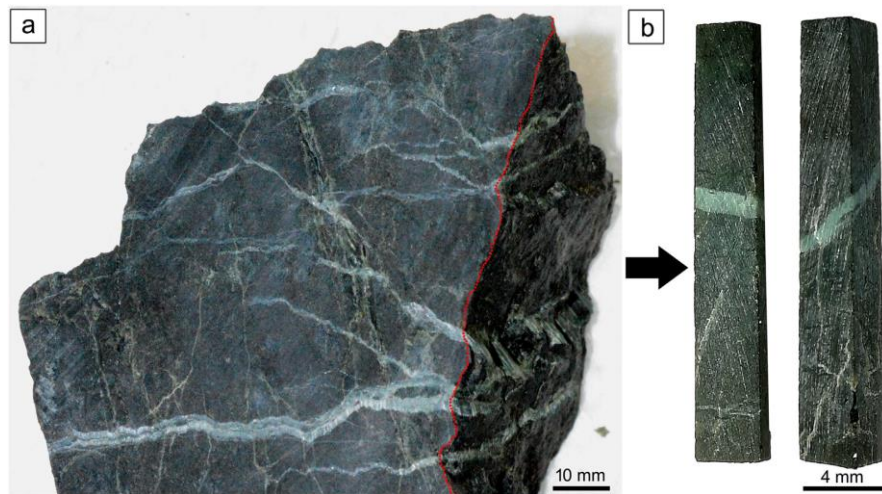
Figure 26: a) cut serpentinite specimen with evident veining (to the left of the red line); serpentinite impregnated with epoxy resin (to the right of the red line); b) prismatic samples cut for SR-μCT analysis. Bloise et al., 2020a.
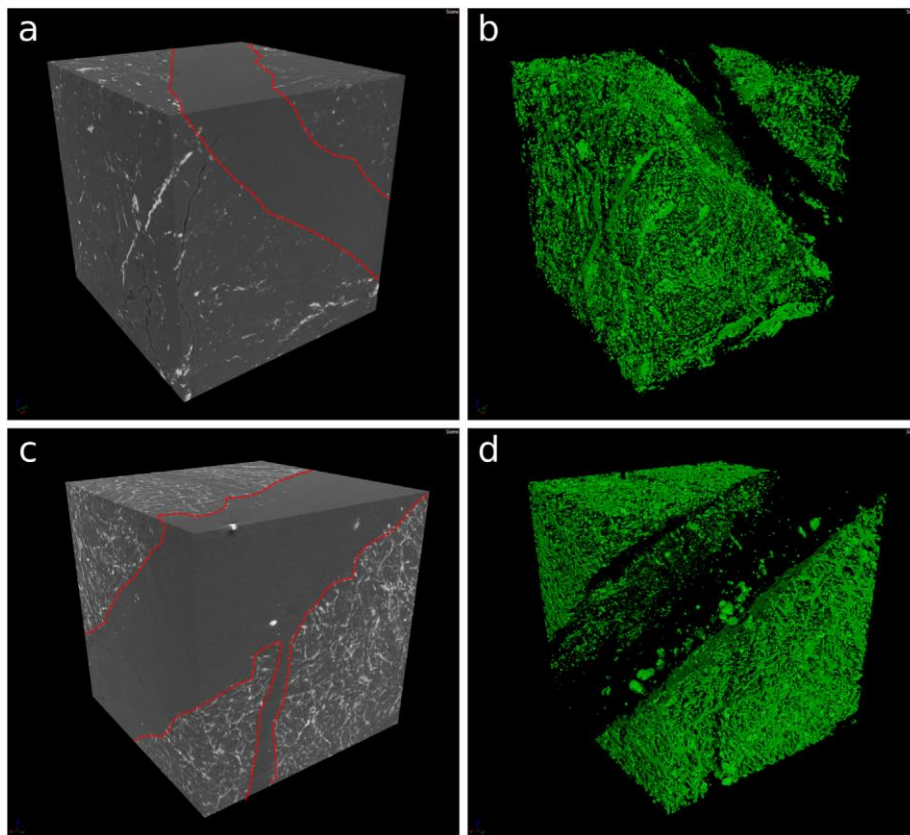
Figure 27: volume rendering of extracted VOIs from: a) $T2\_{GMR2}$ (7 MM3) and c) $T2\_{GMRU12}$. The red lines highlight the contact between veins and matrix. Images b) and d) show the spatial distribution of the veins, which are reported as empty spaces, for $T2\_{GMRU2}$ and $T2\_{GMRU12}$ respectively. The matrix is indicated with green color. Bloise et al., 2020a.
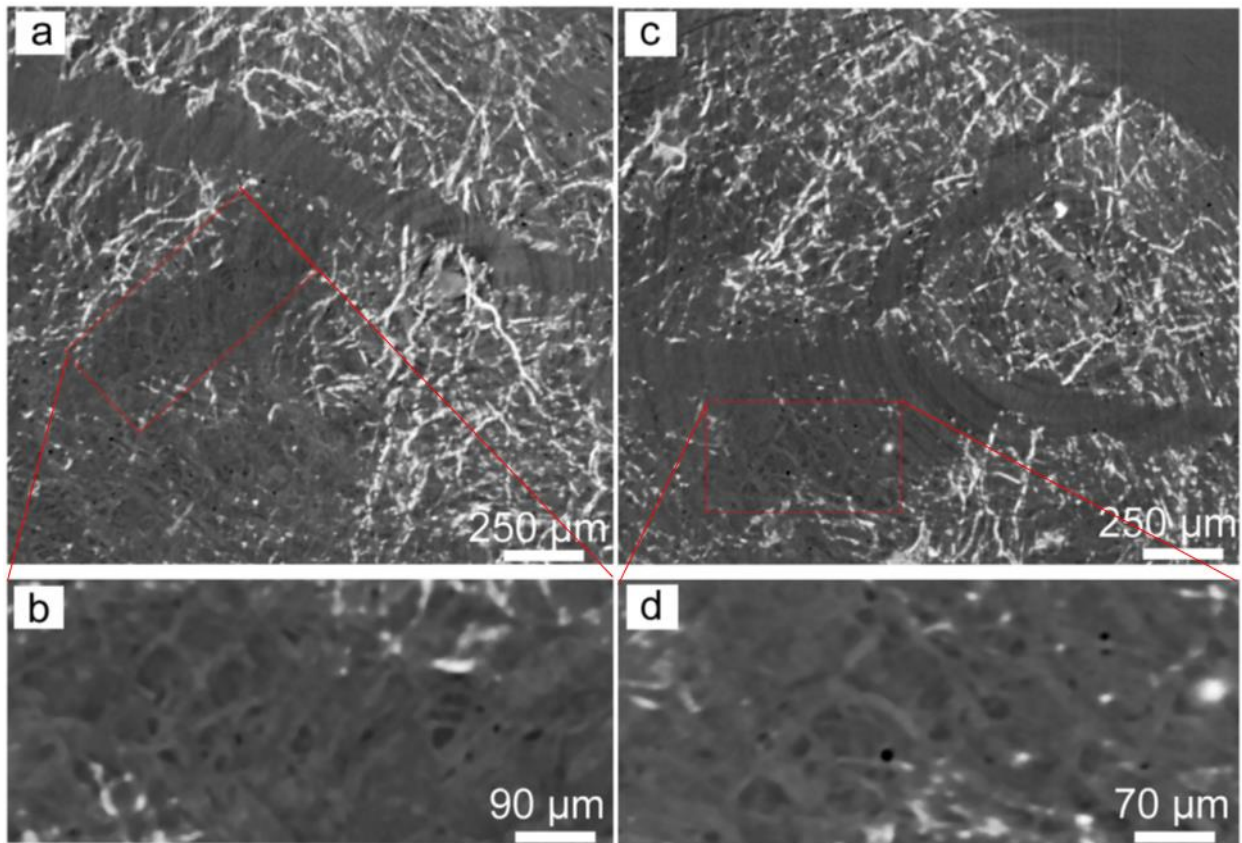
Figure 28: axial slices of T2_GMRU12 sample. a) vein system filled by chrysotile fibres; b) detail of the red rectangle in figure a; c) vein system filled by chrysotile fibres; d) detail of the red rectangle in figure c. Bloise et al., 2020a.

7.2.2   *Rocks from Episcopia village*

The mineralogical study conducted on rocks samples collected in the surroundings of Episcopia village (Administrative province of Potenza, Basilicata Region), aimed to the investigation of the presence of NOA since a detailed characterization of asbestos minerals present in the study area is still lacking in the literature. The eleven serpentinite samples were characterized by means of various analytical techniques such as X-ray powder diffraction (XRPD), scanning electron microscopy combined with energy dispersive spectrometry (SEM-EDS) and derivative thermogravimetry (DTG) to determine the occurrence of asbestos minerals and their morphological characteristics.

The XRPD characterization allowed the determination of the mineralogical phases present in the studied samples. XRPD patterns showed the presence of serpentine minerals, chlorite, talc, tremolite, actinolite, willemseite and dolomite (Table 7). Specifically, the diffractograms showed that serpentinite minerals occur in all samples except in the sample E10 (characterized by talc and tremolite) and in the sample E10b (characterized by actinolite, willemseite and dolomite). Instead, reflections diagnostic of the presence of asbestos amphiboles such as tremolite/actinolite, were found in eight samples out of eleven (Table 7). It is worth mentioning, that the X-ray powder diffraction method did not allow the discrimination of serpentine varieties (i.e., chrysotile, lizardite, antigorite and polygonal serpentine), because of the diffraction peaks overlapping of the serpentine polymorphs. Therefore, the samples in which serpentine minerals were detected have been further investigated by thermal analysis and summarized in Table 7 together with those detected by means of SEM-EDS. Semi-quantitative analysis has also been performed and shown in Table 7 where the detected mineralogical phases in order of decreasing relative abundance are expressed for each sample.

Sample	Phases Detected Max ↔ Min
E1	Ctl > Liz > Atg > Chl > Tlc > Tr
E4	Ctl > PS > Chl > Tlc > Tr
E6	Chl >Tr > Liz > Ctl
E8	Chl > Liz > Ctl
E8b	Chl > Ctl > PS
E10	Tlc > Tr
E10b	Wil > Dol > Act
E10t	Tlc > Ctl > Atg > Act
E11	Tlc > Liz > Ctl
E11b	Liz > Ctl > Tlc > Tr
E12	Tlc > Ctl > PS > Act

Table 7: semi-quantitative mineralogical composition of the serpentinite samples from Episcopia village in order of decreasing relative abundance, detected by X-ray diffraction (XRPD), scanning electron microscopy combined with energy dispersive spectrometry (SEM-EDS) and derivative thermogravimetry

(DTG) analysis. Atg = antigorite, Lz = lizardite, Ctl = chrysotile, Act = asbestos actinolite, Tr = asbestos tremolite, PS = polygonal serpentine, Chl = chlorite, Will = willemseite, Dol = dolomite, and Tlc = talc. Bloise et al., 2019.

7.2.2.2   SEM-EDS characterization

SEM analysis was useful to observe the morphological characteristics of mineral fibres present in the studied samples. As visible in figure 29, chrysotile fibres appear thin and flexible (Figure 29a) with length > 6-8 µm and occur either in isolated fibres or in bundles. Conversely, tremolite and actinolite fibres look straight and exhibit a slender needle-like crystal habit with length > 10 µm (Figure 29b).

In all samples, the presence of both chrysotile and amphibole asbestos (i.e., tremolite, actinolite) having size matching with those of regulated asbestos (L > 5 µm; D < 1 µm; WHO, 1986) has been detected (Table 7). Moreover, the splitting of larger fibres into thinner ones is often visible, thus leading to even smaller diameters and therefore to an increasing risk for human health related to the inhalation when they become airborne.

The correct identification of the mineral species was allowed by the use of EDS spot analysis (Figure 29a, b inserts) by means of which the presence of chrysotile, tremolite asbestos and actinolite asbestos has been confirmed. Specifically, EDS chemical analyses revealed low amounts of Al replacing Mg in chrysotile octahedral sites and an iron content ranging from a minimum of 3.51 wt % (sample E11) of FeO to 8.71 wt % (sample E12) with an average value of 4.90 wt %.

As for amphiboles, their chemical composition (obtained by EDS) was plotted in the diagram Si vs. $Mg/(Mg + Fe^{2+})$ (Figure 30) and what comes out is that: i) three samples (E10b, E10t, and E12) fall in the field of actinolite with Si values ranging from 7.94 a.p.f.u (atoms per formula unit) and $Mg/(Mg + Fe^{2+})$ values from 0.87 to 0.89; and ii) five samples are in the field of tremolite with Si values ranging from 7.94 to 7.99 a.p.f.u and $Mg/(Mg + Fe^{2+})$ value > 0.9.
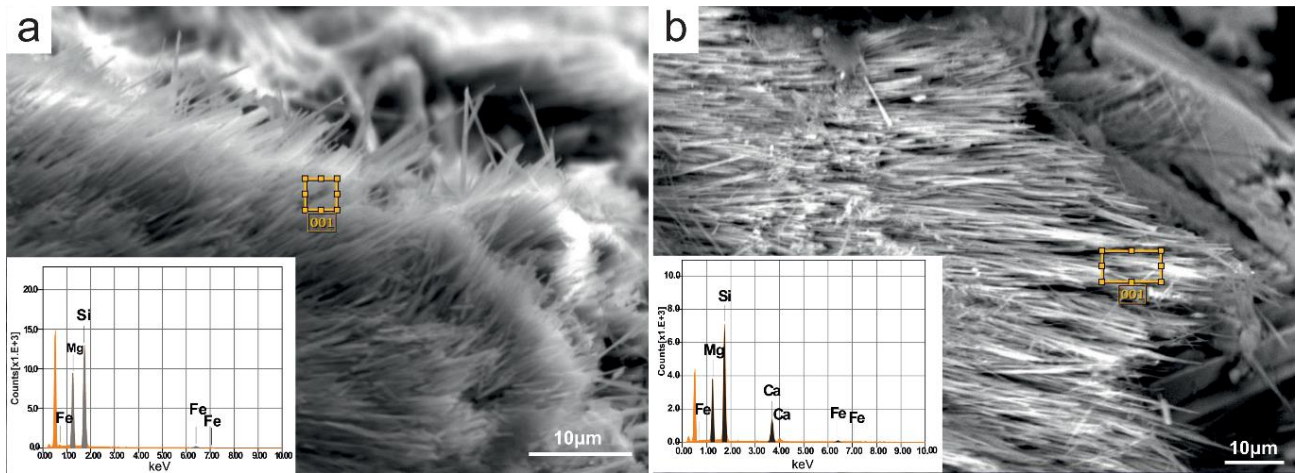
Figure 29: SEM images of asbestos detected in the studied samples. a) chrysotile in sample E11; b) tremolite in sample E4. The graphical inserts illustrate the EDS point analysis. Bloise et al., 2019.
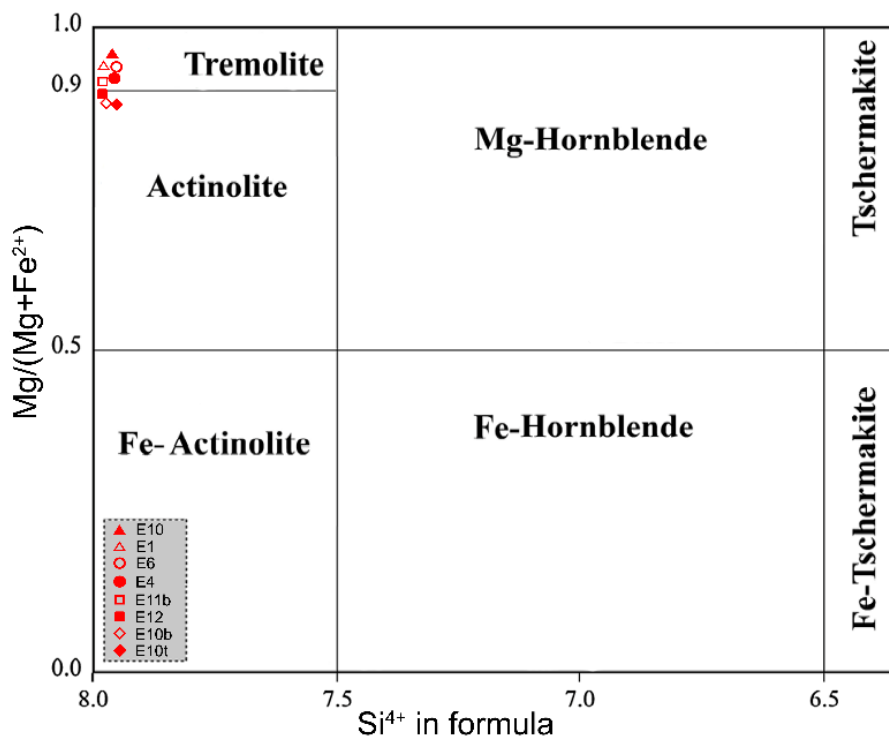
Figure 30: data plot on the Amphibole classification diagram by Leake et al., 1997 (From Bloise et al., 2019).

Thermal analysis allowed the discrimination among serpentine varieties (chrysotile, lizardite, antigorite, polygonal serpentine; Kusiorowski et al., 2012) in those sample in which serpentine minerals were detected by the other analytical techniques.

Figure 31 shows the DTG curves of the samples E1, E4, E6, E8, E8b, E10t, E11, E11b, E12 in the temperature range between 550 °C and 850 °C.

All the analyzed samples seem to show the same behavior showing the maximum mass loss rate in the T range of 605-690 °C that is due to the loss of the chemical bonded water of chrysotile. Instead, the DTG peaks in the T range of 705-731 °C are related to the dihydroxylation of lizardite while that of antigorite occur at higher temperatures (770 °C average value).

Based on the thermal analysis results, chrysotile was detected in nine out of eleven samples, lizardite was identified in five samples, antigorite in two samples, while polygonal serpentine was detected in three samples (Table 7).
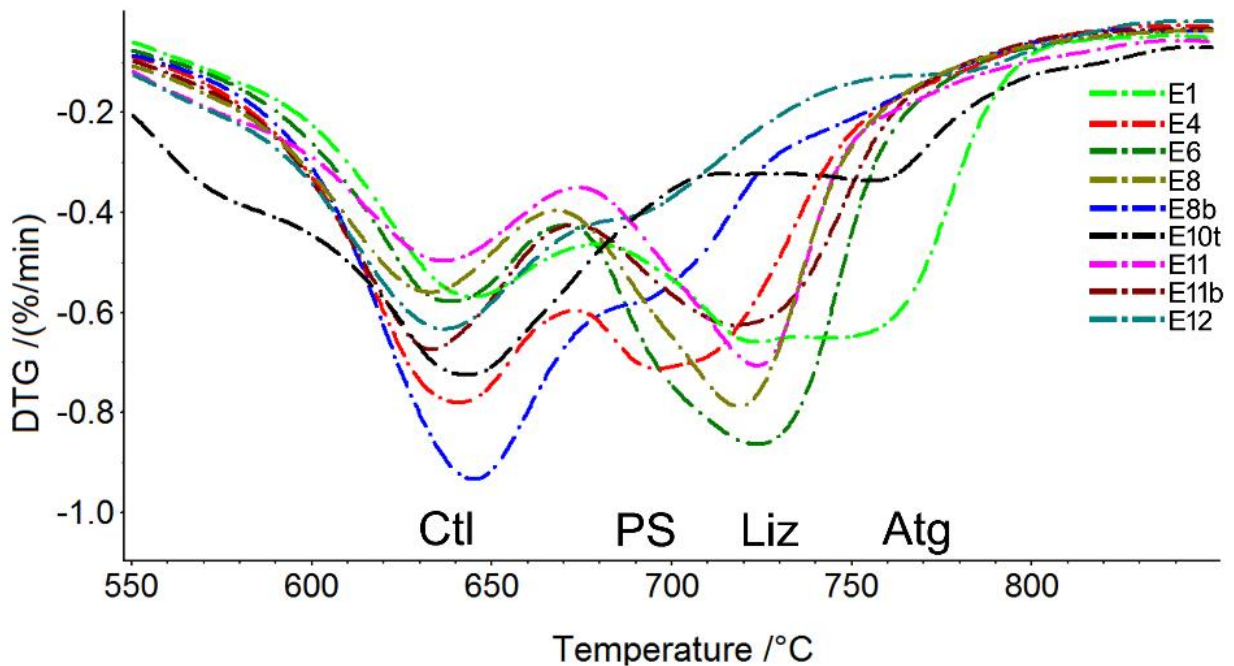
Figure 31: DTG curves of the nine analyzed samples, in the T range of 500-850 °C. Endothermic peaks related to Ctl = chrysotile; PS = polygonal serpentine; Liz = lizardite; Atg = antigorite. Bloise et al., 2019.

7.2.3 Rocks and Soils from San Severino Lucano village

Serpentinite rocks and agricultural derivative soil samples have been collected in the surroundings of San Severino Lucano village (administrative province of Potenza, Basilicata region, southern Italy) and fully characterized by the mineralogical and geochemical point of view.

Specifically, Polarized Light Microscopy (PLM), X-Ray Powder Diffraction (XRPD), Scanning Electron Microscopy combined with Energy Dispersive Spectrometry (SEM/EDS), Transmission Electron Microscopy with Energy Dispersive Spectrometry (TEM/EDS), Differential Scanning Calorimetry (DSC), Derivative Thermogravimetry (DTG) X-Ray Fluorescence (XRF), have been used for the samples analyses. Special attention has been paid on soil samples characterization, since they inherit the mineralogical and geochemical composition of the bed-rock and subsequently it was object of a great interests the investigation of inherited fibrous minerals, if any.

7.2.3.1   Petrographic characterization

The observations of the serpentinite thin sections at the polarizing microscope, show that serpentine group minerals represent the main constituents of the samples and magnetite ± talc ± Cr-spinel ± chlorite are also present. In most cases, original minerals have been completely replaced by serpentine pseudomorph aggregates and small magnetite grains, but rare relics of olivine and pyroxene have been found (Figure 32a).

Where olivine has been replaced by serpentine minerals, the fractures in which the serpentinization occur are well visible and the mesh textures is shown (Figure 32b). The former olivine grain-boundaries and fractures are emphasized by secondary magnetite formed by the serpentinization process, thus making the mesh core of olivine grains well distinguishable (Figure 32c).

As for pyroxene, the replacement by serpentine minerals begins from grain boundaries and fractures by following the cleavage planes as shown in figure 32d.

Finally, many vein systems filled by serpentine minerals (Figure 32e) oriented perpendicular to the vein elongation direction (cross-fibres) together with talc (Figure 32f) are visible in thin section.
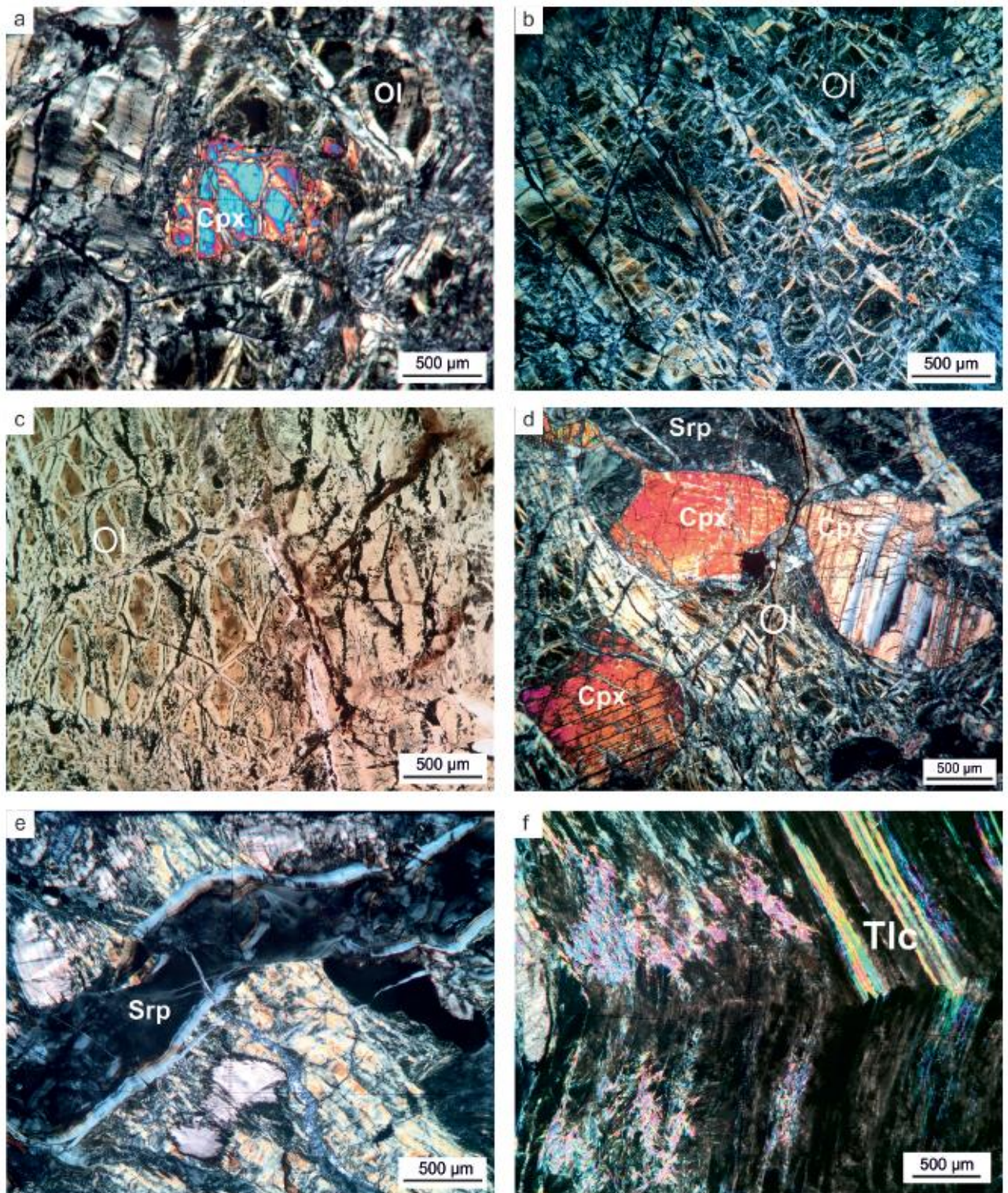
Figure 32: photomicrograph of serpentinite samples showing: a) clinopyroxene relic, olivine partially replaced by serpentine; b) mesh structure of olivine pseudomorph replaced by serpentine (crossed polarizers); c) serpentinized olivine with mesh textures in plane-polarized light; secondary magnetite emphasize the fractures; d) clinopyroxene partially replaced by serpentine, olivine pseudomorph and serpentine matrix visible at the top; e) serpentine vein cross-cutting the main rock; f) serpentine and talc fibres arrangement inside a vein (crossed polarizers). Punturo et al., 2018. Mineral symbols after Whitney and Evans (2010).

7.2.3.2   XRPD characterization

The presence of serpentine minerals as the most abundant phase in all serpentinite rock samples is confirmed by the XRPD analysis. As a matter of fact, the diffractograms interpretation revealed the characteristic diffraction lines of serpentine in all samples, differently to tremolite that has been detected in four samples out of twelve. Other phases such as diopside and magnetite occur in all samples, whereas clay minerals (chlorite, montmorillonite) only in a few (Figure 33a).

As for soil samples, also in this case the X-ray diffraction investigation revealed the presence of serpentine minerals in all samples, whereas diopside, clay minerals (e.g., montmorillonite-chlorite, chamosite, muscovite) and quartz are the other mineral components. It is worth mentioning, that while the reflections diagnostic of tremolite were not well visible in the serpentinite diffraction patterns (likely for the overlapping of serpentine reflections), they are clearly visible in soil patterns. As a matter of fact, tremolite was detected in nine samples out of twelve in serpentinite-derived soils compared to four of rocks samples (Figure 33).
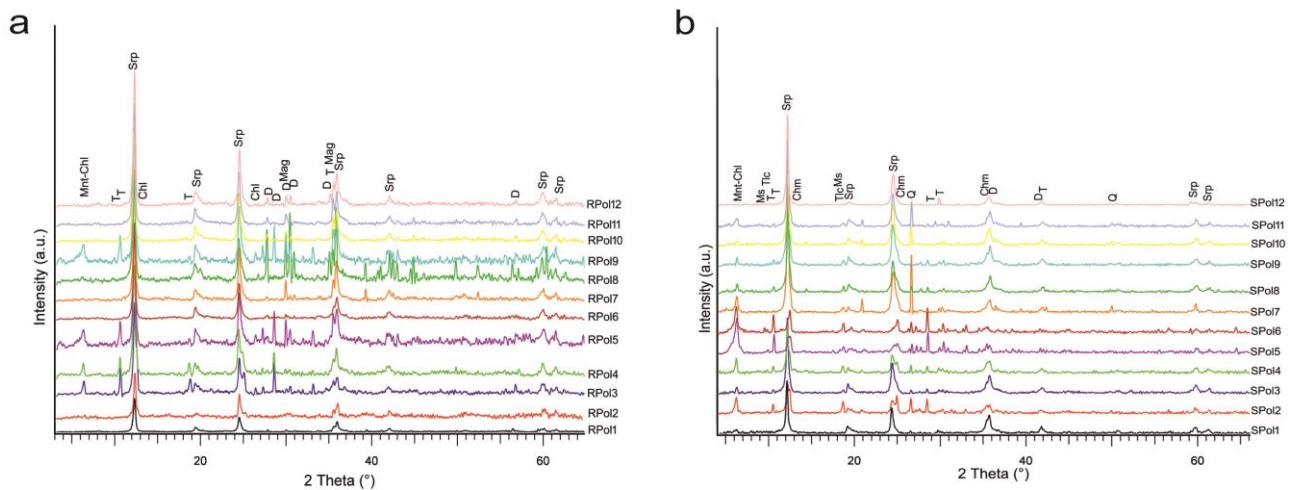
Figure 33: XRPD pattern related to serpentinite rocks (a) and derived soils (b). Peaks were assigned according to literature (Mineral Powder Diffraction File: Data Book, JCPDS-International Centre for Diffraction Data). Punturo et al., 2018.

The morphological characteristics of representative fibrous mineral phases detected in the studied samples are shown in figure 34. With special regard to asbestos minerals in soils, SEM observations revealed many fibrous phases with acicular habit trapped in aggregating agents like organic matter, clay, and iron oxides. The fibres length ranges from 13 to 18 μm while the diameter is about 1 μm, and often the longitudinal splitting of the larger into thinner ones is visible. The EDS analysis was performed to complete the preliminary identification of the mineral phases, showing the presence of chrysotile, amphiboles with tremolite-actinolite main composition, and minor anthophyllite.
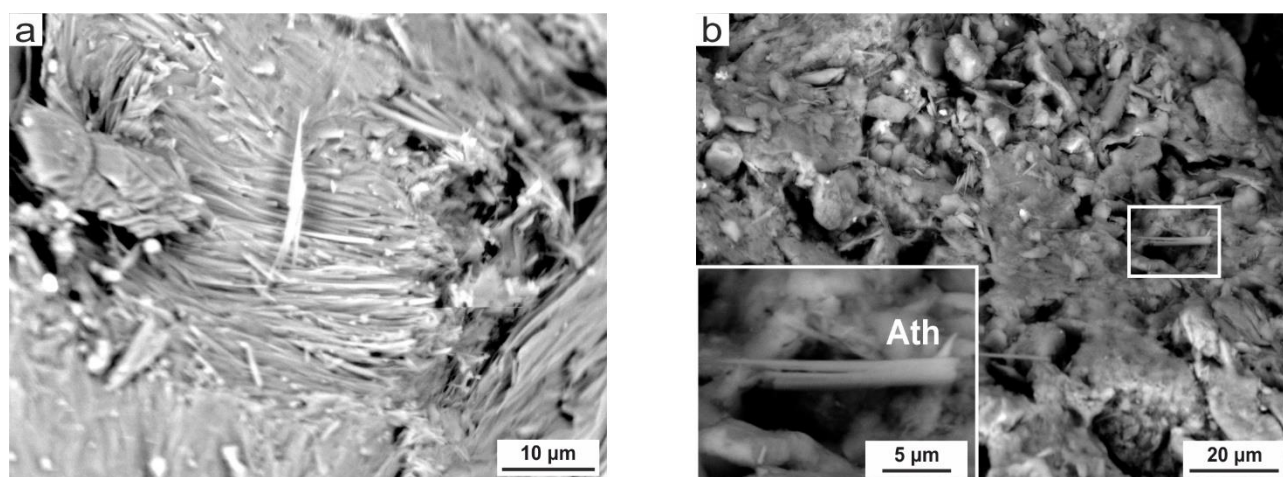
Figure 34: SEM images showing the representative morphology of: a) asbestos fibres in serpentinite rocks; b) asbestos fibres in soil soil samples; Ath = Anthophyllite. Rectangle is zoomed image. Punturo et al., 2018.

7.2.3.4 TEM-EDS characterization

Thanks to high magnification power, TEM observations allowed to determine the presence of serpentine varieties and their morphological features in the studied samples. A representative set of soil samples has been selected and analyzed. Results showed the presence of different fibrous serpentine varieties such as chrysotile, fibrous antigorite, polygonal serpentine as well as that of fibrous amphiboles such as tremolite (Figure 35). The fibrous minerals found, exhibit various shape and size.

As for chrysotile, it occurs as thin individual fibrils and sometimes forms larger longitudinally aligned fibres as visible in figure 35 (a, b). The cylindrical shape of chrysotile is the most common fibre morphology occurring in all the samples and consists of a central core formed by an empty

cavity that extends over the entire length of the fibre (Figure 36). Generally, the fibres are long (from 300 to 1500 nm) with diameters of the inner core of about 20 nm and that of the outer of about 40 nm. Some samples show chrysotile fibres characterized by a wide core and very thin outer walls thus proving that chrysotile suffered an unrolling process from the inside during the alteration process from the rock to soil. This is likely due to the passage of water through the core (Figure 35c).

Low amount of polygonal serpentine has been found in most of the studied samples (Figure 35b,d) while only two samples showed the presence of fibrous antigorite (platy antigorite is the most abundant form) whose fibres occur with the shortest length (1000 nm) and with diameters of about 300 nm (Figure 35b). Few samples are characterized by lizardite with platy morphology.

As for fibrous amphiboles, tremolite fibres have also been observed (Figure 35a). The typical appearance of fibrous tremolite is shown in figure 37. The fibres exhibit prismatic rod-shaped morphology lacking any flexibility, an average length ranging from 2.5 µm to 3µm and diameter of about 0.2 µm.
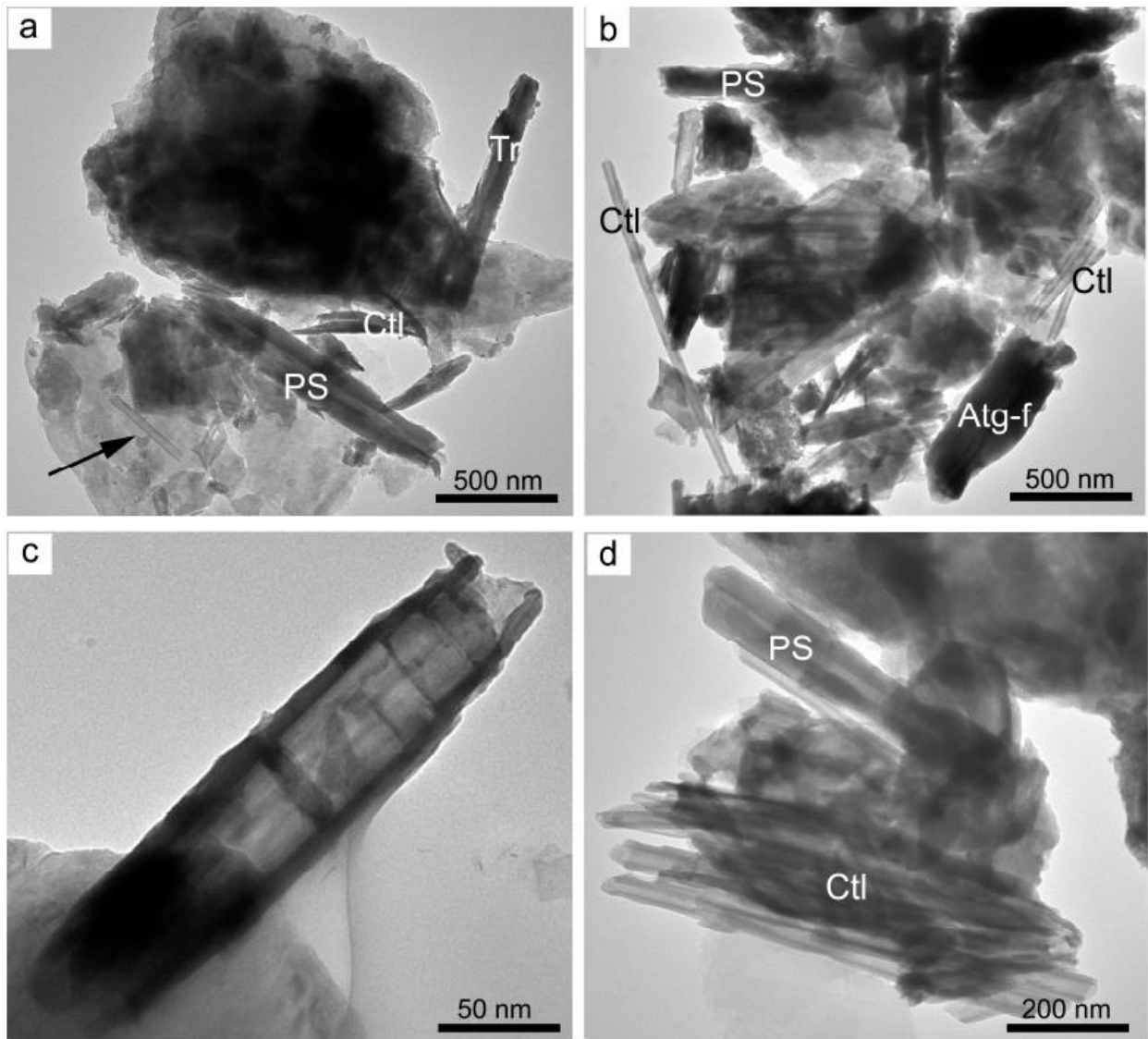
Figure 35: TEM images of fibrous phases detected in the analyzed soil samples: a) bundles of chrysotile fibres (Ctl); polygonal serpentine and fibrous tremolite; the black narrow indicates a chrysotile fiber characterized by the empty central cavity and thin outer walls; (sample Spol1); b) chrysotile fibres, polygonal serpentine and fibrous antigorite (sample Spol3); c) chrysotile fibre partially unrolled from the inside like cylinder-in cylinder morphology (sample Spol10); d) polygonal serpentine and bundles of chrysotile fibres (sample Spol11). Punturo et al., 2019.

Ctl = chrysotile; Tr = tremolite; Atg-f = fibrous antigorite; PS = polygonal serpentine; (mineral symbols after Whitney and Evans 2010).
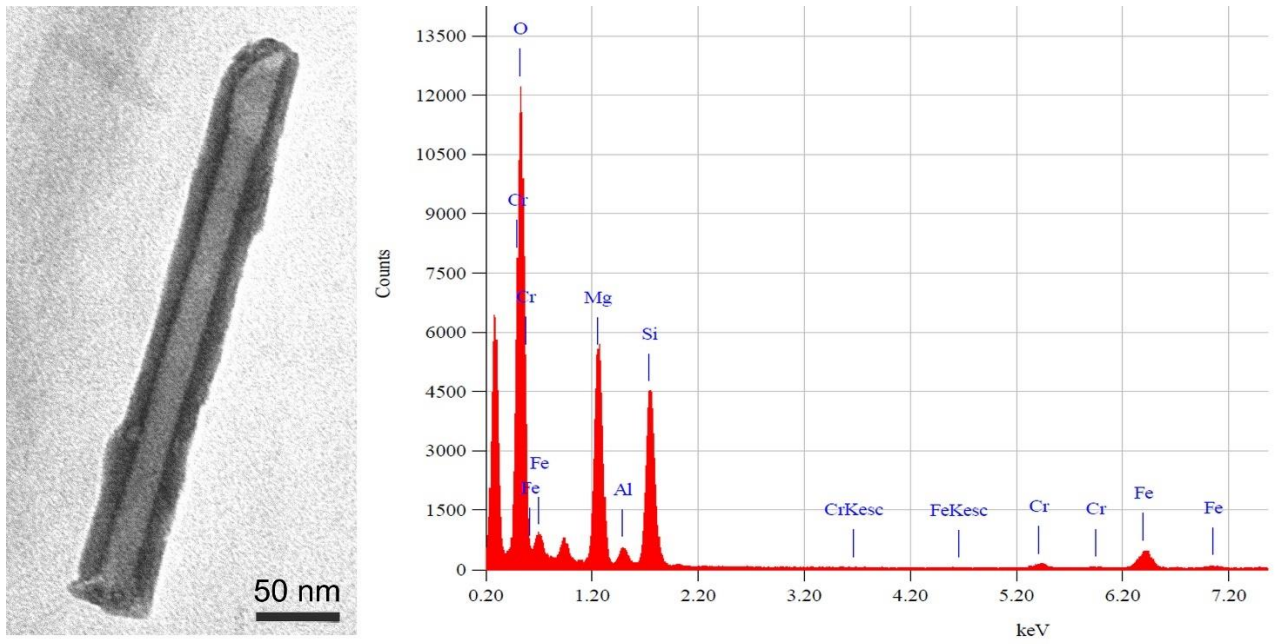
Figure 36: Single cylinder chrysotile with the relative point analysis (sample Spol1). Punturo et al., 2019.
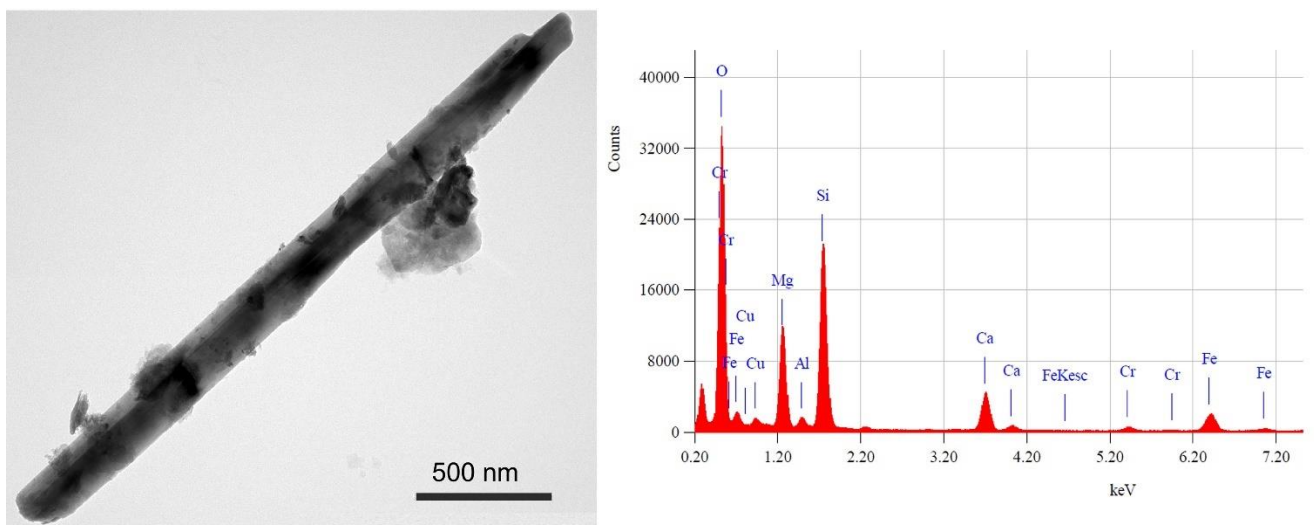
Figure 37: Single tremolite fibre with the relative point analysis (sample Spol1). Punturo et al., 2019.

7.2.3.5   Thermal analyses

In addition to the other analytical techniques, the mineralogical constituents of eight selected soil samples have been determined by means of thermal analysis which also allowed the discrimination of serpentine varieties (i.e., chrysotile, lizardite, antigorite, polygonal serpentine; Kusiorowski et al., 2012). Therefore, the samples have been subjected to progressive heating (up to 1000 °C) to provoke thermic reactions useful for the identification of the present phases.

Figure 38a, displays the differential scanning calorimetry patterns (DSC) of the eight analyzed soil samples in the temperature range of 0 - 1000 °C, showing the endo- and exothermic peaks related to the breakdown of existent phases and the crystallization of new phases, respectively. The mineral phases recognized with relative temperature peaks are listed in Table 8.

Similar behavior is displayed by almost all curves in the graph showing the main peaks at: *i)* T < 110 (endothermic) °C; *ii)* T range of 600-650 °C (endothermic); *iii)* T range of 800-850 °C (exothermic). Generally, an endothermic peak at low temperature (< 110 °C) is a marker of the adsorbed water loss while those at higher temperature indicate chemical combined water loss and therefore the breakdown of the mineral structures. As a matter of fact, the strong endothermic peaks registered between 600 and 650 °C suggest the presence of chrysotile, since the collapse of its structure happen at the average T of 630 °C (Figure 38b). The DSC pattern interpretation also revealed the presence of sharp exothermic peaks at the average T of 830 °C thus indicating the crystallization of forsterite (Figure 38a; Table 8). In fact, by heating the samples to perform the thermal analysis, due to the pseudomorphosis phenomena, chrysotile structure is completely altered at a molecular scale thus leading to the complete transformation of the asbestos mineral into non-hazardous silicate such as forsterite.
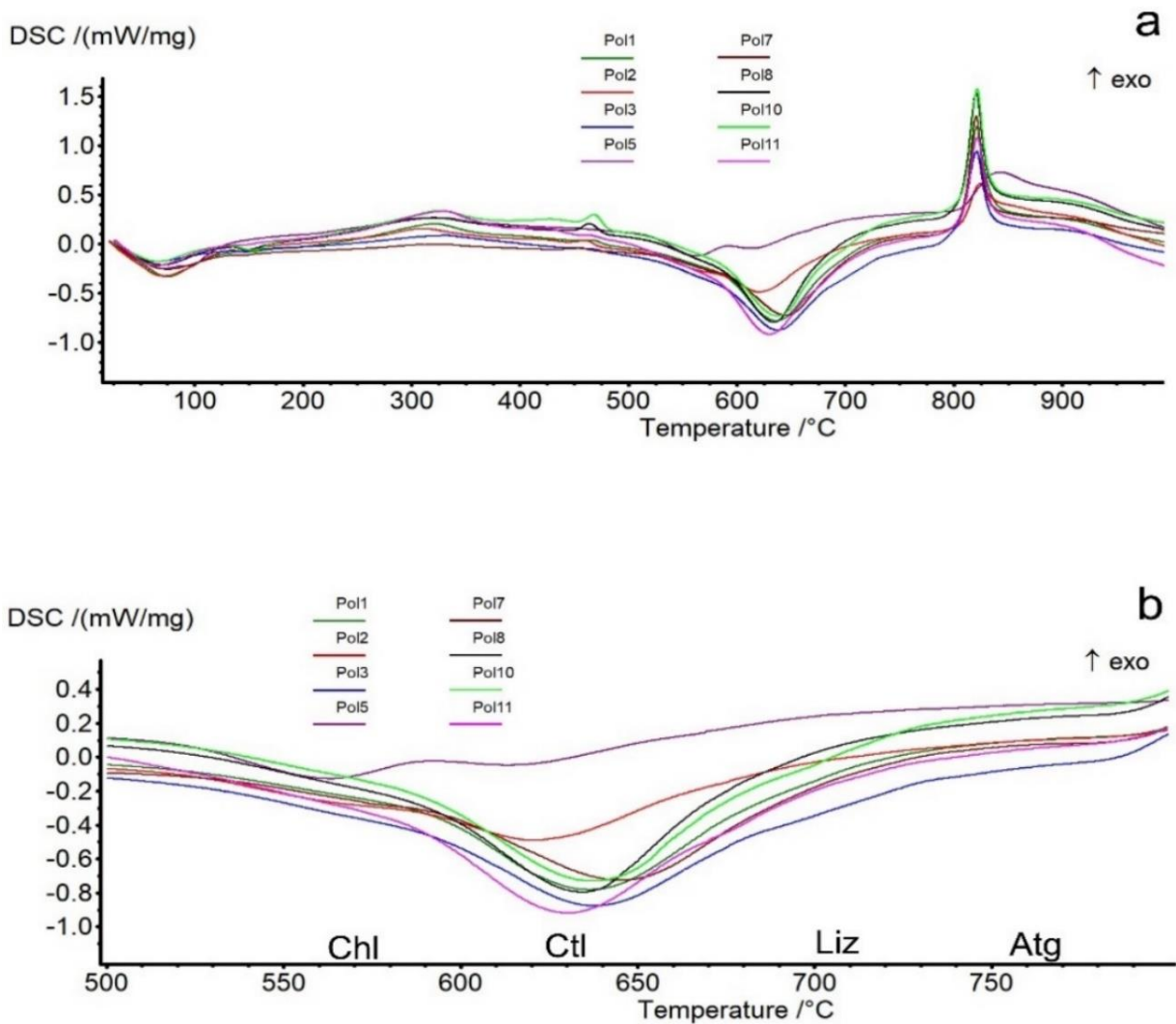
Figure 38: a) differential scanning calorimetry (DSC) curves of soil samples located in the surroundings of Sal Severino village (Basilicata region); b) zoom of DSC curves in the temperature range of 500-800 °C. Punturo et al., 2019.

Similarly, the curves obtained by the Derivative Thermogravimetry (DTG) analysis appear to be comparable in most of the samples showing loss of mass in the temperature range of 500-830 °C (Figure 39). Specifically, samples Spol2 and Spol5 show mass change related to the presence of small amount of chlorite (weak DTG peaks at 563 and 564 °C respectively) while all the analyzed samples showed mass changes in the temperature range of 614-639 °C testifying the presence of chrysotile in high amount (Table 8). Other phases such as polygonal serpentine, lizardite and antigorite have been identified. Most of the samples showed a weak DTG endothermic peak related to the presence of polygonal serpentine in a T range of 677-688 °C, while only the samples Spol3 and Spol5 are characterized by the presence of lizardite, testified by the DTG endothermic shoulder

at 736 and 744 °C respectively. Finally, all samples except for Spol7 and Spol11 contain antigorite which presence is confirmed by the DTG endothermic peak in a T range of 770-790 °C (Table 8). The temperatures of each thermal effect registered with DSC and DTG analyzes are listed in table 8 while the mineralogical assemblage obtained by means of the various analytical techniques adopted in the present study is reported in table 9.
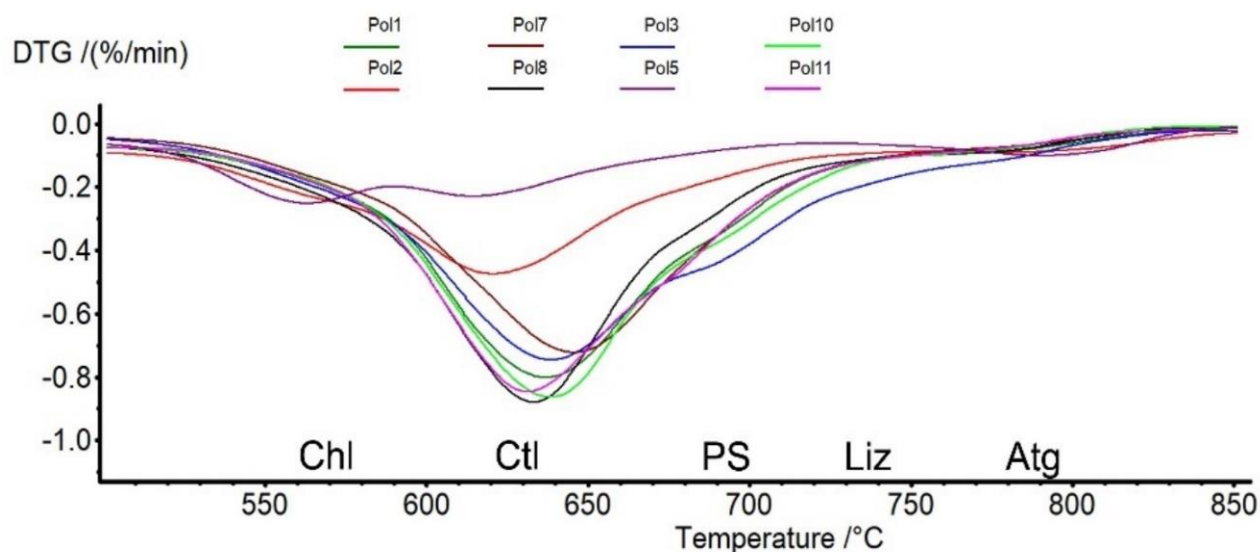
Figure 39: derivative Thermogravimetry (DTG) curves of the analyzed soil samples in the temperature range of 500-850 °C. Endothermic DTG peaks related to chlorite (Chl), polygonal serpentine (PS), lizardite (Liz) and antigorite (Atg) decomposition. Punturo et al., 2019.

Samples	Spol1	Spol2	Spol3	Spol5	Spol7	Spol8	Spol10	Spol11
				DSC				
Chl				563 en(w)				
Ctl	636 en(s)	621 en(s)	638 en(s)	612 en(w)	645 en(w)	634 en(s)	637 en(s)	630 en(s)
Fo	822 ex(ss)	824 ex(ss)	821 ex(ss)	844 ex(s)	821 ex(ss)	821 ex(ss)	822 ex(ss)	822 ex(ss)
				DTG				
Chl		564 en(vw)		563 en(w)				
Ctl	637 en(ss)	619 en(s)	638 en(s)	614 en(w)	647 en(ss)	634 en(s)	639 en(ss)	631 en(ss)
PS	679 en(vw)		686 en(vw)			677 en(vw)	688 en(vw)	679 en(vw)
Liz			736 en(sh)	744 en(sh)				
Ant	774 en(sh)	784 en(vw)	784 en(sh)	790 en(w)		778 en(sh)	770 en(sh)	

Table 8: DSC and DTG peaks of the studied soil samples. w = weak; vw = very weak; s=strong, ss = very strong; sh = shoulder, en = endothermic, ex = exothermic. Punturo et al., 2019.

Sample	Lithotype	Phases detected	Sample	Lithotype	Phases detected
Rpol_1	Serpentinite	Srp, Di, Mag, Chl	Spol_1	Soil	Ctl, PS, Ant, Tr, Di, Qtz, Mnt-Chl
Rpol_2	Serpentinite	Srp	Spol_2	Soil	Ctl, f-Atg, Di, Qtz, Mnt-Chl, Tr
Rpol_3	Serpentinite	Srp, Di, Tr, Chl, Mag, Mnt	Spol_3	Soil	Ctl, PS, Liz, f-Atg, Di, Qtz, Mnt-Chl, Tr
Rpol_4	Serpentinite	Srp, Di, Tr, Chl, Mnt	Spol_4	Soil	Srp, Di, Qtz, Mnt-Chl, Tr, Chm, Chl
Rpol_5	Serpentinite	Srp, Di, Tr, Mag, Mnt	Spol_5	Soil	Ctl, Liz, Ant, Di, Qtz, Mnt-Chl, Tr, Chm, Ms
Rpol_6	Serpentinite	Srp, Di, Mag	Spol_6	Soil	Srp, Di, Qtz, Mnt-Chl, Tr, Chm, Ms, Tlc
Rpol_7	Serpentinite	Srp, Di, Chl, Mag	Spol_7	Soil	Ctl, Tr, Di, Qtz, Mnt-Chl, Chm
Rpol_8	Serpentinite	Srp, Di, Chl, Mag	Spol_8	Soil	Ctl, PS, Atg, Di, Qtz, Mnt-Chl, Tr, Chm
Rpol_9	Serpentinite	Srp, Di, Tr, Mag	Spol_9	Soil	Srp, Di, Qtz, Mnt-Chl, Tr, Chm
Rpol_10-11	Serpentinite	Srp, Di, Chl, Mag	Spol_10	Soil	Ctl, PS, Atg, Di, Qtz, Mnt-Chl, Tr, Chm
			Spol_11	Soil	Ctl, PS, Di, Qtz, Mnt, Tr, Chm
Rpol_12	Serpentinite	Srp, Di, Mag	Spol_12	Soil	Srp, Di, Qtz

Table 9: mineralogical assemblage in rock and soil samples detected by X-ray powder diffraction (XRPD), scanning electron microscopy combined with energy dispersive spectrometry (SEM/EDS), transmission electron microscopy combined with energy dispersive spectrometry (TEM/EDS), differential scanning calorimetry (DSC) and Derivative Thermogravimetry (DTG).

Table 10 shows the data obtained by the thermogravimetric analysis (TG) which allowed to determine the mass loss in the analyzed samples in a certain temperature range. Specifically, the data showed the values of 1-4 % mass loss at a T < 110 °C due to the adsorbed water loss, and a total weight loss up to 1000 °C of ranging from 12 to 18 %, mainly caused by the loss of chemical bonded water of serpentine minerals constituting the analyzed soils.

The samples showing the highest values of mass loss at 1000 °C are Spol1 (17.44 %), Spol10 (15.40 %) and Spol11 (15.42 %); this could be caused either by the presence of other hydrated minerals in addition to serpentine minerals (see table 9) or by the presence of water (physically bound) trapped between the fibrous bundles of chrysotile (Loomis et al., 2010).

Spol1		Spol2	
T range (°C)	TG loss %	T range (°C)	TG loss %
< 110 °C	3.57	< 110 °C	3.30
TOT loss at 1000 °C	17.44	TOT loss at 1000 °C	14.80
Spol3		**Spol5**	
T range (°C)	TG loss %	T range (°C)	TG loss %
< 110 °C	1.47	< 110 °C	3.94
TOT loss at 1000 °C	13.13	TOT loss at 1000 °C	12.08
Spol7		**Spol8**	
T range (°C)	TG loss %	T range (°C)	TG loss %
< 110 °C	2.16	< 110 °C	2.39
TOT loss at 1000 °C	12.24	TOT loss at 1000 °C	14.90
Spol10		**Spol11**	
T range (°C)	TG loss %	T range (°C)	TG loss %
< 110 °C	1.96	< 110 °C	2.78
TOT loss at 1000 °C	15.40	TOT loss at 1000 °C	15.42

Table 10: TG data of the analyzed soil samples. The weight loss % at T < 110 °C and Total loss at 1000 °C is reported. Punturo et al., 2019.

7.2.3.6   *XRF characterization*

The geochemical composition of bulk serpentinite rock and derived soil samples carried out by means of X-ray fluorescence analysis, provided the concentration levels (oxide values) of major, minor and trace elements (Tables 11 and 12).

Results revealed similar average values in both rocks and soils, with $SiO_{2average} \approx 40$ wt%, $MgO_{average}$ wt% of 41.6 (rock) and 39.7 (soil), $FeO_{average}$ wt % of about 8.3 (rock) and 5.5 (soil), and $CaO_{average}$ of 2.7 wt% in rocks versus lower amount in soil (1.98 wt%). Differently, the highest concentration of $Al_2O_{3average}$ was detected in soils with values of 4.48 vs 1.07 wt %, as well as that of K_2O (up to 0.4 wt % in soils) that was detected with amounts below the detection limits in rock samples.

Special attention has been paid on some selected minor (Cr, Ni) and trace (Co, V) elements since they are potentially harmful to human health (Nemery, 1990; Censi et al., 2006, 2011a, b). The concentration levels of Co, Cr, Ni, and V detected in rock and soil samples are comparable except for Ni that is more abundant in rocks (Table 12). As a matter of fact, the average value of Ni is

2041 ppm in rock samples versus 1691.5 ppm in soils while Co, Cr and V are slightly more abundant in soils, in which they reached average values of about 115 ppm, 2359.2 and 95.6 respectively, compared to rocks that showed average amount of 95.4 ppm (Co), 2338 ppm (Cr) and 86,8 ppm (V).

Wt%	SiO_2	Al_2O_3	MgO	CaO	K_2O	Fe_2O_3	L.O. I
Rock							
RPOL1	39.80	0.90	41.20	2.20	0.00	8.70	7.40
RPOL2	39.10	0.70	40.30	0.60	0.00	9.10	10.10
RPOL3	40.70	1.70	42.20	3.50	0.00	7.90	4.00
RPOL4	40.70	1.00	43.20	3.00	0.00	8.90	3.20
RPOL5	41.90	1.30	40.90	4.60	0.00	10.10	1.30
RPOL6	39.60	0.90	41.70	1.70	0.00	8.10	8.00
RPOL7	40.10	1.00	41.20	2.10	0.00	8.60	7.10
RPOL8	43.20	1.70	43.20	5.20	0.00	4.30	2.40
RPOL9	38.60	0.80	40.20	2.30	0.00	8.80	9.20
RPOL10_11	40.00	0.90	42.20	2.40	0.00	8.40	6.10
RPOL12	39.90	0.90	41.50	2.20	0.00	8.10	7.40
Soil							
SPOL_1	38.50	3.80	40.00	2.00	0.10	6.10	9.60
SPOL_2	41.00	5.90	36.70	3.20	0.40	6.00	6.70
SPOL_3	40.20	4.20	41.20	1.90	0.10	5.50	6.90
SPOL_4	39.30	5.50	39.40	1.20	0.30	7.20	7.20
SPOL_5	41.00	5.00	39.20	2.90	0.10	5.30	6.50
SPOL_6	40.90	4.20	39.60	2.30	0.20	5.30	7.50
SPOL_7	45.40	4.40	38.70	0.60	0.30	5.20	5.30
SPOL_8	39.10	4.70	41.10	1.80	0.10	5.00	8.30
SPOL_9	39.80	3.80	42.20	2.10	0.00	5.50	6.60
SPOL_10	40.00	4.90	39.10	2.00	0.30	4.60	9.10
SPOL_11	40.80	5.20	38.60	1.90	0.30	5.10	8.10
SPOL_12	39.90	3.40	41.00	1.80	0.10	5.90	8.00

Table 11: Major oxide values (wt%) in bulk serpentinite rock and derived soil samples and Loss On Ignition (L.O.I.) values. Punturo et al., 2018.

ppm	Co	Cr	Ni	V
Rock				
RPOL1	88	2658	2281	91
RPOL2	107	1725	2489	66
RPOL3	87	2175	1726	88
RPOL4	97	2622	2379	67
RPOL5	112	2865	2073	82
RPOL6	97	3077	2074	65
RPOL7	105	2553	2100	68
RPOL8	62	1065	1177	217
RPOL9	99	2247	2004	62
RPOL10_11	99	2527	2140	76
RPOL12	97	2207	2018	73
Soil				
SPOL_1	122	2680	2131	91
SPOL_2	137	2942	1735	117
SPOL_3	79	1888	1576	75
SPOL_4	123	3425	1670	137
SPOL_5	139	2652	1203	144
SPOL_6	148	3828	1942	139
SPOL_7	103	1644	1505	78
SPOL_8	125	1997	1854	86
SPOL_9	71	1956	1547	78
SPOL_10	116	1711	1718	65
SPOL_11	103	2052	1574	81
SPOL_12	111	1536	1843	56

Table 12: Selected heavy metals values (ppm) in bulk serpentinite rock and derived soil samples. Punturo et al., 2018.

7.3 Discussion

The mineralogical and geochemical characterization of serpentinite rocks and derivative agricultural soils occurring in Southern Apennines (i.e., Calabria and Basilicata regions), was the main goal of the first section of the present study since they may contain asbestos minerals potentially hazardous to human health. As a matter of fact, serpentinites are among the main lithotypes associated with the presence of NOA (Natural Occurrence of Asbestos) as they develop from low-temperature hydration of ultramafic rocks (i.e., dunite, peridotite or pyroxenite) and they are composed essentially of serpentine minerals (Caillaud et al., 2006).

The data obtained revealed that serpentine minerals are the main constituents of both analyzed rock and soil samples, followed by tremolite and actinolite in minor amount.

The serpentinization process provokes the transformation of olivine and pyroxenes into serpentine minerals (chrysotile, lizardite and antigorite) as well as the development of veining systems able of providing information related to the rock deformation history, process of mass transfer, and to the mineral crystallization sites (Andreani et al., 2004).

Rocks samples from Gimigliano-Mount Reventino Unit (Calabria region) appear ideal to the vein investigation and to their infill since the presence of various vein systems with different size and shape crosscutting the rock was already well visible at the mesoscopic scale.

It is worth mentioning, that the veins formation process requires three sequential stages: *i)* the crack opening, whose opening-rate is linked to the stress/strain overall regime; *ii)* the transport of elements (by advection and/or diffusion) to the vein forming; *iii)* the crystallization of the vein minerals.

The mechanism usually proposed to explain the vein formation process is known as "Crack-seal mechanism" and consists of an incremental opening followed by full sealing of small consecutive cracks (Ramsay, 1980; Andréani et al., 2004).

Both polarized light microscope (PLM) and scanning electron microscope (SEM-EDS) observations highlighted the presence of veins filled by fibrous minerals whose orientation was mainly perpendicular (cross fibres) to the vein elongation directions. More specifically, chrysotile fibres were mainly found inside the veins while lizardite (non-fibrous serpentine) occur in the massive portion of the analyzed rocks. This is mainly because the veins provide favorable conditions for the fibre's growth, since chrysotile formation is favored by the presence of porosity and that of a supersaturate fluid (Evans, 2004). As a matter of fact, the transfer of matter either from the nearby wall rocks (by diffusion or dissolution process), or through the fluid's circulation

is needed for the crystallization of chrysotile into the veins (Deschamps et al., 2013) and in both cases, the vein formation reflects different stages of serpentinization (Andréani et al., 2007).

The electron probe micro-analysis allowed to determine the element's distribution into the studied samples and therefore to observe the chemical variations between the veins and the matrix. Serpentine minerals are essentially magnesian but, depending on the chemical composition of their growing environment (O'Hanley, 1996; Mével, 2003), they may contain considerable amounts of Fe, Al, Cr, Ni, and other trace elements.

From a chemical point of view, Si^{4+} and Mg^{2+} of chrysotile present in the T and O sheets respectively, may be substituted by Al^{3+} (Wicks and Plant, 1979), as well as Fe^{2+} may replace Mg (located in the O sheet Bloise et al., 2009; Hardy and Aust, 1995; Wicks and Plant, 1979) and Fe^{3+} may substitute Si even though this position may preferentially host Al^{3+}(Bloise et al., 2014, 2017; O'Hanley and Dyar, 1998). As for Mn, Ni and Cr, they almost exclusively replace Mg (isomorph substitution) (Bloise et al., 2010, 2016b).

The elemental maps obtained with the EPMA investigation, showed lower content of Fe in chrysotile filling the vein (T2 class) compared to the serpentinite matrix that instead retains part of their initial Fe in relict minerals, as olivine and pyroxene, and in magnetite that marks the vein borders. Differently, a higher Al content has been registered in chrysotile into the vein, thus suggesting the presence of Al-rich fluid (formed by the alteration of Al-rich phases such as spinel) at the time of chrysotile formation.

Thanks to these compositional differences it was possible to distinguish the vein from the matrix in the analyzed section and to follow the vein trend since the high Al content is maintained along their entire length. The chemical data observed, match with those obtained by Andréani et al. (2007) relating to the latest generation veins (V4) whose formation takes place at shallow conditions (T < 200 °C; Depth < 2 km) and testifying a serpentinization degrees >50% in an open system of hydrothermal circulation.

Basically, the model proposed by Andréani et al. (2007) recognizes two different stages during the veins formation*: i)* a first stage with Al-poor fluids, and *ii)* a second stage with Al-richer fluids.

In the first stage takes place the formation of iron oxide (mainly observed in mesh textures) that are associated to the hydration of olivine to form serpentine minerals. The abundance of iron oxide suggests the first hydration of the protolith in which primary minerals were dominant in the rock and therefore the primary opening of a crack system by brittle deformation (Andréani et al., 2007). At this stage, local mass transfer and diffusion processes within a closed system are dominant.

As the serpentinization process evolves, an environment with a different fluid influences the crystallization. As a matter of fact, the second stage (upper ∼2 km of the lithosphere) is

characterized by Al-rich fluid resulting from the alteration of Al-rich minerals (i.e., pyroxenes and spinels), and with higher fluid/rock ratios that documents an open system of hydrothermal circulation. Therefore, the hydration reactions with the transfer of excess elements take place and subsequently the full serpentinization process is allowed.

Additionally, the SR-μCT provided a better discrimination of the veins with special regards to their fibrous infill whose size was preserved thanks to the lack grinding during the sample preparation. As a matter of fact, 3D images showed the spatial distribution of the veins (often branched) into the sample as well as their shape in massive serpentinite matrix. Moreover, the 2D slices observations highlighted the presence of voids in which chrysotile fibres crystallized as long bundles of woven fibres and therefore well visible. Conversely, other parts of the rocks showed veins filled by compact chrysotile fibres thus making the fibrous habit hard to identify.

The measurements of fibres revealed that their size (i.e., width, length) match with those of regulated asbestos and therefore classified as asbestos under European law (Directive, 2003/18/CE, 2003).

Morphological observations have also been carried out by other analytical techniques such as TEM-EDS that allowed to examine the various characteristics of asbestos fibres (i.e., chrysotile, tremolite, actinolite) and other mineral phases present in the studied samples. Specifically, as showed in TEM images collected from serpentinite and derivative soils from Episcopia and San Severino villages (Basilicata region), cylindrical shape (consisting of an empty central cavity) represents the most common morphology of chrysotile. Sometimes, soil samples showed chrysotile fibres with a wide central tube and thin outer walls thus proving to have undergone unrolling process from the inside during the rock-soil transition likely because of the passage of water through the core. Differently, tremolite and actinolite asbestos that are the other main fibrous phases recognized in the samples, exhibit prismatic rod-shaped morphology lacking any flexibility.

It is worth mentioning, that in addition to regulated minerals, asbestiform phases (potentially harmful as well) have been identified by TEM investigation. As a matter of fact, fibrous antigorite and polygonal serpentine that is another structural variety of serpentine was found in most of the investigated soil samples.

Their presence has also been confirmed by thermal analyses which allowed the serpentine varieties discrimination. The DTG and DSC curves interpretation revealed similar behavior for most of the samples, showing endothermic peaks corresponding to polygonal serpentine, lizardite and antigorite in addition to chrysotile that always represents the most abundant phase (strong endothermic peak at about 630 °C). Moreover, TG data showed total wight losses of about 12-

18% up to 1000 °C which are mainly caused by the breakdown of serpentine minerals according to literature data (Ballirano et al., 2017). The highest percentage of total water loss (i.e., 18%) registered in some samples, may be explained by: *i)* the presence of hydrated phases in addition to serpentine minerals; and *ii)* the presence of water (physically bound) caught between the chrysotile fibrous bundles (Loomis et al., 2010).

Besides the mineralogical characterization of the analyzed samples, the comparison of the geochemical composition of rocks and derivative soil samples was of great interest in the present study. As a matter of fact, soils developed on serpentinite inherit the mineralogical and geochemical composition of the bedrock and therefore may contain asbestos fibres as well as potentially toxic elements (PTEs; Zupančič, 2017). These characteristics make serpentine soils potentially harmful especially if used for agricultural purposes since the terrain mobilization provoke the formation of dust containing fibres potentially inhalable. Moreover, heavy metals in soils can be transferred to other environmental matrixes depending on their mobility and bioavailability (e.g., circulating water, plant; Zupančič, 2012) thus posing serious environmental risks.

Chemical results of the analyzed samples revealed high concentration of chromium, vanadium cobalt and nickel in both bulk serpentinite and derived soils whose origin can be defined geogenic since no anthropogenic sources characterize the study area.

To compare the PTEs amounts of the studied rock and soil samples to the maximum admissible contents established by the Italian law (Italian Legislative Decree No. 152 of 03/04/2006), the concentration of V, Cr, Co, and Ni have been plotted in diagrams in which the concentration of SiO_2 is taken as the reference variable (Figure 40). Results showed that the amounts of Co and V in both soils and rocks exceed the regulatory thresholds for public, private, and residential green use (limit A corresponding to 20 and 90 ppm respectively), while Cr and Ni (limit A: 150 and 120 respectively) exceed the legal limit for industrial and commercial use (limit B: 800 and 500 respectively).

Therefore, it is possible to assess that the population living within serpentinite rich geological context as the inhabitants of San Severino village could be exposed to health risks due to soil pollution from heavy metals.
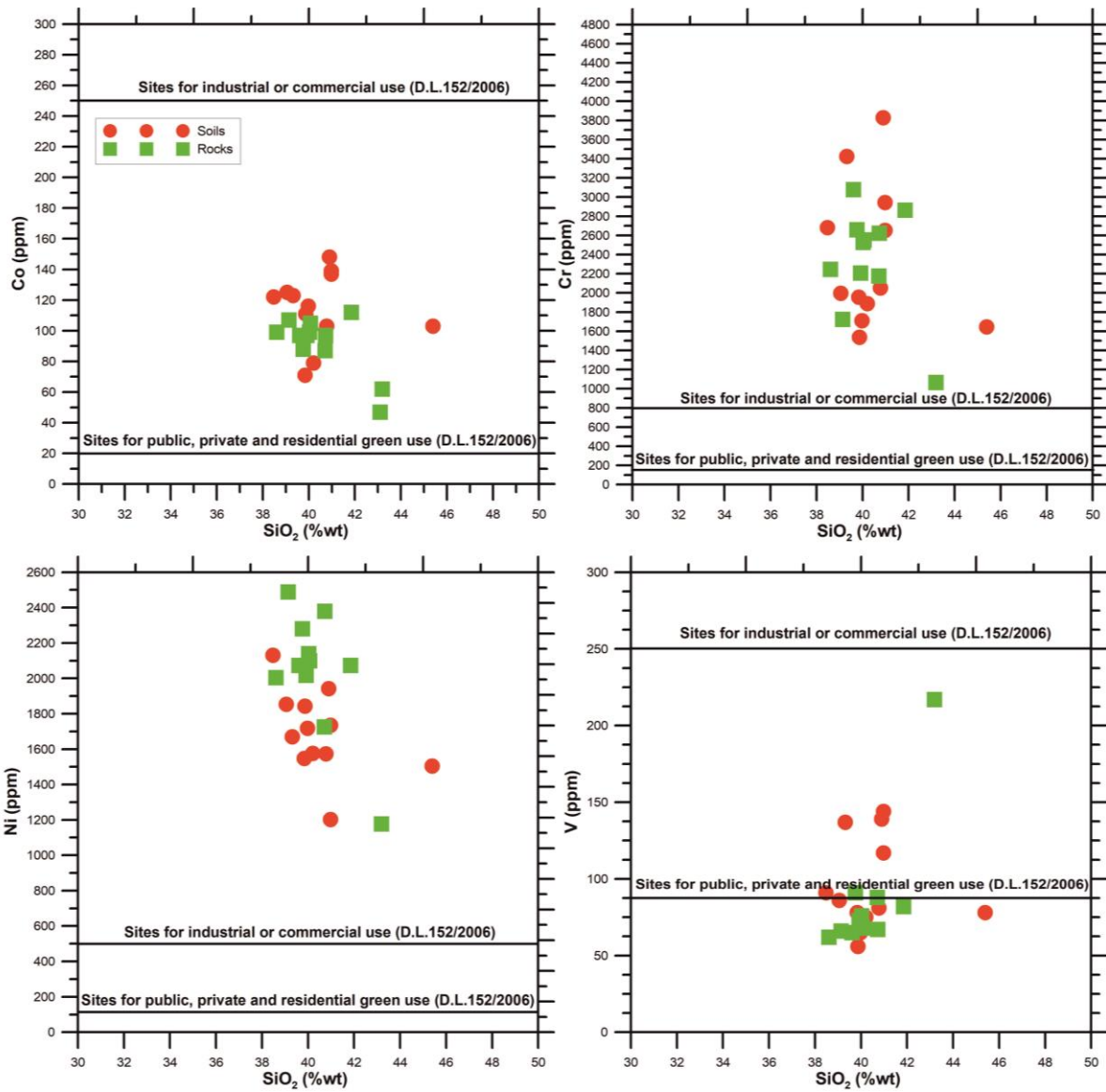
Figure 40: correlation diagrams of SiO2 versus Co, Cr, Ni and V for rocks and soils of the studied area. Thresholds contents regulated by Italian law (D.L. 152/2006) are also shown for each heavy metal.

8. Section 2 – Individual asbestos fibres: chemical characterization

8.1 Methods

Due to the important role played by potentially toxic elements (PTEs) in asbestos toxicity, micro-X-ray fluorescence (μ-XRF), inductively coupled plasma mass spectrometry (ICP-MS), and inductively coupled plasma spectrometry with Optical Emission Spectrometry (ICP-OES) have been used to obtain the chemical characterization of asbestos fibres samples (Table 13). Chrysotile, tremolite asbestos, and actinolite asbestos extracted from serpentinite rocks occurring in the Gimigliano Mount-Reventino Unit (GMRU; Calabria region) and two tremolite asbestos extracted from serpentinite rocks from the Pollino Massif in the surrounding of Episcopia (TR_EPS) and San Severino Lucano (Tr_SSL) villages (Basilicata region) have been characterized in term of major, minor (Si, Mg, Ca, Al, Fe, Mn) and trace elements (As, Ba, Be, Cd, Co, Cr, Cu, Li, Mo, Ni, Pb, Sb, Sn, Sr, Ti, Te, V, W, Zn, Zr).

	Samples				
Methods	**Fibres_GMRU**			**Fibres_Pol**	
	Ctl	Tr	Act	TR_EPS	TR_SSL
μ-XRF	X	X	X	X	X
ICP-MS	X	X	X		
ICP-OES				X	X

Table 13: list of the analytical techniques used for the analysis of asbestos fibre samples. Fibres_GMRU = asbestos fibres coming from Gimigliano Mount-Reventino Unit (Calabria region); Fibres_Pol = asbestos fibres coming from Pollino Massif area (Basilicata region).
Ctl = chrysotile; Tr = tremolite asbestos; Act = actinolite asbestos; TR_EPS = tremolite asbestos from Episcopia village (Basilicata region); TR_SSL = tremolite asbestos from San Severino village (Basilicata region).

8.1.1 *Micro X-ray fluorescence (μ-XRF)*

Micro-X-ray fluorescence (μ-XRF) analysis was useful for the quantification of major and minor elements (Si, Mg, Ca, Fe, Al, Mn) in terms of oxides by means of a Bruker M4 Tornado spectrometer equipped with two X-ray tubes (Rh and W) and two SDD detectors, active area of 60mm2. The Rh tube has a polycarpellary optic to concentrate the radiation in a spot < 20 μm (Mo - Kα). Vacuum conditions (2 mbar) have been set for the data acquisition using Rh radiation with the generator operating at 50 kV and 150 μA, using two detectors to enhance the intensity of the received signal. An acquisition time of 60s has been set for each measurement. A total of sixty spot analyses were performed on each sample of the present study. Spot chemical analyses allowed to observe the micrometric compositional variations. For the element's detection, a double measurement has been performed for each point, first without a primary filter for the quantification of major elements, then with a primary filter composed of three superimposed layers of Al (100 μm), Ti (50 μm) and Cu (25 μm). This method allowed to reduce the background up to 15 keV thus improving sensitivity to minor and trace elements, particularly for those ones whose spectral lines are between 4 and 14 keV. ESPRIT M4 v. 1.5.2.65 software was used for processing the acquired spectra to obtain a semi-quantitative analysis expressed as wt% of major elements (oxides) and ppm for minor elements.

8.1.2 *Inductively coupled plasma mass spectrometry (ICP-MS)*

ICP-MS analysis has been conducted with ICP-MS AGILENT 7800 for Fibres_GMRU (Ctl, Tr, Act) samples. An amount of 0.1 g of sample powder has been digested with HNO_3 + HF in high pressure (90 bar) vessels in Milestone Microwave. The accuracy (i.e., the relative difference from reference values) was generally better than 8%. To calibrate the equipment, the analytical service has used certified standard dilutions (Panreac) of the different elements (1000 mg/l each) grouped in a multi-elemental patron. Data collection was possible by using the common experimental procedure used in the Mass Spectroscopy Laboratory of the University of Calabria (Italy) (e.g., Bloise et al., 2016a).

8.1.3 *Inductively coupled plasma spectrometry with Optical Emission Spectrometry (ICP-OES)*

ICP-OES Agilent 710 Technology was employed for the determination of trace elements in Fibres_Pol (TR_EPS and TR_SSL) samples using a microwave Milestone MLS Mega 1200 with HPR 1000/10 vessels. An amount of 100 mg of sample powder were dissolved in a mixture of Merck "suprapur" quality acids, nitric acid (0.5 mL) and hydrofluoric acid (1.5 mL). A small amount of boric acid is added to the composition after the complete dissolution, to neutralize the samples before the ICP-OES analysis. The calibration curve was prepared using the "multielement smart solutions" for As, B, Ba, Bi, Cd, Co, Cr, Cu, Li, Mo, Ni, Pb, Sb, Se, Sn, Sr, Ti, Tl, V, W, Zn, Zr. The instrumental limit of quantification considered (LOQ) for each element was determined with the white method, the values obtained correspond to those provided by the ISO-11885. All the measurements were performed in triplicate to ensure reproducibility.

8.2 Results

8.2.1 Fibres from GMRU

The concentrations of major and minor elements (Si, Mg, Ca, Fe, Al, Mn) detected in chrysotile, tremolite asbestos and actinolite asbestos samples from Gimigliano Mount-Reventino Unit (GMRU) obtained by µ-XRF analysis (Figure 41) are listed in table 14.
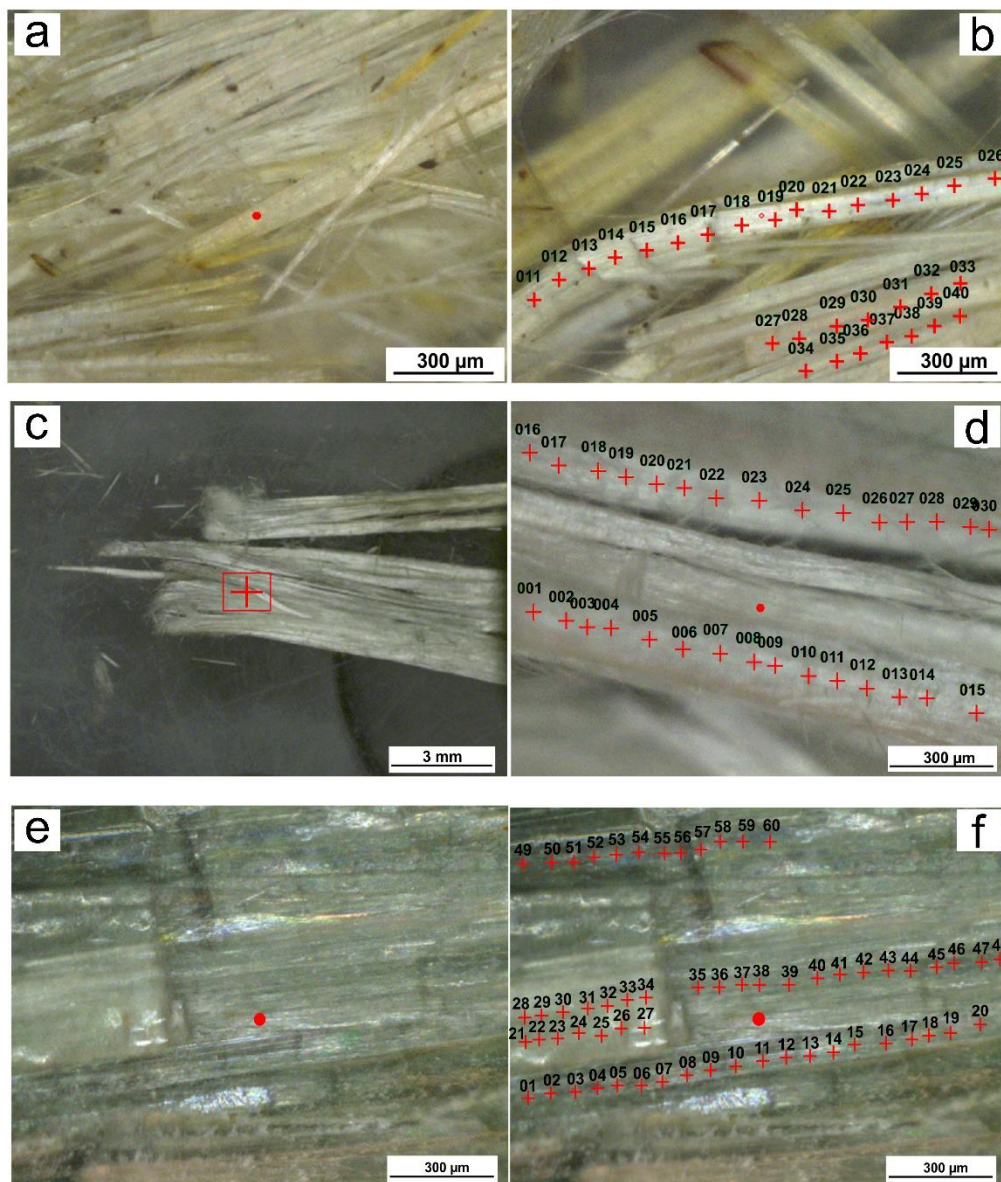
Figure 41: micro X-ray fluorescence (µ-XRF) images of a,b) chrysotile from San Mango D'Aquino (Ctl_GMRU sample; Calabria region); c,d) white tremolite asbestos from abandoned quarry in Mt. Reventino (Tr_GMRU; Calabria region); e,f) green actinolite asbestos fron abandoned quarry close to Conflenti town (Act_GMRU sample; Calabria region). Red crosses indicate the analysis points. Modified after Bloise et al., 2020b.

As for chrysotile, major and minor elements detected agree with literature data (Morgan and Cralley, 1973; Bloise et al., 2016a) showing SiO_2 and MgO amounts of 46.41 wt% and 48.78 % respectively and minor amounts of CaO (1.37 wt %) and FeO (3.22 wt %) (Figure 42).

Amphibole asbestos samples revealed average values of 55.8 wt% (SiO_2) and 27.12 wt% (MgO) in tremolite, while actinolite showed an amount of 54.06 wt% of SiO_2 and 22.96 wt% of MgO (Figure 42; Table 14). CaO content was higher in tremolite (15.0 wt%) compared to actinolite (11.3 wt%) that, as expected, showed higher FeO concentrations, with values of 9.07 wt% versus 1.80 wt% in tremolite and 3.22 wt% in chrysotile (Figure 43).

Regarding minor elements, results revealed Mn amounts > 1000 ppm in all the analyzed samples and Al > 1000 ppm in tremolite asbestos and actinolite asbestos. Specifically, Mn in chrysotile was 0.17 wt%, 0.20 wt% in tremolite, and 0.75 wt% in actinolite asbestos while smaller amounts of Al were detected in chrysotile (0.02 wt%) compared to tremolite (0.34 wt%) and actinolite (0.38 wt%) asbestos (Figure 43).

	Fibres_GMRU		
wt %	Ctl	Tr	Act
MgO	48.78 (0.72)	27.12 (3.90)	22.96 (0.56)
SiO_2	46.41 (0.82)	55.79 (5.81)	54.06 (0.70)
CaO	1.37 (0.96)	14.99 (1.86)	11.29 (0.64)
FeO	3.22 (0.82)	1.80 (0.20)	9.07 (0.76)
Al_2O_3	0.02 (0.01)	0.34 (0.16)	0.38 (0.12)
MnO	0.17 (0.05)	0.20 (0.05)	0.75 (0.11)

Table 14: Average values of major and minor elements amounts (wt%) in the studied samples from Gimigliano Mount-Reventino (GMRU) obtained by μ-XRF. Ctl = chrysotile, Tr = tremolite asbestos, Act = actinolite asbestos. Standard deviations in brackets. Bloise et al., 2020b.
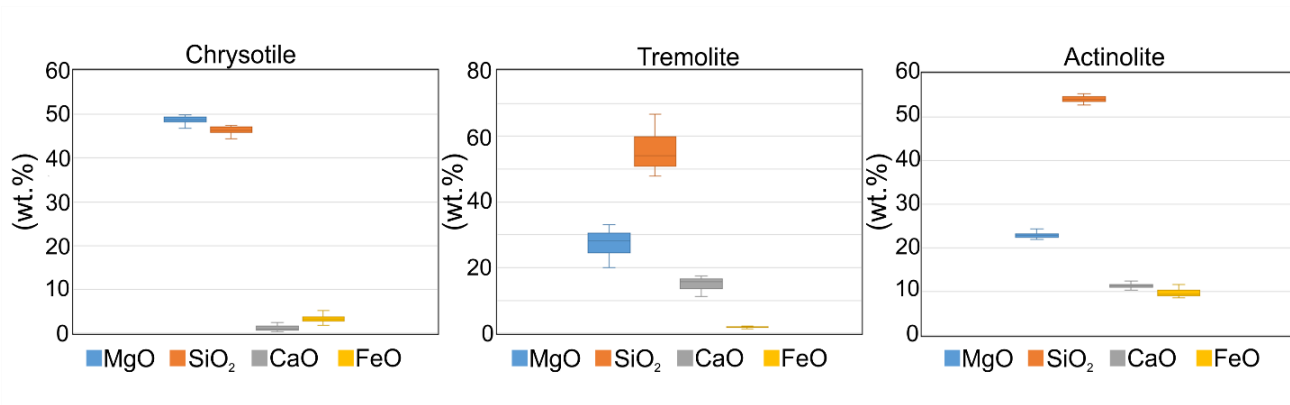
Figure 42: box plots showing MgO, SiO2, CaO, FeO contents in chrysotile, tremolite and actinolite asbestos from GMRU. Statistical parameters are based on 60 analyses. In the box plot numerical data are divided into quartiles, the range content is marked by vertical lines. Median value is represented by the horizontal line inside the box. Bloise et al., 2020b.
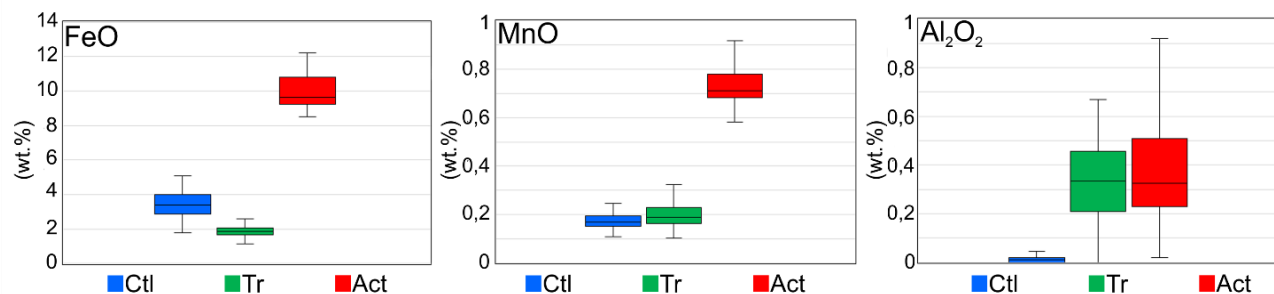
Figure 43: box plots showing FeO, MnO and Al_2O_3 in chrysotile, tremolite and actinolite asbestos from GMRU. Statistical parameters are based on 60 analyses. In the box plot numerical data are divided into quartiles, the range content is marked by vertical lines. Median value is represented by the horizontal line inside the box. Bloise et al., 2020b.

The concentrations of trace elements (Cr, Co, Ni, Cu, Zn, Be, V, As, Rb, Sb, Ba, Pb, Sr) obtained by means of ICP-MS (Table 15) revealed different content in the analyzed asbestos samples as visible in figure 44. The amounts of Fe and Mn have also been acquired with ICP-MS revealing to match with those obtained by using µ-XRF.

Special regard has been dedicated on some metals (i.e., Cr, Ni, Co, Cu, Zn) due to their high amount in the studied samples. In fact, high concentrations of Cr and Ni were detected in tremolite (171 ppm and 308.63 ppm respectively) followed by actinolite (15 ppm and 14.50 ppm respectively) and chrysotile (5.5 ppm and 4.32 respectively). Similarly, tremolite showed the highest amounts of Co (22.64 ppm) and Cu (24.53 ppm) followed by actinolite with 4.69 ppm (Co) and 19.39 ppm (Cu), and chrysotile (1.89 ppm and 10.52 ppm respectively). As for Zn, the highest

amount has been detected in chrysotile reaching values of 65.47 ppm followed by actinolite (46.56 ppm) and tremolite (28.42 ppm).

As for the other trace elements, figure 45 shows the concentration (ppm) patterns of Be, V, As, Rb, Sb, Ba, Pb and Sr detected in chrysotile, tremolite and actinolite asbestos. As, Pb, Sr and Be are the elements showing the most heterogenous values while V, Rb and Ba were quite similar in all three samples. As a matter of fact, As and Be were detected with the highest amount in chrysotile in which reached 7.0 ppm and 2.90 respectively, Pb and V in actinolite asbestos (23.29 ppm and 11.06 respectively) and Sr in tremolite asbestos with an amount of 200.0 ppm. Therefore, in summary, results highlighted that chrysotile is characterized by the highest amounts of As (7.0 ppm) and Be (2.9 ppm), tremolite asbestos showed the highest amount of Sr (200 ppm) and Ba (14.8 ppm) and actinolite asbestos contained highest concentrations of Pb (23.29 ppm) and V (11.06 ppm) (Figure 45).

(ppm)	Concentration range in human lungs*	Ctl	Tr	Act	D.L.
Fe**	40 - 500	25000	14000	75100	0.01
Mn**	0.01 - 3	1186.8	678.2	3874.2	0.01
Cr	0.002 - 0.50	5.50	170.91	14.86	0.20
Co	0.002 - 0.1	1.89	22.64	4.69	0.05
Ni	0.01 - 1.00	4.32	308.63	14.50	0.09
Cu	1 - 5.00	10.52	24.53	19.39	0.06
Zn	1 - 30.00	65.47	28.42	46.56	1.90
Pb	0.02 - 0.50	2.40	4.44	23.29	0.04
V	0.0005 - 0.50	6.88	7.07	11.06	0.10
Be	0.0001 - 0.03	2.90	0.30	1.10	0.01
As	0.001 - 0.10	7.00	1.20	1.50	0.40
Rb	0.5 - 10.00	0.70	0.40	0.70	0.30
Sb	0.002 - 0.10	0.20	0.20	0.60	0.01
Ba	>1.10	11.40	14.8	14.1	0.07
Sr	0.01 - 1.00	10.70	200.0	47.0	0.03

Table 15: concentration values (ppm) in the investigated asbestos samples from Gimigliano Mount-Reventino Unit (GMRU) obtained by ICP-MS. Ctl = chrysotile, Tr = tremolite, Act = actinolite. *Indicative baseline data for some trace elements in normal human lung tissues (Vanoeteren et al., 1986). D.L. = detection limit; n.d. = not detected; ** Minor elements. Bloise et al., 2020b.
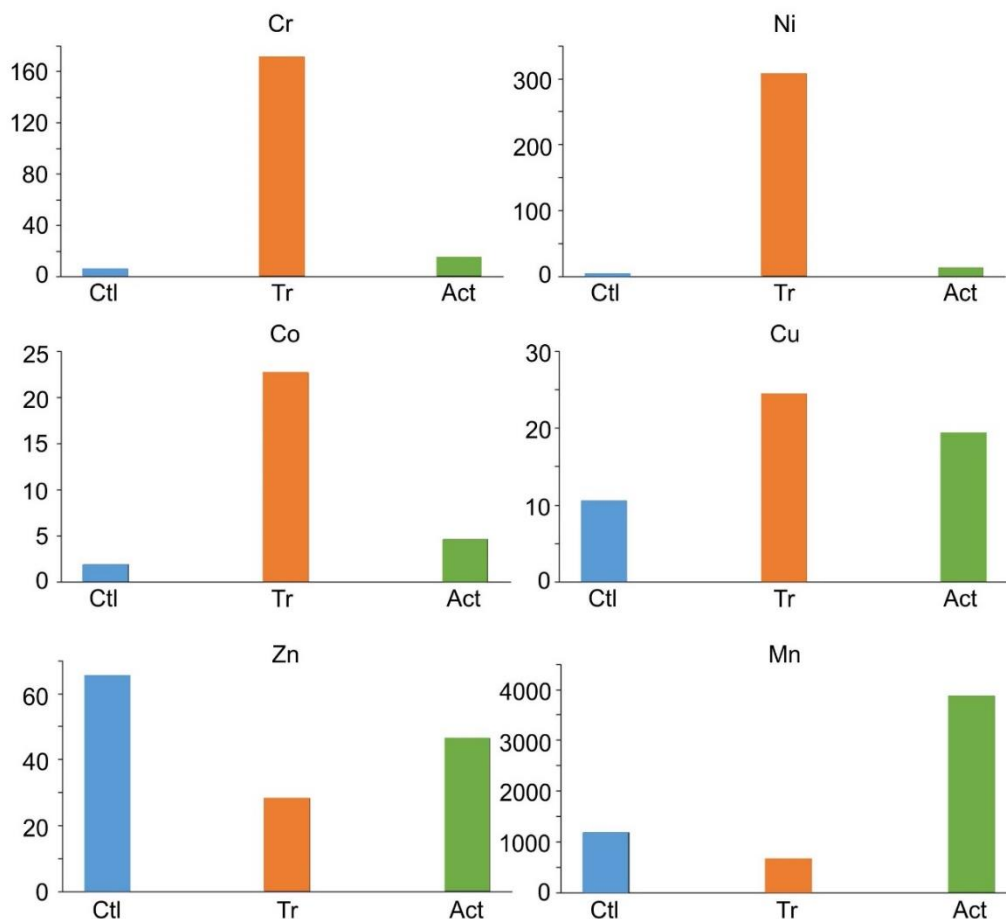
Figure 44: bar diagrams showing the concentration of heavy metals (ppm) in the studied asbestos samples from Gimigliano Mount-Reventino Unit. Ctl = chrysotile, Tr = tremolite; Act = actinolite. Each element has an error, measured as relative standard deviation (RSD%), of around 1%. Bloise et al., 2020b.
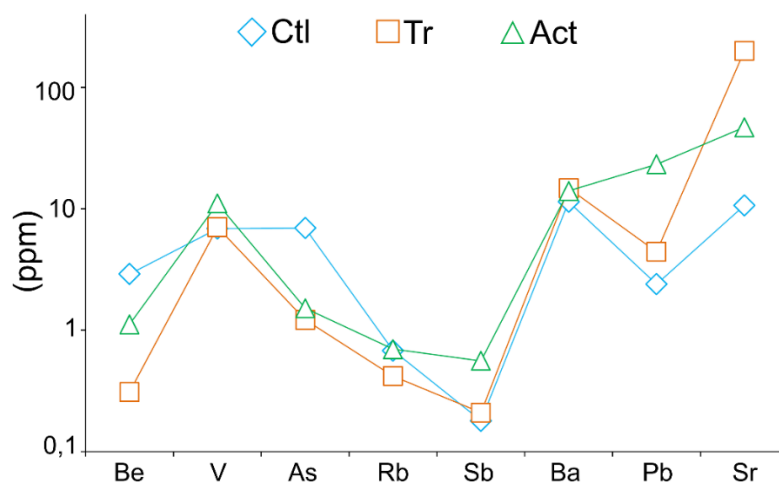
Figure 45: concentration patterns of trace elements (ppm) in the investigated asbestos samples from Gimigliano Mount-Reventino Unit. Ctl = chrysotile, Tr = tremolite, Act = actinolite. Logarithmic scale is used for the Y axis. Each element has an error, measured as relative standard deviation (RSD%), of around 1%. Bloise et al., 2020b.

8.2.2. Fibres from Pollino Massif

Tremolite asbestos samples from Episcopia (TR_EPS sample) and San Severino Lucano (TR_SSL) villages (Pollino Massif, Basilicata region), have been characterized by means of μ-XRF (Figure 46) to measure the concentrations of major, minor (Si, Mg, Ca, Fe, Al, Mn), and trace elements (As, Ba, Cd, Co, Cr, Cu, Li, Mo, Ni, Pb, Sb, Sn Sr, Ti, Te, V, W, Zn, Zr). Figure 46 shows the fibrous appearance of tremolite asbestos samples (a, c, d) and some analysis points of the fibres (b).

As for major and major elements, TR_EPS showed SiO_2 and MgO amounts of 53.3 wt% and 26.0 wt% respectively, and concentrations of 16.8 wt% for CaO and 3.3 wt% for FeO (Figure 47, Table 16).

TR_SSL sample revealed SiO_2 and MgO amounts of 54.1 wt% and 26.1 wt% respectively, while the concentration of CaO (14.1 wt%) was lower than those detected in TR_EPS. Conversely, the amounts of FeO were higher reaching values of 5.2 wt% (Figure 47, Table 16).
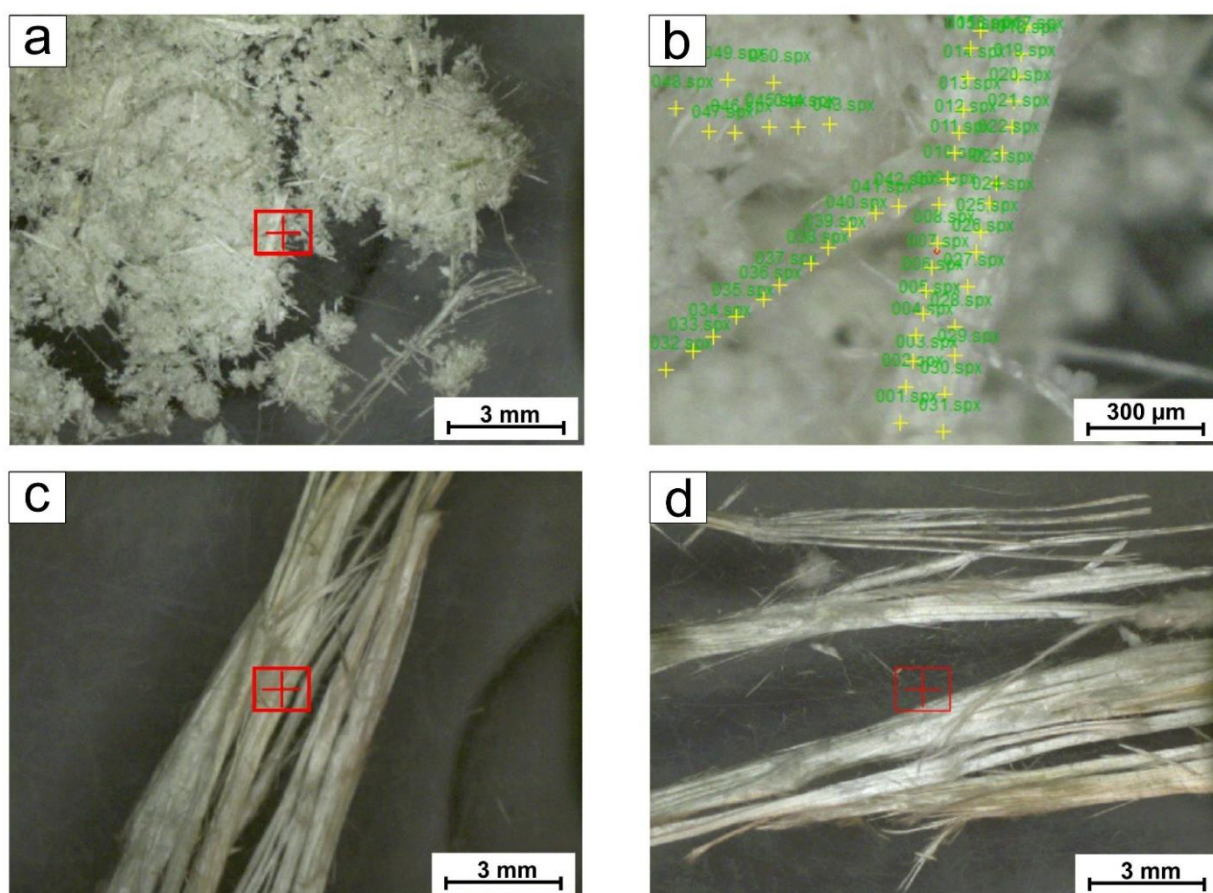
Figure 46: micro X-ray fluorescence (μ-XRF) images of the analyzed tremolite asbestos samples. (a,b) tremolite asbestos from Episcopia village (TR_EPS sample); (c,d) tremolite asbestos from San Severino Lucano village (TR_SSL sample). Crosses indicate the analysis points. Ricchiuti et al., 2021.
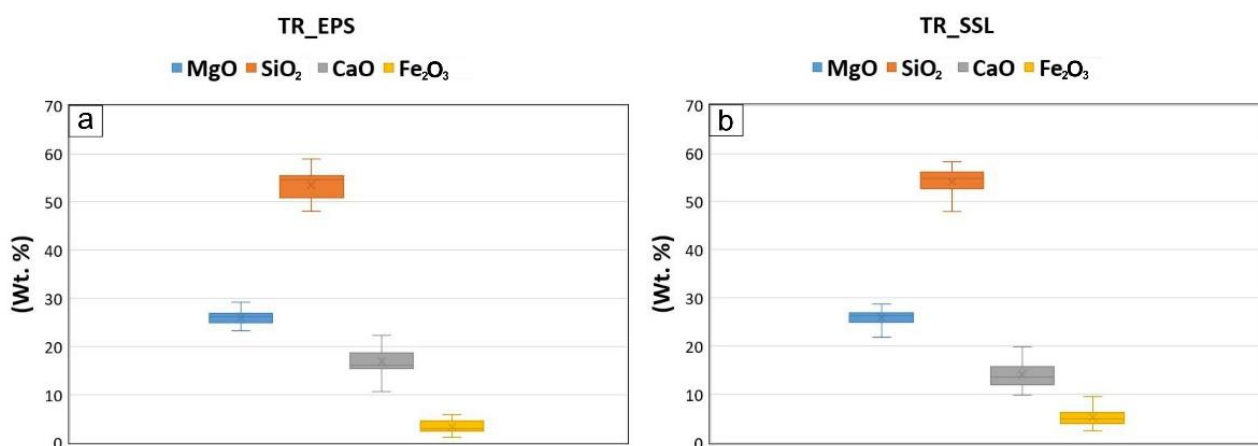
Figure 47: Box plots showing statistical parameter for major elements in: a) tremolite asbestos from Episcopia village (TR_EPS), and b) tremolite asbestos from San Severino Lucano village (TR_SSL). Statistical parameters are based on 60 spot analyses. In the box plot numerical data are divided into quartiles, the vertical lines indicate the range in contents. The horizontal line inside the box shows the median value. The cross indicates the mean value. Ricchiuti et al., 2021.

(wt%)	TR_EPS	TR_SSL
MgO	26.00	26.10
SiO$_2$	53.32	54.12
CaO	16.80	14.12
FeO	3.33	5.20
Al$_2$O$_3$	0.32	0.35
MnO	0.23	0.11

Table 16: average values of major and minor elements amounts (wt%) of tremolite asbestos samples obtained by using μ-XRF. TR_EPS = tremolite asbestos from Episcopia village; TR_SSL = tremolite asbestos from San Severino Lucano village (Pollino Massif, Basilicata region). Ricchiuti et al., 2021.

Regarding trace elements concentrations, As, Ba, Cd, Co, Cr, Cu, Li, Mo, Ni, Pb, Sb, Sn, Sr, Ti, Te, V, W, Zn, Zr, showed heterogenous values in the two investigated tremolite asbestos samples (Table 17). Due to the well-known negative impact of some heavy metals on human health (IARC, 1993, 2012a), special attention has been pain on Cr, Ni, Co, V, As, Ti, Cu and Zn amounts (Figure 48).

Results revealed that Cr and Ni represent the most abundant elements of both the studied samples with concentrations of 1120 ppm (Cr) and 1830 (Ni) in TR_EPS that are higher than those detected in TR_SSL in which Cr content is 550 ppm and that of Ni reaches 480 ppm. TR_EPS also showed

the highest values of Co (31.9 ppm), V (6.3 ppm), Ti (430 ppm) and Cu (23.2 ppm) while TR_SSL revealed higher values of As (7.9 ppm) and Zn (37.7 ppm).

The concentration levels of the other trace elements investigated (i.e., Ba, Cd, Li, Mo, Sb, Sn, Sr, Te, W and Zr) are showed in Figure 49. As revealed by ICP-OES data, the highest amounts of all these elements have been detected in TR_SSL sample except for Li and Sb which are more abundant in TR_EPS with values of 20.50 ppm and 15.10 ppm respectively. As a matter of fact, TR_EPS showed 1.10 ppm of Ba, 1.1 ppm of Cd, 20.50 ppm of Sn, 1.50 ppm of Sr, and 7.20 ppm of Zr (Table 17).

Nevertheless, the concentrations of Mo, Te and W are not much different (Table 17).

In summary, as showed in figure 50 in which the concentration levels of all trace elements detected in the investigated tremolite asbestos are reported, the most abundant elements are Cr and Ni that occur in higher amount in TR_EPS.

(ppm)	TR_EPS	TR_SSL
As	3.20	7.90
Ba	1.10	16.50
Cd	1.11	9.90
Co	31.90	7.80
Cr	1120	550
Cu	23.20	17.80
Li	20.50	5.30
Mo	2.50	6.70
Ni	1830	480
Pb	11.50	20.50
Sb	15.10	11.20
Sn	20.50	51.70
Sr	1.50	16.10
Ti	430	92.90
Te	6.40	8.80
V	6.30	2.60
W	6.30	8.80
Zn	34.30	37.70
Zr	7.20	32.20
Σ_{TOT}	**3573**	**1384**

Table 17: contents f trace elements (ppm) in the investigated tremolite asbestos from Episcopia (TR_EPS) and San Severino Lucano (TR_SSL) villages (Pollino Massif, Basilicata region) obtained by ICP-OES. Ricchiuti et al., 2021.

Figure 48: bar diagrams showing the concentrations of selected potentially toxic elements (PTEs; ppm) in tremolite asbestos from Episcopia (TR_EPS) and San Severino Lucano (TR_SSL) villages (Pollino Massif, Basilicata region). Ricchiuti et al., 2021.

Figure 49: concentration levels (ppm) of some trace elements detected in tremolite asbestos from Episcopia (TR_EPS) and San Severino Lucano (TR_SSL) villages (Pollino Massif, Basilicata region). Ricchiuti et al., 2021.

Figure 50: comparison of trace elements contents in tremolite asbestos from Episcopia (TR_EPS) and San Severino Lucano (TR_SSL) villages (Pollino Massif, Basilicata region). Ricchiuti et al., 2021.
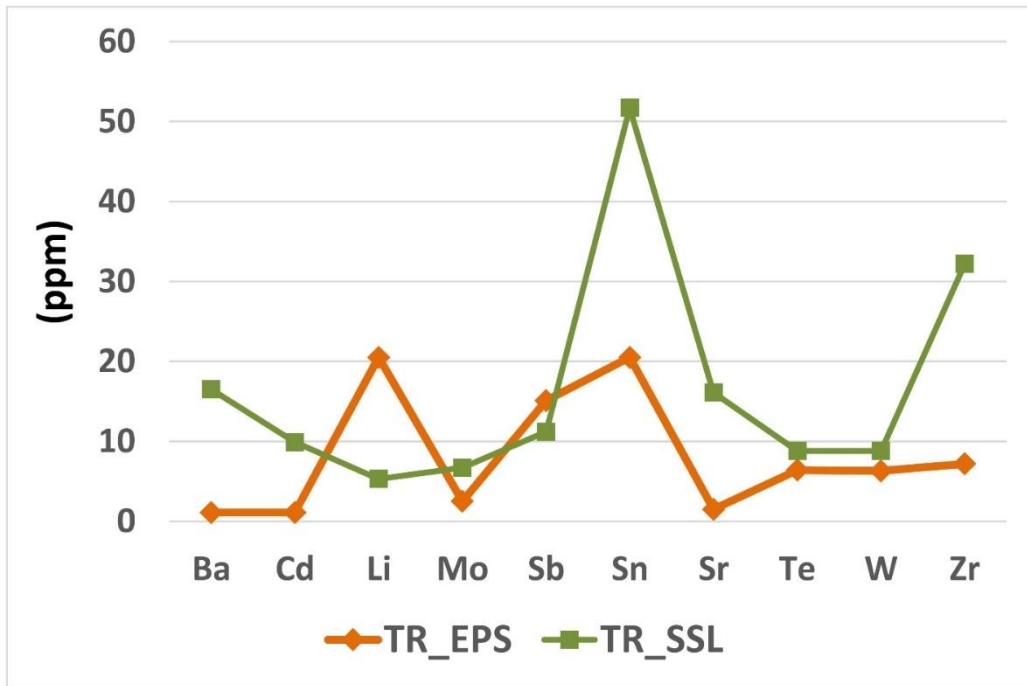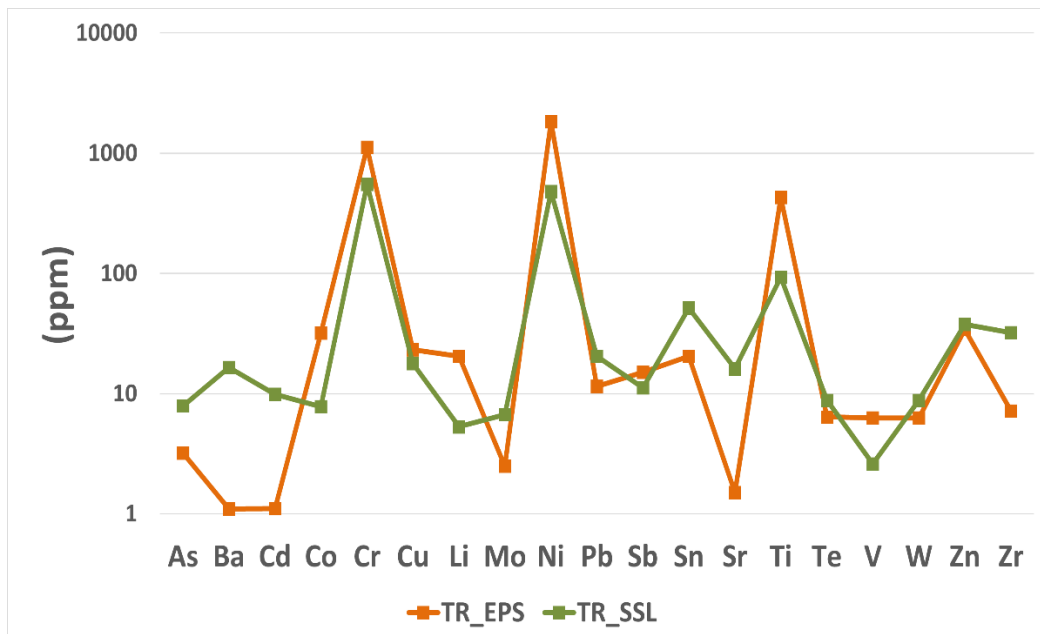
8.3 Discussion

The chemical characterization conducted on asbestos fibres extracted from serpentinites occurring in southern Apennines (Calabria and Basilicata regions) revealed significant data useful for the fibres toxicity definition. In fact, in addition to parameters such as morphology, biodurability and surface activity, the presence of high amount of potentially toxic elements (PTEs) in fibre structure play an important role to the toxic potential of the fibres.

The study areas are of great scientific interest due to the wide occurrence of ophiolitic rocks which are known to contain asbestos fibres and PTEs (e.g., Mn, Cr, Ni, Co) that can become bioavailable (Mistikawy et al., 2020) and mobilized. The Italian National Mesothelioma Register reports 70 mesothelioma deaths caused by both occupational and environmental exposure to asbestos registered in the Calabria region between 1993 and 2015 (INAIL, 2015). Similarly, epidemiological studies conducted on twelve villages of the Basilicata region, revealed relevant excess of negative health effect NOA-correlated cases. High number of mesothelioma cases were documented in the area 20 km far away from Episcopia village recognizing the exposure to asbestos minerals as the main cause.

After the mineralogical and geochemical characterization of asbestos-containing rocks and soils occurring in the Calabria and Basilicata regions described in session I, the quantification of potentially toxic elements (PTEs) specifically in asbestos fibre structure was the main goal of the session II. Since there are scientific evidence demonstrating the relationship between negative health effects (e.g., lung cancer) and the exposure to PTEs, the definition of trace elements amounts such as heavy metals is necessary to define the fibre toxicity and subsequently their potential impact to human health. In fact, once inhaled the fibres release the PTEs more or less quickly, depending due to the dissolution processes when in contact with body fluids. With this investigation, we have hypothesized which of the studied fibres could be the most harmful according to the PTEs content considering equal the other factors influencing the fibre toxicity (e.g., morphometry, biodurability, surface activity). Moreover, the comparative evaluation of PTEs contents in the samples allowed us to consider which elements play a role in asbestos toxicity.

As for asbestos fibre samples collected from Gimigliano Mount-Reventino Unit (Fibres_GMRU samples, Calabria region), chrysotile, tremolite asbestos and actinolite asbestos showed heterogenous values of PTEs. In fact, chrysotile revealed the highest content of Zn and the lowest amounts of Cr, Ni, Co, and Cu compared to those detected in amphiboles. By considering the sum of the most abundant trace elements $\sum$ (Cr, Co, Ni, Cu, Zn) for each analyzed sample comes out

that tremolite is the asbestos fibre with the highest content of trace metals reaching 555 ppm, followed by actinolite asbestos (100 ppm) and chrysotile (88 ppm). However, the concentrations of heavy metals such as Mn and Fe present as minor elements (>1000 ppm) in the studied samples, influence the balance content of toxic metals (Table 18). In fact, considering the sum $\sum$ (Cr, Co, Ni, Cu, Zn, Mn), actinolite asbestos (3974 ppm) > chrysotile (1274 ppm) > tremolite asbestos (1233 ppm) is the fibres order according to the highest content of these elements. The same order is maintained considering the sum $\sum$ (Cr, Co, Ni, Cu, Zn, Mn, Fe) with values of 79074 ppm (actinolite), 26275 ppm (chrysotile), 15233 ppm (tremolite). Literature studies showed the negative impact of excessive dose of Mn which may induce permanent neurological damage as well as the presence of Fe and its coordination together with surface ferrous ions trigger the formation of toxic hydroxyl radicals thus inducing cyto- and genotoxic effects (Bonneau et al., 1986; Fantauzzi et al., 2010; Pacella et al., 2020).

Other trace elements potentially hazardous to human health such as Be, V, As, Rb, Sb, Ba, Pb and Sr occur in various amount in the investigated fibres. For instance, Be may have effect on the interaction of the fibres with the biological system as well as As may intake and increase the development of cancer (Chen et al., 2003; IARC, 2012c). The highest amounts of these elements ($\sum$ Be, V, As, Rb, Sb, Ba, Pb, Sr) have been detected in tremolite asbestos (228 ppm) followed by actinolite (99 ppm) and chrysotile (42 ppm). These differences in content in the three asbestos fibres may be due to the geochemical variability involved during their genesis (e.g., pressure, temperature, elements availability and mobility) in distinct locations or for crystallographic reasons. The lower amounts of Sb, Ba, Pb and Sr detected in chrysotile may be explained by crystallographic reasons due to the big ionic radii (> 1 Å) of these elements that cannot replace Si or Mg in T or O sites but rather they are hosted in the hollow core of the fibrils (Ballirano et al., 2017). Conversely, since elements with smaller ionic radii (< 1 Å) can be hosted into crystallographic sites of both chrysotile and tremolite, in this case the variations are mainly due to their geochemical availability rather than crystallographic reasons.

At this point, it can be useful to consider the total amount of all PTEs detected in the samples (Figure 51; Table 18) that revealed the highest concentrations in actinolite asbestos (79173 ppm), followed by chrysotile (26317 ppm) and tremolite asbestos (15461 ppm).
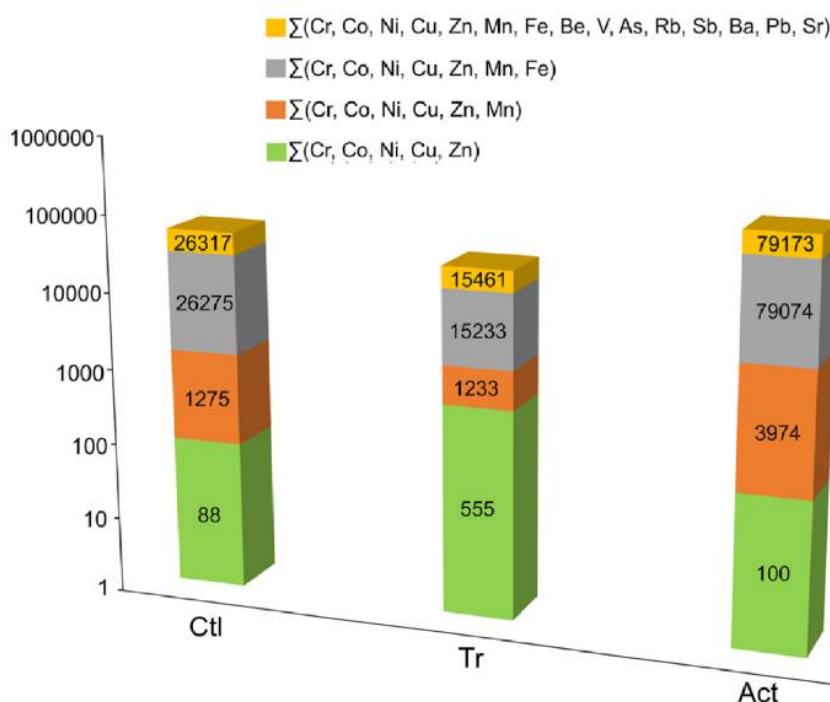
Figure 51: sum of PTEs amounts (ppm) detected in the investigated asbestos fibres samples. Logarithmic scale is used for Y axis. Ctl = chrysotile; Tr = tremolite asbestos; Act = actinolite asbestos. Bloise et al., 2020b.

(ppm)	Σ (Cr, Co, Ni, Cu, Zn)	Σ (Cr, Co, Ni, Cu, Zn, Mn)	Σ (Cr, Co, Ni, Cu, Zn, Mn, Fe)	Σ (Be, V, As, Rb, Sb, Ba, Pb, Sr)	Σ (Cr, Co, Ni, Cu, Zn, Mn, Fe, Be, V, As, Rb, Sb, Ba, Pb, Sr)
Ctl	88	1275	26275	42	26317
Tr	555	1233	15233	228	15461
Act	100	3974	79074	99	79173

Table 18: sum of elements concentrations (ppm) of asbestos fibre samples from Gimigliano Mount-Reventino (GMRU; Calabria region). Ctl = chrysotile; Tr = tremolite; Act = actinolite. Bloise et al., 2020b.

As for chemical characterization of the two tremolite asbestos samples from Episcopia (TR_EPS) and San Severino Lucano (TR_SSL) villages (Pollino Massif, Basilicata region), results revealed concentrations of potentially toxic elements even greater than those found in asbestos fibres from Gimigliano Mount-Reventino Unit.

Focusing on trace elements amounts, Cr and Ni are the most abundant ones with the highest concentrations in TR_EPS sample which showed also high levels of Co, V, Ti and Cu, while As and Zn are more in TR_SSL. If the total balance of PTEs (i.e., ∑ As, Ba, Cd, Co, Cr, Cu, Li, Mo, Ni, Pb, Sb, Sn, Sr, Ti, Te, V, W, Zn, Zr) in the studied samples is considered, TR_EPS specimen is more enriched than TR_SSL (Figure 52) reaching values of 3572.61 ppm vs. 1384.4 ppm (Table

19). The estimation of the total amount of PTEs allowed us to assume that TR_EPS is potentially more dangerous than TR_SSL, considering equal the other factors contributing to the fibre toxic potential definition (e.g., morphometry, dissolution rate, biodurability, surface activity).

At this point, the comparison of PTEs detected in tremolite asbestos from Episcopia and San Severino villages (Basilicata region) with those of tremolite asbestos from Gimigliano Mount Reventino Unit (Calabria region) was useful to observe the difference in PTEs content. A further comparison has been made with tremolite asbestos from Val d'Ala (TR_VLA; Piedmont region, northern Italy) detected by Bloise et al. (2016a) to examine the differences with samples from another geographic location (Figure 53; Table 19). Most of the potentially toxic elements investigated, have been detected with higher amount in tremolite asbestos from Episcopia (TR_EPS). Specifically, Cr and Ni concentrations were much higher in TR_EPS then the other samples, reaching values of 1120 ppm (Cr) and 1830 ppm (Ni), together with Co (31.9 ppm) and Sb (15.10 ppm). Conversely, Cu (24.53) and Sr (200 ppm) are more abundant in TR_GMRU while the highest amount of V were found in TR_VLA. Table 19 also displays the Indicative baseline data for some trace elements in normal human lung tissues (Biedermann et al., 1987) showed for comparison.

Considering the PTEs total amounts in tremolite asbestos samples (Figure 53), comes out that the specimen with the highest concentrations of PTEs is TR_EPS (3078.1 ppm) followed by TR_SSL (1168.1 ppm), TR_GMRU (782.83 ppm) and TR_VLA (707.08 ppm). The reason why we found these difference in PTEs concentrations may be explained by the various geochemical/petrological processes involved during the genesis of the asbestos fibres (Bloise et al., 2017; Tiepolo et al., 2007).
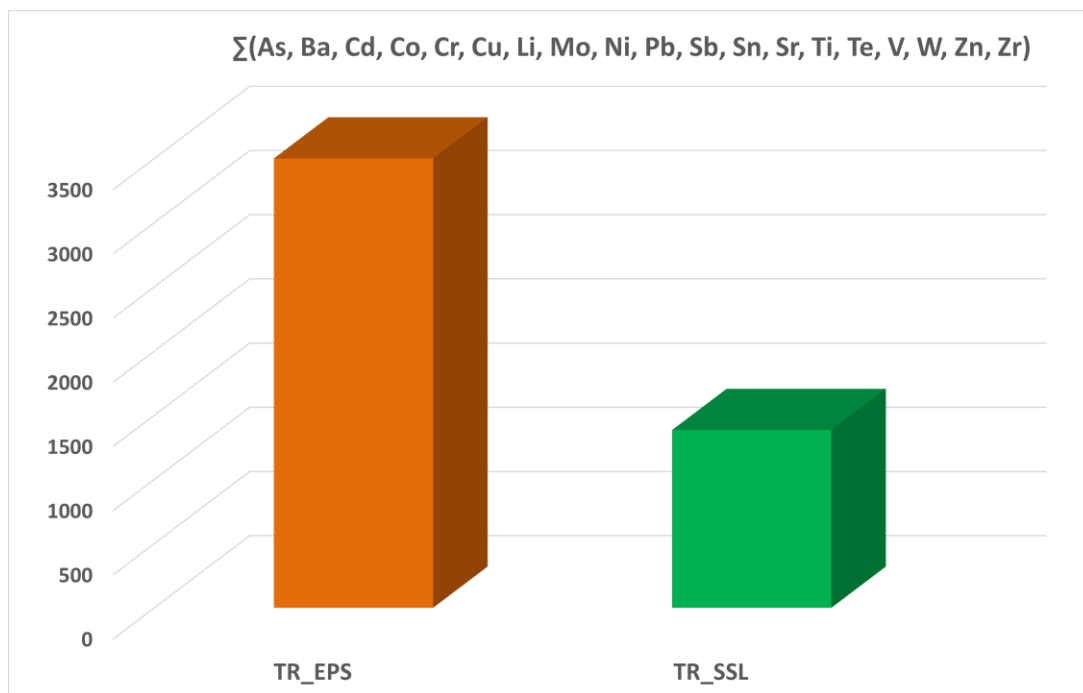
Figure 52: total concentrations of trace elements (ppm) in the investigated tremolite asbestos samples from Basilicata region. TR_EPS = tremolite asbestos from Episcopia; TR_SSL = tremolite asbestos from San Severino Lucano. Ricchiuti et al., 2021.
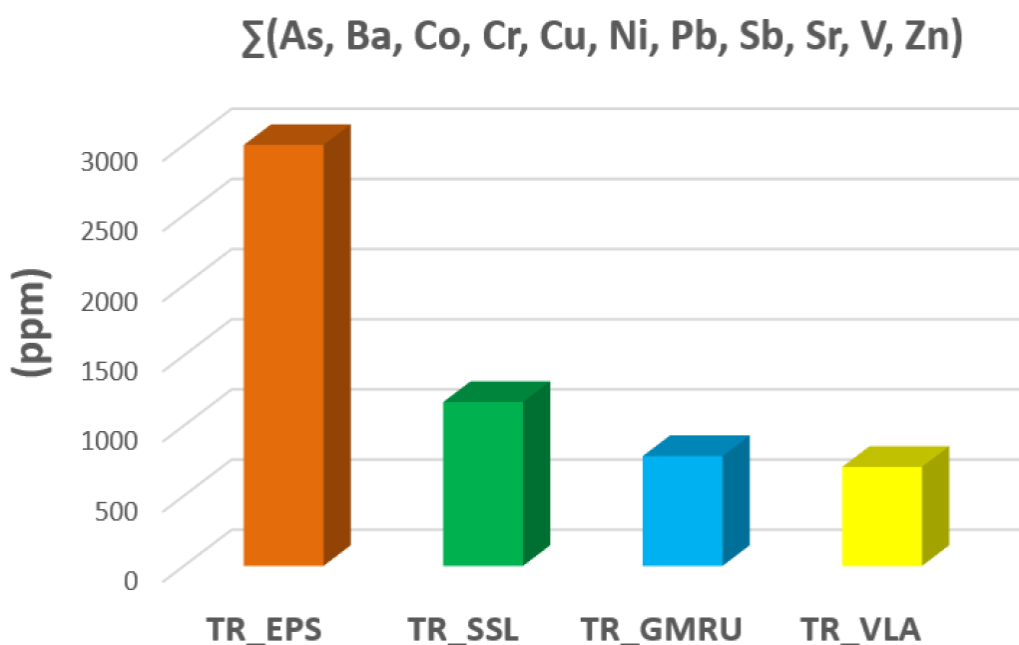
Figure 53: comparison of the trace elements total amounts (ppm) in the investigated tremolite asbestos from Episcopia (TR_EPS), San Severino Lucano (TR_SSL), tremolite asbestos from Gimigliano Mount-Reventino Unit (TR_GMRU) and Val d'Ala (TR_VLA) studied by Bloise et al 2016a, 2020b. Ricchiuti et al., 2021.

ppm	TR_EPS	TR_SSL	TR_GMRU	TR_VLA	Concentration range in human lungs*
As	3.20	7.90	1.20	n.d.	0.001-0.10
Ba	1.10	16.50	14.80	0.61	> 1.10
Co	31.90	7.80	22.64	26.92	0.002-0.10
Cr	1120	550	170.91	165	0.002-0.50
Cu	23.20	17.80	24.53	3.23	1-5.00
Ni	1830	480	308.63	473	0.01-1.00
Pb	11.50	20.50	4.40	0.45	0.02-0.50
Sb	15.10	11.20	0.20	0.03	0.002-0.10
Sr	1.50	16.10	200	6.59	0.01-1.00
V	6.30	2.60	7.10	13.06	0.0005-0.50
Zn	34.30	37.70	28.42	17.19	1-30.00
Σ_{TOT}	3078.10	1168.10	782.83	706.08	

Table 19: trace elements (ppm) detected in the studied tremolite asbestos from Episcopia (TR_EPS), San Severino Lucano (TR_SSL), and tremolite asbestos from Gimigliano Mount-Reventino Unit (TR_GMRU) and Val d'Ala (TR_VLA) studied by Bloise et al 2016a, 2020b, showed for comparison. *Indicative baseline data for some trace elements in normal human lung tissues (Biedermann et al., 1987). Ricchiuti et al., 2021.

9. Summary considerations and conclusion

The multidisciplinary investigation conducted on serpentinite rocks, derivative soils, and individual asbestos fibres (i.e., chrysotile, tremolite, actinolite) occurring in geological outcrops in southern Italy (Calabria and Basilicata regions) allowed to make significant considerations to asbestos-related hazard.

The multiscale approach provided an overview of the environmental impact due to the presence naturally occurring asbestos (NOA) in the study areas as well as providing the basis to assess the risks to human health due to the potential inhalation of asbestos fibres released from asbestos-containing rocks and soils.

The mineralogical investigation of serpentinite rocks and derivative agricultural soils occurring in the Gimigliano Mount-Reventino Unit (GMRU; Calabria region) and Pollino Massif (Episcopia and San Severino Lucano villages, Basilicata region) revealed that among the six asbestos minerals, chrysotile, tremolite and actinolite fibres occur in the studied samples. Moreover, asbestiform mineral species such as polygonal serpentine and fibrous antigorite have been detected.

In serpentinite samples, asbestos fibres were mainly found inside the veins rather than the massive portion with an orientation mainly perpendicular (cross-fibres) to the vein elongation directions. A broad characterization of the veins and their infill has been conducted on serpentinites from GMRU. In these samples, vein systems with various size and shape crosscutting the rock were well visible even at the mesoscopic scale and those ones with average width ranging between 0.3 mm to 1 mm represents the most abundant vein type. As shown by microscopic observations, the veins were filled by chrysotile fibres whose dimensions (i.e., width, length) match with those of regulated asbestos and therefore classified as asbestos under European law (Directive, 2003/18/CE, 2003). Accordingly, asbestos fibres (chrysotile, tremolite, actinolite) detected in serpentinite samples and derivative soils from Pollino Massif, occur with dimensions of regulated asbestos (length > 5 µm, width < 3 µm; WHO, 1986).

In addition to the mineralogical composition, the geochemical characteristics of serpentinite rocks and derived soils inherited from the mother rock revealed significant information related to the presence of potentially toxic elements (PTEs) harmful to human health. As a matter of fact, analyzed bulk rocks and derived soils showed concentration of Cr, V, Co, and Ni exceeding the maximum admissible contents established by the Italian law (Italian Legislative Decree No. 152/2006) for public, private, and residential green use (Co, V) as for industrial and commercial use (Cr, Ni). These results represent significant fundings since heavy metals can be mobilized and

discharged into various environmental matrixes (e.g., water, soils) thus expanding the contamination source and the potential interaction with human body. Scientific studies conducted in the GMRU area, revealed that water interacting with ophiolite rocks is characterized by high amounts of PTEs (i.e., Cr, Ni, Cu, Zn, Pb) due to the dissolution of primary phases such as serpentine and amphiboles (Apollaro et al., 2011) thus emphasizing the importance of asbestos minerals characterization for assessing contaminated groundwater and soil in ophiolitic outcrops. The quantification of PTEs in asbestos fibres extracted from serpentinites rocks from GMRU (chrysotile, tremolite, actinolite) and Poillino Massif (tremolite from Episcopia and San Severino villages, respectively) revealed high concentrations of toxic elements (Cr, Ni, Co, Cu, Zn, V, As, Ti) as well. Specifically, Cr and Ni were the most abundant trace elements detected in the samples and, among the three asbestos species from GMRU, tremolite showed the highest content of trace metals followed by actinolite and chrysotile. It is worth mentioning, that potentially toxic minor elements such as Fe and Mn influence the balance content of toxic metals. If we wanted to suppose which fibre is more potentially dangerous based on the PTEs total amount, we would assume that tremolite is the most hazardous one due to the highest content of heavy metals. However, other important factors such as the biodurability influence the toxic potential of the fibres. For instance, chrysotile, which is considered by many countries less toxic than amphiboles, due to its shorter bio-persistence into the lungs, can quickly release its PTEs high content into the body thus causing negative effects. If this condition is exact, the toxic potential of metal-rich chrysotile asbestos should be reevaluated (Gualtieri et al., 2017b).

As for the two tremolite from Pollino Massif, the concentrations of PTEs were even higher than those ones found in asbestos fibres from GMRU. Specifically, tremolite from Episcopia revealed the highest amounts of trace elements, followed by tremolite from San Severino Lucano and tremolite from GMRU. In this case, other conditions being equal (e.g., biodurability, surface activity), among the two tremolite asbestos investigated it is possible to assume that based on PTEs content, tremolite from Episcopia is more dangerous than tremolite from San Severino Lucano village.

Therefore, what comes out from the present work of thesis, is that population living within serpentinite rich geological context could be exposed to health risks due to the presence of asbestos mineral species as well as that of high concentrations of potentially toxic elements in rocks and soils and individual fibres. In this context, local maps indicating areas with environmental concern should be published by the institutions thus avoiding hazardous exposures.

References

Allison, A.C., 1974. Pathogenic effects of inhaled particles and antigens. *Ann. N. Y. Acad. Sci.,* 221, 299-308.

Amodio Morelli, L., Bonardi, G., Colonna, V., Dietrich, D., Giunta, G., Ippolito, F., Liguori, V., Lorenzoni, S., Paglioncino, A., Perrone, V., 1976. L' arco Calabro Peloritano nell' orogene Appenninico-Maghrebide. *Mem. Soc. Geol. It.,* 17, 1–60.

Andréani, M., Baronnet, A., Boullier, A.M., Gratier, J.P., 2004. A microstructural study of a crack-seal type serpentine vein, using SEM and TEM techniques. *Eur. J. Mineral.,* 16, 585–595.

Andréani, M., Mével, C., Boullier, A.M., Escartin, J., 2007. Dynamic control on serpentine crystallization in veins: constraints on hydration processes in oceanic peridotites. *Geochem. Geophy. Geosy.*, 8 (2), 2–24. https://doi.org/10.1029/ 2006GC001373.

Apollaro, C., Marini, L., Critelli, T., Barca, D., Bloise, A., De Rosa, R., Liberi, F., Miriello, D., 2011. Investigation of rock-to-water release and fate of major, minor, and trace elements in the metabasalt–serpentinite shallow aquifer of Mt. Reventino (CZ, Italy) by reaction path modelling. *Appl. Geochem.*, 26 (9–10), 1722–1740.

Asbestos.com Brought to you by Mesothelioma Center. Textile Mill Workers and Asbestos, by Michelle Whitmer. https: //www.asbestos.com/occupations/textile-mill-workers/

Baker, D.R., Mancini, L., Polacci, M., Higgins, M.D., Gualda, G.A.R., Hill, R.J., Rivers, M.L., 2012. An introduction to the application of X-ray microtomography to the three-dimensional study of igneous rocks. *Lithos*, 148, 262–276.

Ballirano, P., Bloise, A., Gualtieri, A.F., Lezzerini, M., Pacella, A., Perchiazzi, N., Dogan, M., Dogan, A.U. The Crystal Structure of Mineral Fibers. In Mineral Fibers: Crystal Chemistry, Chemical-Physical Properties, Biological Interaction and Toxicity; In: Gualtieri, A.F. (Ed.), European Mineralogical Union: London, UK, 2017; Volume 18, pp. 17–53.

Belluso, E., Baronnet, A., Capella, S., 2020. Naturally Occurring Asbestiform Minerals in Italian Western Alps and in Other Italian Sites. *Environ. Eng. Geosci.*, 26 (1): 39–46.

Belluso, E., Cavallo, A., Halterman, D. Crystal habit of mineral fibres. In Mineral Fibers: Crystal Chemistry, Chemical-Physical Properties, Biological Interaction and Toxicity; In: Gualtieri, A.F. (Ed.), European Mineralogical Union: London, UK, 2017; pp. 65–109.

Bernstein, D., Castranova, V., Donaldson, K., Fubini, B., Hadley, J., Hesterberg, T., Kane, A., Lai, D., McConnell, E.E., Muhle, H., and others, 2005. Testing of Fibrous Particles: Short-Term Assays and Strategies. *Inhal. Toxicol.*, 17, 497–537.

Biedermann, A., Koch, B., Pettke, C., Hirt, T., 2015. Magnetic anisotropy in natural amphibole crystals. *Am Min*, 100. 10.2138/am-2015-5173.

Biedermann, K.A., Landolph, J.R., 1987. Induction of anchorage independence in human diploid foreskin fibroblasts by carcinogenic metal salts. *Cancer Res.*, 47, 3815–3823.

Blaauw, C., Stroink G., Leiper W., Zentilli M., 1979. Mössbauer analysis of some canadian chrysotiles, *Canad Mineral*, 17, 713-717.

Bloise, A, Ricchiuti C, Lanzafame G, Punturo R. 2020a. X-ray synchrotron microtomography: a new technique for characterizing chrysotile asbestos. *Sci Total Environ.*, 10; 703:135675.

Bloise, A., Barca, D., Gualtieri, A.F., Pollastri, S., and Belluso, E., 2016a. Trace elements in hazardous mineral fibres. *Environ. Pollut.,* 216, 314–323.

Bloise, A., Belluso, E., Barrese, E., Miriello, D., Apollaro, C., 2009. Synthesis of Fe-doped chrysotile and characterization of the resulting chrysotile fibers. *Crys. Res. Tec.*, 44(6), 590–596.

Bloise, A., Belluso, E., Catalano, M., Barrese, E., Miriello, D., and Apollaro, C., 2012. Hydrothermal alteration of glass to chrysotile. *J. Am. Ceram. Soc.*, 95, 3050–3055.

Bloise, A., Belluso, E., Fornero, E., Rinaudo, C., Barrese, E., Capella, S., 2010. Influence of synthesis condition on growth of Ni-doped chrysotile. *Microporous Mesoporous Mat.*, 132, 239–245.

Bloise, A., Catalano, M., and Gualtieri, A., 2018a. Effect of grinding on chrysotile, amosite and crocidolite and implications for thermal treatment. *Minerals*, 8, 135.

Bloise, A., Catalano, M., Critelli, T., Apollaro, C., Miriello, D., 2017. Naturally occurring asbestos: potential for human exposure, San Severino Lucano (Basilicata, southern Italy). *Environ. Earth Sci.,* 76, 648–661.

Bloise, A., Critelli, T., Catalano, M., Apollaro, C., Miriello, D., Croce, A., Barrese, A., Liberi, F., Piluso, E., Rinaudo, C., 2014. Asbestos and other fibrous minerals contained in the serpentinites of the Gimigliano-Mount Reventino unit (Calabria, S-Italy). *Environ. Earth. Sci.* 71, 3773–3786.

Bloise, A., Fornero, E., Belluso, E., Barrese, E., Rinaudo, C., 2008. Synthesis and characterization of tremolite asbestos fibres. *Eur. J. Mineral.,* 20, 1027−1033.

Bloise, A., Kusiorowski, R., Gualtieri, A., 2018b. The effect of grinding on tremolite asbestos and anthophyllite asbestos. *Minerals*, 8, 274.

Bloise, A., Punturo, R., Catalano, M., Miriello, D., Cirrincione, R., 2016b. Naturally occurring asbestos (NOA) in rock and soil and relation with human activities: the monitoring example of selected sites in 121 Calabria (southern Italy). *Ital. J. Geosci.*, 135, 268–279.

Bloise, A., Ricchiuti, A., Giorno, E., Zumpano, P., Miriello, D., Apollaro, C., Crispini, A., De Rosa, R., and Punturo, R., 2019. Assessment of Naturally Occurring Asbestos in the area of Episcopia (Lucania, Southern Italy). *Fibers*, 7, 703

Bloise, A., Ricchiuti, C., Punturo, R., Pereira, D., 2020b. Potentially toxic elements (PTEs) associated with asbestos chrysotile, tremolite and actinolite in the Calabria region (Italy). *Chem. Geol.*, 558.

Bonneau, L., Malard, C. and Pezerat, H., 1986. Studies on surface properties of asbestos. II. Role of dimensional characteristics and surface properties of mineral fibers in the induction of pleural tumors. *Environ. Res.*, 41, 268_275.

Broaddus, V., 2001. Apoptosis and asbestos-induced disease: Is there a connection? *J Lab Clin Med.*, 137, 314–315.

Brun, F., Massimi, L., Fratini, M., Dreossi, D., Billé, F., Accardo, A., Pugliese, R., Cedola, A., 2017. SYRMEP tomo project: a graphical user interface for customizing CT reconstruction workflows. *Adv. Struct. Chem. Imag.* 3 (1).

Buck, B., Goossens, D., Metcalf, R.V., McLaurin, B., and Freudenberger, M., 2013. Naturally Occurring Asbestos: Potential for Human Exposure, Southern Nevada, USA. *Soil Sci Soc Am J.*, 77, 2192−2204.

Burragato, F., Ballirano, P., Fiori, S., Papacchini, L., Sonno, M., 2001. Segnalazione di tremolite asbestiforme nel Lazio. Il Cercapietre Notiziario del Gruppo Mineralogico Romano, 1-2, 33-35.

Caicedo, M., Jacobs, J.J., Reddy, A., Hallab, N.J., 2007. Analysis of metal ion-induced DNA damage, apoptosis, and necrosis in human (Jurkat) T-cells demonstrates Ni2+ and V3+ are more toxic than other metals: Al3+, Be2+, Co2+, Cr3+, Cu2+, Fe3+, Mo5+, Nb5+, Zr2+. *J. Biomed. Mat. Res.*, Part A, 905–913.

Caillaud, J., Proust, D. & Righi, D., 2006. Weathering sequences of rock-forming minerals in a serpentinite: Influence of microsystems on clay mineralogy. *Clays Clay Miner.* 54**,** 87–100.

Campopiano, A., Bruno, M., Olori, A., Angelosanto, F., Iannò, A., Casciardi, S., and Spadafora, A., 2018. Fibrous antigorite in mount reventino area of central calabria. *J. Mediterr. Earth Sci.,* 10, 17−25.

Capella, S., Belluso, E., Bursi Gandolfi, N., Tibaldi, E., Mandrioli, D., and Belpoggi, F., 2017. In vivo biological activity of mineral fibres. In EMU Notes in Mineralogy, 18, 307–345.

Caputo, A, De Santis, M., Manno, V., Cauzillo, G., Bruni, BM., Palumbo, L., Conti, S., Comba, P., 2018. Impatto sulla salute delle fibre di amianto presenti in affioramenti naturali nell'area del Pollino (Basilicata). *Epidemiol Prev.*, 42(2), 142-150.

Cardile, V., Renis, M., Scifo, C., Lombardo, L., Gulino, R., Mancari, B., Panico, A., 2004. Behaviour of the new asbestos amphibole fluoro-edenite in different lung cell systems. *Int J Biochem Cell Biol,* 36:849–860.

Case, B.W., Abraham, J.L., Meeker, G., Pooley, F.D., and Pinkerton, K.E., 2011. Applying definitions of 'asbestos' to environmental and 'low-dose' exposure levels and health effects, particularly malignant mesothelioma. Journal of toxicology and environmental health. Part B, *Crit Rev*, 14, 3–39.

Cavallo, A., Rimoldi, B., 2013. Chrysotile asbestos in serpentinite quarries: A case study in Valmalenco, Central Alps, Northern Italy. *Environ. Sci. Process. Impacts*, 15, 1341–1350.

Censi, P., Spoto, S.E., Saiano, F., Sprovieri, M., Mazzola, S., Nardone, G., Di Geronimo, S.I., Punturo, R., Ottonello, D., 2006. Heavy metals in coastal water systems. A case study from the northwestern Gulf of Thailand. *Chemosphere,* 64(7), 1167–1176.

Censi, P., Tamburo, E., Speziale, S., Zuddas, P., Randazzo, L.A., Punturo, R., Cuttitta, A., Arico, P., 2011a. Yttrium and lanthanides in human lung fluids, probing the exposure to atmospheric fallout. *J. Hazard. Mater.,* 186(2–3), 1103–1110.

Censi, P., Zuddas, P., Randazzo, L.A., Tamburo, E., Speziale, S., Cuttitta, A., Punturo, R., Arico, P., Santagata, R., 2011b. Source and nature of inhaled atmospheric dust from trace element analyses of human bronchial fluids. *Environ. Sci. Technol.* 45(15), 6262–6267.

Chen, L., Yang, X., Jiao, H., Zhao, B., 2003. Tea catechins protect against lead-induced ROS formation, mitochondrial dysfunction, and calcium dysregulation in PC12 cells. *Chem. Res. Toxicol.* 16, 1155–1161.

Chesworth, W., 1992. Weathering systems, in Martini I.P., and Chesworth W., eds., Weathering, soils and paleosols, Amsterdam, Netherlands, *Elsevier*, p. 19–39.

Cloetens, P., Pateyron-Salome, M., Buffière, J.Y., Peix, G., Baruchel, J., Peyrin, F., Schlenker, M., 1997. Observation of microstructure and damage in materials by phase sensitive radiography and tomography. *J. App. Phys,.* 81.

Colombino, E., Capella, S., Casalinuovo, F., Racco, R., Pruiti, F., Volante, M., Di Marco, V., Belluso, E., Capucchio, M., 2019. Malignant peritoneal mesothelioma in a boar who lived in Calabria (Italy): Wild animal as sentinel system of human health. *Sci. Total Environ.,* 683, 267−274.

Compagnoni R, Ferraris G, Flora L., 1983. Balangeroite, a new fibrous silicate related to gageite from Balangero, Italy. *Am. Mineral.,* 68, 214-219.

Compagnoni, R., Groppo, C., 2006. The asbestos in the rocks of the Susa Valley (Torino Province, Plemonte, Italy). *Rend. Online Soc. Geol. Ital*, 3, 21-28.

Cooke, W.E., 1924. Fibrosis of the lung due to the inhalation of asbestos dust. *BMJ*, 2, 147–148.

Cralley, L.J., Keenan, R.G., Lynch, J.R., 1967. Exposure to Metals in the Manufacture of Asbestos Textile Products. *Am. Ind. Hyg. Assoc. J.*, 28, 452–461.

Cressey, B.A., Cressey, G., Cernik, R.J., 1994. Structural Variations in Chrysotile Asbestos Fibers Revealed by Synchrotron X-Ray Diffraction and High-Resolution Transmission Electron Microscoy. *Canad Mineral,* 32, 257–270.

De Waele, J. K., Luys, M. J., Vansant, E. F., Adams, F.C., 1984. Analysis of chrysotile asbestos by LAMMA and Mossbauer spectroscopy: a study of the distribution of iron. *J. Trace Microprobe Tech.,* 2, 87-102.

Dement, J.M., and Brown, D.P., 1994. Lung cancer mortality among asbestos textile workers: a review and update. *Ann. Occup. Hyg,* 38, 412, 525-532.

Deschamps, F., Godard, M., Guillot, S., Hattori, K., 2013. Geochemistry of subduction zone serpentinites: a review. *Lithos*, 178, 96–127.

Di Giuseppe, D., Zoboli, A., Vigliaturo, R., Gieré, R., Bonasoni, M.P., Sala, O., Gualtieri, A.F., 2019. Mineral Fibres and Asbestos Bodies in Human Lung Tissue: A Case Study. *Minerals, 9*, 618.

Diandini, R., Takahashi, K., Park, E.K., Jiang, Y., Movahed, M., Le, G.V., Lee, L.J., Delgermaa, V. Kim, R., 2013. Potential years of life lost (PYLL) caused by asbestos-related diseases in the world. *Am. J. Ind. Med.,* 56, 993-1000.

Dichicco, M.C., Laurita, S., Sinisi, R., Battiloro, R., Rizzo, G., 2018. Environmental and Health: The Importance of Tremolite Occurence in the Pollino Geopark (Southern Italy). *Geosci*, 8. 98.

Dichicco, M.C., Paternoster, M., Rizzo, G., Sinisi, R., 2019. Mineralogical Asbestos Assessment in the Southern Apennines (Italy): A Review. *Fibers*, 7, 24.

Directive 2003/18/CE of the European Parliament and of the European Council of 27 March 2003.

Directive, 2003/18/CE 27 March 2003 del Parlamento Europeo e del Consiglio, che modifica la direttiva 83/477/CEE, del Consiglio sulla protezione dei lavoratori contro i rischi connessi con un'esposizione all'amianto durante il lavoro. Available online https://www.ambientediritto.it/Legislazione/amianto/2003/dir%202003%2018%20CE.pdf

Dixon, J. R., Lowe, D. B., Richards, D. E., Cralley, L. J., Stokinger, H. E., 1970. The role of trace metals in chemical carcinogenesis: asbestos cancers. *Cancer Res*., 30, 1068–1074.

Dodson, R.F., Atkinson, M.A., Levin, J.L., 2003. Asbestos fiber length as related to potential pathogenicity: a critical review. *Am. J. Ind. Med.,* 44, 291-297.

Donaldson, K., Murphy, F.A., Duffin, R., Poland, C.A., 2010. Asbestos, carbon nanotubes and the pleural mesothelium: a review of the hypothesis regarding the role of long fibre retention in the parietal pleura, inflammation and mesothelioma. Part. *Fibre Toxicol.* 7(1), 1–17.

Driscoll, T., Nelson, D.I., Steenland, K., Leigh, J., Concha-Barrientos, M., et al., 2005. The global burden of disease due to occupational carcinogens. *Am. J. Ind. Med.,* 48, 419–31

Drummond, G., Bevan, R., Harrison, P., 2016. A comparison of the results from intra-pleural and intraperitoneal studies with those from inhalation and intratracheal tests for the assessment of pulmonary responses to inhalable dusts and fibres. *RTP*, 81, 89-105.

EPA, Environmental Protection Agency, 1986. *Airborne Asbestos Health Assessment Update. EPA/6000/8–84/003E*, Washington, DCEPA

EPA, Environmental Protection Agency, 2009. Soil, Sediment and Surface Water sampling Sumas Mountain Naturally-Occurring Asbestos site, Whatcom county, Washington. U.s. EPA region 10 Office of Environmental Assessment, Seattle, 98101−3140.

Evans, W.B., 2004. The serpentinite multisystem revisited: chrysotile is metastable. *Int. Geol. Rev.,* 46(6), 479–506.

Famoso, D.A., Mangiameli, M., Roccaro, P., Mussumeci, G., Vagliasindi, F., 2012. Asbestiform fibers in the Biancavilla site of national interest (Sicily, Italy): Review of environmental data via GIS platforms. *Rev. Environ. Sci. Biotechnol.,* 11, 417-427.

Fantauzzi, M., Pacella, A., Atzei, D., Gianfagna, A., Andreozzi, G.B. Rossi, A., 2010. Combined use of Xray photoelectron and Mo¨ssbauer spectroscopic techniques in the analytical characterization of iron oxidation state in amphibole asbestos. *Anal. Bioanal. Chem.,* 396, 2889-2898.

Fantauzzi, M., Pacella, A., Fournier, J., Gianfagna, A., Andreozzi, G.B., Rossi, A., 2012. Surface chemistry and surface reactivity of fibrous amphiboles that are not regulated as asbestos. *Anal. Bioanal. Chem.,* 404, 821-833.

Fubini, B., 1993. In: Wahreit DB (Ed) Fiber toxicology. Academic, San Diego.

Fubini, B., Mollo, L., 1995. Role of iron in the reactivity of mineral fibers. *Toxicol. Lett.,* 82, 951-960.

Gaggero, L., Crispini, L., Isola, E., Marescotti, P., 2013. Asbestos in natural and anthropic ophiolitic environments: A case study of geohazards related to the Northern Apennine ophiolites (Eastern Liguria, Italy). *Ofioliti*, 38, 29–40.

Gaggero, L., Sanguineti, E., Gonzalez, A. Y., Militello, G.M., Scuderi, A., Parisi, G., 2017. Airborne asbestos fibres monitoring in tunnel excavation. *J. Environ. Manage.*, 196, 583–593.

García-Barriuso, M., Bernado, S., Nabais, C., Pereira, D., Amich, F., 2011. The Paleosubtropical element Notholaenamarantae (L.) Desv subsp. marantae in serpentine areas in the west of Iberian Peninsula: Phytogeochemical study, distribution and conservation. *Biologia*, 66, 258-265.

Gianfagna, A., Ballirano, P., Bellatreccia, F., Bruni, B.M., Paoletti, L., and Oberti, R., 2003. Characterization of amphibole fibers linked to mesothelioma in the area of Biancavilla, Eastern Sicily, Italy. *Mineral. Mag.*, 67, 1221-1229.

Gladney, E.E., Roelandts, I., 1988a. 1987 compilation of elemental concentration data for USGS BIR-1, DNC-1 and W-2. *Geostand. newsl*, 12, 63-118.

Gladney, E.S., Jones, E.A., Nickell, E.J., Roelandts, I., 1991. 1988 compilation of elemental concentration data for USGS DTS-1, G-1, PCC-1 and W-1. *Geostand newsl*, 15, 199-396.

Gualtieri A.F. 2012, Mineral fibre-based building materials and their health hazards. In Pacheco-Torgal F., Jalali S., and Fucic A. (Eds.). Toxicity of building materials. Elsevier, pp. 166-195. Woodhead, Cambridge.

Gualtieri, 2017a. Mineral fibres: Crystal chemistry, chemical-physical properties. Biological interaction and toxicity. In EMU notes (Gualtieri, A.F. Ed.), chapter 1 Vol. 18.

Gualtieri, A., Mangano, D., Gualtieri, M., Ricchi, A., Foresti, E., Lesci, G., Roveri, N., Mariotti, M., and Pecchini, G., 2009. Ambient monitoring of asbestos in selected Italian living areas. *J. Environ. Manage.,* 90, 3540−3552.

Gualtieri, A., Mossman, B.T., Roggli, V.L., 2017b. Towards a general model for predicting the toxicity and pathogenicity of mineral fibres. In: Mineral Fibres: Crystal Chemistry, Chemical-Physical Properties, Biological Interaction and Toxicity, A. F. Gualtieri (Eds) European Mineralogical Union, Volume 18.

Gualtieri, A.F., Bursi Gandolfi, N., Pollastri, S., Burghammer, M., Tibaldi, E., Belpoggi, F., Pollok, K., Langenhorst, F., Vigliaturo, R., Dražić, G., 2017c. New insights into the toxicity of mineral fibres: A combined in situ synchrotron μ-XRD and HR-TEM study of chrysotile,

crocidolite, and erionite fibres found in the tissues of Sprague-Dawley rats. *Toxicol Lett.,* 15, 274-20-30.

Gualtieri, A.F., Pollastri, S., Bursi Gandolfi, N., and Lassinantti Gualtieri, M., 2017d. In vitro acellular dissolution of mineral fibers. A comparative study. *Nanotoxicology*, 0–36.

Guthrie, G.D. Jr., 1997. Mineral properties and their contributions to particle toxicity. *Environ. Health Perspect.,* 105, 1003-1011.

Hardy, J.A., Aust, A.E., 1995. Iron in asbestos chemistry and carcinogenicity. *Chem. Rev.* 95(1), 97–118.

Harington, J.S., Roe, F.J.C., Walters, M., 1967. No Title Studies of the mode of action of asbestos as a carcinogen. *SAMJ*, 41, 800–804.

Harper, M., 2008. 10th Anniversary critical review: naturally occurring asbestos. *J. environ. monit.,* 10, 1394−1408.

Hawthorne, F.C., Oberti, R., Harlow, G.E., Maresch, W.V., Martin, R.F., Schumacher, J.C., Welch, M.D., 2012. Ima report: Nomenclature of the amphibole supergroup. *Am Min*, 97, 2031–2048.

Herman, G.T., 1980. Image Reconstruction from Projections. The Fundamentals of Computerized Tomography. first ed. Academic Press, New York.

Horie, M., Nishio, K., Fujita, K., Kato, H., Nakamura, A., Kinugasa, S., Endoh, S., Miyauchi, A., Yamamoto, K., Murayama, H., Niki, E., Iwahashi, H., Yoshida, Y., Nakanishi, J., 2009. Ultrafine NiO particles induce cytotoxicity *in vitro* by cellular uptake and subsequent Ni(II) release. *Chem. Res. Toxicol.,* 22, 1415–1426.

Huang, J., Hisanaga, N., Sakai, K., Iwata, M., Ono, Y., Shibata, E., Takeuchi, Y., 1988. Asbestos fibers in human pulmonary and extrapulmonary tissues. *Am J Ind Med*, 14, 331–339.

IARC, 2009. Asbestos (chrysotile, amosite, crocidolite, tremolite, actinolite, and anthophyllite) IARC Monographs. Arsenic, Metals, fibres and dusts, International Agency for Research on Cancer, Lyon, 147-167.

IARC, International Agency for Research on Cancer, 1984. Polynuclear Aromatic Compounds. Part 3. Industrial Exposures in Aluminium Production, Coal Gasification, Coke Production, Iron and Steel Founding. International Agency for Research on Cancer, Lyon, France.

IARC, International Agency for Research on Cancer, 1993. Beryllium, Cadmium, Mercury, and Exposures in the Glass Manufacturing Industry. International Agency for Research on Cancer, Lyon, France.

IARC, International Agency for Research on Cancer, 2012. Working Group on the Evaluation of Carcinogenic Risk to Humans. IARC Monographs on the Evaluation of Carcinogenic Risks to Humans; No. 100C; International Agency for Research on Cancer: Lyon, France.

IARC, International Agency for Research on Cancer, 2012a Metals, arsenic, dusts and fibres. Monographs on the Evaluation of Carcinogenic Risks to Humans, 100C, 527 pp, Lyon, France.

IARC, International Agency for Research on Cancer, 2012b. Asbestos (chrysotile, amosite, crocidolite, tremolite, actinolite and anthophyllite). Pp. 219_309 in: Arsenic, Metals, Fibres, and Dusts. Monographs on the evaluation of carcinogenic risks to humans, Vol. 100C. World Health Organization (WHO), Lyon (F), France.

IARC, International Agency for Research on Cancer, 2012c. Working Group on the Evaluation of Carcinogenic Risk to Humans. IARC Monographs on the Evaluation of Carcinogenic Risks to Humans, no. 100C. International Agency for Research on Cancer, Lyon, France.

IBAS, International Ban Asbestos Secretariat, 2019. http://www.ibasecretariat.org/alpha_ban_list.php

INAIL, Istituto Nazionale Assicurazione Infortuni sul Lavoro, 2015. V rapporto Registro Nazionale Mesoteliomi (Re.NaM). pubblicazioni/catalogo-generale/il-registro-nazionale-dei-mesoteliomi-v-rapporto. Accessed date: 3 April 2019. https://www.inail.it/cs/internet/comunicazione/

International Centre for diffraction data. Mineral Powder Diffraction File: Data Book, JCPDS

Kamp, D.W., Weitzman, S.A., 1999. The molecular basis of asbestos induced lung injury. *Thorax,* 54, 638-652.

Keeling, J.L., Raven, M.D., Self, P.G., Eggleton, R.A., Bruker, 2008. Asbestiform antigorite occurrence in South Australia. 9th International Congress for Applied Mineralogy, ICAM 2008, 329–336.

Koerten, H.K., Hazekamp, J., Kroon, M., and Daems, W.T., 1990. Asbestos body formation and iron accumulation in mouse peritoneal granulomas after the introduction of crocidolite asbestos fibers. *Am. J. Pathol.,* 136, 141–57.

Kusiorowski, R., Zaremba, T., Piotrowski, J. Et al., 2012. Thermal decomposition of asbestos-containing materials. *J Therm Anal Calorim,* 113, 179–188.

Kusiorowski, R., Zaremba, T., Piotrowski, J. Et al., 2012. Thermal decomposition of different types of asbestos. *J Therm Anal Calorim,* 109**,** 693–704.

L. 257/1992 - *Norme Relative alla Cessazione Dell'impiego Dell'amianto*; Suppl. Ord. alla Gazzetta Ufficiale—Serie Generale n. 87 del 13 Aprile 1992. Available online: http://www.salute.gov.it/resources/static/primopiano/amianto/normativa/Legge_27_ marzo_1992.pdf.

Lafay, R., Montes-Hernandez, G., Janots, E., Chiriac, R., Findling, N., Toche, F., 2014. Simultaneous precipitation of magnesite and lizardite from hydrothermal alteration of olivine under high-carbonate alkalinity. *Chem. Geol*., 368, 63–75.

Laurita, S., Rizzo, G., 2019. The first occurrence of asbestiform magnesio- riebeckite in schists in the frido unit (pollino unesco global geopark, southern italy). *Fibers*, 7, 79.

Law 23 March 2001, n. 93 – Disposizioni in campo ambientale. Gazzetta Ufficiale n. 79 del 4 aprile 2001. Arc. 20 "Censimento dell'amianto e interventi di bonifica". Available online https://www.mite.gov.it/sites/default/files/legge_23_03_2001_93.pdf

Leake, B.E., Woolley, A.R., Arps, C.E., Birch, W.D., Gilbert, M.C., Grice, J.D., Linthout, K., Laird, J., Mandarino, J., Maresch, W.V., et al., 1997. Nomenclature of amphiboles: Report of the subcommittee on amphiboles of the international mineralogical association, commission on new minerals and mineral names. *Can. Mineral*., 35, 219–246

Lee, R. J., Strohmeier, B.R., Bunker, K.L., Van Orden, D.R., 2008, Naturally occurring asbestos—A recurring public policy challenge. *J. Hazard. Mater.,* 153, 1–21.

Legislative Decree 3 April 2006, n. 152 on Environmental Regulations. (GU n.88 del 14-4-2006 – Suppl. Ordinario n. 96), Vigente al: 17-2-2020. Available online http://extwprlegs1.fao.org/docs/pdf/ita192848.pdf

Legislative Decree No 277, 15/08/1991. Attenuazione delle direttive n 80/1107/CEE, n. 82/605/CEE, n. 83/477/CEE, n. 86/188/CEE e n. 88/642/CEE, in materia di protezione dei lavoratori contro i rischi derivanti da esposizione ad agenti chimici, fisici e biologici durante il lavoro, a norma dell'art. 7 legge 30 luglio 1990, n. 212.

Leyssens, L., Vinck, B., Van Der Straeten, C., Wuyts, F., Maes, L., 2017. Cobalt toxicity in humans— a review of the potential sources and systemic health effects. *Toxicology,* 387, 43–56.

Lippmann, M., 2014. Toxicological and epidemiological studies of cardiovascular effects of ambient air fine particulate matter (PM 2.5) and its chemical components: Coherence and public health implications. *Crit. Rev. Toxicol.,* 44, 299–347.

Loomis, D., Dement, J., Richardson, D., Wolf, S., 2010. Asbestos fibre dimensions and lung cancer mortality among workers exposed to chrysotile. *Occup. Environ. Med*., 67, 580–584.

Maire, E., Withers, P.J., 2014. Quantitative X-ray tomography. *Int. Mat. Rev*., 59, 1–43.

Manning, C.B., Vallyathan, V. Mossman, B.T., 2002. Diseases caused by asbestos: mechanisms of injury and disease development. *Int. Immunopharmacol.,* 2, 191-200.

Martra, G., Tomatis, M., Fenoglio, I., Coluccia, S., Fubini, B., 2003. Ascorbic acid modifies the surface of asbestos: possible implications in the molecular mechanisms of toxicity. *Chem. Res. Toxicol*., 16, 328-335.

Massaro, T., Baldassarre, A., Pinca, A, Martina, G., Fiore, S., Lettino, A., Cassano, F., Musti, M., 2013. [Exposure to asbestos in buildings in areas of Basilicata characterized by the presence of rocks containing tremolite]. *G Ital Med Lav Ergon.,* 34. 568-70.

McDonald, J.C., Liddell, F.D., Gibbs, G.W., Eyssen, G.E., McDonald, A.D., 1980. Dust exposure and mortality in chrysotile mining, 1910-75. *Br. J. Ind. Med*., 37, 11–24.

McDonald, J.C., McDonald, A.D., 1997. Chrysotile, tremolite and carcinogenicity. *Ann Occup Hyg*, 41, 699-705.

McDonald, R., 2003. Introduction to Natural and Man-made Disasters and Their Effects on Buildings (1st ed.). Routledge.

Meni, F., 2012. Eternit factory at Casale Monferrato. In Allen D., and Kazan-Allen L. (Eds.), International Ban Asbestos Secretariat (IBAS), Eternit and the Great Asbestos Trial, 31-34.

Metintas, S., Batirel, H., Bayram, H., Yilmaz, U., Karadag, M., Ak, G., and Metintas, M., 2017. Turkey National Mesothelioma Surveillance and Environmental Asbestos Exposure Control Program. *Int. J. Environ. Res.,* 14, E1293.

Mével, C., 2003. Serpentinization of abyssal peridotites at mid-ocean ridges, C.R. *Geosci.,* 335, 825–852.

Militello, G., Sanguineti, E., Gonzalez, A., Mantovani, F., and Gaggero, L., 2019. The concentration of asbestos fibers in bulk samples and its variation with grain size. *Minerals*, 9.

Ministerial Decree No 257, 06/09/1994: Normative e metodologie tecniche di applicazione dell'art. 6, comma 3, e dell'art. 12, comma 2, della legge 27 marzo 1992, n. 257, relativa alla cessazione dell'impiego dell'amianto.

Miserocchi, G., Sancini, G., Mantegazza, F., and Chiappino, G., 2008. Translocation pathways for inhaled asbestos fibers. *J. Environ. Health*, 7, 4.

Mistikawy, J.A., Mackowiak, T.J., Butler, M.J., Mischenko, I.C., Cernak, R.S., Richardson, J.B., 2020. Chromium, manganese, nickel, and cobalt mobility and bioavailability from mafic-to-ultramafic mine spoil weathering in western Massachusetts. USA. *Environ. Geochem. Health* 1–17.

Monaco, C., Tortorici, L., 1995. Tettonica estensionale quaternaria nell'Arco Calabro e in Sicilia orientale. *Studi geol. camerti*, 2, 351–362.

Monaco, C., Tortorici, L., Paltrinieri, W., 1998. Structural evolution of the Lucanian Apennines, southern Italy. *J. Struct. Geol.*, 20, 617–638.

Morgan, A., Cralley, L., 1973. Chemical characteristics of asbestos and associated trace elements. In: Bogovski, P., Gilson, J.C., Timbrell, V., Wagner, J.C. (Eds.), Biological Effects of Asbestos. IARC Sci. Publ, Lyon, France, pp. 113–131.

Mossman, B.T., Bignon, J., Corn, M., Seaton, A., and Gee, J.B., 1990. Asbestos: scientific developments and implications for public policy. *Science*, 247, 294–301.

Mossman, B.T., Pugnaloni, A., 2017. In vitro biological activity and mechanisms of lung and pleural cancers induced by mineral fibres. In EMU Notes in Mineralogy, Vol. 18 pp. 261–306.

Musumeci, G., Cardile, V., Fenga, C., Caggia, S., Loreto, C., 2011. Mineral fibre toxicity: expression of retinoblastoma (Rb) and phospho-retinoblastoma (pRb) protein in alveolar epithelial and mesothelial cell lines exposed to fluoro-edenite fibres. *Cell Biol Toxicol,* 27, 217–225.

Nackerdien, Z., Kasprzak, K.S., Rao, G., Halliwell, B., Dizdaroglu, M., 1991. Nickel (II)- and cobalt (II)-dependent damage by hydrogen peroxide to the DNA bases in isolated human chromatin. *Cancer Res.,* 51, 5837–5842.

Nemery, B., 1990. Metal toxicity and the respiratory tract. *Eur. Respir. J.,* 3, 202–219.

Newhouse, M.L., Thompson, H., 1965. Mesothelioma of pleura and peritoneum following exposure to asbestos in the London area. *Br. J. Ind. Med.,* 22, 261-269.

Nichols, M.D., Young, D., Gray, D., 2002. Guidelines for geologic investigations of naturally occurring asbestos in California. *California Geological Survey, Special Publication,* 124, 85.

Nicholson,W.J., 1986. 'Airborne asbestos health assessment update'. Report EPA-600/8-84-003F.Washington, D.C: Office of Health and Environmental Assessment, US Environmental Protection Agency, 200 pp.

NIOSH, National Institute for Occupational Safety and Health, 2008, Current Intelligence Bulletin (June 2008-Revised Draft) Asbestos and Other Elongated Mineral Particles: State of the Science and Roadmap for Research.

NIOSH, National Institute for Occupational Safety and Health, 2011. DHHS Publication 2011-159). *Current Intelligence Bulletin 62: asbestos fibers and other elongate mineral particles: state of the science and roadmap for research.* Mar.

Nordman, M., 1938. Occupational cancer of asbestos workers. *Zischr J. Krebsforsch*, 47, 288–302.

O'Hanley D.S., Dyar, M.D., 1998. The composition of chrysotile and its relationship with lizardite. *Canad Mineral,* 36, 727-740.

O'Hanley, D.S., 1996. Serpentinites: Records of Tectonic and Petrological History, Oxford Univ. Press, New York.

Oberdörster, G., 2000. Determinants of the pathogenicity of man-made vitreous fibers (MMVF). Int *Arch Occup Environ Health*, 73 Suppl, S60–S68.

Pacella, A., Andreozzi, G.B., Fournier, J., 2010. Detailed crystal chemistry and iron topochemistry of asbestos occurring in its natural setting: A first step to understanding its chemical reactivity. *Chem. Geol.*, 277, 197-206.

Pacella, A., Andreozzi, G.B., Fournier, J., Stievano, L., Giantomassi, F., Lucarini, G., Rippo, M.R., Pugnaloni, A., 2012. Iron topochemistry and surface reactivity of amphibole asbestos: relations with in vitro toxicity. *Anal. Bioanal. Chem.*, 402, 871-881.

Pacella, A., Tomatis, M., Viti, C., Bloise, A., Arrizza, L., Ballirano, P., Turci, F., 2020. Thermal inertization of amphibole asbestos modulates Fe topochemistry and surface reactivity. *J. Hazard. Mater*, 398, 123119.

Paganin, D., Mayo, S.C., Gureyev, T.E., Miller, P.R., Wilkins, S.W., 2002. Simultaneous phase and amplitude extraction from a single defocused image of a homogeneous object. *J. Microsc.* 206, 33–40.

Paoletti, L., Batisti, D., Bruno, C., Di Paola, M., Gianfagna, A., Mastrantonio, M., Nesti, M., Comba, P., 2000. Unusually high incidence of malignant pleural mesothelioma in a town of the eastern Sicily: an epidemiological and environmental study. *Arch. Environ. Health*, 55(6), 392-398.

PHE, Public Health England, P.H.E.C. for R.C. and E.H. (2007) Asbestos Toxicological Overview.

Pugnaloni, A., Giantomassi, F., Lucarini, G., Capella, S., Bloise, A., Di Primio, R., and Belluso, E., 2013. Cytotoxicity induced by exposure to natural and synthetic tremolite asbestos: An in vitro pilot study. *Acta histochem.,* 115, 100–112.

Punturo R., Bloise A., Critelli T., Catalano M., Fazio E., Apollaro C., 2015. Environmental implications related to natural asbestos occurrences in the ophiolites of the Gimigliano-Mount Reventino Unit (Calabria, Southern Italy). *Int J Environ Res.,* 9 (2), 405-418.

Punturo, R., Ricchiuti, C., and Bloise, A., 2019**,** Assessment of Serpentine Group Minerals in Soils: A Case Study from The Village of San Severino Lucano (Basilicata, Southern Italy). *Fibers*, 7, 18.

Punturo, R., Ricchiuti, C., Mengel, K., Apollaro., C., De Rosa, R., and Bloise, A., 2018. Serpentinite-derived soils in southern Italy: potential for hazardous exposure. *J. Mediterr. Earth Sci.,* 10.

Qi, F., Okimoto, G., Jube, S., Napolitano, A., Pass, H.I., Laczko, R., Demay, R.M., Khan, G., Tiirikainen, M., Rinaudo, C., and others, 2013. Continuous exposure to chrysotile asbestos can cause transformation of human mesothelial cells via HMGB1 and TNF-α signaling. *Am. J. Pathol.,* 183, 1654–1666.

Ramsay, J.G., 1980. The crack-seal mechanism of rock deformation. *Nature*, 284, 135-139.

Ricchiuti, C., Bloise, A., Punturo, R**.,** 2020. Occurrence of asbestos in soils: state of the art**.** *Episodes*, 43, 881-891.

Ricchiuti, C., Pereira, D., Punturo, R., Giorno, E., Miriello, D., Bloise, A., 2021. Hazardous Elements in Asbestos Tremolite from the Basilicata Region, Southern Italy: A First Step. *Fibers*, *9*, 47.

Ross, M., Nolan, R.P., 2003. History of asbestos discovery and use and asbestosrelated disease in context with the occurrence of asbestos within ophiolite complexes. *Geol. Soc. Am. Spec. Pap.*, 373, 447-470.

Rozalén, M., Huertas, F., Pacella, A. Ballirano, P., 2017. Dissolution and biodurability of mineral fibres. Pp. 347_366 in: Mineral Fibres: Crystal Chemistry, Chemical-physical Properties, Biological Interaction and Toxicity (A.F. Gualtieri, editor). EMU Notes in Mineralogy, 18. European Mineralogical Union and Mineralogical Society of Great Britain & Ireland, London.

Rozalén, M., Ramos, M.E., Fiore, S., Gervilla, F., Huertas, F.J., 2014. Minerals in the human body effect of oxalate and pH on chrysotile dissolution at 25 °C: An experimental study. *Am. Mineral.*, 99, 589–600.

Salnikow, K., Su, W., Blagosklonny, M.V., Costa, M., 2000. Carcinogenic metals induce hypoxia-inducible factor-stimulated transcription by reactive oxygen species-independent mechanism. *Cancer Res.*, 60, 3375–3378.

Scambelluri, M., Piccardo, G.B., Philippot, P., Robbiano, A. Negretti, L., 1997. High salinity fluid inclusions formed from recycled seawater in deeply subducted alpine serpentinite. *Earth Planet Sci Lett*, 148, 485-499.

Schindelin, J., Arganda-Carreras, I., Frise Fiji, E., 2012. An open-source platform for biological-image analysis. *Nat. Methods.*, 9(7), 676–682.

Schinwald, A., Chernova, T., Donaldson, K., 2012. Use of silver nanowires to determine thresholds for fibre length-dependent pulmonary inflammation and inhibition of macrophage migration in vitro. *Part. Fibre Toxicol.*, 9, 47.

Schreier, H., Northcote, T.G., Hall, K., 1987. Trace metals in fish exposed to asbestos rich sediments. *Water Air Soil Pollut.*, 35(3–4), 279–291.

Schwarz, E. J., and Winer, A.A., 1971. Magnetic properties of asbestos, with special reference to the determination of absolute magnetite contents. *CIM Bull.,* 64, 55-59.

Seilkop, S.K., Oller, A.R., 2003. Respiratory cancer risks associated with low-level nickel exposure: an integrated assessment based on animal, epidemiological, and mechanistic data. *Regul. Toxicol. Pharmacol.*, 37, 173–190.

Standard for Microanalysis. Standards Ref. # 02757-AB. SPI Supplies, Metals & Minerals Standard, serial 4AK.Stanton, F., Layard, M., Tegeris, A., Smith, A., Miller, E., and May, M., 1981. Relation of Particle Dimension to Carcinogenicity in Amphibole Asbestoses and Other Fibrous Minerals. *J. Natl. Cancer Inst.,* 67, 965–975.

Stayner, L., Welch, L.S., Lemen, R., 2013. The worldwide pandemic of asbestos-related diseases. *Annu. Rev. Public Health*, 34, 205-216.

Stayner, L.T., Danhovic, D.A., Lemen, R.A., 1996. Occupational exposure to chrysotile asbestos and cancer risk: A review of the amphibole hypothesis. *Am. J. Public Health*, 86, 179–186.

Stroink, G., Blaauw, C., White, C.G., Leiper, W., 1980. Mössbauer characteristics of UICC standard reference asbestos samples. Canad Mineral, 18, 285-290.

Sturm, R., Hofmann, W., 2009. A theoretical approach to the deposition and clearance of fibers with variable size in the human respiratory tract. *J. Hazard. Mater.*, 170, 210-218.

Thompson, B.D., Gunter, M.E., Wilson, M.S., 2011. Amphibole asbestos soil contamination in the USA: A matter of definition. *Am. Mineral*, 96, 690−693.

Tiepolo, M., Oberti, R., Zanetti, A., Vannucci, R., Foley, S.F., 2007. Trace-element partitioning between amphibole and silicate melt. Pp. 417-452 in Amphiboles: Crystal Chemistry, Occurrence, and Health Issues (F.C. Hawthorne, R. Oberti, G. Della Ventura and A. Mottana,

editors). Reviews in Mineralogy and Geochemistry, 67, Mineralogical Society of America and Geochemical Society, Chantilly, Virginia, USA.

Travaglione, S., Bruni, BM., Falzano, L., Filippini, P., Fabbri, A., Paoletti, L., Fiorentini, C., 2006. Multinucleation and proinflammatory cytokine release promoted by fibrous Fluoroedenite in lung epithelial A549 cells. *Toxicol In Vitro*, 20, 841–850.

Turci, F., Avataneo, C., Botta, S., Marcelli, I., Barale, L., Tomatis, M., Cossio, R., Tallone, S., Piana, F., Compagnoni, R., 2020. New Tools for the Evaluation of Asbestos-Related Risk during Excavation in an NOA-Rich Geological Setting. *Environ. Eng. Geosci.*, 26(1), 113–120.

Turci, F., Tomatis, M., Gazzano, E., Riganti, C., Martra, G., Bosia, A., Ghigo, D. Fubini, B., 2005. Potential toxicity of nonregulated asbestiform minerals: balangeroite from the western Alps. Part 2: Oxidant activity of the fibers. *J. Toxicol. Environ. Health - A: Curr. Issues.*, 68, 21-39.

Turci, F., Tomatis, M., Lesci, I.G., Roveri, N., Fubini, B., 2011. The iron-related molecular toxicity mechanism of synthetic asbestos nanofibres: a model study for high-aspect-ratio nanoparticles. *Chem. Eur. J.,* 17, 350-358.

Turci, F., Tomatis, M., Pacella, A., 2017. Surface and bulk properties of mineral fibres relevant to toxicity. In: Gualtieri, A.F. (Ed.), Mineral Fibres: Crystal Chemistry, Chemical-Physical Properties. Biological Interaction and Toxicity. European Mineralogical Union, London, UK, pp. 171–214.

UNI EN ISO-11885: 2009. Qualità dell'acqua – Determinazione di alcuni elementi mediante spettrometria di emissione ottica al plasma accoppiato induttivamente.

USGS, Unitated States Geological Survei, 2001. Some Facts about Asbestos (USGS Fact Sheet FS-012–01), Reston, VA, US Geological Survey.

Vanoeteren, C., Cornelis, R., Sabbioni, E., 1986. Critical Evaluation of Normal Levels of Major and Trace Elements in Human Lung Tissue. Commission of the European Communities, Luxembourg.

Veblen, D.R., 1981. Amphiboles and other hydrous pyriboles-mineralogy. *MSA*, 9.

Vezzani, L., 1966. La sezione tortoniana di Perosa sul fiume Sinni presso Episcopia (Potenza). *Geol. Rom.*, 5, 263–290.

Vezzani, L., 1969. La Formazione del Frido (Neocomiano- Aptiano) tra il Pollino e il Sinni. *Geol. Rom.,* 8, 129–176.

Vignaroli, G., Ballirano, P., Belardi, G., Rossetti, F., 2013. Asbestos fibre identification vs. evaluation of asbestos hazard in ophiolitic rock mélanges, a case study from the Ligurian Alps (Italy). *Environ. Earth Sci.*, 72, 3679–3698.

Virta, R., 2006. Worldwide Asbestos Supply and Consumption Trends from 1900 through 2003, Reston, VA, U.S. Department of the Interior, U.S. Geological Survey. Circular 1298.

Virta, R.L., 2002. Asbestos: Geology, Mineralogy, Mining, and Uses. U.S. Department of the Interior - U.S. *Geol. Surv*, 1–28.

Vogel, L., 2005. Asbestos in the World. *HESA Newsletter*, 27, 7-21.

Wagner, J.C., Sleggs, C.A., Marchand, P., 1960. Diffuse pleural mesothelioma and asbestos exposure in the North Western Cape Province. *Br. J. Ind. Med.,* 17, 260-271.

Wedler, H.W., 1943. Lung cancer in asbestosis patients. *Arch. Klinischen Medizin*, 191, 189–209.

Wei, B., Yang, L., Zhu, O., Yu, J., & Jia, X., 2014. Multivariate analysis of trace elements distribution in hair of pleural plaques patients and health group in a rural area from China. *Hair Therapy & Transplantation*, 4, 2167–3118.

Whitney, D.L., Evans, B.W., 2010. Abbreviations for names of rock-forming minerals. *Am. Mineral*., 95, 185–187.

Whittaker, E.J.W., 1979. Clustering of cations in amphiboles. *Phys. Chem. Miner*., 4, 1–10.

WHO, 1986. Asbestos and other natural mineral fibres. Programme on Chemical Safety. World Health Organization. Environmental Health Criteria 53, Geneva.

WHO, 2010. Asbestos: elimination of asbestos-related diseases. Fact sheet N∘343, July. http://www.who.int/mediacentre/factsheets/fs343/en/index.html

Wicks, F.J., O'Hanley, D.S., 1988. Serpentine minerals; structures and petrology. *Rev. Mineral. Geochem*., 19, 91 LP-167.

Wicks, F.J., Plant, A.G., 1979. Electron-microprobe and X-ray microbeam studies of serpentine textures. *Can. Mineral.* 17(4), 785–830.

Wroble, J., Frederick, T., Vallero, D., 2020. Refinement of Sampling and Analysis Techniques for Asbestos in Soil. *Environ. Eng. Geosci.*, 26(1), 129−131.

Yada, K., 1967. Study of chrysotile asbestos by high resolution electron microscope. *Acta. Cryst.*, 704.

Yespolitical.com Casale e l'Amianto. Morire sorridendo con 18 milioni, by Davide Serafin. https://yespolitical.com/tag/casale-monferrato/

Zakrzewska, M., Capone, PP., Ianno, A., Tarzia, V., Campopiano A., Villella, E., 2008. Calabrian ophiolites: Dispersion of airborne asbestos fibers during mining and milling operations. *Per. Mineral.*, 77. 27-34.

Zupančič, N., 2012. The influence of vegetation type on metal content in soils. *RMZ-materials and geoenvironment, letnik 59, številka 2/3, str. 229-244*.

Zupančič, N., 2017. Influence of climate factors on soil heavy metal content in Slovenia. *J. Soils Sediments*. 17.

Journal of Mediterranean Earth Sciences

Serpentinite-derived soils in southern Italy: potential for hazardous exposure

Rosalda Punturo [1,*], Claudia Ricchiuti [1], Kurt Mengel [3], Carmine Apollaro [2], Rosanna De Rosa [2], Andrea Bloise [2]

[1] *Dipartimento di Scienze Biologiche, Geologiche e Ambientali, Università di Catania, Italy*
[2] *Dipartimento di Biologia, Ecologia e Scienze della Terra, Università della Calabria, Arcavacata di Rende (CS), Italy*
[3] *InstitutfürEndlagerforschung, Technischen Universität Clausthal, Clausthal-Zellerfeld, Germany*
[*] *Corresponding author: punturo@unict.it*

ABSTRACT - The aim of the present study was to investigate on serpentinite rocks and related derivative soil samples in order to understand their potential contribution to the health problems caused by asbestos exposure. With this intent, agricultural soil samples as well as serpentinite rocks from which soils derive have been collected at San Severino Lucano village (Basilicata region, southern Italy); this site was chosen because of spatially isolated from other urban centers as well as any factory. In our study, we adopted different analytical techniques such as Polarized Light Microscopy (PLM), X-Ray Fluorescence (XRF), X-Ray Powder Diffraction (XRPD) and Scanning and Electron Microscopy combined with Energy Dispersive Spectrometry (SEM/EDS). Results pointed out as all of the collected soil samples contain asbestos minerals (e.g., chrysotile, tremolite-actinolite), clay minerals, plagioclase and oxides in various amounts. In our opinion, since the dispersion of fibres could be associated with carcinogenic lung cancer, in areas where Natural Occurring Asbestos (NOA) can be found, the institutions should publish local maps indicating areas with mineralogical concern and take precautions to avoid hazardous exposure of population.

The concentration levels of four toxic elements (Cr, Co, Ni, V) in almost all the serpentinite rocks and their derivative soils developed within San Severino Lucano village exceeds the regulatory thresholds for public, private and residential green use.

Key words: NOA; serpentinite-derived soil; heavy metals; southern Italy.

1. INTRODUCTION

Naturally occurring asbestos fibres are generally associated with serpentinite or altered ultramafic rocks. Over the last decades, many studies have focused on rocks containing NOA with the aim of determining the potential health risks to exposed neighboring populations (Bloise et al., 2012, 2014; Punturo et al., 2015; Baumann et al., 2015). The term "asbestos" represents a group of six fibrous silicate minerals belonging to the serpentinite (chrysotile) and amphibole (tremolite, actinolite, anthophyllite, amosite, crocidolite) mineral groups (e.g., World Health Organization WHO, 1986; NIOSH 2008). It has plenty been exploited for use in industrial and commercial products, mainly in building materials (e.g. insulation), heat-resistant fabrics and friction products (e.g. brake pads). Naturally occurring asbestos (NOA) is a generic term used to refer to both regulated and non-regulated fibrous minerals when encountered in natural geological deposits (Harper, 2008). Nowadays, only the six varieties above listed are considered as potential environmental pollutants by the Italian laws, however also asbestiform minerals such as balangeorite, carlosturanite, antigorite, diopside and fluoro-edenite (Compagnoni et al., 1983, 1985; Gianfagna, 2003; Compagnoni and Groppo, 2006) could be potentially dangerous if inhaled. In Europe and several other countries, asbestiform minerals are currently classified as asbestos when they have length >5 μm and aspect ratio (i.e., length divided by width) ≥3:1 (World Health Organization WHO 1986, Directive 2003/18/CE, NIOSH 2008).

Asbestos fibres dispersion in the environment is extremely dangerous because their inhalation may cause many types of cancer pathologies; it is confirmed by many studies which shown that death from lung diseases such as malignant mesothelioma, can be associated with environmental exposure to asbestos (International Agency for Research on Cancer, IARC, 2009).

On the basis of the effects of asbestos on biological systems, several authors ascribe the asbestos-fibres toxicity

to the synergetic effect of fibre size, bio-persistence and chemical composition (Gualtieri et al., 2017). However, it is generally accepted that none of the theories alone is adequate to explain the pathogenic mechanism of asbestos. Some study suggests that the cytotoxicity of asbestos may be also related to the minor and trace elements present as impurities in their structure (Bloise et al., 2016 a,b). Indeed, asbestos minerals, for different structural reasons, have a high capability to host a large number of toxic elements and some researchers claimed that asbestos fibers may play a passive role in producing diseases as carriers of trace elements. The human health risks are based on the potential fibres inhalation when they become airborne; NOA can be released into the atmosphere by natural weathering processes (e.g. erosion) or with human activities such as excavation, road construction, driving or walking on unpaved surfaces and agricultural activities which may disturb NOA outcrops causing the formation of potentially inhalable airborne dust (Punturo et al., 2015; Bloise et al., 2016c). Moreover, heavy metals may be released to natural water (e.g. Apollaro et al., 2011, 2012), contributing to human health. An association with neighborhood exposure to asbestos and an increased risk of deaths from lung diseases has been documented among the people who live near Naturally Occurring Asbestos (NOA) deposits around the world (e.g. Acosta et al., 1997; Burragato et al., 2005; Constantopoulos, 2008; Pereira et al., 2008; Navarro et al., 2013; Gaggero et al., 2017; Worliceck, 2017), including the Basilicata region (Italy) (Bloise et al., 2017a). Indeed, in this region, an increased number of lung disease were related to the environmental exposure to asbestos tremolite (Bernardini et al., 2003; Burragato et al., 2004; Pasetto et al., 2004).

In this frame, this paper reports the results of a detailed study on rocks and soils that developed on serpentinite bedrocks cropping out within the San Severino Lucano village (Basilicata region, Italy) (Fig. 1), in order to assess the presence of NOA potentially hazardous to human health and environmental quality. The geographic isolation and its distance from other main sources of asbestos for instance, are among some major aspects, which make the village an engrossing case study, besides local interest.

To this aim, we collected twelve serpentinite rocks and twelve related soil samples and cross-checked the data obtained from different analytical techniques (i.e., MOLP, XRPD, XRF, SEM–EDS), in order to perform a detailed characterization and to relate NOA release in the environment due to agricultural activity.

2. AREA DESCRIPTION

This study area (Fig. 1) is comprised within the Pollino National Park, which is located between the Basilicata and Calabria regions of southern Italy. The area is characterized by the terrains of the Liguride Complex which consists of three main tectonic units of Upper Jurassic to Upper Oligocene age (Ogniben, 1969; Vezzani, 1970; Monaco and Tortorici, 1995; Cirrincione et al., 2015): (1) the Calabro-Lucano Flysh (Monaco et al., 1998), a non-metamorphosed ophiolithiferous unit which partly corresponds to the North-Calabrian Unit; (2) the metamorphic terranes of the Frido Unit, characterized by HP/LT metamorphism (Vezzani, 1969; Amodio-Morelli et al., 1976; Cavalcante et al., 2012); (3) syn-orogenic turbiditic sequences, i.e., the Saraceno Formation, the Albidona Formation, and a sequence composed of alternating shales, mudstones and sandstones, the latter corresponding to the Perosa unit as defined by Vezzani (1966). The ophiolites of the Southern Apennine Liguride Units occur in the Frido Unit and in the North-Calabrian Unit. In particular, ophiolitic rocks of the Frido Unit consist of lenticular metabasites interbedded with cataclastic and highly fractured serpentinites (Sansone et al., 2011, 2012) that, together with serpentinites, slates, and metalimestones form sequences with a maximum thickness of several dozen meters In particular, we focused on the Village of San SeverinoLucano (40°1'0" N, 16°8'0" E) and its surroundings, on an area that encompasses about 20 km² (Fig. 1).

3. METHODS AND MATERIAL

Field survey carried out at San Severino Lucano village showed that the serpentinites are green coloured and present mainly two varieties: foliated and massive. Moreover, serpentinite outcrops are rarely covered by vegetation (Fig. 2a) due to the toxic composition of the surface formation (soils) derived from these rocks. Only few plants are able to survive under this extreme chemical composition (García Barriuso et al., 2011). For this reason, serpentine outcrops are highly exposed to weathering. Locally, serpentinites are very brittle, as indicated by the large number of fracture surfaces that may be filled by asbestiform minerals. Either alluvial and residual soils related to the serpentinite parent rock were collected (Fig. 2b) and analyzed, for a total of twelve serpentinite rocks and twelve related soil samples, respectively (Tabs. 1 and 2). Sampling sites are indicated in figure 1. Collected specimens were treated and studied in order to investigate their petrographic and mineralogical features and to highlight the occurrence of asbestiform minerals, if any.

To this aim, on thin sections obtained from the serpentinite collected, we carried out a petrographic and mineralogical investigation by using a Zeiss Axiolab Microscope with Polarized Light (PLM). X-ray powder diffraction patterns (XRPD) were obtained on a Bruker D8 Advance X-ray diffractometer with CuKa radiation, monochromated with a graphite sample monochromator at 40 kV and 40 mA. Scans were collected in the range of 3°-66° 2θ, with a step interval of 0.02° 2θ and step-counting time of 3 s. EVA software (DIFFRACplus EVA) was used to identify the mineral phases in each X-ray powder spectrum, experimental peaks being compared
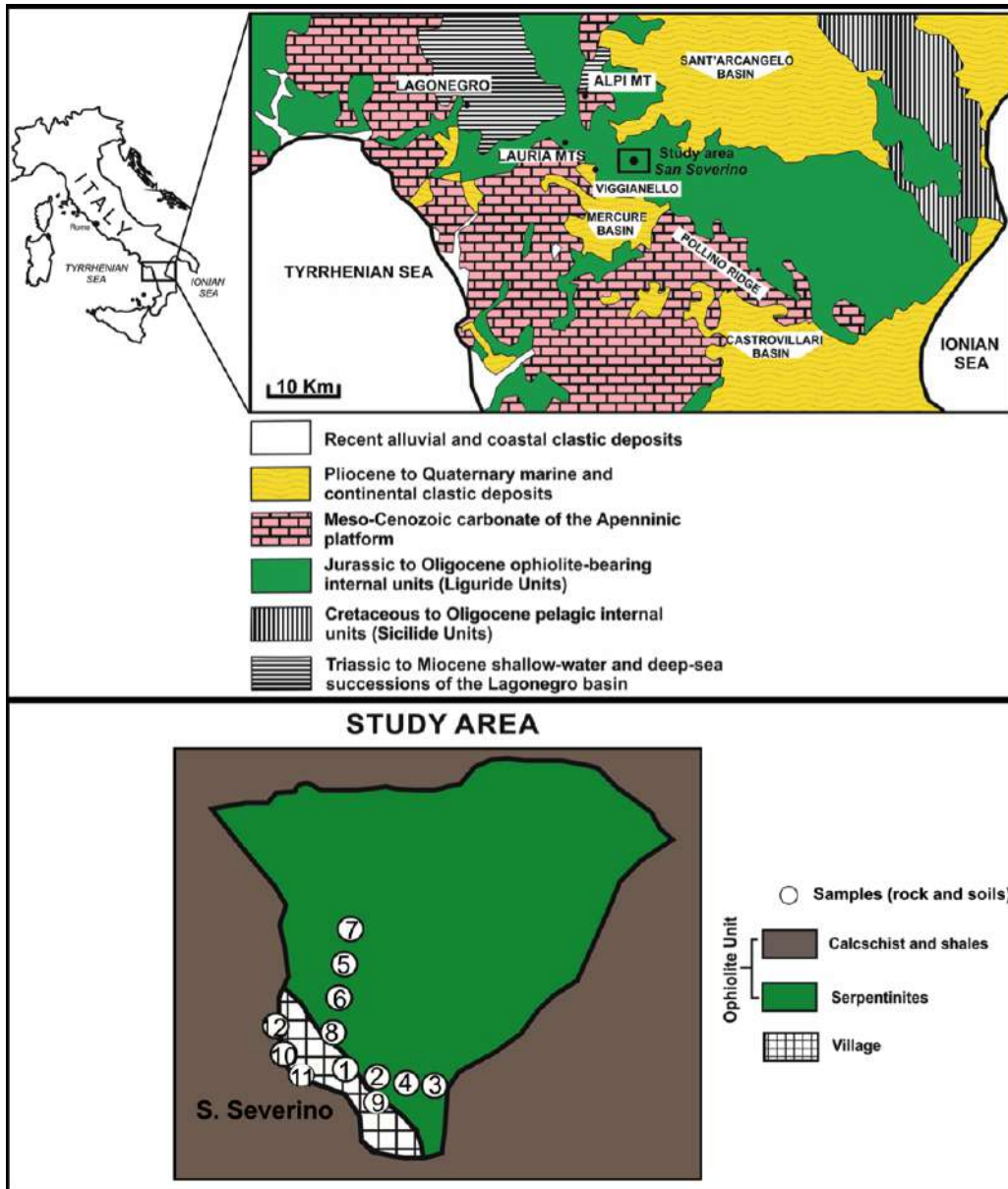
Fig. 1 - Geological map of the Calabria-Lucania border (modified after Bloise et al., 2017a) and study area location with sampling sites.
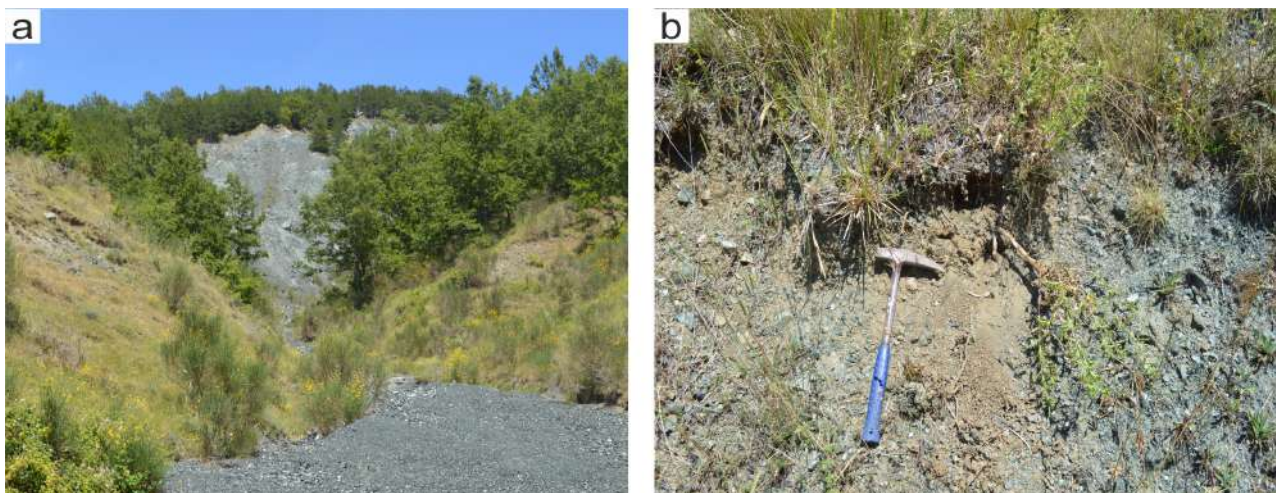

Fig. 2 - Products developed after serpentite alteration: **a)** alluvial debris; and **b)** derivative agricultural soil.

Sample	Lithotype	Locality	Site description	Lon (East)	Lat (North)	Phases detected
Rpol_1	Serpentinite	S. Severino Village	Entry of the Village	597417	4429775	Srp, Di, Mag, Chl
Rpol_2	Serpentinite	S. Severino Village	Entry of the Village	597405	4430523	Srp
Rpol_3	Serpentinite	S. Severino Village	Road cut outside the Village	597808	4430474	Srp, Di, Tr, Chl, Mag, Mnt
Rpol_4	Serpentinite	S. Severino Village	Road cut outside the Village	597569	4430504	Srp, Di, Tr, Chl, Mnt
Rpol_5	Serpentinite	S. Severino Village	Road cut outside the Village	597270	4431103	Srp, Di, Tr, Mag, Mnt
Rpol_6	Serpentinite	S. Severino Village	Road cut outside the Village	597268	4430927	Srp, Di, Mag
Rpol_7	Serpentinite	S. Severino Village	Road cut outside the Village	597323	4431363	Srp, Di, Chl, Mag
Rpol_8	Serpentinite	S. Severino Village	Road cut within the Village	597223	4430711	Srp, Di, Chl, Mag
Rpol_9	Serpentinite	S. Severino Village	At the base of the slop, outside the Village	597569	4430504	Srp, Di, Tr, Mag
Rpol_10-11	Serpentinite	S. Severino Village	Road cut within the Village	596890	4430715	Srp, Di, Chl, Mag
Rpol_12	Serpentinite	S. Severino Village	Road cut within the Village	596831	4430823	Srp, Di, Mag,

Tab. 1 - Studied localities, coordinates and, for each collected serpentinite sample, mineralogical assemblage detected by X-ray powder diffraction (XRPD) and scanning electron microscopy combined with energy dispersive spectrometry (SEM/EDS). Mineral symbols after Kretz (1983). Amphiboles present in the samples were classified according to the amphibole diagram classification (Leake et al., 1997).

Sample	Lithotype	Locality	Site description	Lon	Lat	Phases detected
Spol_1	Soil	S. Severino Village	At the entrance of the Village	597417	4429775	Srp, Di, Qtz, Mnt-Chl,
Spol_2	Soil	S. Severino Village	At the entrance of the Village	597405	4430523	Srp, Di, Qtz, Mnt-Chl, Tr
Spol_3	Soil	S. Severino Village	Road cut outside the Village	597808	4430474	Srp, Di, Qtz, Mnt-Chl, Tr
Spol_4	Soil	S. Severino Village	Road cut outside the Village	597569	4430504	Srp, Di, Qtz, Mnt-Chl, Tr, Chm, Chl,
Spol_5	Soil	S. Severino Village	Road cut outside the Village	597270	4431103	Srp, Di, Qtz, Mnt-Chl, Tr, Chm, Ms
Spol_6	Soil	S. Severino Village	Road cut outside the Village	597268	4430927	Srp, Di, Qtz, Mnt-Chl, Tr, Chm, Ms, Tlc,
Spol_7	Soil	S. Severino Village	Road cut outside the Village	597323	4431363	Srp, Di, Qtz, Mnt-Chl, Chm,
Spol_8	Soil	S. Severino Village	Road cut within the Village	597223	4430711	Srp, Di, Qtz, Mnt-Chl, Tr, Chm,
Spol_9	Soil	S. Severino Village	At the base of the slop, outside the Village	597569	4430504	Srp, Di, Qtz, Mnt-Chl, Tr, Chm,
Spol_10	Soil	S. Severino Village	Road cut within the Village	596890	4430715	Srp, Di, Qtz, Mnt-Chl, Tr, Chm, Mo
Spol_11	Soil	S. Severino Village	Road cut within the Village	596890	4430715	Srp, Di, Qtz, Mnt, Tr, Chm
Spol_12	Soil	S. Severino Village	Road cut within the Village	596831	4430823	Srp, Di, Qtz,

Tab. 2 - Studied localities, coordinates and, for each collected derivative soil sample, mineralogical assemblage detected by X-ray powder diffraction (XRPD) and scanning electron microscopy combined with energy dispersive spectrometry (SEM/EDS). Mineral symbols after Kretz (1983). Amphiboles present in the samples were classified according to the amphibole diagram classification (Leake et al., 1997).

with 2005 PDF2 reference patterns. For a better determination of mineralogical composition by XRPD, the soil samples were pre-treated with H_2O_2 and pre-heated for 24 h at 530 °C, in order to remove the organic compounds. The soil samples have been investigated from a petrographic, mineralogical and geochemical point of view by using various analytical techniques, in order to point out eventual asbestiform minerals and to point out the enrichment in heavy metals respect to the serpentinite rocks from which soils themselves derive. For SEM analysis, samples were examined without any grinding treatment with the Tescan-Vega\\LMU scanning electron microscope, equipped with an energy-dispersive X-ray spectrometer (EDS) Edax Neptune XM4 60,

operating at 15 kV accelerating voltage and 20 nA beam current conditions. X-ray fluorescence spectrometry was carried out with Axios instrument from analyticalon fused glass diluted by $Li_2B_4O_7$ (1:5) and by using external calibration with international rock standards. L.O.I. (Loss on Ignition) was determined by gravimetric method. Values of representative major and trace elements (ppm) are reported in tables 3 and 4, respectively.

4. RESULTS

At the mesoscopic scale, serpentinite rocks show the typical dark green coloration and massive structure, with widespread presence of veins with varying thickness. The main mineral constituting these veins is serpentine whose individuals are in most cases arranged perpendicular to the vein elongation. Thin sections obtained from specimens show at the polarizing microscope that the serpentine group minerals as the main constituents and magnetite±talc±Cr-spinel±chlorite as the other mineral phases present. Rare relics of olivine and pyroxene are observable (Fig. 3a); in most cases, original crystals have been completely replaced by pseudomorphic aggregates

of serpentine minerals and by small magnetite grains. The pseudomorphic replacement of olivine by serpentine causes the formation of fractured olivine grains into which serpentinization advances uniformly, from all fractures and grain boundaries, to produce mesh textures (Fig. 3b); the mesh core is clearly distinguishable from the mesh rim. Secondary magnetite commonly develops along the former olivine grain-boundaries and fractures emphasizing them (Fig. 3c). The pseudomorphic replacement of pyroxene by serpentine begins from grain boundaries and fractures by following along cleavage planes; in most cases the primary pyroxene is easily recognizable because the cleavage is preserved (Fig. 3d). Many vein systems are filled by serpentine group minerals and by talc (Fig. 3 e,f), in particular serpentine fibres are found with perpendicular orientation to the vein elongation ("cross" serpentine).

4.1. XRPD characterization

Results from the XRPD showed that the most abundant minerals in all serpentinite rocks are serpentine minerals, while tremolite was found in four samples out of twelve. Diopside and magnetite are ubiquitous, whereas and

Wt%	SiO_2	Al_2O_3	MgO	CaO	K_2O	Fe_2O_3	L.O.I
Rock							
RPOL1	39.8	0.9	41.2	2.2	0.0	8.7	7.4
RPOL2	39.1	0.7	40.3	0.6	0.0	9.1	10.1
RPOL3	40.7	1.7	42.2	3.5	0.0	7.9	4.0
RPOL4	40.7	1.0	43.2	3.0	0.0	8.9	3.2
RPOL5	41.9	1.3	40.9	4.6	0.0	10.1	1.3
RPOL6	39.6	0.9	41.7	1.7	0.0	8.1	8.0
RPOL7	40.1	1.0	41.2	2.1	0.0	8.6	7.1
RPOL8	43.2	1.7	43.2	5.2	0.0	4.3	2.4
RPOL9	38.6	0.8	40.2	2.3	0.0	8.8	9.2
RPOL10_11	40.0	0.9	42.2	2.4	0.0	8.4	6.1
RPOL12	39.9	0.9	41.5	2.2	0.0	8.1	7.4
Soil							
SPOL_1	38.5	3.8	40.0	2.0	0.1	6.1	9.6
SPOL_2	41.0	5.9	36.7	3.2	0.4	6.0	6.7
SPOL_3	40.2	4.2	41.2	1.9	0.1	5.5	6.9
SPOL_4	39.3	5.5	39.4	1.2	0.3	7.2	7.2
SPOL_5	41.0	5.0	39.2	2.9	0.1	5.3	6.5
SPOL_6	40.9	4.2	39.6	2.3	0.2	5.3	7.5
SPOL_7	45.4	4.4	38.7	0.6	0.3	5.2	5.3
SPOL_8	39.1	4.7	41.1	1.8	0.1	5.0	8.3
SPOL_9	39.8	3.8	42.2	2.1	0.0	5.5	6.6
SPOL_10	40.0	4.9	39.1	2.0	0.3	4.6	9.1
SPOL_11	40.8	5.2	38.6	1.9	0.3	5.1	8.1
SPOL_12	39.9	3.4	41.0	1.8	0.1	5.9	8.0

Tab. 3 - Major oxide values (wt%) in bulk serpentinite rock and derived soil samples. L.O.I. (Loss On Ignition) is also reported.

ppm	Co	Cr	Ni	V
Rock				
RPOL1	88	2658	2281	91
RPOL2	107	1725	2489	66
RPOL3	87	2175	1726	88
RPOL4	97	2622	2379	67
RPOL5	112	2865	2073	82
RPOL6	97	3077	2074	65
RPOL7	105	2553	2100	68
RPOL8	62	1065	1177	217
RPOL9	99	2247	2004	62
RPOL10_11	99	2527	2140	76
RPOL12	97	2207	2018	73
Soil				
SPOL_1	122	2680	2131	91
SPOL_2	137	2942	1735	117
SPOL_3	79	1888	1576	75
SPOL_4	123	3425	1670	137
SPOL_5	139	2652	1203	144
SPOL_6	148	3828	1942	139
SPOL_7	103	1644	1505	78
SPOL_8	125	1997	1854	86
SPOL_9	71	1956	1547	78
SPOL_10	116	1711	1718	65
SPOL_11	103	2052	1574	81
SPOL_12	111	1536	1843	56

Tab. 4 - Selected heavy metals values (ppm) in bulk serpentinite rock and derived soil samples.

clay minerals (chlorite, montmorillonite) were detected in some samples (Fig. 4; Tab. 1). As far as soils, X-ray diffraction study revealed that serpentine group minerals mainly constitute all samples, together with diopside inherited from rocks, secondary clay minerals (e.g. montmorillonite-chlorite; chamosite, muscovite) and quartz. Moreover, the relatively sharp reflections diagnostic of the presence of tremolite probably present in low amount in the serpentinite rocks, which were observed only in fourXRPD pattern from serpentinite rocks due to the overlapping of serpentine reflections, are now clearly visible. Indeed, in serpentinite-derived soils, tremolite was detected in nine samples out of twelve (Fig. 4b; Tab. 2).

4.2. SEM–EDS characterization

Morphological observations by means of SEM in soil samples, show a large amount of fibrous minerals with acicular habit trapped in aggregating agents like organic matter, clay and iron oxides. Morphology of representative fibres is shown in figure 5 a,b. These fibers have variable size (length 13-18 μm and diameter about 1 μm) and in most cases tend to split up along the fibers

elongation axis. Their identification is not easy just by observing images at SEM, therefore, representative chemical analyses by means of EDS have been useful to complete their preliminary characterization. The results of microanalytical investigation carried out on some occurring fibers pointed out that they are chrysotile and amphiboles with tremolite-actinolite main composition and minor anthophyllite.

4.3. Major, minor and trace elements

Selected element values for either serpentinite rocks and derivative soils are set out on tables 3 and 4. Results showed that the average values of most major elements are quite similar in the two groups, being $SiO_{2average} \approx 40$ wt%, $MgO_{average}$ wt% is 41.6 (rock) and 39.7 (soil), and $CaO_{average}$ is 2.7 wt% (rock) and lower in soil (1.98 wt%). On the contrary, soils are enriched in $Al_2O_{3average}$ (4.48 vs 1.07 wt%) and in K_2O (below detection limits in rocks). As far as minor (Cr, Ni) and trace (Co, V) elements values are higher in soils compared to rocks, whereas the opposite happens for Ni, being more abundant in rocks (Tab. 4). The distribution of the selected elements (potentially harmful elements, PHEs) is comparable to results observed in similar lithotypes and derivative soils (e.g. Censi et al., 2011, 2011a; Guagliardi et al., 2013, 2016 a,b).

5. DISCUSSIONS

Considering the results of this case study, we can assess that the population that lives within serpentite rich geological context is clearly exposed to serious health risks due to soil pollution from heavy metals. In particular, chromium could be a cause of several human health problems such as stomach and lung cancer (e.g., Shekhawat et al., 2015). It is also worth mentioning that among the minor elements known as being dangerous for human health, Ni is the toxic metal of greatest concern (Nackerdien et al., 1991). In fact, contact with nickel compounds can cause a variety of adverse effects on human health, such as cardiovascular, kidney diseases and cancer of the respiratory tract (Seilkop and Oller, 2003). Cobalt breathing in high amount may cause several human health problems such as asthma and pneumonia (ATSDR, 2004). Finally, excessive amounts of vanadium in the human body can increase the possibility of uremia and/or lung cancer (e.g., Crans et al., 2004). In the study area, chromium, vanadium, cobalt and nickel are geogenic in serpentine soils and not anthropogenic. In fact, in chrysotile samples, the trace metals represent an almost exclusively isomorphs substitute for magnesium (Bloise et al., 2009, 2010, 2017b; Ballirano et al., 2017). Although, heavy metal substitution in chrysotile is usually more restricted than in the other serpentine minerals (i.e., lizardite and antigorite). Moreover, the concentration of heavy metal is highly variable among the different asbestos detected (i.e., chrysotile and tremolite), due to the different geochemical processes involved in their formation. In a recent work, Bloise et al. (2016b) show that metals, such as
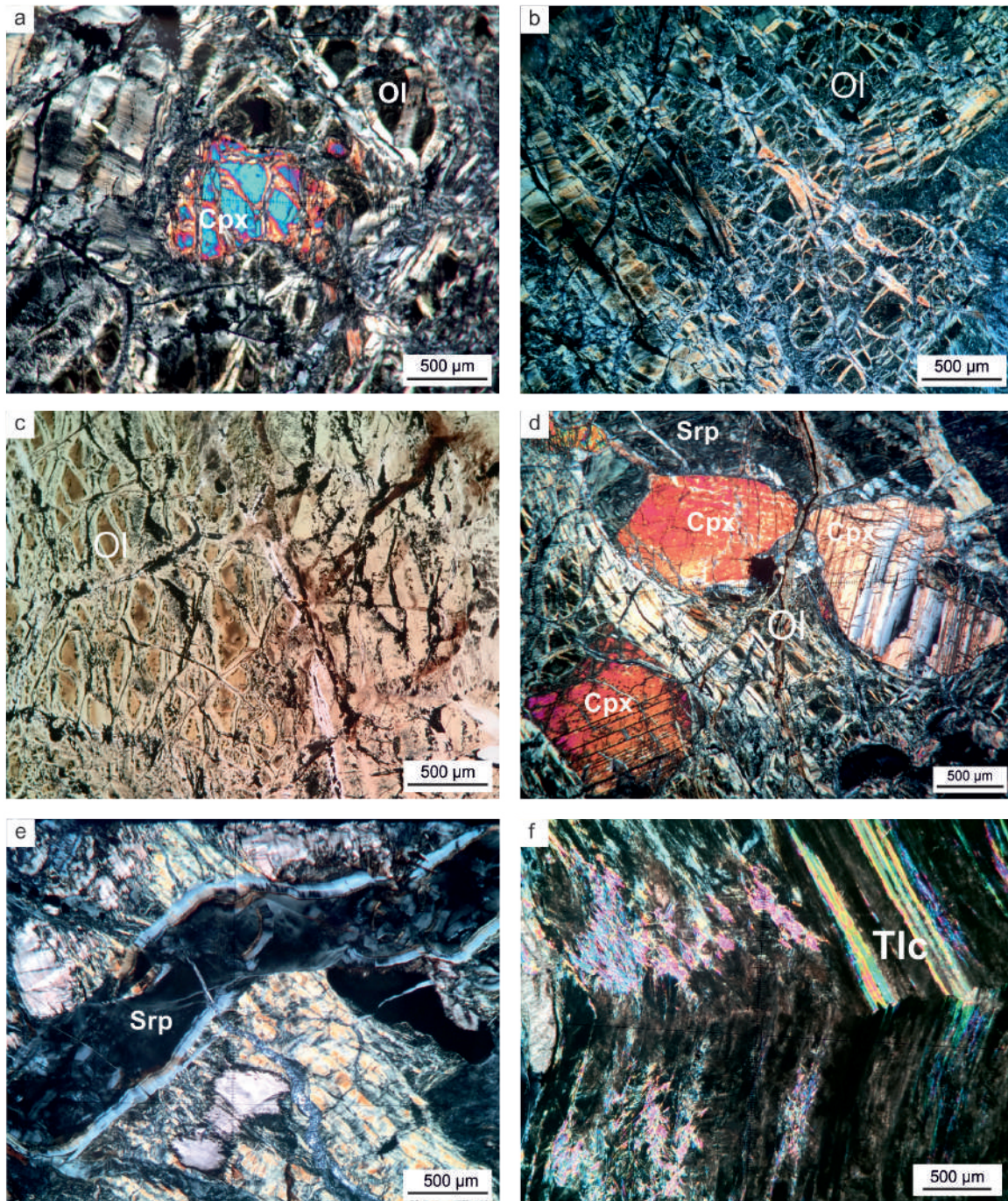
Fig. 3 - Photomicrographs of: a) relic of clinopyroxene and olivine partially replaced by serpentine; b) olivine pseudomorph replaced by serpentine showing mesh texture (crossed polarizers); c) serpentine over olivine with mesh textures in plane-polarized light; fractures are emphasized by secondary magnetite; d) clinopyroxene partially replaced by serpentine with olivine pseudomorph between them; serpentine matrix is observable at the top; e) serpentine vein cross-cutting the main rock); f) arrangement of serpentine and talc fibers inside a vein (crossed polarizers);

Co and Ni in tremolite asbestos from Val d'Ala (Italy) were present in a high amount. Ni and Co in tremolite occupy the specific crystallographic M(1) and M(3) sites as in synthetic calcic amphibole (Ballirano et al., 2017).

Finally, the comparison of the concentrations of PHEs (V, Cr, Co e Ni) is investigated through a series of correlation plots in which the concentration of SiO_2 is taken as the reference variable (Fig. 6). From diagrams, it is evident that in either studied soils and rocks, the maximum admissible contents established by the Italian law shows that these elements in our samples are very high and exceeds the regulatory thresholds (Italian Legislative Decree No. 152 of 03/04/2006) for public, private and residential green use for V, Cr and Co (limit A corresponding to 90, 150, 20 ppm respectively), while nickel (limit A: 120) is also exceeded the legal limit for industrial and commercial use.
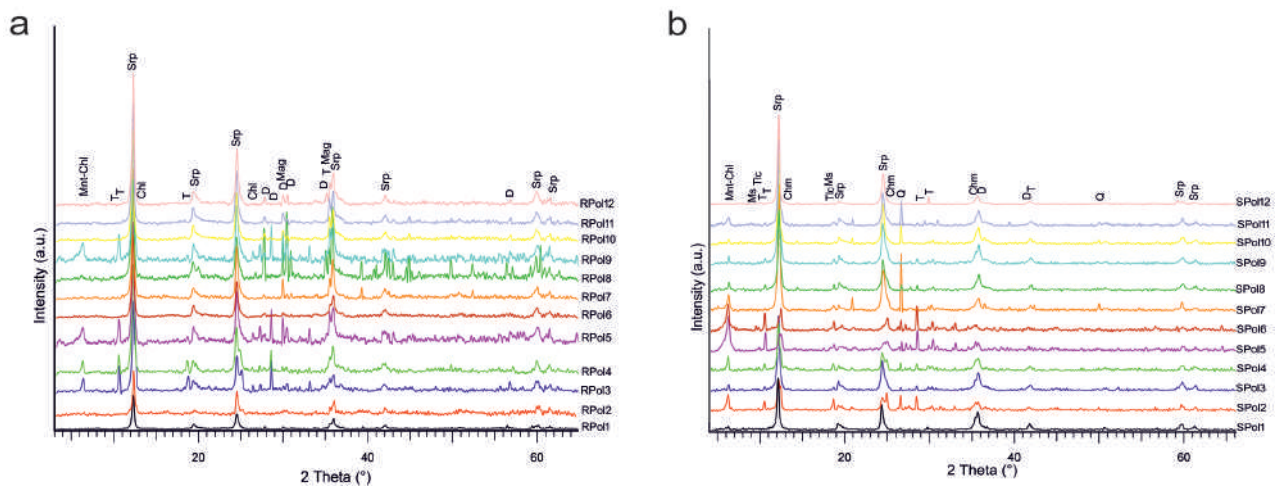
Fig. 4 - XRPD pattern from: a) serpentinite rocks and b) derived soils. Peaks were assigned according to literature (Mineral Powder Diffraction File: Data Book, JCPDS-International Centre for Diffraction Data).
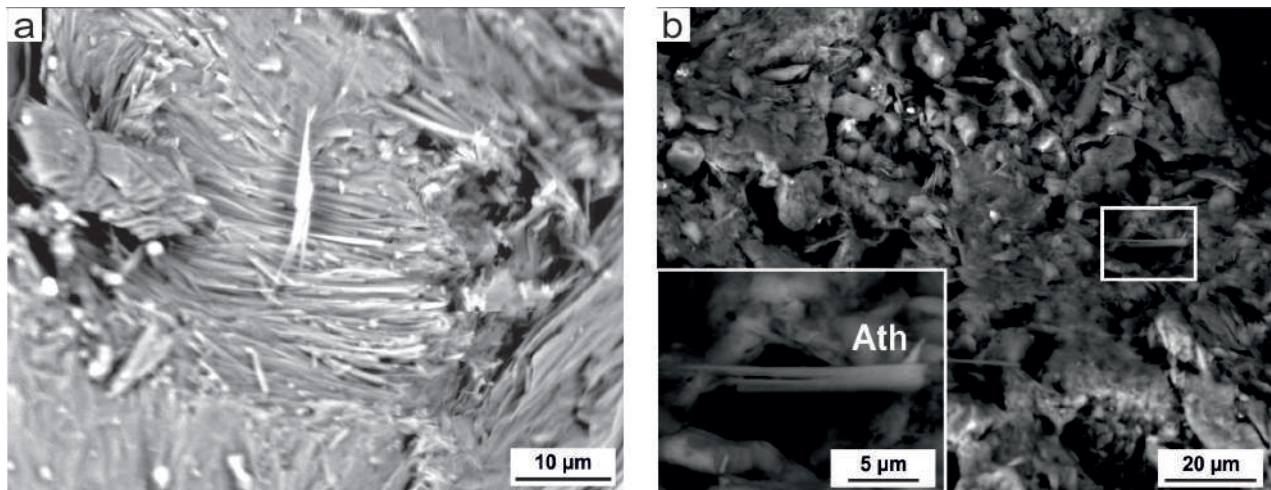

Fig. 5 - Selected Scanning Electron Microscope images of: a) representative morphology of asbestos fibers in serpentinite rocks and b) representative morphology of asbestos fiber in soil samples; Ath=Anthophyllite. Rectangle is zoomed image.

6. CONCLUSIONS

The multidisciplinary study on serpentinite rocks and derivative soils was carried out in the area of San Severino Lucano (Basilicata, Southern Italy) in order to determine the presence of naturally occurring asbestos, by means of different analytical techniques. This study outlined that in both rocks and derivative soils, there are asbestos minerals such as chrysotile and asbestos tremolite. Indeed, either chrysotile and asbestos tremolite were found in soils, suggesting that human activities can disturb and provoke the release of inhalable asbestos in the atmosphere, triggering thus mechanisms of hazardous exposition for population. Even if they usually occur in aggregates that cannot be suspended in the air, agricultural activities can destroy these soil aggregates with the formation of dust containing inhalable asbestos fibres, which evolve into airborne increasing thus the exposure to them.

Moreover, the present study revealed that serpentinite rocks cropping out near to San Severino village towns act as a perennial source of contamination for the agriculture lands. Since the dispersion of fibres could be associated with carcinogenic lung cancer, in our opinion in areas where NOA can be found, the institutions should publish local maps indicating areas with mineralogical concern and realization of constructions (e. g. road) must have dust control measure to avoid hazardous exposures. Finally, the values of trace metals in our samples are very high and by adopting the thresholds for soils, elements such as Cr, Co, Ni and V exceeds the regulatory thresholds for public, private and residential green use.
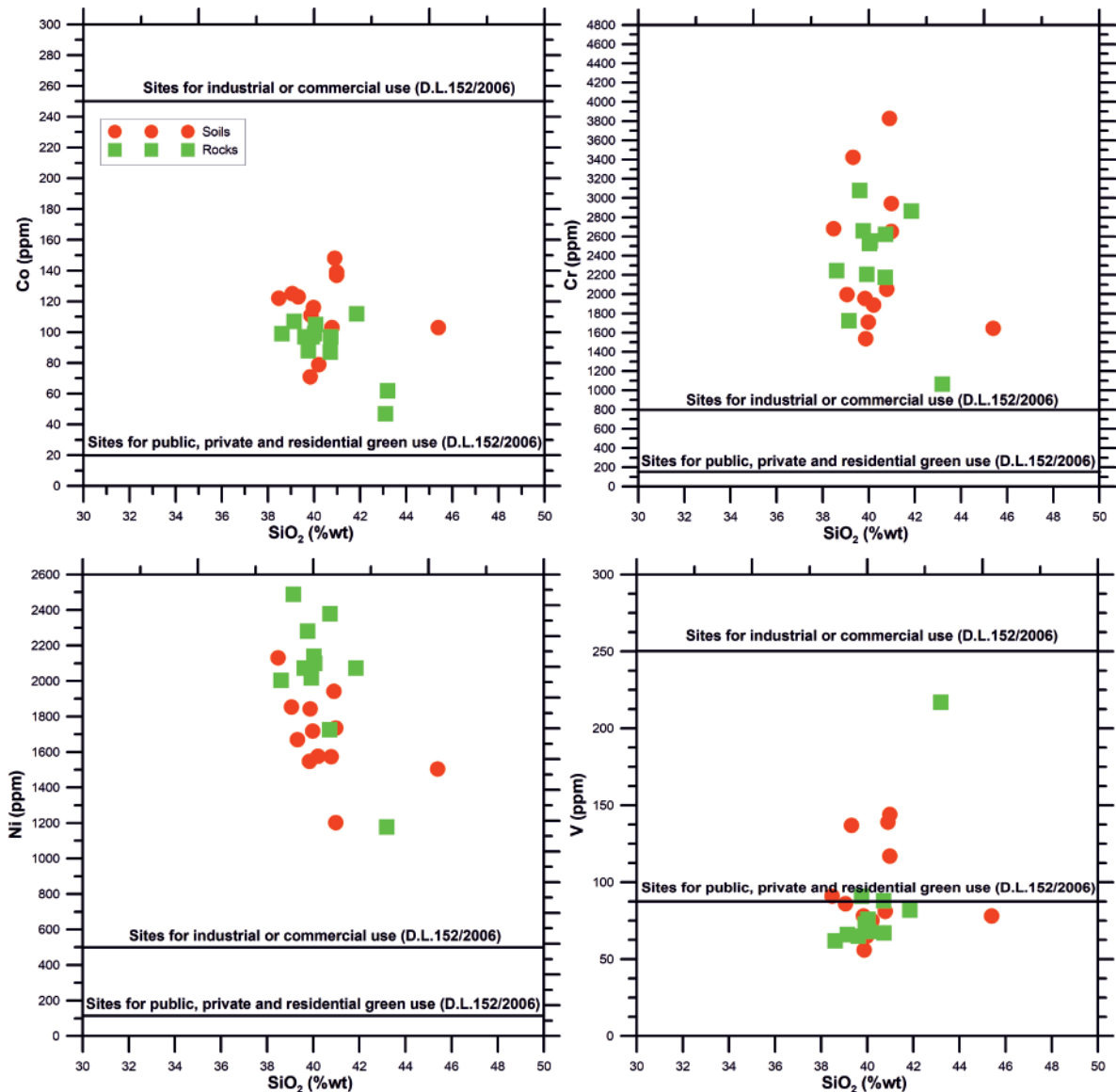
Fig. 6 - Correlation diagrams of SiO$_2$ versus Co, Cr, Ni and V for soils and rocks of the studied area. Thresholds values regulated by Italian law (D.L. 152/2006) are also indicated for each heavy metal.

REFERENCES

Acosta A., Pereira M.D., Shaw D.M., Bea F., 1997. Serpentinización de la peridotita de Ronda (cordillera Betica) comorespuesta a la interacción con fluidosricos en volátiles: comportamiento del boro. Revista de la Sociedad Geológica de España 10, 99-106.

Agency for Toxic Substances and Disease Registry (ATSDR), 2004. Toxicological profile for cobalt. Atlanta, GA: U.S. Department of Health and Human Services, Public Health Service.

Amodio Morelli L., Bonardi G., Colonna V., Dietrich D., Giunta G., Ippolito F., Liguori V., Lorenzoni S., Paglioncino A., Perrone V., 1976. L'arco Calabro Peloritano nell'orogene Appenninico-Maghrebide. Memorie della Società Geologica Italiana 17, 1-60.

Apollaro C., Dotsika E., Marini L., Barca D., Bloise A., De Rosa R., Doveri M., Lelli M., Muto F., 2012. Chemical and isotopic characterization of the thermo mineral watero of Terme Sibarite springs (Northern Calabria, Italy). Geochemical Journal 46, 117-129.

Apollaro C., Marini L., Critelli T., Barca D., Bloise A., De Rosa R., Liberi F., Miriello D., 2011. Investigation of rock-to-water release and fate of major, minor, and trace elements in the metabasalt-serpentinite shallow aquifer of Mt. Reventino (CZ, Italy) by reaction path modeling. Applied Geochemistry 26, 1722-1740.

Ballirano P., Bloise A., Gualtieri A.F., Lezzerini M., Pacella A., Perchiazzi N., Dogan M., Dogan A.U., 2017. The crystal structure of mineral fibres. In Gualtieri A.F. (Ed.), Mineral fibres: crystal chemistry, chemical-physical properties, biological interaction and toxicity. European Mineralogical

Union, London, 18, 17-53.

Baumann F., Buck B.J., Metcalf R.V., McLaurin B.T., Merkler D.J., Carbone M., 2015. The presence of asbestos in the natural environment is likely related to mesothelioma in young individuals and women from Southern Nevada. Journal of Thoracic Oncology 10, 731-737.

Bernardini P., Schettino B., Sperduto B., Giannadrea F., Burragato F., Castellino N., 2003. Tre Casi di mesotelioma pleurico ed inquinamento ambientale da rocce affioranti di tremolite in Lucania. Giornale Italiano di Medicina del Lavoro ed Ergonomia 25, 408-411.

Bloise A., Barrese E., Apollaro C., Miriello D., 2009. Flux growth and characterization of Ti and Ni doped forsterite single crystals. Crystal Research and Technology 44, 463-468.

Bloise A., Belluso E., Fornero E., Rinaudo C., Barrese E., Capella S., 2010. Influence of synthesis conditions on growth of Ni-doped chrysotile. Microporous and Mesoporous Materials 132, 239-245.

Bloise A., Barca D., Gualtieri A.F., Pollastri S., Belluso E., 2016b. Trace elements in hazardous mineral fibres. Environmental Pollution 216, 314-323.

Bloise A., Belluso E., Critelli T., Catalano M., Apollaro C., Miriello D., Barrese E., 2012. Amphiboleasbestos and other fibrous minerals in the meta-basalt of the Gimigliano-Mount Reventino Unit (Calabria, South-Italy). Rendiconti Online della Società Geologica Italiana 21, 847-848.

Bloise A., Catalano M., Barrese E., Gualtieri A.F., Gandolfi N.B., Capella S., Belluso E., 2016a. TG/DSC study of the thermal behaviour of hazardous mineral fibres. Journal of Thermal Analysis and Calorimetry 123, 2225-2239.

Bloise A., Catalano M., Critelli T., Apollaro C., Miriello D., 2017a. Naturally occurring asbestos: potential for human exposure, San Severino Lucano (Basilicata, Southern Italy). Environmental Earth Sciences 76, 648. 10.1007/s12665-017-6995-9

Bloise A., Critelli T., Catalano M., Apollaro C., Miriello D., Croce A., Barrese E., Liberi F., Piluso E., Rinaudo C., Belluso E., 2014. Asbestos and other fibrous minerals contained in the serpentinites of the Gimigliano-Mount Reventino Unit (Calabria, S-Italy). Environmental Earth Sciences 71, 3773-3786.

Bloise A., Kusiorowski R., Lassinantti Gualtieri M., Gualtieri A.F., 2017b. Thermal behaviour of mineral fibres. In Gualtieri A.F. (Ed.), Mineral fibres: crystal chemistry, chemical-physical properties, biological interaction and toxicity. European Mineralogical Union, London, 18, 215-252.

Bloise A., Punturo R., Catalano M., Miriello D., Cirrincione R., 2016c. Naturally occurring asbestos (NOA) in rock and soil and relation with human activities: the monitoring example of selected sites in Calabria (southern Italy). Italian Journal of Geosciences 135, 268-279.

Burragato F., Mastacchi R., Papacchini L., Rossini F., Sperduto B., 2004. Mapping of risks due to particulates of natural origin containing fibrous tremolite: the case of Seluci di Lauria (Basilicata, Italy). Natural Hazard Abstract, poster session NH 11.01 in European Geoscience Union, 1st General Assembly, Nice France 25-30 April 2004.

Burragato F., Comba P., Baiocchi V., Palladino D.M., Simei S., Gianfagna A., Pasetto R., 2005. Geo-volcanological, mineralogical and environmental aspects of quarry materials related to pleural neoplasm in the area of biancavilla, mount Etna (eastern sicily, italy). Environmental Geology 47, 855-868. 10.100

Cavalcante F., Belviso C., Laurita S., Prosser G., 2012. P-T constraints from phyllosilicates of the Liguride complex of the Pollino area (Southern Apennines, Italy): Geological inferences. Ofioliti, 37, 65-75. doi:10.4454/ofioliti.v37i2.406

Censi P., Zuddas P., Randazzo L.A., Tamburo E., Speziale S., Cuttitta A., Punturo R., Santagata R., 2011. Source and nature of inhaled atmospheric dust from trace element analyses of human bronchial fluids. Environmental Science and Technology 45, 6262-6267. 10.1021/es200539p

Censi P., Tamburo E., Speziale S., Zuddas P., Randazzo L.A., Punturo R., Aricò P., 2011a. Yttrium and lanthanides in human lung fluids probing the exposure to atmospheric fallout. Journal of Hazardous Materials 186, 1103-1110. 10.1016/j.jhazmat.2010.11.113

Cirrincione R., Fazio E., Fiannacca P., Ortolano G., Pezzino A., Punturo R., 2015. The Calabria-Peloritani Orogen, a composite terrane in Central Mediterranean; its overall architecture and geodynamic significance for a pre-Alpine scenario around the Tethyan basin. Periodico di Mineralogia 84(3B), 701-749. Special Issue: Progresses in deciphering structures and compositions of basement rocks. 10.2451/2015PM0446

Compagnoni R., Groppo C., 2006. Gli Amianti in Val di Susa e le rocce che li contengono. Rendiconti della Società Geologica Italiana 3, 21-28.

Compagnoni R., Ferraris G., Fiora L., 1983. Balangeorite, a new fibrous silicate related to gageite from Balangero, Italy. American Mineralogist 68, 214-219.

Compagnoni R., Ferraris G., Mellini M., 1985. Carlosturanite, a new asbestiform rock-forming silicate from Val Varaita, Italy. American Mineralogist 70, 767-772.

Constantopoulos S.H., 2008. Environmental mesothelioma associated with tremolite asbestos: Lessons from the experiences of turkey, greece, corsica, new caledonia and cyprus. Regulatory Toxicology and Pharmacology, 52, S110-S115. 10.1016/j.yrtph.2007.11.001

Crans D.C., Smee J.J., Gaidamauskas E., Yang L., 2004. The chemistry and biochemistry of vanadium and the biological activities exerted by vanadium compounds. Chemical Reviews 104, 849-902.

Gaggero L., Sanguineti E., Yus González A., Militello G.M., Scuderi A., Parisi G., 2017. Airborne asbestos fibres monitoring in tunnel excavation. Journal of Environmental Management, 196, 583-593. 10.1016/j.jenvman.2017.03.055

García-Barriuso M., Bernado S., Nabais C., Pereira D., Amich F., 2011. The Paleosubtropical element Notholaenamarantae (L.) Desv subsp. marantae in serpentine areas in the west of Iberian Peninsula: Phytogeochemical study, distribution and conservation. Biologia 66, 258-265.

Gianfagna A., Ballirano P., Bellatreccia F., Bruni B., Paoletti E., Oberti R., 2003. Characterization of amphibole fibres linked to mesothelioma in the area of Biancavilla, eastern

Sicily, Italy. Mineralogical Magazine 67, 1221-1229. 10.1180/0026461036760160

Guagliardi I., Rovella N., Apollaro C., Bloise A., De Rosa R., Scarciglia F., Buttafuoco G., 2016a. Effects of source rocks, soil features and climate on natural gamma radioactivity in the Crati valley (Calabria, southern Italy). Chemosphere 150, 97-108.

Guagliardi I., Rovella N., Apollaro C., Bloise A., De Rosa R., Scarciglia F., Buttafuoco G., 2016b. Modelling seasonal variations of natural radioactivity in soils: A case study in southern Italy. Journal of Earth System Science 125, 1569-1578.

Guagliardi I., Buttafuoco G., Apollaro C., Bloise A., De Rosa R., Cicchella D., 2013. Using gamma-ray spectrometry and geostatistics for assessing geochemical behaviour of radioactive elements in the Lese catchment (Southern Italy). International Journal of Environmental Research 7, 645-658.

Gualtieri A.F., 2017. Mineralfibres: crystalchemistry, chemical-physicalproperties, biologicalinteraction and toxicity. European Mineralogical Union and Mineralogical Society of Great Britain and Ireland, London, pp. 533.

Harper M., 2008. 10th Anniversary critical review: naturally occurring asbestos. Journal of Environmental Monitoring 10, 1394-1408.

IARC, 2009. Asbestos (chrysotile, amosite, crocidolite, tremolite, actinolite, and anthophyllite) IARC Monographs. Arsenic, Metals, fibres and dusts, International Agency for Research on Cancer, Lyon, 147-167.

Kretz R., 1983. Symbols for rock-forming minerals. American Mineralogist 68, 277-279.

Leake B.E. et al., 1997. Nomenclature of amphiboles: report of the subcommittee on amphiboles of the international mineralogical association, commission on new minerals and mineral names. The Canadian Mineralogist 35, 219-246.

Monaco C., Tortorici L., Paltrinieri W., 1998. Structural evolution of the Lucanian Apennines, southern Italy. Journal of Structural Geology 20, 617-638.

Monaco C., Tortorici L., 1995. Tettonica estensionale quaternaria nell'Arco Calabro e in Sicilia orientale. Studi Geologici Camerti 2, 351-362.

Nackerdien Z., Kasprzak K.S., Rao G., Halliwell B., Dizdaroglu M., 1991. Nickel (II)-and cobalt (II)-dependent damage by hydrogen peroxide to the DNA bases in isolated human chromatin. Cancer Research 51, 5837-5842.

Navarro R., Pereira D., Gimeno A., Del Barrio S., 2013. Verde Macael: A serpentinite wrongly referred to as a marble. Geosciences 3-1, 102-113.

NIOSH, 2008. Current Intelligence Bulletin (June 2008-Revised Draft) Asbestos and Other Elongated Mineral Particles: State of the Science and Roadmap for Research.

Ogniben L., 1969. Schema introduttivo alla geologia del confine calabro-lucano. Memorie della Società Geologica Italiana 8, 453-763.

Pasetto R., Bruni B., Bruno C., Cauzillo G., Cavone D., Convertini L., De Mei B., Marconi A., Montagano G., Musti M., Paoletti L., Comba P., 2004. Mesotelioma pleurico ed esposizione ambientale a fibre minerali: il caso di un'area rurale in Basilicata. Annali dell'Istituto Superiore di Sanità 40, 251-265.

Pereira M.D., Peinado M., Blanco J.A., Yenes M., 2008. Geochemical characterization of serpentinites at cabo ortegal, northwestern Spain. Canadian Mineralogist 46, 317-327. 10.3749/canmin. 46.2.317

Punturo R., Bloise A., Critelli T., Catalano M., Fazio E., Apollaro C., 2015. Environmental implications related to natural asbestos occurrences in the ophiolites of the Gimigliano-Mount Reventino Unit (Calabria, southern Italy). International Journal of Environmental Research 9, 405-418.

Sansone M.T.C., Prosser G., Rizzo G., Tartarotti P., 2012. Spinel-peridotites of the Frido unit ophiolites (southern apennine-Italy): Evidence for oceanic evolution. Periodico di Mineralogia 81, 35-59. 10.2451/2012PM0003.

Sansone M.T.C., Rizzo G., Mongelli G., 2011. Petrochemical characterization of mafic rocks from the Ligurian ophiolites, Southern Apennines. International Geology Review 53, 130-156. 10.1080/00206810902954993

Seilkop S.K., Oller A.R., 2003. Respiratory cancer risks associated with low-level nickel exposure: an integrated assessment based on animal, epidemiological, and mechanistic data. Regulatory Toxicology and Pharmacology 37, 173-190.

Shekhawat K., Chatterjee S., Joshi B., 2015. Chromium toxicity and its health hazards. International Journal of Advanced Research 3, 167-172.

Vezzani L., 1966. La sezione tortoniana di Perosa sul fiume Sinni presso Episcopia (Potenza). Geologica Romana 5, 263-290.

Vezzani L., 1969. La Formazione del Frido (Neocomiano-Aptiano) tra il Pollino e il Sinni. Geologica Romana 8, 129-176.

Vezzani L., 1970. Le ofioliti della zona tra Castelluccio Inferiore e S. Severino Lucano (Potenza). Accademia Gioenia di Scienze Naturali in Catania 7, 1-49.

World Health Organization, 1986. Asbestos and other natural mineral fibres. Environmental Health Criteria, 53. Geneva.

Worliczek E., 2017. Naturally occurring asbestos: The perception of rocks in the mountains of new caledonia. Environmental Transformations and Cultural Responses: Ontologies, Discourses, and Practices in Oceania, 187-214. 10.1057/978-1-137-53349-4_8

fibers

MDPI

Assessment of Serpentine Group Minerals in Soils: A Case Study from the Village of San Severino Lucano (Basilicata, Southern Italy)

Rosalda Punturo [1], Claudia Ricchiuti [1] and Andrea Bloise [2],*

[1]   Department of Biological, Geological and Environmental Sciences, University of Catania, Corso Italia, 55, 95129 Catania, CT, Italy; punturo@unict.it (R.P.); claudia.ricchiuti@unict.it (C.R.)
[2]   Department of Biology, Ecology and Earth Sciences, University of Calabria, Via Pietro Bucci, I-87036 Rende, Italy
*   Correspondence: andrea.bloise@unical.it; Tel.: +39-0984-493588

check for updates

Abstract: Naturally occurring asbestos (NOA) is a generic term used to refer to both regulated and un-regulated fibrous minerals when encountered in natural geological deposits. These minerals represent a cause of health hazard, since they have been assessed as potential environmental pollutants that may occur both in rocks and derived soils. In the present work, we focused on the village of San Severino Lucano, located in the Basilicata region (southern Apennines); due to its geographic isolation from other main sources of asbestos, it represents an excellent example of hazardous and not occupational exposure of population. From the village and its surroundings, we collected eight serpentinite-derived soil samples and carried out Differential Scanning Calorimetry (DSC), Derivative Thermogravimetric (DTG) and Transmission Electron Microscopy with Energy Dispersive Spectrometry (TEM-EDS), in order to perform a detailed characterization of serpentine varieties and other fibrous minerals. Investigation pointed out that chrysotile and asbestos tremolite occur in all of the samples. As for the fibrous but non-asbestos classified minerals, polygonal serpentine and fibrous antigorite were detected in a few samples. Results showed that the cultivation of soils developed upon serpentinite bedrocks were rich in harmful minerals, which if dispersed in the air can be a source of environmental pollution.

Keywords: serpentine varieties; naturally occurring asbestos; health hazard; serpentinite soil

1. Introduction

As it is known, the term "asbestos" represents a group of six fibrous silicate minerals: chrysotile (serpentine group) and amphibole group as: tremolite, actinolite, anthophyllite, amosite and crocidolite [1,2]. In the past, asbestos was plenty been exploited and marketed for the use in industrial and commercial products, mainly as building material [3]. All types of asbestos cause lung cancer, mesothelioma, cancer of the larynx and ovary, and asbestosis (fibrosis of the lungs) [2]. It has been assessed that exposure to asbestos occurs through inhalation of airborne fibers in various contexts such as the working environment, ambient air in the vicinity of point sources such as factories handling asbestos, or indoor air in housing and buildings containing friable asbestos materials [4]. Nevertheless, it is worth noting that natural occurrences of asbestos represent a cause of health hazard, which is sometimes overlooked and difficult to properly monitor. Indeed, naturally occurring asbestos (NOA) is a generic term used to refer to both regulated and non-regulated fibrous minerals when encountered in natural geological deposits [5]. Now-a-days, only the six varieties above listed are regulated as potential environmental pollutants by law (in Europe and in several countries

worldwide), even though other asbestiform minerals such as balangeorite, erionite, fibrous antigorite and fluoro-edenite [6–9] are non-asbestos classified and, therefore, not regulated by law but could be potentially dangerous if inhaled. On the basis of the effects of asbestos on biological systems, several authors ascribe the asbestos-fibers toxicity to the synergetic effect of fiber size, bio-persistence and chemical composition [10–13]; this latter is related to the high capability of asbestos minerals to host a large number of toxic elements; for this reason, due to interactions between lung fluids and inhaled atmospheric dust [14,15], some researchers claimed that asbestos fibers may play a passive role in producing diseases as carriers of heavy metals that may be then released into the environment [16]. In general, many factors such as natural weathering processes (e.g., erosion) and human activities (e.g., excavation, road construction, agricultural activities) contribute to NOA release in the environment [13,17], enhancing hazard of people who live near to NOA deposits around the world [18–25].

In the present study we focused on the Basilicata region (Italy) [26], where an increased number of lung disease cases were related to the environmental exposure to asbestos [27–29]. The village and its surroundings represent an excellent example of hazardous and not occupational exposure of population to asbestos, because of the geographic isolation and its distance from other main sources of asbestos for instance.

Recently, a work by Punturo et al. [30] dealt with the characterization by X-Ray Fluorescence (XRF), X-Ray Powder Diffraction (XRPD) and Scanning and Electron Microscopy (SEM) of the soils of San Severino Lucano, reporting their potential for hazardous exposure of population, because of their heavy metal content. However, the discrimination among the serpentine group minerals (i.e., lizardite, antigorite chrysotile, polygonal serpentine) was not achievable by using only X-ray powder diffraction, because the diffraction peaks overlap each other. Moreover, scanning electron microscopy (SEM) alone could not determine the diameter of single fibrils. Since these last techniques were not able to identify the different serpentine varieties, in this work a more targeted characterization of soil samples was performed by Differential Scanning Calorimetry (DSC), Derivative thermogravimetric (DTG) and Transmission Electron Microscopy with Energy Dispersive Spectrometry (TEM-EDS). We collected eight serpentinite soil samples and cross-checked the data obtained from DSC, DTG and TEM-EDS, in order to perform a detailed characterization and discrimination among the serpentine varieties and other fibrous minerals, as well as to relate NOA release in the environment due to agricultural activity. Investigation highlighted that chrysotile and asbestos tremolite are the asbestos minerals occurring in all of the analyzed soils, appearing both as single fibrils and bundles. As for the fibrous but non-asbestos classified minerals, polygonal serpentine and fibrous antigorite were detected in a few samples. Because of the fibrous structure, longitudinal splitting of these minerals is very common, creating thus fibers having the same length as the original one but with smaller diameter. Furthermore, the cultivation of soils developed on serpentinite bedrocks could enhance this process and provoke the release of smaller fibrils into the environment, increasing thus the exposure of population to asbestos risk. Results may provide a useful tool for planning prevention measures during agricultural activities, in order to diminish negative effects of NOA on health.

2. Geological Setting

This study area encompasses approximately 20 km^2 in the Pollino National Park [16], which is located at the borders between the Basilicata and Calabria regions (southern Italy; Figure 1).
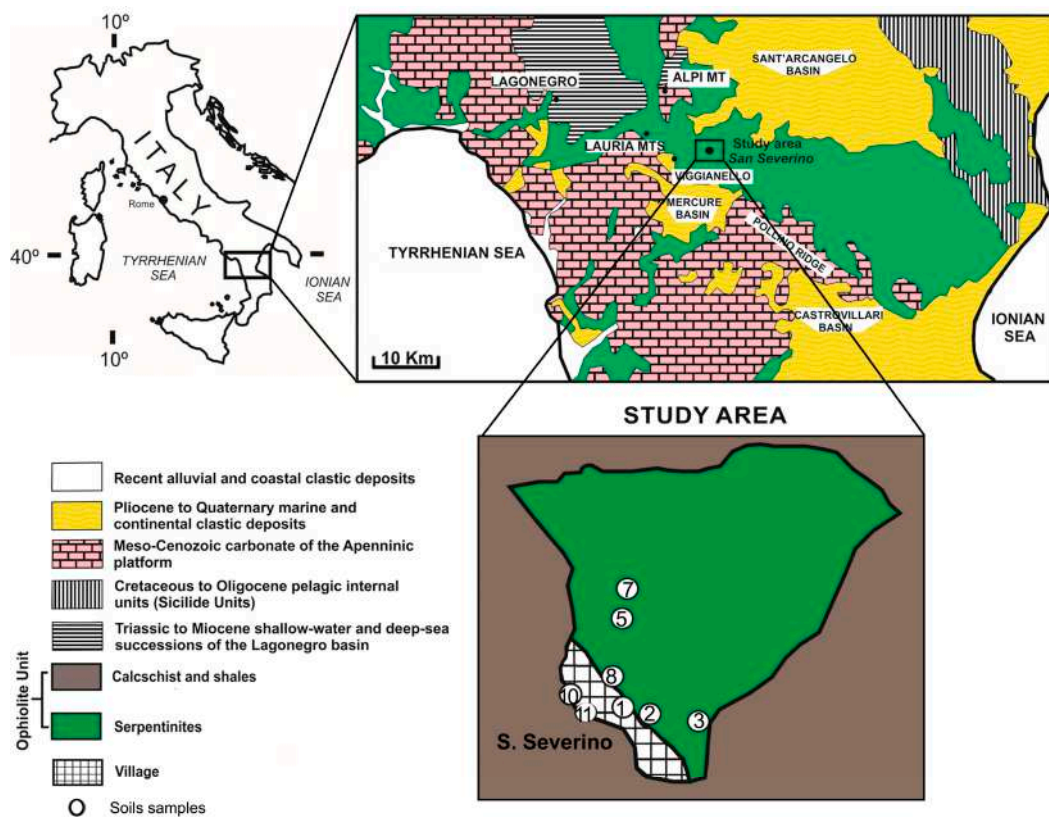
Figure 1. Geological map of the Calabria-Lucania border (modified after [30]) and study area location with sampling sites.

The area is characterized by the terrains of the Liguride Complex, which consists of three main tectonic units of Upper Jurassic to Upper Oligocene age [31]: (1) the Calabro-Lucano Flysch [32], a unit that did not underwent any metamorphism and partly corresponds to the North-Calabrian Unit; (2) the metamorphic terranes of the Frido Unit [33,34]; (3) syn-orogenic turbiditic sequences, i.e., the Saraceno Formation, the Albidona Formation, and a sequence composed of alternating shales, mudstones and sandstones, the latter corresponding to the Perosa Unit as defined by Vezzani [35]. The ophiolites of the Southern Apennine Liguride Units occur in the Frido Unit and in the North-Calabrian Unit. In particular, ophiolitic rocks of the Frido Unit consist of lenticular metabasites interbedded with cataclastic and highly fractured serpentinite rocks [36]. Metabasite rocks are foliated and fine-grained, with rare remnants of porphyritic texture. They are often intercalated with serpentinites, slates and metacarbonate rocks [37], forming sequences with a maximum thickness of several dozen metres. Serpentinite rocks, which are green-bluish in colour, represent mantle peridotites [38]. Locally, serpentinites are very brittle, as indicated by the large number of fractures that are usually filled by amphibole asbestos. As it may be observed on Figure 1, serpentinite lithotypes constitute the bedrock of the village of San Severino Lucano and its surroundings. The detailed field survey carried out along the transect of sampling sites located at San Severino village and its surroundings (Figure 1), highlighted that the area is characterized by sparse vegetation and by soils developed on serpentinite bedrocks (Figure 2a–e).
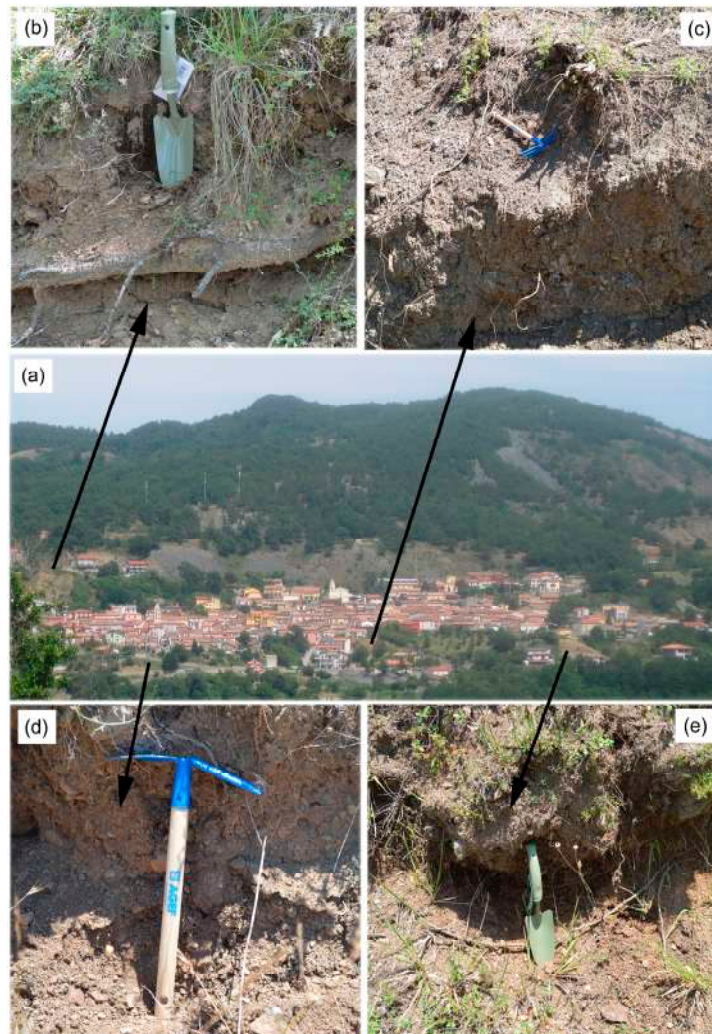
Figure 2. (**a**) Distant view of the San Severino Village (modified after [26]); (**b**) soil outcrop that contain NOA (Spol8); (**c**) soil outcrop (Spol1); (**d**) soil outcrop (Spol10); (**e**) soil outcrop (Spol2).

3. Materials and Methods

Eight serpentinite derivative soil samples (Spol1,2,3,5,7,8,10,11) were collected mainly within to urban center and analyzed by using TEM-EDS and thermal analyzes (DSC, DTG) at the University of Calabria (DiBEST laboratory), in order to investigate their mineralogical features and to assess the occurrence of asbestiform minerals, which are considered to be potentially hazardous for human health [13]. It is worth mentioning that combination of both analytical methodologies, i.e., thermal analysis and TEM-EDS, permitted successful identification of distinct serpentine minerals (antigorite, lizardite, chrysotile, and polygonal serpentine) and the characterization of amphibole asbestos [13]. Moreover, the length of fibrous antigorite and polygonal serpentine fibers has been measured using the TEM micrographs, adding further details to the previous observations carried out with SEM [30]. The soil samples were pre-treated with H_2O_2 and pre-heated for 24 h at 530 °C, in order to remove the organic compounds and so that they could be subsequently ground. Size and chemical composition of single fibers were determined using a Jeol JEM 1400 Plus (120 kV) Transmission Electron Microscope equipped with Jeol large-area silicon drift detector SDD-EDS (Jeol, Tokyo, Japan) for microanalyses. For TEM investigation, each sample was put into isopropyl alcohol and then sonicated. Three drops of the obtained suspension were deposited on a Formvar carbon-coated copper grid.

Thermogravimetry (TG) and differential scanning calorimetry (DSC) were performed in an alumina crucible under a constant aseptic air flow of 30 mL·min^{-1} with a Netzsch STA 449 C

Jupiter (Netzsch-Gerätebau GmbH, Selb, Germany) in the 25–1000 °C temperature range with a heating rate of 10 °C·min^{-1} and 20 mg of sample powder. Instrumental precision was checked by 5 repeated collections on a kaolinite reference sample revealing good reproducibility (instrumental theoretical T precision of ±1.2 °C). Netzsch Proteus thermal analysis software (Netzsch-Gerätebau GmbH, Selb, Germany) was used to identify exo- and endothermic peaks, weight loss and derivative thermogravimetric (DTG).

4. Results

4.1. TEM Characterization

TEM has been mainly useful to determine the occurrence of serpentine varieties and their morphological features in the soil samples; indeed, distinct fibrous serpentine varieties have been found such as chrysotile, fibrous antigorite, polygonal serpentine and tremolite (Figure 3). They exhibit various shape and size. Chrysotile appears as thin individual fibers (known as fibrils) and often forms relatively larger longitudinally aligned fibers (Figure 3a,b).
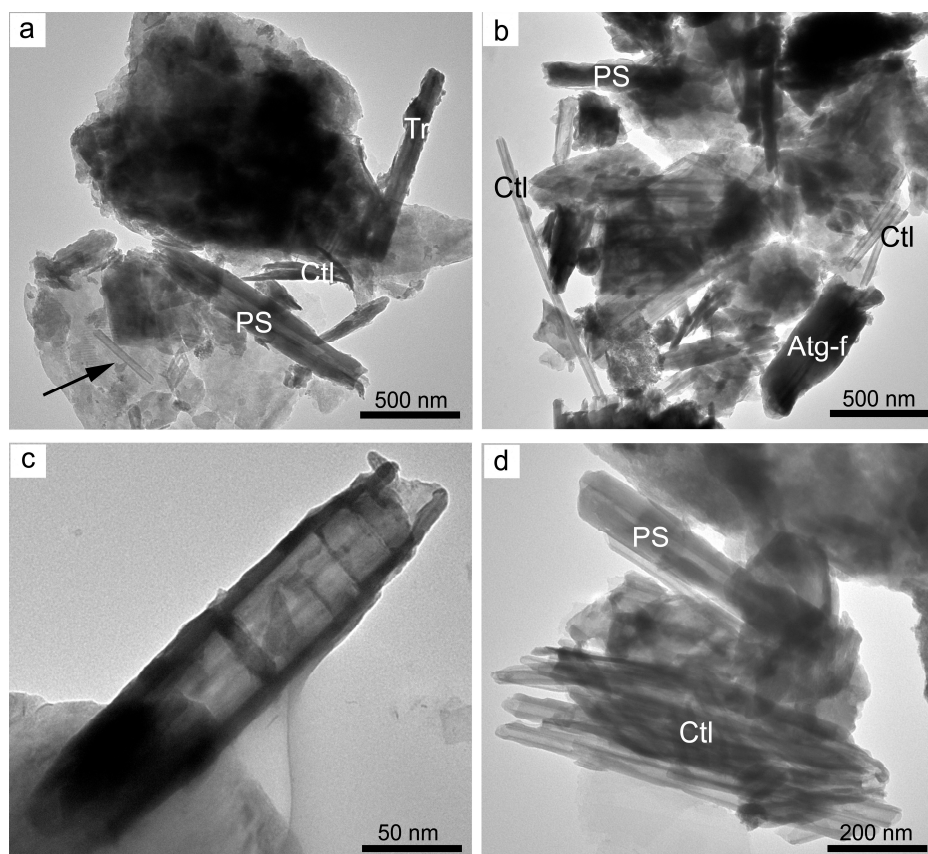

Figure 3. Representative TEM images of fibrous mineral detected in the soil samples: (**a**) bundles of chrysotile fibers; chrysotile fiber characterized by the empty central cavity and thin outer walls indicated by black arrow; polygonal serpentine and fibrous tremolite (sample Spol1); (**b**) chrysotile fibers, polygonal serpentine and fibrous antigorite (Spol3); (**c**) chrysotile fiber partially unrolled from the inside like cylinder-in-cylinder morphology (Spol10); (**d**) polygonal serpentine and bundles of chrysotile fibers (Spol11). Ctl = chrysotile; Tr = tremolite; Atg-f = fibrous antigorite; PS = polygonal serpentine (mineral symbols after Whitney and Evans [39]).

From Figures 3 and 4 it is evident the classical cylindrical shape of chrysotile fibers; this is the most common morphology in all of the samples, consisting of an empty central cavity (core) along throughout their length. The length varies from 300 to 1500 nm and the diameter of the core is about

20 nm and 40 nm inner and outer, respectively. In some samples the outer walls of chrysotile are very thin and the central tube (core) is wide, measuring about 40 nm (Figure 3a,b). This proves that the chrysotile underwent an unrolling process from the inside during the process of alteration from rock to soil, likely caused by the passage of water through the core (Figure 3c). Chrysotile with cylinder-en-cylinder and proto-cylinder morphologies have also been found with TEM investigation; these do not show the well-defined wrapping of layers and cylindrical shape that the chrysotile fibers exhibited (Figure 4).
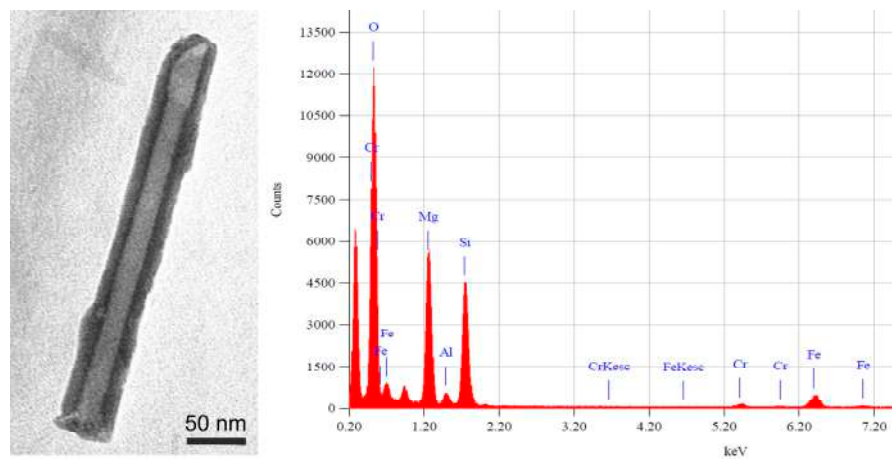

Figure 4. Single cylinder chrysotile with the relative point analysis (Spol1).

Fibrous polygonal serpentine is another structural variety that has been found in most of the studied samples (Table 1); it occurs in lower amount and has very often a diameter larger than 100 nm and wider than the chrysotile individuals (Figure 3a,b,d). Antigorite fibers are the shortest, with length and width of 1000 and 300 nm respectively. However, fibrous antigorite has been identified only in two samples (Figure 3b; Table 1), with platy antigorite the most abundant morphology observed in all of the studied specimens. Lizardite with platy morphology was also detected in a few samples (Table 1). Tremolite fibers have also been observed. TEM micrographs reported on Figures 3a and 5, show the typical morphology of tremolite fibers, which exhibit prismatic rod-shaped morphology lacking of any flexibility. In these fibers, the average length ranges from 2.5 μm to 3 μm and the diameter is about 0.2 μm.
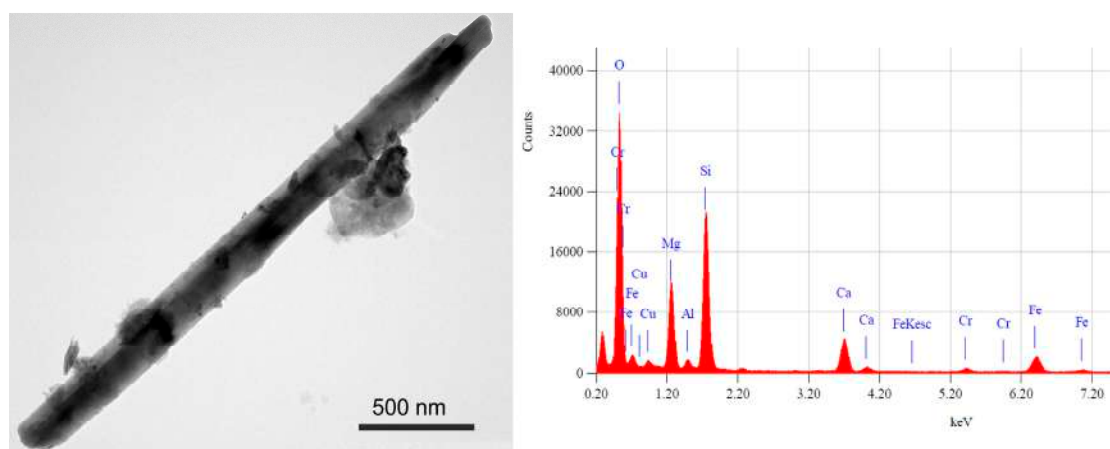

Figure 5. Single tremolite fiber with the relative point analysis (Spol1).

Table 1. Studied localities, reference coordinates and, for each collected soil sample, mineralogical assemblage detected by X-ray powder diffraction (XRPD) and by scanning electron microscopy combined with energy dispersive spectrometry (SEM-EDS) * after [30]. Serpentine minerals varieties and amphiboles detected by DSC, DTG and TEM-EDS. Chlorite (Chl), chrysotile (Ctl), polygonal serpentine (PS), lizardite (Liz), fibrous antigorite (f-Ant), antigorite (Atg) and tremolite (Tr) (mineral symbols after Whitney and Evans [39]). Amphiboles present in the samples were classified according to the amphibole diagram classification [40].

Sample	Site Description	Longitude (East)	Latitude (North)	Phases Detected
Spol1	At the entrance of the Village	597,417	4,429,775	Ctl, PS, Ant, Tr (Di, Qtz, Mnt-Chl) *
Spol2	At the entrance of the Village	597,405	4,430,523	Ctl, f-Ant (Di, Qtz, Mnt-Chl, Tr) *
Spol3	Road cut outside the Village	597,808	4,430,474	Ctl, PS, Liz, f-Ant (Di, Qtz, Mnt-Chl, Tr) *
Spol5	Road cut outside the Village	597,270	4,431,103	Ctl, Liz, Ant (Di, Qtz, Mnt-Chl, Tr, Chm, Ms) *
Spol7	Road cut outside the Village	597,323	4,431,363	Ctl, Tr, (Di, Qtz, Mnt-Chl, Chm) *
Spol8	Road cut within the Village	597,223	4,430,711	Ctl, PS, Ant (Di, Qtz, Mnt-Chl, Tr, Chm) *
Spol10	Road cut within the Village	596,890	4,430,715	Ctl, PS, Ant (Di, Qtz, Mnt-Chl, Tr, Chm, Mo) *
Spol11	Road cut within the Village	596,890	4,430,715	Ctl, PS (Di, Qtz, Mnt, Tr, Chm) *

4.2. Thermal Analysis Characterization

Thermal analysis of all representative soil samples enabled us to recognize the constituent mineralogical phases, and in particular the serpentine varieties (i.e., antigorite, lizardite, chrysotile, polygonal serpentine) (Table 1). In Figure 6a, the DSC patterns describe the thermal behavior of the investigated samples. In the temperature range between 500 and 850 °C, chrysotile lost its chemical-bonded water (strong endothermic peak on average temperature at 630 °C, Figure 6b) causing the complete breakdown of the mineral structure. At higher temperature value, the crystallization of forsterite [41] generates a sharp exothermic peak recorded at about 830 °C (Figure 6a; Table 2). After thermal analysis, the chrysotile structure has completely changed at a molecular scale because of a phenomenon called pseudomorphosis, which leads to the complete transformation of asbestos minerals into non-hazardous silicates such as forsterite [42,43].
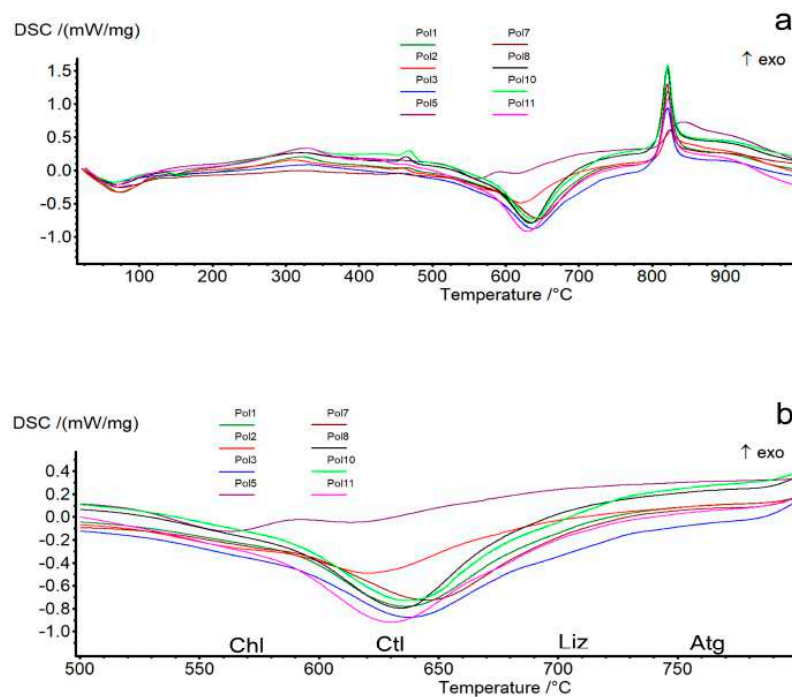

Figure 6. (**a**) Comparison among differential scanning calorimetry (DSC) curves of the soils located within or near the village of San Severino Lucano Village (Basilicata, Southern Italy); (**b**) zoom of (**a**) in the temperature range of 500–800 °C.

Table 2. Peak temperatures in DSC and DTG curves. W = weak, vw = very weak, s = strong, ss = very strong, sh = shoulder, en = endothermic, ex = exothermic.

Samples	Spol1	Spol2	Spol3	Spol5	Spol7	Spol8	Spol10	Spol11
				DSC				
Chl				563 en(w)				
Ctl	636 en(s)	621 en(s)	638 en(s)	612 en(w)	645 en(w)	634 en(s)	637 en(s)	630 en(s)
Fo	822 ex(ss)	824 ex(ss)	821 ex(ss)	844 ex(s)	821 ex(ss)	821 ex(ss)	822 ex(ss)	822 ex(ss)
				DTG				
Chl		564 en(vw)		563 en(w)				
Ctl	637 en(ss)	619 en(s)	638 en(s)	614 en(w)	647 en(ss)	634 en(s)	639 en(ss)	631 en(ss)
PS	679 en(vw)		686 en(vw)			677 en(vw)	688 en(vw)	679 en(vw)
Liz			736 en(sh)	744 en(sh)				
Ant	774 en(sh)	784 en(vw)	784 en(sh)	790 en(w)		778 en(sh)	770 en(sh)	

DTG curves appear to be similar for most of the samples and show the main endothermic peaks related to the mineralogical phases decomposition between 500 and 830 °C (Figure 7). A weak endothermic peak at 563 and 564 °C for Spol2 and Spol5 respectively, is linked to the presence of a small amount of chlorite. For all samples, the very strong endothermic peak in a temperature range of 614–639 °C, clearly showed the presence of chrysotile in high amount (Table 2).

Polygonal serpentine occurs in most of the samples showing a weak endothermic peak in a range of 677–688 °C, whereas only two samples, Spol3 and Spol5, are characterized by an endothermic shoulder at 736 and 744 °C related to the presence of lizardite (Table 2). Finally, the occurrence of antigorite is confirmed by the endothermic peak in a T range of 770–790 °C (Table 2).
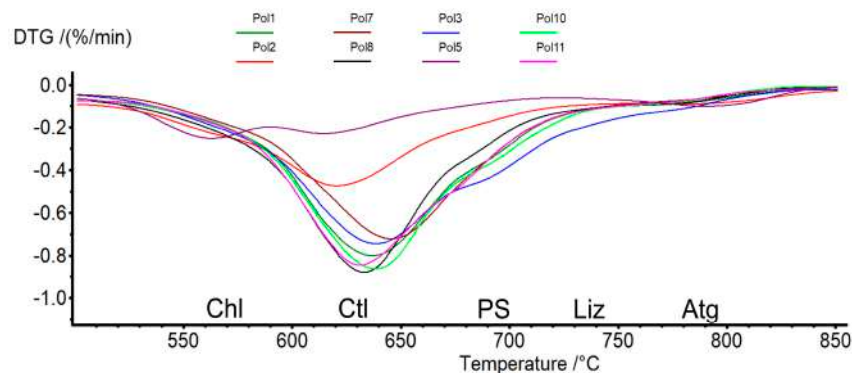

Figure 7. Comparison among DTG curves in the temperature range of 500–850 °C: endothermic peaks related to chlorite (Chl), chrysotile (Ctl), polygonal serpentine (PS), lizardite (Liz) and antigorite (Atg) decomposition.

The TG data reported on Table 3, show the values of 1–4% mass loss at a temperature up to 110 °C due to the adsorbed water and total weight losses of about 12–18% up to 1000 °C in all of the samples, mainly due to the breakdown of serpentine minerals according to the literature data [44,45]. Some samples have high values of total water loss at 1000 °C (i.e., 18%) due to two reasons: (i) presence of other hydrated minerals in addition to the serpentine polymorphs (Table 1); and (ii) the presence of water (physically bound) trapped between the fibrous bundles of chrysotile [46].

Table 3. TG data (weight loss % up to 110 °C and up to 1000 °C) for the analyzed samples.

Spol1		Spol2	
T range (°C)	TG loss %	T range (°C)	TG loss %
<110	3.57	<110	3.30
TOT loss at 1000	17.44	TOT loss at 1000	14.80
Spol3		Spol5	
T range (°C)	TG loss %	T range (°C)	TG loss %
<110	1.47	<110	3.94
TOT loss at 1000	13.13	TOT loss at 1000	12.08
Spol7		Spol8	
T range (°C)	TG loss %	T range (°C)	TG loss %
<110	2.16	<110	2.39
TOT loss at 1000	12.24	TOT loss at 1000	14.90
Spol10		Spol11	
T range (°C)	TG loss %	T range (°C)	TG loss %
<110	1.96	<110	2.78
TOT loss at 1000	15.40	TOT loss at 1000	15.42

5. Discussion and Conclusions

The results obtained by thermal analysis and transmission electron microscope showed that chrysotile and asbestos tremolite are the asbestos minerals occurring in all of the analyzed soil samples in the area of san Severino Lucano village (southern Apennines). Chrysotile appears both as bundles and single fibrils with typical cylindrical shape with diameter and length shorter of 0.25 and 5 μm, respectively; it is interesting to point out as the most common morphology of chrysotile fibers is the classical cylindrical shape consisting of an empty central cavity throughout the length. Moreover, some chrysotile fibers are characterized by very thin outer walls and by wide central tube, proving that chrysotile, during the process of alteration in the passage from rock to soils underwent unrolling process from the inside; this is likely caused by the passage of water through the core. As far as occurring amphibole, results showed that it is tremolite, whose fibers exhibit prismatic rod-shaped morphology lacking of any flexibility. The average length ranges from 2.5 μm to 3 μm and the diameter is about 0.2 μm.

According to many authors, fibers shorter than 5 μm and very thin <0.25 μm may have considerable carcinogenic potential [47–49]. Therefore, both techniques applied revealed to be a useful tool for determining the occurrence of asbestiform varieties and their morphological features in the studied soil samples, permitting asbestos minerals to be univocally identified and investigated in detailed, revealing that the fibers found within the studied soil samples show a size that may be associated with carcinogenesis when breathed.

It is important to specify that, in addition to the minerals regulated as asbestos by the Italian law, also asbestiform minerals such as fibrous antigorite could be potentially dangerous if inhaled [9]. In this work, polygonal serpentine and antigorite were the fibrous minerals detected in five and two samples respectively, while the other minerals identified were non-fibrous and most of them showing platy morphology (e.g., lizardite, chlorite). The village of San Severino is a significant example of a settlement built on NOA-bearing outcrops [50,51] and the risk of inhaling airborne fibers of asbestos around the village increases due to the agricultural activities which are among the main resources for the economy of the area. The cultivation of soils developed on serpentinite bedrocks could provoke the fiber splitting into smaller fibrils that are widely spread out into the environment, increasing thus the exposure to them. Since asbestos occurrence in soils is a serious health problem, in many parts of the world, asbestos-containing land has been abandoned and countries with this problem have suffered economic losses due to depreciation of properties. The use of soils containing asbestos for agricultural purposes can increase the presence of fibers in the air, necessitating adequate attention to ensuring the protection of workers and general public, as already pointed out by dedicated agencies. It is useless to

create unjustified alarmism in population; at the same time, inhabitants who live in countryside areas where NOA is present, should be aware that as now-a-days various techniques are available to limit or eliminate the presence of airborne fibers deriving from the processing of the soil, thus diminishing the risks related; among them, it is worth mentioning: (i) the use of tractors with air-conditioned and filtered cabins; (ii) wet the ground before hoeing it; (iii) wear overalls and masks suitable for protection from airborne asbestos fibers.

In conclusion, results presented in this work may provide a useful tool for planning prevention measures during human activities, in order to diminish negative effects of NOA on health.

References

1. World Health Organization (WHO). *Asbestos and Other Natural Mineral Fibers. Environmental Health Criteria, 53*; World Health Organization: Geneva, Switzerland, 1986; p. 194.

2. National Institute for Occupational Safety and Health (NIOSH). *Asbestos and Other Elongated Mineral Particles: State of the Science and Roadmap for Research*; Current Intelligence Bulletin, June 2008-Revised Draft; National Institute for Occupational Safety and Health (NIOSH): Washington, DC, USA, 2008.

3. Punturo, R.; Cirrincione, R.; Pappalardo, G.; Mineo, S.; Fazio, E.; Bloise, A. Preliminary laboratory characterization of serpentinite rocks from Calabria (southern Italy) employed as stone material. *J. Mediterr. Earth Sci.* **2018**, *10*, 79–87.

4. International Agency for Research on Cancer (IARC). *Asbestos (Chrysotile, Amosite, Crocidolite, Tremolite, Actinolite, and Anthophyllite) IARC Monographs. Arsenic, Metals, Fibers and Dusts*; International Agency for Research on Cancer: Lyon, France, 2009; pp. 147–167.

5. Harper, M. 10th Anniversary critical review: naturally occurring asbestos. *J. Environ. Monit.* **2008**, *10*, 1394–1408. [CrossRef] [PubMed]

6. Compagnoni, R.; Ferraris, G.; Fiora, L. Balangeroite, a new fibrous silicate related to gageite from Balangero, Italy. *Am. Mineral.* **1983**, *68*, 214–219.

7. Ballirano, P.; Pacella, A.; Bloise, A.; Giordani, M.; Mattioli, M. Thermal Stability of Woolly Erionite-K and Considerations about the Heat-Induced Behaviour of the Erionite Group. *Minerals* **2018**, *8*, 28. [CrossRef]

8. Gianfagna, A.; Ballirano, P.; Bellatreccia, F.; Bruni, B.; Paoletti, E.; Oberti, R. Characterization of amphibole fibers linked to mesothelioma in the area of Biancavilla, eastern Sicily, Italy. *Mineralog. Mag.* **2003**, *67*, 1221–1229. [CrossRef]

9. Cardile, V.; Lombardo, L.; Belluso, E.; Panico, A.; Capella, S.; Balazy, M. Toxicity and Carcinogenicity Mechanisms of Fibrous Antigorite. *Int. J. Environ. Res. Public Health* **2007**, *4*, 1–9. [CrossRef] [PubMed]

10. Gualtieri, A.F. *Mineral Fibers: Crystalchemistry, Chemical-Physicalproperties, Biological Interaction and Toxicity*; European Mineralogical Union and Mineralogical Society of Great Britain and Ireland: London, UK, 2017; p. 533.

11. Pugnaloni, A.; Giantomassi, F.; Lucarini, G.; Capella, S.; Bloise, A.; Di Primio, R.; Belluso, E. Cytotoxicityinduced by exposure to natural and synthetic tremolite asbestos: An in vitro pilot study. *Acta Histochem.* **2013**, *115*, 100–112. [CrossRef] [PubMed]

12. Bloise, A.; Catalano, M.; Barrese, E.; Gualtieri, A.F.; Gandolfi, N.B.; Capella, S.; Belluso, E. TG/DSC study of the thermal behaviour of hazardous mineral fibers. *J. Therm. Anal. Calorim.* **2016**, *123*, 2225–2239. [CrossRef]

13. Bloise, A.; Punturo, R.; Catalano, M.; Miriello, D.; Cirrincione, R. Naturally occurring asbestos (NOA) in rock and soil and relation with human activities: The monitoring example of selected sites in Calabria (southern Italy). *Ital. J. Geosci.* **2016**, *135*, 268–279. [CrossRef]

14. Censi, P.; Zuddas, P.; Randazzo, L.A.; Tamburo, E.; Speziale, S.; Cuttitta, A.; Punturo, R.; Santagata, R. Source and nature of inhaled atmospheric dust from trace element analyses of human bronchial fluids. *Environ. Sci. Technol.* **2011**, *45*, 6262–6267. [CrossRef] [PubMed]

15. Censi, P.; Tamburo, E.; Speziale, S.; Zuddas, P.; Randazzo, L.A.; Punturo, R.; Aricò, P. Yttrium and lanthanides in human lung fluids, probing the exposure to atmospheric fallout. *J. Hazard. Mater.* **2011**, *186*, 1103–1110. [CrossRef] [PubMed]

16. Bloise, A.; Barca, D.; Gualtieri, A.F.; Pollastri, S.; Belluso, E. Trace elements in hazardous mineral fibres. *Environ. Pollut.* **2016**, *216*, 314–323. [CrossRef] [PubMed]

17. Punturo, R.; Bloise, A.; Critelli, T.; Catalano, M.; Fazio, E.; Apollaro, C. Environmental implications related to natural asbestos occurrences in the ophiolites of the Gimigliano-Mount Reventino Unit (Calabria, southern Italy). *Int. J. Environ. Res.* **2015**, *9*, 405–418.

18. Acosta, A.; Pereira, M.D.; Shaw, D.M.; Bea, F. Serpentinización de la peridotita de Ronda (cordillera Betica) comorespuesta a la interacción con fluidosricos en volátiles: comportamiento del boro. *Rev. Soc. Geol. Esp.* **1997**, *10*, 99–106.

19. Burragato, F.; Comba, P.; Baiocchi, V.; Palladino, D.M.; Simei, S.; Gianfagna, A.; Pasetto, R. Geo-volcanological, mineralogical and environmental aspects of quarry materials related to pleural neoplasm in the area of Biancavilla, Mount Etna (Eastern Sicily, Italy). *Environ. Geol.* **2005**, *47*, 855–868. [CrossRef]

20. Constantopoulos, S.H. Environmental mesothelioma associated with tremolite asbestos: Lessons from the experiences of Turkey, Greece, Corsica, New Caledonia and Cyprus. *Regul. Toxicol. Pharmacol.* **2008**, *52*, 110–115. [CrossRef] [PubMed]

21. Pereira, M.D.; Peinado, M.; Blanco, J.A.; Yenes, M. Geochemical characterization of serpentinites at cabo ortegal, northwestern Spain. *Can. Mineral.* **2008**, *46*, 317–327. [CrossRef]

22. Bloise, A.; Belluso, E.; Critelli, T.; Catalano, M.; Apollaro, C.; Miriello, D.; Barrese, E. Amphibole asbestos and other fibrous minerals in the meta-basalt of the Gimigliano-Mount Reventino Unit (Calabria, south-Italy). *Rend Online Soc Geol It.* **2012**, *21*, 847–848.

23. Navarro, R.; Pereira, D.; Gimeno, A.; Barrio, S.D. Verde Macael: A Serpentinite Wrongly Referred to as a Marble. *Geosciences* **2013**, *3*, 102–113. [CrossRef]

24. Gaggero, L.; Sanguineti, E.; Yus González, A.; Militello, G.M.; Scuderi, A.; Parisi, G. Airborne asbestos fibers monitoring in tunnel excavation. *J. Environ. Manag.* **2017**, *196*, 583–593. [CrossRef] [PubMed]

25. Worliczek, E. Naturally occurring asbestos: The perception of rocks in the mountains of New Caledonia. In *Environmental Transformations and Cultural Responses: Ontologies, Discourses, and Practices in Oceania*; Dürr, E., Pascht, A., Eds.; Springer: Berlin, Germany, 2017; pp. 187–214.

26. Bloise, A.; Catalano, M.; Critelli, T.; Apollaro, C.; Miriello, D. Naturally occurring asbestos: Potential for human exposure, San Severino Lucano (Basilicata, Southern Italy). *Environ. Earth Sci.* **2017**, *76*, 648. [CrossRef]

27. Bernardini, P.; Schettino, B.; Sperduto, B.; Giannadrea, F.; Burragato, F.; Castellino, N. Tre Casi di mesotelioma pleurico ed inquinamento ambientale da rocce affioranti di tremolite in Lucania. *GIMLE* **2003**, *25*, 408–411.

28. Burragato, F.; Mastacchi, R.; Papacchini, L.; Rossini, F.; Sperduto, B. Mapping of risks due to particulates of natural origin containing fibrous tremolite: The case of Seluci di Lauria (Basilicata, Italy). In Proceedings of the 1st General Assembly, Nice, France, 25–30 April 2004.

29. Pasetto, R.; Bruni, B.; Bruno, C.; Cauzillo, G.; Cavone, D.; Convertini, L.; De Mei, B.; Marconi, A.; Montagano, G.; Musti, M.; et al. Mesotelioma pleurico ed esposizione ambientale a fibre minerali: Il caso di un'area rurale in Basilicata. *Ann. Ist. Super. Sanita.* **2004**, *40*, 251–265. [PubMed]

30. Punturo, R.; Ricchiuti, C.; Mengel, K.; Apollaro, C.; De Rosa, R.; Bloise, A. Serpentinite-derived soils in southern Italy: Potential for hazardous exposure. *J. Mediterr. Earth Sci.* **2018**, *10*, 51–61.

31. Monaco, C.; Tortorici, L. Tettonica estensionale quaternaria nell'Arco Calabro e in Sicilia orientale. *Studi Geologici Camerti* **1995**, *2*, 351–362.

32. Monaco, C.; Tortorici, L.; Paltrinieri, W. Structural evolution of the Lucanian Apennines, southern Italy. *J. Struct. Geol.* **1998**, *20*, 617–638. [CrossRef]

33. Vezzani, L. La Formazione del Frido (Neocomiano- Aptiano) tra il Pollino e il Sinni. *Geol. Rom.* **1969**, *8*, 129–176.

34. Amodio Morelli, L.; Bonardi, G.; Colonna, V.; Dietrich, D.; Giunta, G.; Ippolito, F.; Liguori, V.; Lorenzoni, S.; Paglioncino, A.; Perrone, V. L' arco Calabro Peloritano nell' orogene Appenninico-Maghrebide. *Mem. Soc. Geol. It.* **1976**, *17*, 1–60.

35. Vezzani, L. La sezione tortoniana di Perosa sul fiume Sinni presso Episcopia (Potenza). *Geol. Rom.* **1966**, *5*, 263–290.

36. Sansone, M.T.C.; Rizzo, G.; Mongelli, G. Petrochemical characterization of mafic rocks from the Ligurian ophiolites, Southern Apennines. *Int. Geol. Rev.* **2011**, *53*, 130–156. [CrossRef]

37. Rizzo, G.; Cristi Sansone, M.T.; Perri, F.; Laurita, S. Mineralogy and petrology of the metasedimentary rocks from the frido unit (southern apennines, Italy). *Period. Mineral.* **2016**, *85*, 153–168.

38. Sansone, M.T.C.; Prosser, G.; Rizzo, G.; Tartarotti, P. Spinel-peridotites of the frido unit ophiolites (southern apennine-italy): Evidence for oceanic evolution. *Period. Mineral.* **2012**, *81*, 35–59.

39. Whitney, D.L.; Evans, B.W. Abbreviations for names of rock-forming minerals. *Am. Mineral.* **2010**, *95*, 185–187. [CrossRef]

40. Leake, B.E.; Woolley, A.R.; Arps, C.E.S.; Birch, W.D.; Gilbert, M.C.; Grice, J.D.; Hawthorne, F.C.; Kato, A.; Kisch, H.J.; Krivovichev, V.G.; et al. Nomenclature of amphiboles: Report of the subcommittee on amphiboles of the international mineralogical association, commission on new minerals and mineral names. *Can. Mineral.* **1997**, *35*, 219–246.

41. Bloise, A.; Barrese, E.; Apollaro, C.; Miriello, D. Flux growth and characterization of Ti and Ni doped forsterite single crystals. *Cryst. Res. Technol.* **2009**, *44*, 463–468. [CrossRef]

42. Bloise, A.; Catalano, M.; Gualtieri, A.F. Effect of Grinding on Chrysotile, Amosite and Crocidolite and Implications for Thermal Treatment. *Minerals* **2018**, *8*, 135. [CrossRef]

43. Bloise, A.; Kusiorowski, R.; Gualtieri, A.F. The Effect of Grinding on Tremolite Asbestos and Anthophyllite Asbestos. *Minerals* **2018**, *8*, 274. [CrossRef]

44. Ballirano, P.; Bloise, A.; Gualtieri, A.F.; Lezzerini, M.; Pacella, A.; Perchiazzi, N.; Dogan, M.; Dogan, A.U. The Crystal Structure of Mineral Fibers. In *Mineral Fibers: Crystal Chemistry, Chemical-Physical Properties, Biological Interaction and Toxicity*; Gualtieri, A.F., Ed.; European Mineralogical Union: London, UK, 2017; Volume 18, pp. 17–53.

45. Bloise, A.; Kusiorowski, R.; Lassinantti Gualtieri, M.; Gualtieri, A.F. Thermal behaviour of mineral fibers. In *Mineral Fibers: Crystal Chemistry, Chemical-Physical Properties, Biological Interaction and Toxicity*; Gualtier, A.F., Ed.; European Mineralogical Union: London, UK, 2017; Volume 18, pp. 215–252.

46. Loomis, D.; Dement, J.; Richardson, D.; Wolf, S. Asbestos fibre dimensions and lung cancer mortality among workers exposed to chrysotile. *Occup. Environ. Med.* **2010**, *67*, 580–584. [CrossRef] [PubMed]

47. Suzuki, Y.; Yuen, S.R.; Ashley, R. Short, thin asbestos fibersc ontribute to the development of human malignant mesothelioma: Pathological evidence. *Int. J. Hyg. Environ. Health* **2005**, *208*, 201–210. [CrossRef] [PubMed]

48. Bernstein, D.; Castranova, V.; Donaldson, K.; Fubini, B.; Hadley, J.; Hesterberg, T.; Kane, A.; Lai, D.; McConnell, E.E.; Muhle, H.; et al. Testing of fibrous particles: Short-term assays and strategies. *Inhal. Toxicol.* **2005**, *17*, 497–537. [CrossRef] [PubMed]

49. Stanton, M.F.; Layard, M.; Tegeris, A.; Miller, E.; May, M.; Morgan, E.; Smith, A. Relation of particle dimension to carcinogenicity in amphibole asbestoses and other fibrous mineral. *J. Natl. Cancer. Inst.* **1981**, *67*, 965–975. [PubMed]

50. Dichicco, M.C.; Laurita, S.; Sinisi, R.; Battiloro, R.; Rizzo, G. Environmental and Health: The Importance of Tremolite Occurence in the Pollino Geopark (Southern Italy). *Geosciences* **2018**, *8*, 98. [CrossRef]

51. Bellomo, D.; Gargano, C.; Guercio, A.; Punturo, R.; Rimoldi, B. Workers' risks in asbestos contaminated natural sites. *J. Mediterr. Earth Sci.* **2018**, *10*, 97–106.

Mineralogical and Microstructural Features of Namibia Marbles: Insights about Tremolite Related to Natural Asbestos Occurrences

Rosalda Punturo [1],*, Claudia Ricchiuti [1], Marzia Rizzo [2] and **Elena Marrocchino [2]**

[1] Department of Biological, Geological and Environmental Sciences, University of Catania, Corso Italia 55, 95129 Catania, Italy; claudia.ricchiuti@unict.it

[2] Department of Physics and Earth Science—University of Ferrara, Via Saragat 1, 44122 Ferrara, Italy; marzia.rizzo@unife.it (M.R.); mrrlne@unife.it (E.M.)

* Correspondence: punturo@unict.it; Tel.: +39-095-719-5757

Abstract: The Mg-rich marbles of Precambrian rocks of Namibia are widely exploited and marketed abroad for ornamental purposes. Karibib marbles, named after the locality where the most important quarries are located, are commercially known as "White Rhino Marble". They formed under greenschist facies metamorphic conditions and may be characterized by the presence of veins of tremolite. Although the quarries, whose exploited marbles contain tremolite, do not seem to be abundant, we decided to carry out a detailed mineralogical and petrographic study on Karibib marbles in order to point out the occurrence of tremolite, whose shape may vary from prismatic to acicular, even sometimes resembling the asbestiform habitus and its geometry within the rock. With this aim, we carried out optical microscopy, X-ray diffractometry, X-ray scanning electron microscopy, and micro-Raman investigations, and also imaged the 3D fabric with micro computed X-ray tomography. The study of white marbles from Namibia and their mineral phases has an important impact, since tremolite might split into thin fibers and, therefore, being potentially harmful, the presence of tremolite requires an analysis of the risks of exposure to asbestos.

Keywords: rhino white marble of Namibia; tremolite; fibrous habitus; health hazard

1. Introduction

In the last century, Namibia has been one of the favorable mining contexts for the exploration and evaluation of geo-resources. From 1990 to 2000, in Namibia, the production of marble and granite was about 20,000 tons per year. Since 2004, thanks to modern methods and processing machinery, there has been a continuous increase in production, and the production has exceeded the threshold of 50,000 tons/year [1]. The geo-mining industry of Namibia includes several ornamental stones: marbles (calcite and/or dolomite-bearing metacarbonate rocks); magmatic rocks such as granites, granodiorites, and gabbros; serpentinites; and onyxes and alabasters. The firms linked to the ornamental stone that are gathered around the Karibib have become a benchmark for the high quantity and quality of marble.

Since 1900, railway construction has led to great development in mining and, in the past 10 years, the Karibib has become one of the most productive international marble districts that includes extraction, processing, and marketing activities of marble and granite rocks.

In the Karibib district, the most important marble and granite reserves are located in the Karibib quarry area of the northwest sector of town, where the White Rhino and Karibib marble varieties are exploited; in the Nonidas quarry area, which consists of small extractive sites that sit between the northern part of the town of Nonidas and the eastern area of Swakopmund; and the Arandis quarry

area, where the extraction activities mainly concern the domes of intrusive magmatic rocks (pink granite).

At present, there is growing interest due to the ornamental exploitation of these Neoproterozoic carbonate rocks, and many quarries are contributing to the socio-economic development of Namibia and other regions—indeed, extensive outcrops of carbonate rocks are part of Namibia's geological resources and are therefore recalling the interest of mining companies (see also the website of the Namibian Ministry of Mines and Energy [2]).

In this work, mineralogical and petrographic characteristics of the main commercial marble in the Karibib area, known as "Rhino White Marble", are described. It is a dolomite-bearing marble from the Neoproterozoic, which belongs to the Swakop group (Damara sequence). It is exploited and marketed in many European countries, and it is appreciated because of its pearly white appearance, sometimes cut by creamy yellow veins. However, some concerns related to the commercial use of Rhino White Marble are due to the occurrence of tremolite-rich veins, as revealed by preliminary petrographic investigation [3]. Indeed, tremolite, $Ca_2Mg_5Si_8O_{22}(OH)_2$, belongs to the calcic amphibole group of minerals and, when occurring with fibrous habitus, it is considered a dangerous naturally-occurring asbestos—a term applied to six specific silicate minerals that also comprises tremolite—the critical dimension is: length > 5 μm, diameter < 3 μm, length:diameter > 3:1 [4–6].

This mineral usually occurs with elongated and/or bladed prismatic habitus, but it may also be acicular or even fibrous-shaped. According to the literature, tremolite toxicology, as for all asbestos minerals, has been associated with size, durability, and chemical composition (e.g., [7–15]). According to [16], "In mineralogy, acicular is the term applied to straight, free-standing (i.e., individual) and highly elongated crystals; these ones can be bordered and delimited by crystal faces. As far as the acicular crystals, they are characterized by aspect ratio comparable to those ones of fibrous crystals, even though their diameter may extend up to 7 mm". A fiber is defined as an elongate particle that is longer than 5.0 μm, with a minimum aspect ratio (length of the particle divided by its width) of 3:1 [6]. Indeed, when used as building stone, the studied marbles are washed with aggressive detergents and also exposed to accelerated weathering, so the mineral fibers contained within could break and may be spread out in the environment and make them dangerous for the environment and human health [17–26].

Although the quarries of the Karibib area that sit on tremolite-bearing marbles do not seem to be abundant, we considered it necessary to carry out a detailed mineralogical and microstructural investigation in order to characterize the white marbles of Namibia and to detect the eventual occurrence of asbestos tremolite. For the above reasons, the present study has several implications, since the presence of tremolite with asbestiform habitus might be linked to health problems and asbestosis. Therefore, it is a useful tool for initiating an analysis of the risks to occupational and non-occupational activities concerning the use of the tremolite-bearing marble, providing useful suggestions for safe marble exploitation.

2. Materials and Methods

2.1. Geological Setting and Samples

The Namibia marbles belong to the Neoproterozoic carbonate succession, dating 665 ± 34 million years, which constitute the Pan-African Damara Belt. The latter was generated during the orogenic events that produced the Gondwana supercontinent. The sedimentary successions of the Damara Belt, siliciclastic and carbonate in composition, were deposited in an environment of passive continental margin (i.e., Neoproterozoic rift basins) related to the Rodinia break-up on a global scale. In some sectors, the thickness of deposits exceeds 1000 m [27–30]. According to the literature [31–34], the Damara Belt is considered as an asymmetric double-vergent orogen, which separates the Angola-Congo and Kalahari cratons (Figure 1), formed during the Neoproterozoic to early Paleozoic tectonic events related to the closure of the Damara Ocean. In Namibia, the Damara

Orogen (Figure 1) is constituted by three orogenic belts: The intracontinental Damara belt and the coastal belt, the Kaoko belt, and the Gariep belts [35–38].
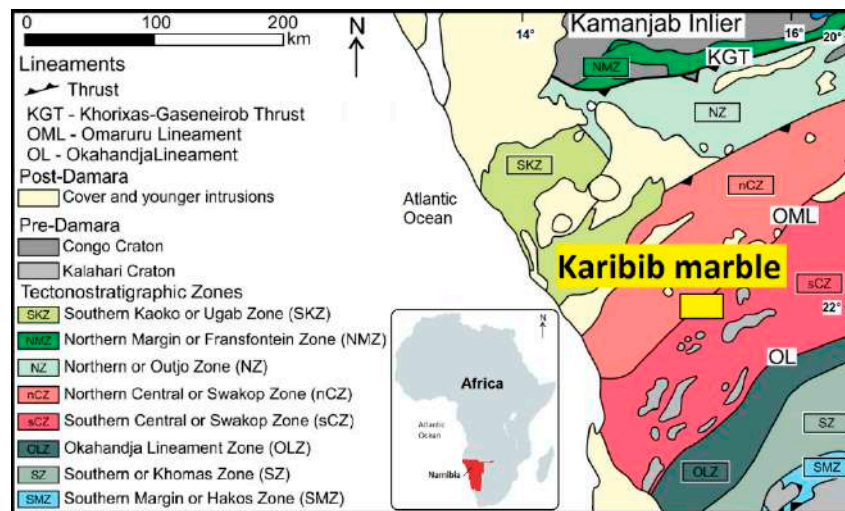

Figure 1. Simplified tectonic map of the Damara Belt (Namibia (Africa). showing the distribution of the main tectono-stratigraphic zones according to [28]. Modified after [35].

In the Central Zone of the Damara Belt, the successions were deformed and metamorphosed to greenschist facies conditions reaching, in some sectors, metamorphic conditions of up to ca. 590 °C and 0.5 GPa [39]. Moreover, a detailed structural mapping [40–45], highlighted as the most striking structural feature of the Central zone, is the northeast trending domes elongated at kilometer-scale [37,40,42,45,46], where the most important quarries are located (Figure 2).
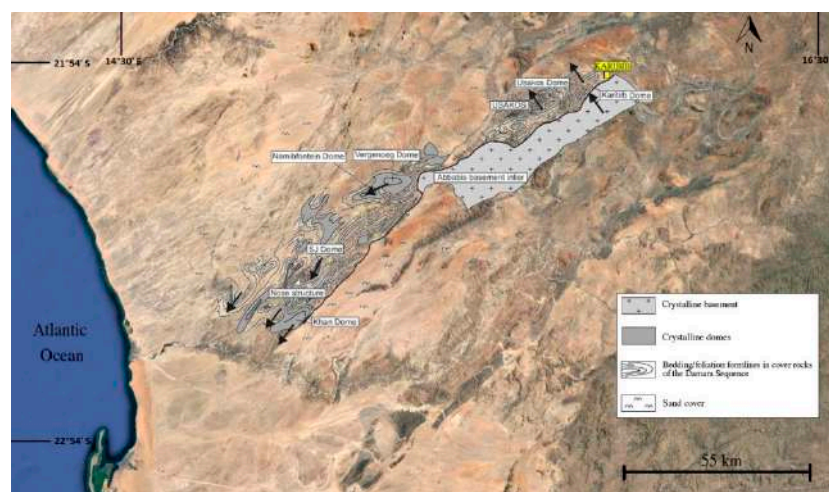

Figure 2. Schematic map showing the northeast trending dome structures covered by the geological map, by [40]. The gneisses and/or the Pan-African granitoids constitute the cores of the dome structures, whereas the surrounding supracrustals of the Damara sequence are draped around the domes. The solid black arrows indicate the tectonic transport direction for domes [41–44] and the Karibib district in the northeast. The yellow rectangle indicates the area where the marble quarries are located.

Deformation and metamorphism have not completely obliterated structures and textures inherited from sedimentary environments, so the planar surfaces due to tectonic deformation overprint the contacts between lithofacies [35,47–49].

Within the carbonate protolith, which represents a pelagic environment with main carbonate sedimentation and a lower contribution of siliceous organisms in relation to the oscillations of Carbonate Compensation Depth, the derived magnesium-rich marbles—which underwent greenschist facies metamorphism—can be characterized by the occurrence of tremolite as one of the main constituting minerals. Conversely, the portions closest to the continental margins do not have tremolite because the Al and Fe terrigenous sediments, metamorphosed under greenschist facies conditions, give chlorite in the metamorphic assemblage.

At the scale of the quarry, White Rhino Marbles of the Karibib area look pearly white and are extracted as dimension stones (Figure 3a)—at the mesoscopic scale, marbles show a saccaroid fabric and are cut by yellowish veins (Figure 3b,c).
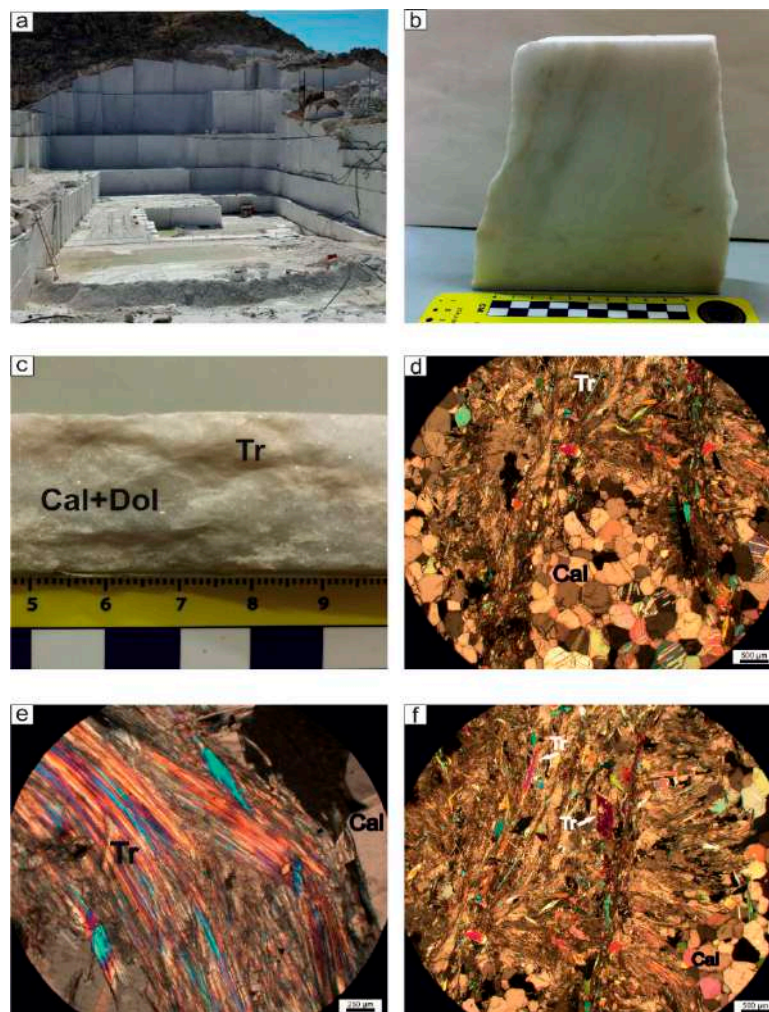

Figure 3. The main features of Karibib white marbles. (**a**) Front of a quarry where marble is exploited as dimensional stone; (**b**) Appearance of the marble at the mesoscopic scale, note the yellow-greenish veins across the pearly portion; (**c**) Particular of a cross section of a brick; (**d**–**f**): Photomicrographs of thin sections of marbles; (**d**) Coexistence of granoblastic portions constituted by calcite with nematoblastic portions constituted by tremolite; (**e**) Blow-up of acicular tremolite-rich level; (**f**) Nematoblastic level showing various habitus types of tremolite, from prismatic to acicular. Mineral symbols after [50].

2.2. Methodologies

In order to describe the microstructural features of the investigated marbles, we selected some specimens for optical microscopy (OM), scanning electron microscopy (SEM/EDS), X-ray diffractometry (XRD), micro-Raman spectrometry, and synchrotron radiation X-ray microtomography

(SR X-ray μCT) investigations. A polarizing microscope Zeiss Axiolab and a Tescan-Vega\\LMU scanning electron microscope (Tescan-Vega, Brno – Kohoutovice, Czech Republic) equipped with an Edax Neptune XM4 60 energy-dispersive X-ray spectrometer (EDS), Edax, Mahwah, NJ, 07430 USA) operating at 20 kV accelerating voltage and 20 nA beam current conditions, were employed to obtain microstructural features, morphoscopic images, and elemental microanalyses. Investigation was carried out on polished thin sections as well as on small chips of marble specimens.

Some specimens were also examined through the X-ray diffractometry (XRD) technique to establish the mineralogical composition. The XRD analysis was performed on rock powder using a Philips PW1860/00 diffractometer (Philips Panalytical Canton, MA, USA), with graphite-filtered Cu Kα radiation (1.54 Å), allowing determination of the mineralogical phases within the constituents. Diffraction patterns were collected in the 2θ angular range 5–50°, with 5 s/step (0.02° 2θ). Moreover, XRD data were quantified by the RIR (Reference Intensity Ratio) method of powder X-ray diffraction data in order to establish the quantities of the constituting minerals according to [51].

A LabRam HR800 micro-Raman instrument from Horiba Jobin Yvon (Horiba, Kyoto, Japan), equipped with an air-cooled CCD detector (1024×256 pixels) at -70 °C, an Olympus BXFM microscope, a 600 groove/mm grating, and a $50\times$ objective, was used to collect the Raman scattering signals. The excitation source was a He–Ne laser (632.8 nm line) whose maximum power was 20 mW. The spectrometer was calibrated with silicon at 520 cm^{-1} and the exposure time was varied from 50 to 100 s. Data obtained were compared with the RRUFF^{TM} project database [52]. Moreover, one selected sample considered to be representative of the microstructural features of marbles was imaged by synchrotron radiation X-ray microtomography (SR X-ray μCT) at the SYRMEP (SYnchrotron Radiation for MEdical Physics) beamline of the Elettra synchrotron (Elettra - Sincrotrone Trieste S.C.p.A, Trieste, Italy) in white-beam configuration mode at high spatial resolution. To this aim, we cut a parallelepiped with a size of about 4 mm. The X-ray spectrum was filtered for low energies with 1 mm of Si + 1 mm of Al, and the sample-to-detector distance was set to 200 mm. For each measurement, 1800 projections were acquired over a total scan angle of 180° with an exposure time/projection of 2 s. The detector consisted of a 16-bit air-cooled sCMOS camera (Hamamatsu C11440 22C, Hamamatsu City, Japan) with a 2048°—2048° pixels chip. The effective pixel size of the detector was set at 1.952 μm^2, yielding a maximum field of view of ca. 3.22 mm^2. Since the lateral size of the samples was larger than the detector field of view, the X-ray tomographic microscans were acquired in local or region-of-interest mode [53]. A single distance phase retrieval-preprocessing algorithm [54] was applied to the white beam projections in order to improve the reliability of the quantitative morphological analysis and enhance the image contrast.

The obtained 3D volumes were then imported in VGStudio Max 2.2 (Volume Graphics, Charlotte, NC, USA) for the 3D rendering and segmentation by manual thresholding.

3. Results

At the scale of the microscope, the White Rhino Marbles of the Karibib area had relatively fine grain size with a very heterogeneous distribution of white and yellowish levels, as was revealed by previous mesoscopic observation (Figure 3b,c). Indeed, two main domains, whose thickness ranged from 2 mm up to 1–2 cm, were distinguished on the basis of evident microstructures and constituting minerals: granoblastic levels, given by calcite +/− dolomite (Figure 3d), which are the most abundant portions of the rocks, as also highlighted by mesoscopic observations. Conversely, the nematoblastic levels that occurred to a minor extent, were characterized by tremolite, occurring with various habitus types—indeed, there were levels in which tremolite crystals were made of well-developed prismatic to acicular minerals and minor levels in which this mineral phase tended to constitute fiber belts (Figure 3e,f).

The granoblastic portions, prevalently constituted by calcite and dolomite, showed straight grain boundaries. They were also sutured, even embayed, resulting in an interlocked texture (Figure 3d)—the greenish-yellowish nematoblastic levels, showing marked microstructural anisotropy, were given by

tremolite, occurring as either acicular crystals and/or highly elongated fiber aggregates in belts with radial disposition (Figure 3d,f), together with hetero-granoblastic calcite and dolomite grains elongated parallel to foliation.

XRD and micro-Raman analyses (Figures 4 and 5) showed the coexistence of calcite, tremolite, and dolomite and the absence of other mineral phases also in the finest-grained nematoblastic portions of the yellowish bands, without secondary or accessory minerals occurring. Quantitative phase analyses with the RIR method showed that, on average, the abundances of constituent minerals determined on powders obtained from representative bricks were calcite 70%, tremolite 26%, and dolomite 4%.
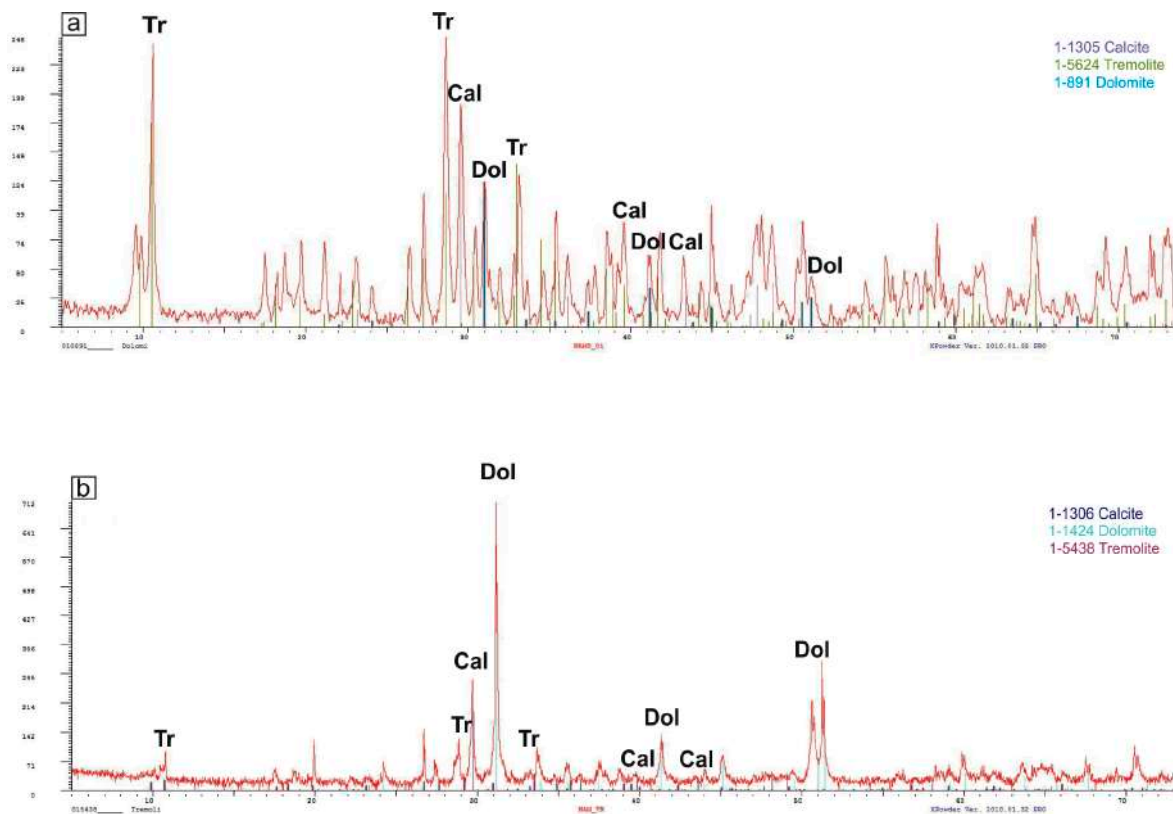

Figure 4. X-ray diffractograms on representative portions of the Karibib white marbles, showing calcite, tremolite, and dolomite as constituting mineral phases. The peak color of each mineral is indicated in the legend. (**a**) main vein; (**b**) massive part.
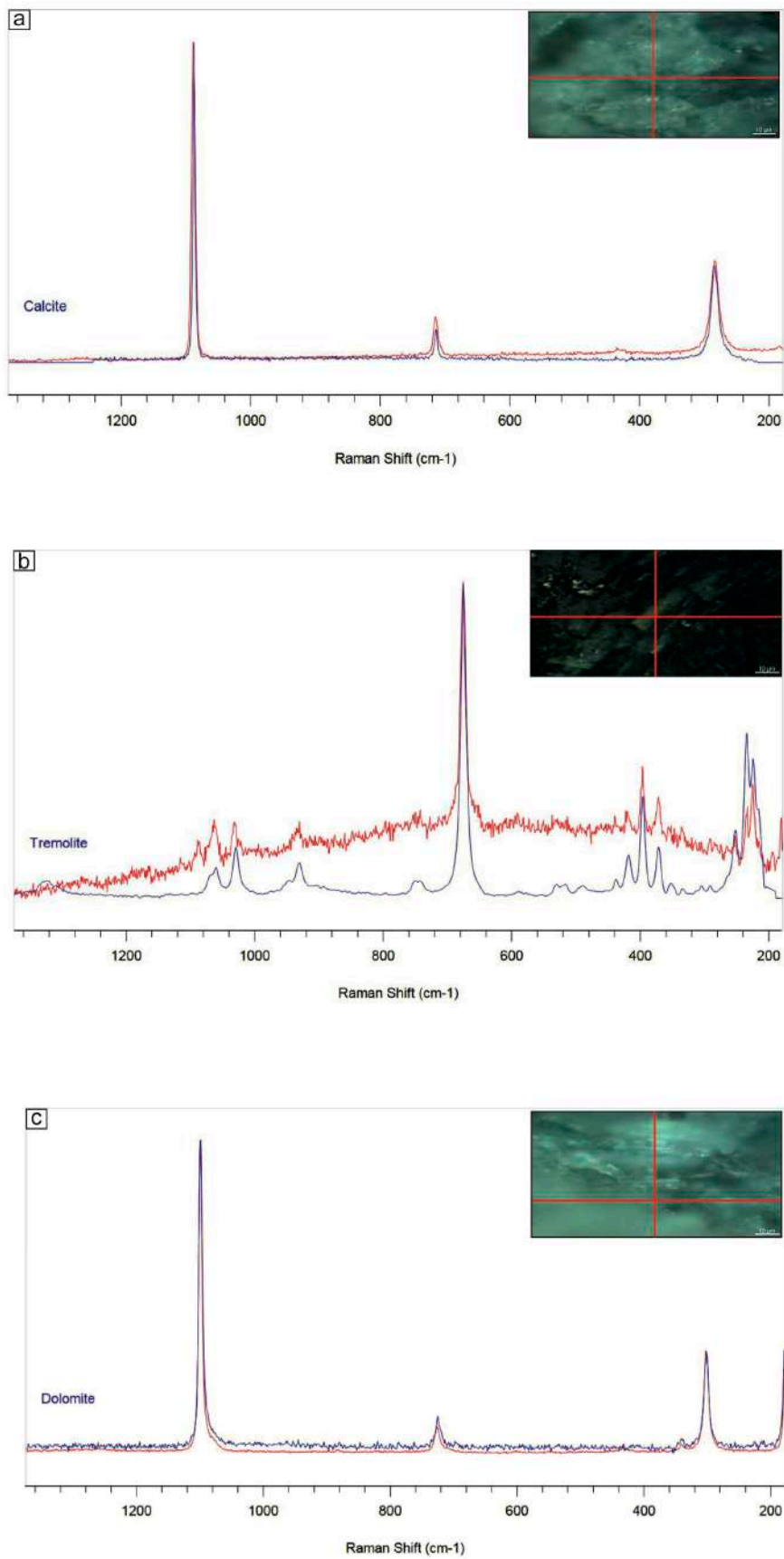
Figure 5. Micro-Raman spectra of selected areas of the Karibib white marbles, showing (**a**) calcite; (**b**) tremolite; and (**c**) dolomite as constituting mineral phases (red spectra). The blue reference spectra are after [52]. Pictures of boxes indicate the investigated points.

The rock exhibited a friable appearance, especially at the contact areas between amphibole and carbonate minerals, with tremolite occurring either with prismatic elongated habitus or elongated fibers, closely bound to carbonate minerals, as can be seen in the SEM images (Figure 6a–c). The SEM/EDS elemental microanalysis suggested that tremolite individuals were pure Mg-member $Ca_2Mg_5(OH)_2Si_8O_{22}$ without any iron detected [55]. Moreover, the SEM images did show that, as a consequence of disaggregation, tremolite might also split into fibers and cleavage fragments, whose shape parameters may resemble asbestiform habitus (Figure 6d–f).
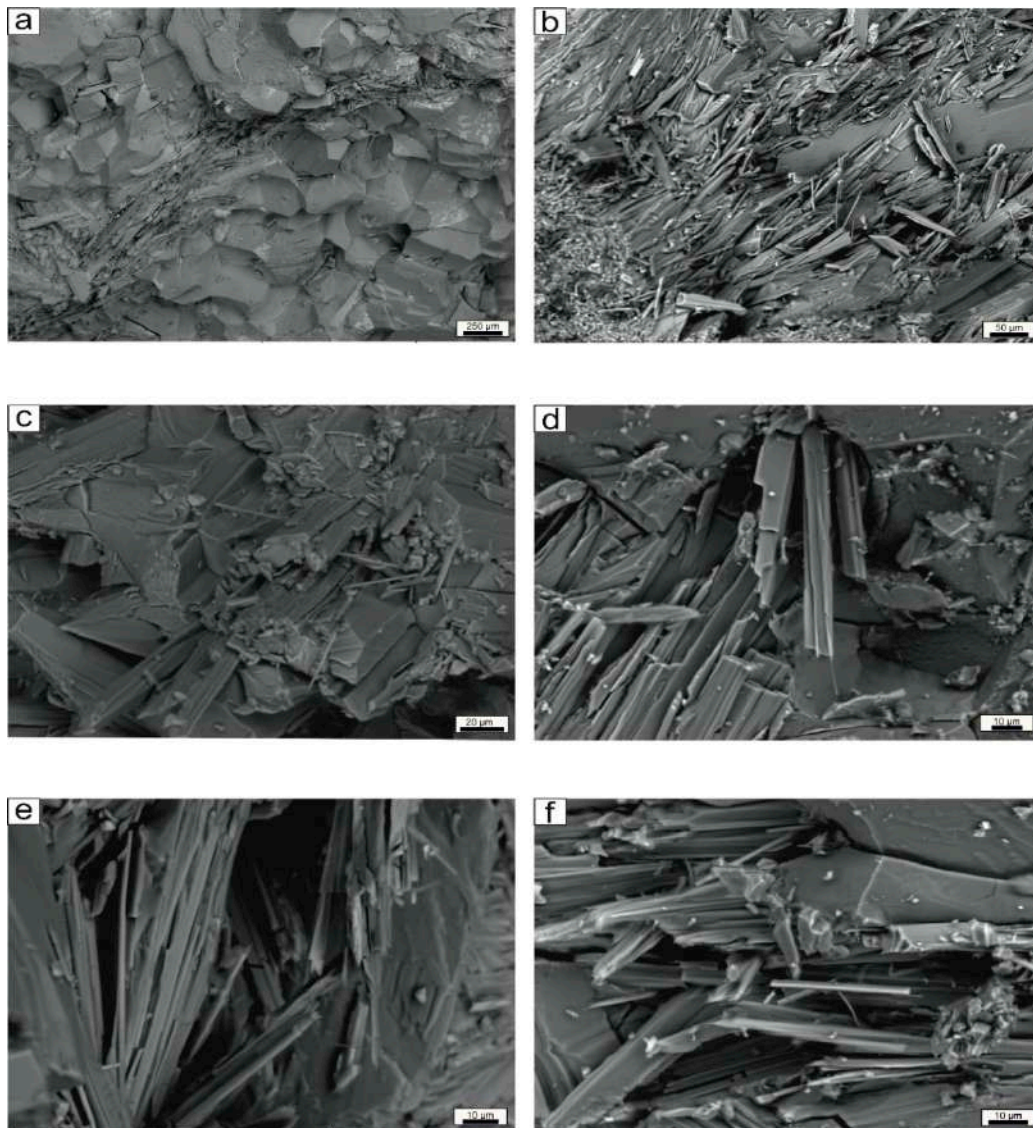

Figure 6. Scanning electron photomicrographs. (**a**) Calcite-rich granoblastic levels cut by tremolite veins; (**b**) Elongated tremolite crystals, sometimes showing radial disposition; (**c**) Tremolite splitting into fibers; (**d**) Tremolite cleavage fragments prone to split; (**e**,**f**) tremolite fibers whose shape parameters may resemble asbestiform habitus. Mineral symbols after [50].

Finally, on one selected small brick measuring about 30 mm × 4 mm, we carried out synchrotron radiation X-ray microtomography (SR X-ray μCT). X-ray microtomography is a non-destructive technique that improves the observation of the arrangement of fibers in the three-dimensional space, thus avoiding any morphological variations of the sample as a result of comminution. Indeed, this technique allowed us to image the three-dimensional enveloping and intergrowth of nematoblastic

and granoblastic levels as well as the geometry and reciprocal arrangement of constituting minerals into the marble, with special regard to the spatial relationship between calcite and tremolite, the latter sometimes showing radial disposition, as can be clearly seen in Figure 7.
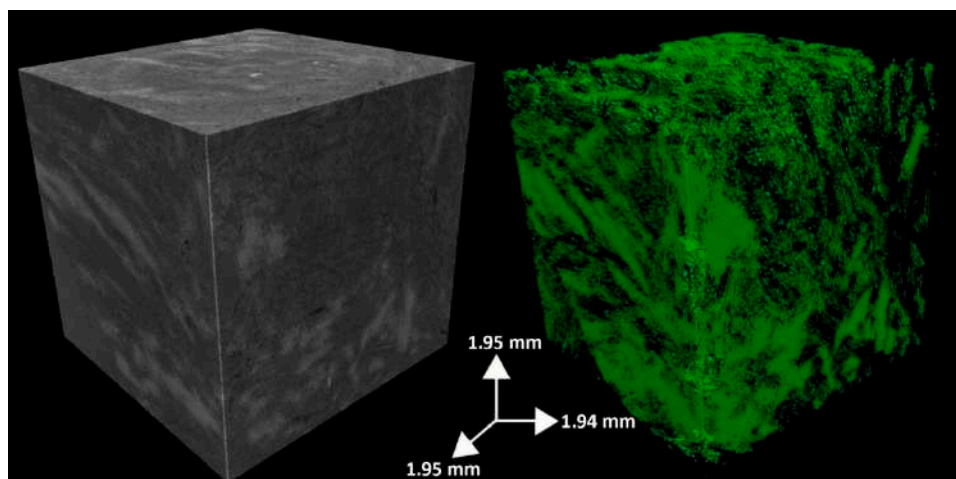

Figure 7. 3D rendering of a selected part of one specimen analyzed by means of synchrotron radiation X-ray micro-tomography: in the left picture, light colors correspond to high-density phases, while dark colors correspond to low-density phases; in the right picture, a green color is associated with the highest-density phase (i.e., tremolite). Note the 3D interlock between tremolite- and carbonate-rich portions.

4. Discussion and Conclusions

The multi-analytical investigation carried out on White Rhino Marbles exploited in the Karibib area (Namibia), which consisted of a detailed petrographic, microstructural, and mineralogical characterization of their fabric and microstructural features, permitted us to highlight the occurrence and to depict the geometry of amphibole minerals in the yellow veins that cut the rock. From the petrological point of view, the Neoproterozoic White Rhino Marbles are characterized by a mineralogical assemblage that proves the absence of terrigenous contributions in their protolith, as they do not contain any aluminum or iron, even in nematoblastic levels in which silicate mineral phases (i.e., amphibole) are found.

During the metamorphic event, the high-silica (e.g., diatomaceous) levels reacted with the Mg-rich carbonates, giving rise to amphibole tremolite $Ca_2Mg_5Si_8O_{22}(OH)_2$. Therefore, the paragenesis of the White Rhino Marbles is given by calcite + tremolite ± dolomite. Calcite and minor dolomite grains are the constituent of the granoblastic levels, which are certainly the most abundant portions of the marble rocks exploited. Conversely, tremolite is the principal constituent of the nematoblastic levels, where it is mainly found with acicular (i.e., needle-like) habitus, which means it is characterized by sectional dimensions that are small relative to its length. Moreover, no secondary minerals formed on primary minerals have been detected or observed, proving that no weathering process has been affecting the studied marbles.

Nevertheless, the detailed microstructural and morphological analyses carried out on marbles highlighted that, despite non-asbestos tremolite exhibiting acicular habitus, it is the most common mineral phase that was found. Asbestos tremolite fibers were also detected within veins. Tremolite-rich veins were easy to distinguish at the mesoscopic and at the optical microscopic scale, where they defined the microstructural anisotropy of marbles. Scanning the electron microscopy highlighted that tremolite fibers, resembling the asbestiform habitus, occurred as fibrous aggregates with radial arrangement, prone to split into thinner fibers and ultimately into fibrils, often formed after cleavage fragments. Despite its occurring habitus, tremolite appeared as straight and stiff crystals (i.e., needles

and fibers). Moreover, 3D imaging showed the tight interlock between the nematoblastic microdomains (i.e., tremolite-rich) and the granoblastic portions (i.e., carbonate-rich) and their contact geometry.

The asbestos hazard related to the occurrence of fibrous tremolite veins that cross-cut the studied marbles arises when either natural weathering processes (e.g., erosion and mobilization) or human activities (e.g., exploitation of dimension blocks and subsequent use as building stones) separate tremolite fibers and break them down, making them dispersed into the environment as airborne and easily breathable.

For instance, during the steps of marble quarrying, non-asbestos tremolite can break along preferred cleavage planes and be released in the air. For this reason, it is ultimately possible for workers to be exposed to asbestos during these activities. Therefore, before any exploitation and subsequent process of marble containing non-asbestos minerals, which may otherwise develop into minerals with asbestiform habitus, it is necessary that mining companies adopt monitoring surveys, in situ tests, as well as safety measures and prevention practices for each recognized hazardous situation. Among them it is worth noting the avoidance of asbestos veins during exploitation, maintenance of devices, use of protective personal equipment, planning sanitary surveillance, and envisaging dust abatement and remediation systems [21,56–58]. As far as the non-occupational point of view states, it is important to assess the extent of exposure to those airborne particles, whose morphology may resemble asbestos, to populations who live close to the quarry as well as to family members of workers. Finally, we suggest that weathering and ageing tests should be carried out on vein-rich marble, in order to detect any deterioration forms that may cause the release of fibers, and to plan eventual remediation practices.

References

1. Ministry of Mines and Energy. Available online: http://www.mme.gov.na (accessed on 20 January 2019).
2. Ministry of Mines and Energy. Available online: http://www.mme.gov.na/directorates/mine/ (accessed on 20 January 2019).
3. Vaccaro, C.; Punturo, R.; Volpe, L.; Marrocchino, E.; Rizzo, M.; Ricchiuti, C.; Mannino, M. *Tremolite—Bearing Marbles from Namibia Exploited as Dimension Stone: Preliminary Mineralogical and Petrographic Characterization*; Abstract Book; Congresso SGI-SIMP: Catania, Italy, 2018.
4. World Health Organization (WHO). *Asbestos and Other Natural Mineral Fibres*; Environmental Health Criteria, 53; World Health Organization: Geneva, Switzerland, 1986; p. 194.
5. National Institute for Occupational Safety and Health (NIOSH). *Asbestos and Other Elongated Mineral Particles: State of the Science and Roadmap for Research*; Revised Draft; NIOSH Current Intelligence Bulletin: Washington, DC, USA, 2008.
6. International Agency for Research on Cancer (IARC). *Asbestos (Chrysotile, Amosite, Crocidolite, Tremolite, Actinolite, and Anthophyllite) IARC Monographs*; Arsenic, Metals, Fibres and Dusts; International Agency for Research on Cancer: Lyon, France, 2009; pp. 147–167.
7. Mossman, B.T.; Lippmann, M.; Hesterberg, T.W.; Kelsey, K.T.; Barchowsky, A.; Bonner, J.C. Pulmonary endpoints (lung carcinomas and asbestosis) following inhalation exposure to asbestos. *J. Toxicol. Environ. Health* **2011**, *14*, 76–121. [CrossRef] [PubMed]

8. Pugnaloni, A.; Giantomassi, F.; Lucarini, G.; Capella, S.; Bloise, A.; Di Primio, R.; Belluso, E. Cytotoxicity induced by exposure to natural and synthetic tremolite asbestos: An in vitro pilot study. *Acta Histochem.* **2013**, *115*, 100–112. [CrossRef] [PubMed]

9. Oberti, R.; Hawthorne, F.C.; Cannillo, E.; Camara, F. Long-range order in amphiboles. In *Amphiboles: Crystal Chemistry, Occurrence, and Health Issues Hawthorne*; Oberti, F.C., della Ventura, R., Mottana, G.A., Eds.; Mineralogical Society of America: Chantilly, VA, USA, 2007; pp. 125–172.

10. Ballirano, P.; Bloise, A.; Gualtieri, A.F.; Lezzerini, M.; Pacella, A.; Perchiazzi, N.; Dogan, M.; Dogan, A.U. The Crystal Structure of Mineral Fibres. In *Mineral Fibres: Crystal Chemistry, Chemical-Physical Properties, Biological Interaction and Toxicity*; Gualtieri, A.F., Ed.; European Mineralogical Union: London, UK, 2017; Volume 18, pp. 17–53.

11. Gaggero, L.; Sanguineti, E.; Yus González, A.; Militello, G.M.; Scuderi, A.; Parisi, G. Airborne asbestos fibres monitoring in tunnel excavation. *J. Environ. Manag.* **2017**, *196*, 583–593. [CrossRef] [PubMed]

12. Apollaro, C.; Fuoco, I.; Vespasiano, G.; De Rosa, R.; Cofone, F.; Miriello, D.; Bloise, A. Geochemical and mineralogical characterization of tremolite asbestos contained in the Gimigliano-Mount Reventino Unit (Calabria, south Italy). *JMES* **2018**, *10*, 5–15. [CrossRef]

13. Punturo, R.; Bloise, A.; Critelli, T.; Catalano, M.; Fazio, E.; Apollaro, C. Environmental implications related to natural asbestos occurrences in the ophiolites of the Gimigliano-Mount Reventino Unit (Calabria, southern Italy). *Int. J. Environ. Res.* **2015**, *9*, 405–418.

14. Constantopoulos, S.H. Environmental mesothelioma associated with tremolite asbestos: Lessons from the experiences of Turkey, Greece, Corsica, New Caledonia and Cyprus. *Regul. Toxicol. Pharmacol.* **2008**, *52*, 110–115. [CrossRef] [PubMed]

15. Bloise, A.; Barca, D.; Gualtieri, A.F.; Pollastri, S.; Belluso, E. Trace elements in hazardous mineral fibres. *Environ. Pollut.* **2016**, *216*, 314–323. [CrossRef]

16. Strohmeier, B.R.; Huntington, J.C.; Bunker, K.L.; Sanchez, M.S.; Allison, K.; Lee, R.J. What is asbestos and why is it important? Challenges of defining and characterizing asbestos. *Int. Geol. Rev.* **2010**, *52*, 801–872. [CrossRef]

17. Petriglieri, J.R.; Laporte-Magoni, C.; Gunkel-Grillon, P.; Tribaudino, M.; Bersani, D.; Sala, O.; Salvioli-Mariani, E. Mineral fibres and environmental monitoring: A comparison of different analytical strategies in new caledonia. *Geosci. Front.* **2019**. [CrossRef]

18. Laporte-Magoni, C.; Petriglieri, J.R.; Gunkel-Grillon, P.; Salvioli-Mariani, E.; Selmaoui-Folcher, N.; Le Mestre, M. Weathering Influence on fiber release of asbestos type minerals under subtropical climate. In Proceedings of the XXII Meeting of the International Mineralogical Association, Melbourne, Australia, 13–17 August 2018.

19. Bloise, A.; Kusiorowski, R.; Lassinantti Gualtieri, M.; Gualtieri, A.F. Thermal behaviour of mineral fibres. In *Mineral Fibres: Crystal Chemistry, Chemical-Physical Properties, Biological Interaction and Toxicity*; Gualtier, A.F., Ed.; European Mineralogical Union: London, UK, 2017; Volume 18, pp. 215–252.

20. Bloise, A.; Punturo, R.; Catalano, M.; Miriello, D.; Cirrincione, R. Naturally occurring asbestos (NOA) in rock and soil and relation with human activities: The monitoring example of selected sites in Calabria (southern Italy). *Ital. J. Geosci.* **2016**, *135*, 268–279. [CrossRef]

21. Bellomo, D.; Gargano, C.; Guercio, A.; Punturo, R.; Rimoldi, B. Workers' risks in asbestos contaminated natural sites. *JMES* **2018**, *10*, 97–106.

22. Pacella, A.; Andreozzi, G.B.; Ballirano, P.; Gianfagna, A. Crystal chemical and structural characterization of fibrous tremolite from Ala di Stura (Lanzo Valley, Italy). *Period. Mineral.* **2008**, *77*, 51–62.

23. Belardi, G.; Vignaroli, G.; Trapasso, F.; Pacella, A.; Passeri, D. Detecting asbestos fibres and cleavage fragments produced after mechanical tests on ophiolite rocks: Clues for the asbestos hazard evaluation. *JMES* **2018**, *10*, 63–78. [CrossRef]

24. Punturo, R.; Cirrincione, R.; Pappalardo, G.; Mineo, S.; Fazio, E.; Bloise, A. Preliminary laboratory characterization of serpentinite rocks from Calabria (southern Italy) employed as stone material. *J. Mediterr. Earth Sci.* **2018**, *10*, 79–87. [CrossRef]

25. Punturo, R.; Ricchiuti, C.; Mengel, K.; Apollaro, C.; De Rosa, R.; Bloise, A. Serpentinite-derived soils in southern Italy: Potential for hazardous exposure. *J. Mediterr. Earth Sci.* **2018**, *10*, 51–61. [CrossRef]

26. Censi, P.; Zuddas, P.; Randazzo, L.A.; Tamburo, E.; Speziale, S.; Cuttitta, A.; Punturo, R.; Santagata, R. Source and nature of inhaled atmospheric dust from trace element analyses of human bronchial fluids. *Environ. Sci. Technol.* **2011**, *45*, 6262–6267. [CrossRef]

27. South African Committee for Stratigraphy, SACS. Stratigraphy of South Africa, Part I. Lithostratigraphy of the Republic of South Africa, South West Africa/Namibia and the Republics of Bophuthatswana, Transkei and Venda. *Geol. Surv. S. Afr.* **1980**, *8*, 690.

28. Kröner, A. Late Precambrian diamictites of South Africa and Namibia. In *Earth's Pre-Pleistocene Glacial Record*; Hambrey, M.J., Harland, W.B., Eds.; Cambridge University Press: Cambridge, UK, 1981; pp. 167–177.

29. Paciullo, F.V.P.; Ribeiro, A.; Trouw, R.A.J.; Passchier, C.W. Facies and facies association of the siliciclastic Brak River and carbonate Gemsbok formations in the Lower Ugab River valley, Namibia, W. *Africa. J. Afr. Earth Sci.* **2007**, *47*, 121–134. [CrossRef]

30. Miller, R.M. Neoproterozoic and early Palaeozoic rocks of the Damara Orogen. In *The Geology of Namibia*, 2nd ed.; Miller, R.M., Ed.; Geological Survey of Namibia: Windhoek, Namibia, 2008; pp. 1311–1341.

31. Hoffmann, K.H. *Sedimentary Depositional History of the Damara Belt Related to Continental Breakup, Passive to Active Margin Transition and Foreland Basin Development*; Abstract of the 23rd Earth Science Congress; Geological Society of South Africa: Cape Town, South Africa, 1990; pp. 250–253.

32. Kukla, P.A.; Stanistreet, I.G. Record of the Damara Khomas Hochland accretionary prism in central Namibia: Refutation of an "ensialic" origin of a Late Proterozoic orogenic belt. *Geology* **1991**, *19*, 473–476. [CrossRef]

33. Kukla, P.A. Tectonics and sedimentation of a late Proterozoic Damaran convergent continental margin, Khomas Hochland. *Memoir. Geol. Surv. Namib.* **1992**, *12*, 1–95.

34. Blanco, G.; Germs, G.J.B.; Rajesh, H.M.; Chemale, F., Jr.; Dussin, I.A.; Justino, D. Provenance and paleogeography of the Nama Group (Ediacaran to early Paleozoic, Namibia): Petrography, geochemistry and U-Pb detrital zircon geochronology. *Precambr. Res.* **2011**, *187*, 15–32. [CrossRef]

35. Nascimento, D.B.; Ribeiro, A.; Trouw, R.A.J.; Schmitt, R.S.; Passchier, C.W. Stratigraphy of the Neoproterozoic Damara Sequence in northwest Namibia: Slope to basin sub-marine mass-transport deposits and olistolith fields. *Precambr. Res* **2016**, *278*, 108–125. [CrossRef]

36. Porada, H. The Damara-Ribeira orogen of the Pan-African/Brasiliano cycle in Namibia (South West Africa) and Brazil as interpreted in terms of continental collision. *Tectonophysics* **1979**, *57*, 237–265. [CrossRef]

37. Miller, R.M. The Pan-African Damara orogen of south west Africa/Namibia. In *Evolution of the Damara Orogen of South West Africa/Namibia*; Miller, R.M., Ed.; The Geological Society of South Africa: Johannesburg, South Africa, 1983; Volume 11, pp. 431–515.

38. Prave, A.R. Tale of three cratons: Tectostratigraphic anatomy of the Damara Orogen in northwestern Namibia and the assembly of Gondwana. *Geology* **1996**, *24*, 1115–1118. [CrossRef]

39. Puhan, D. Reverse age relations of talc and tremolite deduced from reaction textures in metamorphosed siliceous dolomites of the southern Damara Orogen (Namibia). *Contrib. Mineral. Petrol.* **1988**, *98*, 24–27. [CrossRef]

40. Smith, D.A.M. The geology around the Khan and Swakop Rivers in South West Africa. *Memoir. Geol. Surv. S. Afr. S.W. Afr. Ser.* **1965**, *3*, 113.

41. Jacob, R.E.; Snowden, P.A.; Bunting, F.J.L. Geology and structural development of the tumas basement dome and its cover rocks. In *Evolution of the Damara Orogen of South West Africa/Namibia*; Milled, R.M., Ed.; Geological Society of South Africa, Special Publisher: Johannesburg, South Africa, 1983; Volume 11, pp. 157–172.

42. Kröner, A. Dome structures and basement reactivation in the Pan-African Damara belt of Namibia/South West Africa. In *Precambrian Tectonics Illustrated*; Kröner, A., Greiling, R.O., Eds.; Naegele and Obermiller: Stuttgart, Germany, 1984; pp. 191–206.

43. Oliver, G.J.H. Mid-crustal detachment and domes in the central zone of the Damara Orogen, Namibia. *J. Afr. Earth Sci.* **1994**, *19*, 331–344. [CrossRef]

44. Poli, L.C.; Oliver, G.J.H. Constrictional deformation in the Central Zone of the Damara Orogen, Namibia. *J. Afr. Earth Sci.* **2001**, *33*, 303–321. [CrossRef]

45. Alexander, F.M.; Kisters, L.; Smith, J.; Kathrin, N. Thrust-related dome structures in the Karibib district and the origin of orthogonal fabric domains in the south Central Zone of the Pan-African Damara belt, Namibia. *Precambri. Res* **2004**, *133*, 283–303. [CrossRef]

46. Jacob, R.E. Geology and Metamorphic Petrology of Part of the Damara Orogen along the Lower Swarkop River, South West Africa. Bulletin of the Precambrian res Unit. Ph.D. Thesis, University of Cape Town, Cape Town, South Africa, 1974.

47. Smith, E.F.; MacDonald, F.A.; Crowley, J.L.; Hodgin, E.B.; Schrag, D.P. Tectonostratigraphic evolution of the *c*. 780–730 Ma Beck Spring Dolomite: Basin Formation in the core of Rodinia. *Geol. Soc. Lond.* **2016**, *424*, 213–239. [CrossRef]

48. Marian, M.L. Sedimentology of the Beck Spring Dolomite, Eastern Mojave Desert, California. Master's Thesis, University of Southern California, Los Angeles, CA, USA, 1979.

49. Corsetti, F.A.; Kaufman, A.J. Stratigraphic investigations of carbon isotope anomalies and Neoproterozoic ice ages in Death Valley, California. *Geol. Soc. Am. Bull.* **2003**, *115*, 916–932. [CrossRef]

50. Whitney, D.L.; Evans, B.W. Abbreviations for names of rock-forming minerals. *Am. Mineral.* **2010**, *95*, 185–187. [CrossRef]

51. Hubbard, C.R.; Snyder, R.L. RIR-measurement and use in quantitative XRD. *Powder Diffr.* **1988**, *3*, 74–77.

52. RRUFF™ Project Database. Available online: http://rruff.info/ (accessed on 20 February 2019).

53. Maire, E.; Withers, P.J. Quantitative X-ray tomography. *Int. Mater. Rev.* **2014**, *59*, 1–43. [CrossRef]

54. Paganin, D.; Mayo, S.C.; Gureyev, T.E.; Miller, P.R.; Wilkins, S.W. Simultaneous phase and amplitude extraction from a single defocused image of a homogeneous object. *J. Microsc.* **2002**. [CrossRef]

55. Leake, B.E.; Woolley, A.R.; Arps, C.E.; Birch, W.D.; Gilbert, M.C.; Grice, J.D.; Hawthorne, F.C.; Kato, A.; Kisch, H.J.; Krivovichev, V.G.; et al. Nomenclature of amphiboles: Report of the subcommittee on amphiboles of the international mineralogical association, commission on new minerals and mineral names. *Can. Mineral.* **1997**, *35*, 219–246.

56. Witek, J.; Psiuk, B.; Naziemiec, Z.; Kusiorowski, R. Obtaining an artificial aggregate from cement-asbestos waste by the melting technique in an arc-resistance furnace. *Fibers* **2019**, *7*, 10. [CrossRef]

57. Witek, J.; Kusiorowski, R. Neutralization of cement-asbestos waste by melting in an arc-resistance furnace. *Waste Manag.* **2017**, *69*, 336–345. [CrossRef]

58. Spasiano, D.; Pirozzi, F. Treatments of asbestos containing wastes. *J. Environ. Manag.* **2017**, *204*, 82–91. [CrossRef]

Assessment of Naturally Occurring Asbestos in the Area of Episcopia (Lucania, Southern Italy)

Andrea Bloise [1],*[iD], **Claudia Ricchiuti** [2], **Eugenia Giorno** [3], **Ilaria Fuoco** [1], **Patrizia Zumpano** [1], **Domenico Miriello** [1][iD], **Carmine Apollaro** [1][iD], **Alessandra Crispini** [3], **Rosanna De Rosa** [1] and **Rosalda Punturo** [2]

[1] Department of Biology, Ecology and Earth Sciences, University of Calabria, Via Pietro Bucci, I-87036 Rende, Italy; ilaria.fuoco@unical.it (I.F.); patrizia85@gmail.com (P.Z.); miriello@unical.it (D.M.); apollaro@unical.it (C.A.); derosa@unical.it (R.D.R.)

[2] Department of Biological, Geological and Environmental Sciences, University of Catania, Corso Italia, 55, 95129 Catania CT, Italy; claudia.ricchiuti@unict.it (C.R.); punturo@unict.it (R.P.)

[3] MAT-InLAB-Department of Chemistry and Chemical Technologies, University of Calabria, 87036 Arcavacata di Rende-Cosenza, Italy; eugenia.giorno@unical.it (E.G.); a.crispini@unical.it (A.C.)

* Correspondence: andrea.bloise@unical.it; Tel.: +39-0984-493588

Abstract: Over the last few years, the risk to human health related to asbestos fiber exposure has been widely demonstrated by many studies. Serpentinites are the main rocks associated with naturally occurring asbestos (NOA). In order to investigate the presence of NOA, a mineralogical study was conducted on eleven serpentinite samples collected nearby the village of Episcopia (Lucania, Southern Italy). Various analytical techniques such as X-ray powder diffraction (XRPD), scanning electron microscopy combined with energy dispersive spectrometry (SEM-EDS) and derivative thermogravimetry (DTG) were used to determine the occurrence of asbestos minerals and to make morphological observations. Results pointed out that all of the samples contain asbestos minerals (e.g., tremolite, actinolite and chrysotile). Moreover, it was observed that both natural processes and human activity may disturb NOA-bearing outcrops and provoke the formation of potentially inhalable airborne dust causing the release of asbestos fibers into the environment, thereby increasing the risk to human health. For this reason, our study aims to highlight the requirement of a natural asbestos survey and periodic update in the area.

Keywords: naturally occurring asbestos; serpentinites; polymorphs; health hazard

1. Introduction

Today, it is widely accepted in the scientific community that exposure to asbestos bring to the development of negative health issues. Indeed, malignant mesothelioma and lung cancers could be caused by the inhalation of asbestos fibers due to environmental exposure [1–4].

The silicate mineral habitus type may be fibrous or non-fibrous and, among the minerals which form the airborne particulate, the most hazardous ones display a fibrous-asbestiform crystal habitus [5]. The term Naturally occurring asbestos (NOA) refers to asbestos minerals contained in rocks and soils to distinguishing them from those contained in asbestos containing materials (ACM) [6–10]. Six fibrous silicate minerals belonging to the serpentine (i.e., chrysotile) and amphibole (i.e., tremolite, actinolite, anthophyllite, amosite, and crocidolite) mineral groups are defined as asbestos by law in Europe and in several countries worldwide [5]. However, many studies demonstrate that besides these six varieties, which are regulated as potential environmental pollutants by law, asbestiform minerals such as erionite, antigorite and fluoro-edenite could also be dangerous if respired by humans, leading to

several respiratory diseases [11–17]. The issue is even more complicated as the US National Institute for Occupational Safety and Health (NIOSH) has lately proposed to extend the definition of asbestos to all elongated mineral particles (EMP) [18].

Chrysotile is one of the three principal serpentine polymorphs (chrysotile, lizardite, and antigorite), and it occurs with a fibrous habit [17]. Structurally, it is constituted by tetrahedral silica-oxygen groups (SiO_4) (T) connected to brucite-type $Mg(OH)_2$ octahedral sheets (O) by sharing of oxygen atoms, forming structures having the ideal formula $Mg_3Si_2O_5(OH)_4$ [17]. Because of the smaller dimension of the tetrahedral sheets to the corresponding octahedral ones, the connection of the TO layers results in a rolled papyrus-like microstructure which may compose a characteristic fibrous habit [18].

Amphiboles are built on double-chains of Si_4O_{11} groups linked to each other by a variety of cations, which may display a fibrous habit being structurally elongated in one preferred crystal direction [17]. The chemical composition of the amphibole group can be expressed by the general formula $AB_2C_5T_8O_{22}(OH)_2$, where A = Na and K; B = Na, Ca, Fe^{2+}, Mg, Mn^{2+}, Li and rarer ions of similar size; C = Fe^{2+}, Mg, Mn^{2+}, Li, Fe^{3+}, Cr^{3+}, Al, Mn^{3+}, Zr^{4+} and Ti^{4+}; T = Si, Al, and Ti^{4+}; and (OH^-) may be replaced by F^-, Cl^- and O^{2-} [17–21]. The A-site is in 10–12-fold coordination, while the B- and C-sites are octahedrally coordinated [17]. Amphiboles can be shown in monoclinic or orthorhombic crystalline system, and for both, modern nomenclature is based on the atomic proportions of the major elements assigned to the A, B, C and T structural sites, following the rules of Leake [19,20]. Among the amphibole group minerals, tremolite, actinolite and anthophyllite occur in both asbestiform and non-asbestiform habit types, whereas crocidolite and amosite occur only in the asbestiform habit [18].

Serpentinite rocks are widely outcropping in the Lucania region (Southern Italy) [22,23] and often they are removed from their natural place of origin to be used as ornamental stones and building materials due to their coloring and physic-mechanical properties [24]. However, asbestos tremolite/actinolite and/or chrysotile are detected in serpentinite outcrops of several urban centers of the region [25], including Episcopia. The release of asbestos fibers in the environment is the result of both natural weathering processes (e.g., erosion) and human activities (e.g., excavation or road construction), which may disturb NOA outcrops and provoke the formation of potentially inhalable airborne dust [6,21], causing one or more respiratory diseases that could occur after a long latency time (e.g., [1]). In particular, about 3000 people living around the study area, comprising Episcopia village and its hamlets (Figure 1), could be exposed to potential sources of airborne asbestos due to the wide distribution of outcrops where serpentinite is exploited.

Previous studies on serpentine rocks, carried out in the central and southern parts of the Basilicata region, highlighted that it is necessary to deepen public health studies in order to characterize and determine the position of NOA [22–26]. Moreover, a recent epidemiological study conducted in twelve villages located in this part of the region showed significant excesses in health problems that are NOA-correlated cases [27]. Particularly, in the geographic area located about 20 km from Episcopia, several mesothelioma cases were documented in which the etiological factor turned out to be exposure to asbestos minerals [28,29]. Therefore, local maps indicating areas where asbestos is present in outcropping rocks, as is established by Italian law (DM 18/03/2003), are crucial to avoid hazardous exposure to populations.

So far, a detailed mineralogical characterization of asbestos minerals present in the area of the Episcopia village is still lacking in the literature. In this context, aiming to point out the eventual presence of asbestos minerals within the serpentinite rocks cropping out in the surroundings of the Episcopia village (Figure 1), we collected eleven rock samples, studied them and crossed the data obtained from different analytical techniques (i.e., X-ray powder diffraction (XRPD), scanning electron microscopy combined with energy dispersive spectrometry (SEM-EDS) and derivative thermogravimetry (DTG)) for a detailed mineralogical characterization.
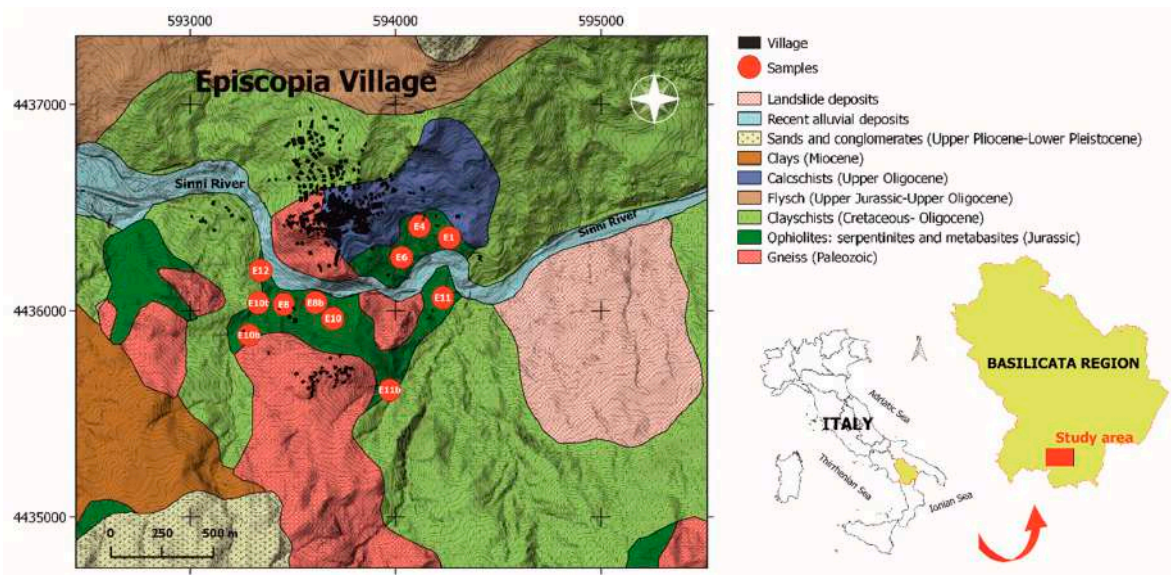
Figure 1. Simplified geological map of the Episcopia village and the study area location with the sample sites.

2. Materials and Methods

The Episcopia village (Figure 1) is located to the south-western part of the San Arcangelo basin in the Pollino National Park of the Basilicata region [30]. The pre-Pleistocene substrate (Episcopia-San Severino mélange) is discriminated by articulated tectonic slices overlapping that belong to different geological units and formations. Along the Sinni River, calc-schists and phyllites to the Unit of Frido crop out [31–35]. Over the Frido Unit, meta-ophiolites, made up of lenticular metabasite interbedded with and highly fractured serpentinites may occur (Figure 1) [32,36]. In a higher stratigraphic position, the Crete Nere and Saraceno formations and the Flysch of Albidona appear, which are non-metamorphic lithotypes referable to the North-Calabrian Unit [37].

With the aim to assess the presence of NOA in the area of the Episcopia village, 11 serpentinite rock samples were collected and characterized by X-ray powder diffraction (XRPD), scanning electron microscopy combined with energy dispersive spectrometry (SEM-EDS) and thermogravimetric analysis (TGA-DTG). Sample collection was conducted in the area surrounding the village, in particular the pieces were taken at the road cuts outside and within the village center and at dirt roads and slops in which serpentinites are well-exposed and display a vivid green color (Figure 2a,b).

X-ray powder diffraction (XRPD) data were obtained by X-ray diffraction acquired on a Bruker D2-Phaser (Bruker, Billerica, MA, USA) equipped with Cu Kα radiation (λ = 1.5418 Å) and a Lynxeye detector, at 30 kV and 10 mA, with a step size of 0.01° (2θ) and between 5 and 66° (2θ). The crystalline phases and semi-quantitative mineralogical composition of samples were obtained using EVA software (DIFFRACPlusEVA), which compares the experimental peaks with the 2005 PDF2 reference patterns. In the laboratory, the samples were recovered under a binocular microscope (20x, ZEISS, Thornwood, NY, USA) in order to choose representative fragments (i.e., more fibrous) to be studied by scanning electron microscopy. Scanning electron microscopy analysis combined with energy dispersive spectrometry (SEM-EDS) for the morphological observations was performed using an Environmental Scanning Electron Microscope FEI QUANTA 200 (Thermo Fisher Scientific, Waltham, MA, USA) equipped with an X-ray EDS suite comprising a Si/Li crystal detector model EDAX-GENESIS4000 (EDAX Inc., Mahwah, NJ, USA). For SEM examinations, a piece of each sample was firmed on an SEM stub utilizing double-sided conductive adhesive tape. In the present paper, the weight change was evaluated by thermogravimetric analysis (TGA: Netzsch STA 449 C Jupiter, Netzsch-Gerätebau GmbH, Selb, Germany). During thermogravimetric analysis (TGA) the samples were heated at a rate of 10 °C·min^{-1} in the 30–850 °C temperature range under an air flow of 30 mL·min^{-1}. About 20 mg of a sample were

used for each run. Instrumental precision was checked by three repeated collections on a kaolinite reference sample revealing good reproducibility (instrumental theoretical T precision of ±1.2 °C). Derivative thermogravimetry (DTG) was obtained using the Netzsch Proteus thermal analysis software (Netzsch-Gerätebau GmbH, Selb, Germany). For X-ray powder diffraction and thermal analysis investigations, samples were mechanically milled using a Bleuler Rotary Mill (Sepor, Los Angeles, CA, USA) for 10 s at a speed of 900 revolutions per min (rpm).
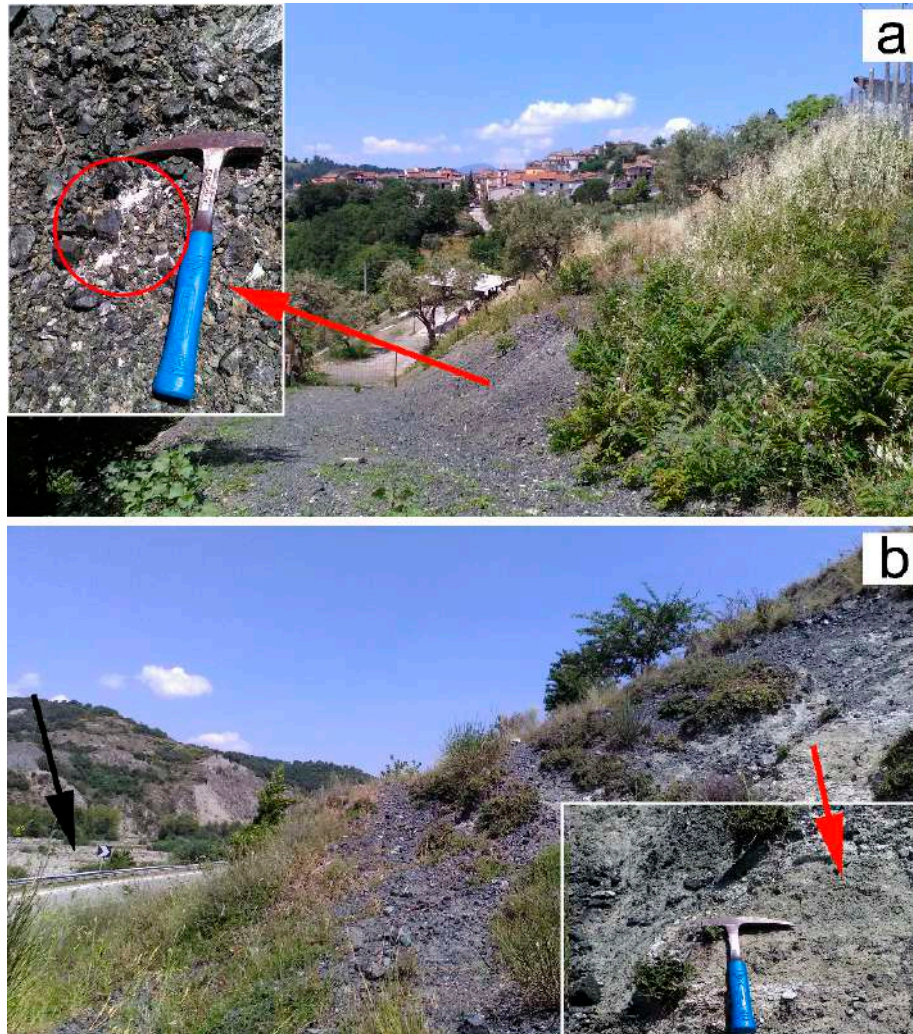
Figure 2. (**a**) Distant view of the Episcopia village, with appearance of serpentinite at the road cut near to the village (the red circle encloses white fibers of asbestos tremolite); and (**b**) pictures show vivid green serpentine at the road cut near to the village of Episcopia (highway 656 indicated by the black arrow). Inserts depict a zoomed-in area.

3. Results and Discussion

The field survey carried out nearby the Episcopia village (Figure 2) showed that serpentinite rocks appear to be characterized by a massive structure and by a dark-green color with widespread white parts consisting of fibrous minerals. Figure 3 shows the details of the studied samples at the mesoscopic scale, where it is possible to appreciate the appearance of white tremolite fibers (Figure 3a) and dark green serpentine (Figure 3b).

Figure 3. (**a**) White and silky tremolite on the surface of a serpentinite sample at the mesoscopic scale; and (**b**) the characteristic blazing surface of serpentinite, looking like a snake's skin.
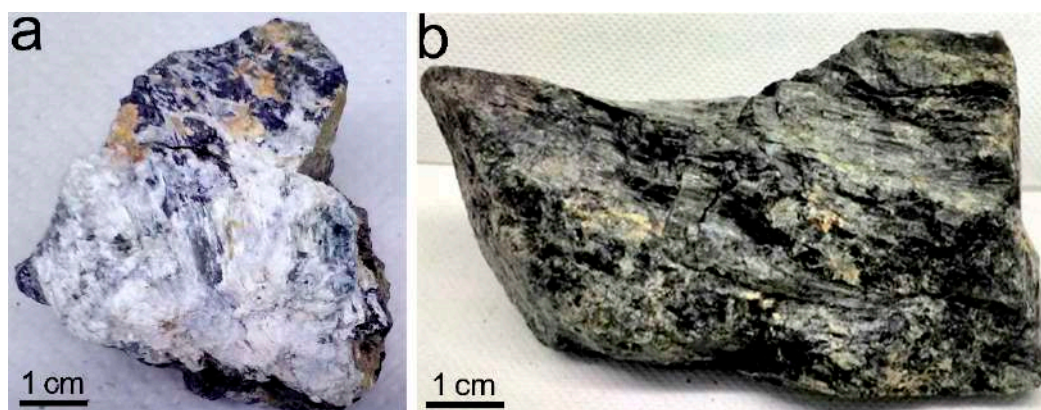
The study conducted through various analytical techniques on eleven samples of serpentinite cropping out in the area of Episcopia village was finalized by determining the presence of NOA. Results of XRPD patterns showed that the investigated specimens are composed of serpentine minerals, chlorite, talc, tremolite, actinolite, willemseite and dolomite (Table 1). In particular, by the diffractograms interpretation the presence of serpentine minerals came out in all of the samples except for two, in which talc and tremolite (sample E10) and actinolite, willemseite, and dolomite (sample E10b) were the only phases detected. It is worth noting that the reflections diagnostic of the presence of asbestos amphiboles (i.e., tremolite/actinolite) were found in eight samples out of eleven (Table 1).

Table 1. Semi-quantitative mineralogical composition of samples in order of decreasing relative abundance, detected by X-ray powder diffraction (XRPD), scanning electron microscopy combined with energy dispersive spectrometry (SEM-EDS) and derivative thermogravimetry (DTG) analysis. Atg = antigorite, Lz = lizardite, Ctl = chrysotile, Act = asbestos actinolite, Tr = asbestos tremolite, PS = polygonal serpentine, Chl = chlorite, Will = willemseite, Dol = dolomite, and Tlc = talc. Mineral symbols after [38].

Sample	Site Description	Longitude East (WGS84)	Latitude North (WGS84)	Phases Detected Max ↔ Min
E1	Slope	594261	4436353	Ctl > Liz > Atg > Chl > Tlc > Tr
E4	Road cut	594118	4436407	Ctl > PS > Chl > Tlc > Tr
E6	Slope	594031	4436259	Chl > Tr > Liz > Ctl
E8	Dirt road	593457	4436029	Chl > Liz > Ctl
E8b	Dirt road	593611	4436038	Chl > Ctl > PS
E10	Slope	593696	4435960	Tlc > Tr
E10b	Road cut	593287	4435880	Wil > Dol > Act
E10t	Dirt road	593332	4436037	Tlc > Ctl > Atg > Act
E11	Road cut	594231	4436063	Tlc > Liz > Ctl,
E11b	Road cut	593973	4435615	Liz > Ctl > Tlc > Tr
E12	Road cut	593342	4436196	Tlc > Ctl > PS > Act

However, discrimination among the serpentine varieties (i.e., chrysotile, lizardite, antigorite, and polygonal serpentine) was not achievable by using only the X-ray powder diffraction method because diffraction peaks of the serpentine polymorphs overlap each other [7]. As reported in the literature, thermal analysis allowed for the discrimination among serpentine varieties [22,39]. Therefore, only samples in which serpentine minerals were detected by XRPD have been further investigated by thermal analysis. The correspondence between the maximum loss rates peaks and the serpentine minerals was defined in agreement with the literature data [40].

In particular, DTG curves showed the maximum peaks loss rate in the temperature range of 605–690 °C due to the chrysotile breakdown (Figure 4). The presence of DTG peaks in a temperature range of 705–731 °C were related to lizardite dehydroxylation, while antigorite occurred at higher temperatures (a 770 °C average value) than lizardite. Based on thermal analysis, chrysotile was identified in nine out of eleven analyzed samples, lizardite was detected in five samples, while antigorite and polygonal serpentine in two and three samples, respectively (Table 1).
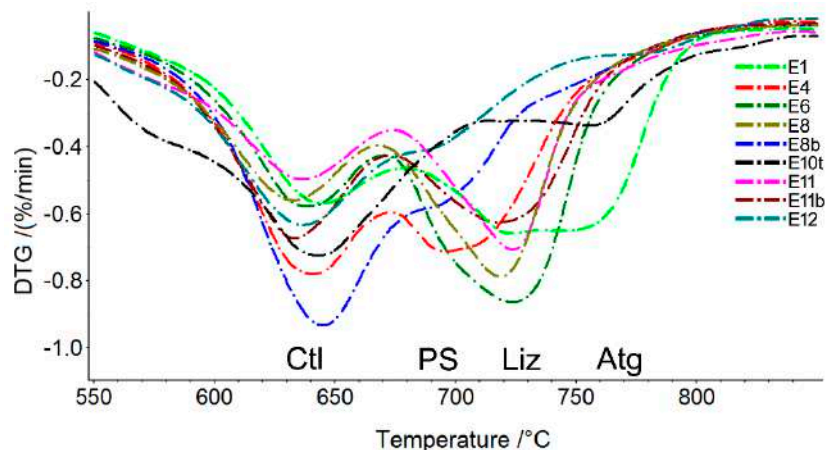

Figure 4. DTG curves for each sample in the temperature range of 500–850 °C. Endothermic peaks related to Ctl = chrysotile, PS = polygonal serpentine, Liz = lizardite, and Atg = antigorite. Mineral symbols after [38].

SEM observations highlighted that chrysotile is made up of either thin and flexible isolated fibril (Figure 5a) with a length longer than 6–8 µm or crystals arranged in bundles. In contrast, tremolite and actinolite appear straight and show a slender needle-like crystal habit with a length longer than 10 µm (Figure 5b). It is worth remembering that fibers are composed of many fibrils, which tend to split up along the fiber elongation axis [18]. This tendency leads to even smaller diameters, thus increasing the risks for human health related to the inhalation when they become airborne. Moreover, fibers having size matching with those of regulated asbestos (length >5 µm and an aspect ratio of 3) of both chrysotile and tremolite/actinolite have been detected in all samples, even if the length of both chrysotile and tremolite/actinolite fibers were sometimes shorter than the length established by law (Italian Legislative Decree 277/9).
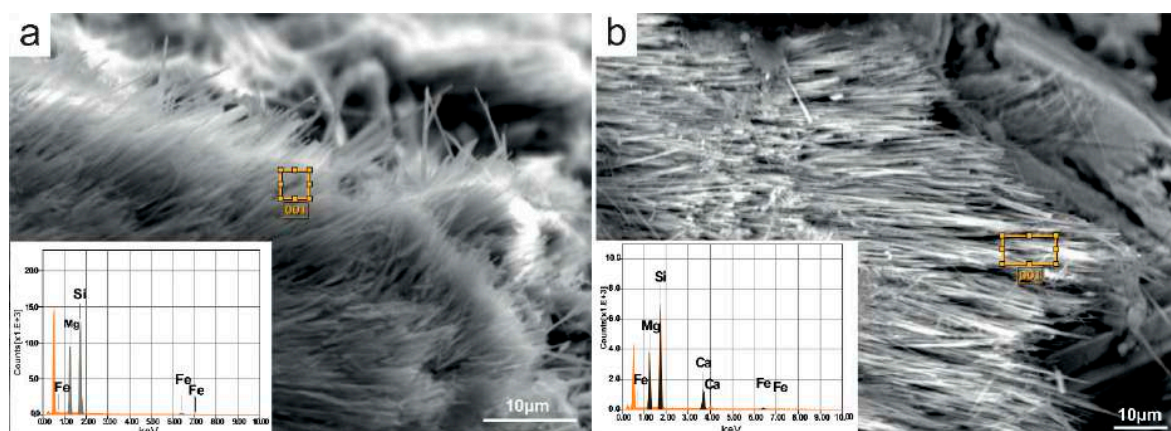

Figure 5. Scanning electron microscopy (SEM) images of asbestos. (**a**) Chrysotile sample E11; and (**b**) tremolite sample E4. Graphical inserts depict energy dispersive spectrometry (EDS) point analysis.

The use of the energy dispersive spectrometry (EDS) spot analysis (Figure 5a,b inserts) is essential for the correct identification of the chrysotile and tremolite/actinolite asbestos fibers. Chrysotile fibers show low amounts of Al, which mainly replaces the Mg in the octahedral sites. The EDS analyses revealed a low percent replacement of Mg for Fe occurs in the octahedral sites of chrysotile [22]. Regarding iron content, it ranges from a minimum of 3.51 wt % (sample E11) of FeO to 8.71 wt % (sample E12) with an mean value of 4.90 wt %. The presence of iron could play an significant function in the biological–mineral system interaction, increasing fiber toxicity, which has been unequivocally related to the effect of surface iron ions acting as catalytic sites generating free radicals and reactive oxygen species (ROS) [41].

The chemical composition of amphiboles detected by EDS was plotted in the diagram Si vs. $Mg/(Mg + Fe^{2+})$ [19], and graphically reported in Figure 6. Three samples (E10b, E10t, and E12) were plotted in the field of actinolite since their composition is: (i) an Si value to 7.94 a.p.f.u. (atoms per formula unit) and $Mg/(Mg + Fe^{2+})$ value to 0.87 (sample E10t); (ii) an Si value to 7.96 a.p.f.u. and $Mg/(Mg + Fe^{2+})$ value to 0.88 (sample E10b); and (iii) an Si value to 7.98 a.p.f.u. and $Mg/(Mg + Fe^{2+})$ value equal to 0.89. Five amphiboles were classified as tremolite (Table 1) since their chemical composition is: an Si range from 7.94 to 7.99 a.p.f.u. and a $Mg/(Mg + Fe^{2+})$ value >0.9.

The presence of iron in actinolite and tremolite could have a preeminent role in the biological–mineral system interaction. Indeed, it is worth pointing out that many researchers suggested that iron is a key component in asbestos toxicity [41–43]. Although some authors consider amphiboles (e.g., tremolite and crocidolite) to be more harmful than chrysotile to human health [43,44], all of the six asbestos minerals are assumed to be harmful. Therefore, in our opinion serpentinite samples containing asbestos are all potentially toxic for humans.
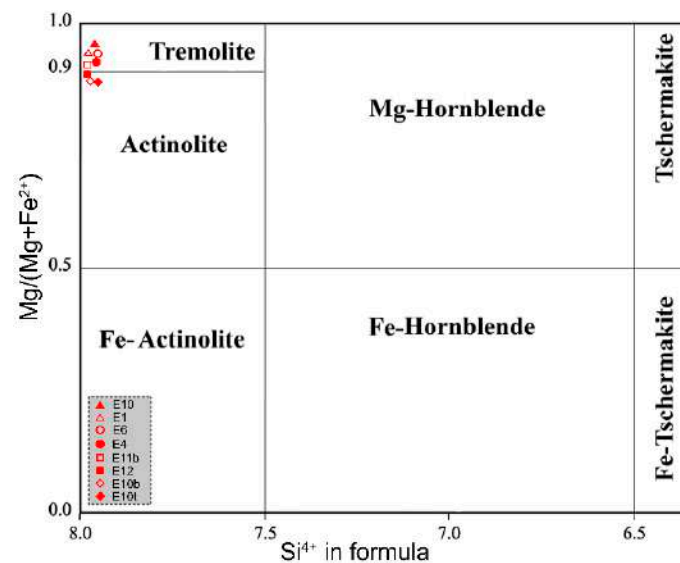
Figure 6. Amphibole classification diagram (after [19]).

Moreover, the analyses carried out by means of XRPD permitted also the identification of a nickelian-talc type named willemseite $(Ni,Mg)_3Si_4O_{10}(OH)_2$ never detected before in the study area (Table 1). Table 1 shows the list of the phases identified in each sample and chrysotile, tremolite and actinolite turn out to be common phases of the serpentinite rocks studied. Since the economy of the area is mainly based on sheep farming and agriculture, it may be assessed that shepherds and farmers are the working figures potentially at highest risk of exposure. The continuous movements of the flocks and the machining of the soil could cause suspension and diffusion of powders containing chrysotile, tremolite and actinolite fibers, with the consequent risk of inhalation by people employed in these activities. A similar situation could occur for farmers who, meanwhile carrying out their business, can breathe dangerous chrysotile, tremolite and actinolite fibers. Furthermore, other figures can suffer

damage as a result of exposure to asbestos dust that is freed during the construction of rural buildings (for example houses) or other construction works (e.g., dirt roads and fences). Moreover, due to its geomorphological, geological and climatic setting, the Basilicata region (Figure 1) is affected by the diffuse presence of landslides [45] that may disturb NOA-bearing outcrops. Indeed, chrysotile together with asbestos tremolite and actinolite may release airborne dust in the neighboring environment, thus increasing population exposure to hazardous air fibers.

4. Conclusions

In this study, serpentinite rocks cropping out nearby the Episcopia village (Lucania, Southern Italy) have been investigated by means of various analytical techniques (i.e., XRPD, SEM-EDS and DTG) with the aim to assess the occurrence of naturally occurring asbestos. The results obtained indicate that the presence of asbestos was detected in all the serpentinite samples, and therefore it may be deduced that all of the analyzed specimens are potentially injurious to human health.

The presence of chrysotile was detected in nine of the eleven samples analyzed, while asbestos tremolite and asbestos actinolite were identified in five and three samples, respectively. The observed dimension of these fibers generally matched with the size of regulated asbestos. Weathering processes and/or human activities are able to produce dust containing asbestos fibers which are potentially inhalable, therefore increasing the human health risks. Their wide dispersion into the environment makes inhalation a risk even for those people not related to occupational purposes. The presence of NOA during working activities should be considered in the preliminary planning step to avoid workers' health risks and sanitary risks for the population living near asbestos sites. The disturbance (excavations, remediation, and moving) of asbestos potentially containing rocks and soils should be foreseen and planned so that adequate control measures may be carried out to avoid the spreading of airborne asbestos dust during work.

It is worth mentioning that, owing to possible health problems due to asbestos fiber dispersion the Italian law regulates these types of outcrops, demanding the asbestos presence identification in order to increase health safeguard. These new knowledge and highlights can be used to provide data for compulsory Italian mapping and should encourage local, regional and national authorities to avoid and to prevent asbestos exposure risks. Moreover, this study could be useful to make the population aware of the geological context in which they live, in order to take adequate prevention measures and good practices in everyday life. Therefore, the asbestos minerals investigation is essential from both scientific and legislative viewpoint, particularly for the administrative agencies, whose task it is to defense public health and to implement construction and safeguard policies.

References

1.　Baumann, F.; Buck, B.J.; Metcalf, R.V.; McLaurin, B.T.; Merkler, D.J.; Carbone, M. The presence of asbestos in the natural environment is likely related to mesothelioma in young individuals and women from Southern Nevada. *J. Thorac. Oncol.* **2015**, *10*, 731–737. [CrossRef] [PubMed]

2. Gamble, J.F.; Gibbs, G.W. An evaluation of the risks of lung cancer and mesothelioma from exposure to amphibole cleavage fragment. *Regul. Toxicol. Pharmacol.* **2008**, *52*, 154–186. [CrossRef]

3. Hillerdal, G. Mesothelioma: Cases associated with non-occupational and low dose exposures. *Int. J. Occup. Environ. Med.* **1999**, *56*, 505–513. [CrossRef]

4. Berry, G.; Gibbs, G.W. Mesothelioma and asbestos. *Regul. Toxicol. Pharmacol.* **2008**, *52*, S223–S231.

5. Gualtieri, A.F. *Mineral Fibers: Crystalchemistry, Chemical-Physical Properties, Biological Interaction and Toxicity*; European Mineralogical Union and Mineralogical Society of Great Britain and Ireland: London, UK, 2017; p. 533.

6. Punturo, R.; Bloise, A.; Critelli, T.; Catalano, M.; Fazio, E.; Apollaro, C. Environmental implications related to natural asbestos occurrences in the ophiolites of the Gimigliano-Mount Reventino Unit (Calabria, southern Italy). *Int. J. Environ. Res.* **2015**, *9*, 405–418.

7. Bloise, A.; Punturo, R.; Catalano, M.; Miriello, D.; Cirrincione, R. Naturally occurring asbestos (NOA) in rock and soil and relation with human activities: The monitoring example of selected sites in Calabria (southern Italy). *Ital. J. Geosci.* **2016**, *135*, 268–279. [CrossRef]

8. Vignaroli, G.; Ballirano, P.; Belardi, G.; Rossetti, F. Asbestos fibre identification vs. evaluation of asbestos hazard in ophiolitic rock mélanges, a case study from the Ligurian Alps (Italy). *Environ. Earth Sci.* **2014**, *72*, 3679–3698. [CrossRef]

9. Bloise, A.; Belluso, E.; Critelli, T.; Catalano, M.; Apollaro, C.; Miriello, D.; Barrese, E. Amphibole asbestos and other fibrous minerals in the meta-basalt of the Gimigliano-Mount Reventino Unit (Calabria, south-Italy). *Rend. Online Soc. Geol. Ital.* **2012**, *21*, 847–848.

10. Harper, M. 10th Anniversary critical review: Naturally occurring asbestos. *J. Environ. Monit.* **2008**, *10*, 1394–1408. [CrossRef] [PubMed]

11. Baumann, F.; Ambrosi, J.-P.; Carbone, M. Asbestos is not just asbestos: An unrecognised health hazard. *Lancet Oncol.* **2013**, *14*, 576–578. [CrossRef]

12. Ballirano, P.; Bloise, A.; Cremisini, C.; Nardi, E.; Montereali, M.R.; Pacella, A. Thermally induced behavior of the K-exchanged erionite: A further step in understanding the structural modifications of the erionite group upon heating. *Period. Mineral.* **2018**, *87*, 123–134.

13. Ballirano, P.; Pacella, A.; Bloise, A.; Giordani, M.; Mattioli, M. Thermal Stability of Woolly Erionite-K and Considerations about the Heat-Induced Behaviour of the Erionite Group. *Minerals* **2018**, *8*, 28. [CrossRef]

14. Cardile, V.; Lombardo, L.; Belluso, E.; Panico, A.; Capella, S.; Balazy, M. Toxicity and carcinogenicity mechanisms of fibrous antigorite. *Int. J. Environ. Res. Public Health* **2007**, *4*, 1–9. [CrossRef] [PubMed]

15. Pinizzotto, M.R.; Cantaro, C.; Caruso, M.; Chiarenza, L.; Petralia, C.; Turrisi, S.; Brancato, A. Environmental monitoring of airborne fluoro-edenite fibrous amphibole in Biancavilla (Sicily, Italy): A nine-years survey. *J. Mediterr. Earth Sci.* **2018**, *10*, 89–95. [CrossRef]

16. Bellomo, D.; Gargano, C.; Guercio, A.; Punturo, R.; Rimoldi, B. Workers' risks in asbestos contaminated natural sites. *J. Mediterr. Earth Sci.* **2018**, *10*, 97–106.

17. Ballirano, P.; Bloise, A.; Gualtieri, A.F.; Lezzerini, M.; Pacella, A.; Perchiazzi, N.; Dogan, M.; Dogan, A.U. The Crystal Structure of Mineral Fibers. In *Mineral Fibers: Crystal Chemistry, Chemical-Physical Properties, Biological Interaction and Toxicity*; Gualtieri, A.F., Ed.; European Mineralogical Union: London, UK, 2017; Volume 18, pp. 17–53.

18. Belluso, E.; Cavallo, A.; Halterman, D. Crystal habit of mineral fibres. In *Mineral Fibres: Crystal Chemistry, Chemical-Physical Properties, Biological Interaction and Toxicity*; Gualtieri, A.F., Ed.; European Mineralogical Union: London, UK, 2017; Volume 18, pp. 65–109.

19. Leake, B.E.; Woolley, A.R.; Arps, C.E.; Birch, W.D.; Gilbert, M.C.; Grice, J.D.; Linthout, K.; Laird, J.; Mandarino, J.; Maresch, W.V.; et al. Nomenclature of amphiboles: Report of the subcommittee on amphiboles of the international mineralogical association, commission on new minerals and mineral names. *Can. Mineral.* **1997**, *35*, 219–246.

20. Bloise, A.; Fornero, E.; Belluso, E.; Barrese, E.; Rinaudo, C. Synthesis and characterization of tremolite asbestos fibres. *Eur. J. Mineral.* **2008**, *20*, 1027–1033. [CrossRef]

21. Bloise, A.; Barca, D.; Gualtieri, A.F.; Pollastri, S.; Belluso, E. Trace elements in hazardous mineral fibres. *Environ. Pollut.* **2016**, *216*, 314–323. [CrossRef]

22. Bloise, A.; Catalano, M.; Critelli, T.; Apollaro, C.; Miriello, D. Naturally occurring asbestos: Potential for human exposure, San Severino Lucano (Basilicata, Southern Italy). *Environ. Earth Sci.* **2017**, *76*, 648. [CrossRef]

23. Punturo, R.; Ricchiuti, C.; Bloise, A. Assessment of Serpentine Group Minerals in Soils: A Case Study from the Village of San Severino Lucano (Basilicata, Southern Italy). *Fibers* **2019**, *7*, 18. [CrossRef]

24. Dichicco, M.C.; Paternoster, M.; Rizzo, G.; Sinisi, R. Mineralogical Asbestos Assessment in the Southern Apennines (Italy): A Review. *Fibers* **2019**, *7*, 24. [CrossRef]

25. Massaro, T.; Baldassarre, A.; Pinca, A.; Martina, G.L.; Fiore, S.; Lettino, A.; Cassano, F.; Musti, M. Exposure to asbestos in buildings in areas of Basilicata characterized by the presence of rocks containing tremolite. *G. Ital. Med. Lav. Ergon.* **2012**, *34* (Suppl. 3), 568–570.

26. Dichicco, M.C.; Laurita, S.; Paternoster, M.; Rizzo, G.; Sinisi, R.; Mongelli, G. Serpentinite Carbonation for CO_2 Sequestration in the Southern Apennines: Preliminary Study. *Energy Procedia* **2015**, *76*, 477–486. [CrossRef]

27. Caputo, A.; De Santis, M.; Manno, V.; Cauzillo, G.; Bruni, B.M.; Palumbo, L.; Conti, S.; Comba, P. Health impact of asbestos fibres naturally occurring in Mount Pollino area (Basilicata Region, Southern Italy). *Epidemiol. Prev.* **2018**, *42*, 142–150. [PubMed]

28. Pasetto, R.; Bruni, B.; Bruno, C.; Cauzillo, G.; Cavone, D.; Convertini, L.; De Mei, B.; Marconi, A.; Montagano, G.; Musti, M.; et al. Mesotelioma pleurico ed esposizione ambientale a fibre minerali: Il caso di un'area rurale in Basilicata. *Annali dell'Istituto Superiore di Sanità* **2004**, *40*, 251–265. [PubMed]

29. Musti, M.; Bruno, C.; Cassano, F.; Caputo, A.; Cauzillo, G.; Cavone, D.; Convertini, L.; De Blasio, A.; De Mei, B.; Marra, M.; et al. Sorve-glianza sanitaria delle popolazioni esposte a fibre di tremolite nel territorio della ASL 3—Lagonegro (PZ). *Annali dell'Istituto Superiore di Sanità* **2006**, *42*, 469–476. [PubMed]

30. Pieri, P.; Vitale, G.; Beneduce, P.; Doglioni, C.; Gallicchio, S.; Giano, S.I.; Loizzo, R.; Moretti, M.; Prosser, G.; Sabato, L.; et al. Tettonica quaternaria nell'area bradanico-ionica. *Il Quaternario* **1997**, *10*, 535–542.

31. Critelli, S.; Le Pera, E. Post-Oligocene sediment dispersal systems and unroofing history of the Calabrian Microplate, Italy. *Int. Geol. Rev.* **1998**, *48*, 609–637. [CrossRef]

32. Vitale, S.; Ciarcia, S.; Tramparulo, F.D.A. Deformation and stratigraphic evolution of the Ligurian Accretionary Complex in the southern Apennines (Italy). *J. Geodyn.* **2013**, *66*, 120–133. [CrossRef]

33. Apollaro, C.; Dotsika, E.; Marini, L.; Barca, D.; Bloise, A.; De Rosa, R.; Doveri, M.; Lelli, M.; Muto, F. Chemical and isotopic characterization of the thermo mineral water of Terme Sibarite springs (Northern Calabria, Italy). *Geochem. J.* **2012**, *46*, 117–129. [CrossRef]

34. Guagliardi, I.; Buttafuoco, G.; Apollaro, C.; Bloise, A.; De Rosa, R.; Cicchella, D. Using gamma-ray spectrometry and geostatistics for assessing geochemical behavior of radioactive elements in the Lese catchment (southern Italy). *Int. J. Environ. Res.* **2013**, *7*, 645–658.

35. Apollaro, C.; Fuoco, I.; Brozzo, G.; De Rosa, R. Release and fate of Cr (VI) in the ophiolitic aquifers of Italy: The role of Fe (III) as a potential oxidant of Cr (III) supported by reaction path modelling. *Sci. Total Environ.* **2019**, *660*, 1459–1471. [CrossRef]

36. Bonardi, G.; Amore, F.O.; Ciampo, G.; Capoa, P.; Miconnet, P.; Perrone, V. Il Complesso Liguride Auct.: Stato delle conoscenze e problemi aperti sulla sua evoluzione pre-appenninica ed i suoi rapporti con l'Arco Calabro. *Mem. Soc. Geol. Ital.* **1988**, *41*, 17–35.

37. Belviso, C.; Lettino, A.; Cavalcante, F.; Fiore, S.; Finizio, F. *Carta Geologica delle Unità Liguridi dell'area del Pollino (Basilicata)*; Digilabs: Bari, Italy, 2009; ISBN 978-88-7522-026-6.

38. Whitney, D.L.; Evans, B.W. Abbreviations for names of rock-forming minerals. *Am. Mineral.* **2010**, *95*, 185–187. [CrossRef]

39. Bloise, A.; Kusiorowski, R.; Lassinantti Gualtieri, M.; Gualtieri, A.F. Thermal behaviour of mineral fibers. In *Mineral Fibers: Crystal Chemistry, Chemical-Physical Properties, Biological Interaction and Toxicity*; Gualtieri, A.F., Ed.; European Mineralogical Union: London, UK, 2017; Volume 18, pp. 215–252.

40. Viti, C. Serpentine minerals discrimination by thermal analysis. *Am. Mineral.* **2010**, *95*, 631–638. [CrossRef]

41. Fubini, B.; Mollo, L. Role of iron in the reactivity of mineral fibers. *Toxicol. Lett.* **1995**, *82*, 951–960. [CrossRef]

42. Shukla, A.; Mossman, B. Cell signalling and transcription factor activation by asbestos in lung injury and disease. *Int. J. Biochem. Cell Biol.* **2003**, *35*, 1198–1209. [CrossRef]

43. Turci, F.; Tomatis, M.; Pacella, A. Surface and bulk properties of mineral fibres relevant to toxicity. In *Mineral Fibers: Crystal Chemistry, Chemical-Physical Properties, Biological Interaction and Toxicity*; Gualtier, A.F., Ed.; European Mineralogical Union: London, UK, 2017; Volume 18, pp. 171–214.

44. Oze, C.; Solt, K. Biodurability of chrysotile and tremolite asbestos in simulated lung and gastric fluid. *Am. Mineral.* **2010**, *95*, 825–831. [CrossRef]

45. Lazzari, M.; Piccarreta, M.; Capolongo, D. Landslide triggering and local rainfall thresholds in Bradanic Foredeep, Basilicata region (southern Italy). In *Landslide Science and Practice*; Springer: Berlin/Heidelberg, Germany, 2013; pp. 671–677.

X-ray synchrotron microtomography: a new technique for characterizing chrysotile asbestos

Andrea Bloise [a,*], Claudia Ricchiuti [b], Gabriele Lanzafame [b], Rosalda Punturo [b]

[a] Department of Biology, Ecology and Earth Sciences, University of Calabria, I-87036 Rende, CS, Italy
[b] Department of Biological, Geological and Environmental Sciences, University of Catania, I-95129 Catania, Italy

HIGHLIGHTS

- Chrysotile asbestos was examined using SR-µCT for the first time.
- 3D analysis provides information on the aspect ratio of chrysotile asbestos.
- 3D analysis provides morphological information of the serpentinite veins.
- Chemical variations were observed between the veins and the serpentinite matrix.

GRAPHICAL ABSTRACT

X-ray synchrotron microtomography: a new technique for characterizing chrysotile that fill the veins found within massive serpentinite rocks
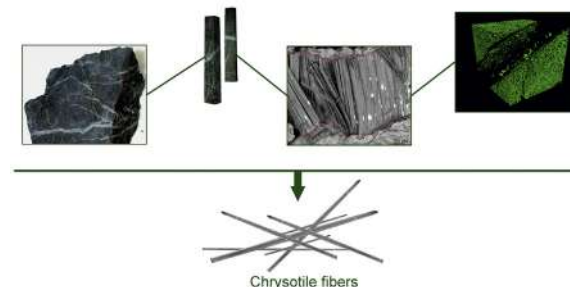
Chrysotile fibers

ARTICLE INFO

ABSTRACT

Over the last decades, many studies have been conducted on rocks containing Naturally Occurring Asbestos (NOA) to determine the potential health risks to exposed neighboring populations. It is difficult to accurately characterize the asbestos fibres contained within the rocks as conventional techniques are not effective and have drawbacks associated with the disturbance of the sample under study. X-ray synchrotron microtomography (SR-µCT) supplemented with polarized light microscope (PLM), scanning electron microscopy analysis combined with energy dispersive spectrometry (SEM/EDS), electron probe micro-analysis (EPMA) were used for identifying asbestos fibres in a mineral matrix. As a case study, we analyzed a representative set of veins and fibrous chrysotile that fills the veins, taken from massive serpentinite outcrops (Southern-Italy). We were able to identify respirable chrysotile fibres (regulated asbestos) within the serpentinite matrix. SR-µCT of NOA veins achieved the resolution and reconstructed 3D structures of infill chrysotile asbestos fibres and other phase structures that were not resolvable with PLM, SEM or EPMA. Moreover, due to differences in chemical composition between veins and matrix, the data obtained enabled us to evaluate the vein shapes present in the massive serpentinite matrix. In particular, iron and aluminum distribution variations between veins and matrix induce different radiation absorption patterns thus permitting a detailed image-based 3D geometric reconstruction. The advantages of the SR-µCT technique as well as limitation of conventional methods are also discussed. These analytical approaches will be used for conducting future research on NOA of other minerals, which exhibit asbestiform and non-asbestiform habits within veins, including asbestos amphiboles.

© 2019 Elsevier B.V. All rights reserved.

* Corresponding author.
    E-mail address: andrea.bloise@unical.it (A. Bloise).

1. Introduction

Serpentinite rocks host Naturally Occurring Asbestos (NOA) which is a potential hazard to human health due to its link to mesothelioma, lung cancer and asbestosis (Baumann et al., 2015; Bloise et al., 2019; Colombino et al., 2019; Harper, 2008; Petriglieri et al., 2019; Punturo et al., 2019a). Serpentinite rocks are formed by the low-temperature hydration of ultramafic rocks (i.e. peridotite, pyroxenite), during which olivine and pyroxenes are transformed into serpentine minerals (chrysotile, lizardite and antigorite) (Bloise et al., 2017; Guillots and Hattori, 2013). Serpentinization significantly alters the physical, mechanical, and chemical properties of ultramafic protoliths, which can be partially or totally serpentinized and therefore exhibit various types of texture (Andréani et al., 2004). Serpentinization is associated with abundant veining development marked by different generations of veins filled with serpentine minerals, which leads to a decrease in density and a possible increase in volume (Andréani et al., 2007; Evans, 2004). Crack-and-seal mechanism is invoked for veins formation which requires three successive stages: i) space opening at a rate linked to the stress/strain overall regime; ii) the transfer of elements to the vein in the presence of a fluid; and iii) a vein-filling episode of mineral crystallization (Andréani et al., 2004, 2007; Ramsay, 1980). Serpentine minerals (generalized formula $Mg_3Si_2O_5(OH)_4$) are of particular geochemical/petrological interest since they contain up to 16 wt% of structurally bound water and inherit specific minor and trace elements such as Ni, Cr, Mn, Sr, Ba, Cs, and Be (Bloise et al., 2014, 2016a; Bloise and Miriello, 2018; Deschamps et al., 2013; Groppo et al., 2006; Punturo et al., 2015; Spandler and Pirard, 2013). Unfortunately, chrysotile, one of the three main forms of serpentine, crystallizes with fibrous shape, and it is included among asbestos minerals along with crocidolite, tremolite, actinolite, anthophyllite and amosite (Bloise et al., 2019). Chrysotile has been classified by the International Agency for Research on Cancer (IARC, 1987) as being carcinogenic to humans (Group 1) and many countries have banned their use (Gualtieri, 2017).

The formation of chrysotile in veins requires the transfer of matter either from the adjacent wall rock by diffusion or dissolution processes, or through the circulation of fluids (Deschamps et al., 2013). The two main factors that appear to enhance chrysotile fibres crystallization (i.e. presence of porosity and fluid supersaturation) are open-system related. Therefore, it is not surprising that veins provide conditions favorable for the growth of chrysotile fibres (Evans, 2004), which has been observed in numerous outcrops of fractured serpentinite worldwide (Bloise et al., 2014; Bloise and Miriello, 2018; Groppo et al., 2006; Punturo et al., 2015).

Infill veins present in the serpentinite rocks are generally studied using polarized light, scanning and transmission electron microscopy (PLM, SEM, TEM), which only perform two-dimensional (2D) imaging of samples. Furthermore, in the case of asbestos mineral fibres contained within serpentinite rocks, PLM, SEM and TEM require sample preparation consisting of sample breakage, grinding or crushing thus causing high levels of sample disturbance. Indeed, the necessary actions for extracting chrysotile fibres from serpentine rocks can also cause size reduction leading to incorrect identification and making the asbestos fibres fall out defined parameters as breathable. Only respirable fibres (i.e., >5 μm long, <3 μm wide and with an aspect ratio >3:1) are defined as "asbestos" under European law (Directive 2003/18/CE). Moreover, the adverse health risks caused by the effects of asbestos are closely related to the dimension of the asbestos fibres (Belluso et al., 2017; Fubini and Arean, 1999; Turci et al., 2017) therefore variations in fibres size represent a fundamental variable in the etiology of the pathological effects of exposure to asbestos fibres.

In recent years, the three-dimensional (3D) textural analysis of rocks, using synchrotron radiation X-ray microtomography (SR-μCT), has proved to be a useful tool for determining their properties (e.g., crystal size distributions, porosity and connectivity) through a non-destructive, characterization (Militello et al., 2019; Punturo et al.,

2019b). Within this framework, this study aims to determine the shape of the veins that form in serpentinite rocks and the size of fibrous chrysotile that fill the veins, without grinding and/or particle size reduction. To obtain this ambitious goal, X-ray synchrotron microtomography (SR-μCT) supplemented with a polarized light microscope (PLM), scanning electron microscopy analysis combined with energy dispersive spectrometry (SEM/EDS) and electron probe microanalysis (EPMA) were used to characterize veins developed in serpentinite rock samples located in Gimigliano-Mount Reventino Unit (GMRU, Calabria, Southern-Italy) (Bloise and Miriello, 2018). We present correlation data that can be obtained from the results of these techniques in the context of characterization of mineral fibres formation in serpentine veins. Moreover, SR-μCT provides 3D morphological details on the vein shape present in massive serpentinite matrix where the chrysotile fibres form. In our opinion, this approach is the best way to analyze the serpentinite vein network filled with fibrous chrysotile as excluding the occurrence of errors derived from the preparation of the sample required in others analytical techniques. These non-destructive techniques prove to be accurate and reliable tools for the environmental monitoring of asbestos.

2. Sampling and characterization

2.1. Dataset and geological provenance of samples

The following samples were used for the analyses:

Seven serpentinite rocks from an abandoned quarry in the Gimigliano-Mount Reventino Unit (GMRU) (Fig. 1), coordinates: 613000 E, 4322500 N, UTM zone 33S; Map Datum: ED50. At the outcrop scale, the dark green serpentinite rocks look massive with a vein network developing inside (Fig. 1). Chrysotile fibres were only detected inside the veins while they were not found within the surrounding rock mass (Bloise and Miriello, 2018). A partial characterization of these serpentinites is reported in literature (Bloise et al., 2012, 2014; Bloise and Miriello, 2018; Cirrincione et al., 2015).

2.2. Petrographic microscope investigation

In order to describe the petrographic and microstructural features of the investigated serpentinite, polished thin sections obtained from the collected samples, were examined using a Zeiss Axiolab Microscope with Polarized Light (PLM). Photomicrographs of main microstructural features were taken with an E3ISPM Industrial Digital Camera equipped with Sony Exmar CMOS sensor. The samples were cut in order to highlight the main fabric features of the serpentinite rocks, such as the massive parts as well as the vein occurrence. The petrographic investigation was carried out at the Dpt of Biological, Geological and Environmental Sciences of the University of Catania.

2.3. SEM-EDS investigation

Scanning electron microscopy analysis combined with energy dispersive spectrometry (SEM/EDS) for the morphological observations was performed using an Environmental Scanning Electron Microscope FEI QUANTA 200 equipped with an X-ray EDS suite comprising a Si/Li crystal detector model EDAX-GENESIS4000. Analytical conditions were: 15 kV accelerating voltage, 10.0 nA probe current, 30 s live time. For the SEM investigations, a fragment for each sample of veins from class T2 (the most abundant type, see below) was fixed onto a SEM stub using a double-sided conductive adhesive tape and subsequently coated by graphite using a Quorum Q150T ES sputter coater.

2.4. EPMA investigation

Microchemical analysis of the minerals was carried out using an Electron Probe Micro Analysis (EPMA) JEOL-JXA 8230 coupled with a
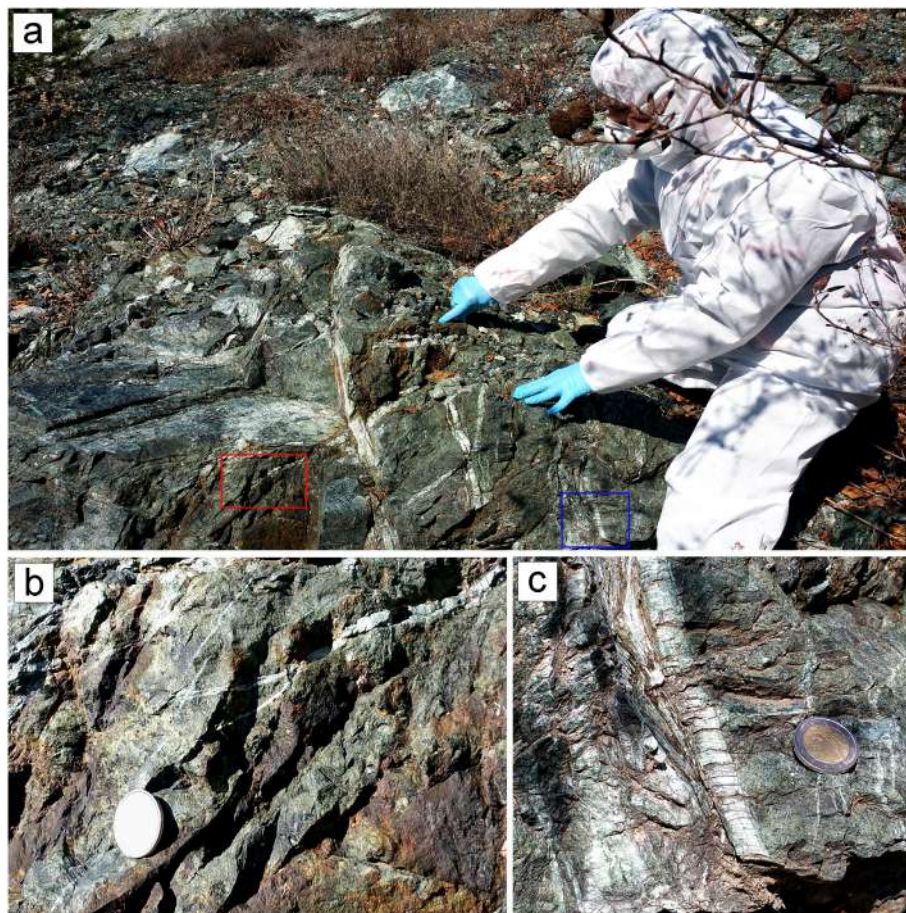
Fig. 1. a) Preliminary site survey (GMRU abandoned quarry); b) the red square indicates the zoom area: the vein network developing inside massive serpentinite; c) the blue square indicates the zoom area: the vein network developing inside massive serpentinite. (For interpretation of the references to colour in this figure, the reader is referred to the web version of this article.)

Spectrometer EDS – JEOL EX-94310FaL1Q and five WDS Spectrometer XCE type equipped with a LDE, TAP, LIF and PETJ crystals. EPMA/WDS single-point analyses were performed using accelerating voltage of 15 kV, probe current of 10 nA, counting times of 30 s for elemental peaks and 5 s for backgrounds. The X-Ray mapping of elements was performed with a WDS system with the following condition: 50.0 nA probe current, 15 keV accelerating voltage, 15 ms dwell time. The area of maps ranged between 1.1 and 0.8 mm^2 with resolutions of 800×600 pixel^2. A set of standards Ref. # 02757-AB (SPI Supplies, Metals & Minerals Standard, serial 4AK) containing minerals with declared compositions was used for quantification. WDS microanalysis was carried out using the standardless ZAF correction method. All samples were polished and carbon coated by graphite using a Quorum Q150T ES sputter coater. All of the SEM/EDS and EPMA analyses were performed at the "Laboratorio di Microscopia Elettronica e Microanalisi" of the University of Calabria, Italy.

2.5. SR-μCT investigation and three-dimensional image analysis

The three-dimensional study of two samples was performed by Synchrotron Radiation X-ray microtomography (SR-μCT) measurements in phase-contrast mode (Cloetens et al., 1997) at the SYRMEP beamline of the Elettra synchrotron laboratory (Trieste, Italy). Veins from class T2 were characterized by SR-μCT cutting the samples in the form of parallelepiped with size of about $4 \times 4 \times 20$ mm. Using a white beam configuration (Baker et al., 2012), a filtered (1 mm Si + 1 mm Al) polychromatic X-ray beam delivered by a bending magnet source illuminated the sample in transmission geometry. For each experiment, sample-to-detector distance was set to 200 mm and 1800

projections were acquired over a total scan angle of 180° with an exposure time/projection of 2 s. The employed detector was a 16 bit, air-cooled, sCMOS camera (Hamamatsu C11440 22C) with a 2048×2048 pixels chip. The effective pixel size of the detector was set at 1.95×1.95 μm^2, yielding a maximum field of view of ca. 4 mm^2. Since the lateral size of the samples was larger than the detector field of view, the microtomographic scans were acquired in local or region-of-interest mode (Maire and Withers, 2014). The reconstruction of the 2D tomographic slices was done with the SyrmepTomo Project (STP) house software suite (Brun et al., 2017), which allows to apply different combinations of filters to reduce ring artefacts caused by detector inhomogeneity (Brun et al., 2013). A single-distance phase-retrieval algorithm (Paganin et al., 2002) based on the Transport of Intensity Equation (TIE) was employed to the sample projections to improve the consistency of the morphological analysis. Combining phase-retrieval and Filtered Back-Projection algorithm (Herman, 1980) allowed obtaining the 3D distribution of the complex refraction index of the imaged samples, in order to reduce edge-enhancement effect at sample borders and preserve the morphology of the smallest features.

The obtained 3D images were investigated to evaluate the arrangement and the geometric relationship between the veins and the massive serpentinite. From the original stack of slices, Volumes of Interest (VOIs) with a size of about $1000 \times 1000 \times 1000$ voxel^3 (corresponding to ~7.4 mm^3) were extracted and inspected by means of 3D renderings using VGStudio Max 2.2 software. The veins part of the samples was segmented from the original volumes by manual thresholding using the Fijii software (Schindelin et al., 2012). Using the Pore3D software library (Brun et al., 2010) the maximum vein thickness was retrieved by the maximal inscribed sphere method, a protocol successfully

developed for measuring the size of objects developing complex networks within the samples (Hildebrand and Rüegsegger, 1997; Lanzafame et al., 2017).

3. Results

3.1. Macroscopic study

The samples were firstly analyzed from the macroscopic point of view paying particular attention to the veins and the infill. At the mesoscopic scale, serpentinite rocks show the typical dark green colour and massive structure, with the widespread presence of veins of various diameters and lengths (Fig. 1). All seven specimens are characterized by the presence of veins that crosscut the serpentinite rock and often intersect each other (Fig. 2a–f). The veins did not seem to possess a preferred texture or orientation thus suggesting that they formed under different mechanisms and conditions of formation (Ningthoujam et al., 2012). This is probably due to the effects that different stages of serpentinization had on the ultramafic protolith, from fracture network development to vein infill (Andréani et al., 2004; Evans, 2004). In particular, some veins decrease in width towards the pointed end (V-shaped) (Fig. 2b, d), while others are similar in shape and crosscut the samples maintaining a constant width (Fig. 2c, f). Sub-parallel distribution of

veins with irregular thicknesses along their length is shown in Fig. 2a and e. Ten measurements on 50 single veins were taken to determine the various widths of the asbestos veins (Fig. S1 Supplementary materials) thus allowing a distinction based on their average distribution width (Fig. S2 Supplementary materials). Using this method, four classes of veins were identified in all of the samples: T1 with average width < 0.3 mm; T2 with average width ranging between 0.3 mm to 1 mm; T3 with average width ranging between 1 mm and 2 mm; T4 with average width > 2 mm. Results highlighted that most vein types belong to classes T1 (37%) and T2 (41%), whereas only 22% of the analyzed population is represented by wider veins (11% per type).

3.2. Petrographic characterization

The sampled serpentinite rocks derive from a peridotite protolith. Despite the almost complete serpentinization process, the original protogranular texture is still locally observed. The serpentine group minerals and small magnetite grains completely replaced the original spinel, olivine and pyroxenes; serpentine and secondary magnetite often appear as pseudomorphic aggregates with typical net-like and mesh texture types (Fig. S3 Supplementary materials). Clusters of olivine, completely retrogressed orthopyroxene and clinopyroxene small grains can be observed in close connection with Cr-spinel grains. At
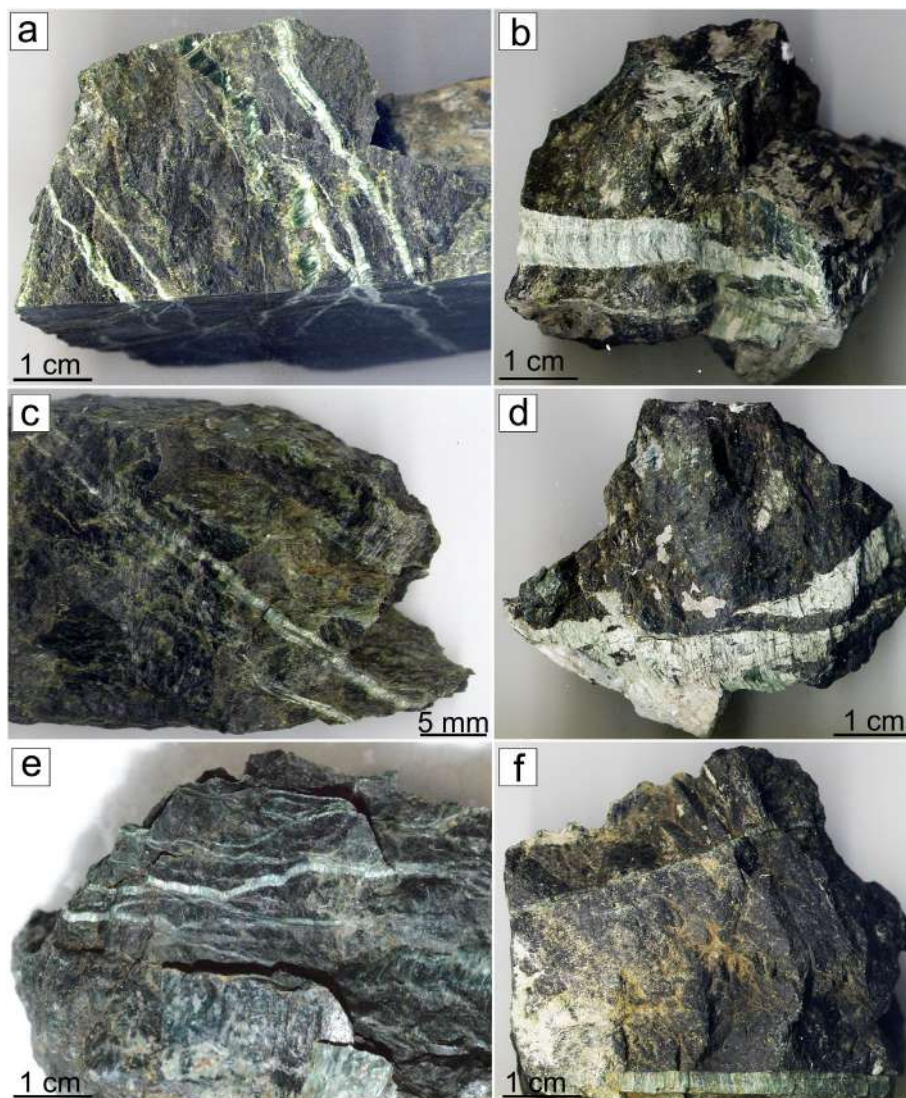

Fig. 2. Vein network developing inside massive serpentinite; a–f) vivid green serpentine veins; a, e) veins crosscut the sample showing variable thicknesses; b, d) V-shaped veins; c, f) veins showing constant thickness. (For interpretation of the references to colour in this figure legend, the reader is referred to the web version of this article.)

the scale of the microscope, it is also possible to observe the different dilatation vein systems filled by chrysotile fibres cross-cutting the rock volumes. In general, chrysotile fibres may be oriented either perpendicular to the vein selvages ("cross" serpentine) or according to their elongation directions. Chrysotile fibres usually fill the veins in syntaxial growth and the motion of the wall rocks causes a curvature of fibres in some veins. Moreover, some veins exhibit evidence of deformation posterior to their emplacement, as shown by kink banding that may be also observed within pseudomorphs (Fig. S3 Supplementary materials). Small magnetite crystals sometimes mark the middle line of the vein.

3.3. SEM/EDS characterization

SEM morphological observations showed that most of the fibres are flexible; from a morphological point of view integrated by the EDS chemical analyses, they were identified as chrysotile. Lizardite with lamellar morphology is present inside the massive serpentinite. Within the veins, the chrysotile fibres were primarily arranged perpendicular to the vein elongation (Fig. 3a) and locally the longitudinal splitting of larger bundles into thinner (Fig. 3a) or isolated fibrils is evident (Fig. 3b) even if chrysotile fibres are generally visible as compact bundles of fine fibrils. At times chrysotile fibres showed inclined fan-shaped orientations with respect to the vein walls.

3.4. EPMA characterization

The chrysotile fibres were characterized using elemental maps (Fig. 4a, b), which were acquired to verify chemical variations between the massive serpentine and the serpentinite veins. As expected, the Si and Mg contents are uniform in the passage between the matrix assemblage and the veins. The chemical map in Fig. 4a–b shows that in addition to Si and Mg, other minor elements of the serpentinite samples are Al and Fe. Other elements such as Ni, Cr and Mn are often found but in smaller quantities. However, there are different concentrations of Al and Fe in the chrysotile that fill the veins and the matrix. Fig. 4a–b shows that the Al content is higher within the veins filled with chrysotile than within the matrix assemblage. Conversely, the Fe content is higher in the matrix assemblage than in the veins, even if Fe is non-homogenously distributed in the matrix and is mainly present in the magnetite matrix. Furthermore, a spot analysis was conducted at the same time, in which only serpentine minerals that fill the veins and in the matrix were analyzed in order to avoid potential matrix effects caused mainly by magnetite. The chemical composition of the chrysotile fibres inside the veins and the chemical composition of the massive serpentinite were established by performing several spot analyses using EPMA (Tables 1, 2). Al concentration did not vary significantly in

chrysotile that fills the veins with an average value of 2.45 wt% (Table 1), while a lower average Al content of 0.72 wt% was found in the matrix (Table 2). The average Fe content was 2.00 wt% within the vein infill (Table 1), while the average Fe content was almost two times higher in the matrix (average 3.67 wt%; Table 2). Mn and Ni were homogenously distributed between chrysotile that fills the veins and the matrix (Tables 1, 2), with an average Ni content approximately 2-fold higher than Mn. Indeed, the Mn content in chrysotile that fills the veins ranges from 0.13 to 0.20 wt% with an average value of 0.16 wt%, showing similar average concentrations of 0.17 wt% in the matrix (Tables 1, 2). The average Ni concentration did not vary significantly with values ranging from 0.25 wt% in the infill veins to 0.31 wt% in matrix. The infill veins and the matrix had highly variable Cr concentrations. The highest Cr values were detected in the matrix (1.04 wt%) with an average value of 0.66 wt%, while it was sometimes below the detection limits within the infill veins.

3.5. Three-dimensional image analysis

Two samples (T2$_{-GMRU2}$; T2$_{-GMRU12}$) of veins from class T2 (i.e., thicknesses ranging from 0.3 to 1 mm) were characterized using SR-µCT (Fig. 5). These specimens were selected for two reasons: i) T2 class is the most abundant veins type; ii) fibrous bundles are visible at the mesoscale in the veins. On observing the 3D rendering (Fig. 6a, c), the geometric shape of the veins is evident (Videos V1, V2; Supplementary material). In particular, four morphologies have been recognized: sub-parallel side, lens-shape, V-shape and irregular-shape. The thickness distributions obtained are in line with the morphological characteristics observed in the 3-D visualizations: in the T2$_{-GMRU2}$ sample (Fig. 6a; video V1 Supplementary material) a small variation of thickness can be seen (Fig. 6a, b) with a maximal thickness of 0.580 mm, while in the T2$_{-GMRU12}$ sample (Fig. 6c), a maximal thickness of 0.566 mm is interconnected by a thin vein with a diameter of approximately 0.350 mm. Moreover, the SR-µCT investigation showed that there are veins of smaller diameters belonging to class T1 within the matrix (Fig. 6c, d; video V2 Supplementary material), which are not visible at mesoscopic scale. Some lens-shaped veins show thicknesses ranging from 0.06 mm in the narrowest parts to 0.15 mm in the widest areas while others are trumpet-shaped and therefore wide at the end (0.32 mm average) and narrow in the center (0.07 mm average). The 3D reconstructions also show the branching of the veins within the serpentinite matrix (Fig. 6b, d; videos V1, V2; Supplementary material). 2D slices of the veins obtained by SR-µCT show voids in some portions of the sample in which chrysotile fibres are evident, as they are not aligned (Fig. 7). In these voids chrysotile fibres crystallized as long bundles of woven fibres (Fig. S4 supplementary materials), whereas in other parts of the sample or in the same slice, the veins appear to be filled
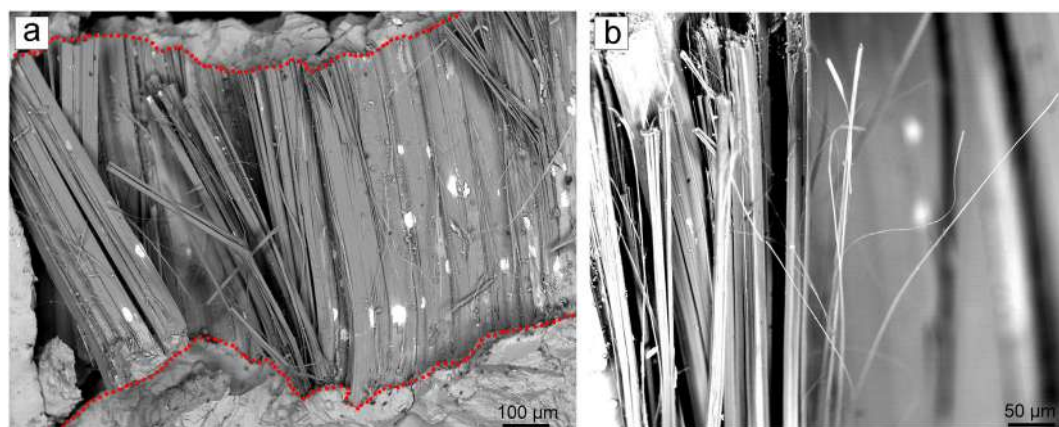

Fig. 3. SEM images of vein infill by chrysotile fibres bundles (a); note the splitting of compact fibres into thinner fibrils; b) chrysotile fibre bundles with their typical wavy appearance. Note the flexibility of the single fibrils.
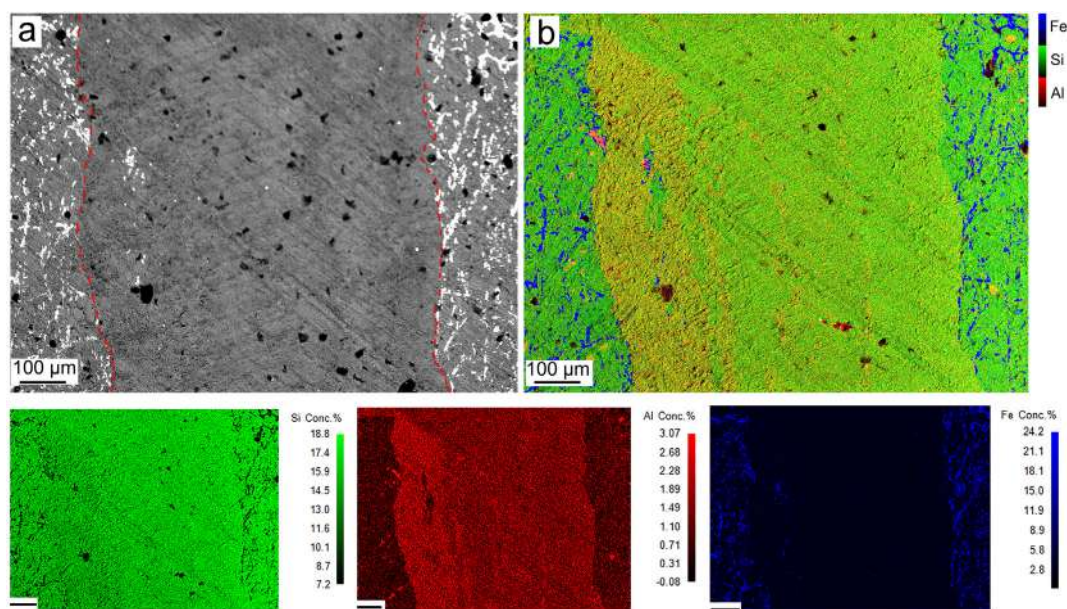
Fig. 4. Element maps of Si, Al, and Fe. The area mapped is indicated in a) red dot line delimited the vein surface. b) Fe/Si/Al ratios. Sample was carefully polished before analysis. Black bar is 100 μm. (For interpretation of the references to colour in this figure legend, the reader is referred to the web version of this article.)

with compact chrysotile fibres (Fig. 7a–d) as there are no voids, which makes the fibrous habit of chrysotile hard to identify. Nevertheless, the vein borders are well distinguished from the matrix (Fig. 7a–d). Fibres width was measured using Fijii software (Schindelin et al., 2012) by direct measurements on 100 slices obtained from SR-μCT. Chrysotile fibres length in all of the samples ranged from 10 to 300 μm, therefore 100% of the fibres were generally longer than 5 μm, with aspect ratios >3:1. However, the best achievable resolution of SR-μCT is not capable of measuring fibres shorter than 2 μm.

4. Discussions

The presence of veins of a specific size and their chemical composition is closely related to serpentinization conditions and rock deformation history (i.e., stress/strain regime) (Andréani et al., 2004; Normand et al., 2002). Compared to the serpentinite matrix, chrysotile fibres inside the veins had little Fe content because the matrix retains part of their initial Fe in relict minerals such as olivine and pyroxene and magnetite marks the boundary between fibrous serpentine infill veins and the matrix (Fig. 4). Moreover, compared to the serpentinite matrix, the chrysotile fibres inside the veins were relatively rich in Al, probably because they formed in the presence of Al-rich liquid created by alterations of the Al-rich phase such as spinel. This means that the veins are visible due to their high Al content along their entire length

(Fig. 4), which is in line with the data obtained for the last vein generation (V4) proposed in the model by Andréani et al. (2007). This stage ($T < 200$ °C; Depth < 2 km) with higher fluid/rock ratios records an open system of hydrothermal circulation that enables the transport of excess elements from hydration reactions and permits full serpentinization process. In this regard, it should be borne in mind that the formation of chrysotile in veins requires the transfer of matter either from the adjacent wall rock by diffusion or dissolution processes, or through the circulation of fluids (Andréani et al., 2007). However, the composition (i.e., Al and Fe content) of veins formed at greater depth and temperature ranges ($T = 300$–350 °C; Depth = 4–8 km) is similar to that one detected in the mesh (matrix). In our opinion, this generation of veins, which seldom contain fibres are hard to discriminate with SR-μCT due to the negligible chemical differences between the veins and the matrix.

From a chemical point of view, in chrysotile Al^{3+} may substitute for both Si^{4+} and Mg^{2+} in the T and O sheets, respectively (Wicks and Plant, 1979). Mg located in the octahedral sheet may be replaced by Fe^{2+} ions (Bloise et al., 2009; Hardy and Aust, 1995; Wicks and Plant, 1979) and Fe^{3+} ions may replace Si ions although this position may preferentially host Al^{3+} (Bloise et al., 2014, 2017; O'Hanley and Dyar, 1998). Mn, Ni and Cr represent an almost exclusively isomorph substitute for magnesium in chrysotile (Bloise et al., 2010, 2016b).

Table 1
Representative EPMA analyses of chrysotile inside the vein.

Oxide wt%	MgO	SiO$_2$	Al$_2$O$_3$	Cr$_2$O$_3$	FeO	MnO	NiO	Total
				Chrysotile inside the veins				
1	40.41	41.64	2.05	0.20	1.90	0.17	0.55	86.91
2	40.28	41.62	2.78	0.35	1.82	0.14	0.00	86.99
3	39.96	41.36	2.08	0.19	3.00	0.15	0.46	87.20
4	40.97	39.99	2.85	0.29	1.93	0.18	0.11	86.32
5	40.77	40.36	2.86	0.00	1.82	0.20	0.38	86.38
6	40.97	41.01	2.44	0.23	2.12	0.13	0.20	87.09
7	40.11	41.37	2.21	0.00	1.76	0.14	0.32	85.91
8	40.14	41.25	3.00	0.67	1.83	0.18	0.00	87.07
9	41.97	41.95	2.03	0.41	1.93	0.16	0.36	88.81
10	40.92	41.40	2.17	0.37	1.89	0.13	0.12	87.01
Average	40.65	41.19	2.45	0.27	2.00	0.16	0.25	86.97

Table 2
Representative EPMA analyses of matrix outside the vein.

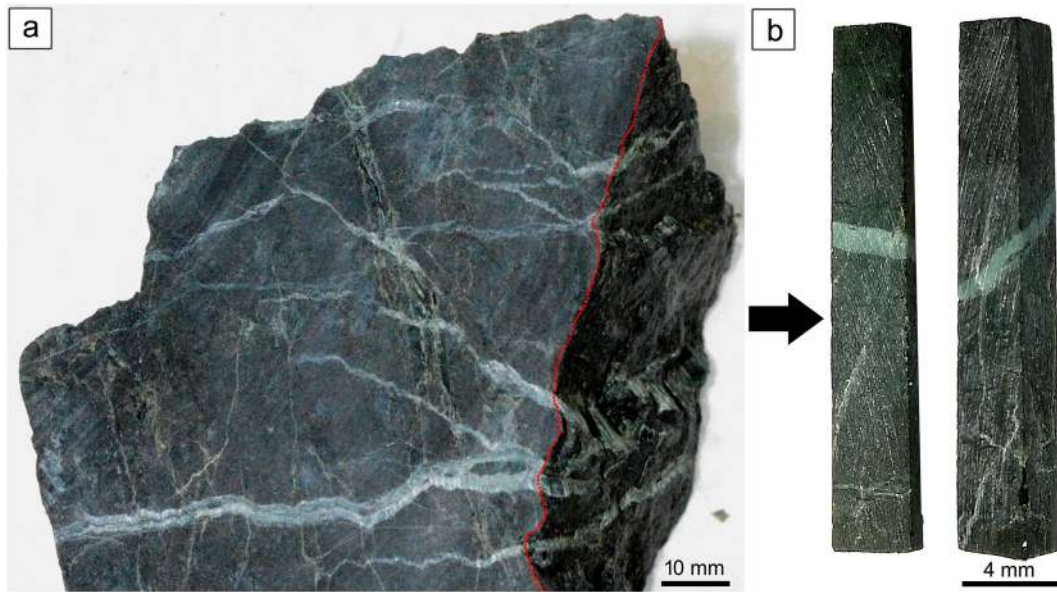| Oxide wt%	MgO	SiO$_2$	Al$_2$O$_3$	Cr$_2$O$_3$	FeO	MnO	NiO	Total
				Matrix outside the veins				
1	41.89	40.68	0.48	0.93	3.42	0.14	0.24	87.78
2	40.42	41.63	1.02	0.84	3.74	0.16	0.29	88.09
3	39.97	42.49	0.85	1.03	3.36	0.13	0.26	88.07
4	40.48	41.09	1.04	0.41	3.54	0.21	0.38	87.14
5	41.60	41.60	1.03	0.72	3.54	0.05	0.25	88.78
6	40.80	41.17	0.56	0.69	3.90	0.18	0.56	87.86
7	41.42	41.09	0.52	0.15	3.87	0.04	0.37	87.44
8	40.57	41.94	0.39	0.11	4.21	0.41	0.33	87.97
9	40.28	41.81	0.46	0.82	3.72	0.26	0.13	87.48
10	39.06	41.95	0.86	1.04	3.38	0.09	0.24	86.60
Average	40.65	41.54	0.72	0.66	3.67	0.17	0.31	87.72

Fig. 5. a) Cut serpentinite specimen, (part to the left of the red dashed line) note veins in massive serpentinite; serpentinite impregnated with epoxy resin (part to the right of the red dashed line). b) Examples of prismatic samples cut for SR-µCT analysis. (For interpretation of the references to colour in this figure legend, the reader is referred to the web version of this article.)

SR-µCT revealed that serpentine veins could be discriminated in massive serpentinite rocks while, routine techniques such as PLM and SEM can only be used for surface observations or to a maximum depth of a few hundred microns. More specifically, a vein network of various shape and size types without any preferred orientation characterizes the analyzed serpentinite samples. The vein-infill represented by chrysotile (Bloise and Miriello, 2018) occurs either parallel (slip-fibre) and perpendicular (cross-fibre) to the vein elongation direction.

The chrysotile fibre dimensions, undisturbed by grinding or milling processes, all matched with the size of regulated asbestos. Indeed,
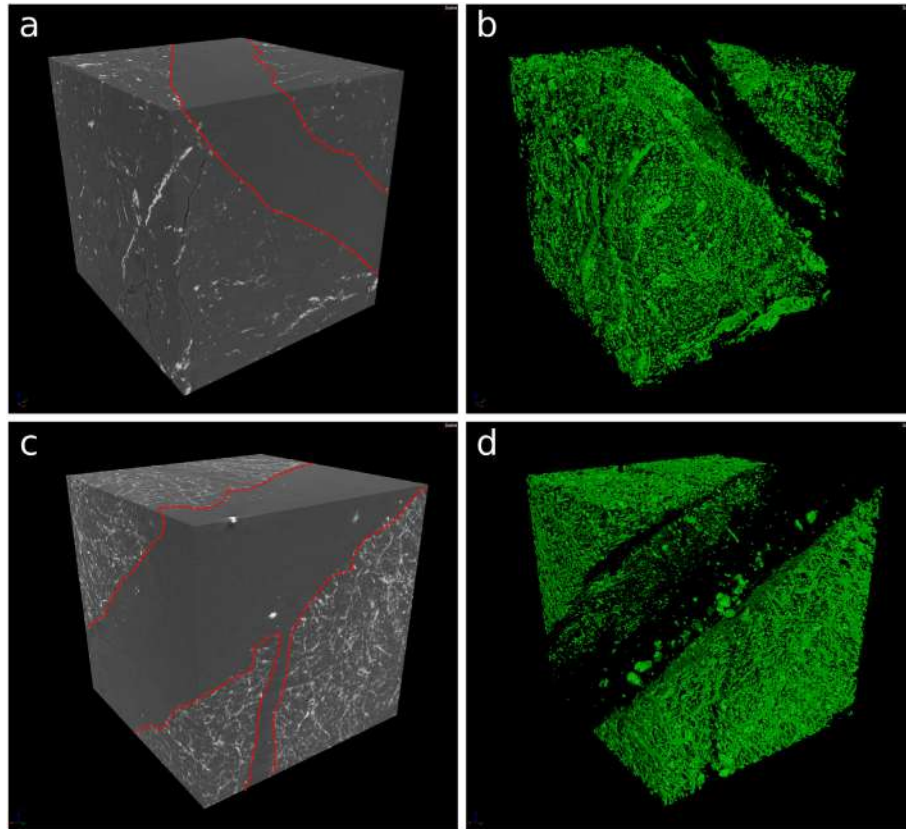
Fig. 6. Volume rendering of extracted VOIs from (a) T2$_{GMRU2}$ (7 mm^3) and (c) T2$_{GMRU12}$ (7 mm^3) with highlighted contact lines (dashed red) between veins and matrix. The spatial distributions of the veins are shown as empty spaces between the matrix (in green) for T2$_{GMRU2}$ (b) and T2$_{GMRU12}$ (d). (For interpretation of the references to colour in this figure legend, the reader is referred to the web version of this article.)
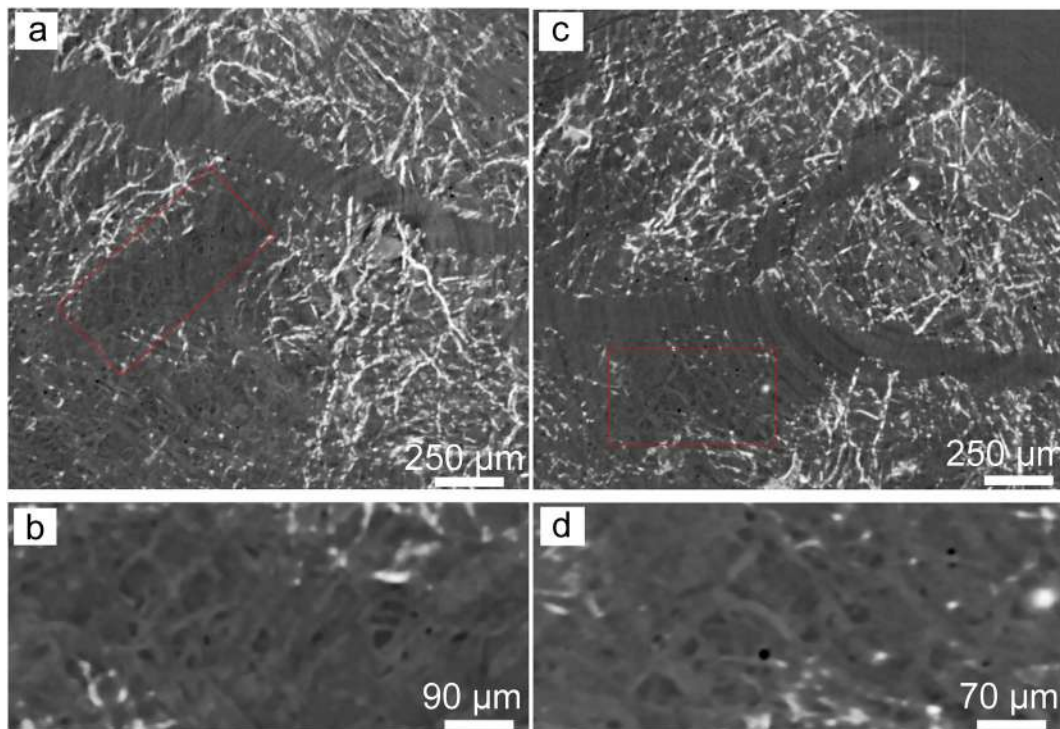
Fig. 7. Axial slices from the original SR-μCT-imaged volume of the prismatic samples (T2_GMRU2). a) venous system filled with chrysotile fibres; b) detail of the figure as indicated by the red rectangle. c) venous system filled with chrysotile fibres; d) zooming of the figure an indicated by the red rectangle. In b and d note the fibrous chrysotile bundles within the veins. (For interpretation of the references to colour in this figure legend, the reader is referred to the web version of this article.)

100% of the chrysotile fibres were longer than 5 μm, with an aspect ratio >3:1 and are therefore classified as asbestos under European law (Directive, 2003/18/CE, 2003) as these particles are more likely to penetrate deeply into the respiratory tract and cause chronic lung disease if inhaled (Turci et al., 2017). 3D images obtained by SR-μCT can be used to determine the size (i.e., width, length) of chrysotile or other asbestos fibres, which is one of the three diagnostic criteria (together with crystallography and chemistry), for identifying asbestiform minerals. However, the measurement of short chrysotile fibres <2 μm long was not allowed since they fall below the SR-μCT detection limit. The correct mineralogical identification of chrysotile within a mineral matrix is essential for preventing NOA hazards and ensuring the safe extraction and processing of asbestos-containing rocks. The mineralogical characterization of chrysotile fibres in a multi-mineral matrix requires the use of several analytical techniques. The combination of PLM, SEM/EDS and EPMA is an effective way to observe and describe the size of chrysotile in a mineral matrix. However, it is not sufficient for risk diagnosis, because PLM, SEM/EDS and EPMA have a limited spatial resolution and sample preparation can cause sample disturbance which may result in changes in size and geometric shape ratios of asbestos chrysotile fibres, leading to the misevaluation of asbestiform fibres findings. Indeed, in most cases, the PLM observation of the veins shows bundles of chrysotile fibres or fibre flakes, which are too complex to resolve internal constituents or individual chrysotile fibres size. As regards the SEM investigation, sample preparation could determine a down-representation in the amount of fibres considered as asbestos due to their reduction in size. Moreover, the length measured by SEM was undervalued because it is not possible to measure the entire fibre length due to fibre geometry.

5. Conclusions

Chrysotile that fills the veins found in serpentinite rocks from an abandoned quarry was investigated using SR-μCT technique. The SR-μCT results are consistent with those obtained through PLM, SEM/EDS and EPMA examination. SR-μCT revealed that serpentine veins could be discriminated in massive serpentinite rocks due to differences in chemical composition between veins and matrix. In particular, iron and aluminum distribution variations inside and outside of the veins induce differently radiation absorption patterns, thus permitting a detailed image-based 3D geometric reconstruction. Furthermore, magnetite which is not present inside the veins, blocked most of the X-ray radiation, thus allowing the vein border to be clearly marked. In particular, the detailed microstructural investigation permitted to recognize, on the basis of shape, four vein types: sub-parallel side, lens-shape, V-shape and irregular-shape.

Moreover, the fibrous form of the chrysotile contained in the veins can be observed without disturbing fibre size. Chrysotile occurs within serpentinite rocks as respirable fibrous phase infill (particles with length > 5 μm, width < 3 μm, length/width ratio > 3:1). Therefore, the sizes of the chrysotile fibres analyzed corresponded with the size of regulated asbestos. It is worth noting that it is essential to measure the size of chrysotile fibres to perform a correct characterization of asbestos-containing rocks, since the size is a key factor in the pathogenicity of asbestos fibres. Weathering processes and/or human activities on serpentinite rocks produce dust containing asbestos chrysotile fibres, which are potentially inhalable and can seriously endanger human health. SR-μCT proved to be a valuable and promising technique for analysing asbestos chrysotile that fill in the veins within massive serpentinite. Combined with conventional analytical techniques, the information obtained from this study could prove useful for performing an accurate characterization of chrysotile-filled veins hosted by serpentinite. In short, the 3D images of veins filled with chrysotile may help us to identify NOA contained within serpentinite rocks. The advantages of this approach include: i) the non-destructivity, which enables us to perform multiple analysis on the same specimen; ii) the ease of analysis, since samples can be analyzed without any specific previous treatment; and iii) the 3D identification, of the inner structure of the samples, including geometrical features of the veins such as volume fraction, size and orientation. This latter is crucial for a correct

characterization of the sample texture and for retrieving the abundance of veins, since the classic two-dimensional (2D) imaging analysis on thin sections cannot accurately determine the true morphology, leaving a large degree of uncertainty for the third dimension.

Future research for improving the SR-μCT approach will focus on the data acquisition protocol, to establish a distinct experimental setting for each type of NOA vein. This will help to fully exploit the potentiality of phase retrieval techniques and therefore improve the quality of 3D images of samples containing phases with similar chemical compositions. Consequently, the reliability and precision of the quantitative analysis will be enhanced. Furthermore, this analytical approach could be tested on other types of rock that contain other asbestos minerals such as amphiboles.

Supplementary data to this article can be found online at https://doi.org/10.1016/j.scitotenv.2019.135675.

Declaration of competing interest

The authors declare that they have no known competing financial interests or personal relationships that could have appeared to influence the work reported in this paper.

Acknowledgments

References

Andréani, M., Baronnet, A., Boullier, A.M., Gratier, J.P., 2004. A microstructural study of a crack-seal type serpentine vein, using SEM and TEM techniques. Eur. J. Mineral. 16, 585–595. https://doi.org/10.1127/0935-1221/2004/0016-0585.

Andréani, M., Mével, C., Boullier, A.M., Escartin, J., 2007. Dynamic control on serpentine crystallization in veins: constraints on hydration processes in oceanic peridotites. Geochem. Geophy. Geosy. 8 (2), 2–24. https://doi.org/10.1029/2006GC001373.

Baker, D.R., Mancini, L., Polacci, M., Higgins, M.D., Gualda, G.A.R., Hill, R.J., Rivers, M.L., 2012. An introduction to the application of X-ray microtomography to the three-dimensional study of igneous rocks. Lithos 148, 262–276.

Baumann, F., Buck, B.J., Metcalf, R.V., McLaurin, B.T., Merkler, D.J., Carbone, M., 2015. The presence of asbestos in the natural environment is likely related to mesothelioma in young individuals and women from Southern Nevada. J. Thorac. Oncol. 10 (5), 731–737. https://doi.org/10.1097/jto.0000000000000506.

Belluso, E., Cavallo, A., Halterman, D., 2017. Crystal habit of mineral fibres. In: Gualtieri, A.F. (Ed.), Mineral Fibres: Crystal Chemistry, Physical–Physical Properties, Biological Interaction and Toxicity. European Mineralogical Union, London, pp. 65–109. https://doi.org/10.1180/EMU-notes.18.3.

Bloise, A., Miriello, D., 2018. Multi-analytical approach for identifying asbestos minerals in situ. Geosci. 8 (4), 133. https://doi.org/10.3390/geosciences8040133.

Bloise, A., Belluso, E., Barrese, E., Miriello, D., Apollaro, C., 2009. Synthesis of Fe-doped chrysotile and characterization of the resulting chrysotile fibers. Crys. Res. Tec. 44 (6), 590–596. https://doi.org/10.1002/crat.200900135.

Bloise, A., Belluso, E., Fornero, E., Rinaudo, C., Barrese, E., Capella, S., 2010. Influence of synthesis condition on growth of Ni-doped chrysotile. Microporous Mesoporous Mat. 132, 239–245. https://doi.org/10.1016/j.micromeso.2010.03.003.

Bloise, A., Belluso, E., Critelli, T., Catalano, M., Apollaro, C., Miriello, D., Barrese, E., 2012. Amphibole asbestos and other fibrous minerals in the meta-basalt of the Gimigliano-Mount Reventino Unit (Calabria, south-Italy). Rend. Online Soc. Geol. It. 21 (2), 847–848.

Bloise, A., Critelli, T., Catalano, M., Apollaro, C., Miriello, D., Croce, A., Barrese, A., Liberi, F., Piluso, E., Rinaudo, C., 2014. Asbestos and other fibrous minerals contained in the serpentinites of the Gimigliano-Mount Reventino unit (Calabria, S-Italy). Environ. Earth. Sci. 71, 3773–3786. https://doi.org/10.1007/s12665-013-3035-2.

Bloise, A., Punturo, R., Catalano, M., Miriello, D., Cirrincione, R., 2016a. Naturally occurring asbestos (NOA) in rock and soil and relation with human activities: the monitoring example of selected sites in Calabria (southern Italy). Ital. J. Geosci. 135, 268–279. https://doi.org/10.3301/IJG.2015.24.

Bloise, A., Barca, D., Gualtieri, A.F., Pollastri, S., Belluso, E., 2016b. Trace elements in hazardous mineral fibres. Environ. Pollut. 216, 314–323. https://doi.org/10.1016/j.envpol.2016.06.007.

Bloise, A., Catalano, M., Critelli, T., Apollaro, C., Miriello, D., 2017. Naturally occurring asbestos: potential for human exposure, San Severino Lucano (Basilicata, southern Italy). Environ. Earth Sci. 76, 648–661. https://doi.org/10.1007/s12665-017-6995-9.

Bloise, A., Punturo, R., Kusiorowski, R., Pereira Gómez, D., 2019. Editorial for special issue "mineral fibres". Fibres 7, 54. https://doi.org/10.3390/fib7060054.

Brun, F., Mancini, L., Kasae, P., Favretto, S., Dreossi, D., Tromba, G., 2010. Pore 3D: a software library for quantitative analysis of porous media. Nucl. Instr. Meth. Phys. Res. A 615, 326–332. https://doi.org/10.1016/j.nima.2010.02.063.

Brun, F., Accardo, A., Kourousias, G., Dreossi, D., Pugliese, R., 2013. Effective implementation of ring artifacts removal filters for synchrotron radiation microtomographic images. In: Ramponi, G., Loncaric, S., Carini, A., Egiazarian, K. (Eds.), Proceedings of the International Symposium on Image and Signal Processing and Analysis (ISPA 2013), Trieste, 2013, pp. 672–676. https://doi.org/10.1109/ISPA.2013.6703823 Trieste.

Brun, F., Massimi, L., Fratini, M., Dreossi, D., Billé, F., Accardo, A., Pugliese, R., Cedola, A., 2017. SYRMEP tomo project: a graphical user interface for customizing CT reconstruction workflows. Adv. Struct. Chem. Imag. 3 (1). https://doi.org/10.1186/s40679-016-0036-8.

Cirrincione, R., Fazio, E., Fiannacca, P., Ortolano, G., Pezzino, A., Punturo, R., 2015. The Calabria-Peloritani Orogen, a composite terrane in Central Mediterranean; its overall architecture and geodynamic significance for a pre-Alpine scenario around the Tethyan basin. Period. Mineral. 84 (3B), 701–749. https://doi.org/10.2451/2015PM0446.

Cloetens, P., Pateyron-Salome, M., Buffière, J.Y., Peix, G., Baruchel, J., Peyrin, F., Schlenker, M., 1997. Observation of microstructure and damage in materials by phase sensitive radiography and tomography. J. App. Phys. 81. https://doi.org/10.1063/1.364374.

Colombino, E., Capella, S., Casalinuovo, F., Racco, R., Pruiti, F., Volante, M., Di Marco Lo Presti, V., Belluso, E., Capucchio, M.T., 2019. Malignant peritoneal mesothelioma in a boar who lived in Calabria (Italy): Wild animal as sentinel system of human health. Sci. Total. Environ. 683, 267–274. https://doi.org/10.1016/j.scitotenv.2019.05.254.

Deschamps, F., Godard, M., Guillot, S., Hattori, K., 2013. Geochemistry of subduction zone serpentinites: a review. Lithos 178, 96–127. https://doi.org/10.1016/j.lithos.2013.05.019.

Directive 2003/18/CE of the European Parliament and of the European Council of 27 March 2003.

Evans, W.B., 2004. The serpentinite multisystem revisited: chrysotile is metastable. Int. Geol. Rev. 46 (6), 479–506. https://doi.org/10.2747/0020-6814.46.6.479.

Fubini, B., Arean, C.O., 1999. Chemical aspects of the toxicity of inhaled mineral dusts. Chem. Soc. Rev. 28, 373–383. https://doi.org/10.1002/chin.200006289.

Groppo, C., Rinaudo, C., Cairo, S., Gastaldi, D., Compagnoni, R., 2006. Micro-Raman spectroscopy for a quick and reliable identification of serpentine minerals from ultramafics. Eur. J. Mineral. 18, 319–329. https://doi.org/10.1127/0935-1221/2006/0018-0319.

Gualtieri, A.F., 2017. Introduction. In: Gualtieri, A.F. (Ed.), Mineral Fibres: Crystal Chemistry, Chemical-Physical Properties. Biological Interaction and Toxicity. European Mineralogical Union, London, UK, pp. 1–15. https://doi.org/10.1180/EMU-notes.18.3.

Guillots, S., Hattori, K., 2013. Serpentinites: essential roles in geodynamics, arc volcanism, sustainable development, and the origin of life. Elements 9 (2), 95–98. https://doi.org/10.2113/gselements.9.2.95.

Hardy, J.A., Aust, A.E., 1995. Iron in asbestos chemistry and carcinogenicity. Chemical Reviews. 95 (1), 97–118. https://doi.org/10.1021/cr00033a005.

Harper, M., 2008. 10th anniversary critical review: naturally occurring asbestos. J. Environ. Monit. 10 (12), 1394–1408. https://doi.org/10.1039/b810541n.

Herman, G.T., 1980. Image Reconstruction from Projections. The Fundamentals of Computerized Tomography. first ed. Academic Press, New York.

Hildebrand, T., Rüegsegger, P., 1997. A new method for the model-independent assessment of thickness in three-dimensional images. J. Microsc. 185 (1), 67–75. https://doi.org/10.1046/j.1365-2818.1997.1340694.x.

IARC, 1987. Overall Evaluations of Carcinogenicity: An Updating of IARC Monographs Volumes 1 to 42. International Agency for Research on Cancer, Lyon, France.

Lanzafame, G., Iezzi, G., Mancini, L., Lezzi, F., Mollo, S., Ferlito, C., 2017. Solidification and turbulence (non-laminar) during magma ascent: insights from 2D and 3D analyses of bubbles and minerals in an Etnean Dyke. J. Petrol. 58 (8), 1511–1534. https://doi.org/10.1093/petrology/egx063.

Maire, E., Withers, P.J., 2014. Quantitative X-ray tomography. Int. Mat. Rev. 59, 1–43. https://doi.org/10.1179/1743280413Y.0000000023.

Militello, G.M., Bloise, A., Gaggero, L., Lanzafame, G., Punturo, R., 2019. Multianalytical approach for asbestos minerals and their non-asbestiform analogues: inferences from host rock textural constraints. Fibers 7, 42. https://doi.org/10.3390/fib7050042.

Ningthoujam, P.S., Dubey, C.S., Guillot, S., Fagion, A.S., Shukla, D.P., 2012. Origin and serpentinization of ultramafic rocks of Manipur Ophiolite Complex in the Indo-Myanmar subduction zone, Northeast India. J. Asian. Earth Sci. 50, 128–140. https://doi.org/10.1016/j.jseaes.2012.01.004.

Normand, C., Williams-Jones, A.E., Martin, R.F., Vali, H., 2002. Hydrothermal alteration of olivine in a flow-through autoclave: nucleation and growth of serpentine phases. Am. Mineral. 87, 1699–1709. https://doi.org/10.2138/am-2002-11-1220.

O'Hanley, D.S., Dyar, M.D., 1998. The composition of chrysotile and its relationship with lizardite. Can. Mineral. 36, 727–740.

Paganin, D., Mayo, S.C., Gureyev, T.E., Miller, P.R., Wilkins, S.W., 2002. Simultaneous phase and amplitude extraction from a single defocused image of a homogeneous object. J. Microsc. 206, 33–40. https://doi.org/10.1046/j.1365-2818.2002.01010.x.

Petrigrieri, J.R., Laporte-Magoni, C., Gunkel-Grillon, P., Tribaudino, M., Bersani, D., Sala, O., Salvioli-Mariani, E., 2019. Mineral fibres and environmental monitoring: a

comparison of different analytical strategies in New Caledonia. Geosci. Front. in press. https://doi.org/10.1016/j.gsf.2018.11.006.

Punturo, R., Bloise, A., Critelli, T., Catalano, M., Fazio, E., Apollaro, C., 2015. Environmental implications related to natural asbestos occurrences in the ophiolites of the Gimigliano-Mount Reventino Unit (Calabria, southern Italy). Int. J. Environ. Sci. 9, 405–418. https://DOI:10.22059/IJER.2015.913

Punturo, R., Ricchiuti, C., Bloise, A., 2019a. Assessment of serpentine group minerals in soils: a case study from the village of San Severino Lucano (Basilicata, Southern Italy). Fibres 7, 18. https://doi.org/10.3390/fib7020018.

Punturo, R., Ricchiuti, C., Rizzo, M., Marrocchino, E., 2019b. Mineralogical and microstructural features of namibia marbles: insights about tremolite related to natural asbestos occurrences. Fibres 7, 31. https://doi.org/10.3390/fib7040031.

Ramsay, J.G., 1980. The crack-seal mechanism of rock deformation. Nature 284, 135–139.

Schindelin, J., Arganda-Carreras, I., Frise Fiji, E., 2012. An open-source platform for biological-image analysis. Nat. Methods. 9 (7), 676–682.

Spandler, C., Pirard, C., 2013. Element recycling from subducting slabs to arc crust: a review. Lithos 170, 208–223. https://doi.org/10.1016/j.lithos.2013.02.016.

Turci, F., Tomatis, M., Pacella, A., 2017. Surface and bulk properties of mineral fibres relevant to toxicity. In: Gualtieri, A.F. (Ed.), Mineral Fibres: Crystal Chemistry, Chemical-Physical Properties. Biological Interaction and Toxicity. European Mineralogical Union, London, UK, pp. 171–214. https://doi.org/10.1180/EMU-notes.18.3.

Wicks, F.J., Plant, A.G., 1979. Electron-microprobe and X-ray microbeam studies of serpentine textures. Can. Mineral. 17 (4), 785–830.

by Claudia Ricchiuti[1]*, Andrea Bloise[2], and Rosalda Punturo[1]

Occurrence of asbestos in soils: State of the Art

[1] Department of Biological, Geological and Environmental Sciences, University of Catania, Corso Italia, 55, 95129 Catania CT, Italy;
  Corresponding author: E-mail: claudia.ricchiuti@unict.it, punturo@unict.it
[2] Department of Biology, Ecology and Earth Sciences, University of Calabria, Via Pietro Bucci, I-87036 Rende, Italy

In the last decades, it has been widely demonstrated the risk to human health related to asbestos fibres exposure. Many studies have mainly focused on the mineralogical and geochemical characterization of ophiolites (i.e., serpentinite and metabasite rocks) since they are the main lithotypes associated with Naturally Occurring Asbestos (NOA). Nevertheless, derivative soil from these rocks inherits the mineralogical and geochemical composition of bed rock and may contain hazardous fibres, thus making its examination necessary as well. This paper provides a summary of asbestos-containing soils investigation worldwide with the purpose of providing an overview of the data obtained so far. To this aim, the most relevant available literature, testifying the presence of fibrous minerals in soils have been considered. This allowed the global territory mapping in order to depict the distribution of natural asbestos in soils worldwide.

Introduction

Asbestos is a term used to indicate six fibrous silicate minerals belonging to serpentine (i.e., chrysotile) and amphibole (i.e., tremolite, actinolite, anthophyllite, amosite that is the fibrous-asbestiform variety of grunerite also known as brown asbestos, and crocidolite that is the fibrous-asbestiform variety of riebeckite, commercially known as blue asbestos; Gualtieri et al., 2017) super-group (WHO, 1986; NIOSH 2008; Ballirano et al., 2017). These minerals have been widely exploited to create Asbestos-Containing Materials (ACMs) due to their physical properties (Bloise et al., 2017a, 2018a, b; Bloise 2019a).

The term NOA means the asbestos fibres present in rocks (i.e., serpentinite or altered ultramafic rocks) and soils, referring to those that have not been extracted for commercial purposes (Bloise et al., 2008; Harper, 2008; Pugnaloni et al., 2013; Belluso et al., 2020; Bailey 2020a,b; Cahill 2020; Cagnard et al., 2020; Erskine 2020; Gualtieri 2020; Léocat 2020; Pierdzig 2020; Wroble et al., 2020). The natural asbestos occurrences is widespread in the environment, some examples include chrysotile deposits in Ural Mountains in the Russian Federation (Ross and Nolan, 2003), Appalachian Mountains (USA), Canada (Virta, 2006) and also in India, China, Italy, South Africa, Australia, Greece, Cyprus (Ross and Nolan, 2003) and other countries. Figure 1a, shows a global map with the main asbestos mines. The most frequent asbestos occurring form is chrysotile, whose fibres are normally found as veins in serpentine rocks, followed by anthophyllite, crocidolite, tremolite, actinolite and amosite (Virta, 2002; Bloise et al., 2019b).

Human activity and weathering processes may disturb NOA and provoke the dispersion of fibres, potentially inhalable, in the environment. Many studies confirmed that death from lung diseases can be associated with environmental exposure to asbestos (IARC, 2009). In fact, the risk to human health is represented by the inhalation of asbestos fibres that penetrate in the lungs and may cause cancer pathologies. It is worth noting that, fibrous minerals such as, erionite, ferrite fluoro-edenite, antigorite (Gianfagna et al., 2003; Cardile et al., 2007; Ballirano et al., 2018a,b; Gualtieri et al., 2018; Petriglieri et al., 2020) and others, may have toxic effects as asbestos fibres and, if inhaled, can be dangerous.

To date, many studies are based on the knowledge of natural asbestos in rocks whereas much less literature refers to asbestos-bearing soils. Asbestos in soils may be found for: i) improperly removal of Asbestos-Containing Materials; ii) proximity to asbestos factory/ mine; iii) inheritance from mother rocks (natural occurrences).

In this scenario, this work aims to provide an overview about the presence of asbestos fibres in soils worldwide pointing to improve knowledge of asbestos global issue. Therefore, the most relevant study from various disciplines (i.e., geology, mineralogy, medicine, etc.) that testified the presence of asbestos in soil were hereby considered, thus making it available an overview of the data obtained so far and providing a contribution to the mapping of the territory (Fig. 1b).

Because of considerable asbestos-related diseases (Skinner et al., 1988) all of the six asbestos minerals are considered toxic to human health and therefore regulated by law. However, currently only in 67 over 195 countries (34%) in the world the use of regulated asbestos minerals is restricted (Table 1). Since many studies provide the epidemiological evidence that asbestos crocidolite and tremolite are apparently more dangerous than chrysotile (Hodgson et al., 2000), many countries employ it since this is considered a "safe use" for industrial purposes. For example, Russia is the biggest producer in the world (tons/year) followed by China, Brazil, Kazakhstan and India as shown by the 2014 (chrysotile) asbestos trade data (Gualtieri, 2017).

The different global use of asbestos is due to the various political and economic situation of countries and it is constantly changing. For instance, some countries like Canada and Colombia have recently changed their regulations relatively to asbestos exploitation and use. Indeed, in

Colombia the new law is taking effect on January 1st, 2021 with five years transition period for companies currently using asbestos minerals. The ban prohibited the mining, commercialization and distribution of all asbestos types including its export. In the case of Canada, despite asbestos fibres have been recognized as hazardous to human health and well-being (World Health Organization's International Agency) for more than 30 years, Canada remained one of the major exporter of this material until 2011. The federal Prohibition of Asbestos and Products Containing Asbestos Regulations (Regulations: SOR/2018-196) came into force in Canada on January 2019, prohibiting the import, sale and use of asbestos as well as of products containing asbestos. However, there are certain exceptions such as asbestos contained in household product intended for personal use or in a military equipment (IBAS, 2019).

Even in the scientific community a division is noted: some scientists promote the "safe use" of chrysotile and assume that it has little potential for causing mesothelioma (e.g., Liddell et al., 1997; McDonald et al., 1997; Camus, 2001) whereas others are totally opposed to this and claim that all six asbestos types may induce lung diseases if inhaled (Skinner et al., 1988; Yarborough, 2007). Therefore, the International Agency for Research on Cancer define them belonging to Group 1 "substance carcinogenic to humans" (IARC, 2012).

It is difficult to univocally define the relationship (cause-effect) between disease and exposure to different fibres types because of the variability in the chemistry, size, molecular arrangement, surface activity (Pollastri et al., 2014; Bloise et al., 2016b) of mineral fibres. For instance, one hypothesis of higher toxicity of amphiboles compared to chrysotile is based on the behavior of fibres in the lungs. In particular, unlike the amphiboles that are more durable and remain in the lungs for a long time, chrysotile dissolves reasonably quickly due to its low biodura-
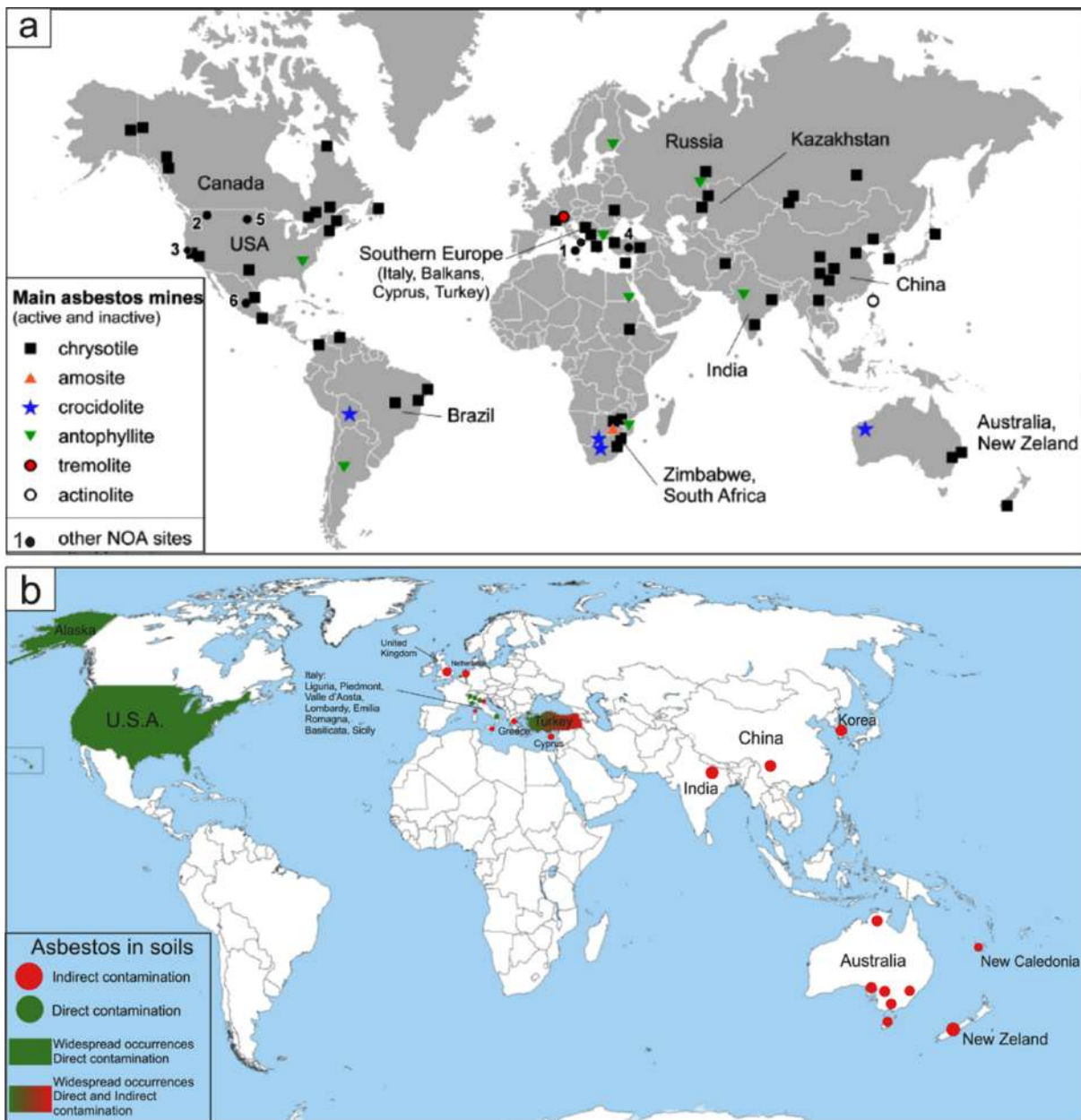

Figure 1. a) global map with the main asbestos mines (active and inactive), modified after Virta 2002; b) global map with the asbestos-containing soil at the state of the knowledge.

Table 1. Exemptions for minor uses are permitted in some countries listed; however, all countries listed must have banned the use of all types of asbestos. List compiled by Laurie Kazan-Allen and modified and revised in July 15, 2019 (http://www.ibasecretariat.org/alpha_ban_list.php)

National Asbestos Bans				
Algeria	Czech Republic	Iraq	Mauritius	Seychelles
Argentina	Denmark	Ireland	Monaco	Slovakia
Australia	Djibouti	Israel	Mozambique	Slovenia
Austria	Egypt	Italy	Netherlands	South Africa
Barain	Estonia	Japan	New Caledonia	Spain
Belgium	Finland	Jordan	New Zeland	Sweden
Brazil	France	Korea (South)	Norway	Switzerland
Brunei	Gabon	Kuwait	Oman	Taiwan5
Bulgaria	Germany	Latvia	Poland	Turkey
Canada	Gibraltar	Liechtenstein	Portugal	United Kingdom
Chile	Greece	Lithuania	Qatar	Uruguay
Colombia	Honduras	Luxembourg	Romania	
Croatia	Hungary	Macedonia	Saudi Arabia	
Cyprus	Iceland	Malta	Serbia	

bility (Hume and Rimstidt, 1992; Bernstein et al., 2008; Oze and Solt 2010). In this work, we summarize and discuss data of the most relevant studies available in literature which testify the presence of asbestos fibres in soils worldwide.

Methods and Materials

In this work, we carried out a literature search on articles of various disciplines that appeared over the past thirty years and subdivided them according to the source of contamination: i) indirect contamination; and ii) direct contamination (Table 2).

Results and Discussion

The articles that reveal the presence of asbestos fibres in soils due to indirect contamination are mainly of three types: i) case-report; ii) case-control study; iii) environmental study.

The first two are mainly epidemiological studies based on the investigation of documented cases of pathologies consequently to the occupational and environmental exposition to asbestos. In particular, case-report consists in a detailed description of an individual case whereas case-control study involves the comparison of two existing groups differing in outcome (e.g., effected by issues: case; non-effected: control).

Case- reports and case-control studies involved in the present work, revealed that in most cases the contamination is due to the presence of fibres in materials used for aims like dirt roads (Baris et al., 1987; Viallat et al., 1991; Luce et al., 2000; Comba et al., 2003; Luo et al., 2003), and whitewash (Constantopoulos et al., 1991; Sichletidis et al., 1992; Sakellariou 1996; Luce et al., 2000; Metintas et al., 2002).

For instance, Luce et al. 2000, carried out a study on respiratory cancers in New Caledonia, where a high incidence of malignant pleural mesothelioma had been observed. In particular, a case-control study has been conducted in regard to the association between tremo-

lite exposure and the risk for respiratory cancer from different sites. Results revealed that the risk of pleural mesothelioma was associated with exposure to whitewash (Table 3) that have widely been used for indoor and outdoor walls of houses.

Differently, the other articles taken into consideration are based on environmental and monitoring study where the source of contamination is mainly represented by asbestos removal operations (Davies et al., 1996; Gualtieri et al., 2009), asbestos in material used for construction (Famoso et al., 2012) or asbestos waste in soil (Driece et al., 2010; Bint et al., 2017), proximity to asbestos mine (Gualtieri et al., 2014; Lee et al., 2015; Turci et al., 2016) as well as asbestos cement factory, widely documented in India (Musthapa et al., 2003; Subramanian et al., 2005; Trivedi et al., 2011, 2013) where the use and production of asbestos is not banned yet.

Gualtieri et al. 2009, presented the results of a monitoring activity conducted on particulate, fall-out and soil samples of selected inhabited areas in Italy (i.e., Emilia Romagna region). The aim of the work was to detect asbestos content in air and the risk of exposure for the population in addition to the assessment of the nature of other mineral phases composing the particulate matrix. To this purpose, various analytical techniques have been used such as XRPD, PLOM, SEM, TEM. In the specific case of the analyzed soils, asbestos fibres were found in samples taken from a residential zone of Sassuolo and near the Bologna Central Railway Station. According to authors, in the first case the contamination is likely due to asbestos removal operations of ACMs whereas in the second case, natural dispersion from ophiolite rock used as track ballast represent the source of contamination. For the results interpretation they elaborate a general model of environmental asbestos pollution (Fig. 2a) referring to the pollution mechanism proposed by Chiappino et al., 1993. The latter consists of a primary and secondary pollution stages. In the primary, the dispersing materials release coarse fibres which settle near to the source because of their higher mass and at the same time release ultra-fine materials. In the secondary, the settled fibres break up into ultra-fine and ultra-short fibrils that are able to remain suspended in the atmosphere for long periods thanks to their minimal mass.

Table 2. Literature data of asbestos-containing soil

Place	Fibres type	Source of contamination	Methods	Reference
Australia	Amosite, Crocidolite, Chrysotile	Indirect (ACMs in the soil)	Case - report	Genever et al., 2017
China (Da-yao)	Crocidolite	Indirect (Dirt roads, stucco, dishes)	Review of clinical/epidemiological studies	Luo et al., 2003
Corsica	Tremolite	Indirect (use in the flooring)	Case - report	Viallat et al., 1991
Cyprus	Tremolite Crisotile	Indirect (Stucco, gutters)	Case - report Radiological studies on population	McConnochie et al., 1989
Greece	Tremolite, Chrysotile	Indirect (Whitewash)	Case – report XRPD	Constantopoulos et al., 1991
Greece (Macedonia)	Tremolite, Chrysotile	Indirect (Whitewash)	Case – report X-ray study on population	Sichletidis et al., 1992
Greece (Metsovo)	Tremolite	Indirect (Whitewash)	Case – report X-ray study on population	Sakellariou et al., 1996
India (Mohanlalganj, Lucknow)	Chrysotile	Indirect (Vicinity to Asbestos cement factory)	PCOM	Subramanian et al., 2005; Trivedi et al., 2011, 2013; Musthapa et al., 2003
Italy (Basilicata)	Tremolite	Direct (Natural occurrences)	Case – report; OM, SEM-EDS, TEM-EDS XRPD, XRF, DTG, DSC	Bernardini et al., 2003; Pasetto et al., 2004; Bloise et al., 2016, 2018; Punturo et al., 2018, 2019
Italy (Emilia-Romagna)	Serpentine asbestos	Indirect (Asbestos removal operations); Direct (Natural occurrences)	PLOM, XRPD, SEM, TEM	Gualtieri et al., 2009
Italy (Liguria)	Tremolite, Actinolite, Chrysotile	Direct (Natural occurrences)	SEM-EDS	Barale et al., 2020; Militello et al., 2019; Turci et al., 2020
Italy (Lombardy)	Chrysotile, Tremolite	Direct (Natural occurrences)	SEM-EDS	Cavallo et al., 2020
Italy (Piedmont)	Chrysotile	Indirect (Vicinity to asbesos mine)	µXRF, XRPD, SEM	Turci et al., 2016
Italy (Sicily)	Fluoro-edenite	Indirect (Quarries, dirt roads, use in mortar and plasters)	Case – report; PCOM, SEM-EDS	Comba et al., 2003; Famoso et al., 2012
Italy (Valle d'Aosta)	Tremolite, Chrysotile	Indirect (Vicinity to asbestos mine)	OM, XRPD, FTIR, SEM, DTA	Gualtieri et al., 2014
Korea (Hongseong; Janghang)	Chrysotile, Tremolite, Actinolite	Indirect (Vicinity to asbestos mine), Direct (Natural occurrences)	PLM, XRD, PCM, FE-EDS, SEM-EDS, TEM-EDS	Lee et al., 2015; Yoon et al., 2020
Netherlands (Hof van Twente)	Crocidolite, Chrysotile	Indirect (Asbestos waste in soil)	TEM on air samples	Driece et al., 2010
New Caledonia	Tremolite	Indirect (Whitewash, dirt roads)	Case – control study	Luce et al., 2000; Petriglieri et al., 2020b
New Zeland	Asbestos fibres	Indirect (Construction waste)	Guidelines	Bint et al., 2017
Turkey (Anatolia)	Tremolite, Actinolite, Chrysotile	Indirect (Whitewash, stucco, terra-cotta); Direct (Natural occurrences)	Cohort study; XRPD	Metintas et al., 2002, 2017
Turkey (Cappadocia)	Erionite	Indirect (Dirt roads, brick)	Case – control study	Baris et al., 1987
United Kingdom	Amosite, Crocidolite	Indirect (Asbestos removal operations)	PCOM quantitative study	Davies et al., 1996
USA	Amphibole asbestos	Direct (Natural occurrences)	XRD, SEM	Thompson et al., 2011
USA (California)	Chrysotile, fibrous amphiboles	Direct (Natural occurrences)	TEM-EDX Electron diffraction analysisi	Bailey 2020a
USA (Nevada)	Actinolite, Fibrous Erionite	Direct (Natural occurrences)	SEM-EDS, FE-SEM, XRD	Buck et al., 2013; Ray 2020
USA (Whashington)	Chrysotile, Actinolite	Direct (Natural occurrences)	PLM	EPA, 2009

Concerning direct contamination, according to the most relevant studies it has been recognized into three countries: Italy, Turkey and USA. In Italy, many studies have been conducted in the Basilicata and Calabria region (Campopiano et al., 2018; Bloise et al., 2019c; Colombino et al., 2019; Dichicco et al., 2019; Laurita and Rizzo, 2019) where tremolite is the main asbestos mineral found in soils (Pasetto et al., 2004; Bloise et al., 2016a; 2018a,b; Punturo et al., 2018, 2019). Tremolite, in actinolite and chrysotile has also been observed in soil sam-

ples investigated by Militello et al., 2019 (Liguria region), whereas samples analysed by Gualtieri et al., 2009, testify the presence of serpentine asbestos in soils occurring in Valle d'Aosta region.

For example, the purpose of the study carried out by Bloise et al., 2016a was to assess the occurrence of asbestiform minerals in serpentinite and serpentinite-derived soils cropping out in the area of Sila Piccola. To this aim, they characterized both serpentinite and agricultural soil samples by means of various analytical techniques such as

Table 3. Pleural mesothelioma risk associated with exposure to whitewash, New Caledonia, 1993-1995. *Odds ratio adjusted for age and gender; Numbers in parentheses, 95% confidence interval (Modified after Luce et al., 2000)

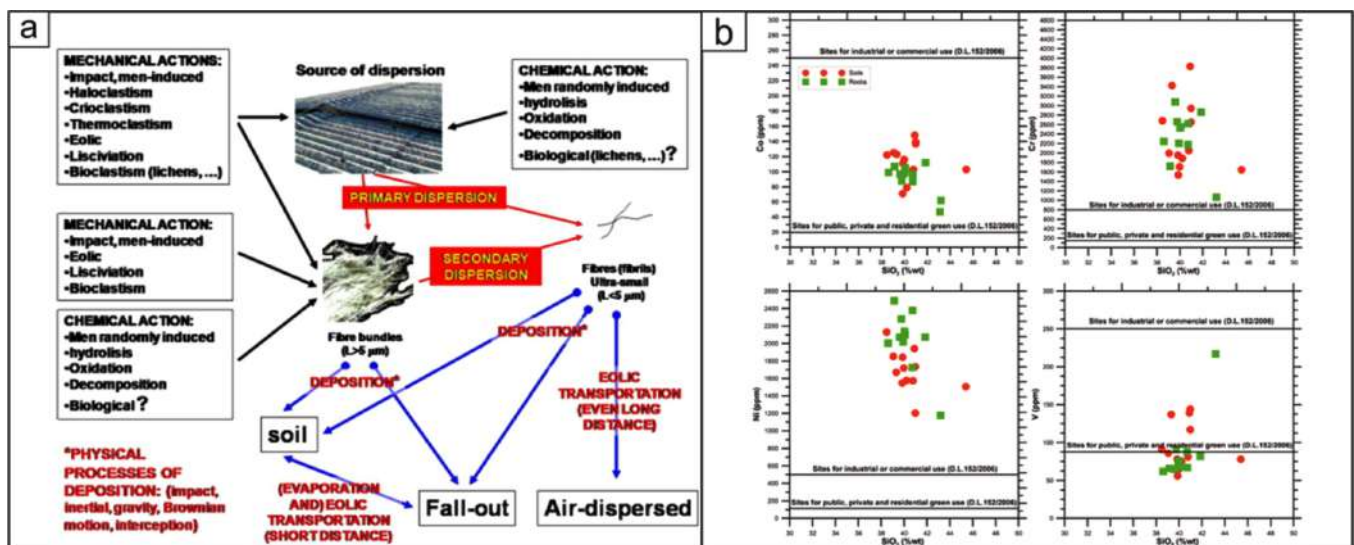| Exposure	No. of cases	No. of controls	Odds ratio*
Never exposed	1	223	1
Ever exposed	14	82	40,9 (5.15, 325)
Exposure duration			
< 20 years	4	38	22.2 (2.33, 211)
≥ 20 years	10	41	65.1 (7.69, 551)
Age at first exposure			
Birth	13	61	52.8 (6.53, 427)
≤ 16	1	11	20.0 (1.09, 368)
> 16	0	10	0

Figure 2. a) Model of asbestos fibre dispersion from cement-asbestos (modified after Gualtieri et al., 2009); b) Correlation diagrams of SiO$_2$ versus Co, Cr, Ni and V for soils and rocks of the studied area (after Punturo et al., 2018). Thresholds values regulated by Italian law (D.L.152/2006) are also indicated for each heavy metal.

Table 4. Mineralogical assemblage detected by PLM, XRPD, SEM/EDS, DSC/TG, µ-R reported in order of decreasing abundance. PS=polygonal serpentine, Atg= antigorite, Lz= lizardite, Ctl=chrysotile, Tr-Act=tremolite-actinolite, Mag=magnetite, Chl=chlorite, Ms=muscovite, Ab=albite, Qtz=quartz, Cal=calcite, Rt=rutile, Sp=spinel (Bloise et al., 2016)

Sample	Phase detected
CNF-S1	Clay>Qtz>Tr-Act>Chl>Ms>Ctl>Liz>Ab>Atg>Rt
CNF-S2	Clay>Qtz>Chl>Ms>Tr-Act>Ctl>Ab>Rt>Liz
GML-S1	Clay>Qtz>Chl>Ms>Tr-Act>Ctl>Ab>Liz>Rt

PLOM, XRPD and SEM/EDS. Moreover, for a better discrimination of serpentine polytypes, Differential Scanning Calorimetry, Thermogravimetric and µ-Raman spectroscopy were used. Results show high amount of chrysotile and asbestos tremolite-actinolite in agricultural soils (Table 4).

Instead, Punturo et al. 2018 conducted a detailed mineralogical and geochemical investigation of both rocks and soil collected in the Basilicata region, with the aim to understand their potential contribution to human health caused by asbestos exposure. Therefore, the presence of asbestos

fibres (chrysotile and asbestos tremolite) and the concentration levels of toxic elements (Cr, Co, Ni, V) have been determined. In the specific case, in almost all samples, detected values exceed the regulatory thresholds for public, private and residential green use (D.L. 152/2006; Fig. 2b).

In the other two countries, fibrous amphiboles and chrysotile are the main fibres detected. In particular, a total of 1251 soil samples in Anatolia region (Turkey) were collected and analyzed by Metintas et al., 2017 (Fig. 3a). XRPD analysis results revealed that chrysotile, tremolite or mixed asbestos fibres were contained in 514 soil samples.

In USA, high occurrence of actinolite and chrysotile has been monitored (EPA, 2009; Thompson et al., 2011; Buck et al., 2013). Thompson et al., 2011 discussed the geographic distribution of amphiboles in the USA, using the mineralogical data from selected sand and/or silt fraction of soils from the USDA-NRCS National Cooperative Soil Survey database, which shows the presence of amphiboles in all states except for Rhode Island. A total of 212,839 horizons (layer within soil with unique morphological characteristics) within 34,326 pedons (body of soil that consists of all the horizons at that location) were sampled (Fig. 3b).
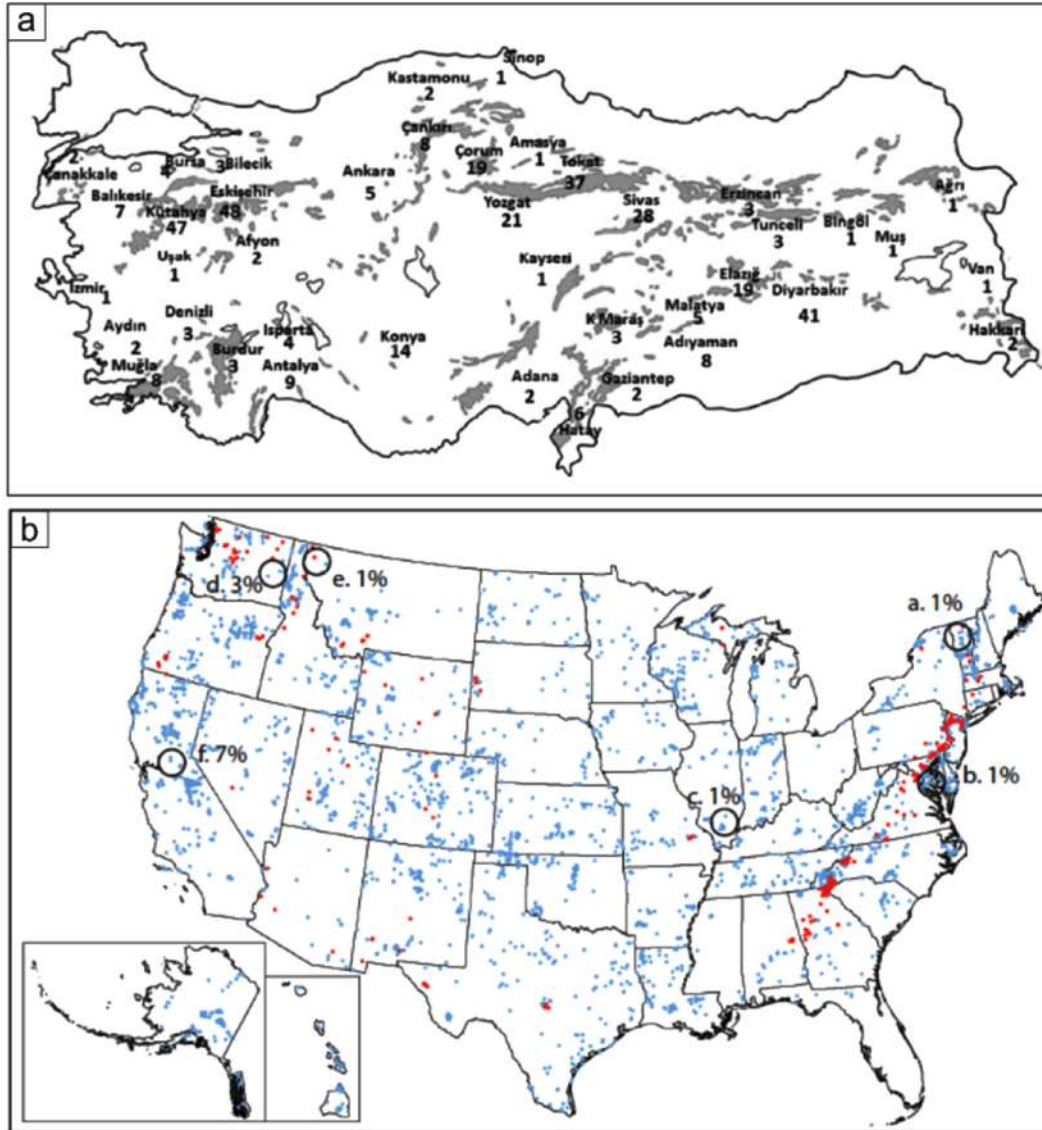
Figure 3. a) Map of Turkey showing the distribution of villages where asbestos exposure was definite (after Metintas et al., 2017; b) Map of the U.S.A. showing asbestos-containing soils (more detail from Thompson et al., 2001))

On the basis of data available in literature of the past thirty years, it is possible to draw up various considerations. First of all, asbestos-related diseases are certainly of significant concern in terms of occupational and public health. Indeed, many studies confirmed a significant malignant mesothelioma risk due to asbestos environmental exposure (Baumann et al., 2016; Liu et al., 2017). Compared to NOA in rocks (Bloise et al., 2019a), asbestos content in soils is today poorly investigated. The soil contamination plays an important role relatively to the environmental exposure especially if soils are used for agricultural purposes, becoming a risk for both workers (Bellomo et al., 2018) and people living near NOA (non-occupational exposure; Bloise et al., 2012; Pugnaloni et al., 2013; Bloise et al., 2017b; Bloise et al., 2018c; Pinizzotto et al., 2018; Punturo et al., 2018). According to Januch et al., 2013, people exposure derived from disturbance of asbestos-contaminated soil, is mainly investigated by measuring asbestos concentration in breathing zone air during soil-disturbance activities. Nevertheless, in our opinion the determination of asbestos content in top-soil or sub-soil is essential as it constitutes the primary threat to health. Indeed, the tendency of fibres is

to settle out of air and water and deposit in soil (EPA, 1979). Moreover, some fibres are sufficiently small to remain in suspension and can be transported for long distance thus increasing the contamination area. It is worth specifying that, asbestos itself is very stable and, if not disturbed can remain in the soil indefinitely (ATSDR, 2001). Indeed, concerning ACMs asbestos is bonded in a matrix which does not favour the release of free respirable fibres unless it is extremely weathered, or exposed to acid material (NEPC, 2011). However, many common forms of asbestos containing materials may slowly degrade if left in soil leading to more asbestos fibres being released over time (Bint et al., 2017). Since the extensive use in the past, ACMs represent a persistent source of environmental pollution despite the cessation of asbestos mining and legal prohibitions adopted by many countries. It is estimated that about 150 million m^2 of asbestos-based products and more than two thousand million m^2 of cement-asbestos roofings are still present today (Gualtieri et al., 2009).

In summary, the source of asbestos contamination in soils can be indirect and direct. In the first case, it is originated by asbestos fac-
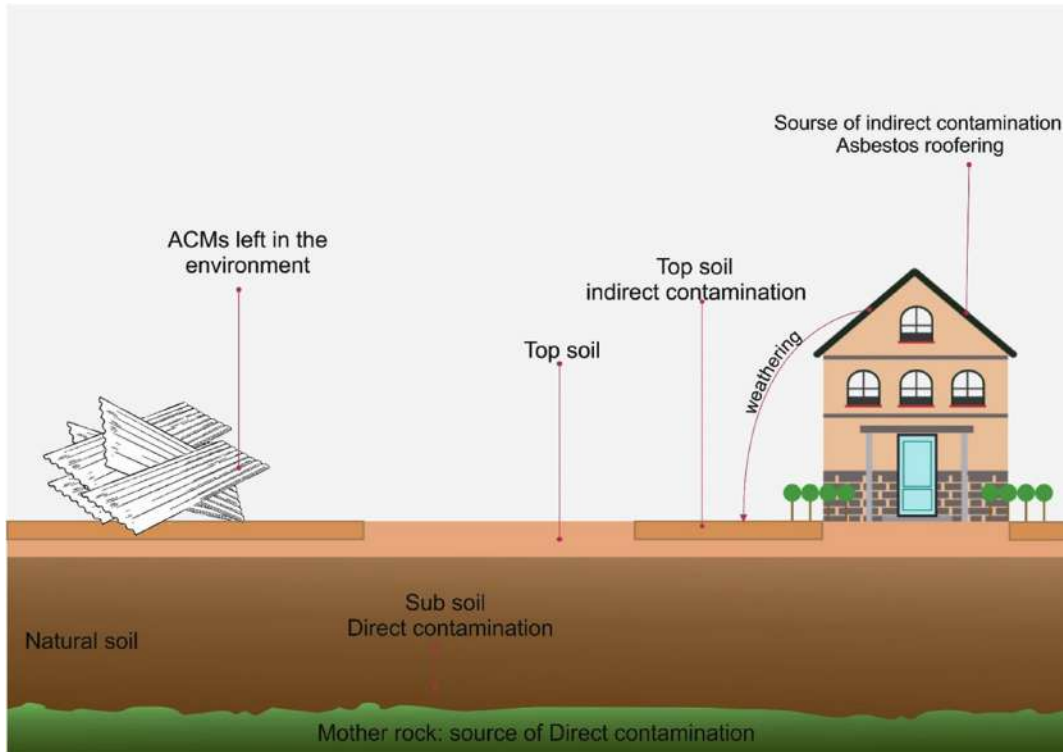
Figure 4. The image shows where asbestos fibres can be found depending on the source of contamination (direct/indirect).

tory, mines and ACMs subject to weathering or improperly removed. Direct contamination instead, derive by the disturbance of natural deposits by weathering or anthropic activity which cause the dispersion of fibres into the environment.

Depending on the source of contamination, asbestos fibres can be found in different portion of soil. Indeed, to verify the presence of fibres in the surrounding of asbestos factory/mine it is important to sample the top-soil in the proximity of the emission point. Differently, in the case of direct contamination, sub-soil samples are more representative since the presence of fibres is not due to deposition but rather to the characteristics of the mother rock. Figure 4, summarize where fibres can be found depending on the contamination source.

Observing the collected data, it is possible to notice that the indirect contamination has been widely detected in the investigated soils and their distribution cover a big range of the territory. This is likely due to the high use and commercialization of asbestos in the past, which resulted in his exportation all over the world.

Instead, since natural asbestos occurrences depends on the geology of the area, the presence of contaminated soils is limited to the distribution of the mother rock outcrops.

In recent years a new line of research asserts that the ingestion of asbestos by drinking water containing fibres, represents another factor that may cause an increase in cancer incidence in expose populations (DHHS Committee, 1987) although this issue is still debated (Rodelsperger et al., 1991; Di, 2017; Li et al., 2019). The possible sources of contamination include erosion of rock, industrial effluents, disintegration of asbestos-containing products (WHO, 2000, 2004). In this context, it is essential to identify the source dispersion and act on it. Therefore, knowledge on contaminated soil as well as territory mapping need to be improved.

Conclusions

In this study, a detailed examination of the most relevant literature studies revealing the presence of asbestos in soils worldwide, has been conducted. The aim of this work is to provide an overview about the distribution of asbestos-containing soils, thus improving the global mapping and the knowledge obtained so far.

Main results from our investigation showed that the presence of asbestos content in soils is still poorly studied. At this time, many studies are mainly based on the measuring of asbestos concentration in breathing zone air during disturbance activities. Moreover, several studies provide epidemiological and experimental evidence that trace metals may provoke lung cancer thus making necessary their investigation. In this scenario, the identification of the source of contamination and actions on it are essential.

For instance, one way to locate the potential "asbestos-containing soil" is to: i) identify the natural outcrops of rocks that may contain asbestos and investigate on derivative soil (natural contamination); and ii) identify old factory and asbestos mine (even the abandoned ones) and examine the surrounding soil (indirect contamination). As far as ACMs is concerned, it may be more difficult because of their high diffusion all over the world due to the extensive use in the past, but removal or renewal action are essential.

Acknowledgements

di Catania, Dipartimento di Scienze Biologiche, Geologiche e Ambientali), scientific responsible Rosalda Punturo.

References

Agency for Toxic Substances and Disease Registry, 2001, Toxicological profile for asbestos. Division of Toxicology/Toxicology Information Branch, Atlanta, 319 p.

Bailey, R.M., 2020a, Asbestiform Minerals of the Franciscan Assemblage in California with a Focus on the Calaveras Dam Replacement Project. Environmental and Engineering Geoscience February 20, v. 26, pp. 21–28. doi.org/10.2113/EEG-2264

Bailey, R.M., 2020b, Overview of Naturally Occurring Asbestos in California and Southwestern Nevada. Environmental and Engineering Geoscience February 20, v. 26, pp. 9–14. doi:org/10.2113/EEG-2282

Ballirano, P., Bloise, A., Cremisini, C., Nardi, E., Montereali, M.R., and Pacella, A., 2018b, Thermally induced behavior of the K-exchanged erionite: a further step in understanding the structural modifications of the erionite group upon heating. Periodico di Mineralogia, v. 87, pp. 123–134.

Ballirano, P., Bloise, A., Gualtieri, A.F., Lezzerini, M., Pacella, A., Perchiazzi, N., Dogan, M., and Dogan, A.U., 2017, The Crystal Structure of Mineral Fibers. In: Gualtieri, A.F., (Eds.), Mineral Fibers: Crystal Chemistry, Chemical-Physical Properties, Biological Interaction and Toxicity. European Mineralogical Union, London, 2017, pp. 17–53.

Ballirano, P., Pacella, A., Bloise, A., Giordani, M., and Mattioli, M., 2018a, Thermal Stability of Woolly Erionite-K and Considerations about the Heat-Induced Behaviour of the Erionite Group. Minerals, v. 8, 28.

Barale, L., Piana, F., Tallone, S., Compagnoni, R., Avataneo, C., Botta S., Marcelli, I., Irace, A., Mosca, P., Cossio, R., and Turci, F., 2020, Geological Model for Naturally Occurring Asbestos Content Prediction in the Rock Excavation of a Long Tunnel (Gronda di Genova Project, NW Italy). Environmental and Engineering Geoscience February 20, v. 26, pp. 107–112. doi:org/10.2113/EEG-2269

Baris, I., Simonato, L., Artvinli, M., Pooley, F., Saracci, R., Skidmore, J., and Wagner, C., 1987, Epidemiological and environmental evidence of the health effects of exposure to erionite fibres: a four-year study in the Cappadocian region of Turkey. International Journal of Cancer, v. 39, pp. 10–17.

Baumann, F., and Carbone, M., 2016, Environmental risk of mesothelioma in the United States: an emerging concern-epidemiological issues. Journal of Toxicology and Environmental Health Part B Critical Reviews, v. 19, pp. 231–249.

Bellomo, D., Gargano, C., Guercio, A., Punturo, R., and Rimoldi, B., 2018, Workers' risks in asbestos contaminated natural sites. Journal of Mediterranean Earth Sciences, v. 10, pp. 97–106.

Belluso, E., Baronnet, A., and Capella, S., 2020, Naturally Occurring Asbestiform Minerals in Italian Western Alps and in Other Italian Sites. Environmental and Engineering Geoscience February 20, v. 26, pp. 39–46. doi:org/10.2113/EEG-2276

Bernardini, P., Schettino, B., Sperduto, B., Giannandrea, F., Burragato, F., and Castellino, N., 2003, Tre casi di mesotelioma pleurico ed inquinamento ambientale da rocce affioranti di tremolite in Lucania. Giornale Italiano di Medicina del Lavoro ed Ergonomia, v. 25, pp. 408–411.

Bernstein, D.M., Donaldson, K., Decker, U., Gaering, S., Kunzendorf, P., Chevalier, J., and Holm, E., 2008, A biopersistence study following exposure to chrysotile asbestos alone or in combination with fine particles. Inhalation Toxicology, v. 20, pp. 1009–1028.

Bint, L., Hunt, S., Dangerfield, D., and Mechaelis, M., 2017, New Zeland Guidelines for Assessing and Managing Asbestos in soil. Branz, Porirua, 96 p.

Bloise, A., 2019a, Thermal behaviour of actinolite asbestos. Journal of Materials Science, v. 54, pp. 11784–11795.

Bloise, A., Barca, D., Gualtieri, A.F., Pollastri, S., and Belluso, E., 2016b, Trace elements in hazardous mineral fibres. Environmental Pollution, v. 216, pp. 314–323.

Bloise, A., Belluso, E., Critelli, T., Catalano, M., Apollaro, C., Miriello, D., and Barrese, E., 2012, Amphibole asbestos and other fibrous minerals in the meta-basalt of the Gimigliano-Mount Reventino Unit (Calabria, south-Italy). Rendiconti Online della Società Geologica Italiana, v. 21, pp. 847–848

Bloise, A., Catalano, M., Critelli, T., Apollaro, C., and Miriello, D., 2017b, Naturally occurring asbestos: potential for human exposure, San Severino Lucano (Basilicata, Southern Italy). Environmental Earth Sciences, v. 76, pp. 648.

Bloise, A., Catalano, M., and Gualtieri, A., 2018, Effect of grinding on chrysotile, amosite and crocidolite and implications for thermal treatment. Minerals, v. 8, pp. 135.

Bloise, A., Fornero, E., Belluso, E., Barrese, E., and Rinaudo, C., 2008, Synthesis and characterization of tremolite asbestos fibres. European Journal of Mineralogy, v. 20, pp. 1027–1033.

Bloise, A., Kusiorowski, R., and Gualtieri, A., 2018a, The effect of grinding on tremolite asbestos and anthophyllite asbestos. Minerals, v. 8, pp. 274. doi:org/10.3390/min8070274

Bloise, A., Kusiorowski, R., Lassinantti, Gualtieri, M., and Gualtieri, A.F., 2017a, Thermal behaviour of mineral fibers. In: Gualtieri, A.F. (Eds)., Mineral Fibers: Crystal Chemistry, Chemical-Physical Properties, Biological Interaction and Toxicity; European Mineralogical Union: London, 2017; 18, pp. 215–252.

Bloise, A., and Miriello, D., 2018c, Multi-analytical approach for identifying asbestos minerals in situ. Geosciences, v. 8, pp. 133

Bloise, A., Punturo, R., Catalano, M., Miriello, D., and Cirrincione, R., 2016a, Naturally occurring asbestos (NOA) in rock and soil and relation with human activities: the monitoring example of selected sites in Calabria (southern Italy). Italian Journal of Geosciences, v. 135, pp. 268–279.

Bloise, A., Punturo, R., Kusiorowski, R., and Pereira Gómez, D., 2019a, Editorial for Special Issue "Mineral Fibres". Fibers, v. 7, pp. 54.

Bloise, A., Ricchiuti, A., Giorno, E., Zumpano, P., Miriello, D., Apollaro, C., Crispini, A., De Rosa, R., and Punturo, R., 2019c, Assessment of Naturally Occurring Asbestos in the area of Episcopia (Lucania, Southern Italy). Fibers, v. 7, pp. 703

Bloise, A., Ricchiuti, C., Lanzafame, G., and Punturo, R., 2019b, X-ray synchrotron microtomography: a new technique for characterizing chrysotile asbestos. Science of The Total Environment, v. 703, pp. 135675. doi:org/10.1016/j.scitotenv.2019.135675

Buck, B., Goossens, D., Metcalf, R.V., McLaurin, B., and Freudenberger, M., 2013, Naturally Occurring Asbestos: Potential for Human Exposure, Southern Nevada, USA. Soil Science Society of America Journal, v. 77, pp. 2192–2204.

Cagnard, F., and Lahondère, D., 2020, Naturally Occurring Asbestos in France: Geological Mapping, Mineral Characterization, and Technical Developments. Environmental and Engineering Geoscience February 20, v. 26, pp. 53–59. doi:org/10.2113/EEG-2277

Cahill, E., 2020, Sampling, Analysis, and Risk Assessment for Asbestos and Other Mineral Fibers in Soil. Environmental and Engineering Geoscience February 20, v. 26, pp. 121–127. doi:org/10.2113/EEG-2286

Campopiano, A., Bruno, M., Olori, A., Angelosanto, F., Iannò, A., Casciardi, S., and Spadafora, A., 2018, Fibrous antigorite in mount reventino area of central calabria. Journal of Mediterranean Earth Sciences, v. 10, pp. 17–25.

Camus, M., 2001, A ban on asbestos must be based on a comparative risk assessment. Journal of the Association of Medicine Canadian, v. 164, pp. 491–494.

Cardile, V., Lombardo, L., Belluso, E., Panico, A., Capella, S., and Balazy, M., 2007, Toxicity and Carcinogenicity Mechanisms of Fibrous Antigorite. International journal of environmental research and public health, v. 4, pp. 1–9.

Cavallo, A., and Petriglieri, J.R., 2020, Naturally Occurring Asbestos in Valmalenco (Central Alps, Northern Italy): From Quarries and Mines

to Stream Sediments. Environmental and Engineering Geoscience February 20, v. 26, pp. 47−52. doi:org/10.2113/EEG-2270

Chiappino, G., Todaro, A., and Blanchard, O., 1993. Atmospheric asbestos pollution in the urban environment: Rome, Orbassano and a control locality (II). La medicina del lavoro, v. 84, pp. 187−192.

Colombino, E., Capella, S., Casalinuovo, F., Racco, R., Pruiti, F., Volante, M., Di Marco, V., Belluso, E., and Capucchio, M., 2019. Malignant peritoneal mesothelioma in a boar who lived in Calabria (Italy): Wild animal as sentinel system of human health. Science of the Total Environment, v. 683, pp. 267−274.

Comba, P., Gianfagna, A., and Paoletti, L., 2003, Pleural mesothelioma cases in Biancavilla are related to a new fluoro-edenite fibrous amphibole. Archives of Environmental & Occupational Health, v. 58, pp. 229−232.

Constantopoulos, S., Theodoracopoulos, P., Dascalopoulos, G., Saratzis, N., and Sideris, K., 1991, Metsovo lung outside Metsovo. Chest, v. 99, pp. 1158−1161.

Davies, L.S.T., Wetherill, G.Z., McIntosh, C., McGonagle, C., and Addison, J., 1996, Development and validation of an analytical method to determine the amount of asbestos in soils and loose aggregates. Institute of Occupational Medicine, Edinburgh, 69 p.

DHHS Committee, 1987, Report on cancer risks associated with the ingestion of asbestos. DHHS Committee to Coordinate Environmental and Related Programs Environmental health perspectives, v. 72, pp. 253−265.

Di Ciaula, A., 2017, Asbestos ingestion and gastrointestinal cancer: A possible underestimated hazard. Expert Review of Gastroenterology and Hepatology, v. 11, pp. 419−425.

Driece, H., Siesling, S., Swuste, P., and Burdorf, A., 2010, Assessment of cancer risks due to environmental exposure to asbestos. Journal of Exposure Science and Environmental Epidemiology, v. 20, pp. 478−485.

EPA, 1979, Water-related environmental fate of 129 priority pollutants. Vol I. Introduction and technical background, metals and inorganics, pesticides and PCBs. Washington, DC: U.S. Environmental Protection Agency, Office of Water Planning and Standards. EPA-440/4-79-029a. NTIS No. PB80-204373

EPA, 2009, Soil, Sediment and Surface Water sampling Sumas Mountain Naturally-Occurring Asbestos site, Whatcom county, Washington. U.s. EPA region 10 Office of Environmental Assessment, Seattle, 98101−3140

Erskine, B.G., 2020, Geologic Investigations for Compliance with the CARB Asbestos ATCM. Environmental and Engineering Geoscience February 20, v. 26, pp. 99−106. doi:org/10.2113/EEG-2290

Famoso, D., Mangiameli, M., Roccaro, P., Mussumeci, G., and Vagliasindi, F., 2012, Asbestiform fibers in the Biancavilla site of national interest (Sicily, Italy): Review of environmental data via GIS platforms. Reviews in Environmental Science and Bio/Technology, v. 11, pp. 417−427.

Genever, M., Allan, M., and Bos, S., 2017, Case studies of contaminated land, final report.

Gianfagna, A., Ballirano, P., Bellatreccia, F., Bruni, B., Paoletti, E., and Oberti, R., 2003, Characterization of amphibole fibers linked to mesothelioma in the area of Biancavilla, eastern Sicily, Italy. Mineralogical Magazine, v. 67, pp. 1221−1229.

Gualtieri A., Pollastri, S., Gandolfi, N., Ronchetti, F., Albonico, C., Cavallo, A., Zanetti, G., Marini, P., and Sala, O., 2014, Determination of the concentration of asbestos minerals in highly contaminated mine tailings: An example from abandoned mine waste of Crètaz and Èmarese (Valle d'Aosta, Italy). American Mineralogist, v. 99. pp. 1233−1247

Gualtieri, A., Mangano, D., Gualtieri, M., Ricchi, A., Foresti, E., Lesci, G., Roveri, N., Mariotti, M., and Pecchini, G., 2009, Ambient monitoring of asbestos in selected Italian living areas. Journal of Environmental Management, v. 90, pp. 3540−3552.

Gualtieri, A., 2017, Mineral fibres: Crystal chemistry, chemical-physical properties, biological interaction and toxicity. In: A.F. Gualtieri (Eds.), Mineralogical Society, EMU Notes in Mineralogy Volume 18 − chapter 1.

Gualtieri, A., Gandolfi, N.B., Passaglia, E., Pollastri, S., Mattioli, M.,

Giordani, M., Ottaviani, M.F., Cangiotti, M., Bloise, A., Barca, D., Vigliaturo, R., Viani, A., Pasquali, L., and Gualtieri, L.M., 2018b, Is fibrous ferrierite a potential health hazard? Characterization and comparison with fibrous erionite. American Mineralogist: Journal of Earth and Planetary Materials, v. 103, pp. 1044−1055.

Gualtieri, A.F., 2020, Naturally Occurring Asbestos: A Global Health Concern? State of the Art and Open Issues. Environmental and Engineering Geoscience February 20, v. 26, pp. 3−8. doi:org/10.2113/EEG-2271

Harper, M., 2008, 10th Anniversary critical review: naturally occurring asbestos. Journal of Environmental Monitoring, v. 10, pp. 1394−1408.

Hodgson, J., Darnton, A., 2000, The quantitative risks of mesothelioma and lung cancer in relation to asbestos exposure. Annals of Occupational Hygiene, v. 44, pp. 565−601. doi:org/10.1016/S0003-4878(01)00029-1

Hume, L., and Rimstidt, J., 1992, The biodurability of chrysotile asbestos. American Mineralogist, v. 77, pp. 1125−1128.

International Agency for Research on Cancer, 2009, Asbestos (chrysotile, amosite, crocidolite, tremolite, actinolite, and anthophyllite) IARC Monographs. Arsenic, Metals, fibres and dusts, International Agency for Research on Cancer, Lyon, pp. 147−167.

International Agency for Research on Cancer, 2012, Asbestos (chrysotile, amosite, crocidolite, tremolite, actinolite, and anthophyllite). IARC Monographs on the Evaluation of Carcinogenic Risks to Human, Lyon, France, v. 100C, pp. 219−309.

International Ban Asbestos Secretariat, 2019. http://www.ibasecretariat.org/alpha_ban_list.php

Januch, J., Brattin, W., Woodburyc, L., and Berry, D., 2013, Evaluation of a fluidized bed asbestos segregator preparation method for the analysis of low-levels of asbestos in soil and other solid media. Analytical Methods, v. 5, p. 1658−1668.

Laurita, S., and Rizzo, G., 2019, The first occurrence of asbestiform magnesio-riebeckite in schists in the frido unit (pollino unesco global geopark, southern italy). Fibers, v. 7, pp. 79.

Lee, Jieun., Yoon, C., Ham, S., and Tsai, P., 2015, Optimal Treatment Condition for Changing Characteristics of Naturally Occurring Asbestos. Aerosol and Air Quality Research, v. 15, pp. 2332−2345.

Léocat, E., 2020, Naturally Occurring Asbestos in France: A Technical and Regulatory Review. Environmental and Engineering Geoscience February 20, v. 26, pp. 61−65. doi:org/10.2113/EEG-2254

Li, J., Li, H., Zheng, B., and Yu, Z., 2019, Comparison of analysis of asbestos fibres in drinking water using phase contrast microscopy and microFTIR spectrometry with scanning electron microscopy and energy-dispersive X-ray spectroscopy. Environmental Science: Water Research and Technology, v. 5, pp. 543−551.

Liddell, F.D.K., McDonald, A.D., and McDonald, J.C., 1997, The 1891-1920 birth cohort of Quebec chrysotile miners and millers: development from 1904 and mortality to 1992. Annals of Occupational Hygiene, v. 41, pp. 13−36.

Liu, B., Van Gerwen M., Bonassi, S., and Taioli, E., 2017, Epidemiology of environmental exposure and malignant mesothelioma. Journal of thoracic oncology: official publication of the International Association for the Study of Lung Cancer Mesothelioma, v. 12, pp. 1031−1045.

Luce, D., Bugel, I., Goldberg, P., Goldberg, M., Salomon, C., Billon- Galland, M., Nicolau, J., Quénel, P., Fevotte, J., and Brochard, P., 2000, Environmental exposure to tremolite and respiratory cancer in New Caledonia: a case-control study. American Hournal of Epidemiology, v. 151, pp. 259−265.

Luo, S., Liu, X., Tsai, S.P., and Wen, C., 2003, Asbestos related diseases from environmental exposure to crocidolite in Da-yao, China. I. Review of exposure and epidemiological data. Occupational and Environmental Medicine, v. 60, pp. 35−42. doi:org/10.1136/oem.60.1.35

McConnochie, K., Simonato, L., Mavrides, P., Christofides, P., Mitha, R., Griffiths, D., and Wagner, J., 1989, Mesothelioma in Cyprus. In: Mignon J, Peto J, Saracci R (Ed.). Non-occupational exposure to mineral fibres. IARC, Science Publications, v. 90, pp. 411−419.

McDonald, A.D., Case, B.W., Churg, A., Dufresne, A., Gibbs, G.W., Sébastien, P., and McDonald, J.C., 1997, Mesothelioma in Quebec chrysotile miners and millers: epidemiology and etiology. Annals of Occupational Hygiene, v. 41, pp. 707−719

Metintas, S., Batirel, H., Bayram, H., Yilmaz, U., Karadag, M., Ak, G., and Metintas, M., 2017, Turkey National Mesothelioma Surveillance and Environmental Asbestos Exposure Control Program. International Journal of Environmental Research and Public Health, v. 14, pp. E1293.

Metintas, S., Metintas, M., Ucgun, I., and Oner, U., 2002, Malignant mesothelioma due to environmental exposure to asbestos. Chest, v. 122(6), pp. 2224−2229.

Militello, G., Sanguineti, E., Gonzalez, A., Mantovani, F., and Gaggero, L., 2019, The concentration of asbestos fibers in bulk samples and its variation with grain size. Minerals, v. 9.

Musthapa, M., Ahmad, I., Trivedi, A., and Rahman, Q., 2003. Asbestos contamination in biota and abiota in the vicinity of asbestos-cement factory. Bulletin of Environmental Contamination and Toxicology, v. 70, pp. 1170–1177.

National Environment Protection Council, 2011, Guideline on investigation levels for soil and groundwater, Assessment of Site Contamination, Measure April 2011, Schedule B1, Adelaide, p. 61

NIOSH, 2008, Current Intelligence Bulletin (June 2008-Revised Draft) Asbestos and Other Elongated Mineral Particles: State of the Science and Roadmap for Research.

Oze, C., and Solt, K., 2010, Biodurability of chrysotile and tremolite asbestos in simulated lung and gastric fluids. American Mineralogist, v. 95, pp. 825−831.

Pasetto, R., Bruni, B., Bruno, C., and Cauzillo, G., 2004, Mesotelioma pleurico ed esposizione ambientale a fibre minerali: Il caso di un'area rurale in Basilicata. Annali Dell'Istituto Superiore Di Sanita, v. 40, pp. 251−265.

Petriglieri, J., Laporte-Magoni, C., Gunkel-Grillon, P., Tribaudino, M., Bersani, D., Sala, O., and Salvioli-Mariani, E., 2020, Mineral fibres and environmental monitoring: A comparison of different analytical strategies in New Caledonia. Geoscience Frontiers, v. 11, pp. 189−202.

Petriglieri, J.R., Laporte-Mangoni, C., Salvioli-Mariani, E., Tomatis, M., Gazzano, E., Turci, F., Cavallo, A., and Fubini, B., 2020b, Identification and Preliminary Toxicological Assessment of a Non-Regulated Mineral Fiber: Fibrous Antigorite from New Caledonia. Environmental and Engineering Geoscience February 20, v. 26, pp. 89−97. doi:org/10.2113/EEG-2274

Pierdzig, S., 2020, Regulations Concerning Naturally Occurring Asbestos (NOA) in Germany—Testing Procedures for Asbestos. Environmental and Engineering Geoscience February 20, v. 26, pp. 67−71. doi:org/10.2113/EEG-2278

Pinizzotto, M., Cantaro, C., Caruso, M., Chiarenza, L., Petralia, C., Turrisi, S., and Brancato, A., 2018. Environmental monitoring of airborne fluoro-edenite fibrous amphibole in biancavilla (sicily, italy): A nine-years survey. Journal of Mediterranean Earth Sciences, v. 10, pp. 89−95.

Pollastri, S., Gualtieri, A., Lassinantti Gualtieri, M., Hanuskova, M., Cavallo, A., and Gaudino, G., 2014, The zeta potential of mineral fibres. Journal of Hazardous Materials, v. 276, pp. 469−479.

Pugnaloni, A., Giantomassi, F., Lucarini, G., Capella, S., Bloise, A., Di Primio, R., and Belluso, E., 2013, Cytotoxicity induced by exposure to natural and synthetic tremolite asbestos: An in vitro pilot study. Acta histochemical, v. 115, pp. 100−112.

Punturo, R., Ricchiuti, C., and Bloise, A., 2019, Assessment of Serpentine Group Minerals in Soils: A Case Study from The Village of San Severino Lucano (Basilicata, Southern Italy). Fibers, v. 7, pp. 18.

Punturo, R., Ricchiuti, C., Mengel, K., Apollaro., C., De Rosa, R., and Bloise, A., 2018, Serpentinite-derived soils in southern Italy: potential for hazardous exposure. Journal of Mediterranean Earth Sciences, v. 10.

Ray, R., 2020, Discerning Erionite from Other Zeolite Minerals During Analysis. Environmental and Engineering Geoscience February 20, v. 26, pp. 133−139. doi:org/10.2113/EEG-2279

Rodelsperger, K., and Woitowitz, H., 1991, Asbestos in drinking water. Deutsche Medizinische Wochenschrift, v. 116, pp. 555−557.

Ross, M., and Nolan, R.P., 2003, History of asbestos discovery and use and asbestos-related disease in context with the occurrence of asbestos within ophiolite complexes. In: Dilek, Y., Newcomb, S. (Eds.), Ophiolite concept and the evolution of geological thought. Boulder, Colorado, Geological Society of America, Special Paper 373, pp. 447−470.

Sakellariou, K., Malamou-Mitsi, V., Haritou, A., Koumpaniou, C., Stachouli, C., Dimoliatis, I., and Constantopoulos, S., 1996, Malignant pleural mesothelioma from non-occupational asbestos exposure in Metsovo (north-west Greece): slow end of an epidemic? European Respiratory Journal, v. 9, pp. 1206−1210.

Sichletidis, I., Daskalopoulou, E., Tsarou, V., Pnevmatikos, I., Chloros, D., and Vamvalis, C., 1992, Five cases of pleural mesothelioma with endemic pleural calcifications in a rural area in Greece. La Medicina del lavoro, v. 83, pp. 326−329.

Subramanian, V., and Madhavan, N., 2005, Asbestos problem in India. Lung Cancer, v. 49 Suppl 1, pp. S9−12.

Thompson, B.D., Gunter, M.E., and Wilson, M.S., 2011, Amphibole asbestos soil contamination in the USA: A matter of definition. American Mineralogist, v. 96, pp. 690−693.

Trivedi, A., and Ahmad, I., 2011, Effects of Chrysotile Asbestos Contaminated Soil on Crop Plants. Soil and Sediment Contamination, v. 20, pp. 767−776.

Trivedi, A., and Ahmad, I., 2013, Impact of chrysotile asbestos contaminated soil on foliar nutrient status of plants. Indian Journal of Plant Physiology, v. 18(3). doi:org/10.1007/s40502-013-0036-9

Turci, F., Avataneo, C., Botta, S., Marcelli, I., Barale, L., Tomatis, M., Cossio, R., Tallone, S., Piana, F., and Compagnoni, R., 2020, New Tools for the Evaluation of Asbestos-Related Risk during Excavation in an NOA-Rich Geological Setting. Environmental and Engineering Geoscience February 20, v. 26, pp. 113−120. doi:org/10.2113/EEG-2272

Turci, F., Favero-Longo, S., Gazzano, C., Tomatis, M., Gentile-Garofalo, L., and Bergamini, M., 2016, Assessment of asbestos exposure during a simulated agricultural activity in the proximity of the former asbestos mine of Balangero, Italy. Journal of hazardous, v. 308, pp. 321−327. doi:org/10.1016/j.jhazmat.2016.01.056

Viallat, J., Boutin, C., Steinbauer, J., Gaudichet, A., and Dufour, G., 1991, Pleural effects of environmental asbestos pollution in Corsica. Annals of the Bew York Academy of Sciences 643 (1 The Third Wav), pp. 438−443.

Virta, R., 2002, Asbestos: Geology, Mineralogy, Mining, and Uses. U.S. Geological Survey Open-File Report 02-149, 35 p.

Virta, R., 2006. Worldwide asbestos supply and consumption trends from 1900 through 2003. U.S. Geological Survery Circular 1298, 80 p.

WHO, 2000, Air quality guidelines for Europe (2nd edition). Regional Office for Europe. World Health Organization, Copenhagen, 274 p.

WHO, 2004, Guidelines for Drinking-Water Quality: Third edition. Volume 1, Recommendations. World Health Organization, Geneva, 494 p.

WHO, 1986, Asbestos and other natural mineral fibres. Programme on Chemical Safety. World Health Organization. Environmental Health Criteria 53, Geneva.

Wroble, J., Frederick, T., and Vallero, D., 2020, Refinement of Sampling and Analysis Techniques for Asbestos in Soil. Environmental and Engineering Geoscience February 20, v. 26, pp. 129−131. doi:org/10.2113/EEG-2283

Yarborough, C., 2007, The risk of mesothelioma from exposure to chrysotile asbestos. Current opinion in pulmonary medicine, v. 13, pp. 334−338.

Yoon, S., Yeom, K., Kim, Y., Park, B., Park, J., Kim, H., Jeong, H., and Roh, Y., 2020, Management of Naturally Occurring Asbestos Area in Republic of Korea. Environmental and Engineering Geoscience February 20, v. 26, pp. 79−87. doi:org/10.2113/EEG-2287

Claudia Ricchiuti is currently a Ph.D. student in mineralogy and petrography at the Department of Biological, Geological and Environmental Sciences at the University of Catania, Italy. Her scientific activity is mainly based on the mineralogical characterization of asbestos fibres in rocks and soils. Since 2015, she improved their knowledge concerning Natural Occurring Asbestos (NOA), through her Master thesis, post-graduated internship at foreign Universities and collaboration with national and international research centres during which she had experience on performing various laboratory analyses (i.e., XRPD, SEM, TEM, TG/DSC, EPMA). She is co-author in scientific international publications, based on petrographic and geochemical investigation of soils and rocks outcropping in southern Apennines with special regards on fibrous minerals.

Rosalda Punturo has research interest in Petrography and Petrophysics and their application to cultural heritage and to environment. She completed her doctoral research on petrophysical properties of mantle and crustal xenoliths in the year 2000. Since 2004 she is an assistant Professor at the University of Catania and is part of the group with special focus on Metamorphic, Igneous and Sedimentary petrology. She is the principal investigator of the group focusing on Natural Asbestos Occurrences. She has extensively carried out research in southern Italy (Calabrian–Peloritani Orogen; Hyblean Plateau) and in southern Rhodope Massif (Greece). Official Homepage http://www.dipbiogeo.unict.it/docenti/rosalda.punturo

Andrea Bloise is currently Associate Professor of mineralogy at the Department of Biology, Ecology and Earth Sciences (DiBEST) at Calabria University, Rende, Italy. He has expertise in X-ray powder diffraction, scanning and transmission electron microscopy, thermal analysis, collaborating on various scientific projects of national and international interest. He has recently also been working in the fields of cultural heritage and geochemical modelling of both natural and thermal waters. He is the author of several international peer reviewed scientific publications and scientific director of the Laboratory of Experimental Mineralogy at the DiBEST.

Potentially toxic elements (PTEs) associated with asbestos chrysotile, tremolite and actinolite in the Calabria region (Italy)

Andrea Bloise[a,*], Claudia Ricchiuti[b], Rosalda Punturo[b], Dolores Pereira[c,d]

[a] *Department of Biology, Ecology and Earth Sciences, University of Calabria, I-87036 Rende, CS, Italy*
[b] *Department of Biological, Geological and Environmental Sciences, University of Catania, I-95129 Catania, Italy*
[c] *CHARROCK Research Group, University of Salamanca, Plaza de los Caídos s/n, 37008 Salamanca, Spain*
[d] *Geology Department, Science Faculty, University of Salamanca, Plaza Merced s/n, Salamanca 37008, Spain*

ARTICLE INFO

ABSTRACT

Potentially toxic elements (PTEs) hosted in asbestos elongate mineral particles is one of the factors that determines their toxic/pathogenic effects.

This study quantifies and compares these elements in terms of major, minor and trace element concentrations (Si, Mg, Ca, Al, Fe, Mn, Cr, Co, Ni, Cu, Zn, Be, V, As, Rb, Sb, Ba, Pb, Sr) in various types of asbestos using micro X-ray fluorescence (μ-XRF) and inductively coupled plasma mass spectrometry (ICP-MS), in order to understand how they contribute to asbestos-related diseases. Chrysotile, tremolite asbestos and actinolite asbestos extracted from the Gimigliano-Mount Reventino Unit (Calabria Region, Southern Italy) were used for this study.

In the minerals analysed, high concentrations of Cr (171 ppm) and Be (2.9 ppm) were found in tremolite asbestos and chrysotile respectively. When calculating the pseudo-total concentrations of trace elements in the samples, the largest amounts were detected in tremolite asbestos, followed by actinolite asbestos and chrysotile. However, since other metals such as Mn and Fe (minor elements) are known to induce toxicity, and considering their input to the overall balance, actinolite contained the largest amount of PTEs and in this case chrysotile proved to be more toxic than tremolite asbestos. Furthermore, the potential leaching of PTEs, released by chrysotile, tremolite and actinolite asbestos-containing rocks, into the soil and water supply is also discussed. Since asbestos elongate mineral particles can be widespread in the environment (i.e. air, rocks, soil, water), it is essential to quantify the toxic elements present in asbestos elongate mineral particles in order to prevent asbestos-related diseases. The knowledge obtained from this study will provide us with a better understanding of asbestos-related lung cancer.

1. Introduction

Asbestos has been classified as a carcinogenic substance (Group 1) by the International Agency for Research on Cancer (IARC, 2012). Five types of asbestos belong to the amphibole group (actinolite asbestos, amosite, anthophyllite asbestos, crocidolite and tremolite asbestos) while chrysotile belongs to the serpentine mineral group (IARC, 2012). The industrial exploitation of asbestos for manufacturing Asbestos Containing Materials (ACMs) began between 1860 and 1875; however, since the late 1970s asbestos demand has dropped considerably due to the health risks associated with asbestos exposure (Alleman and Mossman, 1997). It is important to note that due to the widespread use of ACMs (e.g., hospitals, schools, gyms, cinemas, industrial plants) during the peak period of asbestos consumption around 1977 (Park et al., 2012), the handling of asbestos-containing materials is still a matter of global concern (Paglietti et al., 2012; Spasiano and Pirozzi, 2017; Cannata et al., 2018).

Inhalation of contaminated air is the most common route of asbestos exposure (WHO, 2006). Once the asbestos elongate mineral particles have entered the body, lungs or stomach (Di Ciaula, 2017), they can cause various chronic diseases that mainly affect the respiratory system. For this reason, asbestos has been banned in > 50 countries (International Ban Asbestos Secretariat, 2016; Spasiano and Pirozzi, 2017).

However, since many studies have revealed that amphibole asbestos elongate mineral particles are more dangerous than chrysotile (WHO, 2015), many countries including Russia, China, Brazil (Frank and Joshi, 2014; U.S. Geological Survey, 2016) deem chrysotile to be "safer to use" for industrial purposes. Instead, countries like Canada and Colombia have recently changed their regulations and have introduced a

---

ban on the production, use and sale of asbestos (CEPA, 1999; International Ban Asbestos Secretariat, 2019).

Another aspect to consider is that asbestos may also occur in the environment as natural components of rocks and soils (natural occurrence of asbestos; Gunter, 2018) that are often excavated for numerous civil engineering projects such as housing settlements, railway lines, motorways, etc. These anthropic activities may cause the release of dust particles containing asbestos elongate mineral particles, which pose a significant risk to human health; indeed, it has been widely demonstrated that the onset of diseases such as mesothelioma, lung cancer and asbestosis is linked to asbestos exposure (IARC, 2012; Harper, 2008; Baumann et al., 2015; Bloise et al., 2017a, 2017b). Moreover, ACMs disturbance caused by natural risks (e.g. earthquakes, hurricanes) and anthropic disasters (Perkins et al., 2007; Kashimura et al., 2015) may contribute to the release of elongate mineral particles (NIOSH, 2011; Gunter, 2018; Oberdörster and Graham, 2018).

The mechanisms associated with asbestos elongate mineral particles toxicity depend on various factors such as fibre dimensions, biopersistence, surface reactivity, chemical composition and the ability to generate Reactive Oxygen Species (ROS) (Roggli, 1989; Weiss, 1999; Mossman et al., 2011; Huang et al., 2011; Pugnaloni et al., 2013; Baumann et al., 2013; Liu et al., 2013; Turci et al., 2017; Jablonski et al., 2017). In addition to parameters such as morphometry, biodurability and surface activity, some authors (i.e. Schoonen et al., 2006), consider elongate mineral particles as complex crystal-chemical reservoirs that may release PTEs (e.g. Fe, Ni, Co, Cr) into the intracellular or extracellular environment during dissolution.

Indeed, there is epidemiologic and experimental evidence that PTEs such as some heavy metals are carcinogens and pose a significant threat to human health (e.g., Nemery, 1990; Censi et al., 2006; Censi et al., 2011a, 2011b). Moreover, some researchers theorize that asbestos elongate mineral particles may play only a passive role in producing diseases as carriers of trace elements (Dixon et al., 1970; Upreti et al., 1984; Nemery, 1990; Bowes and Farrow, 1997; Wei et al., 2014; Bloise et al., 2016a). There has recently been much debate on the role of cancer-causing agents, but it was only in the early 70s that some studies invoked the PTEs as an indicator of asbestos pathogenicity (Cralley et al., 1968; Dixon et al., 1970; Bloise et al., 2016a). It has been proved that high concentrations of trace elements in asbestos are capable of inducing lung cancer (Schreier et al., 1987; Wei et al., 2014). These studies are in agreement with the study conducted by Gazzano et al. (2005) who proposed using synthetic stoichiometric chrysotile elongate mineral particles (free of any toxic elements) as a negative control for toxicological studies since synthetic chrysotile elongate mineral particles do not have any in-vitro toxic effects.

In a pioneering study, Cralley et al. (1968) reported data showing the possible role of toxic elements in inducing asbestos-related cancer in bovines and textile workers. Gross et al. (1969) showed that toxic elements induced lung cancers in rats after they were exposed to asbestos dust containing large amounts of Ni, Cr and Co. Medical researchers focused on the physical properties of asbestos as a cause of lung cancer, but plant and animal ecologists have long claimed that trace metals associated with asbestos are the major causes of oxidative stress-induced cell death. For example, a high toxic metal concentration (i.e., Mn) was found in fish exposed to asbestos rich sediments (Schreier et al., 1987), while Pascal and Tessier (2004) showed that Mn is cytotoxic to human normal bronchial epithelial cells in vitro, and Hasegawa et al. (2008) demonstrated that high concentrations of Mn and Cu may increase one's risk of developing lung cancer. Among the asbestos trace elements known to be hazardous to human health, Ni is considered the most hazardous because it damages DNA (IARC, 1984; Caicedo et al., 2007). Several studies have been published on the capability of Ni to generate ROS and on its toxicity at intracellular sites (Nackerdien et al., 1991; Salnikow et al., 2000; Kawanishi et al., 2001; Chen et al., 2003; Horie et al., 2009). More specifically, Ni can cause a variety of adverse health effects, such as lung fibrosis and cancer of the respiratory tract

(Oller et al., 1997; Seilkop and Oller, 2003; Leyssens et al., 2017). The adverse health effects of Cr^{3+} found in chrysotile are mainly due to the production of ROS (Scharf et al., 2014). Cr^{3+} can induce tissue damage, necrosis, and inflammation in patients with Cr associated adverse local tissue reactions. However, Cr^{3+} is not deemed to be as dangerous as Cr^{6+}, which is very harmful to humans due its high mobility and bioavailability. As for Co, although no previous studies have linked Co exposure to lung cancer, it is well-documented in literature that if Co is absorbed into the muscle tissues or the bloodstream, it can cause several neurological, cardiovascular and endocrine deficits (Leyssens et al., 2017). Zn is considered to be an essential element for the human body if people are exposed to small amounts. However, as demonstrated by Vanoeteren et al. (1986), excessive concentrations of Zn can seriously affect human health. The normal (Vanoeteren et al., 1986) Zn values reported for humans lie between 1 and 30 ppm.

Pb is a cumulative toxicant that can also have serious consequences for human health; in fact, if absorbed by the body it affects multiple body systems including the respiratory and digestive systems (Boskabady et al., 2018). Several researchers claim that Be stimulates the formation of ROS, similarly to the redox reactions observed for Fe and Ni, thus increasing asbestos carcinogenesis and lung cancer mortality rates (e.g., Dixon et al., 1970; Mancuso, 1970; Nackerdien et al., 1991; Salnikow et al., 2000; Kawanishi et al., 2001; Chen et al., 2003; Verma et al., 2003).

Asbestos minerals can host a large number of PTEs (i.e., Fe, Cr, Ni, Zn, Mn, Co and Rare Earth Elements) (Scambelluri et al., 1997; Tiepolo et al., 2007; Vils et al., 2008). Previous data concerning ophiolite-derived soils reported in literature (e.g., Bloise et al., 2016b; Punturo et al., 2018) revealed the presence of a significant amount of PTEs such as Mn, Cr, Co, Ni. It is important to note that the leaching of asbestos due to soil deposits in streams and the weathering of asbestos-bearing rocks, reduces the concentrations of PTEs in the elongate mineral particles and increases them in the soil (Holmes et al., 1971; Kumar and Maiti, 2015). In this regard, it has been demonstrated that some acids alter the mineral surface of asbestos and remove considerable amounts of PTEs (Lavkulich et al., 2014). Therefore, resembling the original contents, soils developed from ophiolitic rocks are characterized by high concentrations of PTEs, in particular Mn, Cr, Ni and Co (Lyon et al., 1968; 1970; Atzori et al., 1999; Oze et al., 2004; Smith et al., 2007; Rajapaksha et al., 2012; Kelepertzis et al., 2013; Vithanage et al., 2014; Baumeister et al., 2015; Bloise et al., 2016b). Mistikawy et al. (2020), hypothesized that ultramafic rocks are rich in PTEs that can become bioavailable or easily mobilized. It is well known that in many countries, such as Italy, Argentina, India and Canada, asbestos large scale mining operations have caused toxic heavy metal pollution in soils, water, and the atmosphere (Cavallo and Rimoldi, 2013; Kumar and Maiti, 2015). These heavy metals generally exceed, by up to one order of magnitude, the maximum concentration limits imposed by environmental agencies and governments (Caillaud et al., 2009; Tashakor et al., 2014). For example, it has been documented that in the Gimigliano – Mount Reventino Unit (GMRU), the concentration of some PTEs such as Cr, Ni, Co, V in serpentinite-derived soils, exceed the regulatory thresholds for public, private and green residential use (e.g., Punturo et al., 2018). These toxic elements can be mobilized, discharged into various terrestrial environments and absorbed into the body, thus representing a significant threat to public health. Also Cr contamination is a significant environmental challenge in areas where ophiolitic outcrops are abundant.

Moreover, it is important to note that water interacting with ophiolite rocks is generally characterized by high concentrations of PTEs derived through the dissolution of primary solid phases (e.g., serpentines and amphiboles). Apollaro et al. (2011) claim that ophiolites are known sources of dissolved Cr as well as of Ni, Cu, Zn and Pb in the waters coming from the ophiolitic outcrops of the GMRU. Ophiolitic rocks contain large amounts of Cr^{3+} in their minerals (e.g., chrysotile, tremolite-actinolite asbestos, spinels) which is oxidized to Cr^{6+} due to

the weathering process and become highly mobile. Therefore, the characterization of asbestos minerals represents the first step for assessing contaminated soil and groundwater in ophiolitic outcrops.

In this scenario, the aim of this study was to carry out a systematic and comparative analysis of PTEs in terms of major, minor (Si, Mg, Ca, Fe, Al and Mn, as oxide) and trace elements (Cr, Co, Ni, Cu, Zn, Be, V, As, Rb, Sb, Ba, Pb, Sr) concentrations in three types of asbestos using micro X-Ray Fluorescence (μ-XRF) and Inductively Coupled Plasma mass spectrometry (ICP-MS), in order to understand how they contribute to numerous health problems. Chrysotile, tremolite asbestos and actinolite asbestos were selected for this study and the samples were collected from Gimigliano-Mount Reventino Unit (GMRU) (Calabria Region, Italy) (Zakrzewska et al., 2008; Punturo et al., 2015). In this area several deposits of serpentinite and metabasite rock containing chrysotile, tremolite asbestos and actinolite asbestos have been mapped and reported (Bloise et al., 2012, 2014, 2016b; Bloise and Miriello, 2018; Bloise et al., 2020). According to the Italian National Mesothelioma Register, 70 mesothelioma deaths, caused by occupational and environmental exposure to asbestos minerals, were recorded in the Calabria region between 1993 and 2015 (INAIL, 2015), thus confirming the presence of asbestos in the environment. For example, Campopiano et al. (2017) identified tremolite asbestos in the pulmonary tissue of goats, sheep and two boars living near disused quarries in the Calabria Region. Recently, Colombino et al. (2019) described a case of malignant peritoneal mesothelioma caused by asbestos exposure (chrysotile and tremolite/actinolite) in a wild boar living in the same area, thus demonstrating a relationship between the neoplasia and exposure to natural occurrence of asbestos outcrops in the Mount Reventino (Calabria Region). Since there is strong evidence of a relationship between lung cancer and asbestos and co-occurring PTEs (Dixon et al., 1970; Nemery, 1990; Wei et al., 2014), the comparative evaluation of the amount of PTEs contained in the samples enabled us to determine which elements play a role in asbestos toxicity. Until now no studies have evaluated PTEs concentration associated with actinolite asbestos, in this regard, this paper attempts to fill this gap in academic literature.

2. Materials and methods

The Calabria region (southern Italy) is characterized by wide occurrence of ophiolitic rocks which are used as building and ornamental stones; "Verde Calabria" is the commercial name for this local stone (Bloise et al., 2014; Punturo et al., 2015; Bloise et al., 2016b; Punturo et al., 2018). The exploitation sites of these rocks, some of which are still active, are located in the Gimigliano-Mount Reventino Unit (GMRU) (Punturo et al., 2018). In this study, asbestos minerals coming from ophiolitic outcrops belonging to the GMRU have been investigated; specifically:

a) Chrysotile, from a road cut close to San Mango D'Aquino town. This specimen, also contains minor impurities of antigorite (Punturo et al., 2015); b) tremolite asbestos from an abandoned metabasite quarry located in the area of Mount Reventino (Bloise and Miriello, 2018); c) actinolite asbestos from an abandoned quarry close to the towns of Conflenti. This specimen contains very minor impurities of talc and cordierite (Bloise, 2019). The complete and exhaustive mineralogical and physical characterization of the asbestos considered in this study, can be found in: (Punturo et al., 2015; Bloise and Miriello, 2018; Bloise, 2019).

Using an optical Zeiss Axioskop 40 reflected light microscope, elongate mineral particles were manually selected and disaggregated with the aim of choosing those without evident chemical alterations or impurities.

Major and minor elements (Si, Mg, Ca, Fe, Al, Mn) as oxide were quantified by means of micro X-ray fluorescence (μ-XRF) analysis. The equipment used is a Bruker M4 Tornado spectrometer, equipped with two X-ray tubes (Rh and W) and two SDD detectors, active area of 60mm^2. The Rh tube has a polycapillar optic to concentrate the

radiation in a spot < 20 μm (Mo-Kα). The data for each point has been acquired in vacuum conditions (2 mbar) using Rh radiation with the generator operating at 50 kV and 150 μA, using two detectors to increase the intensity of the received signal. The acquisition time for each measurement was 60 s. In this study, sixty spot analyses were performed on each sample. Spot chemical analyses enable us to study micrometric compositional variations. In order to facilitate the detection of elements, each point was measured twice, once without a primary filter for the quantification of major elements and once with a primary filter composed of three superimposed layers of Al (100 μm), Ti (50 μm) and Cu (25 μm). This significantly reduces the background up to 15 keV, improving sensitivity to minor and trace elements, especially those ones whose spectral lines are between 4 and 14 keV. The acquired spectra were processed with the software ESPRIT M4 v. 1.5.2.65 to obtain a semi-quantitative analysis expressed as wt% of major elements (oxides) and ppm for minor elements.

Cr, Co, Ni, Cu, Zn, Be, V, As, Rb, Sb, Ba, Pb and Sr were determined by Inductively Coupled Plasma-Mass Spectrometry (ICP-MS). Fe and Mn analyses were also obtained using ICP-MS as well as μ-XRF. Analyses were conducted by means of ICP-MS AGILENT 7800. For this analysis, 0.1 g of sample powder is digested with HNO$_3$ + HF in high pressure (90 bar) vessels in Milestone Microwave. The accuracy (i.e., the relative difference from reference values) was generally better than 8%. To calibrate the equipment, the analytical service has used certified standard dilutions (Panreac) of the different elements (1000 mg/l each) grouped in a multi-elemental patron. Data collection was possible by using the common experimental procedure used in the Mass Spectroscopy Laboratory of the University of Calabria (Italy) (e.g., Bloise et al., 2016a). Cr, Co, Ni, Cu, Zn, Be, V, As, Rb, Sb, Ba, Pb and Sr were determined using Inductively Coupled Plasma-Mass Spectrometry (ICP-MS) due to its low detection limits (Table 2) compared to μ-XRF.

3. Results

3.1. Major and minor elements

Major and minor elements (Si, Mg, Ca, Fe, Al and Mn) as oxide were measured in chrysotile, tremolite and actinolite asbestos (Figs. 1, 2 and 3) contained in rocks that belong to the Gimigliano - Mount Reventino Unit (Calabria Region, Italy) by means μ-XRF. As regards the major elements in chrysotile, SiO$_2$ and MgO contents were 46.41 wt% and 48.78 wt% respectively, with minor amounts of CaO (1.37 wt%) and FeO (3.22 wt%) (Fig. 4a, Table 1). These values are in agreement with those detected in chrysotile and reported in literature (Morgan and Cralley, 1973; Bloise et al., 2016a).

For the amphiboles, the tremolite asbestos samples show SiO$_2$ and MgO average values of 55.8 wt% and 27.12 wt%, while in actinolite asbestos samples the content is 54.06 wt% and 22.96 wt% (Fig. 4b, Table 1) respectively. CaO was more abundant in tremolite asbestos, with values of 15.0 wt%, compared to actinolite asbestos whose concentration was 11.3 wt%. As expected, actinolite asbestos showed higher FeO contents, reaching 9.07 wt% (Fig. 4c; Table 1) versus 1.80 wt% of tremolite asbestos and 3.22 wt% of chrysotile (Fig. 5). As far as, the minor elements are concerned, the data revealed a Mn content > 1000 ppm in all of the samples as well as Al in tremolite asbestos and actinolite asbestos (Fig. 5, Table 1). In particular, the data showed a Mn content of 0.17 wt% in chrysotile, 0.20 wt% in tremolite asbestos and 0.75 wt% in actinolite asbestos. Al was present in small amounts in chrysotile (0.02 wt%) and was more abundant in tremolite asbestos (0.34 wt%) and actinolite asbestos (0.38 wt%) (Fig. 5).

3.2. Trace elements

Table 2 shows the concentrations of the trace elements (Cr, Co, Ni, Cu, Zn, Be, V, As, Rb, Sb, Ba, Pb, Sr) in each sample, obtained using ICP-MS. The results show that the trace metal concentrations found in
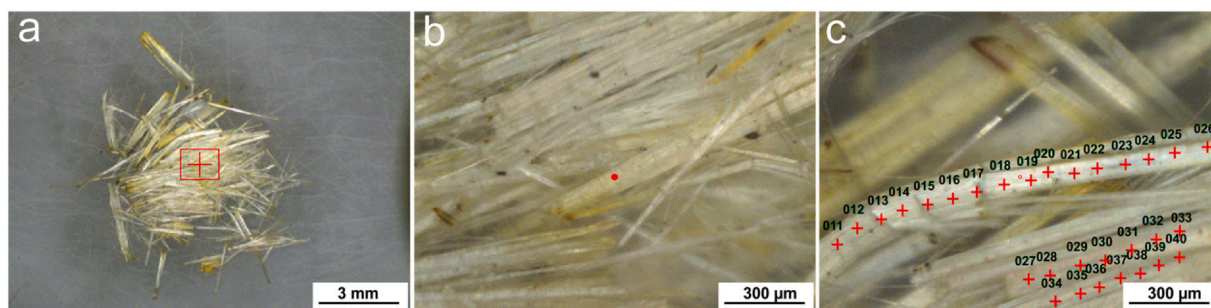
Fig. 1. Micro-X-ray fluorescence (μ-XRF) images of chrysotile from GMRU. a) Straw-yellow chrysotile elongate mineral particles, from San Mango D'Aquino (Calabria Region, Italy). b) chrysotile bundles, c) chrysotile elongate mineral particles with some analysis points, note (top left corner) the curvature that demonstrates the flexibility of the elongate mineral particle. (For interpretation of the references to colour in this figure legend, the reader is referred to the web version of this article.)

chrysotile, tremolite and actinolite asbestos differ (Fig. 6). Fe and Mn whose concentrations were also acquired by means ICP-MS, were in line with the data acquired by means μ-XRF.

Special attention has been paid to the content of some metals (i.e. Cr, Co, Ni, Cu, Zn) whose summation Σ(Cr, Co, Ni, Cu, Zn) was the highest in tremolite asbestos, reaching a value of 555 ppm, followed by actinolite asbestos (100 ppm) and chrysotile (88 ppm). In particular, Cr concentration was 5.5 ppm in chrysotile, 171 ppm in tremolite asbestos and 15 ppm in actinolite asbestos, while Co showed lower values of 1.89 ppm in chrysotile, 22.64 ppm in tremolite asbestos and 4.69 ppm in actinolite asbestos. The highest concentrations of Ni and Cu were found in tremolite asbestos, followed by actinolite asbestos and chrysotile. Ni content was 4.32 ppm in chrysotile, 308.63 in tremolite asbestos and 14.50 in actinolite asbestos, while Cu was present at a concentration of 10.52 ppm in chrysotile, at 24.53 ppm in tremolite asbestos and at approximately 19.39 ppm in actinolite asbestos. Zn was detected in chrysotile reaching values of 65.47 ppm, followed by actinolite asbestos (46.56 ppm) and tremolite asbestos (28.42 ppm).

Fig. 7 shows the concentration (ppm) patterns of trace elements Be, V, As, Rb, Sb, Ba, Pb, and Sr found in chrysotile, tremolite and actinolite asbestos. It is important to note that the concentrations of the trace elements V, Rb and Ba were quite similar in all three samples or showed slight differences (e.g. Be, Sb). However, As, Pb and Sr data highlight more heterogeneous values. In fact, the highest concentration of As was detected in chrysotile with a value of 7.0 ppm, while similar concentrations were found in tremolite and actinolite asbestos: 1.20 ppm and 1.50 ppm respectively. As regards the Pb and V values, the data revealed that the highest concentrations were detected in actinolite asbestos followed by tremolite asbestos and chrysotile. Pb content was approximately 2.40 ppm in chrysotile and reached 4.44 and 23.29 ppm in tremolite and actinolite asbestos respectively. V was present at concentrations of approximately 6.88 in chrysotile, 7.07 ppm in tremolite asbestos and 11.06 ppm in actinolite asbestos. The Sr content was higher in tremolite asbestos in which reached 200.0 ppm compared

to actinolite asbestos (47.0 ppm) and chrysotile (10.7 ppm). For Be content, it was 2.90 ppm in chrysotile which was higher than the Be concentrations found in tremolite asbestos (0.30 ppm) and actinolite asbestos (1.10 ppm). As a resume, the obtained data highlight that chrysotile sample contained the highest concentrations of As (7.0 ppm) and Be (2.9 ppm), tremolite asbestos had the highest amount of Sr (200 ppm) and Ba (14.8 ppm) while actinolite asbestos is characterized by the highest values of Pb (23.29 ppm) and V (11.06 ppm) (Fig. 7).

4. Discussion

4.1. Potentially toxic elements for the human body

Due to the scientific evidence demonstrating the relationship between lung cancer mortality and cumulative exposure to PTEs, the asbestos toxicity model proposed by Gualtieri (2018) states that it is essential to quantify the toxic elements present in the asbestos. In this study, lower concentrations of the trace metals Cr, Co and Ni were found in the chrysotile samples than those found in the tremolite and actinolite asbestos samples. The role of Mn in the balance content of toxic metals in the studied samples is crucial. As illustrated in Fig. 6, considering the contribution of Mn (Σ Cr, Co, Ni, Cu, Zn, Mn), the sample containing the largest amount of trace metals was actinolite asbestos (3974 ppm) followed by chrysotile (1274 ppm) and tremolite asbestos (1233 ppm). However, without taking the contribution of Mn into consideration, the highest concentrations of trace metals were found in tremolite asbestos at a total value of 553 ppm, followed by actinolite asbestos (100 ppm) and chrysotile (88 ppm). Therefore, the Mn content influences the most hazardous fibre definition related to the content of PTEs. The other trace elements like Be, V, As, Rb, Sb, Ba, Pb and Sr are present in different amounts in the samples. Considering the total amount of these elements (Table 3) in the samples, tremolite asbestos showed the highest value (228 ppm) followed by actinolite asbestos (99 ppm) and chrysotile (42 ppm). The high concentration of Be
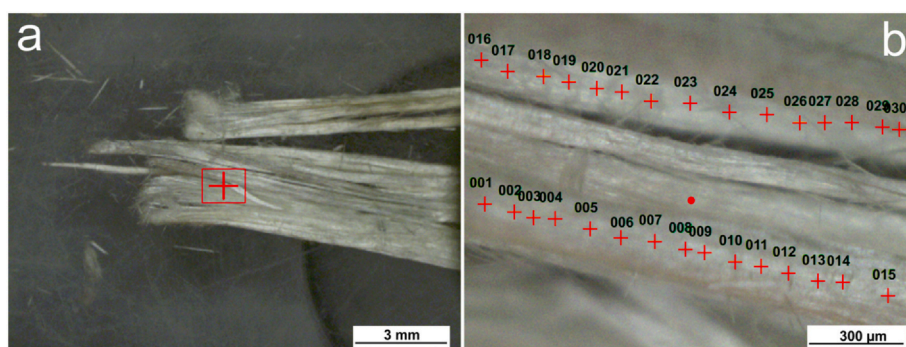

Fig. 2. Micro-X-ray fluorescence (μ-XRF) images on the tremolite asbestos from GMRU. a) white tremolite asbestos, from an abandoned quarry in Mt. Reventino (Calabria Region, Italy), b) tremolite asbestos with some analysis points.
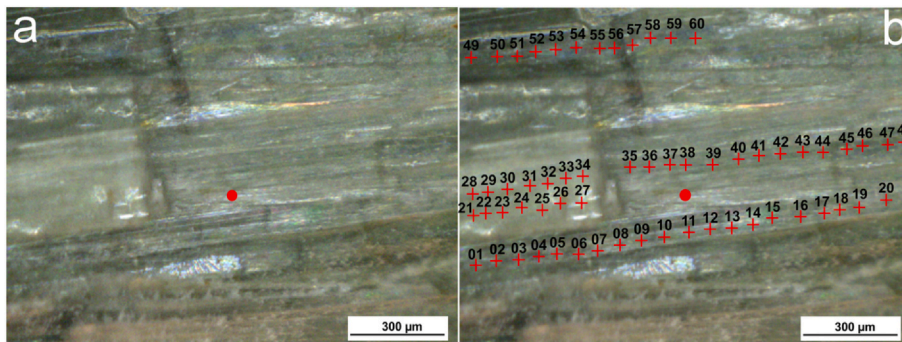
Fig. 3. Micro-X-ray fluorescence (μ-XRF) images of actinolite asbestos from GMRU. a) green actinolite asbestos, from an abandoned quarry close to the town of Conflenti (Calabria Region, Italy), b) actinolite asbestos with some analysis points. (For interpretation of the references to colour in this figure legend, the reader is referred to the web version of this article.)

in chrysotile (3 ppm) may have an effect on the interaction of the elongate mineral particles with the biological system. In addition to Be, the highest concentrations of As which is considered a cytotoxic element, were found in chrysotile (Fig. 7). Numerous studies have examined the relationship between arsenic exposure and intake and increased lung cancer mortality (Nackerdien et al., 1991; Salnikow et al., 2000; Kawanishi et al., 2001; Chen et al., 2003; IARC, 2012). There is still much debate on the genotoxic properties of vanadium. Previous studies have found associations between airborne vanadium particles in the air and lung cancer (Leonard and Gerber, 1994; Rodríguez-Mercado et al., 2011). Another aspect highlighted by Gualtieri et al. (2019) is that the contents of V released from asbestos fibres are very low and should not represent a major health concern. The differences in the PTEs (Be, V, As, Pb, Sb, Ba, Pb and Sr) concentration patterns of chrysotile, tremolite asbestos and actinolite asbestos were mainly attributed to the geochemical variable involved in their genesis (e.g., pressure, temperature, availability of elements) in different locations. However, Be, V, As, Pb, Sb, and Ba showed similar concentration patterns for both tremolite asbestos and actinolite asbestos, except for Pb and Sr. As regards chrysotile, in addition to the geochemical variability involved in its genesis, the different concentrations from amphiboles is also due to crystallographic differences between them (Ballirano et al., 2017). Indeed, chrysotile showed lower Sb, Ba, Pb and Sr concentrations (Fig. 7) than amphiboles, due to the fact that elements with large ionic radii (> 1 Å, e.g., Sb, Ba, Pb and Sr) cannot replace Si or Mg in tetrahedral or octahedral sites, since in chrysotile elements with large ionic radii (> 1 Å) were hosted in the hollow core within its fibrils, which act as trapping locations for elements with large ionic radii (Ballirano et al., 2017). Contrastingly, elements such as Be, V and As (ionic radius < 1 Å) can be hosted into the crystallographic sites of both amphiboles and chrysotile, and therefore variations of these elements are due to their geochemical availability rather than crystallographic reasons.

4.2. The role of iron

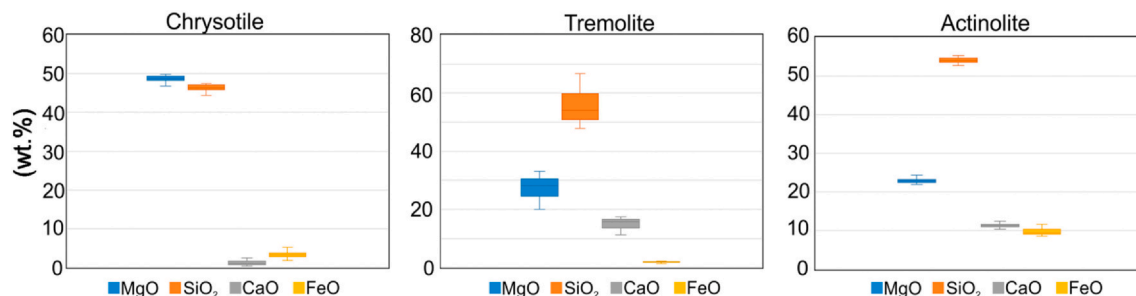In addition to the metals mentioned above, several researchers have

Table 1

Average values of major and minor element concentrations (wt%) in the investigated asbestos elongate mineral particles from GMRU obtained by μ-XRF. Ctl = chrysotile, Tr = tremolite asbestos, Act = actinolite asbestos. Standard deviations in brackets.

(wt%)	Ctl	Tr	Act
MgO	48.78 (0.72)	27.12 (3.90)	22.96 (0.56)
SiO$_2$	46.41 (0.82)	55.79 (5.81)	54.06 (0.70)
CaO	1.37 (0.96)	14.99 (1.86)	11.29 (0.64)
FeO	3.22 (0.82)	1.80 (0.20)	9.07 (0.76)
Al$_2$O$_3$	0.02 (0.01)	0.34 (0.16)	0.38 (0.12)
MnO	0.17 (0.05)	0.20 (0.05)	0.75 (0.11)

suggested that, even in trace amounts, iron plays an important role in asbestos-induced cytotoxicity (Shukla et al., 2003).

There is experimental evidence that demonstrates that iron on the surface of elongate mineral particles (Pollastri et al., 2015; Andreozzi et al., 2017) as well as iron content and its structural coordination are essential factors which trigger the formation of toxic hydroxyl radicals inducing cyto- and genotoxic effects (Bonneau et al., 1986; Fantauzzi et al., 2010; Pacella et al., 2020). In fact, all natural asbestos elongate mineral particles contain iron either as a substitution for Mg (e.g. chrysotile, tremolite) ions or as a constituent of the mineral structure (crocidolite, amosite; Turci et al., 2017). It has also been demonstrated, that surface ferrous ions constitute the catalytic sites where ROS and free radicals are produced (Pezerat et al., 1989; Fubini and Otero Areán, 1999; Favero-Longo et al., 2005; Gazzano et al., 2005). It is important to note that free radical generation may be induced by reactions in the presence of H$_2$O$_2$ (Fenton reaction) and in the absence of H$_2$O$_2$ (Haber-Weiss Cycle). After chrysotile has been inhaled, it dissolves and releases Fe as well as other metals (i.e. Ni, Cr, Mn; Turci et al., 2010), inducing toxic effects such as ROS production, oxidative stress, DNA damage, lipid peroxidation and protein modification (Jomova and Valko, 2011). When amphibole asbestos is inhaled, it suffers a limited surface dissolution creating a persistent physical response and biochemical action (in terms of surface activity of iron prompting ROS production; Bernstein et al., 2013; Turci et al., 2017). Consequently, it is possible to
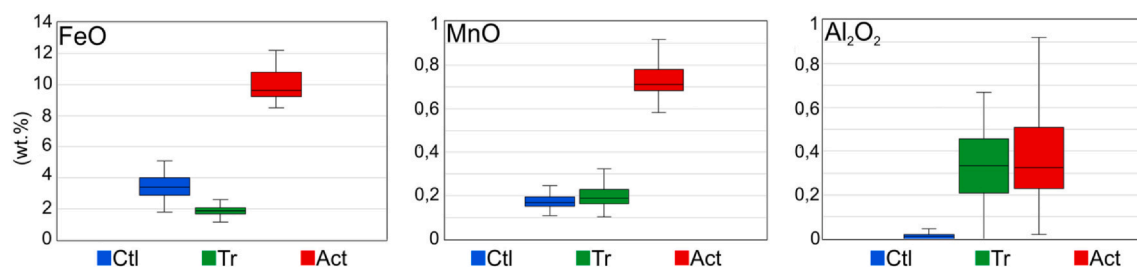

Fig. 4. Box plots showing statistical parameters for contents (wt%) of MgO, SiO$_2$, CaO, FeO, in chrysotile, tremolite and actinolite asbestos from GMRU. Statistical parameters are based on 60 analyses. Vertical lines show the range in contents, the horizontal line inside the box represents the median value.

Fig. 5. Box plots showing statistical parameters for contents (wt%) of FeO, MnO and Al_2O_3, in chrysotile, tremolite and actinolite asbestos from GMRU. Statistical parameters are based on 60 analyses. Vertical lines show the range in contents, the horizontal line inside the box represents the median value.

Table 2

Trace element concentrations (ppm) in the investigated asbestos elongate mineral particles from GMRU obtained by ICP-MS. Ctl = chrysotile; Tr = tremolite asbestos; Act = actinolite asbestos. *Indicative baseline data for some trace elements in normal human lung tissues (Vanoeteren et al., 1986). D.L. = detection limit; **Minor element.

(ppm)	Concentration range in human lungs*	Ctl	Tr	Act	D.L.
Fe**	40–500	25,000	14,000	75,100	0.01
Mn**	0.01–3	1186.8	678.2	3874.2	0.01
Cr	0.002–0.50	5.50	170.91	14.860	0.20
Co	0.002–0.1	1.89	22.64	4.69	0.05
Ni	0.01–1.00	4.32	308.63	14.50	0.09
Cu	1–5.00	10.52	24.53	19.39	0.06
Zn	1–30.00	65.47	28.42	46.56	1.90
Pb	0.02–0.50	2.40	4.44	23.29	0.04
V	0.0005–0.50	6.88	7.07	11.06	0.10
Be	0.0001–0.03	2.90	0.30	1.10	0.01
As	0.001–0.10	7.00	1.20	1.50	0.40
Rb	0.5–10.00	0.70	0.40	0.70	0.30
Sb	0.002–0.10	0.20	0.20	0.60	0.01
Ba	> 1.10	11.40	14.8	14.1	0.07
Sr	0.01–1.00	10.70	200.0	47.0	0.03

deduce that the fast dissolution rate of chrysotile should prompt increased release of available surface-active Fe in the first stage of dissolution despite the small differences in the Fe concentrations in chrysotile (ideally 0–4 wt%), tremolite asbestos (ideally 0–4 wt%) and actinolite asbestos (ideally 7–10%; Gualtieri, 2018; Gualtieri et al., 2018). Our results showed that the highest concentration of Fe was in the actinolite asbestos (9.07 wt%), followed by chrysotile (3.20 wt%) and tremolite asbestos (1.80 wt%) (Table 1). As shown in Fig. 8 and Table 3, considering the contribution of Fe (Σ Cr, Co, Ni, Cu, Zn, Mn, Fe), the sample containing the largest amount of heavy metals proved to be actinolite asbestos (79,074 ppm) followed by chrysotile (26,275 ppm) and tremolite asbestos (15,233 ppm).

4.3. Bio-durability

An important factor that influences the degree of fibre toxicity is asbestos bio-durability. In fact, the elevated levels of PTEs in the human body caused by inhaling elongate mineral particles is strictly dependent on various factors, including the solubility of elongate mineral particles. The solubility is defined as the maximum amount of the fibre that dissolves in body fluids (Turci et al., 2017). It determines the bio-durability, that is the residence time of the elongate mineral particles in the organism, and therefore it is probable that adverse interactions occur between the mineral fibre and its biological surroundings (Turci et al., 2017). The chemical properties of asbestos change in the chemical properties below pH 8.0 (i.e., Bernstein et al., 2013) and PTEs associated with asbestos elongate mineral particles can be released into the lungs. As demonstrated by many authors (Hesterberg et al., 1998; Bernstein et al., 2013; Rozalen et al., 2014; Gualtieri et al., 2018; Gualtieri, 2018), the solubility of chrysotile is higher than that for amphibole asbestos. For example, in a recent study Gualtieri et al.

(2018) carried out an in-vitro comparative study of chrysotile asbestos (UICC, standard Chrysotile "B", Canadian NB #4173-111-1) and amphibole asbestos (i.e., crocidolite and amosite) at pH 4, in order to determine their dissolution rates. Chrysotile undergoes fast dissolution (few months) and releases its PTEs cargo into the lung environment in a short period of time, while amphibole slowly releases its toxic cargo over a long time span (tens of years). Therefore, in our case, it is highly probable that PTEs contained in chrysotile elongate mineral particles are rapidly released into the extracellular medium (Bloise et al., 2016a). In this scenario, under the hypothesis that the other parameters are equal (e.g., fibre dimensions, biopersistence, surface reactivity), our samples with various concentrations of PTEs in their structure, should show different in-vitro toxicity levels. Observing the concentrations of Σ Cr, Co, Ni, Cu, Zn, Mn, Fe, Be, V, As, Rb, Sb, Ba, Pb and Sr which were considered representative of the family of all of the toxic elements present in these natural elongate mineral particles, actinolite asbestos (79,173 ppm) proved to be the sample with the highest concentration of PTEs, followed by chrysotile (26,317 ppm) and tremolite asbestos (15,461 ppm) (Fig. 8; Table 3). Moreover, it should also be considered that chrysotile showed higher values of Be and As compared to other samples, and it is less bio-durable than amphibole asbestos. These potentially toxic elements present in asbestos elongate mineral particles could play an important role in the pathogenesis of human lung cancer (Dixon et al., 1970; Nemery, 1990; Wei et al., 2014). If these trace elements accumulate in sufficient amounts in the lungs, via fibre dissolution, they may cause lung cancer (e.g., mesothelioma and bronchogenic carcinoma) (Dixon et al., 1970; Nemery, 1990; Wei et al., 2014), as it will alter the baseline levels of these elements in normal human lung tissue, that has not been damaged by disease (Table 2; Vanoeteren et al., 1986).

4.4. Toxic elements in the environment

A considerable number of PTEs could be partly contained in the structure of amphibole and chrysotile asbestos as isomorphic substitutions in certain crystallographic sites (Morgan and Cralley, 1973; Bloise et al., 2009, 2010; Ballirano et al., 2017) and partly as components of magnetite and chromite contamination in asbestos (Kumar and Maiti, 2015; Bloise et al., 2020).

The Calabria region is characterized by numerous areas of ophiolite outcrops (Punturo et al., 2004; Cirrincione et al., 2015; Ricchiuti et al., 2020) which are potential sources of asbestos elongate mineral particles and PTEs (e.g. Mn, Cr, Co and Ni) and are released into the environment due to naturally occurring processes (drainage, leaching) and also due to anthropic activities (mining, excavation, landscape modification), resulting in the contamination of soil, water and air (e.g., Bloise et al., 2016b; Cannata et al., 2018; Gwenzi, 2019; Ricchiuti et al., 2020).

The relatively high concentrations of PTEs found in the studied asbestos samples (Fig. 8; Table 3) makes them potentially available for subsequent accumulations in water and soil that can adversely affect human health. These toxic elements could be leaching off ophiolitic host rocks and their respective sediments causing a significant increase in PTEs concentrations in soils and groundwaters. A strong correlation
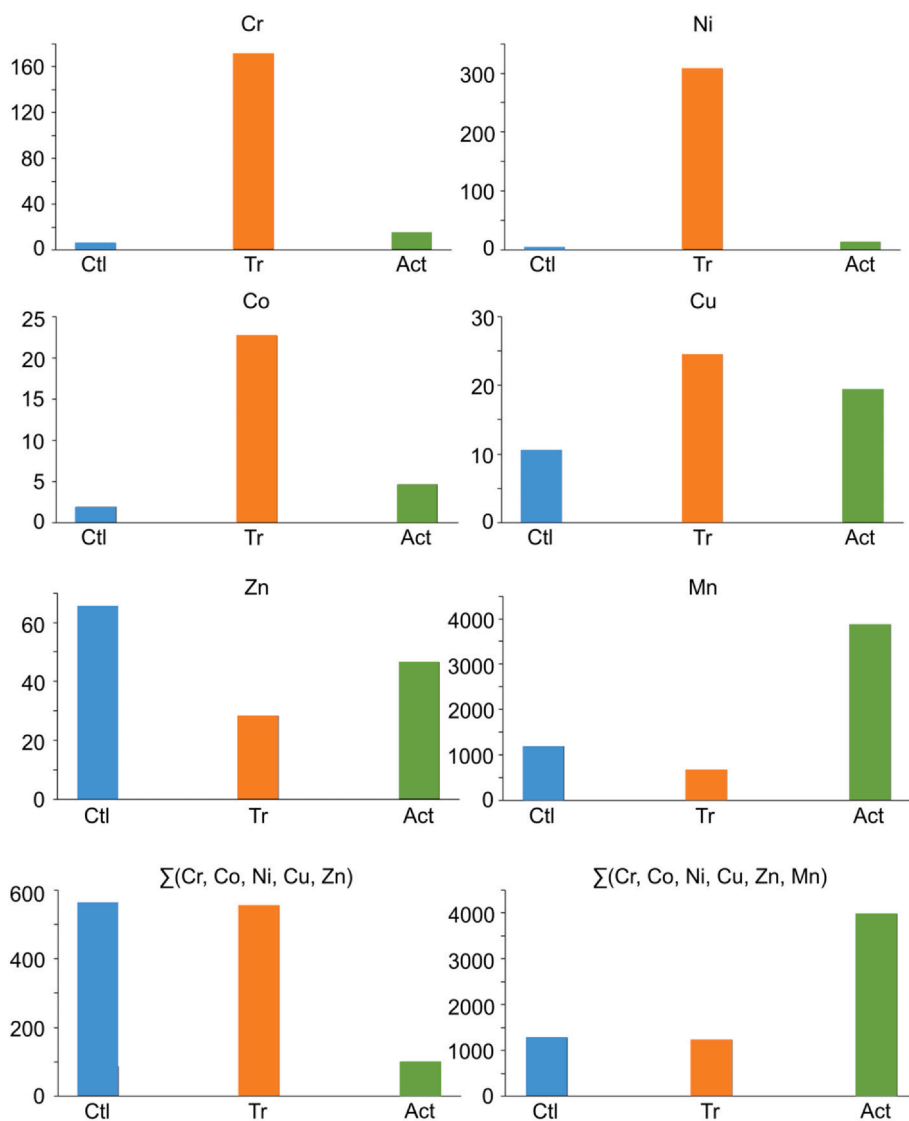
Fig. 6. Concentration of heavy metals (ppm) in the investigated asbestos elongate mineral particles from GMRU. Ctl = chrysotile; Tr = tremolite asbestos; Act = actinolite asbestos. Each element has an error, measured as relative standard deviation (RSD%), of around 1%.
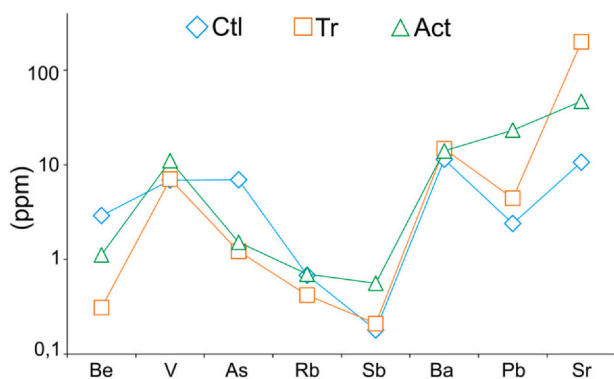

Fig. 7. Trace elements concentration (ppm) patterns in the investigated asbestos elongate mineral particles from GMRU. Ctl = chrysotile; Tr = tremolite asbestos; Act = ac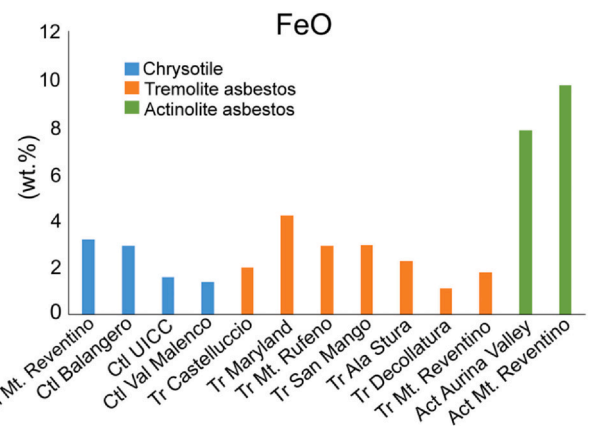tinolite asbestos. Logarithmic scale is used for the Y axis. Each element has an error, measured as relative standard deviation (RSD%), of around 1%.

has been found between high levels of PTEs in the air, water and soil and human disease (e.g., Gwenzi, 2019) as they can trigger deadly pathologies.

4.5. Cross-country comparison of asbestos samples

Even if different analytical techniques were used, we compared our data to those obtained by other authors for the same mineral species in order to gain a better understanding of how toxic elements may contribute to the overall toxicity of the elongate mineral particles. The data regarding the iron content of actinolite asbestos from GMRU are in line with the data previously reported in literature (Table 4; Pollastri et al., 2017; Bloise, 2019). As expected, actinolite asbestos is the mineral with the highest iron content of all of the minerals analysed (Fig. 9).

The FeO found in the chrysotile samples from GMRU is slightly higher than the amounts found in chrysotile from Canada, Balangero (Italy) and Val Malenco (Italy), (Table 4) studied by Pollastri et al. (2016). As regards tremolite asbestos, the FeO content of the sample analysed in this study was 1.8 wt% (Fig. 9) which is lower than the values obtained for the tremolite asbestos from Castelluccio (Italy), Maryland (USA), Mount Rufeno (Italy), San Mango (Italy) and Ala Stura (Italy) studied by Pacella et al. (2010) and in line with the data

Table 3

Sum (Σ) elements concentration (ppm) of Ctl = chrysotile; Tr = tremolite asbestos; Act = actinolite asbestos, from GMRU.

(ppm)	Σ(Cr, Co, Ni, Cu, Zn)	Σ(Cr, Co, Ni, Cu, Zn, Mn)	Σ(Cr, Co, Ni, Cu, Zn, Mn, Fe)	Σ(Be, V, As, Rb, Sb, Ba, Pb, Sr)	Σ(Cr, Co, Ni, Cu, Zn, Mn, Fe, Be, V, As, Rb, Sb, Ba, Pb, Sr)
Ctl	88	1275	26,275	42	26,317
Tr	555	1233	15,233	228	15,461
Act	100	3974	79,074	99	79,173

Fig. 8. Sum of PTEs concentrations (ppm) in the investigated asbestos elongate mineral particles samples Ctl = chrysotile; Tr = tremolite asbestos; Act = actinolite asbestos from GMRU. Logarithmic scale is used for the Y axis.

Fig. 9. FeO (wt%) in the analysed asbestos samples from GMRU (Mt. Reventino). Ctl = chrysotile; Tr = tremolite asbestos; Act = actinolite asbestos. Reference data of chrysotile from Balangero, UICC Canadian chrysotile, chrysotile from Val Malenco, tremolite asbestos from Castelluccio, from Maryland, from San Mango, from Ala Stura, from Decollatura, actinolite asbestos from Aurina Valley are shown for comparison.

obtained for tremolite asbestos from Decollatura (Italy) (Table 4). Finally, similar amounts of FeO were found in the actinolite asbestos analysed in this study (9.07 wt%) and the actinolite asbestos samples studied by Pollastri et al. (2017) collected from the Aurina Valley which was 7.77 wt% (Fig. 9; Table 4).

As regard, Cr, Co, Ni, Cu, Zn and Mn, different results were obtained when we compared the values of the analysed samples, with those reported in literature (Morgan and Cralley, 1973; Bloise et al., 2016a), which depended on the outcrop where the chrysotile specimens were collected (Table 5). In fact, as shown in Fig. 10a, chrysotile from GMRU is characterized by Σ Cr, Co, Ni, Cu, Zn, Mn at 1274 ppm, which is lower than in UICC Canadian chrysotile (1750 ppm), Balangero (2574 ppm) and Val Malenco (2725 ppm) studied by Bloise et al., 2016a using the ICP-MS technique (Table 5).

As regards tremolite asbestos, the sample analysed showed the highest PTEs. By comparing our data set with the data obtained for tremolite asbestos from Val D'Ala studied by Bloise et al. (2016a), tremolite asbestos from GMRU contained a total amount of toxic metals (Cr, Co, Ni, Cu, Zn) equal to 555 ppm while it reached 685 ppm in tremolite asbestos from Val D'Ala.

Based on the results of the present study and those reported in literature (Table 5), actinolite from GMRU proved to be the asbestos sample with the highest concentration of PTEs while the similar values observed for the chrysotile samples collected from the GMRU and Canada outcrops (Bloise et al., 2016a) and tremolite asbestos from GMRU and the ophilitic outcrops of Ala Stura demonstrated that they could be less toxic samples as they contain the lowest concentrations of PTEs. Nevertheless, it is important to note that due to their different matrix structures, chrysotile is not as biodurable as amphiboles (i.e. tremolite

Table 4

FeO (wt%) in the asbestos samples from GMRU (Gimigliano Mount Reventino Unit). Reference data of chrysotile from Balangero, from UICC Canadian chrysotile, from Val Malenco, tremolite asbestos from Castelluccio, from Maryland, from San Mango, from Ala Stura, from Decollatura, actinolite asbestos from Aurina Valley, are shown for comparison; (estimated standard deviations are shown in brackets). n.d. = not detected; μ-XRF = micro X-ray fluorescence; EMPA = electron microprobe analysis; MS = Mössbauer spectroscopy.

Sample	FeO	Detected by	References
Chrysotile GMRU(Calabria, Italy)	3.22 (0.82)	μ-XRF	This work
Chrysotile Balangero (Piedmont, Italy)	2.9 (5)	EMPA	Pollastri et al., 2016
Chrysotile UICC (Quebec, Canada)	1.6 (3)	EMPA	Pollastri et al., 2016
Chrysotile Val Malenco (Lombardy, Italy)	1.4 (1)	EMPA	Pollastri et al., 2016
Tremolite asbestos Castelluccio (Basilicata, Italy)	2.06 (16)	EMPA	Pacella et al., 2010
Tremolite asbestos Maryland (Maryland, USA)	4.50 (77)	EMPA	Pacella et al., 2010
Tremolite asbestos Mount Rufeno (Latium, Italy)	2.23 (8)	EMPA	Pacella et al., 2010
Tremolite asbestos San Mango (Calabria, Italy)	2.97 (9)	EMPA	Pacella et al., 2010
Tremolite asbestos Ala Stura (Piedmont, Italy)	2.42(25)	EMPA	Pacella et al., 2010
Tremolite asbestos Decollatura (Calabria, Italy)	1.10 (n.d.)	EDS/SEM	Apollaro et al., 2018
Tremolite asbestos GMRU(Calabria, Italy)	1.80 (0.20)	μ-XRF	This work
Actinolite asbestos Aurina Valley (Trentino, Italy)	7.77 (5)	MS	Pollastri et al., 2017
Actinolite asbestos GMRU (Calabria, Italy)	9.07 (0.76)	μ-XRF	This work

Table 5

Trace element concentrations (ppm) in the asbestos samples from GMRU obtained using ICP-MS. Reference data of chrysotile from Balangero, UICC Canadian chrysotile, chrysotile from Val Malenco, tremolite asbestos from Ala Stura are shown for comparison, as this sample was previously studied by Bloise et al., 2016a, all obtained using ICP-MS.

(ppm)	Cr	Co	Ni	Cu	Zn	Mn	Σ(Cr, Co, Ni, Cu, Zn)	Σ(Cr, Co, Ni, Cu, Zn, Mn)
Chrysotile GMRU (Calabria, Italy)	5.50	1.89	4.32	10.52	65.47	1186.80	88	1274
Chrysotile Balangero (Piedmont, Italy)	1078.20	40.40	445.80	14.50	33.10	962.00	1612	2574
Chrysotile UICC (Quebec, Canada)	360.50	45.30	866.10	1.70	17.40	459.00	1291	1750
Chrysotile Val Malenco (Lombardy, Italy)	153.60	52.40	1576.20	29.70	22.70	890.00	1835	2725
Tremolite asbestos GMRU (Calabria, Italy)	170.91	22.64	308.63	24.53	28.42	678.20	555	1233
Tremolite asbestos Ala Stura (Piedmont, Italy)	165.00	26.90	473.00	3.20	17.20	879.90	685	1565
Actinolite asbestos GMRU (Calabria, Italy)	14.86	4.69	14.50	19.39	46.56	3874.20	100	3974

and actinolite asbestos) in simulated lung fluids (Bernstein et al., 2013, Gualtieri et al., 2018; see Bio-durability section). The fast chrysotile dissolution rate triggers the full release of available PTEs in the host organism in a few months. However, thanks to this comparison, it was observed that Pb, V, As, Sb, Be were not always present in large amounts in our samples (Fig. 10b). In fact, chrysotile from GMRU revealed a total amount of Pb, V, As, Sb and Be of 19.40 ppm which is higher than the amounts reported for chrysotile collected from Val Malenco (5.70 ppm) and lower than those reported for chrysotile from Balangero (56.10 ppm) and UICC Canadian chrysotile (20.40 ppm). As regards the tremolite asbestos from GMRU and Val D'Ala, the samples contained similar concentrations equal to 13.20 ppm and 13.80 ppm respectively.

These differences in PTEs concentrations may be due to the common chemical variability exhibited by amphibole elongate mineral particles (e.g., Hawthorne and Oberti, 2007; Andreozzi et al., 2009) and to the various geochemical/petrological processes involved in the formation of chrysotile and amphiboles (Bloise et al., 2020). It is important to note that small variations in the amounts of PTEs may also be due to the different degrees of accuracy of the instruments used in the various laboratories.

5. Conclusions

The aim of this study was to determine the presence and quantity of PTEs that may play a role in asbestos toxicity as demonstrated in literature. To this aim, the chemical data obtained by analysing three natural asbestos samples (chrysotile, tremolite asbestos, actinolite asbestos) from Gimigliano-Mount Reventino Unit (Calabria Region, southern Italy) were analysed. The results show that, taking into account the contribution of heavy metals (i.e. Cr, Co, Ni, Cu, Zn) and their toxicity levels, it is possible to speculate that tremolite asbestos is the most toxic form of asbestos among the investigated minerals, followed by actinolite asbestos and chrysotile. The same trend has been observed with other trace elements such as Be, V, As, Rb, Sb, Ba, Pb and Sr. However, considering the contribution of other metals such as Mn and Fe to the overall balance (i.e. Mn, Fe, Cr, Co, Ni, Cu, Zn, Be, V, As, Rb, Sb, Ba, Pb, Sr), actinolite asbestos proved to have the most toxic elongate mineral particles of all the investigated minerals, while chrysotile should be more toxic than tremolite asbestos in this case. Moreover, it should also be considered that chrysotile showed higher values of Be and As and it is less biodurable than amphibole asbestos and therefore releases its PTEs cargo into the lung environment in a short period of time.

In view of the mesothelioma deaths caused by asbestos exposure in the Calabria region, this study supports the hypothesis that the PTEs hosted in asbestos elongate mineral particles could be one of the factors which determines their toxic/pathogenic effects.

The data obtained from this study may prove useful for determining the toxicity/pathogenicity potential of asbestos and for interpreting the results of in-vitro testing. As regards environmental pollution, it is essential to quantify the PTEs present in asbestos minerals in order to limit exposure and minimize the public health risks for people living in these geological contexts, since exposure to asbestos minerals and toxic
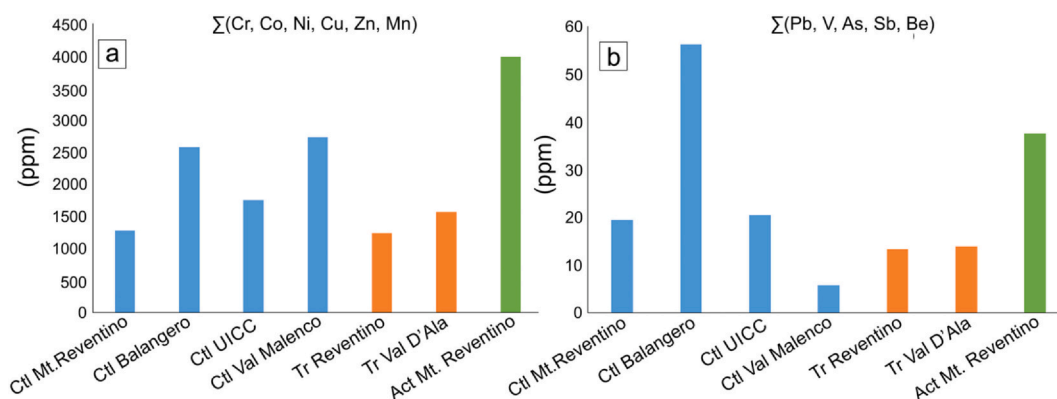

Fig. 10. a) Sum of PTEs (Cr, Co, Ni, Cu, Zn, Mn) concentrations (ppm) in the investigated asbestos samples from GMRU (Mt. Reventino), Ctl = chrysotile; Tr = tremolite asbestos; Act = actinolite asbestos. b) Sum of PTEs (Pb, V, As, Sb, Be) concentrations (ppm) in the investigated asbestos samples from GMRU. Reference data of a chrysotile from Balangero, from Canada UICC (standard Chrysotile "B", NB #4173-111-1), from Val Malenco, asbestos tremolite from Ala di Stura are shown for comparison, as this sample was previously studied by Bloise et al., 2016a.

elements can cause lung cancer in humans. In conclusion, the concomitant presence of asbestos minerals and PTEs in the environment poses a serious health threat to local populations. Due to the abundance of ophiolite outcrops worldwide, the results obtained from this study will be of global interest.

Declaration of competing interest

The authors declare that they have no known competing financial interests or personal relationships that could have appeared to influence the work reported in this paper.

Acknowledgments

References

Alleman, J.E., Mossman, B.T., 1997. Asbestos revisited. Sci. Am. 277, 70–75.

Andreozzi, G.B., Balliran, P., Gianfagna, A., Mazziotti-Tagliani, S., Pacella, A., 2009. Structural and spectroscopic characterization of a suite of fibrous amphiboles with high environmental and health relevance from Biancavilla (Sicily, Italy). Am. Mineral. 94, 1333–1340.

Andreozzi, G.B., Pacella, A., Corazzari, I., Tomatis, M., Turci, F., 2017. Surface reactivity of amphibole asbestos: a comparison between crocidolite and tremolite. Sci. Rep. 7 (1), 1–9.

Apollaro, C., Marini, L., Critelli, T., Barca, D., Bloise, A., De Rosa, R., Liberi, F., Miriello, D., 2011. Investigation of rock-to-water release and fate of major, minor, and trace elements in the metabasalt–serpentinite shallow aquifer of Mt. Reventino (CZ, Italy) by reaction path modelling. Appl. Geochem. 26 (9–10), 1722–1740.

Apollaro, C., Fuoco, I., Vespasiano, G., De Rosa, R., Cofone, F., Miriello, D., Bloise, A., 2018. Geochemical and mineralogical characterization of tremolite asbestos contained in the Gimigliano-Monte Reventino Unit (Calabria, south Italy). J. Mediterr. Earth Sci 10, 5–15.

Atzori, P., Mazzoleni, P., Punturo, R., Scribano, V., 1999. Garnet-spinel-pyroxenite xenoliths from Hyblean Plateau (South-eastern Sicily, Italy). Mineral. Petrol. 66 (4), 215–226.

Balliran, P., Bloise, A., Gualtieri, A.F., Lezzerini, M., Pacella, A., Perchiazzi, N., Dogan, M., Dogan, A.U., 2017. The crystal structure of mineral fibres. In: Gualtieri, A.F. (Ed.), Mineral Fibres: Crystal Chemistry, Chemical-Physical Properties, Biological Interaction and Toxicity. European Mineralogical Union, London, pp. 17–53.

Baumann, F., Ambrosi, J.-P., Carbone, M., 2013. Asbestos is not just asbestos: an unrecognised health hazard. Lancet Oncol 14, 576–578.

Baumann, F., Buck, B.J., Metcalf, R.V., McLaurin, B.T., Merkler, D.J., Carbone, M., 2015. The presence of asbestos in the natural environment is likely related to mesothelioma in young individuals and women from Southern Nevada. J. Thorac. Oncol. 10 (5), 731–737.

Baumeister, J.L., Hausrath, E.M., Olsen, A.A., Tschauner, O., Adcock, C.T., Metcalf, R.V., 2015. Biogeochemical weathering of serpentinites: an examination of incipient dissolution affecting serpentine soil formation. Appl. Geochem. 54, 74–84.

Bernstein, D., Dunnigan, J., Hesterberg, T., Brown, R., Velasco, J.A.L., Barrera, R., Hoskins, J., Gibbs, A., 2013. Health risk of chrysotile revisited. Crit. Rev. Toxicol. 43 (2), 154–183.

Bloise, A., 2019. Thermal behaviour of actinolite asbestos. J. Mater. Sci. 54, 11784–11795.

Bloise, A., Miriello, D., 2018. Multi-analytical approach for identifying asbestos minerals in situ. Geosciences 8 (4), 133.

Bloise, Andrea, Belluso, E., Barrese, E., Miriello, D., Apollaro, C., 2009. Synthesis of Fe-doped chrysotile and characterization of the resulting chrysotile fibers. Cryst. Res. Technol. 44 (6), 590–596.

Bloise, A., Belluso, E., Fornero, E., Rinaudo, C., Barrese, E., Capella, S., 2010. Influence of synthesis conditions on growth of Ni-doped chrysotile. Microporous Mesoporous Mater. 132 (1–2), 239–245.

Bloise, A., Belluso, E., Critelli, T., Catalano, M., Apollaro, C., Miriello, D., Barrese, E., 2012. Amphibole asbestos and other fibrous minerals in the meta-basalt of the Gimigliano-Mount Reventino Unit (Calabria, south-Italy). Rend. Online Soc. Geol. It. 21, 847–848.

Bloise, A., Critelli, T., Catalano, M., Apollaro, C., Miriello, D., Croce, A., Belluso, E., 2014. Asbestos and other fibrous minerals contained in the serpentinites of the Gimigliano-Mount Reventino Unit (Calabria, S-Italy). Environ. Earth Sci 71 (8), 3773–3786.

Bloise, A., Barca, D., Gualtieri, A.F., Pollastri, S., Belluso, E., 2016a. Trace elements in

hazardous mineral fibres. Environ. Pollut. 216, 314–323.

Bloise, A., Punturo, R., Catalano, M., Miriello, D., Cirrincione, R., 2016b. Naturally occurring asbestos (NOA) in rock and soil and relation with human activities: the monitoring example of selected sites in Calabria (southern Italy). Ital. J. Geosci. 135 (2), 268–279.

Bloise, A., Catalano, M., Critelli, T., Apollaro, C., Miriello, D., 2017a. Naturally occurring asbestos: potential for human exposure, San Severino Lucano (Basilicata, Southern Italy). Environ. Earth Sci. 76, 648. https://doi.org/10.1007/s12665-0 17-6995-9.

Bloise, A., Kusiorowski, R., Lassinantti Gualtieri, M., Gualtieri, A.F., 2017b. Thermal behaviour of mineral fibres. In: Gualtieri, A.F. (Ed.), Mineral Fibres: Crystal Chemistry, Chemical–Physical Properties, Biological Interaction and Toxicity. European Mineralogical Union, London, pp. 215–252.

Bloise, A., Ricchiuti, C., Lanzafame, G., Punturo, R., 2020. X-ray synchrotron microtomography: a new technique for characterizing chrysotile asbestos. Sci. Total Environ. 703, 135675.

Bonneau, L., Malard, C., Pezerat, H., 1986. Studies on surface properties of asbestos. II. Role of dimensional characteristics and surface properties of mineral fibers in the induction of pleural tumors. Environ. Res 41, 268–275.

Boskabady, M., Marefati, N., Farkhondeh, T., Shakeri, F., Farshbaf, A., Boskabady, M.H., 2018. The effect of environmental lead exposure on human health and the contribution of inflammatory mechanisms, a review. Environ. Int. 120, 404–420.

Bowes, D.R., Farrow, C.M., 1997. Major and trace element compositions of the UICC standard asbestos samples. Am. J. Ind. Med. 32, 592–594.

Caicedo, M., Jacobs, J.J., Reddy, A., Hallab, N.J., 2007. Analysis of metal ion-induced DNA damage, apoptosis, and necrosis in human (Jurkat) T-cells demonstrates Ni^{2+} and V^{3+} are more toxic than other metals: Al^{3+}, Be^{2+}, Co^{2+}, Cr^{3+}, Cu^{2+}, Fe^{3+}, Mo^{5+}, Nb^{5+}, Zr^{2+}. J. Biomed. Mat. Res. Part A 905–913.

Caillaud, J., Proust, D., Philippe, S., Fontaine, C., Fialin, M., 2009. Trace metals distribution from a serpentinite weathering at the scales of the weathering profile and its related weathering microsystems and clay minerals. Geoderma 149, 199–208.

Campopiano, A., Cannizzaro, A., Olori, A., Angelosanto, F., Iannò, A., Bruno, M.R., Bruni, B.M., Casalinuovo, F., Ciambrone, L., Esposito, A., Iavicoli, S., 2017. Valutazione indiretta di fibre di amianto respirabili in aree del territorio calabrese con presenza di pietra verde: primi risultati. 80° Congresso Nazionale SiMLii, Padova 20-22/09/2017.

Cannata, C.B., Bloise, A., De Rosa, R., 2018. Outdoor fibres air pollution monitoring in the Crotone area (Southern Italy). J. Mediterr. Earth Sci 10, 27–36.

Cavallo, A., Rimoldi, B., 2013. Chrysotile asbestos in serpentinite quarries: a case study in Valmalenco, Central Alps, Northern Italy. Environ Sci Process Impacts 15, 1341–1350.

Censi, P., Spoto, S.E., Saiano, F., Sprovieri, M., Mazzola, S., Nardone, G., Di Geronimo, S.I., Punturo, R., Ottonello, D., 2006. Heavy metals in coastal water systems. A case study from the northwestern Gulf of Thailand. Chemosphere 64 (7), 1167–1176.

Censi, P., Tamburo, E., Speziale, S., Zuddas, P., Randazzo, L.A., Punturo, R., Cuttitta, A., Aricò, P., 2011a. Yttrium and lanthanides in human lung fluids, probing the exposure to atmospheric fallout. J. Hazard. Mater. 186 (2–3), 1103–1110.

Censi, P., Zuddas, P., Randazzo, L.A., Tamburo, E., Speziale, S., Cuttitta, A., Punturo, R., Aricò, P., Santagata, N., 2011b. Source and nature of inhaled atmospheric dust from trace element analyses of human bronchial fluids. Environ. Sci. Technol. 45 (15), 6262–6267.

CEPA (Canadian Environmental Protection Act), 1999. Prohibition of Asbestos and Products Containing Asbestos Regulations. SOR/2018–196.

Chen, L., Yang, X., Jiao, H., Zhao, B., 2003. Tea catechins protect against lead-induced ROS formation, mitochondrial dysfunction, and calcium dysregulation in PC12 cells. Chem. Res. Toxicol. 16, 1155–1161.

Cirrincione, R., Fazio, E., Fiannacca, P., Ortolano, G., Pezzino, A., Punturo, R., 2015. The Calabria-Peloritani Orogen, a composite terrane in Central Mediterranean; its overall architecture and geodynamic significance for a pre-Alpine scenario around the Tethyan basin. Period. di Mineral. 84 (3B), 701–749.

Colombino, E., Capella, S., Casalinuovo, F., Racco, R., Pruiti, F., Volante, M., Di Marco Lo Presti, V., Belluso, E., Capuccio, M.T., 2019. Malignant peritoneal mesothelioma in a boar who lived in Calabria (Italy): Wild animal as sentinel system of human health. SSci. Total Environ. 683, 267–274.

Cralley, L.J., Keenan, R.G., Kupel, R.E., Kinser, R.E., Lynch, J.R., 1968. Characterization and solubility of metals associated with asbestos fibers. Am. Ind. Hyg. Assoc. J. 29, 569–573.

Di Ciaula, A., 2017. Asbestos ingestion and gastrointestinal cancer: a possible underestimated hazard. Expert. Rev. Gastroenterol Hepatol. 11 (5), 419–425.

Dixon, J.R., Lowe, D.B., Richards, D.E., Cralley, L.J., Stokinger, H.E., 1970. The role of trace metals in chemical carcinogenesis: asbestos cancers. Cancer Res. 30, 1068–1074.

Fantauzzi, M., Pacella, A., Atzei, D., Gianfagna, A., Andreozzi, G.B., Rossi, A., 2010. Combined use of X-ray photoelectron and Mössbauer spectroscopic techniques in the analytical characterization of iron oxidation state in amphibole asbestos. Anal. Bioanal. Chem. 396, 2889.

Favero-Longo, S.E., Castelli, D., Salvadori, O., Belluso, E., Piervittori, R., 2005. Pedogenic action of the lichens Lecidea atrobrunnea. Rhizocarpon geographicum gr. And Sporastatia testudinea on serpentinized ultramafic rocks in an alpine environment. Int. Biodeterior. Biodegrad. 56, 17–27.

Frank, A.L., Joshi, T.K., 2014. The global spread of asbestos. Ann. Glob. Health 80 (4), 257–262.

Fubini, B., Otero Aréan, C., 1999. Chemical aspects of the toxicity of inhaled mineral dusts. Chem. Soc. Rev. 28, 373–382.

Gazzano, E., Riganti, C., Tomatis, M., Turci, F., Bosia, A., Fubini, B., Ghigo, D., 2005. Potential toxicity of nonregulated asbestiform minerals: balangeroite from the western Alps. Part 3: depletion of antioxidant defenses. J. Toxicol. Environ. Health 68, 41–49.

Gross, P., DeTreville, R.T., Tolker, E.B., Kaschak, M., Babyak, M.A., 1969. The pulmonary macrophage response to irritants: an attempt at quantitation. Arch. Environ. Occup. Health 18, 174–185.

Gualtieri, A.F., 2018. Towards a quantitative model to predict the toxicity/pathogenicity potential of mineral fibers. Toxicol. Appl. Pharmacol. 361, 89–98.

Gualtieri, A.F., Andreozzi, G.B., Tomatis, M., Turci, F., 2018. Iron from a geochemical viewpoint. Understanding toxicity/pathogenicity mechanisms in iron-bearing minerals with a special attention to mineral fibers. Free Radic. Biol. Med. 133, 21–37.

Gualtieri, A.F., Lusvardi, G., Zoboli, A., Di Giuseppe, D., Gualtieri, M.L., 2019. Biodurability and release of metals during the dissolution of chrysotile, crocidolite and fibrous erionite. Environ. Res. 171, 550–557.

Gunter, M.E., 2018. Elongate mineral particles in the natural environment. Toxicol. Appl. Pharmacol. 361, 57–164.

Gwenzi, W., 2019. Occurrence, behaviour, and human exposure pathways and health risks of toxic geogenic contaminants in serpentinitic ultramafic geological environments (SUGEs): a medical geology perspective. Sci. Total Environ. 700, 134622.

Harper, M., 2008. 10th anniversary critical review: naturally occurring asbestos. J. Environ. Monit. 10 (12), 1394–1408.

Hasegawa, S., Koshikawa, M., Takahashi, I., Hachiya, M., Furukawa, T., Akashi, M., Yoshida, S., Saga, T., 2008. Alterations in manganese, copper, and zinc contents, and intracellular status of the metal-containing superoxide dismutase in human mesothelioma cells. J. Trace Elem. Med. Biol. 22, 248–255.

Hawthorne, F.C., Oberti, R., 2007. Amphiboles: Crystal chemistry. In: Hawthorne, F.C., Oberti, R., Della Ventura, G., Mottana, A. (Eds.), Amphiboles: Crystal Chemistry, Occurrence, and Health Issues. Reviews in Mineralogy and Geochemistry, Mineralogical Society of America, Chantilly, pp. 1–54.

Hesterberg, T.W., Chase, G., Axten, C., Miller, W.C., Musselman, R.P., Kamstrup, O., Hadley, J., Morscheidt, C., Bernstein, D.M., Thevenaz, P., 1998. Biopersistence of synthetic vitreous fibers and amosite asbestos in the rat lung following inhalation. Toxicol. Appl. Pharmacol. 151 (2), 262–275.

Holmes, A., Morgan, A., Sandalls, F.J., 1971. Determination of iron, chromium, cobalt, nickel, and scandium in asbestos by neutron activation analysis. Am. Ind. Hyg. Assoc. J. 32 (5), 281–286.

Horie, M., Nishio, K., Fujita, K., Kato, H., Nakamura, A., Kinugasa, S., Endoh, S., Miyauchi, A., Yamamoto, K., Murayama, H., Niki, E., Iwahashi, H., Yoshida, Y., Nakanishi, J., 2009. Ultrafine NiO particles induce cytotoxicity *in vitro* by cellular uptake and subsequent Ni(II) release. Chem. Res. Toxicol. 22, 1415–1426.

Huang, S.X., Jaurand, M.C., Kamp, D.W., Whysner, J., Hei, T.K., 2011. Role of mutagenicity in asbestos fibre-induced carcinogenicity and other diseases. J. Toxicol. Environ. Health B Crit. Rev. 14, 179–245.

IARC, 1984. Polynuclear Aromatic Compounds. Part 3. Industrial Exposures in Aluminium Production, Coal Gasification, Coke Production, Iron and Steel Founding. International Agency for Research on Cancer, Lyon, France.

IARC, 2012. Working Group on the Evaluation of Carcinogenic Risk to Humans. IARC Monographs on the Evaluation of Carcinogenic Risks to Humans, no. 100C. International Agency for Research on Cancer, Lyon, France.

International Ban Asbestos Secretariat, 2016. http://ibasecretariat.org/lka_alpha_asb_ban_280704.php, 2016 > (accessed 19.12.16).

International Ban Asbestos Secretariat, 2019. http://www.ibasecretariat.org/alpha_ban_list.php.

Istituto Nazionale Assicurazione Infortuni sul Lavoro (INAIL), 2015. V rapporto Registro Nazionale Mesoteliomi (Re.NaM). https://www.inail.it/cs/internet/comunicazione/pubblicazioni/catalogo-generale/il-registro-nazionale-dei-mesoteliomi-v-rapporto, Accessed date: 3 April 2019.

Jablonski, R.P., Kim, S., Cheresh, P., Liu, G., Kamp, D.W., 2017. Insights into mineral fibre-induced lung epithelial cell toxicity and pulmonary fibrosis. In: Gualtieri, A.F. (Ed.), Mineral Fibres: Crystal Chemistry, Chemical–Physical Properties, Biological Interaction and Toxicity. European Mineralogical Union, London, pp. 447–500.

Jomova, K., Valko, M., 2011. Advances in metal-induced oxidative stress and human disease. Toxicology 283, 65–87.

Kashimura, K., Yamaguchi, T., Sato, M., Yoneda, S., Kishima, T., Horikoshi, S., Yoshikawa, N., Mitani, T., Shinohara, N., 2015. Rapid transformation of asbestos into harmless waste by a microwave rotary furnace: application of microwave heating to rubble processing of the 2011 Tohoku earthquake. J. Hazard Toxic. Radioact. Waste 19 (3), 04014041–04014048.

Kawanishi, S., Hiraku, Y., Oikawa, S., 2001. Mechanism of guanine-specific DNA damage by oxidative stress and its role in carcinogenesis and aging. Mutat. Res. Rev. Mutat. Res. 488, 65–76.

Kelepertzis, E., Galanos, E., Mitsis, I., 2013. Origin, mineral speciation and geochemical baseline mapping of Ni and Cr in agricultural topsoils of Thiva valley (central Greece). J. Geochem. Explor. 125, 56–68.

Kumar, A., Maiti, S.K., 2015. Assessment of potentially toxic heavy metal contamination in agricultural fields, sediment, and water from an abandoned chromite-asbestos mine waste of Roro hill, Chaibasa, India. Environ. Earth Sci. 74 (3), 2617–2633.

Lavkulich, L.M., Schreier, H.E., Wilson, J.E., 2014. Effects of natural acids on surface properties of asbestos minerals and kaolinite. J. Environ. Sci. Heal. A 49 (6), 617–624.

Léonard, A., Gerber, G.B., 1994. Mutagenicity, carcinogenicity and teratogenicity of vanadium compounds. Mut. Res./Reviews in Genetic Toxicology 317 (1), 81–88.

Leyssens, L., Vinck, B., Van Der Straeten, C., Wuyts, F., Maes, L., 2017. Cobalt toxicity in humans—a review of the potential sources and systemic health effects. Toxicology 387, 43–56.

Liu, C., Cheresh, P., Kamp, D.W., 2013. Molecular basis of asbestos-induced lung disease. Annu. Rev. Pathol. 8, 161–187.

Lyon, G.L., Brooks, R.R., Peterson, P.J., Butler, G.W., 1968. Trace elements in a New Zealand serpentine flora. Plant. Soil 29, 225–240.

Lyon, G.L., Brooks, R.R., Peterson, P.J., 1970. Some trace elements in plants from serpentine soils. New Zeal. J. Sci 13, 133–139.

Mancuso, T.F., 1970. Relation of duration of employment and prior respiratory illness to respiratory cancer among beryllium workers. Environ. Res. 3, 251–275.

Mistikawy, J.A., Mackowiak, T.J., Butler, M.J., Mischenko, I.C., Cernak, R.S., Richardson, J.B., 2020. Chromium, manganese, nickel, and cobalt mobility and bioavailability from mafic-to-ultramafic mine spoil weathering in western Massachusetts. USA. Environ. Geochem. Health 1–17. https://doi.org/10.1007/s10653-020-00566-7.

Morgan, A., Cralley, L., 1973. Chemical characteristics of asbestos and associated trace elements. In: Bogovski, P., Gilson, J.C., Timbrell, V., Wagner, J.C. (Eds.), Biological Effects of Asbestos. IARC Sci. Publ, Lyon, France, pp. 113–131.

Mossman, B.T., Lippmann, M., Hesterberg, T.W., Kelsey, K.T., Barchowsky, A., Bonner, J.C., 2011. Pulmonary endpoints (lung carcinomas and asbestosis) following inhalation exposure to asbestos. J. Toxicol. Environ. Health B Crit. Rev. 14, 76–121.

Nackerdien, Z., Kasprzak, K.S., Rao, G., Halliwell, B., Dizdaroglu, M., 1991. Nickel (II)- and cobalt (II)-dependent damage by hydrogen peroxide to the DNA bases in isolated human chromatin. Cancer Res. 51, 5837–5842.

National Institute for Occupational Safety and Health (NIOSH), 2011. Asbestos fibers and other elongate mineral particles: State of the science and roadmap for research. Revised Edition. Department of Health and Human Services. DHHS (NIOSH) Publication No. 2011,159. Current Intelligence Bulletin 62, 1–159.

Nemery, B., 1990. Metal toxicity and the respiratory tract. Eur. Respir. J. 3, 202–219.

Oberdörster, G., Graham, U., 2018. Predicting EMP hazard: Lessons from studies with inhaled fibrous and non-fibrous nano- and micro-particles. Toxicol. App. Pharm. 361, 50–61.

Oller, A.R., Costa, M., Oberdörster, G., 1997. Carcinogenicity assessment of selected nickel compounds. Toxicol. Appl. Pharmacol. 143, 152–166.

Oze, C., Fendorf, S., Bird, D.K., Coleman, R.G., 2004. Chromium geochemistry in serpentinized ultramafic rocks and serpentine soils from the Franciscan complex of California. Am. J. Sci. 304, 67–101.

Pacella, A., Andreozzi, G.B., Fournier, J., 2010. Detailed crystal chemistry and iron topochemistry of asbestos occurring in its natural setting. A first step to understand its chemical reactivity. Chem. Geol. 277, 197–206.

Pacella, A., Tomatis, M., Viti, C., Bloise, A., Arrizza, L., Ballirano, P., Turci, F., 2020. Thermal inertization of amphibole asbestos modulates Fe topochemistry and surface reactivity. J. Hazard. Mater. 123119.

Paglietti, F., Malinconico, S., Molfetta, V.D., Bellagamba, S., Damiani, F., Gennari, F., De Simone, P., Sallusti, F., Giangrasso, M., 2012. Asbestos risk: from raw material to waste management: the Italian experience. Crit. Rev. Environ. Sci. Technol. 42 (17), 1781–1861.

Park, E.K., Takahashi, K., Jiang, Y., Movahed, M., Kameda, T., 2012. Elimination of asbestos use and asbestos-related diseases: a n unfinished story. Cancer Sci. 103 (10), 1751–1755.

Pascal, L.E., Tessier, D.M., 2004. Cytotoxicity of chromium and manganese to lung epithelial cells in vitro. Toxicol. Lett. 147 (2), 143–151.

Perkins, R.A., Hargesheimer, J., Fourie, W., 2007. Asbestos release from wholebuilding demolition of buildings with asbestos-containing material. J. Occup. Environ. Hyg. 4, 889–894.

Pezerat, H., Zalma, R., Guignard, J., Jaurand, M.-C., 1989. Production of oxygen radicals by the reduction of oxygen arising from the surface activity of mineral fibres. In: Bignon, J., Peto, J., Saracci, R. (Eds.), Non Occupational Exposure to Mineral Fibers. 90. IARC Scientific Publication, Lyon, pp. 100–110.

Pollastri, S., D'Acapito, F., Trapananti, A., Colantoni, I., Andreozzi, G.B., Gualtieri, A.F., 2015. The chemical environment of iron in mineral fibers. A combined X-ray absorption and Mössbauer spectroscopic study. J. Hazard. Mater. 298, 282–293.

Pollastri, S., Perchiazzi, N., Lezzerini, M., Plaisier, J.R., Cavallo, A., Dalconi, M.C., Bursi Gandolfi, N., Gualtieri, A.F., 2016. The crystal structure of mineral fibres: 1. Chrysotile. Period. di Mineral. 85 (3), 249–259.

Pollastri, S., Gigli, L., Ferretti, P., Andreozzi, G.B., Gandolfi, N.B., Pollok, K., Gualtieri, A.F., 2017. The crystal structure of mineral fibres. 3. Actinolite asbestos. Period. di. Mineral 86 (2), 89–98.

Pugnaloni, A., Giantomassi, F., Lucarini, G., Capella, S., Bloise, A., Di Primio, R., Belluso, E., 2013. Cytotoxicity induced by exposure to natural and synthetic tremolite asbestos: an in vitro pilot study. Acta Histochem. 115 (2), 100–112.

Punturo, R., Fiannacca, P., Lo Giudice, A., Pezzino, A., Cirrincione, R., Liberi, F., Piluso, E., 2004. Le cave storiche della "Pietra Verde" di Gimigliano e Monte Reventino (Calabria): studio petrografico e geochimico. Boll. Acc. Gioenia Sci. Nat. 37 (364), 35–59.

Punturo, R., Bloise, A., Critelli, T., Catalano, M., Fazio, E., Apollaro, C., 2015. Environmental implications related to natural asbestos occurrences in the ophiolites of the Gimigliano-Mount Reventino Unit (Calabria, Southern Italy). Int. J. Environ. Sci. 9 (2), 405–418.

Punturo, R., Ricchiuti, C., Mengel, K., Apollaro, C., De Rosa, R., Bloise, A., 2018. Serpentinite-derived soils in southern Italy: potential for hazardous exposure. J. Mediterr. Earth Sci 10, 51–61.

Rajapaksha, A.U., Vithanage, M., Oze, C., Bandara, W.M.A.T., Weerasooriya, R., 2012. Nickel and manganese release in serpentine soil from the Ussangoda Ultramafic complex, Sri Lanka. Geoderma 189–190, 1–9.

Ricchiuti, C., Bloise, A., Punturo, R., 2020. Occurrence of asbestos in soils: State of the Art. Episodes 43 (3), 881–891.

Rodríguez-Mercado, J.J., Mateos-Nava, R.A., Altamirano-Lozano, M.A., 2011. DNA damage induction in human cells exposed to vanadium oxides in vitro. Toxicol. in Vitro 25 (8), 1996–2002.

Roggli, V.L., 1989. Pathology of human asbestosis: A critical review. In: Fenoglio-Preiser, C.M. (Ed.), Advances in Pathology. vol. 2. pp. 31–60 Chicago.

Rozalen, M., Ramos, M.E., Gervilla, F., Kerestedjian, T., Fiore, S., Huertas, F.J., 2014.

Dissolution study of tremolite and anthophyllite: pH effect on the reaction kinetics. Appl. Geochem. 49, 46–56.

Salnikow, K., Su, W., Blagosklonny, M.V., Costa, M., 2000. Carcinogenic metals induce hypoxia-inducible factor-stimulated transcription by reactive oxygen species-in-dependent mechanism. Cancer Res. 60, 3375–3378.

Scambelluri, M., Piccardo, G.B., Philippot, P., Robbiano, A., Negretti, L., 1997. High salinity fluid inclusions formed from recycled seawater in deeply subducted alpine serpentinite. Earth Planet. Sci. Lett. 148, 485–499.

Scharf, B., Clement, C.C., Zolla, V., Perino, G., Yan, B., Elci, G., Purdue, E., Goldring, S., Macaluso, F., Cobelli, N., Vachet, R.W., Santambrogio, L., 2014. Molecular analysis of chromium and cobalt-related toxicity. Sci. Rep. 4, 5729.

Schoonen, M.A., Cohn, C.A., Roemer, E., Laffers, R., Simon, S.R., 2006. Mineral-induced formation of reactive oxygen species. In: Sahai, N., Schoonen, M.A. (Eds.), Medical mineralogy and geochemistry. Reviews in Mineralogy and Geochemistry, Mineralogical Society of America, Chantilly, pp. 179–221.

Schreier, H., Northcote, T.G., Hall, K., 1987. Trace metals in fish exposed to asbestos rich sediments. Water Air Soil Pollut. 35 (3–4), 279–291.

Seilkop, S.K., Oller, A.R., 2003. Respiratory cancer risks associated with low-level nickel exposure: an integrated assessment based on animal, epidemiological, and mechan-istic data. Regul. Toxicol. Pharmacol. 37, 173–190.

Shukla, A., Gulumian, M., Hei, T.K., Kamp, D., Rahman, Q., Mossman, B.T., 2003. Multiple roles of oxidants in the pathogenesis of asbestos-induced diseases. Free Radic. Biol. Med. 34, 1117–1129.

Smith, I.M., Hall, K.J., Lavkulich, L.M., Schreier, H., 2007. Trace metal concentrations in an intensive agricultural watershed in British Columbia, Canada. J. Am. Water Resour. Assoc 43 (6), 1455–1467.

Spasiano, D., Pirozzi, F., 2017. Treatments of asbestos containing wastes. J. Environ. Manag. 204, 82–91.

Tashakor, M., Yaacob, W.Z.W., Mohamad, H., Ghani, A.A., 2014. Geochemical char-acteristics of serpentinite soils from Malaysia. Malays. J. Soil Sci. 18, 35–49.

Tiepolo, M., Oberti, R., Zanetti, A., Vannucci, R., Foley, S.F., 2007. Trace-element par-titioning between amphibole and silicate melt. In: Hawthorne, F.C., Oberti, R., Della Ventura, G., Mottana, A. (Eds.), Amphiboles: Crystal Chemistry, Occurrence, and Health Issues. Mineralogical Society of America, Chantilly, pp. 417–452.

Turci, F., Pavan, C., Leinardi, R., Tomatis, M., Pastero, L., Garry, D., Anguissola, S., Lison, D., Fubini, B., 2010. Revisiting the paradigm of silica pathogenicity with synthetic quartz crystals: the role of crystallinity and surface disorder. Part. Fibre Tox. 13, 32.

Turci, F., Tomatis, M., Pacella, A., 2017. Surface and bulk properties of mineral fibres relevant to toxicity. In: Gualtieri, A.F. (Ed.), Mineral Fibres: Crystal Chemistry, Chemical-Physical Properties, Biological Interaction and Toxicity. European Mineralogical Union, London, pp. 171–214.

Upreti, R.K., Dogra, R., Shanker, R., Murti, C.K., Dwivedi, K.K., Rao, G.N., 1984. Trace elemental analysis of asbestos with an X-ray fluorescence technique. Sci. Total Environ. 40, 259–267.

U.S. Geological Survey, 2016. Mineral Commodity Summaries. https://www.usgs.gov/centers/nmic/mineral-commodity-summaries.

Vanoeteren, C., Cornelis, R., Sabbioni, E., 1986. Critical Evaluation of Normal Levels of Major and Trace Elements in Human Lung Tissue. Commission of the European Communities, Luxembourg.

Verma, D.K., Ritchie, A.C., Shaw, M.L., 2003. Measurement of beryllium in lung tissue of a chronic beryllium disease case and cases with sarcoidosis. Occ. Med. 53, 223–227.

Vils, F., Pelletier, L., Kalt, A., Müntener, O., Ludwig, T., 2008. The lithium, boron and beryllium content of serpentinized peridotites from ODP Leg 209 (Sites 1272A and 1274A): implications for lithium and boron budgets of oceanic lithosphere. Geochim. Cosmochim. Acta 72, 5475–5504.

Vithanage, M., Rajapaksha, A.U., Oze, C., Rajakaruna, N., Dissanayake, C.B., 2014. Metal release from serpentine soils in Sri Lanka. Environ. Monit. Assess. 186, 3415–3429.

Wei, B., Yang, L., Zhu, O., Yu, J., Jia, X., 2014. Multivariate analysis of trace elements distribution in hair of pleural plaques patients and health group in a rural area from China. Hair Ther. Transpl. 4, 2167–3118.

Weiss, W., 1999. Asbestosis: a marker for the increased risk of lung cancer among workers exposed to asbestos. Chest 115 (2), 536–549.

WHO, 2015. Mesothelial tumours - diffuse malignant mesothelioma - epithelioid me-sothelioma. In: Travis, W.D., Müller-Hermelink, H., Harris, C. (Eds.), Classification of Tumours of the Lung, Pleura, Thymus and Heart, pp. 130–138.

WHO (World Health Organization), 2006. Elimination of Asbestos- Related Diseases. Geneva. http://www.who.int/occupational_health/publications/asbestosrelateddisease/en/index.html, Accessed date: 27 April 2010.

Zakrzewska, M., Capone, P.P., Iannò, A., Tarzia, V., Campopiano, A., Villella, E., Giardino, R., 2008. Calabrian ophiolites: dispersion of airborne asbestos fibres during mining and milling operations. Period. di Mineral. 77 (2), 27–34.

ORIGINAL PAPER

Natural occurrence of asbestos in serpentinite quarries from Southern Spain

Andrea Bloise [ID] **· Claudia Ricchiuti · Rafael Navarro · Rosalda Punturo ·
Gabriele Lanzafame · Dolores Pereira**

Abstract The nevado-filábride complex (NFC) (southern Spain) is well known for its widespread mining and quarrying activities. Serpentinite and metabasite rocks are extracted, processed and traded as building and ornamental stones. Due to the possible presence of natural occurrence of asbestos (NOA) in these rocks, the aim of this paper is to conduct an in-depth characterisation of fibrous minerals. To this aim, seven serpentinite rock samples were collected in four quarries located in the Sierra Nevada and Sierra de los Filabres (South-eastern Spain), which were then analysed by X-ray powder diffraction (XRPD), scanning electron microscopy combined with energy-dispersive spectrometry (SEM/EDS), differential scanning calorimetry (DSC), derivative thermogravimetry (DTG) and X-ray synchrotron microtomography (SR-μCT). It is essential to investigate asbestos minerals from both scientific and legal perspective, especially for public health officials that implement occupational health and safety policies, in order to safeguard the health of workers (e.g. quarry excavations, road yards, civil constructions, building stones).

Keywords Quarries · Serpentinite · Asbestos · NOA · Spain

A. Bloise (✉)
Department of Biology, Ecology and Earth Sciences,
University of Calabria, Cubo 15b, 87036 Rende,
CS, Italy
e-mail: andrea.bloise@unical.it

C. Ricchiuti · R. Punturo · G. Lanzafame
Department of Biological, Geological and Environmental
Sciences, University of Catania, 95129 Catania, Italy

R. Navarro · D. Pereira
CHARROCK Research Group, University of Salamanca,
Plaza de los Caídos s/n, 37008 Salamanca, Spain

D. Pereira
Geology Department, Science Faculty, University of
Salamanca, Plaza Merced s/n, 37008 Salamanca, Spain

Introduction

Ophiolites are fragments of oceanic lithosphere composed of mafic and ultramafic rocks (i.e. metabasite and serpentinite), commonly known as greenstone (Punturo et al. 2018; Pereira 2012) because of their typical dark greenish colour. Due to their aesthetic features and to their mechanical properties (i.e. high tensile strength, flexibility, high thermal stability), these rocks have been used extensively as building and dimension stones and have therefore been important natural resources for many countries (Pereira et al. 2013). In fact, greenstone rocks have been mined intensively worldwide and traded internationally (Kazan-Allen 2005) for centuries. Nevertheless, since ophiolites are the main source of asbestos minerals, many studies have revealed that the greenstone mining

could represent a significant risk to human health if dust containing asbestos fibres is inhaled (Mossman and Marsh 1989; Kamp, 2009; Baumann et al. 2015; Case et al. 2017; Bernstein and Pavlisko 2017; Colombino et al. 2019). The term "asbestos" (i.e. regulated-asbestos) refers to a group of six fibrous silicate minerals belonging to the serpentine (i.e. chrysotile) and amphibole (i.e. tremolite, actinolite, anthophyllite, amosite, crocidolite) mineral groups (IARC 2012). As regards the dimensional definition of asbestos, the World Health Organization (WHO, 1997) established that fibres > 5 μm long and with aspect ratio (i.e. length divided by width) ≥ 3:1, are classed as respirable fibres. The health risk is that depending on their size, these fibres may penetrate the lungs and consequently cause asbestos-related diseases (IARC 2012; Pavlisko and Sporn 2014; Case et al. 2017). Besides, it is important to note that some authors (Schoonene et al. 2006) consider fibres as complex chemical reservoirs of potentially toxic elements (PTEs) such as Fe, Ni, Cr and fibres might only passively cause disease as carriers of toxic elements, which tend to be released into the intracellular or extracellular environment during the dissolution process. Epidemiological and experimental evidence (e.g., Nemery, 1990) prove that PTEs such as some heavy metals are carcinogens and therefore hazardous to human health. It has been demonstrated that the high concentrations of PTEs in asbestos minerals may induce lung cancer (Schreier et al. 1987; Wei et al. 2014). More specifically, if sufficient amounts of trace elements (e.g. Ni, Cr) accumulate in the lungs, they may alter the baseline levels of these elements in normal human lung tissue, which has not been damaged by disease (Vanoeteren et al. 1986), thus causing lung cancer (e.g. mesothelioma and bronchogenic carcinoma) (Dixon et al. 1970; Nemery 1990; Wei et al. 2014). Moreover, since excessive amount of Ni can damage DNA (Caicedo et al. 2007), it is regarded as one of the most dangerous trace elements to human health to be found in asbestos. Indeed, several studies have been conducted on the ability of Ni to generate Reactive Oxygen Species (ROS) and on the toxic effects of Ni at intracellular sites (e.g. Chen et al. 2003; Horie et al. 2009). In addition to Ni, high concentrations of other trace elements such as Cr may be hazardous to human health as they can stimulate the production and transformation of ROS as well as iron (e.g. Jomova and Valko

2011). Indeed, Gross et al (1969) observed that toxic elements induced lung cancers in rats after they were exposed to asbestos dust containing large amounts of Ni, Cr and Co. Ophiolitic rocks contain large amounts of some trace elements and even ophiolite derived soils may contain toxic elements such as Cr and Ni, being a risk to human health as reported in literature (e.g. Gwenzi 2019; Bloise et al. 2020a). Epidemiological studies have reported numerous cases of cancer among asbestos workers (Ross and Nolan 2003). The three main asbestos-related diseases are: (1) asbestosis; (2) lung cancer; and (3) mesothelioma (Dixon et al. 1970; Mossman and Marsh 1989; Nemery 1990; Kamp 2009; IARC 2012; Wei et al. 2014; Pavlisko and Sporn 2014; Baumann et al. 2015; Case et al. 2017; Bernstein and Pavlisko 2017). Furthermore, an association has been observed between the increase in the incidence of lung disease and non-occupational exposure to asbestos fibres, thus indicating an elevated risk for both asbestos workers and people who live near to Natural Occurrence of Asbestos (NOA) outcrops (Acosta et al. 1997; Constantopoulos 2008; Pugnaloni et al. 2013; Berk et al. 2014; Baumann et al. 2015; Bellomo et al. 2018; Gunter 2018; Cagnard and Lahondère 2020). The term NOA refers to both regulated and non-regulated fibrous minerals present in rocks (i.e. serpentinite or altered ultramafic rocks) and soils that have not been extracted for commercial purposes (Harper 2008). Excavation activities (e.g. road constructions and building foundation excavation) as well as weathering processes may disturb NOA bearing rocks (e.g., Bloise et al. 2012; Vignaroli et al. 2014; Gaggero et al. 2017; Pierdzig 2019) and cause the release of potentially respirable fibres into the environment. The scientific community has observed that fibrous minerals may have toxic effects on human health even if they do not belong to the asbestos category such as erionite (Ballirano et al. 2017; 2018a, b). Due to the health problems associated with asbestos exposure, in Spain, the quarrying of rocks located in greenstone lithotypes is regulated by Spanish law (Real Decreto 396/2006), as there is evidence that if inhaled, these fibres can pose serious health risks to miners. In addition, several studies (Agudo et al. 2000; López-Abente et al. 2005; Fernández-Navarro et al. 2012) have pointed out that, although the main risk is derived from the exposure in the manufacturing industry (especially those derived from the fibre-cement and talc industry), the mine

workers are also exposed to risk, increasing the cancer prevalence with respect to the average risk of the population. Awareness of the health risks associated with asbestos exposure has generated considerable interest in the identification of regulated and non-regulated mineral fibres in rocks. In order to highlight the presence of asbestos minerals within serpentinite rocks, the aim of this study is to carry out a comprehensive mineralogical characterization of seven serpentinite rock samples collected from quarries located in the Sierra Nevada and the Sierra de los Filabres (South-eastern Spain) (Navarro et al. 2018). These serpentinite rocks have long been used in various construction works as building and as ornamental stones, aggregates and inert material (Pereira et al. 2013; Navarro et al. 2018). In this scenario, the identification of asbestos minerals located in the NFC area can provide a contribution to the territorial mapping.

Geological setting

The studied samples were collected at several quarries of serpentinite from Sierra Nevada and Sierra de los Filabres (South-eastern Spain). In particular, these quarries are located in the Nevado-Filabride Complex (NFC) (Fig. 1), an allochthonous metamorphic complex placed in the lowest position of the internal zones of the Betic Cordillera (Martin-Algarra et al. 2004). This complex can be subdivided into two tectonic units: the lower unit (or Veleta Unit) and the upper unit (or Mulhacen Unit). According to Sanz de Galdeano and López-Garrido (2016), both units share the same sequence from bottom to top: dark schist with interbedded quartzites (Carboniferous), quartzites, mica schist with garnets (Permian) and interbedded quartzites, schist and marble (Permian–Triassic). Interlayered within the sequence, metamorphosed igneous rocks, principally metabasite and tourmaline-bearing orthogneisses are common. This metabasites are mainly composed of serpentinites (the potential source of asbestos studied in this paper) with various degree of serpentinization. This serpentinite bodies, whose thickness ranges from several centimetres to hundreds of metres, occur within the mica schist and marble units, with the exception of the "Barranco de San Juan" outcrop, which is placed in the dark schist unit. According to Sanz de Galdeano

and López-Garrido (2016), the metabasite rocks correspond to former basic volcanic extrusions interlayered in metasediments. In this metabasites bodies, together with serpentinite rocks, it is also possible to observe eclogites, amphibolites and metadolerite dikes that can be found as lenticular bodies of decimetric thickness partially rodingitized and transformed into metarodingite or eclogite during metamorphism (Puga et al. 2011).

Sampling

The rock samples were collected as follows: two were collected in the Sierra Nevada: "Barranco de San Juan" (samples VG1 and VG2) and "Nigüelas" (sample NG), while the other four came from the Sierra de los Filabres: "Virgen del Rosario" (samples VM1 and VM2) and "La Carrasca" (samples CA1 and CA2) (Fig. 1). The number of samples is statistically representative, as the authors have gone through detailed characterizations of the same rocks in papers on different research topics (Navarro et al. 2018 and references therein). The "Barranco de San Juan" quarry is located in Güejar Sierra (Granada). It is the oldest serpentinite quarry for dimension stones in Spain. The quarry began operating in the sixteenth century and it was closed in the middle of the twentieth century. The variety of rock quarried was known as "Verde Granada", which has been used to construct numerous Spanish monuments, such as the Monastery of El Escorial (sixteenth century), the Royal Palace (eighteenth century) in Madrid, the Palace of Carlos V (sixteenth century) and the Royal Chancellery (sixteenth century) in Granada (Navarro et al. 2015). The quarry is of particular importance since it is a potential source of materials for restoring historic buildings and monuments. The "Nigüelas" quarry is a small quarry located in Nigüelas (Granada); opened in the 1970s for extracting dimension stones, but had to be closed down due to the high asbestos content of the rock. The "Virgen del Rosario" quarry is located in Macael (Almería) where white, grey and yellow marble as well as serpentinite that are extracted. The latter is commercialized under the name "Verde Macael" and it has been used as a building material in numerous national and international monuments. Some well-known examples are the Almudena Cathedral (Twenteeth century) in Madrid and in many public and civic
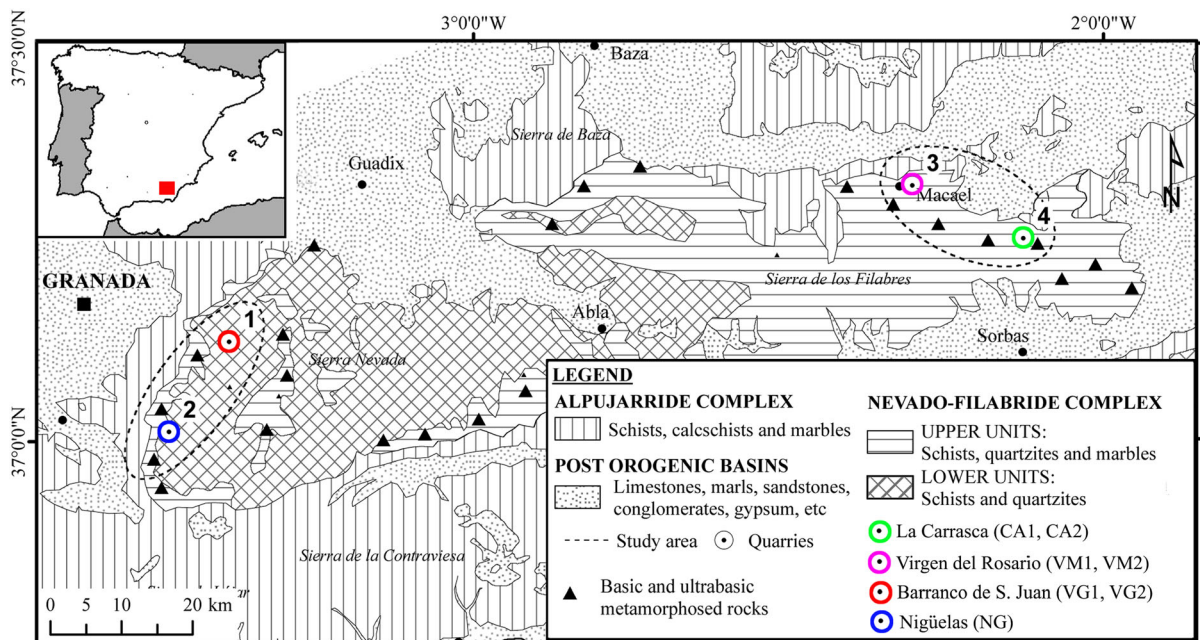
Fig. 1 Geological setting and location of the quarries: 1 = Barranco de San Juan, 2 = Nigüelas, 3 = Virgen del Rosario, 4 = La Carrasca (Modified after Martin-Algarra et al. 2004)

buildings across Spain. Lastly, the "La Carrasca" quarry is located in Albanchez (Almería) and the serpentinite extracted is marketed as dimension stones. Depending on demand, extraction operations are limited and unlike the other mentioned serpentinite rocks, the serpentinite marketed here does not have any commercial name. In the specific case of this study, the samples analysed are serpentinite rocks showing, in some cases (VM1 and VM2), a high degree of carbonation (Navarro et al. 2018), therefore many varieties of these rocks are included in the technical datasheet of marbles even if they have different mineralogical, geochemical, physical and mechanical properties (Navarro et al. 2018).

Analytical methods

The seven serpentinite rock samples have been studied by means of several laboratory techniques such as X-Ray Powder Diffraction (XRPD), scanning electron microscopy (SEM) equipped with an energy-dispersive x-ray spectrometer (EDS), differential scanning calorimetry (DSC), derivative thermogravimetry (DTG) and X-ray synchrotron microtomography (SR-μCT). Thermal analysis has been very useful

either for the identification of the serpentine group (i.e. chrysotile, lizardite, antigorite and polygonal serpentine) and for the characterization of amphibole asbestos (Bloise et al. 2017; Viti 2010). The XRPD analysis was performed by using the Rigaku SmartLab (Rigaku Europe SE, Germany) diffractometer, equipped with CuKa radiation and SC-70 detector at 40 kV and 100 mA. Scans were collected in the range of 6°–75° 2θ with a step interval of 0.01° and step counting time of 2 s. SmarlLab Studio II software was used to identify the mineral phases in each x-ray powder spectrum, experimental peaks being compared with ICDD (PDF2.DAT) reference patterns. DSC/DTG analyses were performed with a Netzsch STA 449 C Jupiter (Netzsch-Gerätebau, Germany) in the temperature range 30–1200 °C with a heating rate of 10 °C min⁻¹ and under air flow of 30 mL min⁻¹. Instrumental precision has been verified by five repeated collections on a kaolinite reference sample, revealing acceptable reproducibility (instrumental theoretical T precision of ± 1.2 °C), DSC detection limit < 1 μW. Netzsch proteus thermal analysis software (Netzsch-Gerätebau, Germany) was used to identify exothermic, endothermic and derivative thermogravimetry (DTG) peaks. For SEM analysis, a fragment of each specimen was coated with graphite

after being fixed on SEM stub using double-sided conductive adhesive tape. All measurements were done at the Dipartimento di Scienze Biologiche, Geologiche e Ambientali of the University of Catania (Italy) by using a Tescan Vega-LMU scanning electron microscope. The microscope is equipped with an EDAX Neptune XM4–60 EDS micro-analyzer using an energy-dispersive system coupled with an EDAX WDS LEXS (wavelength dispersive low energy x-ray spectrometer) calibrated for light elements (although WDS was not used in the data acquisition for minerals analysed in this work). Operating conditions were set at 20 kV accelerating voltage and ~ 8 nA beam current for obtaining high-contrast BSE images and 20 kV accelerating voltage and ~ 2 nA beam current for the analysis of major element abundances in the studied mineral phases. Given the rather low energy applied for sample volume excitation, a focused beam was used. Repeated analyses on SPI 02,753-AB Serial KF certified standards (Fo-rich olivine, An-rich plagioclase, augitic-clinopyroxene and glass) during the analytical runs provided precision for all measured elements of around 3–5%. Accuracy is on the order of 5%. The 3D study of the samples was carried out by using Synchrotron Radiation X-ray computed microtomography (SR-μCT) in phase-contrast mode (Cloetens et al. 1997) at the SYRMEP beamline of the Elettra synchrotron laboratory (Basovizza, Trieste, Italy). Samples were cut parallelepiped shaped with size of about $4 \times 4 \times 20$ mm. Experiments were performed in white beam configuration (Baker et al. 2012), employing a filtered (1 mm Si + 1 mm Al) polychromatic X-ray beam delivered by a bending magnet source in transmission geometry. For each experiment, 1800 projections were acquired over a total scan angle of 180° with an exposure time/projection of 2 s and sample-to-detector distance fixed at 150 mm. The employed detector was a 16 bit, air-cooled, sCMOS camera (Hamamatsu C1144022C) with a 2048×2048 pixels chip. The effective pixel size of the detector was set at 1.95×1.95 μm^2, yielding a maximum field of view of ca. 4 mm^2. Microtomographic scans were acquired in local region of interest mode (Maire and Withers 2014). The reconstruction of the 2D tomographic slices was done with the Syrmep Tomo Project (STP) house software suite (Brun et al. 2017). A single-distance phase-retrieval algorithm (Paganin et al. 2002) combined with Filtered Back-

projection algorithm (Herman 1980) was employed to the sample projections to improve the consistency of the quantitative analysis. The reconstructed volumes were investigated to evaluate the veins/void of the samples. The 3D image treatment and analysis were performed by means of Fiji software (Schindelin et al. 2012) using the procedure described by Bloise et al. (2020a). The original stacks of slices were first cropped for extracting, for each sample, the volumes of interests (VOIs). To retrieve the veins/voids phase, VOIs were segmented by manual thresholding. This procedure allowed to obtain binary (black and white) 3D images of the phase of interest that were analysed for retrieving the porosity values, calculated as volume of pores/total volume. The 3D renderings of the VOIs were obtained by means of VGStudio Max 2.2 software.

Results

Mesoscale properties of serpentinite rocks

Based on the mesoscopic observations, serpentinite rocks collected from the different mentioned outcrops may vary considerably (Figs. 2a, b, c, d and 3a, b, c, d), mainly due to their complex origin (Navarro et al. 2018). Figure 2 shows views of the quarries, and Fig. 3 shows close ups of the outcrops where the samples were collected. Several blocks of decimetric dimensions were collected directly in the faces of the quarries. For this work, the selected samples were affected by fractures filled with apparently fibrous material in the blocks, except for the sample NG, made of asbestos that was taken directly from a fracture in the field. The blocks that contained the samples that were analysed in this work are shown in Fig. 4. The samples have various microstructural features: (1) massive, (2) with evident presence of veins and (3) totally fibrous (Figs. 3 and 4). Moreover, serpentinite rocks come in various shades of green depending on the degree of carbonation. Both samples from the "Barranco de San Juan" (VG1 and VG2) quarry are massive and are dark green and light green in colour, respectively; contrastingly, sample NG from the "Nigüelas" quarry shows a clear fibrous habit. The samples collected from the "Virgen de Rosario" quarry show a massive structure (VM1) and evident veins (VM2). The rocks collected from the "La
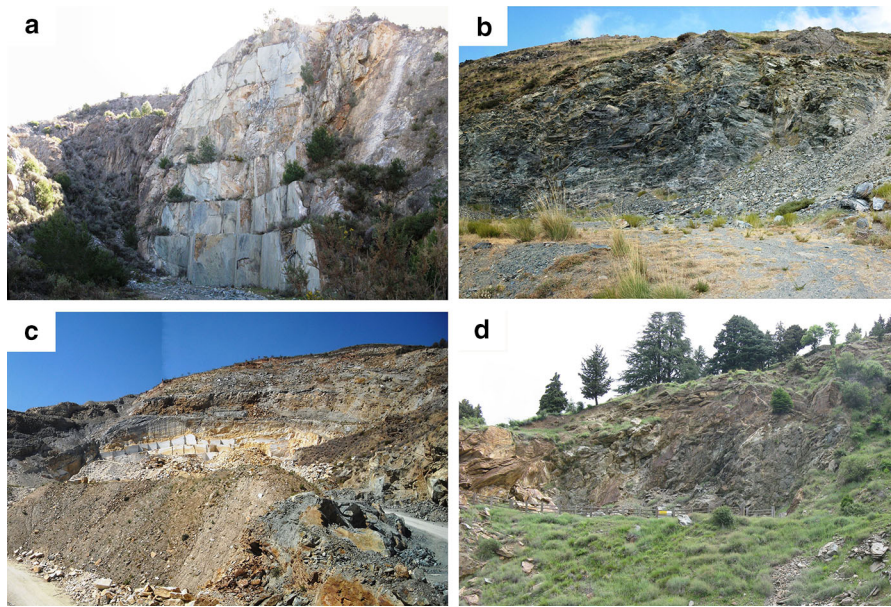
Fig. 2 Distant view of the quarries: **a** Barranco the San Juan, **b** Nigüelas, **c** Virgen de Rosario, **d** La Carrasca
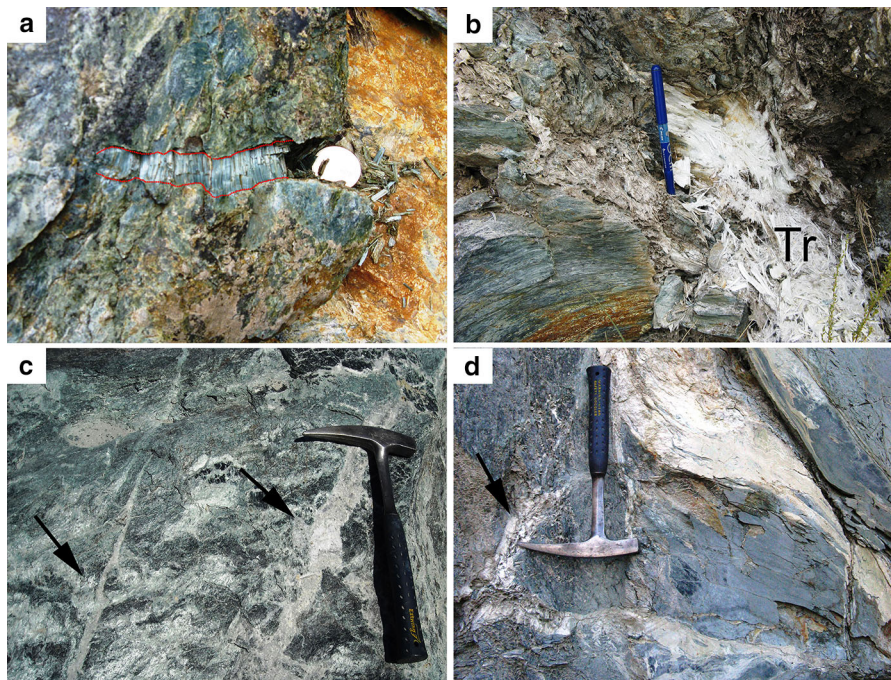

Fig. 3 Pictures taken at the quarry of: **a** Barranco the San Juan, detail of a tremolite vein (between the dashed red lines) cross-cutting serpentinite, **b** Nigüelas, outcrop with white asbestos tremolite (Tr), **c** Virgen de Rosario, network of veins developed inside the massive serpentinite, indicated by the black arrows, **d** La Carrasca, appearance of green serpentinite cut by veins filled with tremolite, indicated by the black arrow
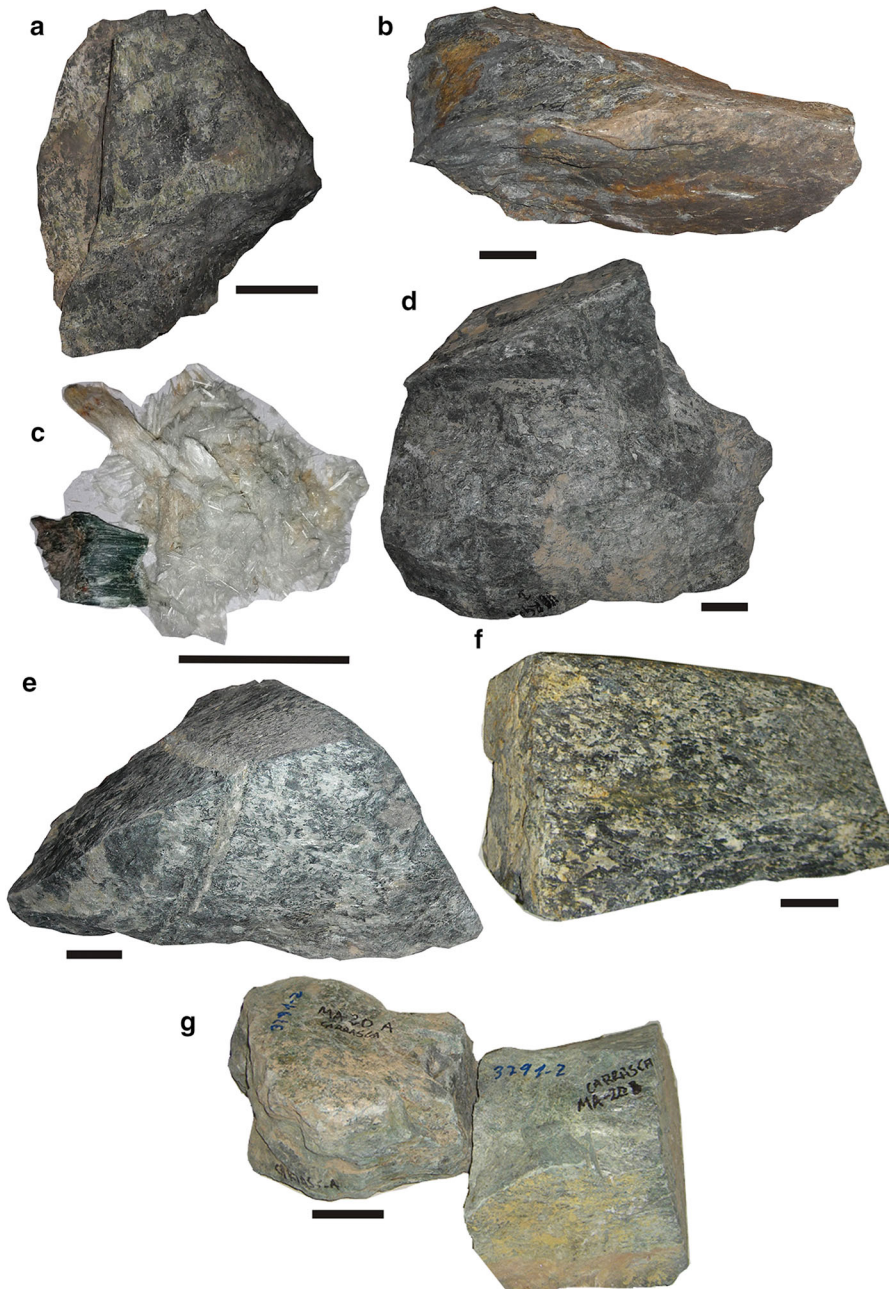
Fig. 4 Serpentinite blocks where the fibrous samples were taken from: **a** VG1; **b** VG2; **c** NG; **d** VM1; **e** VM2; **f** CA1; **g** CA2. Scale bar: 5 cm

Carrasca" quarry differs considerably from one to other; CA1 is fibrous while CA2 is massive.

XRPD characterization

XRPD patterns show that the samples analysed are composed of serpentine minerals, amphiboles,

Table 1 Semi-quantitative mineralogical composition of samples in order of decreasing relative abundance, detected by XRPD, DSC/DTG and EDS/SEM. Ctl = chrysotile, Liz = lizardite, Ant = antigorite, PS = polygonal serpentine, Tr = tremolite, Hbl = hornblende, Ts = tschermakite, Mag = Magnetite, Dol = dolomite, Cal = calcite, Qz = quartz, Chl = Chlorite, Clay = Clay minerals. Mineral symbols after Whitney and Evans (2010)

Sample	Mesoscopic description	Locality	Quarry	Phases detected
VG1	Massive	Granada	Barranco de San Juan	Liz > PS > Ctl
VG2	Massive	Granada	Barranco de San Juan	Ant > Cal > Liz > Ctl > Mag
NG	Fibrous	Granada	Nigüelas	Tr > > Cal > Chl > Ant > PS > Mag
VM1	Massive	Macael	Virgen del Rosario	Dol > Ts > Chl > Clay > Qtz
VM2	Evident fibrous veins	Macael	Virgen del Rosario	Liz > > Hbl-Tr > Chl > Ctl > Dol > Ant > Mag
CA1	Fibrous	Almeria	La Carrasca	Tr > > Ctl > Chl > Qtz > Mag > Dol
CA2	Massive	Almeria	La Carrasca	Ant > > Chl > Liz > Cal > PS > Mag > Clay

dolomite, calcite, followed by chlorite, magnetite, quartz and clay minerals, which were detected less frequently and in smaller amounts (Table 1). Since XRPD was not able to distinguish among the different types of serpentine minerals, a further characterization was carried out on each sample using thermal analysis methods (DSC/DTG).

DSC/DTG characterization

The data obtained using thermal analysis reduced the ambiguities regarding serpentine polymorph identification. The correspondence between the endothermic and exothermic reactions in the DSC curves and

minerals is in accordance with the literature data (Földvári 2011; Bloise et al. 2017). Similarly, the maximum loss rate recorded on the DTG curves was in line with the literature data (Bloise et al. 2017; Viti 2010). As regards asbestos minerals, the endothermic peaks in a temperature range of 605–650 °C (Figs. 4 and 5) were due to chrysotile breakdown, whereas amphiboles showed endothermic peaks in the 1039–1070 °C temperature range (Figs. 5 and 6). Samples NG, VM1 and CA2 were the only samples that did not contain chrysotile. Other serpentine polymorphs such as lizardite (samples VG1, VG2 and CA2) and antigorite (samples VG2, NG, VM2 and CA2) were also detected. Polygonal serpentine was
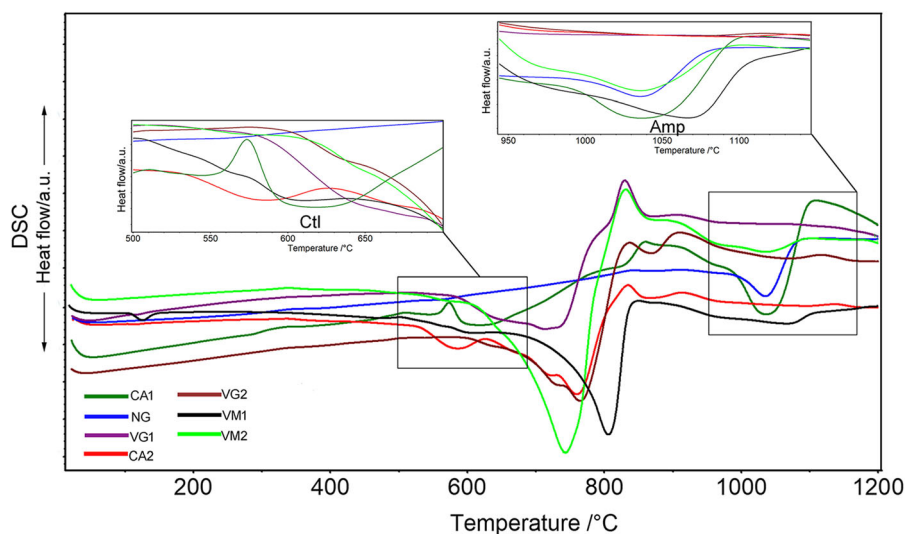

Fig. 5 Comparison between differential scanning calorimetry (DSC) curves of the studied samples; the insets show magnification of DSC curves with arbitrary unit of the heat flow
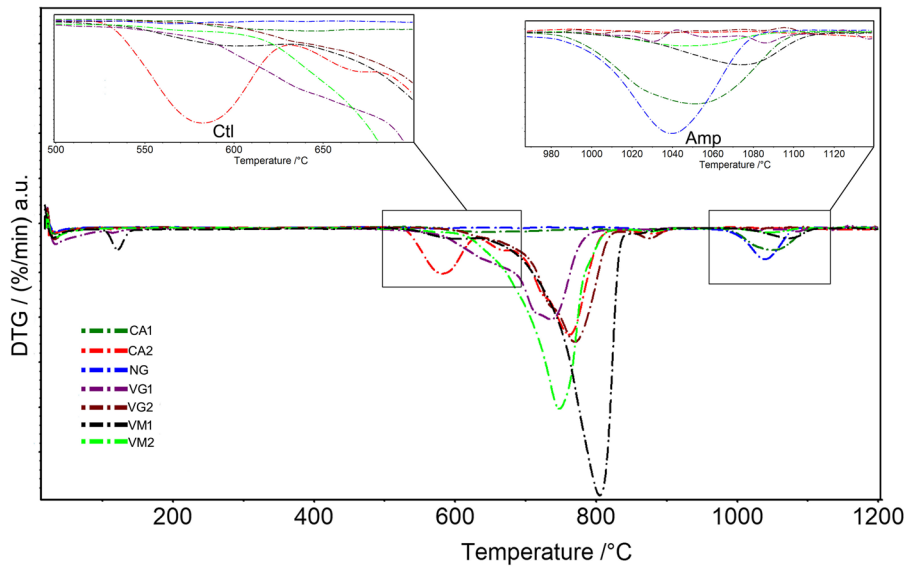
Fig. 6 Comparison between differential scanning calorimetry (DTG) curves of the studied samples; the insets show magnification of DTG curves

only detected in three samples (VG1, NG, CA2). Magnetite, chlorite, calcite, dolomite and quartz were also found in varying amounts in some of the samples (Table 2). The exothermic peaks at approximately 850 °C and 1100 °C (Table 2) were interpreted as forsterite and pyroxene crystallization deriving from serpentine and amphibole breakdown (Bloise et al. 2017).

SEM/EDS investigation

SEM imaging enabled us to carry out a thorough investigation of the morphological features of the minerals (i.e. fibrous or non-fibrous) and a qualitative evaluation of the fibre size. The results highlighted that serpentine and amphibole were present in all of the samples in either fibrous or non-fibrous form. Chrysotile was observed both in single fibrils and in fibre bundles (Fig. 7a-c) or as fibres composed of numerous small fibrils that tend to split up along their elongation axis (Fig. 6b; sample CA1). As regards amphiboles, the samples show the presence of tremolite that occurs either as individual prismatic crystals or with a fibrous habit (Fig. 7a, b, c, d) with small diameters and > 5 µm long. At the mesoscale, sample NG had appeared as fibrous due to the presence of tremolite (Fig. 8a) since chrysotile had not been detected.

Regarding fibres morphology, it is possible to observe very long and thin fibres that tend to split into thinner fibres due to their high flexibility (asbestiform tremolite; Fig. 8b, c, d); these fibres occur simultaneously as long and thin prismatic crystals but lacking in flexibility (non-asbestiform tremolite, Figure 8a, d). Because of their size, prismatic crystals may be mistaken for fibril bundles. Similarly, cleavage fragments, which are the result of fractures that occur along the cleavage planes of larger crystals, may look like fibril bundles. Since these particles are so small that they can be inhaled, several studies have recently focused on the toxicity of non-asbestos fibrous minerals (Belluso et al. 2017). The morphology of chrysotile asbestos particles is quite different from the structure of amphibole asbestos; the former occurs either in single fibres or bundles of fine crystal fibrils, while amphibole asbestos minerals generally occur in narrow, parallel-sided fibres (Figs. 7 and 8).

Table 3 shows the chemical composition (oxide and atom per formula unit) of the chrysotile fibres in samples VG1, VG2, VM2 and CA1. The data revealed that the samples had a similar chemical composition, with SiO_2 values ranging from 42.14 to 47.34 wt% and MgO ranging from 42.12 to 46.85 wt%. Al_2O_3 content ranged from a minimum of 2.46 wt% to a maximum of 4.97 wt%. FeO was always found in variable concentrations in the chrysotile samples (Table 3), which

Table 2 Peak temperature values in DSC and DTG curves; w = weak, s = strong, sh = shoulder, endo = endothermic, exo = exothermic, Atg = antigorite, Lz = lizardite, Ctl = chrysotile, PS = polygonal serpentine, Chl = chlorite, Tr = tremolite, Hbl = hornblende, Ts = tschermakite, Fo = forsterite, Px = pyroxene, Dol = dolomite, Cal = calcite, Qz = quartz, Mag = magnetite, Clay m = clay minerals. *New phases formed after the breakdown. Mineral symbols after Whitney and Evans (2010)

Phases	VG1	VG2	NG	VM1	VM2	CA1	CA2
DSC (T °C)							
Clay				121 endo			125 endo
Mag		340 exo	349 exo		338 exo	339 exo	373 exo
Chl			563 endo	562 endo	574 endo w	543 endo	595 endo
Qz				502 exo		573 exo s	
Ctl	640 endo	622 endo w			644 endo vw	620 endo	
PS	717 endo						
Liz	735 endo w	720 endo			744 endo s		722 endo
Atg		770 endo					760 endo
Fo*	828 exo	823 exo			878 endo w	858 exo	
Dol/cal		875 endo	880 endo	806 endo	800 sh	860 endo	870 endo
Tr/Hbl/ Ts			1039 endo	1070 endo	1043 endo	1053 endo	
Px*			1135 v w	1143 w exo	1110 exo	1103 exo	
DTG (T °C)							
Clay				122 endo			123 endo
Chl			564 endo	560 endo	565 endo	544 endo	585 endo s
Ctl	638 endo	636 endo w			640 sh	622 endo	
PS	717 endo		699 endo vw				670 endo
Liz	735 endo w	732 endo					722 endo
Atg		770 endo	781 endo vw		744 endo		760 endo s
Dol				806, 863 endo s	805, 860 sh	831, 862 endo	
Cal		876 endo	880 endo				878 endo
Tr/Hbl/Ts			1039 endo s	1074 endo	1045 endo w	1053 endo	

ranged between 2.67 and 7.36 wt. % with an average of 4.73 wt%. According to the current cation distribution model (Stroink et al. 1980; Hardy and Aust 1995), Al^{3+} may substitute both Si^{4+} and Mg^{2+} in the tetrahedral and octahedral sheets, respectively, and both Fe^{2+} and Fe^{3+} ions can replace Mg^{2+} in the octahedral sheet, although in limited amounts (Ballirano et al. 2017). In three out of four samples, small amounts of Cr were detected (approximately 0.29 wt%) although not in all analysis points (Table 3). A similar trend was observed for Ni, which was inconsistently detected in all samples (Table 3) at an average value of 1.68 wt%.

The energy-dispersive spectrometry (EDS) spot analysis proved to be essential for identifying amphibole asbestos. The chemical analyses of the amphiboles were plotted on the binary Si vs Mg/ $(Mg + Fe^{2+})$ diagram, which is a standard presentation for classifying calcic amphiboles (Leake et al. 1997; Hawthorne and Oberti 2007). Amphibole compositions plot in the field of tremolite, tremolite-hornblende, actinolite-hornblende, fibrous magnesium-hornblende and tschermakite (Fig. 9). However, only samples CA1 and NG plot in the tremolite domain. The semi-quantitative chemical composition of several tremolite fibres determined by SEM/EDS analyses are reported in Table 4. The chemical composition of tremolite is consistent with the elements present in its stoichiometric composition (Si, Mg, Ca). The ferrous iron content in tremolite in sample CA1 ranges from a minimum of 1.63 wt% to a maximum of 4.98 wt% with average value of 3.34 wt%, while the Fe content in the tremolite detected in
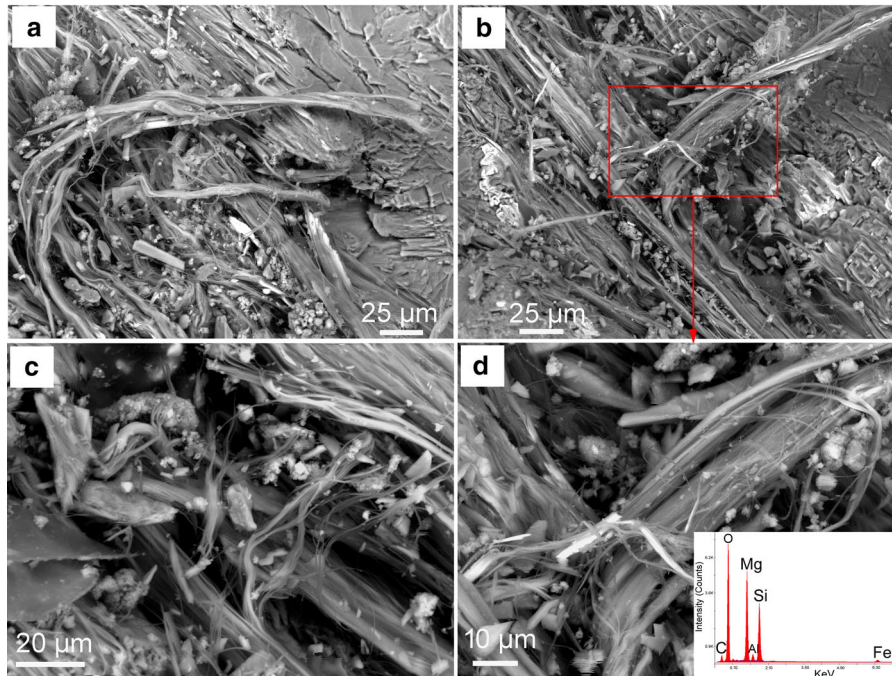
Fig. 7 Scanning electron micrographs: **a** chrysotile bundles (sample VG1), **b** chrysotile bundles (sample CA1), **c** chrysotile bundles (sample VG2), **d** zoom of **b** showing chrysotile separable fibres with the relative energy-dispersive spectrometry (EDS) point analysis

sample NG ranges from 1.52–4.24 wt% with an average value of 2.34 wt%.

From a chemical point of view, the average amount of iron detected in the tremolite extracted from the NFC quarries is in agreement with the iron content of other tremolite samples collected worldwide (e.g. Pacella et al. 2010). Moreover, small amounts of Cr were detected in one sample (CA1).

SR-µCT investigation and three-dimensional image analysis

In recent years, synchrotron radiation X-ray computed microtomography (SR-µCT) has increasingly being used as a non-destructive technique for analysing complex rock textures, since it is possible to obtain high-resolution 3D reconstructions of the inner structure of the samples from micrometric to nanometric resolution, while preserving the specimens for further studies. Indeed, 3D microscopic image visualisation and analysis enables us to conduct high quality quantitative analysis of the size and shape of rock components such as crystals and pores (Baker et al. 2012; Lanzafame et al. 2020) and textures such as

veins and fibres (Militello et al. 2019; Punturo et al. 2019; Bloise et al. 2020a). The DSC/DTG and SEM results were consistent with SR-µCT data. In fact, in line with the study by Bloise et al. (2020a), fibrous chrysotile and amphibole veins were detected in all of the samples in which veins and/or voids were present as shown in Fig. 10a, b (sample CA1). Visual inspection of the 2D slices of the veins acquired by SR-µCT show that there are sections of the samples in which the fibres are clearly visible as they can be oriented both across or along the vein (i.e. oriented in different directions). The asbestos fibres (chrysotile and tremolite) crystallize in the veins as bundles of fibres, while in other parts of the sample the veins are filled with non-fibrous phases since there are no voids. The 3D reconstructions also reveal the branching of the veins/voids within the serpentinite matrix. Contrastingly, the growth of fibrous phases was hindered in the samples with no veins (Fig. 10c, d), (Table 1, sample CA2). Lamellar antigorite and lizardite phases were found predominantly in sample CA2, while no fibrous phases were observed. Small magnetite crystals visible as bright dots were also identified (Fig. 10c, d).
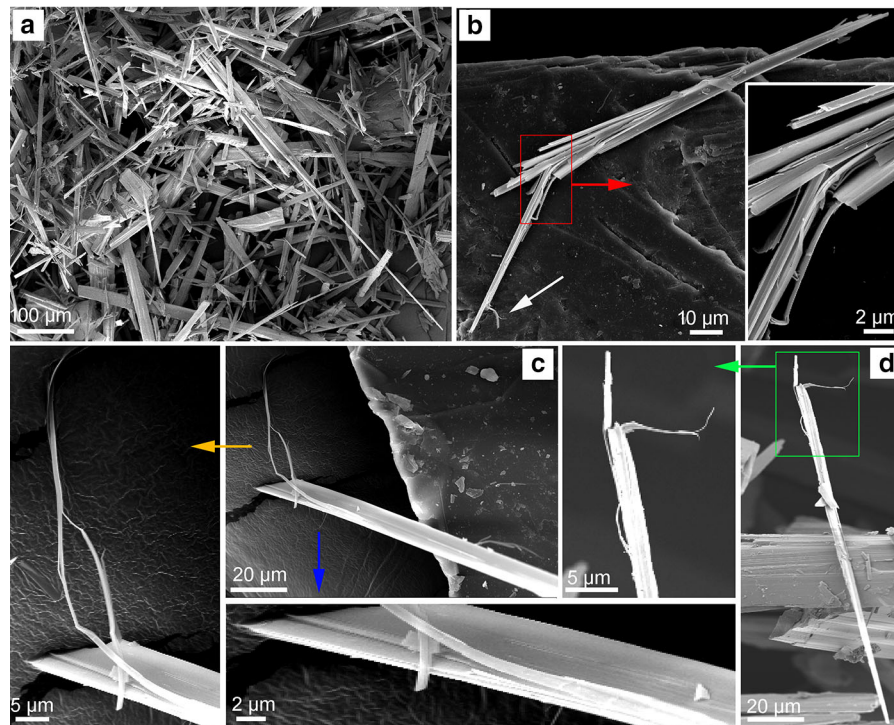
Fig. 8 a Scanning electron micrograph of tremolite, **a** fibrous and prismatic habit (NG sample). **b** fibrous tremolite (CA1 sample), the insert shows fibre flexibility. **c** fibrous tremolite (CA1 sample), the inserts indicated by the orange and blue arrows show longitudinal splitting of the fibre. **d** fibrous tremolite over prismatic tremolite (NG sample) the insert indicated by green arrow shows both flexibility and easiness of the fibre to split

Discussion

The main mineralogical characteristics of the serpentinite samples analysed for this work are similar to those of similar lithotypes found in quarries located all over the world (e.g. Belluso et al. 2020; Pacella et al. 2010; Punturo et al. 2019), which mainly contained chrysotile and tremolite asbestos. Despite the fibrous morphology detected at the outcrop scale, some fibres did not meet the definition (i.e. chemical, flexibility) of asbestos fibres (Gualtieri 2017). However, combining several analytical techniques (XRPD, EDS/SEM, DSC/DTG and SR-μCT) constrains the mineralogical, chemical and morphological properties of lamellar and fibrous phases, thus confirming the mentioned fibrous minerals can be classified as asbestos. As regards fibrous but non-asbestos classified minerals, polygonal serpentine and magnesium-hornblende were also detected. Among the minerals classified as asbestos, chrysotile and tremolite were detected. Various factors affect fibre toxicity such as the size of the inhaled fibres and the potentially toxic elements they contain (Turci et al. 2017). Numerous studies have highlighted that length is a key factor in the pathogenicity of mineral asbestos. More specifically, fibres longer than 5 μm in length have been found to increase the risk of developing asbestos-related lung disease (Mossman and Pugnaloni 2017). Most of the chrysotile and tremolite fibres analysed in this study exceeded 5 μm in length. Moreover, chrysotile and tremolite asbestos contain potentially toxic elements such as Fe, Cr and Ni as minor elements in their crystalline structure and therefore pose a significant threat to human health. It has been demonstrated that asbestos toxicity may depend on the heavy metal content (i.e., Fe, Ni, Cr) as catalysts of the Fenton reaction leading to the creation of free radicals and reactive oxygen species (ROS) (Dixon et al. 1970; Nemery, 1990; Wei et al. 2014; Turci et al. 2017). The relatively high concentrations of these metals in the chrysotile and tremolite asbestos samples analysed is in agreement with the literature data, which show that the detected metals (Fe, Cr, Ni) are often present in concentrations over 1000 ppm (Bloise et al. 2016;

Table 3 Three representative EDS/SEM analyses point of chrysotile fibres from four samples, normalized oxide weight percent and cation number calculated on the basis of seven oxygens, Fe is considered as Fe^{2+}

Samples	VG1			VG2			VM2			CA1		
Oxide wt%	Ctl	Ctl	Ctl	Ctl	Ctl	Ctl	Ctl	Ctl	Ctl	Ctl	Ctl	Ctl
SiO_2	44.61	44.63	44.96	44.01	42.14	43.83	47.34	43.17	44.5	44.97	42.15	44.66
Al_2O_3	2.49	4.71	3.17	4.97	4.10	4.28	2.83	4.69	2.51	3.15	4.00	2.46
MgO	44.58	46.85	46.27	45.48	42.12	42.66	44.32	44.29	44.47	46.29	42.13	44.63
FeO	4.40	3.81	2.68	3.76	7.34	5.55	5.51	4.80	4.60	2.67	7.36	4.33
CaO	2.26	0.00	2.92	1.78	2.05	1.98	0.00	1.65	2.24	2.92	2.09	2.23
Cr_2O_3	0.28	0.00	0.00	0.00	0.00	0.00	0.00	0.00	0.29	0.00	0.00	0.29
NiO	1.38	0.00	0.00	0.00	2.25	1.70	0.00	1.40	1.39	0.00	2.27	1.40
CATIONS calculated on the basis of 7 oxygens												
Si	1.86	1.83	1.85	1.82	1.79	1.84	1.95	1.80	1.86	1.85	1.80	1.86
Al	0.12	0.23	0.15	0.24	0.21	0.21	0.14	0.23	0.12	0.15	0.20	0.12
Mg	2.77	2.87	2.84	2.80	2.67	2.67	2.72	2.76	2.77	2.84	2.67	2.78
Fe^{2+}	0.15	0.13	0.09	0.13	0.26	0.20	0.19	0.17	0.16	0.09	0.26	0.15
Ca	0.00	0.00	0.13	0.08	0.09	0.09	0.00	0.07	0.10	0.13	0.10	0.10
Cr	0.01	0.00	0.00	0.00	0.00	0.00	0.00	0.00	0.01	0.00	0.00	0.01
Ni	0.05	0.00	0.00	0.00	0.08	0.06	0.00	0.05	0.05	0.00	0.08	0.05
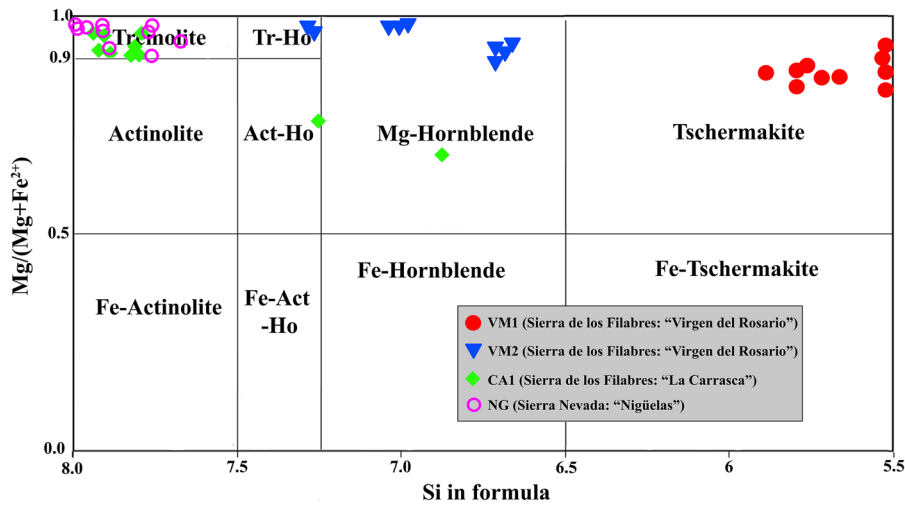
Fig. 9 Amphibole diagram classification (after Leake et al. 1997)

2020b) in these two types of asbestos. It is also important to note that these toxic elements can be mobilized, spread into various terrestrial environments and enter the human body. Indeed, due to its co-occurrence with toxic metals, asbestos is known to introduce metals into soil, water and air systems thus posing a threat to human health (Gwenzi 2019; Mistikawy et al. 2020). Another aspect to consider is

that when released into the environment, both types of fibres can travel considerable distance due to their aerodynamic features (Kohyama 1989). The long distances fibres can travel reveal the potential for non-occupational human exposure which can pose a threat to human health far from the quarry of origin. However, if these rocks are not disturbed by human activities (e.g. road construction, excavations), fibres

Table 4 Representative EDS/SEM analyses of tremolite fibres (CA1 and NG samples), normalized oxide weight percent and cation number calculated on the basis of 23 oxygens

| Samples	CA1_Tremolite							NG_Tremolite										
MgO	25.55	22.32	25.96	25.69	24.65	24.03	23.84	24.25	23.84	24.99	24.92	23.89	27.01	25.84	25.62	22.88	22.53	26.57
Al_2O_3	1.22	2.26	0.29	0.25	1.00	0.32	0.01	2.20	0.74	1.06	1.30	0.54	2.48	2.30	2.08	2.02	2.02	0.48
SiO_2	60.00	58.79	60.68	59.00	60.32	58.82	59.24	60.19	60.00	60.02	60.09	60.99	59.08	58.02	58.62	59.79	58.45	61.08
CaO	10.98	11.76	11.44	11.9	9.83	12.01	11.93	11.53	13.48	11.62	12.06	12.75	9.91	11.02	12.03	11.76	12.76	9.99
Cr_2O_3	0.00	0.56	0.00	0.00	0.00	0.00	0.00	0.00	0.00	0.00	0.00	0.00	0.00	0.00	0.00	0.00	0.00	0.00
FeO	2.25	3.87	1.63	3.16	4.20	4.82	4.98	1.83	1.93	2.31	1.63	1.83	1.52	2.82	1.65	3.55	4.24	1.88
Na_2O	0.00	0.44	0.00	0.00	0.00	0.00	0.00	0.00	0.00	0.00	0.00	0.00	0.00	0.00	0.00	0.00	0.00	0.00
Mg	5.01	4.42	5.09	5.08	4.83	5.08	4.72	4.75	4.71	4.91	4.89	4.69	5.28	5.09	5.05	4.50	4.46	5.15
Al^{3+}	0.11	0.20	0.02	0.04	0.07	0.05	0.002	0.09	0.04	0.09	0.08	0.01	0.25	0.33	0.25	0.11	0.23	0.003
Si	7.90	7.80	7.98	7.82	7.93	7.82	7.87	7.91	7.96	7.91	7.92	8.04	7.75	7.67	7.75	7.89	7.76	7.95
Ca	1.55	1.67	1.61	1.70	1.39	1.71	1.70	1.62	1.92	1.64	1.70	1.8	1.39	1.56	1.70	1.66	1.82	1.40
Cr	0.00	0.06	0.00	0.00	0.00	0.00	0.00	0.00	0.00	0.00	0.00	0.00	0.00	0.00	0.00	0.00	0.00	0.00
Fe^{2+}	0.25	0.43	0.18	0.35	0.46	0.54	0.50	0.20	0.14	0.26	0.18	0.20	0.17	0.31	0.18	0.39	0.47	0.21
Na	0.00	0.11	0.00	0.00	0.00	0.00	0.00	0.00	0.00	0.00	0.00	0.00	0.00	0.00	0.00	0.00	0.00	0.00
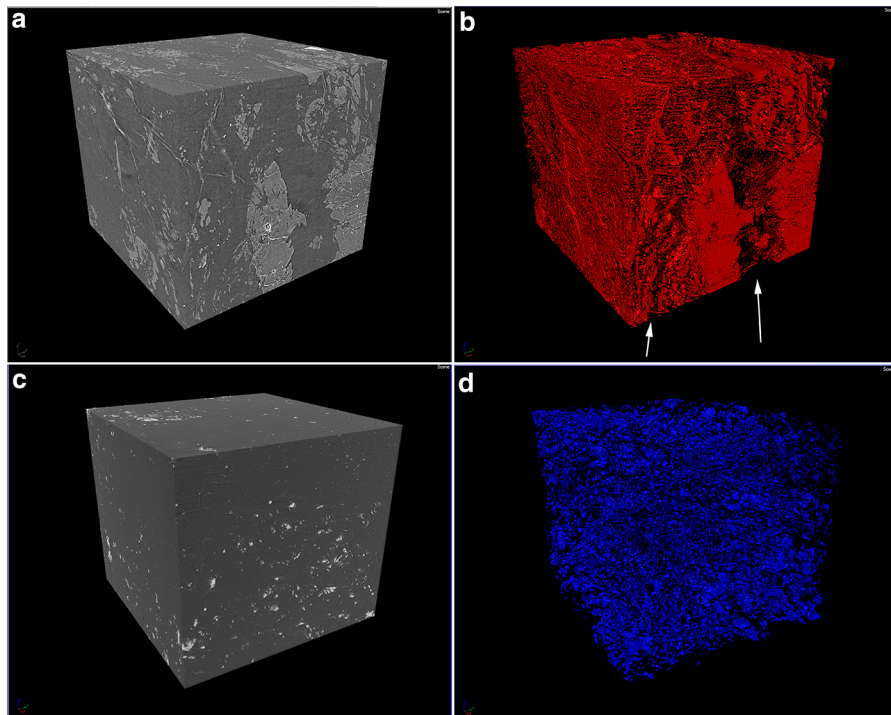
Fig. 10 Left column: Volume renderings of extracted VOIs from samples CA1 (**a**, **b**-5.24 mm³) and CA2 (**c**, **d**-5,67mm³). Right column: corresponding segmented veins/pore phase. The white arrows indicate the veins/voids

are unlikely to become airborne and would therefore not endanger human health. But, rocks can also be disturbed by natural events such as natural weathering processes, earthquakes and by human-caused disasters (Perkins et al. 2007; Kashimura et al. 2015). In this perspective, the voluntary closure of Nigüelas quarry by its owners is a good example of the synergy between asbestos risk assessment by scientists and employers' responsibility for the health and safety of their workers. In our opinion, stone monuments or artefacts built with the rocks extracted from the quarries of Barranco de San Juan, Nigüelas, Virgen del Rosario and La Carrasca are not going to release fibres into the environment for the following reasons: (1) monuments are usually treated with protective encapsulating coatings; (2) stone artefacts are not generally exposed to weathering because they are kept inside buildings (i.e. church altars, columns and holy water fonts) (e.g. Navarro et al. 2015; 2018). However, it is good practise to monitor the state of conservation of monuments and artefacts built with these materials to restore them if they appear damaged or weathered since fractures filled with fibrous minerals can act as weakness planes and cause the breakage of the stones,

with unexpected consequences (Navarro et al. 2018; Yoon et al. 2020; Erskine 2020).

Conclusion

In this study, seven serpentinite blocks from different quarries were investigated in order to determine the presence of natural occurrence of asbestos. XRPD, DSC/DTG, SEM/EDS and SR-µCT methods were successfully used to identify asbestos hosted in complex serpentinite multi-phase samples. The identified asbestos minerals are tremolite and chrysotile. The results obtained by comparing the data obtained reveal that five out of seven samples contain potentially harmful fibres, tremolite was only found in two samples (CA1 and NG), while chrysotile was detected in four samples (CA1, VM2, VG2, VG1). This study highlights asbestos occurrence in the following quarries: Barranco de San Juan (Granada) and Nigüelas (Granada). The Virgen del Rosario and La Carrasca quarries were only partially contaminated by asbestos as two of the samples (VM1 and CA2) did not contain any asbestos. However, sample CA1 (extracted from

La Carrasca-quarry) proved to be the most harmful to human health due to the concomitant presence of chrysotile and tremolite asbestos. These differences observed in the La Carrasca quarry may be due to the diverse geochemical/petrological processes involved in asbestos formation. Therefore, workers should take appropriate safety precautions when extracting rocks from quarries. In this regard, any further extension to the operation of the quarries requires detailed mineralogical studies, aimed at minimizing the risk of asbestos exposure. In conclusion, the results of this study could be used to define a sampling plan for identifying asbestos-contaminated land near quarries. Moreover, the analytical approach employed could attract much interest due to the abundance of ophiolite outcrops worldwide.

Availability of data and materials All the raw data and material used for this research are available at the University of Calabria and University of Catania for request.

Compliance with ethical standards

Conflict of interest The authors declares that there is no conflict of interest.

Ethical Human Participants and/or Animals Not applicable, no human participants and/or animals were used in this research.

References

Acosta, A., Pereira, M. D., Shaw, D. M., & Bea, F. (1997). Serpentinización de la peridotita de Ronda (cordillera Betica) comorespuesta a la interacción con fluidos ricos en volátiles: comportamiento del boro. *Revista de la Sociedad Geológica de España, 10,* 99–106.

Agudo, A., Gonzáles, C. A., Bleda, M. J., Ramírez, J., Hernández, S., López, F., et al. (2000). Occupation and risk of malignant pleural mesothelioma: A case-control study in Spain. *American Journal of Industrial Medicine, 37*(2), 159–168. https://doi.org/10.1002/(sici)1097-0274(200002)37:2%3c159::aid-ajim1%3e3.0.co;2-0.

Baker, D. R., Mancini, L., Polacci, M., Higgins, M. D., Gualda, G. A. R., Hill, R. J., et al. (2012). An introduction to the application of x-ray microtomography to the three-dimensional study of igneous rocks. *Lithos, 148,* 262–276.

Ballirano, P., Bloise, A., Cremisini, C., Nardi, E., Montereali, M. R., & Pacella, A. (2018b). Thermally induced behavior of the K-exchanged erionite: a further step in understanding the structural modifications of the erionite group upon heating. *Periodico di Mineralogia, 87,* 123–134.

Ballirano, P., Bloise, A., Gualtieri, A. F., Lezzerini, M., Pacella, A., Perchiazzi, N., et al. (2017). The Crystal Structure of Mineral Fibers. In A. F. Gualtieri (Ed.), *Mineral fibers: Crystalchemistry, chemical-physical properties, biological interaction and toxicity* (pp. 17–53). London, UK: Mineralogical Society of Great Britain and Ireland.

Ballirano, P., Pacella, A., Bloise, A., Giordani, M., & Mattioli, M. (2018a). Thermal stability of woolly erionite-K and considerations about the heat-induced behaviour of the erionite group. *Minerals, 8,* 28.

Baumann, F., Buck, B. J., Metcalf, R. V., McLaurin, B. T., Merkler, D. J., & Carbone, M. (2015). The presence of asbestos in the natural environment is likely related to mesothelioma in young individuals and women from Southern Nevada. *Journal of Thoracic Oncology, 10*(5), 731–737.

Bellomo, D., Gargano, C., Guercio, A., Punturo, R., & Rimoldi, B. (2018). Workers' risks in asbestos contaminated natural sites. *Journal of Mediterranean Earth Science, 10,* 97–106.

Belluso, E., Baronnet, A., & Capella, S. (2020). Naturally occurring asbestiform minerals in italian western alps and in other Italian sites. *Environmental & Engineering Geoscience, 26*(1), 39–46.

Belluso, E., Cavallo, A., & Halterman, D. (2017). Crystal habit of mineral fibres. In A. F. Gualtieri (Ed.), *Mineral fibers: Crystal chemistry, chemical-physical properties, biological interaction and toxicity* (pp. 65–109). London: European Mineralogical Union.

Berk, S., Yalcin, H., Dogan, O. T., Epozturk, K., Akkurt, I., & Seyfikli, Z. (2014). The assessment of the malignant mesothelioma cases and environmental asbestos exposure in Sivas province Turkey. *Environmental geochemistry and health, 36*(1), 55–64.

Bernstein, D., & Pavlisko, E. N. (2017). Differential pathological response and pleural transport of mineral fibres. In A. Sisko & B. Paolo (Eds.), *Mineral fibres: crystal chemistry, chemical-physical properties biological interaction and toxicity: European Mineralogical Union and the*

Mineralogical Society of Great Britain & Ireland (pp. 417–434). Berlin: Springer.

Bloise, A., Barca, D., Gualtieri, A. F., Pollastri, S., & Belluso, E. (2016). Trace elements in hazardous mineral fibres. *Environmental Pollution, 216,* 314–323.

Bloise, A., Belluso, E., Critelli, T., Catalano, M., Apollaro, C., Miriello, D., & Barrese, E. (2012). Amphibole asbestos and other fibrous minerals in the meta-basalt of the Gimigliano-Mount Reventino Unit (Calabria, south-Italy). *Rendiconti Online della Società Geologica Italiana, 21,* 847–848.

Bloise, A., Kusiorowski, R., Lassinantti Gualtieri, M., & Gualtieri, A. F. (2017). Thermal behaviour of mineral fibers. In A. F. Gualtieri (Ed.), *Mineral fibers: crystal-chemistry, chemical-physical properties, biological interaction and toxicity* (pp. 215–252). London: Mineralogical Society of Great Britain and Ireland.

Bloise, A., Ricchiuti, C., Lanzafame, G., & Punturo, R. (2020a). X-ray synchrotron microtomography: a new technique for characterizing chrysotile asbestos. *Science of the Total Environment, 703,* 135675.

Bloise, A., Ricchiuti, C., Punturo, R., & Pereira, D. (2020b). Potentially toxic elements (PTEs) associated with asbestos chrysotile, tremolite and actinolite in the Calabria region (Italy). *Chemical Geology, 558,* 119896.

Brun, F., Massimi, L., Fratini, M., Dreossi, D., Billé, F., Accardo, A., et al. (2017). SYRMEP tomo project: a graphical user interface for customizing CT recon-struction workflows. *Advanced Structural and Chemical Imaging, 3*(1), 4.

Cagnard, F., & Lahondère, D. (2020). Naturally Occurring Asbestos in France: Geological Mapping, Mineral Characterization, and Technical Developments. *Environmental & Engineering Geoscience, 26*(1), 53–59.

Caicedo, M., Jacobs, J. J., Reddy, A., & Hallab, N. J. (2007). Analysis of metal ion-induced DNA damage, apoptosis, and necrosis in human (Jurkat) T-cells demonstrates Ni2+ and V3+ are more toxic than other metals: Al3+, Be2+, Co2+, Cr3+, Cu2+, Fe3+, Mo5+, Nb5+, Zr2+. *Journal of Biomedical Materials Research Part A, 36,* 905–913.

Case, B. W., Marinaccio, A., & Gualtieri, A. F. (2017). *Epidemiological approaches to health effects of mineral fibres: Development of knowledge and current practice* (pp. 376–406). Mineral Fibers: Crystal Chemistry, Chemical-Physical Properties, Biological Interaction and Toxicity.

Chen, L., Yang, X., Jiao, H., & Zhao, B. (2003). Tea catechins protect against lead-induced ROS formation, mitochondrial dysfunction, and calcium dysregulation in PC12 cells. *Chemical Research in Toxicology, 16,* 1155–1161.

Cloetens, P., Pateyron-Salome, M., Buffiére, J. Y., Peix, G., Baruchel, J., Peyrin, F., et al. (1997). Observation of microstructure and damage in materials by phase sensitive radiography and tomography. *Journal of Applied Physics, 81,* 5878. https://doi.org/10.1063/1.364374.

Colombino, E., Capella, S., Casalinuovo, F., Racco, R., Pruiti, F., Volante, M., et al. (2019). Malignant peritoneal mesothelioma in a boar who lived in Calabria (Italy): Wild animal as sentinel system of human health. *Science of the Total Environment, 683,* 267–274.

Constantopoulos, S. H. (2008). Environmental mesothelioma associated with tremolite asbestos: Lessons from the experiences of turkey, greece, corsica, new caledonia and cyprus. *Regulatory Toxicology and Pharmacology, 52,* S110–S115.

Pugnaloni, A., Giantomassi, F., Lucarini, G., Capella, S., Bloise, A., Di Primio, R., & Belluso, E. (2013). Cytotoxicity induced by exposure to natural and synthetic tremolite asbestos: An in vitro pilot study. *Acta histochemical, 115,* 100–112. https://doi.org/10.1016/j.acthis.2012.04.004.

Dixon, J. R., Lowe, D. B., Richards, D. E., Cralley, L. J., & Stokinger, H. E. (1970). The role of trace metals in chemical carcinogenesis: asbestos cancers. *Cancer Research, 30,* 1068–1074.

Erskine, B. G. (2020). Geologic investigations for compliance with the CARB asbestos ATCM. *Environmental & Engineering Geoscience, 26*(1), 99–106.

Fernández-Navarro, P., García-Péreza, J., Ramisa, R., Boldo, E., & López-Abentea, G. (2012). Proximity to mining industry and cancer mortality. *Science of the Total Environment, 435–436*(10), 66–73. https://doi.org/10.1016/j.scitotenv.2012.07.019.

Földvári, M. (2011). Handbook of thermogravimetric system of minerals and its use in geological practice. In T. Fancsik (Ed.), *Occasional papers of the Geological Institute of Hungary*. Budapest: Geological Institute of Hungary.

Gaggero, L., Sanguineti, E., Yus González, A., Militello, G. M., Scuderi, A., & Parisi, G. (2017). Airborne asbestos fibres monitoring in tunnel excavation. *Journal of Environmental Management, 196,* 583–593.

Gross, P., DeTreville, R. T., Tolker, E. B., Kaschak, M., & Babyak, M. A. (1969). The pulmonary macrophage response to irritants: an attempt at quantitation. *Archives of Environmental and Occupational Health, 18,* 174–185.

Gualtieri, A. F. (2017). Introduction. In A. F. Gualtieri (Ed.), *Mineral fibers: crystalchemistry, chemical-physical properties, biological interaction and toxicity* (pp. 1–15). London, UK: Mineralogical Society of Great Britain and Ireland.

Gualtieri, A. F. (2018). Towards a quantitative model to predict the toxicity/pathogenicity potential of mineral fibers. *Toxicology and applied pharmacology, 361,* 89–98.

Gunter, M. E. (2018). Elongate mineral particles in the natural environment. *Toxicology and Applied Pharmacology, 361,* 57–164.

Gwenzi, W. (2019). Occurrence, behaviour, and human exposure pathways and health risks of toxic geogenic contaminants in serpentinitic ultramafic geological environments (SUGEs): A medical geology perspective. *Science of The Total Environment, 15,* 700.

Hardy, J. A., & Aust, A. E. (1995). Iron in asbestos chemistry and carcinogenicity. *Chemical Reviews, 95,* 97–118.

Harper, M. (2008). 10th Anniversary critical review: naturally occurring asbestos. *Journal of Environmental Monitoring, 10,* 1394–1408.

Hawthorne, F. C., Oberti, R., Della Ventura, G., & Mottana, A. (2007). Amphiboles: Crystal chemistry, occurrence and health issues. In F. C. Hawthorne, R. Oberti, G. Della Ventura, & A. Mottana (Eds.), *Reviews in Mineralogy and Geochemistry*. VA: Mineralogical Society of America and Geochemical Society.

Herman, G. T. (1980). *Fundamentals of computerized tomography. Image reconstruction from projections*. London: Springer-Verlag.

Horie, M., Nishio, K., Fujita, K., Kato, H., Nakamura, A., Kinugasa, S., et al. (2009). Ultrafine NiO particles induce cytotoxicity in vitro by cellular uptake and subsequent Ni(II) release. *Chemical Research in Toxicology., 22,* 1415–1426.

IARC Working Group on the Evaluation of Carcinogenic Risk to Humans, (2012). IARC Monographs on the Evaluation of Carcinogenic Risks to Humans, No. 100C. Lyon: International Agency for Research on Cancer.

Jomova, K., & Valko, M. (2011). Advances in metal-induced oxidative stress and human disease. *Toxicology, 283,* 65–87.

Kamp, D. W. (2009). Asbestos-induced lung diseases: an update. *Translational Research, 153*(4), 143–152.

Kashimura, K., Yamaguchi, T., Sato, M., Yoneda, S., Kishima, T., Horikoshi, S., et al. (2015). Rapid transformation of asbestos into harmless waste by a microwave rotary furnace: Application of microwave heating to rubble processing of the 2011 Tohoku earthquake. *Journal of Hazardous, Toxic & Radioactive Waste, 19,* 04014041–04014048.

Kazan-Allen, L, (2005). Asbestos and mesothelioma: Worldwide trends. Lung Cancer, 49S1, S3-S8.

Kohyama, N. (1989). Airborne asbestos levels in non-occupational environments in Japan. *IARC Scientific Publication, 90,* 262–276.

Lanzafame, G., Casetta, F., Giacomoni, P. P., Donato, S., Mancini, l., Coltorti, M., , et al. (2020). The Skaros effusive sequence at Santorini (Greece): Petrological and geochemical constraints on an interplinian cycle. *Lithos, 362–363,* 105504. https://doi.org/10.1016/j.lithos.2020.105504.

Leake, B. E., Wolley, A., Arps, C. E. S., Birch, W., Gilbert, C. M., Grice, J. D., et al. (1997). Nomenclature of amphiboles: report of the subcommittee on amphiboles of the international mineralogical association, commission on new minerals and mineral names. *The Canadian Mineralogist, 35,* 219–246.

López-Abente, G., Hernández-Barrera, V., Pollán, M., Aragonés, N., & Pérez-Gómez, B. (2005). Municipal pleural cancer mortality in Spain. *Occupational and Environmental Medicine, 62,* 195–199. https://doi.org/10.1136/oem.2004.015743.

Maire, E., & Withers, P. J. (2014). Quantitative X-ray tomography. *International Materials Reviews, 59,* 1–43.

Martín-Algarra, A.C., Alonso-Chaves, F.M., Andreo, B., Azañón, J.M., Balanyá, J.C., Booth-Rea, G., et al. (2004). Zonas Internas Béticas. In J.A. Vera (Ed.), Geología de España (pp. 395–444). Madrid, Spain: Sociedad Geológica de España (S.G.E.)-Instituto Geológico y Minero de España (I.G.M.E.).

Militello, G. M., Bloise, A., Gaggero, L., Lanzafame, G., & Punturo, R. (2019). Multi-analytical approach for asbestos minerals and their non-asbestiform analogues: Inferences from host rock textural constraints. *Fibers, 7,* 42. https://doi.org/10.3390/fib7050042.

Mistikawy, J. A., Mackowiak, T. J., Butler, M. J., Mischenko, I. C., Cernak, R. S., & Richardson, J. B. (2020). Chromium, manganese, nickel, and cobalt mobility and bioavailability from mafic-to-ultramafic mine spoil weathering in western Massachusetts, USA. *Environmental Geochemistry & Health, 42,* 1–17.

Mossman, B. T., & Marsh, J. P. (1989). Evidence supporting a role for active oxygen species in asbestos-induced toxicity and lung disease. *Environmental Health Perspectives, 81,* 91–94.

Mossman, B. T., & Pugnaloni, A. (2017). In vitro biological activity and mechanisms of lung and pleural cancers induced by mineral fibres. In A. F. Gualtieri (Ed.), *Mineral Fibers: Crystal Chemistry, Chemical-Physical Properties, Biological Interaction and Toxicity* (pp. 261–306). London, UK: European Mineralogical Union.

Navarro, R., Pereira, D., Gimeno, A., & Del Barrio, S. (2018). Influence of natural carbonation process in serpentinites used as construction and building materials. *Construction & Building Materials, 170,* 537–546. https://doi.org/10.1016/j.conbuildmat.2018.03.100.

Navarro, R., Pereira, D., Rodríguez-Navarro, C., & Sebastian-Pardo, E. (2015). The Sierra Nevada serpentinites: the serpentinites most used in Spanish heritage buildings. In D. Pereira, B. Marker, S. Kramar, B. Cooper, & B. Schouenborg (Eds.), *Global heritage stone: towards international recognition of building and ornamental stones*. London: Geological Society.

Nemery, B. (1990). Metal toxicity and the respiratory tract. *European Respiratory Journal, 3,* 202–219.

Pacella, A., Andreozzi, G. B., & Fournier, J. (2010). Detailed crystal chemistry and iron topochemistry of asbestos occurring in its natural setting: A first step to understanding its chemical reactivity. *Chemical Geology, 277*(3–4), 197–206.

Paganin, D., Mayo, S. C., Gureyev, T. E., Miller, P. R., & Wilkins, S. W. (2002). Simultaneous phase and amplitude extraction from a single defocused image of a homogeneous object. *Journal of Microscopy, 206,* 33–40.

Pavlisko, E. N., & Sporn, T. A. (2014). Mesothelioma. In T. D. Oury, T. A. Sporn, & V. L. Roggli (Eds.), *Pathology of asbestos-associated disease* (pp. 81–140). Berlin, Heidelberg: Springer-Verlag.

Pereira, D. (2012). A report on serpentinites in the context of heritage stone resources. *Episodes, 35*(4), 478–480.

Pereira, M. D., Blanco, J. A., & Peinado, M. (2013). Study on Serpentinites and the consequence of the misuse of natural stone in buildings for construction. *Journal of Materials in Civil Engineering, 25*(10), 1563–1567. https://doi.org/10.1061/(ASCE)MT.1943-5533.0000689.

Perkins, R. A., Hargesheimer, J., & Fourie, W. (2007). Asbestos release from whole building demolition of buildings with asbestos-containing material. *Journal of Occupational and Environmental Hygiene, 4,* 889–894.

Pierdzig, S. (2019). Regulations concerning naturally occurring asbestos (NOA) in Germany—testing procedures for asbestos. *Environmental & Engineering Geoscience, 26*(1), 67–71.

Puga, E., Fanning, M., Díaz de Federico, A., Nieto, J. M., Beccaluva, L., Bianchini, G., et al. (2011). Petrology, geochemistry and U-Pb geochronology of the Betic Ophiolites: Inferences for pangaea break-up and birth of

the westernmost Tethys Ocean. *Lithos, 124*(3–4), 255–272. https://doi.org/10.1016/j.lithos.2011.01.002.

Punturo, R., Cirrincione, R., Pappalardo, G., Mineo, S., Fazio, E., & Bloise, A. (2018). Preliminary laboratory characterization of serpentinite rocks from Calabria (southern Italy) employed as stone material. *Journal of Mediterranean Earth Science, 10,* 79–87.

Punturo, R., Ricchiuti, C., Rizzo, M., & Marrocchino, E. (2019). Mineralogical and microstructural features of namibia marbles: insights about tremolite related to natural asbestos occurrences. *Fibers, 7,* 31.

Ross, M., & Nolan, R. P. (2003). History of asbestos discovery and use and asbestos-related disease in context with the occurrence of asbestos within ophiolite complexes. *Geological Society of America Special paper, 373,* 447–470.

Sanz de Galdeano, C., & López Garrido, A. C. (2016). The Nevado-Filábride Complex in the western part of Sierra de los Filabres (Betic Internal Zone) structure and lithologic succession. *Boletìn Gològico y Minero, 127*(4), 823–836.

Schindelin, J., Arganda-Carreras, I., Frise, E., Kaynig, V., Longair, M., Pietzsch, T., et al. (2012). Fiji: an open-source platform for biological-image analysis. *Nature Methods, 9*(7), 676–682.

Schoonen, M. A., Cohn, C. A., Roemer, E., Laffers, R., Simon, S. R., & O'Riordan, T. (2006). Mineral-induced formation of reactive oxygen species. *Reviews in mineralogy and geochemistry, 64*(1), 179–221.

Schreier, H., Northcote, T. G., & Hall, K. (1987). Trace metals in fish exposed to asbestos rich sediments. *Water, Air and Soil Pollution, 35*(3–4), 279–291.

Stroink, G., Blaauw, C., White, C. G., & Leiper, W. (1980). Mössbauer characteristics of UICC standard reference asbestos samples. *Canadian Mineralogist, 18,* 285–290.

Turci, F., Tomatis, M., & Pacella, A. (2017). Surface and bulk properties of mineral fibres relevant to toxicity. In A. F. Gualtieri (Ed.), *Mineral Fibers: Crystal Chemistry, Chemical-Physical Properties, Biological Interaction and Toxicity* (pp. 171–214). London, UK: European Mineralogical Union.

Vanoeteren, C., Cornelis, R., & Sabbioni, E. (1986). *Critical Evaluation of Normal Levels of Major and Trace Elements in Human Lung Tissue*. Luxembourg: Commission of the European Communities.

Vignaroli, G., Ballirano, P., Belardi, G., & Rossetti, F. (2014). Asbestos fibre identification vs evaluation of asbestos hazard in ophiolitic rock mélanges, a case study from the Ligurian Alps (Italy). *Environmental Earth Sciences, 72*(9), 3679–3698.

Viti, C. (2010). Serpentine minerals discrimination by thermal analysis. *American Mineralogist, 95*(4), 631–638.

Wei, B., Yang, L., Zhu, O., Yu, J., & Jia, X. (2014). Multivariate analysis of trace elements distribution in hair of pleural plaques patients and health group in a rural area from China. *Hair Therapy & Transplantation, 4,* 2167–3118.

Whitney, D., & Evans, B. W. (2010). Abbreviations for names of rock-forming minerals. *American Mineralogist, 95*(1), 185–187.

WHO. (1997). *Determination of airborne fibre number concentrations; a recommended method, by phase contrast optical microscopy*. Geneva, Switzerland: World Health Organization.

Yoon, S., Yeom, K., Kim, Y., Park, B., Park, J., Kim, H., et al. (2019). Management of naturally occurring asbestos area in Republic of Korea. *Environmental & Engineering Geoscience, 26*(1), 79–87.

Hazardous Elements in Asbestos Tremolite from the Basilicata Region, Southern Italy: A First Step

Claudia Ricchiuti [1] [iD], Dolores Pereira [2,3] [iD], Rosalda Punturo [1], Eugenia Giorno [4], Domenico Miriello [5] [iD] and Andrea Bloise [5,*] [iD]

1 Department of Biological, Geological and Environmental Sciences, University of Catania, 95129 Catania, Italy; claudia.ricchiuti@unict.it (C.R.); punturo@unict.it (R.P.)
2 CHARROCK Research Group, University of Salamanca, Plaza de los Caídos s/n, 37008 Salamanca, Spain; mdp@usal.es
3 Geology Department, Science Faculty, University of Salamanca, Plaza Merced s/n, 37008 Salamanca, Spain
4 MAT-INLAB-Department of Chemistry and Chemical Technologies, University of Calabria, 87036 Rende, CS, Italy; eugenia.giorno@unical.it
5 Department of Biology, Ecology and Earth Sciences (DiBest), University of Calabria, 87036 Rende, CS, Italy; domenico.miriello@unical.it
* Correspondence: andrea.bloise@unical.it

Abstract: In this paper, we report the quantification of potentially toxic elements (PTEs) hosted into two tremolite asbestos from Episcopia and San Severino Lucano villages (Basilicata region, Southern Italy). Micro X-ray fluorescence and Inductively Coupled Plasma spectroscopy with Optical Emission Spectrometry techniques were used to quantify the concentration of major, minor (Si, Mg, Ca, Al, Fe, Mn) and trace elements (As, Ba, Cd, Co, Cr, Cu, Li, Mo, Ni, Pb, Sb, Sn Sr, Ti, Te, V, W, Zn, Zr), with the aim of providing available data useful for the determination of the asbestos fibers toxicity. Results show that in the two studied samples there exist high concentrations of Fe, Mn, Cr and Ni which could lead to the high toxicity of the mineral fibers. By considering the pseudo-total PTEs amounts in each tremolite asbestos, it is possible to affirm that one of the samples is more enriched in toxic elements than the other one (3572 ppm versus 1384 ppm). These PTEs can represent a source of risk to human health since they may be transported away from the geological outcrops, through asbestos in the air, water and soils and thus encountering the human body.

Keywords: potentially toxic elements; tremolite asbestos; trace elements; Basilicata region; southern Italy

1. Introduction

"Asbestos" is a commercial term that includes six fibrous silicate minerals. The Italian law established that chrysotile, actinolite, tremolite, amosite, anthophyllite and crocidolite were included under the definition of asbestos (i.e., regulated asbestos) [1]. Epidemiological studies proved that the development of pathologies, such as malignant mesothelioma and lung cancer, is often linked to occupational or environmental exposure to asbestos [2]. Although many countries have banned the use and marketing of asbestos [3], the environmental exposure of populations still represents an unsolved concern. In addition to asbestos-containing materials (ACMs) that, if not properly handled, release fibers into the atmosphere, the natural occurrence of asbestos (NOA) represents an important source of fibers dispersion. The global territory is interested in the widespread presence of NOA outcrops (e.g., USA, Canada, India, China, Italy, Spain) [4,5] that may be disturbed by natural weathering processes (e.g., erosion) or by human activities (e.g., road construction, excavation, agricultural activities) and release dust containing respirable fibers into the atmosphere [6]. The risks to human health are represented by the potential inhalation of the fibers that become airborne. Depending on their size, the fibers can penetrate deeply into

the lung alveoli and can no longer be eliminated [7]. Once inhaled, the fibers are in contact with body fluids, which promote their physical–chemical transformation. Depending on parameters such as bio durability and bio persistence, biological reactions may require a shorter or longer time. For instance, it was demonstrated that chrysotile is less bio durable than amphibole asbestos, as well as the retention (bio persistence) of amphiboles in the lung, is higher than chrysotile [8].

To date, it is not completely understood the mechanism by which these fibers induce adverse effects on human health as well as on the environment. Major difficulties in understanding arise from the wide variability of the size, bio durability, molecular arrangement, surface reactivity and chemistry of asbestos fibers [8].

However, it is accepted by the scientific community that, in addition to many other interacting factors, the potentially toxic elements (PTEs) content may contribute to increasing the toxic potential of those fibers which have a high dissolution rate [8]. For instance, Dixon et al. [9] present the results of an in vitro study relating to the effects of chrysotile asbestos and heavy metals on the BP hydroxylase system, supporting the hypothesis that trace metals play an active role in the induction of asbestos cancer while the passive role as the metal carrier is played by asbestos fibers. Moreover, epidemiological studies and experimental evidence, provide indications of the possible onset of lung cancer due to the action of heavy metals [10,11]. Asbestos minerals are capable to host PTEs (i.e., Fe, Cr, Ni, Mn, Co) [12,13], which can be released into the intracellular or extracellular environment during dissolution processes and induce lung cancer [14]. Literature studies, highlighted the importance of the quantification of toxic elements present in asbestos fiber structures since it can be considered an important factor that provides a contribution to the fibers toxicity [15,16]. For instance, it was proved that the presence of PTEs increase the risk of developing lung disease in animals and people that have been exposed to asbestos containing large amounts of Ni, Cr, Co, Cu and Mn [9,17,18], as well as other research, showed that, even in trace amounts, the presence of Fe and its structural coordination may induce cyto- and genotoxic effects, thus covering an important role in asbestos toxicity [19,20]. Recently Gualtieri [8], proposed a model on asbestos toxicity, based on parameters such as their physical/chemical and morphological characteristics and stating the importance of quantifying the PTEs present within asbestos. Considering that the presence of PTEs within the mineral structure are primary factors for pathological effects, the identification and quantification of PTEs bearing asbestos tremolite in the investigated area are of paramount relevance for modeling the reactivity of such fibers.

In this scenario, for the first time, this work aims to determine the PTEs concentration in tremolite asbestos from the Basilicata region (Southern Italy), using micro X-ray Fluorescence (μ-XRF) and Inductively Coupled Plasma spectroscopy with Optical Emission Spectrometry (ICP-OES).

2. Materials and Methods

In the present study, tremolite asbestos coming from serpentinite rocks cropping out in the surroundings of San Severino Lucano and Episcopia villages (Basilicata region, southern Italy), were investigated. The mineralogical characterization of the tremolite samples has already been carried out by our research group and published elsewhere [6,21]. More specifically, TR-EPS comes from the sample E10 [21] and TR-SSL comes from the sample S18 [6]. The sample E10 is characterized by the presence of tremolite and talc [21] whereas sample S18 mainly consists of tremolite and minor chrysotile and chlorite [6].

With the aim of avoiding the possible contamination by other mineral impurities, the collected samples: (i) asbestos tremolite from Episcopia village (sample TR_EPS) and (ii) asbestos tremolite from San Severino Lucano village (sample TR_SSL), were selected using binocular microscopy and then analyzed by μ-XRF and ICP-OES to determine the concentration of major, minor (Si, Mg, Ca, Fe, Al, Mn) and trace elements (As, Ba, Cd, Co, Cr, Cu, Li, Mo, Ni, Pb, Sb, Sn Sr, Ti, Te, V, W, Zn, Zr). It is worth specifying, that even though the manual removal of impurities under the microscope, it is not possible to

exclude the presence of nano-sized those ones and consequently their small contribution to the chemical composition, if any.

Micro-fluorescence energy dispersion (μ-XRF) was performed by using a Bruker M4 Tornado spectrometer, equipped with two X-ray tubes (Rh and W) and two SDD detectors, active area of 60 mm^2. The Rh tube has a polycapillary optic to concentrate the radiation in a spot <20 μm (Mo-Kα). Vacuum conditions (2 mbar) were applied for data acquisition, using Rh radiation with the generator operating at 50 kV and 150 μA, using two detectors to increase the intensity of the received signal. The acquisition time for each measurement was 60 s. An average of 60 spot analyses were performed on each sample and a double measurement of each point was executed with the aim of improving the element detection. The acquired spectra were processed with the software ESPRIT M4 v. 1.5.2.65 to obtain a semi-quantitative analysis expressed as wt% of major elements (oxides) and ppm for traces elements.

Inductively coupled plasma spectroscopy with Optical Emission Spectrometry (ICP-OES), Agilent 710 Technology, was used to determine the trace of elements in mineral asbestos fibers.

Using a microwave Milestone MLS Mega 1200 with HPR 1000/10 vessels, 100 mg of powder of sample were dissolved in a mixture of Merck "suprapur" quality acids, nitric acid (0.5 mL) and hydrofluoric acid (1.5 mL). After complete dissolution, a small amount of boric acid is added to the composition to neutralize samples before ICP-OES analysis. The calibration curve was prepared using the "multielement smart solutions" for As, B, Ba, Bi, Cd, Co, Cr, Cu, Li, Mo, Ni, Pb, Sb, Se, Sn, Sr, Ti, Tl, V, W, Zn, Zr. The instrumental limit of quantification considered (LOQ) for each element was determined with the white method, the values obtained correspond to those provided by the ISO-11885. All the measurements were performed in triplicate to ensure reproducibility.

3. Results

3.1. Major and Minor Elements

The micro-fluorescence energy-dispersive techniques (μ-XRF) allowed to measure the concentration of major and minor elements (Si, Mg, Ca, Fe, Al, Mn) as oxides, in both tremolite asbestos samples (Figure 1).
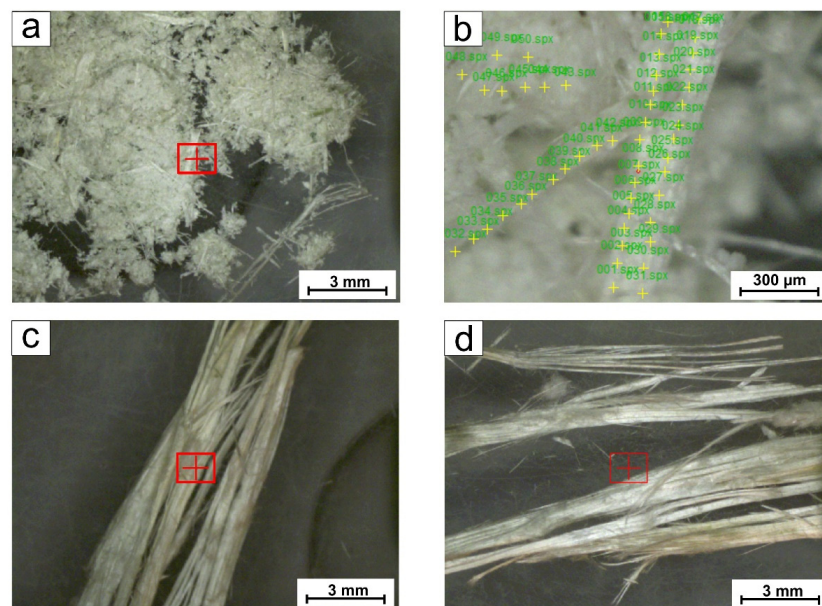

Figure 1. Micro X-ray fluorescence (μ-XRF) images of: (**a**,**b**) tremolite asbestos from Episcopia village (TR_EPS specimen), crosses are drawn to indicate the analysis points; (**c**,**d**) tremolite asbestos from San Severino Lucano village (TR_SSL specimen).

As for major elements, the data of TR_EPS specimen showed SiO_2 and MgO contents of 53.3 wt% and 26.0 wt%, respectively, and an amount of 16.8 wt% for CaO and 3.3 wt% for FeO (Figure 2a, Table 1).
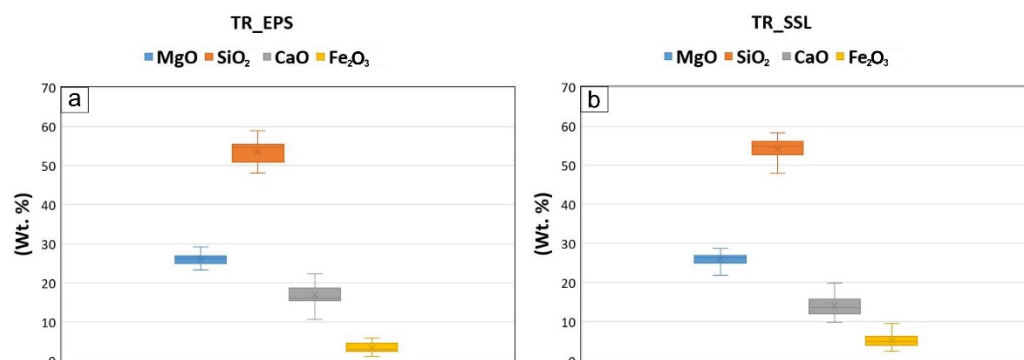

Figure 2. Box plots illustrating statistical parameters for major elements in: (**a**) tremolite asbestos from Episcopia (TR_EPS); and (**b**) tremolite asbestos from San Severino Lucano village (TR_SSL). Statistical parameters are based on 60 spot analyses. The range in contents is represented by the vertical lines, the median value is shown by the horizontal line inside the box, the cross indicates the mean values.

Table 1. Average values of major and minor element amounts (wt%) in the examined tremolite obtained by μ-XRF. TR_EPS = tremolite asbestos from Episcopia; TR_SSL = tremolite asbestos from San Severino Lucano.

(wt%)	TR_EPS	TR_SSL
MgO	26.00	26.10
SiO_2	53.32	54.12
CaO	16.80	14.12
FeO	3.33	5.20
Al_2O_3	0.32	0.35
MnO	0.23	0.11

Regarding the TR_SSL sample, results revealed SiO_2 and MgO values of 54.1 wt% and 26.1 wt% respectively, with a minor amount of CaO (14.1 wt%) and higher content of FeO (5.2 wt%) compared to those of TR_EPS (Figure 2b, Table 1). As for minor elements, data showed concentrations of Mn and Al_2O_3 >1000 ppm in both samples (Table 1). Specifically, the data showed Mn content of 0.23 wt% in TR_EPS and 0.11 wt% in TR_SSL and higher values of Al_2O_3: 0.32 wt% in TR_EPS and 0.35 wt% in TR_SSL (Table 1). These results are in agreement with those ones reported by literature, regarding the chemical composition of tremolite asbestos occurring in the surrounding of the study area [22–24].

3.2. Trace Elements

The concentrations of trace elements (As, Ba, Cd, Co, Cr, Cu, Li, Mo, Ni, Pb, Sb, Sn, Sr, Ti, Te, V, W, Zn, Zr) in the two studied samples revealed heterogeneous values (Table 2).

Particular attention was given to some heavy metals such as Cr, Ni, Co, V, As, Ti, Cu and Zn (Figure 3) since their impact on human health is well known [1,25]. Results revealed that Cr and Ni are the elements reaching the highest amounts in both the studied samples.

More specifically, TR_EPS is the sample characterized by a higher concentration of Cr (1120 ppm) and Ni (1830 ppm) than TR_SSL, in which the concentrations are 550 ppm (Cr) and 480 ppm (Ni). Similarly, Co and V as well as Ti and Cu show the higher amounts in TR_EPS, while As and Zn are found in higher concentrations in the TR_SSL sample (Figure 3). In particular, the TR_EPS sample showed 31.9 ppm of Co, 6.3 ppm of V, high level of Ti (430 ppm) and 23.2 ppm of Cu, while TR_SSL reveals values of 7.8 ppm (Co),

2.6 ppm (V), 92.9 ppm (Ti) and 17.8 ppm of Cu. The other heavy metals considered, such as As and Zn, occur in high amounts in the TR_SSL sample: As is present at a concentration of 7.9 ppm in TR_SSL and 3.2 ppm in TR_EPS while Zn is 37.7 ppm and 34.3 ppm in TR_EPS and TR_SSL respectively. Figure 4 shows the concentration (ppm) levels of the other trace elements detected in the studied samples such as Ba, Cd, Li, Mo, Sb, Sn, Sr, Te, W and Zr.

Table 2. Trace element concentrations (ppm) in the studied tremolite asbestos from Episcopia (TR_EPS) and San Severino Lucano villages (TR_SSL) obtained by ICP-OES.

(ppm)	TR_EPS	TR_SSL
As	3.20	7.90
Ba	1.10	16.50
Cd	1.11	9.90
Co	31.90	7.80
Cr	1120	550
Cu	23.20	17.80
Li	20.50	5.30
Mo	2.50	6.70
Ni	1830	480
Pb	11.50	20.50
Sb	15.10	11.20
Sn	20.50	51.70
Sr	1.50	16.10
Ti	430	92.90
Te	6.40	8.80
V	6.30	2.60
W	6.30	8.80
Zn	34.30	37.70
Zr	7.20	32.20
Σ_{TOT}	3573	1384

Figure 3. *Cont.*
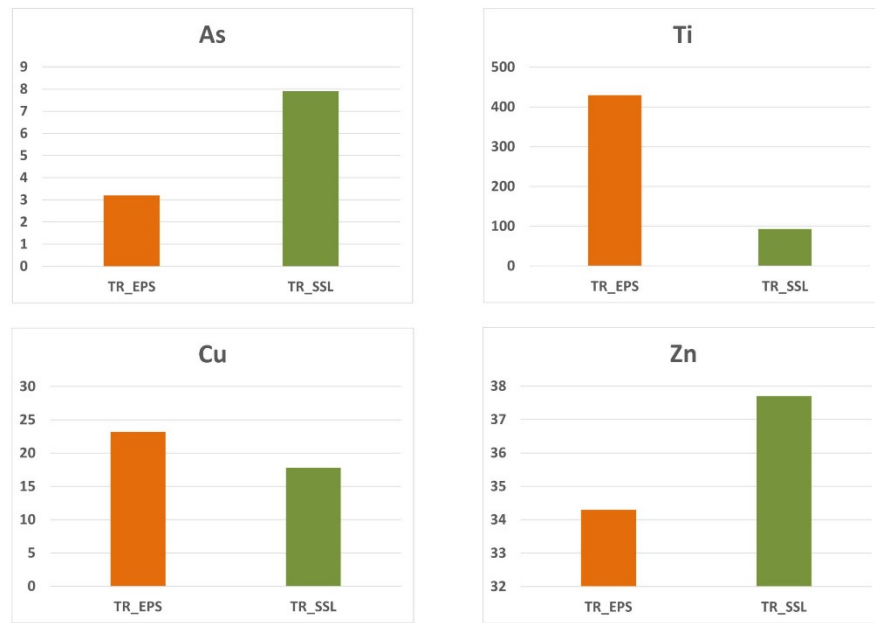
Figure 3. Bar diagrams showing the concentration of some PTEs (heavy metals expressed in ppm) in tremolite asbestos from Episcopia (TR_EPS) and San Severino Lucano (TR_SSL).
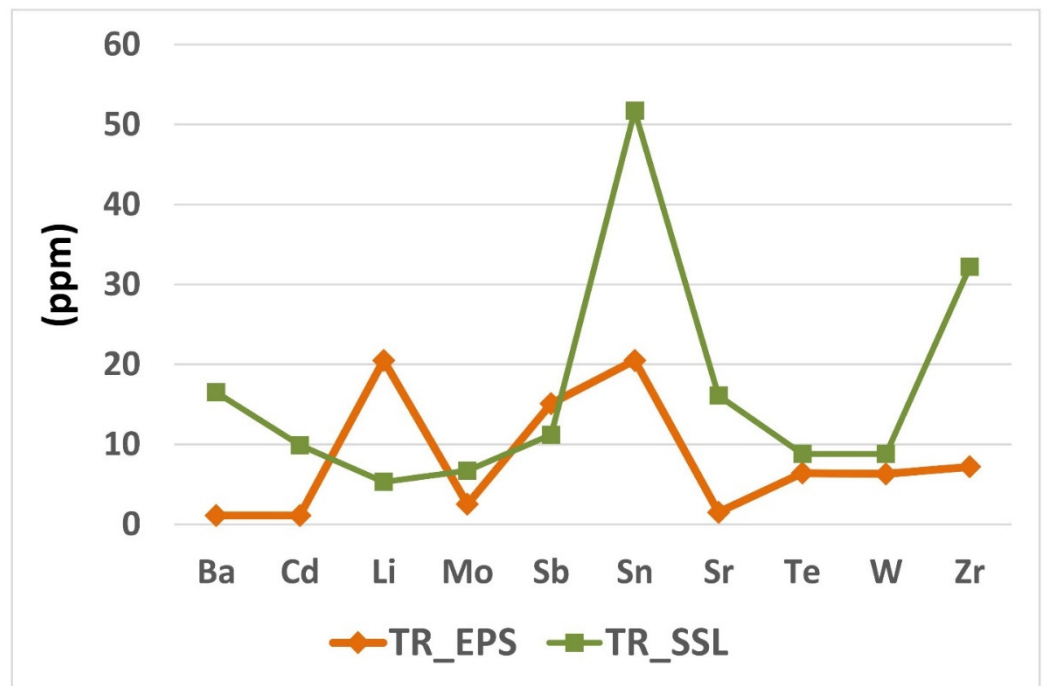

Figure 4. Trace elements concentration (ppm) in tremolite asbestos from Episcopia (TR_EPS) and San Severino Lucano (TR_SSL).

All these elements are present in a higher amount in the TR_SSL rather than TR_EPS sample, except for Li and Sb. Indeed, Ba and Cd in TR_EPS are present at about 1.0 ppm, versus 16.5 ppm and about 10 ppm in TR_SSL, respectively, as well as the amount of Sn (20.5 ppm), Sr (1.5 ppm) and Zr (7.2 ppm) are lower than those ones detected in TR_SSL (51.7 ppm, 16.1 ppm, 32.2 ppm of Sn, Sr, and Zr respectively). However, the difference in Mo, Te and W concentration amounts between the studied samples is not very obvious. Indeed, Mo values are 2.5 ppm versus 6.7 ppm, Te 6.4 ppm versus 8.8 ppm and 6.3 ppm and W 8.8 ppm for TR_EPS and TR_SSL respectively. As for Li and Sb, they were detected

with higher amounts in TR_EPS showing values of 20.5 ppm and 15.1 ppm respectively versus 5.3 ppm (Li) and 11.2 ppm (Sb) in TR_SSL (Figure 4, Table 2). The concentration levels of all the trace elements detected in the studied samples are reported in Figure 5, in which it is possible to observe the amounts of Cr and Ni much higher than the other ones.
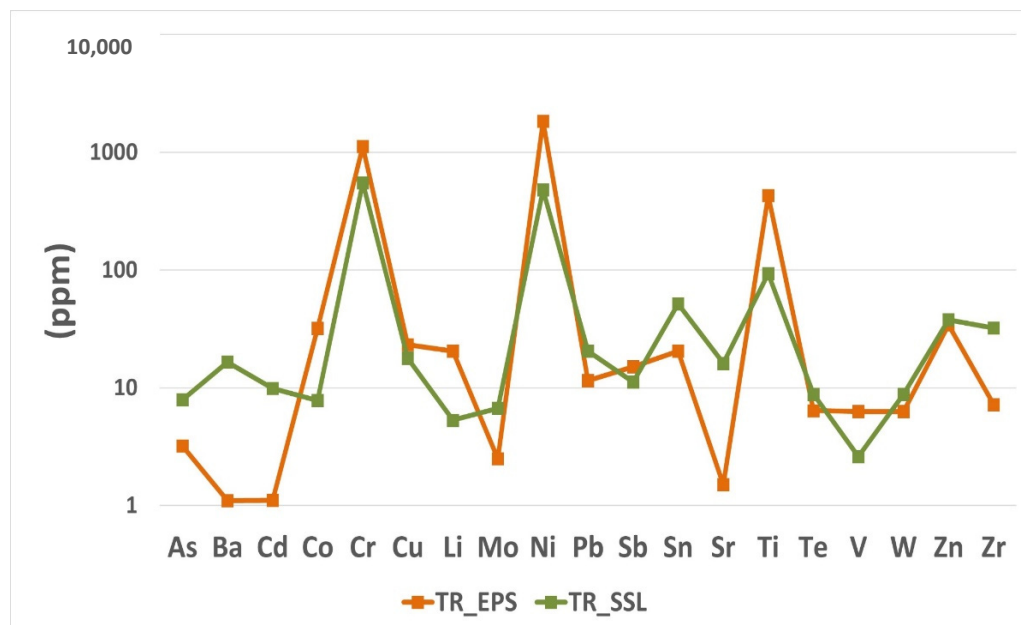

Figure 5. Comparison of trace elements concentration in tremolite asbestos from Episcopia (TR_EPS) and San Severino Lucano (TR_SSL) villages.

4. Discussion

4.1. PTEs in Tremolite Fibers

Chemical results of the analyzed tremolite asbestos samples from Episcopia (TR_EPS) and San Severino Lucano (TR_SSL) villages in the Basilicata region (southern Italy) revealed a relevant concentration of PTEs. Specifically, among major and minor elements, high values of Fe and Mn, whose role in inducing toxicity is well known [19,20,26,27], stand out in both samples. The presence as well as the structural coordination of Fe, together with surface ferrous ions were considered as important factors in carcinogenicity, because of their ability to catalyse the production of reactive oxygen species (ROS) [20,26,27].

As for Mn, despite it represents an essential nutrient for the human body, an excessive dose can otherwise cause some adverse health effects [28]. Literature studies showed that chronic exposure to high levels of Mn provokes permanent neurological damage, as also observed in former manganese mining workers and smelters [29].

As far as trace elements are concerned, Cr and Ni were detected in significant amounts in the studied samples, thus suggesting the high toxicity character of the fibers. Several studies showed that Cr in the hexavalent redox state is highly toxic and may cause adverse effects on human health [1]; similarly, Ni may induce tumors especially at primary cell cultures, where Ni ions cause significant cellular damage and apoptosis [29,30]. Beyond these two most abundant elements, the high amounts of other heavy metals such as Co, V, Ti, Cu in TR_EPS and As and Zn in TR_SSL contribute to increasing the toxicity character of the studied samples. For instance, V has the capacity to affect the activities of various intracellular enzyme systems and to the respiratory, circulatory and central nervous systems whereas As may cause the poor functioning of cell respiration as well as that of cell enzymes and mitosis since it primarily affects the sulfhydryl group of cells of the body [31]. By taking into account the many factors affecting the health effects relating to the presence of PTEs in asbestos fibers structure, it may be useful to consider the total balance of PTEs in the studied samples (i.e., $\sum$(As, Ba, Cd, Co, Cr, Cu, Li, Mo,

Ni, Pb, Sb, Sn, Sr, Ti, Te, V, W, Zn, Zr)), which may assist to the toxicity of the different types of tremolite studied in the present work. Indeed, high amounts of heavy metals can contribute to the toxic potential, provided that the fibers are allowed to release their content according to the extent of their dissolution rate. As shown in Figure 6, the TR_EPS specimen is more enriched in PTEs than TR_SSL; therefore, it could be likely assumed that TR_EPS is potentially more dangerous than TR_SSL. In fact, the sum of the PTEs detected in TR_EPS is 3572.61 ppm vs. 1384.4 ppm of TR_SSL (Figure 6, Table 2). As far as the toxic potential of the different types of tremolite is regarded, the presence of high content of heavy metal can contribute, provided that the fibers will be allowed to release their content according to the extent of their dissolution rate. On this basis, the presence of PTEs in asbestos tremolite in the investigated area may constitute a potential risk for human health. Nevertheless, it is worth noting that TR_SSL is highly enriched in Fe (Figure 2b, Table 1), which plays an important role in asbestos-induced cytotoxicity [19,20]. These results can be used in the predictive model realized by Gualtieri [8] to obtain the fiber's potential toxicity/pathogenicity index (FPTI). It is worth mentioning, that the combination of various factors such as the dose of the pollutant, the duration of the exposure as well as the various impact of the PTEs on the organism, contribute to the definition of the negative health effects. Indeed, if enough of these elements cumulate into the lungs, because of the fibers dissolution processes, they may provoke the development of cancer (e.g., mesothelioma and bronchogenic carcinoma) [8–11], since they may change the baseline concentrations of these elements in the lungs (Table 3; [32]).
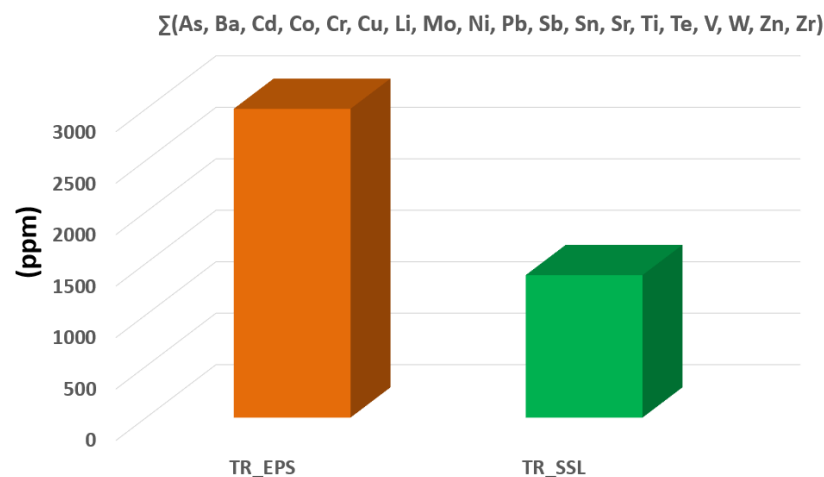

Figure 6. Total trace elements concentration (ppm) in the investigated samples. TR_EPS = tremolite asbestos from Episcopia; TR_SSL = tremolite asbestos from San Severino Lucano.

Table 3. Trace elements (ppm) in the analyzed tremolite asbestos from Episcopia (TR_EPS), San Severino (TR_SSL), and tremolite asbestos from GMRU (TR_GMRU) and Val d'Ala (TR_VLA) studied by Bloise et al. [15,16] showed for comparison. * Indicative baseline data for some trace elements in normal human lung tissues [29].

ppm	TR_EPS	TR_SSL	TR_GMRU	TR_VLA	Concentration Range in Human Lungs *
As	3.20	7.90	1.20	n.d.	0.001–0.10
Ba	1.10	16.50	14.80	0.61	>1.10
Co	31.90	7.80	22.64	26.92	0.002–0.10
Cr	1120	550	170.91	165	0.002–0.50
Cu	23.20	17.80	24.53	3.23	1–5.00

Table 3. *Cont.*

ppm	TR_EPS	TR_SSL	TR_GMRU	TR_VLA	Concentration Range in Human Lungs *
Ni	1830	480	308.63	473	0.01–1.00
Pb	11.50	20.50	4.40	0.45	0.02–0.50
Sb	15.10	11.20	0.20	0.03	0.002–0.10
Sr	1.50	16.10	200	6.59	0.01–1.00
V	6.30	2.60	7.10	13.06	0.0005–0.50
Zn	34.30	37.70	28.42	17.19	1–30.00
$\sum_{TOT}$	3078.10	1168.10	782.83	706.08	

PTEs can be present in asbestos fibers (i.e., chrysotile and amphiboles) structure as isomorphic substitutions. Moreover, the significant capability of amphiboles for hosting trace elements in octahedral sites (specifically M1, M2, M3) confirms the high amounts of heavy metals detected in the studied samples [12]. For instance, Ni and Co in tremolite likely occupy the specific crystallographic M1 and M3 sites while Cr mainly occupies the M2 site.

4.2. Environmental Impact of PTEs

PTEs are usually found in the environment and, in small concentrations, they are needed for maintaining good health; nevertheless, in excessive doses, they can become toxic or hazardous. Indeed, heavy metals can hurt the functioning of organs such as the brain and lungs or affect the blood composition [33–35]. By considering that ophiolite rocks constitute a source of asbestos and widely occur worldwide [5], the quantification of PTEs contained in asbestos fibers is crucial to limit human exposure, especially that one of people living near NOA outcrops. In fact, under specific environmental conditions, potentially toxic elements can be released into the environment, thus constituting a serious hazard for human health. As documented by literature, both areas of Episcopia and San Severino Lucano villages are characterized by a wide occurrence of asbestos [6,21,36], which can become bioavailable and cause the pollution of soils, water as well as the atmosphere. Punturo et al. [36], carried out a multidisciplinary study on serpentinite rocks and derivative soils cropping out in the surroundings of San Severino Lucano, with the aim of determining their bulk chemistry. Results showed, in both rocks and soils, a number of toxic elements (i.e., Cr, Co, Ni, V) exceeding the regulatory threshold for public, private and residential green use [Italian Legislative Decree N°.152 of 03/04/2006]. Moreover, a significant excess of health problem NOA-correlated cases [2] was verified by epidemiological studies conducted on twelve villages of this part of the region. Specifically, several mesothelioma cases were documented in the area 20 km far away from Episcopia village and the main cause recognized was the exposure to asbestos minerals [37,38].

Based on the results of this work, the studied samples from Episcopia (TR_EPS) and San Severino Lucano (TR_SSL) villages are characterized by significant amounts of PTEs hosted into asbestos, which may be potentially harmful to humans. The presence of the high amount of these elements in the fiber structure, not only increases the toxicity character of the studied tremolite asbestos but also makes the environmental exposure riskier, due to the occurrence of the mother rock from which they were extracted.

4.3. PTEs Comparison

With the aim of observing the difference in PTEs content of tremolite asbestos occurring in another part of the Italian territory, our data were compared to those collected by Bloise et al. [15,16] (Table 3) on tremolite from Gimigliano-Mount Reventino Unit (GMRU; Calabria region, Southern Italy), and tremolite from Val d'Ala (TR_VLA; Piedmont region, Northern Italy) in order to assess, based on the total amount of toxic elements, which one could potentially be more dangerous to human health. As shown in Figure 7, compared to those ones detected by Bloise et al. [15,16], the samples of the present work revealed a

higher amount of most potentially toxic elements. In particular, Cr and Ni values of the samples studied in the present work are much higher than those detected in the other ones, especially in TR_EPS in which their concentration reaches 1120 ppm (Cr) and 1830 ppm (Ni). Moreover, a higher amount of Co and Sb characterize TR_EPS whereas tremolite from San Severino Lucano results enriched in As, Ba, Pb and Zn. Differently, TR_GMRU shows a high concentration of Cu (24.53 ppm) and Sr (200 ppm) while TR_VLA is more enriched in V which amount is about 13 ppm (Table 3). By considering the total amount of toxic elements in tremolite asbestos samples (Figure 7), it is possible to assess that TR_EPS is the specimen with the highest amount of PTEs (3078.1 ppm) followed by TR_SSL (1168.1 ppm), TR_GMRU (782.83 ppm) and TR_VLA (706.08 ppm). Therefore, on the basis of the results of the present study and of those conducted by Bloise et al. [20,28], tremolite asbestos from Episcopia and San Severino Lucano are the samples with the highest amount of most PTEs. Therefore, considered equal to the other conditions (e.g., size, duration of exposure), they are potentially toxic to a greater extent. The different concentrations of toxic elements in the tremolite asbestos samples observed, may be due to both the chemical variability of amphiboles and to the geochemical/petrological processes involved in the formation of asbestos fibers [6,12,16].
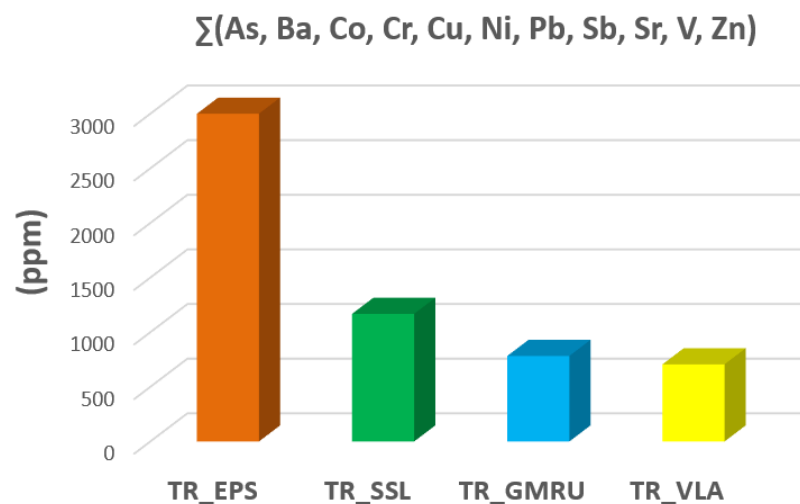

Figure 7. Total amount of trace elements (ppm) in the analyzed tremolite asbestos from Episcopia (TR_EPS), San Severino (TR_SSL), and tremolite asbestos from Gimigliano–Mount Reventino Unit, Calabria (TR_GMRU) and Val d'Ala, Piedmont (TR_VLA) studied by Bloise et al. [15,16] and showed for comparison.

5. Conclusions

In the current study, the concentration of PTEs in two different tremolite asbestos samples coming from serpentinite rocks cropping out in the surroundings of Episcopia and San Severino Lucano villages (Basilicata region, Southern Italy) were analyzed. Micro X-ray fluorescence (μ-XRF) and Inductively Coupled Plasma spectroscopy with Optical Emission Spectrometry (ICP-OES) techniques were used to determine the concentration of major, minor (Si, Mg, Ca, Al, Fe, Mn) and trace elements (As, Ba, Cd, Co, Cr, Cu, Li, Mo, Ni, Pb, Sb, Sn Sr, Ti, Te, V, W, Zn, Zr).

The intrinsic toxicity of asbestos tremolite fibers added to the fact that one of the PTEs results in an extremely dangerous combination for humans and the long-term exposure for the inhabitants of the surrounding areas could derive from the development of different kinds of diseases. The various element concentrations into the two samples allow us to further distinguish them in terms of PTEs amount. High concentrations of trace elements were detected and, by considering the total balance of PTEs in the studied samples (∑(As, Ba, Cd, Co, Cr, Cu, Li, Mo, Ni, Pb, Sb, Sn, Sr, Ti, Te, V, W, Zn, Zr)), TR_EPS results to be the asbestos sample with the highest amount of PTEs. The data of our study have general

implications regarding their possible use to calculate fiber potential toxicity/pathogenicity index (FPTI) which can be a helpful tool for the interpretation of results of in vitro and in vivo testing. Moreover, our study highlights the importance of quantifying PTEs present in asbestos minerals since they increase the toxic character of fibers and can cause lung cancer in humans.

References

1. IARC; Working Group on the Evaluation of Carcinogenic Risk to Humans. *IARC Monographs on the Evaluation of Carcinogenic Risks to Humans*; No. 100C; International Agency for Research on Cancer: Lyon, France, 2012.
2. Baumann, F.; Buck, B.J.; Metcalf, R.V.; McLaurin, B.T.; Merkler, D.J.; Carbone, M. The presence of asbestos in the natural environment is likely related to mesothelioma in young individuals and women from Southern Nevada. *J. Thorac. Oncol.* **2015**, *10*, 731–737. [CrossRef] [PubMed]
3. International Ban Asbestos Secretariat. Available online: http://www.ibasecretariat.org/alpha_ban_list.php (accessed on 15 July 2019).
4. Virta, R. *Worldwide Asbestos Supply and Consumption Trends from 1900 through 2003*; U.S. Geological Survery: Reston, VA, USA, 2006; p. 80.
5. Ricchiuti, C.; Bloise, A.; Punturo, R. Occurrence of asbestos in soils: State of the Art. *Episodes* **2020**, *43*, 881–891. [CrossRef]
6. Bloise, A.; Catalano, M.; Critelli, T.; Apollaro, C.; Miriello, D. Naturally occurring asbestos: Potential for human exposure, san Severino Lucano (Basilicata, southern Italy). *Environ. Earth Sci.* **2017**, *76*, 648. [CrossRef]
7. Feder, I.S.; Tischoff, I.; Theile, A.; Schmitz, I.; Merget, R.; Tannapfel, A. The asbestos fibre burden in human lungs: New insights into the chrysotile debate. *Eur. Respir. J.* **2017**, *49*, 1602534. [CrossRef] [PubMed]
8. Gualtieri, A.F. Towards a quantitative model to predict the toxicity/pathogenicity potential of mineral fibers. *Toxicol. Appl. Pharmacol.* **2018**, *361*, 89–98. [CrossRef]
9. Dixon, J.R.; Lowe, D.B.; Richards, D.E.; Cralley, L.J.; Stokinger, H.E. The role of trace metals in chemical carcinogenesis: Asbestos cancers. *Cancer Res.* **1970**, *30*, 1068–1074.
10. Nemery, B. Metal toxicity and the respiratory tract. *Eur. Respir. J.* **1990**, *3*, 202–219. [CrossRef]
11. Wei, B.; Yang, L.; Zhu, O.; Yu, J.; Jia, X. Multivariate analysis of trace elements distribution in hair of pleural plaques patients and health group in a rural area from China. *Hair Ther. Transplant.* **2014**, *4*, 2167–3118. [CrossRef]
12. Tiepolo, M.; Oberti, R.; Zanetti, A.; Vannucci, R.; Foley, S.F. Trace-element partitioning between amphibole and silicate melt. In *Amphiboles: Crystal Chemistry, Occurrence, and Health Issues*; Hawthorne, F.C., Oberti, R., Della Ventura, G., Mottana, A., Eds.; Mineralogical Society of America: Chantilly, VA, USA, 2007; Volume 67, pp. 417–452.
13. Vils, F.; Pelletier, L.; Kalt, A.; Muntener, O.; Ludwig, T. The lithium, boron and beryllium content of serpentinized peridotites from ODP Leg 209 (Sites 1272A and 1274A): Implications for lithium and boron budgets of oceanic lithosphere. *Geochim. Cosmochim. Acta* **2008**, *72*, 5475–5504. [CrossRef]
14. Bargagli, E.; Monaci, F.; Bianchi, N.; Bucci, C.; Rottoli, P. Analysis of trace elements in bronchoalveolar lavage of patients with diffuse lung diseases. *Biol. Trace Elem. Res.* **2008**, *124*, 225–235. [CrossRef]

15. Bloise, A.; Barca, D.; Gualtieri, A.F.; Pollastri, S.; Belluso, E. Trace elements in hazardous mineral fibres. *Environ. Pollut.* **2016**, *216*, 314–323. [CrossRef] [PubMed]

16. Bloise, A.; Ricchiuti, C.; Punturo, R.; Pereira, D. Potentially toxic elements (PTEs) associated with asbestos chrysotile, tremolite and actinolite in the Calabria region (Italy). *Chem. Geol.* **2020**, *558*, 119896. [CrossRef]

17. Cralley, L.J.; Keenan, R.G.; Kupel, R.E.; Kinser, R.E.; Lynch, J.R. Characterization and solubility of metals associated with asbestos fibers. *Am. Ind. Hyg. Assoc. J.* **1968**, *29*, 569–573. [CrossRef]

18. Schreier, H.; Northcote, T.G.; Hall, K. Trace metals in fish exposed to asbestos rich sediments. *Water Air Soil Pollut.* **1987**, *35*, 279–291. [CrossRef]

19. Shukla, A.; Gulumian, M.; Hei, T.K.; Kamp, D.; Rahman, Q.; Mossman, B.T. Multiple roles of oxidants in the pathogenesis of asbestos-induced diseases. *Free Radic. Biol. Med.* **2003**, *34*, 1117–1129. [CrossRef]

20. Pacella, A.; Tomatis, M.; Viti, C.; Bloise, A.; Arrizza, L.; Ballirano, P.; Turci, F. Thermal inertization of amphibole asbestos modulates Fe topochemistry and surface reactivity. *J. Hazard. Mater.* **2020**, *398*, 123119. [CrossRef] [PubMed]

21. Bloise, A.; Ricchiuti, C.; Giorno, E.; Fuoco, I.; Zumpano, P.; Miriello, D.; Apollaro, C.; Crispini, A.; De Rosa, R.; Punturo, R. Assessment of Naturally Occurring Asbestos in the Area of Episcopia (Lucania, Southern Italy). *Fibers* **2019**, *7*, 45. [CrossRef]

22. Dichicco, M.C.; De Bonis, A.; Mongelli, G.; Rizzo, G.; Sinisi, R. μ-Raman spectroscopy and X-ray diffraction of asbestos' minerals for geo-environmental monitoring: The case of the southern Apennines natural sources. *Appl. Clay Sci.* **2017**, *141*, 292–299. [CrossRef]

23. Dichicco, M.C.; Laurita, S.; Sinisi, R.; Battiloro, R.; Rizzo, G. Environmental and Health: The Importance of Tremolite Occurence in the Pollino Geopark (Southern Italy). *Geosciences* **2018**, *8*, 98. [CrossRef]

24. Dichicco, M.C.; Paternoster, M.; Rizzo, G.; Sinisi, R. Mineralogical Asbestos Assessment in the Southern Apennines (Italy): A Review. *Fibers* **2019**, *7*, 24. [CrossRef]

25. IARC. *Beryllium, Cadmium, Mercury, and Exposures in the Glass Manufacturing Industry*; International Agency for Research on Cancer: Lyon, France, 1993.

26. Fantauzzi, M.; Pacella, A.; Atzei, D.; Gianfagna, A.; Andreozzi, G.B.; Rossi, A. Combined use of X-ray photoelectron and Mossbauer spectroscopic techniques in the analytical characterization of iron oxidation state in amphibole asbestos. *Anal. Bioanal. Chem.* **2010**, *396*, 2889. [CrossRef]

27. Liu, G.; Cheresh, P.; Kamp, D.W. Molecular Basis of Asbestos-Induced Lung Disease. *Annu. Rev. Pathol. Mech. Dis.* **2013**, *8*, 161–187. [CrossRef] [PubMed]

28. Williams, M.; Todd, G.D.; Roney, N.; Crawford, J.; Coles, C.; McClure, P.R.; Garey, J.D.; Zaccaria, K.; Citra, M. Health Effects. In *Toxicological Profile for Manganese*; Agency for Toxic Substances and Disease Registry: Atlanta, GA, USA, 2012; pp. 39–360.

29. Biedermann, K.A.; Landolph, J.R. Induction of anchorage independence in human diploid foreskin fibroblasts by carcinogenic metal salts. *Cancer Res.* **1987**, *47*, 3815–3823.

30. Lee, Y.J.; Lim, S.S.; Baek, B.J.; An, J.M.; Nam, H.S.; Woo, K.M.; Cho, M.K.; Kim, S.H.; Lee, S.H. Nickel (II)-induced nasal epithelial toxicity and oxidative mitochondrial damage. *Environ. Toxicol. Pharmacol.* **2016**, *42*, 76–84. [CrossRef] [PubMed]

31. Gordon, J.J.; Quastel, G.H. Effect of organic arsenicals on enzyme system. *Biochem. J.* **1948**, *42*, 337–350. [CrossRef] [PubMed]

32. Vanoeteren, C.; Cornelis, R.; Sabbioni, E. *Critical Evaluation of Normal Levels of Major and Trace Elements in Human Lung Tissue*; Commission of the European Communities: Luxembourg, 1986.

33. Censi, P.; Zuddas, P.; Randazzo, L.A.; Tamburo, E.; Speziale, S.; Cuttitta, A.; Punturo, R.; Aricò, P.; Santagata, R. Source and nature of inhaled atmospheric dust from trace element analyses of human bronchial fluids. *Environ. Sci. Technol.* **2011**, *45*, 6262–6267. [CrossRef] [PubMed]

34. Jaishankar, M.; Tseten, T.; Anbalagan, N.; Mathew, B.B.; Beeregowda, K.N. Toxicity, mechanism and health effects of some heavy metals. *Interdiscip. Toxicol.* **2014**, *7*, 60–72. [CrossRef] [PubMed]

35. Bloise, A.; Kusiorowski, R.; Lassinantti Gualtieri, M.; Gualtieri, A.F. Thermal behaviour of mineral fibers. In *Mineral Fibers: Crystal Chemistry, Chemical-Physical Properties, Biological Interaction and Toxicity*; Gualtieri, A.F., Ed.; European Mineralogical Union: London, UK, 2017; Volume 18, pp. 215–252.

36. Punturo, R.; Ricchiuti, C.; Mengel, K.; Apollaro, C.; De Rosa, R.; Bloise, A. Serpentinite-derived soils in southern Italy: Potential for hazardous exposure. *J. Mediterr. Earth Sci.* **2018**, *10*, 51–61.

37. Musti, M.; Bruno, C.; Cassano, F.; Caputo, A.; Cauzillo, G.; Cavone, D.; Convertini, L.; De Blasio, A.; De Mei, B.; Marra, M.; et al. Sorve-glianza sanitaria delle popolazioni esposte a fibre di tremolite nel territorio della ASL 3—Lagonegro (PZ). *Ann. Dell'istituto Super. Sanità* **2006**, *42*, 469–476.

38. Caputo, A.; De Santis, M.; Manno, V.; Cauzillo, G.; Bruni, B.M.; Palumbo, L.; Conti, S.; Comba, P. Health impact of asbestos fibres naturally occurring in Mount Pollino area (Basilicata Region, Southern Italy). *Epidemiol. Prev.* **2018**, *42*, 142–150.